SHEAR DISTRIBUTION IN PRESTRESSED CONCRETE GIRDER BRIDGES

A DISSERTATION
SUBMITTED TO THE FACULTY OF THE GRADUATE SCHOOL
OF THE UNIVERSITY OF MINNESOTA
BY

Benjamin Z. Dymond

IN PARTIAL FULFILLMENT OF THE REQUIREMENTS
FOR THE DEGREE OF
DOCTOR OF PHILOSOPHY

Dr. Catherine E. W. French
Dr. Carol K. Shield

October 2015

ACKNOWLEDGEMENTS

I would first like to acknowledge Drs. Cathy French and Carol Shield within the structural engineering group at the University of Minnesota. Their mentorship, technical expertise, and interest in both my well-being and the research topic were greatly appreciated throughout my time as a University of Minnesota graduate student. I would like to extend a sincere thank you to my committee members Drs. Perry Leo and Henryk Stolarski. Dr. Henryk Stolarski was an exceptional mentor as I completed the teaching aspects within the University's Preparing Future Faculty program.

Funding for this research was provided by the Minnesota Department of Transportation (MnDOT) and it is gratefully acknowledged. This research would not have been possible without the expertise of the MnDOT technical advisory panel; their knowledge and assistance were appreciated. Numerical computations were performed using resources provided by the University of Minnesota Supercomputing Institute.

Materials, equipment, and technical expertise was also generously provided by the following groups at various times during the project: ABC Coating Co., Advance Shoring, Ambassador Steel, the Cement Masons, Plasterers & Shophands Local No. 633 union, Cemstone Concrete, Cretex Concrete Products, Graham Construction, Lametti & Sons, Inc., Minnesota Prestressing Association, PCiRoads, and RebarFab Inc.

I would like to acknowledge the assistance of numerous graduate and undergraduate students throughout the project; support was provided by more people than I can count on two hands and two feet. Without their help and advice related to laboratory testing, field testing, and finite element modeling, this project would not have been completed. I also greatly appreciate the assistance provided by Paul Bergson, Chris Bruhn, Rachel Gaulke, and Jane Govro in all aspects of experimental testing.

Finally, I would like to acknowledge the support that family and friends have provided over the years. My time as a graduate student at the University of Minnesota was incredible. I am extremely thankful that I have an extraordinary wife, Salli, and daughter, Cece. Without their smiles and unwavering support, I would not have be able to complete this journey. They certainly deserve more accolades than can be written here.

TABLE OF CONTENTS

LIST OF TABLES

LIST OF FIGURES

CHAPTER 1. INTRODUCTION

1.1 Background and Motivation

Moderate length (45 to 180 ft) straight and skewed highway bridges with precast, prestressed concrete girders and reinforced concrete decks are common in bridge construction because of a lower initial material cost relative to other bridge systems and relatively low maintenance costs through the life of the structure (Barnes et al. 2003). An engineer uses load rating information related to load carrying capacity of a bridge to decide if a bridge needs to be posted with the safe live load carrying capacity. The safe live load capacity of an *in situ* bridge is determined using visual inspection and load rating techniques. Similar to bridge design, load rating requires an estimate of live load distribution through the bridge system to individual girders. Because shear deterioration is known to be an abrupt process that is difficult to monitor through visual inspection and may occur without warning (Nilson 1987), it is especially important to use accurate shear distribution factors to estimate the bridge capacity and avoid brittle failures.

The American Association of State Highway and Transportation Officials (AASHTO) requirements for the consideration of shear in prestressed concrete girders have changed considerably over the last 50 years. In the 1970 edition of the AASHTO Standard Specifications, it was permissible to use the stirrup spacing required at the quarter point for all locations in the girder between the support and the quarter point. More recent specifications changed the critical location from the quarter point to a location much closer to the support. When girders designed using the 1970 specification are rated with current methods, the structure may rate poorly for shear. Bridges that rate poorly for shear do not often show signs of distress under normal traffic conditions. They are often deemed to be in good condition, and therefore, the resulting shear rating may be neglected as outlined in the AASHTO Manual for Bridge Evaluation (2011), which states that "in-service concrete bridges that show no visible signs of shear distress need not be checked for shear when rating for the design load or legal loads."

Many primary bridge parameters affect live load distribution at service and ultimate such as beam depth and spacing, deck thickness, skew angle, span length, and aspect ratio. Puckett et al. (2007) stated that "secondary [bridge] elements, such as diaphragms and

barriers, have been shown to make a significant difference in lateral load distribution in some cases. However, the literature shows conflicting results with respect to their degree of effectiveness." Specifically, conflicting numerical analysis results are presented by Huo et al. (2003) and Puckett et al. (2007) for the same prestressed concrete girder bridge. Results from Huo et al. (2003) indicated that abutment support diaphragms caused a decrease in the shear distribution factor in conflict with the study done by Puckett et al. (2007) that indicated abutment support diaphragms slightly increased the shear distribution factor.

These conflicting results led Dereli et al. (2010) to recommend that the accuracy of the shear live load distribution factors be further assessed through experimental testing of prestressed concrete girder bridges. A better understanding of the shear distribution in prestressed concrete girder bridges is needed to more accurately assess *in situ* capacity using load rating techniques. This goal was reinforced by Tobias (2011) who stated that "the subject of load distribution has been and continues to be somewhat controversial and has seen several efforts at improvement and refinement over the years."

1.2 Objectives and Scope

The research described herein was part of a project sponsored by the Minnesota Department of Transportation (MnDOT) to investigate the accuracy of existing shear distribution factors and to provide recommendations regarding shear distribution to be used in Minnesota. Distribution factors from the AASHTO Load and Resistance Factor Design (LRFD) Specifications (2010) were developed in relation to the critical section for shear (near a support) and may be overly conservative for loads and critical sections further into the span. The goals of the research were to experimentally and numerically investigate live load shear distribution and develop recommendations that might be used to more accurately rate for shear and permit truck crossings on prestressed concrete bridge girders while maintaining adequate safety. This study involved an in-depth investigation regarding the effects of design parameters (e.g., girder size and spacing, bridge length and width, skew, longitudinal and transverse stiffness, and deck thickness) and secondary elements (e.g., barriers and diaphragms) on the live load distribution of shear.

To achieve the goals of the project, Figure 1-1 illustrates the integrated experimental and numerical research approach. The experimental research components

involved both *in situ* field and laboratory tests to assess shear distribution. Numerical analyses were used to identify the variables to be investigated experimentally and to refine the instrumentation and loading plans for the experimental studies. The *in situ* field tests involved truck load tests of six *in situ* prestressed concrete bridge structures in the MnDOT inventory. The laboratory tests involved the construction and testing of a full-scale single span bridge and a single companion girder in the University of Minnesota Theodore V. Galambos Structural Engineering Laboratory. Prior to taking the laboratory bridge into the inelastic range of behavior, a number of elastic tests were conducted to investigate the effects of loading position, as well as the effects of the presence/absence of end diaphragms and barrier railings on shear distribution. The elastic tests were used to validate the numerical modeling approach, which was used to conduct a parametric study to examine how shear forces distribute in different types of prestressed concrete girder bridge structures. Core parameters (e.g., girder spacing and depth, span length, and deck thickness) were de-coupled and a single parameter was varied from a base configuration in the parametric study. The integrated research approach, taking into account other sources of data from the literature, provided the basis for development of recommendations for shear live load distribution.

1.3 Document Organization

Chapter 2 contains a literature review including discussion of shear specifications related to prestressed concrete beams, load rating of existing bridges, and methods for predicting shear distribution.

Chapter 3 is a discussion of the numerical analysis tools used throughout the project. Three types of computer modeling were used: three-dimensional grillage models to determine a rational instrumentation plan, three-dimensional finite element analysis during and after experimental testing to understand complex structural behavior, and two-dimensional grillage analysis as a simplified tool for rating.

Chapter 4 contains details related to the design and test setup of the laboratory bridge. This chapter includes an explanation of the bridge structural design and construction, instrumentation used, and details regarding the experimental test setup.

Chapter 5 describes the results of the laboratory bridge tests in both the elastic and inelastic range. Validation of the finite element modeling technique with respect to the elastic bridge test results is also described.

Chapter 6 discusses the field bridge live load testing methodology and results for six structures from the MnDOT inventory. Details are provided regarding the field location of instrumentation and live load trucks for each of the bridges tested. A description of how the field bridge data were used to validate the finite element modeling technique and the effects of torsion on field bridge data are included. A section is included with recommendations for future live load tests used to collect shear distribution data.

Chapter 7 details the numerical parametric study and introduces the proposed methodology for rating prestressed concrete girder bridges. The parametric study, which was conducted with a validated finite element modeling technique, was used to characterize shear distribution in several bridge configurations. The proposed method for rating prestressed concrete girder bridges was based on a comparison of finite element model live load shear demand and live load shear demand obtained using AASHTO distribution factor methods. The proposed method for rating uses a simplified 2D grillage analysis to calculate the live load shear demand for interior girders.

Chapter 8 synthesizes results from the various parts of the project and provides the final recommendations. The key findings and how they affect shear distribution are included and discussed.

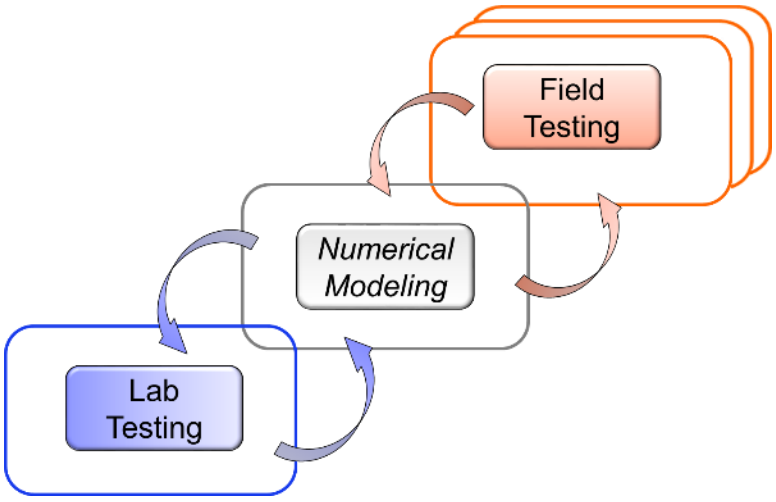

Figure 1-1. Integrated Experimental and Numerical Research Techniques

CHAPTER 2. LITERATURE REVIEW

2.1 Shear Capacity

Prestressed concrete members are commonly subjected to shear and flexural loading. Each of these load effects causes a different type of ultimate failure. Shear failures are sudden, typically without any visible warning. This type of brittle failure is undesirable and has caused costly premature and catastrophic failures of reinforced and prestressed concrete members (Collins and Mitchell 1997). Brittle shear failures can be avoided by providing an adequate web thickness and transverse shear reinforcement in members with high shear forces. Shear degradation and stress redistribution after cracking are complex phenomena. Many factors affect shear transfer in cracked, prestressed concrete beams, including: shear transfer in the uncracked compression zone, aggregate interlock, vertical dowel action of longitudinal reinforcement, resistance provided by transverse shear reinforcement, and the vertical component of the draped prestressing strands (ASCE 1973, ASCE 1998).

This section provides a brief description of empirical sectional models from the AASHTO Standard Specifications (2002) and the AASHTO LRFD Specifications (2010). The AASHTO Standard Specifications (1989) were also used for design in this project, but are the same as the 2002 AASHTO Standard Specifications. More detail on historical AASHTO Standard Specifications can be found in Runzel et al. (2007) and Dereli et al. (2010).

2.1.1 AASHTO Standard Specification Provisions

The AASHTO Standard Specifications 17th Edition (2002) states that the nominal shear strength, V_n, multiplied by a resistance factor, ϕ, must be greater than or equal to the factored shear force at the section of consideration, V_u. The nominal shear strength consists of shear resistance provided by the concrete, V_c, and shear resistance provided by the transverse reinforcement, V_s.

The concrete shear strength, V_c, is the lower of the flexure-shear strength, V_{ci}, and the web-shear strength, V_{cw}. The flexure-shear strength, V_{ci} in pounds, specified in AASHTO Standard (2002) Article 9.20.2.2, is computed using:

$$V_{ci} = 0.6\sqrt{f'_c}b'd + V_d + \frac{V_i M_{cr}}{M_{\max}} \geq 1.7\sqrt{f'_c}b'd \qquad (2.1)$$

where f'_c is the specified compressive strength of the concrete at 28 days (psi), b' is the web width of a flanged member (in.), d is the distance from the extreme compressive fiber to the centroid of the prestressing force (in.), V_d is the shear force at the section due to unfactored dead load (lb), V_i is the factored shear at the section due to applied loads occurring simultaneously with M_{max} (lb), M_{cr} is the moment that causes flexural cracking at the section due to externally applied loads (lb-in.), and M_{max} is the maximum factored moment at the section due to externally applied loads (lb-in.).

The value of d need not be taken less than $0.8h$ with h being the overall depth of the member. The moment causing flexural cracking at the section due to externally applied loads, M_{cr} in inch-pounds, can be computed from AASHTO Standard (2002) Article 9.20.2.2:

$$M_{cr} = \frac{I}{Y_t}\left(6\sqrt{f'_c} + f_{pe} - f_d\right) \qquad (2.2)$$

where I is the moment of inertia about the centroid of the cross section (in.^{4}), Y_t is the distance from the centroidal axis of the gross section to extreme fiber in tension (in.), f_{pe} is the stress in concrete from effective prestress at extreme tensile stress fiber (psi), and f_d is the stress due to unfactored dead load at extreme tensile stress fiber (psi). The maximum factored moment and factored shear at the section due to externally applied loads, M_{max} and V_i, are computed using the load combination causing the maximum moment at the section of interest.

The web-shear strength, V_{cw} in pounds, specified in AASHTO Standard (2002) Article 9.20.2.3 is computed using:

$$V_{cw} = \left(3.5\sqrt{f'_c} + 0.3f_{pc}\right) b'd + V_p \qquad (2.3)$$

where f_{pc} is the effective compressive stress in the concrete at centroid of cross section (or at the top flange-web intersection if the centroid lies in the top flange) (psi), and V_p is the vertical component of effective prestress force at the section (lb).

AASHTO Article 9.20.2.4 states that in the equation for the web-shear strength, the compressive stress at the centroid of the cross section, f_{pc}, shall include a reduced prestress force between the end of the beam and the transfer length, where the transfer length for this reduction can be taken as 50 strand diameters.

The shear strength provided by the transverse reinforcement, V_s in pounds, is calculated using AASHTO Standard (2002) Article 9.20.3.1:

$$V_s = \frac{A_v f_y d}{s} \leq 8\sqrt{f'_c}\, b' d \tag{2.4}$$

where f_y is the yield stress of nonprestressed web reinforcement in tension ($\leq$ 60,000 psi) (psi), s is the longitudinal spacing of the transverse reinforcement (in.), and A_v is the area of web reinforcement (in.^{2}), no less than:

$$A_v \geq \frac{50 b' s}{f_y} \tag{2.5}$$

The spacing of the transverse reinforcement should not be greater than $0.75h$ or 24 in. If V_s is greater than $4\sqrt{f'_c}b'd$ the maximum spacing of $0.75h$ or 24 in. should be reduced by one half. No shear reinforcement is needed in the section of interest if the factored shear force, V_u, is less than half of ϕV_c.

Finally, the factored shear force at the section of consideration, V_u, must be less than the nominal shear strength, V_n multiplied by the resistance factor, ϕ.

2.1.2 AASHTO LRFD Specification Provisions

The fifth edition of the AASHTO LRFD Specifications (2010) has three methods for determining shear resistance. The first method is only applicable to nonprestressed sections and is essentially identical to methods traditionally used for evaluating shear

resistance. The second method is derived from the modified compression field theory (MCFT) as introduced by Vecchio and Collins (1986) and discussed as a design procedure by Collins et al. (1996). This method can be presented as two approaches. First, the iterative design procedure discussed by Collins et al. (1996) is available for use in AASHTO LRFD Appendix B5 and requires the use of tables for the evaluation of β and θ. Second, a simplified design procedure outlined by Bentz et al. (2006) was introduced in the 2008 Interim AASHTO LRFD Specifications to simplify the iterative, tabulated version of the MCFT. With the 2008 revisions, this design procedure was modified to be non-iterative and algebraic equations were introduced for evaluation of β and θ.

Finally, a third method available in the AASHTO LRFD Specifications was introduced in 2007 to determine shear resistance entitled "Simplified Procedure for Prestressed and Nonprestressed Sections." This procedure was developed by Hawkins et al. (2005) and is discussed in depth by Kuchma et al. (2008). This method provided engineers an alternative to the AASHTO LRFD Specifications based on the MCFT and resembles the AASHTO Standard Specifications procedure.

In the simplified method, the nominal shear resistance, V_n in pounds, consists of shear resistance provided by the concrete, V_c, and shear resistance provided by the transverse reinforcement, V_s. Furthermore, V_n has an upper limit in the simplified method equal to:

$$V_n = V_c + V_s \le \left(2.5\times10^{-4} f'_c\right) b_v d_v \tag{2.6}$$

where b_v is the web width, and d_v is the effective shear depth which need not be taken less than the greater of $0.9d_e$ or $0.72h$ where d_e is the effective depth from extreme compression fiber to the centroid of the tensile force in the tensile reinforcement. The upper limit of V_n was added to ensure that the concrete in the web of the beam will not crush prior to yielding of the transverse reinforcement.

The concrete shear strength, V_c, is the lower of the flexure-shear strength, V_{ci}, and the web-shear strength, V_{cw}. The flexure-shear strength (V_{ci} in pounds), the web shear strength (V_{cw} in pounds), and the shear strength provided by the transverse reinforcement

(V_s in pounds) are specified in AASHTO LRFD (2010) Article 5.8.3.4.3 and computed using:

$$V_{ci} = 0.63\sqrt{f'_c}\,b_v d_v + V_d + \frac{V_i M_{cr}}{M_{\max}} \geq 1.9\sqrt{f'_c}\,b_v d_v \tag{2.7}$$

$$V_{cw} = \left(1.9\sqrt{f'_c} + 0.3 f_{pc}\right) b_v d_v + V_p \tag{2.8}$$

$$V_s = \frac{A_v f_y d}{s}\cot\theta \tag{2.9}$$

where cotθ is equal to unity if $V_{ci} < V_{cw}$, otherwise cotθ is taken as:

$$\cot\theta = 1 + 0.095\frac{f_{pc}}{\sqrt{f'_c}} \leq 1.8 \tag{2.10}$$

Methods from the simplified AASHTO LRFD Specifications and the AASHTO Standard Specifications are compared in Table 2-1. Two changes were incorporated into the simplified AASHTO LRFD calculation for shear capacity, compared to that of the AASHTO Standard method, that make the shear capacity near beam ends more dependent on the transverse reinforcement contribution and less dependent on the web-shear concrete contribution. First, the transverse reinforcement contribution to shear, V_s, is based on the angle of diagonal cracking, θ, obtained from a variable angle truss model. Inclusion of the term based on the angle of diagonal cracking increases the steel contribution to shear in prestressed members by up to 80 percent (due to the upper limit of 1.8 on cotθ) depending on the effective compressive stress in the concrete, f_{pc}, due to both prestress and dead load moments. The AASHTO Standard method does not include a cotθ factor, or more specifically, the angle of diagonal cracking is assumed to be 45 degrees such that the cotangent term reduces to unity.

Second, the concrete contribution to shear from web-shear cracking, V_{cw}, as specified in the simplified AASHTO LRFD is more conservative than the term for V_{cw} in the AASHTO Standard Specifications due to the lower coefficient on $\sqrt{f'_c}$. For girders controlled by V_{cw}, this conservative coefficient decreases the concrete contribution to shear at the critical section compared to results calculated using the AASHTO Standard method.

2.2 Load Rating

The methodology behind new bridge design transitioned from the AASHTO Standard (STD) Specifications to the AASHTO LRFD Specifications after October 1, 2007. However, for modifications or analysis of existing structures, a state department of transportation (DOT) has the option of using the LRFD Specifications or the specifications which were used for the original design (Densmore 2000). The methodology behind evaluation of existing bridges is in transition from the AASHTO Manual for Condition Evaluation of Bridges (2003), which uses load factor rating (LFR) aligned with the AASHTO Standard Specifications, to the Manual for Bridge Evaluation (MBE) (2011), which contains load and resistance factor rating (LRFR) aligned with the AASHTO LRFD Specifications. Data collection for the Federal Highway Administration's (FHWA) April 2005 National Bridge Inventory (NBI) allowed for the inventory rating and operating rating to be reported as a rating factor using either LFR or LRFR. Prior to this date, the LFR rating method was the national standard for calculating inventory and operating ratings reported to the NBI (Zheng et al. 2007). The general equations for load factor rating and load and resistance factor rating are given in Eqn. (2.11) and Eqn. (2.12), respectively:

$$\text{LFR} = \frac{\phi V_n - A_1 V_{DL}}{A_2 V_{LL}} \tag{2.11}$$

$$\text{LRFR} = \frac{\varphi_c \varphi_s \phi V_n - \gamma_{DC} V_{DC} - \gamma_{DW} V_{DW}}{\gamma_{LL} V_{LL}} \tag{2.12}$$

where V_{DL} is the shear force due to dead loads (lb), V_{LL} is the shear force due to live load (lb), V_{DC} is the dead load shear force due to structural components and attachments (lb),

V_{DW} is the dead load shear force due to wearing surface and utilities (lb), A_1, γ_{DC}, and γ_{DW} are the load factors for dead loads and vary for inventory or operating rating, A_2 and γ_{LL} are the load factors for live loads and vary for inventory or operating rating, φ_c is the condition factor, and φ_s is the system factor.

There are three differences between the rating factor equations for LFR and LRFR shown in Table 2-2 that are immediately visible. First, the dead load has been separated in LRFR to account for a low variability in structural component dead loads (DC) compared to a high variability in bridge deck wearing surface thicknesses (DW). Second, the differences in the load factors (A_1, γ_{DC}, γ_{DW}, A_2, γ_{LL},) for LFR, LRFR, inventory rating, and operating rating are shown in Table 2-2. The load factor on the dead load is not significantly different between LFR and LRFR, but the load factor on the live load is much larger for inventory rating using LFR compared to LRFR. Third, rating with the LRFR method involves making an assessment of the structural deterioration and the redundancy of the system through the use of the φ_c and φ_s factors, respectively. The condition factor, φ_c, is used to account for resistance uncertainty associated with member deterioration due to natural causes (not damage due to accidents). A condition factor of 1.0, 0.95 or 0.85 is used to account for the level of section deterioration during the period between inspection cycles (MBE 2011). The system factor, φ_s, is used to account for ductility and redundancy and penalizes older, non-redundant structures with lower load ratings. The system factor is required to be taken as unity for shear evaluation due to a lack of system reserve capacity and the fact that shear failures are typically brittle.

Furthermore, there are three key differences between the LFR and LRFR methodologies that are more subtle and embedded in the calculation of both design live load plus impact and ultimate shear capacity. First, the notional design live load was changed to the HL-93 truck plus design lane in LRFR from the HS20 truck in LFR. Researchers have noted that the HL-93 design live load increases the shear demand on shorter bridges and produces a larger live load effect than the HS20 vehicle (Goodrich and Puckett 2002, Moen and Fernandez 2009). The static design live load effects are amplified with an impact factor that accounts for dynamic effects due to moving vehicles. The LRFR impact factor is 1.33 and may be reduced depending on the roadway roughness and vehicle speeds, but the LFR impact factor is equation based and decreases as span length increases.

The factored live load is also influenced by the live load distribution factors, which is the second key difference. There are new equations used to calculate the distribution factors for shear using LRFR compared to LFR. Distribution factors are used to estimate the live load distribution through the bridge system to individual girders and are discussed in detail in Section 2.3. Third, new techniques discussed in Section 2.1 to calculate the shear capacity are available for LRFR and can affect the comparison between LFR and LRFR.

The LRFR evaluation manual is consistent with the LRFD Specifications in using a reliability based limit state philosophy (Moses 2001, Lichtenstein Consulting Engineers 2001, Minervino et al. 2004, Mertz 2005). The LRFD philosophy promotes a more uniform level of safety and reliability across different bridge types and force effects by using calibrated load and resistance factors to account for the variability of system parameters, such as applied loads and material properties.

Poor assumptions prescribed in bridge design that create discrepancies in shear rating have been identified by Runzel et al. (2007), Pei et al. (2008), and Dereli et al. (2010). These assumptions may include design for shear at one quarter of the span length (rather than the critical section near the support) and continuation of the quarter-point stirrup spacing to the supports or not specifying a maximum amount of transverse reinforcement that could be used to resist shear. Many of these assumptions arise because requirements for the consideration of shear in prestressed concrete girders have changed simultaneously with advancements to bridge design and rating philosophies over the last half century. Shear ratings lower than unity for bridges that do not show any visible signs of shear distress may be neglected as discussed in Section 6A.5.8 of the AASHTO MBE (2011). Bradberry (2015) stated that "Texas bridge engineers typically load rate bridges for flexure on the assumption that the structures have sufficient shear capacity to reach flexural capacity. An exception warranting further investigation occurs when some distress (cracking) is found or [when] a particular beam type built in a certain time period (certain old prestressed I-beams lightly reinforced in shear beyond their immediate end regions) [may warrant investigation due to a design error uncovered]. In those cases, repairs have been made (though rarely) to reduce or eliminate the shear deficiency, or the shear capacity has been allowed to control the load rating."

The ability to calculate accurate shear load ratings is important with a growing inventory of structures that no longer rate well. The main factors that affect load rating include the member capacity and the member demand. To rate beam elements, dead and live load shear forces are calculated at the system (bridge) level and applied to an individual girder via distribution factors.

2.3 Shear Distribution

2.3.1 Codified Distribution Factors

Codified live load shear distribution factors (DFs) are based on linear elastic results and have been used in bridge design and evaluation since the early 1930's as a method to estimate system live load effects on individual girders. The first flexural distribution principles published in the AASHTO Standard Specifications (1931) for concrete slabs and beams were developed by Westergaard (1930) and Newmark et al. (1946) and were based on elastic plate theory. The 1931 AASHTO Standard Specifications stated that no lateral distribution of the wheel loads shall be assumed for shear distribution. The last published edition of the AASHTO Standard Specification (2002) stated that lateral shear distribution "at ends of beams" should be calculated using the lever rule, which assumes that in any cross section the bridge deck acts as a simple span between beams. Furthermore, the 2002 AASHTO Standard stated that lateral shear distribution at other locations should use the "S-over" equations (expressed in an *S*/*D* format, where *S* is the girder spacing and *D* is a constant based on superstructure type and the type of lane loading) specified for flexural distribution. The constant *D* for prestressed concrete girders is equal to 7.0 and 5.5 for one lane loaded and two lanes loaded, respectively. The "S-over" equations give the shear distribution in units of wheel lines/beam; it is assumed that two wheel lines travel in one lane. Therefore, the shear distribution factor calculated using *S*/*D* must also be divided by two to obtain the shear distribution in units of lanes per beam. These simple and easy to apply formulas have been used for shear distribution with only minor changes made as research results became available.

The "S-over" procedures in the 2002 AASHTO Standard Specifications became less applicable over time for two reasons. First, the distribution factor equations were developed considering only straight, non-skewed, simply supported bridges (Zokaie 2000).

Second, changes to the specifications were made annually and resulted in a patchwork document with discrepancies in the load distribution criteria, including: inconsistent reduction in load intensity for multiple lane loading, inconsistent changes in distribution factors reflecting changes in the design lane width, and inconsistent verification of accuracy of wheel load distribution factors for various new bridge types (Zokaie 1991a). It was shown by Zokaie et al. (1991a) that these simplified formulas for shear distribution can produce unconservative distribution factors (up to 6 percent) and, in other cases, conservative distribution factors (up to 17 percent) when comparing the 2002 AASHTO Standard Specification results to a detailed finite element model (FEM).

New equations for live load distribution factors were presented in 1994 when the first AASHTO LRFD Specifications for Highway Bridges was adopted as an alternative to the Standard Specifications. The shear distribution factors for precast concrete I or bulb-tee sections are specified in AASHTO LRFD (2010) Article 4.6.2.2.3 and are solely based on the girder spacing (S) in units of feet. The shear distribution factor (units of lanes per beam) for interior girders (g_{int}) for one lane loaded is:

$$g_{\text{int}} = 0.36 + \frac{S}{25} \tag{2.13}$$

and the shear distribution factor for an interior girder for two lanes loaded is:

$$g_{\text{int}} = 0.2 + \frac{S}{12} - \left(\frac{S}{35}\right)^{2.0} \tag{2.14}$$

The shear distribution factor for exterior girders (g_{ext}) for one lane loaded is calculated using the lever rule and the shear distribution factor for an exterior girder for two lanes loaded is calculated using:

$$g_{ext} = \left(0.6 + \frac{d_e}{10}\right) g_{\text{int}} \tag{2.15}$$

where d_e is the horizontal distance from exterior beam centerline to the interior edge of curb or barrier (ft). Furthermore, the AASHTO LRFD Specifications introduced a factor for skewed structures as shown in AASHTO LRFD (2010) Article 4.6.2.2.3, calculated with:

$$skew\ factor = 1.0 + 0.20\left(\frac{12Lt_s^3}{K_g}\right)^{0.3} \tan\theta, \text{with } K_g = n\left(I + Ae_g^2\right) \qquad (2.16)$$

where θ is the skew angle (degrees), L is the girder span length (ft), t_s is the deck thickness (in.), K_g is the longitudinal stiffness parameter (in.^{4}), n is the girder to deck modular ratio, I is the noncomposite girder moment of inertia (in.^{4}), A is the noncomposite girder area (in.^{2}), and e_g is the distance between the centers of gravity of the basic girder and deck (in.).

The equations in the current AASHTO LRFD Specifications (2010), compared to historical Specifications in Table 2-3, were based on the results of a parameter study by Zokaie et al. (1991b) and consider variations in number of beams, girder spacing, girder stiffness, span length, skew, and slab thickness. The LRFD formulas in Table 2-3 generally produce results within five percent of those from a detailed finite-element analysis (Zokaie 1991b). These formulas were developed based on results from loading bridges with the standard AASHTO HS20 truck and were calibrated against a database of constructed bridges to verify their applicability.

Currently, distribution factors for live load shear rating of *in situ* highway bridges are commonly determined either using the 2002 AASHTO Standard Specifications, the 2010 AASHTO LRFD Specifications, or a state-specified method. For example, Henry's equal distribution factor (EDF) method is a simplified method for calculating distribution factors of live load moment and shear. This method was developed by Henry Derthick, a former engineer of the Structures Division within the Tennessee Department of Transportation, and has been in use in Tennessee since 1963 (Huo et al. 2005). Henry's Method makes use of equal distribution of live load in all girders, exterior and interior. This method is easily applied to different types of bridges because it only requires the width of the bridge, the number of traffic lanes, and the number of beam lines for calculation of

distribution factors without limitations on the range of key parameters of bridges. The calculations in Henry's Method for prestressed concrete I-beams is as follows:

1. Divide roadway width by ten (10 ft) to determine the fractional number of traffic lanes.
2. Reduce the value from Step 1 by a factor obtained from a linear interpolation of multiple presence factors to determine the total number of traffic lanes considered for carrying live load on bridge. The multiple presence factor for live load equals 100 percent for a two-lane bridge, 90 percent for a three-lane bridge, or 75 percent for a four-or-more lane bridge.
3. Divide the total number of lanes by the number of beams to determine the number of lanes of live load per beam, or the distribution factor of lane load per beam.
4. Multiply the value from Step 3 by a ratio of 6/5.5 or 1.09 to determine the distribution factor of lane load per beam.

Step 1 indicates that the bridge is considered to be fully loaded with all possible traffic lanes. Step 2 applies a multiple presence factor to the live load, and Step 3 calculates the equal distribution factor for the live load. The value obtained in Step 3 is essentially the basic distribution factor for a girder based on the EDF method. Step 4 provides a constant multiplier of 6/5.5 to amplify the distribution factor for steel and prestressed I-beams only because the live load distribution factor for those types of beams is expected to be higher than the value obtained in Step 3.

Huo et al. (2005) stated that it was specified in the Tennessee DOT design guides that the designer should use the smaller value of the lateral distribution factors from the AASHTO Standard Specifications or from Henry's Method in the design of primary beams. Since the method was introduced in 1963, this resulted in the majority of Tennessee bridges being designed using Henry's Method because it typically yielded smaller distribution factors. Huo et al. (2005) also found that Henry's Method was consistently unconservative for shear distribution factors compared to finite element analysis results.

Huo et al. (2003 and 2005) reexamined Henry's Method for live load moment and shear distribution and developed modification factors for both live load moment and shear. In the Huo et al. method developed, the shear modification factor was unrelated to the

moment modification factor and included a skew correction formula. The modification factors contain different multipliers based on structure type, as outlined below:

1. Basic Equal Distribution Factor – same as Step 3 in original method.
2. Superstructure Type Modification for Shear – Multiply the value from Step 3 in the original method by an appropriate structure modification factor (for precast concrete I-sections this factor is 1.20) to obtain the shear distribution factor. This step and superstructure modification factor replaces Step 4 in the original method.
3. Skew Angle Modification – Multiply the value from Step 2a by the appropriate skew modification factor to get the final shear distribution factor. The skew modification factor is equal to $1.0 + 0.2\tan\theta$, where θ is the skew angle, for all structure types.

Both versions of Henry's method are less complex and less restrictive than AASHTO LRFD Specifications. The modified Henry's Method is less conservative than the AASHTO Standard methods (Huo et al. 2003).

Researchers have worked on developing new and simplified equations for live load shear distribution (Sanders and Elleby 1970, Bakht and Jaeger 1992, Ebeido and Kennedy 1995, Ebeido and Kennedy 1996, Huo et al. 2005). Most of the proposed methods were applicable to the particular type of bridge studied and most methods proposed moderate changes to the AASHTO Standard Specifications. Recently, the National Cooperative Highway Research Program (NCHRP) supported Puckett et al. (2007) to develop less complex live-load distribution equations with accuracy appropriate for linear elastic design through NCHRP Project 12-62.

In an effort to make use of existing simplified methods, Puckett et al. (2007) compared calculated distribution factors from several methods to those obtained from grillage analyses. In NCHRP Report 592, which describes outcomes from NCHRP Project 12-62, Puckett et al. (2007) found that a calibrated lever rule was accurate for calculation of shear live load distribution factors for one and multiple lanes loaded. Puckett et al. calibrated lever rule results with the mean of results from two-dimensional (2D) grillage analyses using affine transformations. In other words, the slope and *y*-intercept of the best fit line of the lever rule results was calibrated to match the slope and *y*-intercept of the best fit line from average 2D grillage results. A discussion of affine transformations is provided

by Weisstein (2015). Use of the lever rule involves investigating a transverse cross section of the structure assuming the bridge deck is simply supported (hinged) over the interior girders. At exterior girders, it is assumed that the deck panel is continuous with the cantilever. These assumptions render the deck cross section statically determinate and support reactions can be determined with statics. Limitations on the research done within NCHRP Project 12-62 were indicated by the authors. Importantly, use of the proposed method was not recommended for direct evaluation of existing structures because it was developed for conservative design of new structures. Puckett et al. (2007) further emphasized that simplifications in this study may render overly conservative decisions associated with a bridge closure, retrofit/maintenance, or permit vehicle assessment.

The LRFD code language suggested by Puckett et al. (2007) was considered by the AASHTO Loads and Load Distribution (T-5) Technical Committee in 2007 but failed to garner enough support for approval (Tobias 2011). Hida (2010) stated that the committee felt it was a step backward to go from exponential curve-fitting distribution factor equations developed with finite element modeling by Zokaie (1991b), used in the AASHTO LRFD Specifications, to linear curve-fitting distribution factor equations as suggested by Puckett et al. (2007). Tobias (2011) noted that the distribution methods did not appear to the committee members to have been as wide-ranging or simplified as they could have been. For example, during a pilot study, the proposed distribution methodology was difficult to use and understand in normal engineering design practice. Furthermore, the new distribution methodology could be iterative and require significant interpretation making its application non-uniform from designer to designer. The committee noted that bridge owners had no indication that bridges were suffering from under-design, and they also recognized that the future of load distribution was influence surfaces, that is, grillage or shell modeling as opposed to girder-line analysis (Hida 2010).

2.3.2 Experimental Investigations

Despite some agencies finding that shear controlled the load rating of their bridges (Al-Mahaidi et al. 2000, Rogers and Jáuregui 2005, Bradberry 2015), only limited experimental research on shear live load distribution can be found. The characteristics of the bridges used to experimentally investigate shear distribution are summarized in Table 2-4. Cross et al. (2006 and 2009) conducted field tests using three-axle loaded dump trucks

on ten steel girder bridges and two prestressed concrete girder bridges at service load levels. Cross et al. (2009) obtained shear distribution factors, at a distance *d* from the support, from field test data by dividing the calculated shear force (generated assuming an effective deck width equal to the girder spacing) in a single girder by the sum of calculated shear forces in all girders at the cross section of interest. The authors found that, in some cases, the experimentally-obtained shear distribution factors were greater than those predicted using AASHTO LRFD Specifications by up to 16 percent.

Idriss and Liang (2010) evaluated the in-service shear distribution factors in a simple span prestressed concrete girder bridge using a three-axle dump truck (6 ft 7 in. gage) and a pair of 3.3 ft long optical fiber sensors in a rosette configuration embedded in each girder web at the support. Idriss and Liang (2010) obtained distribution factors at the support by dividing the calculated shear strain in a single girder by the sum of shear strain on a vertical face in all girders at the support. The authors determined that AASHTO Standard shear distribution factors closely predicted the shear distribution under regular traffic loading while the AASHTO LRFD distribution factors were conservative.

Suksawang et al. (2013) strived to develop a simplified "S-over" equation (similar to AASHTO Standard distribution factor equations which were expressed in an *S*/D format) to determine load distribution factors for shear in both steel and prestressed concrete I-girder bridges using finite element models validated with girder flexural strain data from field testing seven steel girder bridges. No modifications were made to the FEM to account for prestressed concrete girder bridges versus steel girder bridges. Prestressed concrete girder bridge results were generated from the finite element models using the HL-93 truck and distribution factors were calculated by dividing the shear force in any beam by the sum of shear forces at the same cross section. The beam shear force was multiplied by the appropriate number of lanes loaded and multiple presence factor. The authors presented simplified equations based the girder spacing, *S*, divided by D_v which was defined as: (X + *S* / Y) where X and Y were constants determined from best-fit analysis of finite element results; the value of X did not change and the value of Y was dependent on the number of lanes loaded.

2.3.3 Analytical Investigations

Several numerical studies have also been conducted to determine whether AASHTO Specifications accurately predict shear distribution factors and to assess the effect of secondary bridge elements on shear distribution (Arockiasamy and Amer 1998, Huo et al. 2003, Puckett et al. 2007, Zhuang et al. 2011). These studies take into account important characteristics for shear distribution, including: girder spacing, skew, aspect ratio, and secondary elements such as end diaphragms and barriers. The characteristics of the bridges used to analytically investigate shear distribution are summarized in Table 2-5. Arockiasamy and Amer (1998) conducted a parametric study using a 2D grillage model and found that the grillage analogy gave smaller shear distribution factors compared to both the AASHTO LRFD and AASHTO Standard Specifications at the critical section for shear. Zhuang et al. (2011) created finite element models for bridges with three different levels of skew. The authors found that distribution factors calculated using FEM were lower than those calculated with AASHTO LRFD Specifications (including the skew correction factor) and AASHTO Standard Specifications at the critical section for shear.

Huo et al. (2003) and Puckett et al. (2007) obtained conflicting numerical analysis results in studies of Bridge No. 24, which was a prestressed concrete girder bridge described by Huo et al. Huo et al. (2003) used three-dimensional (3D) FEM with frame elements for the girders and shell elements for the deck and Puckett et al. (2007) used 2D grillage models. Both research groups used the following: one or more HS20 design trucks (depending on the number of lanes loaded) configured in the transverse and longitudinal position that maximized shear response in the girder (at the end of the span), an effective deck width equal to the girder spacing, and distribution factors calculated by dividing the maximum shear from an interior girder in the bridge system by the shear generated from a beam-line analysis with the truck load at the same longitudinal location on the span. A beam-line analysis refers to a model where the bridge is idealized as a one-dimensional (1D) structure along its length to determine the shear across a section of the bridge. Huo et al. (2003) found that the shear distribution factors from analysis without end diaphragms were normally larger than those with end diaphragms by up to 20 percent. In contrast, Puckett et al. (2007) found that support diaphragms caused a slight increase in the shear distribution factor. The biggest difference between the two studies was the type of

modeling used to generate the shear distribution results. Furthermore, the boundary conditions related to how the end diaphragm was connected to the support may have varied between the two studies. Huo et al. (2003) indicated that use of "line supports [connecting the diaphragm to the support along its length]…instead of individual point support [only] under beams" were used to consider diaphragm effects. This type of connectivity was not mentioned by Puckett et al. (2007) and a picture displaying a representative grillage model only showed supports under girder elements. Differences in the modeling techniques may be responsible for the discrepancies related to the effects of the end diaphragm.

2.3.4 Inelastic Shear Distribution

There is a dearth of both experimental and analytical research on shear live load distribution in prestressed concrete girder bridges in the inelastic range and near ultimate failure. However, it is recognized that reserve strength relative to predicted capacity may exist and is often attributed to the fact that current design and rating procedures use elastic distribution and consider the resistance of individual members at the component level rather than at the system level, where load redistribution occurs during inelastic behavior (Bechtel et al. 2011).

2.4 Filling Knowledge Gaps in the Literature

The subject of load distribution has been and continues to be somewhat controversial, and there have been several efforts at improvement and refinement over the years. Questions remain as to whether the AASHTO Specification procedures accurately and efficiently predict shear distribution for rating and design of prestressed concrete girder bridges.

The laboratory study and field testing in the elastic range during this project provided the opportunity to experimentally investigate shear distribution in seven prestressed concrete girder bridges of varying geometry. Furthermore, experimental laboratory and field results from this study were used to validate a finite element modeling technique specifically considering shear distribution behavior. The laboratory testing in the inelastic range to ultimate capacity provided an opportunity to study shear redistribution after initial web-shear and flexural cracking before failure; shear behavior in the inelastic range and at ultimate capacity was not well documented in the literature for prestressed

concrete girder bridge systems. Use of linear elastic load distribution factors may be conservative when considering shear distribution at ultimate capacity. Finally, the parametric study in this project, conducted with a validated modeling technique, allowed for research related to how individual bridge parameters affect shear distribution. Finite element model results provided insight related to the accuracy of AASHTO shear distribution factors compared to results from refined analyses.

Table 2-1. Shear Resistance for AASHTO STD and LRFD Specifications (units of lb and in.)

	STD General Procedure	LRFD Simplified Procedure
V_n	$= V_c + V_s$	$= V_c + V_s \le \left(2.5\times10^{-4} f'_c\right) b_v d_v$
V_{ci}	$= 0.6\sqrt{f'_c}\, b' d + V_d + \dfrac{V_i M_{cr}}{M_{\max}} \ge 1.7\sqrt{f'_c}\, b' d$	$= 0.63\sqrt{f'_c}\, b_v d_v + V_d + \dfrac{V_i M_{cr}}{M_{\max}} \ge 1.9\sqrt{f'_c}\, b_v d_v$
V_{cw}	$= \left(3.5\sqrt{f'_c} + 0.3 f_{pc}\right) b' d + V_p$	$= \left(1.9\sqrt{f'_c} + 0.3 f_{pc}\right) b_v d_v + V_p$
V_s	$= \dfrac{A_v f_y d}{s} \le 8\sqrt{f'_c}\, b' d$	$= \dfrac{A_v f_y d_v}{s} \cot\theta$ if $V_{ci} < V_{cw}$ $\cot\theta = 1$, otherwise $\cot\theta = 1 + 0.095 \dfrac{f_{pc}}{\sqrt{f'_c}} \le 1.8$

Note: V_c is taken as the lesser of V_{ci} and V_{cw}

Table 2-2. Inventory and Operating Rating Factors for LFR and LRFR

	Load Factor Rating (LFR)	Load and Resistance Factor Rating (LRFR)
Inventory RF	$= \dfrac{\phi V_n - 1.3 V_{DL}}{2.17 V_{LL}}$	$= \dfrac{\varphi_c \varphi_s \phi V_n - 1.25 V_{DC} - 1.5 V_{DW}}{1.75 V_{LL}}$
Operating RF	$= \dfrac{\phi V_n - 1.3 V_{DL}}{1.3 V_{LL}}$	$= \dfrac{\varphi_c \varphi_s \phi V_n - 1.25 V_{DC} - 1.5 V_{DW}}{1.35 V_{LL}}$

Table 2-3. Shear Distribution Factors for Precast Concrete I or Bulb-Tee Sections from AASHTO Standard and LRFD Specifications.

	1931 AASHTO Standard	2002 AASHTO Standard*		2010 AASHTO LRFD			
	Any Beam	Any Beam		Interior Beams		Exterior Beams	
No. lanes loaded	*n/a*	1	2+	1	2+	1	2+
Shear DF, g (lanes/beam)	*no dist.*	$= \dfrac{S}{2 * 7.0}$	$= \dfrac{S}{2 * 5.5}$	$= 0.36 + \dfrac{S}{25}$	$= 0.2 + \dfrac{S}{12} - \left(\dfrac{S}{35}\right)^{2.0}$	*= lever rule*	$= \left(0.6 + \dfrac{d_e}{10}\right) g_{\text{int}}$
Skew Correction	*n/a*	*n/a*	*n/a*	$= 1.0 + 0.20\left(\dfrac{12 L t_s^3}{K_g}\right)^{0.3} \tan\theta$, with $K_g = n\left(I + A e_g^2\right)$			
Applicability Criteria	*n/a*	$S \le 10^{\dagger}$	$S \le 14^{\dagger}$	$3.5 \le S \le 16.0$ $20 \le L \le 240$ $4.5 \le t_s \le 12.0$	$N_b \ge 4^{\ddagger}$ $0 \le \theta \le 60$	$-1.0 \le d_e \le 5.5$	

* at ends of beams use the lever rule; the S-over equations must be divided by 2 for a comparison to AASHTO LRFD equations.

† if spacing limit is exceeded use the lever rule

‡ if number of girders (N_b) < 4 use the lever rule

Table 2-4. Geometry of Prestressed Girder Bridges used to Experimentally Investigate Shear Distribution

Researcher	Bridge	Number of Girders	Girder Spacing (ft)	Deck Width (ft)	Span Length (ft)	Skew (deg)	Deck Thickness (in.)
Cross et al. (2009)	054-0043	9	6.5	58.0	66.0	0	7.5
	060-0319	6	7.4	43.2	54.5	17	7.5
Idriss and Liang (2010)	I-25 South	6	7.3	43.0	112.5	n/a	7.5
Suksawang et al. (2013)*	US23	6	6.2	35.9	78.7	14	7.5
	M14	8	6.1	44.5	52.5	25	8.0
	I-94 W	9	5.8	47.6	51.7	33	7.5
	I-94 E	10	5.0	47.6	34.4	29	7.0
	DOREMUS	10	4.8	74.8	147.6	0	8.7
	NEWARK BAY	10	6.9	67.3	160.2	35	9.0
	NJTA 16E	8	6.0	44.5	52.5	25	8.0

* These seven steel girder bridges were used to validate the FEM and study shear distribution in prestressed concrete girder bridges.

Table 2-5. Geometry of Prestressed I-beam of Bulb-Tee Girder Bridges used to Analytically Investigate Shear Distribution

Researcher	Bridge	Number of Girders	Girder Spacing (ft)	Deck Width (ft)	Span Length (ft)	Skew (deg)	Deck Thickness (in.)
Arockiasamy and Amer (1998)	940115	9	6.6	58.8	125	45	7
	Parametric Study Base	9	6	54	70	0	7
	116 Bridges	5-9	6-12	54	70-140	0-60	7
Huo et al. (2003)	5	5	8.8	44	124.3	15	8.25
	6	5	9	44	67.4	21.3	8.25
	7	5	9	44	67.4	33.5	8.25
	8	8	10.3	80.7	115.5	0	8.25
	22	4	8.3	32	159	26.7	8.25
	23	4	8.33	32	151.3	17.5	8.25
	24*	5	10.6	51.3	74.3	0	8.75
Zokaie et al. (1991b)†	94 Bridges	n/a	3-10.5	n/a	19-136	0-48	5-9
Puckett et al. (2007)	101 Bridges	Used bridges from Huo et al. (2003) and Zokaie et al. (1991b)					

* Used for parameter studies to investigate skew and end diaphragms by Puckett et al. (2007).
† Taken from Puckett et al. (2007) who listed the parameter ranges by superstructure type.

CHAPTER 3. NUMERICAL ANALYSIS TOOLS

3.1 Introduction

Codified equations for live load distribution provide a fast method for estimating the amount of load carried by individual girders in a bridge superstructure. However, due to the inherent complexity of bridge structures, determining an accurate distribution of forces may require a more refined method such as a grillage method or a finite element method. Numerical analysis tools were integrated throughout this research program to provide a more detailed understanding of shear distribution and to generate final shear distribution recommendations for load rating.

In this project, three-dimensional grillage models were used prior to experimental testing to determine the optimal strain gage locations for the field tested bridges and the laboratory bridge. Furthermore, three-dimensional grillage models were modified to replace bridge deck beam elements with shell elements for use during initial design of the laboratory bridge. The complexity of numerical modeling techniques increased to include three-dimensional solid element finite element models which were used to understand complex bridge behavior related to shear distribution in the laboratory bridge and field bridges. A simplified two-dimensional grillage model, similar to the three-dimensional technique employed prior to conducting experiments, was used to develop final recommendations for the project. Two-dimensional grillage model results were compared to those obtained from three-dimensional finite element models.

3.2 Three-Dimensional Grillage Model

Simplified three-dimensional grillage models were developed due to their computational efficiency. Grillage modeling is often used to represent a three-dimensional continuum of the bridge deck by an assemblage of small frame elements or a grillage of beams. Without shell or solid elements, grillage analysis is computationally inexpensive and has been proven to be reliably accurate for a wide range of bridge types (Hambly 1991). Research has been done using two-dimensional grillage analyses with frame elements for both the beams and deck to predict the shear distribution (Puckett et al. 2007). Sotelino et al. (2004) noted that two-dimensional grillage analysis has limitations that do not account

for physical phenomena, including: the interaction between girders and deck slab, support location, and shear lag. Many limitations can be overcome with three-dimensional grillage modeling with vertical rigid links connecting the barrier to the deck and the deck to the girders (Altay et al. 2003).

In this project, three-dimensional grillage models were used prior to experimental testing as a tool for development of the instrumentation plans. Specifically, model-generated shear and moment results were used to estimate horizontal, vertical, and diagonal strains at potential locations for rosette strain gages in the field bridges. These results were used to determine: (1) the optimal vertical location of strain gage rosettes on a girder web to capture maximum magnitude strain data, and (2) the magnitude of load needed to obtain shear strain data that was not within the expected noise levels of selected strain gages.

3.2.1 3D Grillage Geometry and Elements

Grillage models used in this research program were constructed in SAP2000 (Computers and Structures, Inc. 2009) with frame elements to model the concrete bridge deck, girders (including haunch), traffic barrier, and diaphragms. Geometry for the models was created using the three-dimensional capabilities of AutoCAD and imported into SAP2000 using a drawing exchange format (.dxf) file type. Longitudinal and transverse rebar and prestressing reinforcement was not modeled implicitly or explicitly in the 3D grillage models. The geometry and structural characteristics of frame elements used to model the girders, traffic barrier, and diaphragms were generated using the Section Designer in SAP2000.

The deck was modeled with a grillage of both longitudinal and transverse frame elements as shown in Figure 3-1 and Figure 3-2. Longitudinally, the primary deck frame elements were always placed directly above the girder frame elements and had a width equal to the effective flange width specified by the AASHTO Standard Specifications (2002). Additional longitudinal deck frame elements, shown in Figure 3-1, were used to model both the remaining deck width between AASHTO specified effective flange widths and the section of deck directly beneath the traffic barrier, which had the same transverse width as the barrer. Other methods of numerical modeling in this project, described in Sections 3.3 and 3.4, used the girder spacing as the effective flange width of composite deck rather than values calculated with the AASHTO Standard. Transversely, the bridge

deck for 3D grillage models was divided with slightly more refinement than discussed in guidelines by Hambly (1991) and Zokaie et al. (1991b). Hambly (1991) suggested transverse bridge deck discretization of at least one quarter of the span length with a smaller spacing near regions of sudden change such as over internal supports or at supports near the end of a span. For 3D grillage models in this project, transverse bridge deck grillage elements were spaced at approximately one-eighth of the span length. The one-eighth span length sections near supports were divided into approximately ten equal sections to capture more detailed shear distribution behavior as shown in Figure 3-2.

The grillage models were constructed in a three-dimensional space using vertical rigid links shown in Figure 3-2 to connect the barrier to the bridge deck, the bridge deck to the girders, and the girders to the support. The vertical rigid links were connected at the centroid of each member cross section. The vertical rigid links were modeled as generic frame elements with a circular cross section, but a frame property/stiffness modifier equal to 1,000,000 was used to increase the axial area, shear area, torsional constant, and moment of inertias to obtain rigid behavior. The property/stiffness modifiers for rigid link mass and weight were set to zero.

Figure 3-1 and Figure 3-2 show the grillage connectivity at the end of a span where the end diaphragm and supports interact with the girder and deck. Various details regarding the connectivity between the end diaphragm, girders, and girder supports were considered and evolved over the course of the project. Initially, the girder frame element, the end diaphragm frame element, and the girder support all coincided at a single node located at the centroid of the girder as shown in Figure 3-2. This produced unresolved anomalies in the shear force data near the end of the span length, specifically the girder reaction data. To model this region more precisely, the girder support was lowered to the elevation of the girder sole plate and connected to the centroid of the girder cross section with a rigid link as shown in Figure 3-1 and Figure 3-3. Furthermore, the end diaphragm was relocated to the correct longitudinal position in accordance with the location of the end diaphragm cross section centroid, which was generally a few inches into the span and not directly over the supports. The end diaphragm was always connected to the bridge deck with vertical rigid links. Figure 3-1 also shows the end diaphragm at the correct vertical location considering the cross section centroid. However, locating the end diaphragm at the correct vertical

elevation versus locating it at the same height as the girder centroid was found to produce negligible differences in the results.

Figure 3-2 and Figure 3-3 show the support boundary conditions modeled as ideal pins. The opposite end of the span in Figure 3-2 and Figure 3-3 was supported on rollers (not shown in the figures). This was achieved in SAP2000 using nodal joint restraints that limited translation in *x*, *y*, and *z* for a pin and allowed translation longitudinally (*x*-direction) for a roller. For the 3D grillage models, idealized support conditions were used as a simplification due to a lack of information about the stiffness of various bearing assemblies in the MnDOT inventory (elastomeric bearing pads, guided or non-guided pot type bearings, curved plate bearings, or tapered bearings).

3.2.2 3D Grillage Applied Load

One of the primary benefits of creating grillage models in SAP2000 was use of the built-in moving vehicular live load package. Using this feature in SAP2000, the user specifies the axle weight, longitudinal axle spacing, transverse axle width, and number of locations to place the vehicle along the length of the bridge. Because vehicles were defined by number and spacing of axles, programming unusual configurations of trucks for live loading was straightforward. For example, two dump trucks with three axles each placed back-to-back could be modeled by a 'single truck' that had six axles at appropriate spacing. The vehicular live load was moved along the length of the structure using a multi-step static load case and followed the centerline of a user specified traffic lane that was the same width as the truck axles. Vehicular live load was applied directly to the group of elements representing the bridge deck.

Discretization of the multi-step load case within the bridge live load pattern included specifying the vehicle speed, time duration of vehicle loading, and load discretization time increment. Starting from one end of the bridge, the travel distance was always calculated to be the length of the structure plus the length of the vehicle. This allowed the vehicle to travel along the entire length of the bridge and continue until it was completely off of the deck. The vehicle was automatically positioned to start off of the bridge deck at the beginning of the span. The vehicle speed was always specified to be 20 in./s, the time increment for load discretization was generally defined as one half of a second, and the start distance for the loading was always set to zero (edge of bridge deck).

Thus, by defining the required travel distance in inches, the time duration of loading was calculated. Each step in the analysis corresponded to a specific position of the vehicle along the bridge length. For example, determining the location of the vehicle leading axle for any given step was computed using:

(known load step – 1)(speed)(load discretization time increment) + (start location) (3.1)

For complex structures, the primary benefit of applying multi-step live load with the built-in SAP2000 analysis package was eliminating the need to calculate individual nodal forces at each load step by hand. The inefficiency of hand calculations becomes more prominent when considering multiple transverse lane positions. An individual concentrated load from a vehicle axle was automatically decomposed by SAP2000 into equivalent concentrated forces and eccentric moments applied to the nearest frame element representing the deck.

3.2.3 Modifications of 3D Grillage for Deck Shell Elements

Many researchers have made modifications to basic three-dimensional grillage modeling by replacing the deck frame elements with more complex elements from finite element modeling. Barr et al. (2006) and Bae and Oliva (2012) each independently compared various three-dimensional modeling techniques, including:

- Shell elements for the concrete bridge deck and frame elements for the girders.
- Solid elements for the concrete bridge deck and frame elements for the girders.
- Shell elements to model both the bridge deck and girders.

The modeling objective of Barr et al. (2006) was to quantify the effects of girder spacing, span length, overhang distance and skew angle on the shear live-load distribution factor for bridges constructed with steel I-beams and a composite concrete slab. One objective of the modeling by Bae and Oliva (2012) was to propose shear distribution factor equations for multigirder bridges subjected to overload vehicles carrying industrial freight. Both groups independently came to the conclusion that the modeling technique appropriate for their structural system used shell elements to model the concrete bridge deck and frame elements to model the girders. The modeling technique was deemed appropriate by Barr et

al. (2006) because results matched measured shear strain data of a laboratory bridge within 4 percent; furthermore, the modeling technique was deemed appropriate by Bae and Oliva (2012) when modeling results accurately simulated the measured deflection within 8 percent of a verification structure tested in the field. Of the three techniques, this model arrangement was preferred because it was easiest to implement and also produced results similar to more rigorous models and data from previous experimental load tests.

In this project, three-dimensional grillage models were modified to replace bridge deck members with shell elements for use during initial design of the laboratory bridge. Three-dimensional grillage models created in SAP2000 were changed to have thick-plate Mindlin/Reissner shell elements instead of frame elements representing the concrete bridge deck as shown in Figure 3-3. Similar to the 3D grillage models, vertical rigid links were used to connect the bridge deck to the girder, end diaphragm, and barrier frame elements.

3.3 Three-Dimensional Finite Element Model

With the advances in computer technology and modern FEM programs that support user-friendly graphical interfaces, it is possible to efficiently model bridge structures using a complete solid element model. This analytical approach may still be inefficient for use in design or rating of hundreds of individual bridges in a DOT inventory, but FEM provides an appropriate level of detail for comparison to experimental research results.

In this project, three-dimensional solid finite element models were created in parallel with laboratory experimental testing to develop an understanding of complex structural behavior related to shear distribution, torsion of prestressed concrete girders, boundary conditions, and interactions between structural elements. Specifically, FEM models provided the ability to directly compare measured strains to FEM strains rather than converting strain gage data to stress data which required an assumption of composite cross section dimensions, including the effective flange width. FEM models were also generated for select field tested bridges to compare results and validate the FEM technique. Three-dimensional solid element models were used to broaden the results of the shear distribution study beyond experimental results and were used to develop the final shear distribution recommendations.

3.3.1 FEM Geometry, Mesh, and Material Properties

Three-dimensional finite element models were created using Abaqus/Standard 6.11 (Dassault Systèmes 2010) and were used to model the elastic tension and compression behavior of prestressed concrete girder bridges. The Abaqus bridge superstructures were divided into five parts, including: neoprene bearing pads, traffic barriers, end or intermediate diaphragms, bridge deck, and girders. The geometry of each part was adequately subdivided using partitions for two reasons. First, prior to meshing, individual surfaces were defined to ensure that surface-to-surface constraints were easy to create and to ensure that applied loads could be placed at the correct locations. Second, subdividing each part allowed for use of hexahedral elements and the structured meshing technique in Abaqus, which was preferred because it was more efficient. The mesh for each part was constructed independently using automatic seeding and mesh generation in Abaqus. All parts for non-skewed bridges were meshed using element type C3D8R which is an eight node three-dimensional linear continuum element with reduced integration. Skewed bridge decks utilized a sweep meshing technique with hex-dominated elements. Generally, the majority of skewed bridge deck elements were hexahedral shaped, however select elements were six noded three-dimensional linear triangular prism wedge elements (element type C3D6) used to complete the meshing in areas of unusual geometry.

Characteristic element sizes were approximately 3 in. or smaller for bridge decks and approximately 2 in. or less for bridge girders, traffic barriers, and diaphragms. The mesh of each individual part was deemed satisfactory after verifying that no element had an aspect ratio greater than 2.5. Select elements on skewed bridge decks had aspect ratios larger than 2.5. However, less than two percent of the total elements in skewed bridge decks had an aspect ratio larger than 2.5. For these specific elements, an aspect ratio less than or equal to 4.0 was considered acceptable.

Each part was composed of solid, homogenous sections that included materials defined by their density, Young's modulus, and Poisson's ratio. The uniformly distributed density for all concrete components was assumed to equal 150 pcf (0.0868 lb/in.^{3}) which was 5 pcf greater than the density of plain concrete (145 pcf) to account for the weight of the steel reinforcement as suggested by the AASHTO LRFD Bridge Design Specifications (2010). The Poisson's ratio for all concrete components was assumed to be 0.2 as stated in

Section 5.4.2.5 of the AASHTO LRFD Specifications (2010). The Poisson's ratio for neoprene bearing pad parts was assumed to be 0.49995 as discussed by Roeder et al. (1987) and the density was specified as 0.0813 lb /in.^{3}.

Longitudinal rebar, transverse rebar, and prestressing strands were not discretely modeled. However, the effect of steel stiffness was accounted for in two ways: (1) prescribing transversely isotropic engineering constants (Young's modulus and shear modulus) for girders, end diaphragms, and barriers, and (2) increasing the Young's modulus of concrete parts using a steel and concrete volumetric ratio similar to those used for fiber-reinforced composite materials:

$$E_{longitudinal} = E_{conc}\left(\frac{V_{conc\ only}}{V_{total}}\right) + E_{steel}\left(\frac{V_{steel\ only}}{V_{total}}\right) \tag{3.2}$$

Traffic barriers and end diaphragms were assigned a longitudinal Young's modulus calculated with Eqn. (3.2) based on the amount of longitudinal steel reinforcement. Additionally, the bridge girders were assigned two different materials, one for elements in the bottom flange (concrete plus the additional stiffness of prestressing steel) and one for elements in the remainder of the cross section (concrete only). The transverse Young's modulus of these elements was set equal to the Young's modulus of concrete for all elements in each respective part. In the bridge deck, it was assumed that the amount of longitudinal and transverse reinforcing steel was approximately equal. Therefore, the transversely isotropic elastic material properties were equal, with the Young's modulus value accounting for the volumetric ratio of steel and concrete.

After meshing and assigning material properties, each part was assembled into a single composite structure using master-slave surface-to-surface tie constraints. Typically, the master surface was chosen in the following order: (1) bridge deck, (2) girder, (3) end diaphragm or traffic barrier, (4) bearing pad. The following surface-to-surface tie constraints were used with appropriate partitioning so that surface areas matched:

- Top of bridge deck to bottom of traffic barrier
- Bottom of bridge deck to top of haunch and top of end diaphragm
- Top of girder to bottom of haunch

- Girder web and top flange to end diaphragm (amount of connectivity dependent on desired fixity condition i.e., pinned, fixed, or free)
- Bottom of girder bottom flange to top of bearing pad
- End diaphragms in bays between adjacent girders were connected to each other behind the end of the girder web and top flange

Displacement/rotation boundary conditions were applied in the initial step, prior to any applied loads. The bottom surface of each bearing pad was restrained to have zero vertical displacement and a similar single bottom corner node on each bearing pad (e.g., only the southwest bottom node on each individual bearing pad) was restrained to have zero longitudinal and transverse displacement.

3.3.2 FEM Applied Load

Force was applied to the bridge deck using a static, general pressure load in sequential steps after the initial boundary condition step. Applied patch loads were defined by the total force rather than pressure (force divided by patch area). Load was typically applied to the bridge deck using pre-defined geometry-type surface areas to model patch loads (tire loads or actuator plate loads). For skewed bridge decks, the patch load area was defined by groups of elements after the deck mesh geometry was delineated rather than defining the surface with rectangular surfaces which did not align with the skewed geometry. This alleviated the need to use several longitudinal and transverse partitions to define the patch load areas. An increased density of partitions on a skewed bridge deck created too much geometric complexity for automatic meshing and often led to poor meshes.

Generally, many loading scenarios were created within one comprehensive model database. To reduce computational effort, loads were set to inactive in any load step except where they were created and, when submitting jobs for analysis, only steps and loading scenarios of interest were not suppressed. An intermediary step between application of boundary conditions and application of load was utilized to request stress, strain, and displacement output results from Abaqus. Nodal forces due to element stresses (NFORC

data in Abaqus) were utilized to calculate the vertical shear force on any desired composite cross section.

3.4 Two-Dimensional Grillage Model

A simplified two-dimensional grillage model, similar to the 3D grillage model, was used to develop final recommendations for the project. Two-dimensional grillage models, shown in Figure 3-4, did not include the depth of the structure or utilize rigid links to connect elements at different elevations. Simplified grillage elements were constructed with only longitudinal members that contained a single beam, the haunch, and a section of composite bridge deck with width equal to the girder spacing. The geometry of the longitudinal composite cross section was defined in the SAP2000 Section Designer (Computers and Structures, Inc. 2009) and transformed composite section properties were automatically determined; the deck concrete was converted to beam concrete using the modular ratio. The modulus of elasticity of the bridge deck and girder materials were defined separately. Transverse grillage members were constructed to represent 12 in. wide rectangular sections of bridge deck that spanned the girder spacing. The modulus of elasticity of these sections was equal to the deck modulus of elasticity (i.e., E of the longitudinal composite system was different than E of the transverse deck system). Two-dimensional grillage models did not contain rebar, end diaphragms, intermediate diaphragms, or traffic barriers to maintain simplicity. All sections were constructed using gross section properties. Support boundary conditions for the 2D grillage models were the same as those used in the 3D grillage models.

3.5 Summary

This chapter outlined the various types of numerical modeling used for different tasks within the project. Details related to creation of each model type were discussed in this chapter; additional, specific details only applicable to individual parts of the study are discussed where appropriate in other chapters. Computationally efficient three-dimensional grillage models were used to determine instrumentation plans at the beginning of the project; these models were modified to contain shell elements for the bridge deck during design of the laboratory bridge. Detailed three-dimensional solid element finite element models were used to develop a better understanding of the complex behavior

associated with shear distribution in the laboratory bridge and field bridges. Simplified two-dimensional grillage models were used to develop final recommendations for rating prestressed concrete girder bridges at the end of the project.

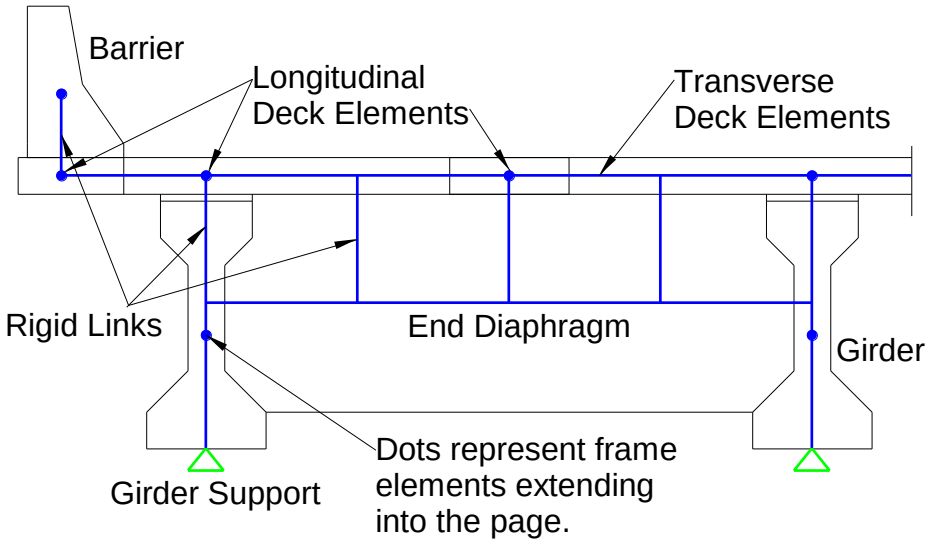

Figure 3-1. Cross Section of Three-Dimensional Grillage Frame Elements

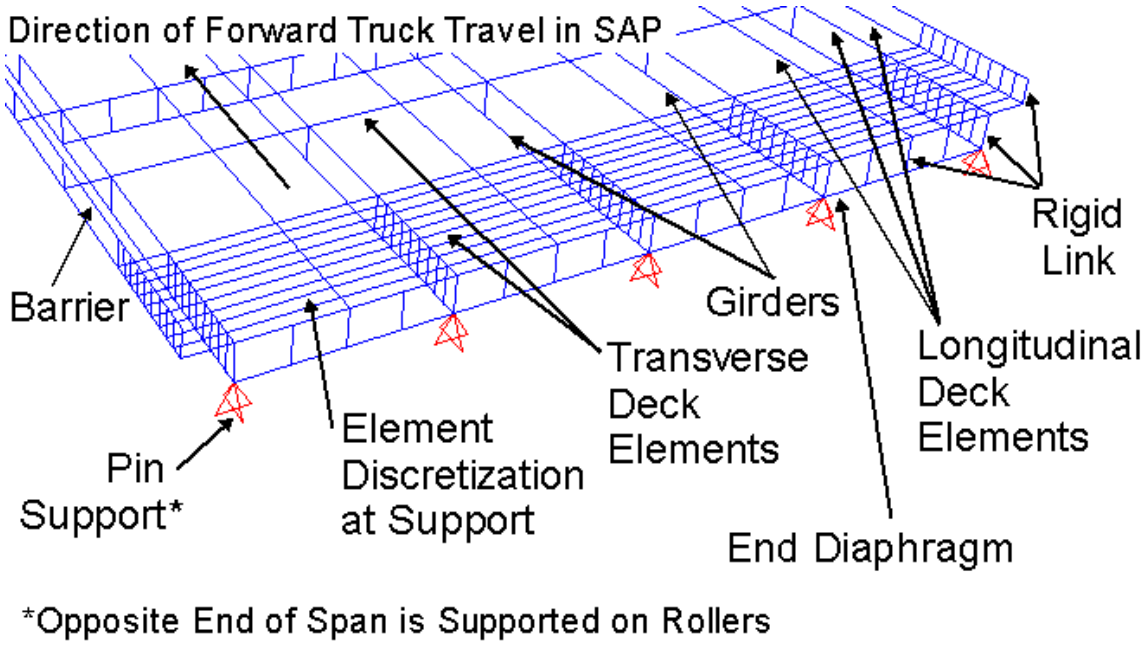

Figure 3-2. Three-Dimensional Grillage Model near Supports

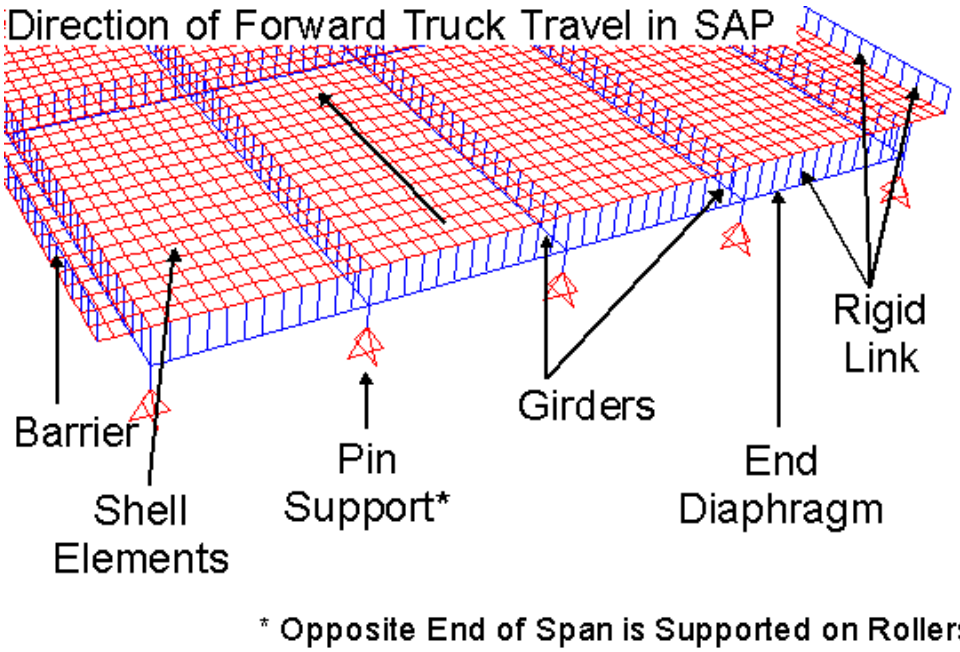

Figure 3-3. Three-Dimensional Grillage Model with Shell Elements for Bridge Deck

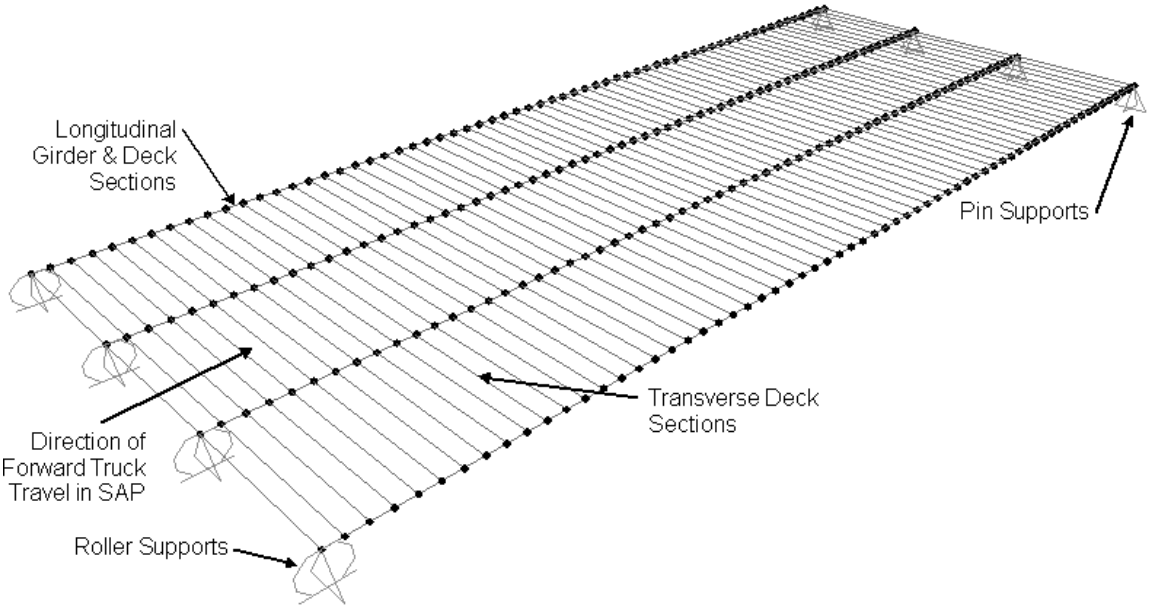

Figure 3-4. Simplified Two-Dimensional Grillage Model

CHAPTER 4. LABORATORY BRIDGE DESIGN, CONSTRUCTION, AND TESTING METHODS

4.1 Introduction

This chapter summarizes the design and construction of the laboratory bridge as well as the experimental test setup used to investigate shear behavior in both the elastic and inelastic range. The elastic laboratory bridge tests were used to validate the numerical modeling techniques in a controlled environment, with known material properties, and with variations of secondary bridge elements in four quadrants to determine the effects of end diaphragms and barriers. The bridge was representative of end span structures in the MnDOT inventory that were designed sometime in the 1960's, 1970's, and early 1980's. Furthermore, the bridge specifications allowed for comparison of data collected in the laboratory with data collected from field testing for a skewed and non-skewed structure of similar specification, as described in Chapter 6.

The bridge needed to fit within the available space in the Theodore V. Galambos Structural Engineering Laboratory at the University of Minnesota, while ensuring that the available loading from a single 77 kip actuator would produce measurable shear strains and that a combination of three actuators producing a maximum load of 440 kips could take the bridge to ultimate shear failure. The ability to subject the laboratory bridge to increased loads causing inelastic response allowed for observation of how shear distribution changes as the bridge girders and deck become damaged and redistribute the loads.

Initial analysis indicated that the maximum bridge girder depth that could be tested to near ultimate strength in the bridge system, with appropriate over-strength factors, was 36 in. Many secondary bridge parameters were considered during the design process, and the laboratory bridge was designed with the following features:

- Four 36 in. deep bridge girders similar to AASHTO Type II (fabricated using MnDOT 36M girder formwork with top and bottom flange blockouts)
- Nine inch thick deck
- Girders spaced at 9 ft center-to-center
- Bridge length of 32 ft and aspect ratio (L/W) of 0.94

- Specified 28-day concrete compressive strength of 7,500 psi in the beams and 4,000 psi in the deck
- Partial depth end diaphragm on one end of the bridge, no diaphragm on the other end of the bridge
- A traffic barrier along one side of the bridge
- Elastomeric bearing pads supporting each girder similar to those used for structures in the MnDOT inventory
- Zero degrees skew

Furthermore, uncoated rebar was used throughout the project to simulate construction standards used during the 1960's, 1970's, and early 1980's. The following sections provide details on the design, fabrication, measured material properties, instrumentation, and test setup for the full-scale laboratory bridge. In addition to the four girders constructed for the bridge, a fifth single companion girder was fabricated and independently tested to investigate the girder behavior at the component level. Documentation on the design, fabrication, instrumentation, and testing of the companion girder can be found in Appendix A.

4.2 Bridge Structural Design

4.2.1 Composite Bridge Girders

The 36 in. deep bridge girders were designed using the AASHTO Standard Specifications (1989) with 1991 Interim Revisions and the Precast/Prestressed Concrete Institute (PCI) Bridge Design Manual (1997). Four girders were used to construct the laboratory bridge, and are referred to as Girder 1 through 4 or G1 through G4. An AASHTO Type II shape was selected to replicate structures in the MnDOT inventory that rate poorly for shear and that were designed in the 1960's, 1970's, or early 1980's. Due to the lack of AASHTO Type II formwork available in Minnesota, formwork for a 36 in. deep Minnesota "M" series I-beam (36M) was modified to create a beam cross section that was similar to the AASHTO shape. Top and bottom flange blockouts were installed at the prestressing plant inside the 36M formwork to create the cross section shown in Figure 4-1. As was typical of current MnDOT practice, the deck was specified to be 9 in. thick.

The bridge girder design was completed using a capacity design approach. The maximum load that could be applied during ultimate testing was limited to 440 kips based on the capacity of the hydraulic actuators. To achieve the desired shear span-to-depth ratio of 2.5 during ultimate testing, which was the smallest recommended by Hawkins et al. (2005) to avoid arching action, the patch load of 440 kips was located 9 ft 7 in. from the centerline of support. To avoid a flexural failure, the girder flexural capacity (M_n) was required to be larger than the maximum flexural demand from the applied load of 440 kips, assuming the largest AASHTO Standard flexural distribution factor considering both one and two lanes loaded. To further ensure a flexural failure would not occur, the flexural demand at ultimate was amplified by 1.10 (i.e., $M_{n\text{-}reqd} \geq 1.1M_{DL}+1.1DF_{max}M_{LL}$). The increase of ten percent was selected after discussion with the MnDOT TAP for additional conservatism. To ensure a shear failure within 440 kips of applied load, it was assumed that the girder shear capacity at ultimate was 30 percent greater than would be predicted using AASHTO Specifications ($1.30V_n$), which was based on the findings of Hawkins et al. (2005) and confirmed with results from Runzel et al. (2007). Furthermore, the shear demand expected to fail a girder in the bridge was conservatively estimated using the smallest AASHTO Standard shear distribution factor considering both one and two lanes loaded ($V_{DL}+DF_{min}V_{LL}$). The assumption of greater shear distribution (i.e., smaller shear distribution factor) provided conservatism because a smaller nominal shear capacity would be required to achieve ultimate shear failure at an applied load of 440 kips.

The girder was designed with a concrete mixture that mimicked those used in bridges from the MnDOT inventory that rate poorly for shear and that were designed in the 1960's, 1970's, and early 1980's. The desired normal weight concrete mixture had a 28-day compressive strength of 6,000 psi and a release strength of 4,600 psi; the design unit weight was assumed to be 155 pcf for dead load and 150 pcf for elastic modulus calculations. Recognizing that concrete compressive strength increases over time (Wood 1991, Dereli et al. 2010), a realistic compressive strength for a 30-year-old bridge cast with this concrete was targeted at 7,500 psi. This targeted strength was based on the recommendation put forth by Dereli et al. (2010) who stated that "a lower bound of 20 percent increase in concrete compressive strength over 20 years was conservative." This became the specified 28-day strength for the bridge girders because it was the current

expected strength of the younger girders in the field that were found to rate poorly for shear from the 1980's. Furthermore, the specified 28-day concrete compressive strength for the bridge deck was 4,000 psi, which was consistent with current practice representative of replaced decks on these structures.

The number of prestressing strands in the girder cross section was chosen to ensure sufficent flexural capacity when the bridge was loaded with 440 kips located 9 ft 7 in. from the centerline of support. Flexural reinforcement was designed using strain compatibility with recommendations from the PCI Bridge Design Manual (1997) for guidance to calculate prestressing strand stress. Strain in the prestressing strands was converted to stress based on the relationship developed by Devalapura and Tadros (1992) for 270 ksi low relaxation strands. A total of 22 strands distributed as shown in Figure 4-2 and Figure 4-3 were used to achieve adequate flexural capacity. The prestressing strands were 0.5 in. diameter, 270 ksi, 7-wire low relaxation strands with a nominal strand area equal to 0.153 in.^{2}. Low relaxation strands were used instead of stress relieved strands (which were more common in the 1960's, 1970's, and early 1980's) due to their availability. The cross-sectional flexural strength was estimated to provide a nominal resistance of approximately 2,860 kip-ft compared to the demand of approximately 2,480 kip-ft at the location of maximum applied moment.

The large number of strands ensured that the girder would not fail in bending during inelastic testing, but a low prestress level was desired to meet allowable stress limits at release for the small girder cross section. The jacking force was limited by the capacity of the hardware used to secure draped prestressing strands at a single hold-down point on the prestressing bed that was scheduled for use during fabrication at Cretex Concrete Products. For ease and consistency, stressing all of the straight and harped strands to the same level of initial prestress was desired. Stress levels for each of the 22 strands were set to 25 kips (i.e., $0.61f_{pu}$) because that was the maximum jacking force allowed per draped strand by the prestressing plant (Fink 2013). This value of prestress resulted in concrete tensile stresses, calculated using gross sections, in excess of the smaller of 200 psi or $3\sqrt{f'_{ci}}$ at the top of the section at midspan, violating the AASHTO Standard Specification (1989) limit for tensile stresses when bonded reinforcement is not present. However, the AASHTO Standard Specification (1989) allowed for a tensile stress of $7.5\sqrt{f'_{ci}}$ if bonded

reinforcement is added to resist the total tension force in the concrete (in this case, at the top of the cross section at midspan). To meet this stress limit, four No. 5 uncoated bars were added to the top flange of the girder and extended one quarter of the beam length on either side of the centerline. All rebar was assumed to have yield strengths of 60 ksi in accordance with ASTM A615-12 (2012). Six of the strands were harped at the end of the girder to reduce the tensile stresses that develop at the top of the section; a single hold down point for these strands was located at midspan of the girder. At service, the calculated stresses, which included an estimate of prestress loss, did not approach the allowable stress limits in the AASHTO Standard Specifications (1989). A comparison of the final design stresses versus AASHTO Standard Specification (1989) allowable stress limits for transfer and service is given in Table 4-1.

Prestress losses were estimated using the AASHTO Standard Specifications (1989). The assumed section properties used for calculation of prestress losses are given in Table 4-2 and are included in the design calculations outlined in Appendix B. This procedure was consistent with MnDOT design practices from the 1960's, 1970's, and early 1980's. The AASHTO Specifications (1989) outline an iterative method to determine the elastic shortening (*ES*) losses, and provide simplified relations to determine shrinkage (*SH*) and creep (CR_c) losses. Steel relaxation (CR_s) losses were dependent on the prestressing strand type.

To complete the primary shear design using No. 4 U-shaped stirrups, which were common in bridges from the 1960's, 1970's, and early 1980's, a spacing, *s*, that satisfied the required minimum area of web reinforcement, the maximum allowable stirrup spacing, and the requirements for horizontal shear design was selected. Preliminary horizontal shear design indicated that the shear demand required to fail the girder was greater than the horizontal shear capacity for a roughened surface calculated using $350 b_v d_p$, where b_v is the width of the horizontal shear interface (top flange) and d_p is the distance from the extreme compressive fiber to the centroid of the prestressing force. However, the AASHTO Standard Specification (1989) allowed for an increase in the horizontal shear capacity by $(160 f_y/40{,}000) b_v d_p$ for each percent of tie reinforcement crossing the contact surface in excess of the minimum required for horizontal shear design. The minimum tie spacing required for horizontal shear design was either four times the 6 in. web width or 24 in.;

selection of a No. 4 stirrup spaced at 24 in., as shown in Figure 4-2 and Figure 4-3, satisfied the minimum tie spacing, minimum tie area (at least $50b_v s/f_y$), and horizontal shear requirements. All of the transverse reinforcement extended 5 in. out of the top flange of the beam to approximately mid-depth of the 9 in. thick deck to develop composite action between the girder and deck. Anchorage zone reinforcement requirements were satisfied at the beam ends by using stirrups spaced at 3 in. and two No. 5 uncoated C-shaped bars beginning 2 in. from the beam end. Confinement reinforcement consisted of two No. 3 uncoated bars bent and spliced together, enclosing all of the straight strands at the ends of the beam. The shear capacity of the composite girder was estimated as 200 kips including a 1.3 over-strength factor ($1.3V_n$) at one half of the composite depth away from the interior face of the support compared to the demand of approximately 215 kips generated by an applied patch load of 440 kips (using $V_{DL}+DF_{min}V_{LL}$).

No lifting devices or lift hooks were installed in the girders. Typically, bundles of three strands are bent into an inverted V-shape and embedded near the ends of beams to move prestressed concrete beams after fabrication. The location and amount of extra reinforcement in the web is not considered in design. Runzel et al. (2007) reported that capacity predictions might be conservative due to the addition of these lift hooks. In lieu of the lift hooks, three holes were located through the web at each end of the beams to accept rigging equipment for moving the beams. Two of these holes, in addition to another two drilled in the laboratory, were used for attachment of the diaphragm at one end of the laboratory bridge.

4.2.2 Deck Reinforcement

Deck reinforcement was chosen by reviewing the deck reinforcement in six bridges from the MnDOT inventory designed in the 1960's, 1970's, and 1980's, the concrete slab reinforcement tables from the MnDOT Bridge Design Manual (1996), Table 9.2.1.1 from the MnDOT LRFD Bridge Design Manual (2013), and AASHTO LRFD Specifications (2010). The bridges reviewed had a girder spacing similar to the spacing specified for the laboratory bridge. Table 4-3 summarizes the deck details reviewed and the final laboratory bridge deck details, which are shown in Figure 4-4. Generally, the amount of longitudinal steel specified using each method was the same because the girder spacing was approximately the same (9 to 11 ft), while the amount of transverse reinforcement was

slightly lower using newer methods compared to methods used between 1968 and 1983 (smaller bar size, approximately same spacing).

The top and bottom transverse reinforcement, No. 5 bars at 5.5 in., and the bottom longitudinal reinforcement, No. 5 bars at 8 in., aligned with details from both the MnDOT Bridge Design Manual (1996) design table and select structures in the MnDOT inventory. Bottom longitudinal reinforcement details were selected considering that bridges designed and constructed in that era typically had a wider bar spacing near the girders and a tighter bar spacing between the girders.

The laboratory bridge represented a single simply-supported bridge span designed to investigate two different types of abutment end details (i.e., with and without end diaphragms). This was atypical of most prestressed bridge girder construction, which consists of multiple simply-supported spans continuous through the deck, where negative moment deck reinforcement extends into the next span over the pier. The final top longitudinal reinforcement details of the laboratory bridge, No. 4 bars at 18 in., did not include extra reinforcement at a tighter spacing over what would typically be considered the negative moment region at a pier.

4.2.3 End Diaphragm

To investigate the effects of end diaphragms, the west end of the laboratory bridge incorporated a partial depth end diaphragm and the east end had no end diaphragm. The partial depth end diaphragm was selected for the study instead of a full depth end diaphragm for three reasons. First, results from initial numerical analyses using 3D grillage models modified to include shell elements for the bridge deck indicated that the amount of shear distributed was not dependent on the stiffness of the diaphragm. Second, many full depth end diaphragms *in situ* are cracked at the interface of the girder and end diaphragm. These cracking patterns are particularly evident in semi-integral abutment bridges where the upward girder deflection due to solar radiation may be constrained by the end diaphragm. Use of an uncracked full depth end diaphragm in the laboratory was not considered to be representative of full depth end diaphragm behavior in the field. Cracked full depth end diaphragms may have a stiffness value and behavior between an uncracked full depth end diaphragm and a partial depth end diaphragm. Third, from a constructability standpoint, either a full depth or a partial depth end diaphragm had to encompass the ends

of the four bridge girders. A full depth end diaphragm offset from the end of the girders interfered with movement of the load frame and the base plates on the bottom of the columns. To remedy this problem, a full depth end diaphragm would have needed to be constructed on a smaller scale at a longitudinal location not representative of practice. A partial depth end diaphragm extending beyond the end of the girders did not interfere with movement of the load frame columns and was constructed at the same scale as partial depth end diaphragms of *in situ* structures.

The partial depth end diaphragm design was based on MnDOT detail B803 used for many bridges designed and built in the 1970's. Longitudinal reinforcement in the bottom of the diaphragm consisted of two straight No. 7 bars placed at the edges of the rebar cage and one bent No. 6 bar placed at the center of the diaphragm cross section. The No. 6 bent bar was shaped such that it extended from the bottom of the diaphragm at midspan between the adjacent girders up to the bridge deck above each girder. The partial depth end diaphragm was made composite with the bridge deck through the use of No. 4 transverse stirrups spaced at approximately 18 in. that extended out of the end diaphragm. Two additional No. 4 longitudinal bars were placed 14 in. above the bottom layer of longitudinal reinforcement for ease of constructability and to maintain the shape of the hoop confinement. Details and spacing of reinforcement can be seen in Figure 4-5 and Figure 4-6.

4.2.4 Barrier

A barrier was designed for the north side of the bridge. The barrier was made composite through the use of No. 5 bent bars spaced at approximately 12 in. that protruded out from the cast-in-place deck. Barrier reinforcement details were taken from bridges that were built during the 1960's and 1970's. Barrier specifications for the laboratory bridge included a construction joint (typically denoted as a deflection joint) at midspan, which was similar to bridges from the time period of interest. Details and spacing of reinforcement are shown in Figure 4-7 and Figure 4-8.

4.3 Bridge Construction

4.3.1 Girder Fabrication

Fabrication of the bridge girders began on June 25, 2013 on Bed 1 at Cretex Concrete Products in Elk River, MN. Construction of the beams was completed by University of Minnesota personnel with assistance from Cretex Concrete employees. The girders were aligned and numbered sequentially in Bed 1 such that Girder 1 was nearest the dead end and Girder 5 (the companion girder) was nearest the live end. An abbreviated timeline for fabrication and other significant events for the girders is given in Table 4-4. Foil and vibrating wire strain gages were embedded in the girder during fabrication to evaluate prestress losses and stirrup strains, more information on the internal instrumentation is given in Section 4.5.2.

Construction of the girders is summarized in the following sequence. On June 25, 2013, the prestressing strands were placed in the bed and four strain gages were installed on the strands with no prestressing force. All of the strands were lightly pretensioned to approximately 4,000 lb each for ease of placing the remaining strain gages on the strands. After gage installation, all of the strands were jacked to approximately 25 kips and end forms were installed. Mild steel reinforcement, including the stirrups, top flange longitudinal rebar, and the confinement bars were placed.

On June 26, 2013, after the rebar cage was complete, the vibrating wire strain gages were installed. Bottom blockouts were installed on the bed before installation of the MnDOT 36M formwork and the top blockouts were installed in the MnDOT 36M formwork the following day prior to concrete placement to achieve the AASHTO Type II section shape. Concrete was mixed at the plant batch station. Each girder contained approximately 3.2 yd^3 of concrete. The total girder volume of approximately 16 yd^3 was delivered in five main 3 yd^3 batches. A sixth batch was used to complete the very end of the fifth (companion) girder. The girders were consolidated using only hand-held vibrators, inserted into the formwork between stirrups. External form vibration was not used due to space limitations and concern for the stability of the wooden blockouts. The top surface of the beams was intentionally roughened using a metal rake. Immediately following concrete

placement, tarpaulins were used to cover the formwork. No external heat or steam was applied during curing.

On June 29, 2013 the formwork was removed after the concrete reached the required concrete compressive strength for release. To release the strands, the following pattern was specified by Cretex Concrete: (1) flame cut four of the straight prestressing strands, (2) flame cut four of the harped prestressing strands, (3) release the harped strand hold down points, (4) flame cut the two remaining harped prestressing strands, and (5) flame cut the remaining 12 straight prestressing strands. No pre- or post-release cracks were observed. On July 3, 2013 the beams were removed from the casting bed and relocated to a storage site in the prestressing yard until they were delivered to the University of Minnesota in two shipments on July 26, 2013. No stability problems or cracks were observed due to transportation.

4.3.2 Girder Placement

The girders were individually placed on the supports in the laboratory and aligned in the east-west direction. The live ends of the girders were oriented to the west and were connected via the partial depth end diaphragm. Girder 1 was the northern exterior girder, Girder 2 was the northern interior girder, Girder 3 was the southern interior girder, and Girder 4 was the southern exterior girder. Final girder positioning on the abutments was completed using the overhead crane for the interior beams and a single Hilman roller under each sole plate for the exterior beams (positioned out of reach of the overhead crane). Once in place, the exterior girders were lifted vertically off the rollers using a hydraulic actuator under each end and placed on the bearing pads. Girder position was adjusted until measurements made diagonally, transversely, and longitudinally indicated the girders were positioned to within a 0.5 in. tolerance. The four girder structure is shown in Figure 4-9 and Figure 4-10. Details regarding the concrete abutments can be found in Appendix B.

The boundary conditions at the ends of all four girders were constructed such that the girder sole plates rested on 2.5 in. thick steel laminated elastomeric bearing pads donated to the project by the MnDOT materials office. The bridge bearing pads contained four steel laminate sheets that were 1/8 in. thick, layered with three interior rubber layers that were 0.5 in. thick and two exterior rubber layers that were 0.25 in. thick. The pads were cut to a 16 in. width and 10 in. length, and they were aligned such that the 16 in.

direction was transversely centered under the end of the girder creating a 1 in. overhang on each side. The 10 in. dimension was parallel to the length of the bridge girders and centered on the sole plate; the centerline of the sole plate was 7.5 in. from the end of the 32 ft girder. This geometry created a span length of 30 ft 9 in. from center of bearing to center of bearing. The elastomeric bearing pads rested directly on the concrete bridge abutments as shown in Figure 4-11.

4.3.3 Deck Fabrication

Approximately 40 yd^3 of deck concrete was placed on March 5, 2014 to cast the laboratory bridge deck. Details regarding the formwork are discussed in Appendix B. Concrete was delivered starting at 8 am in four trucks at 30 minute intervals, each carrying 10 yd^3, and pumped into the laboratory using a 100 ft telescoping Z-boom truck and 4 in. diameter hose as shown in Figure 4-12. Placement and finishing of the concrete deck was completed by volunteers from the Cement Masons, Plasterers, and Shophands Local No. 633 Union apprentice training program. Volunteers from the University of Minnesota coordinated the effort and made companion cylinder test specimens. Figure 4-13 shows a diagram of the bridge deck outlining approximately where concrete from each truck was placed. The bridge deck was subjected to a seven-day moist cure using wet burlap that was periodically remoistened covered by polyethylene plastic.

4.3.4 End Diaphragm Fabrication

Figure 4-6 highlights the composite reinforcement details connecting the end diaphragm to the girders. The four bridge girders were constructed with three 1.5 in. diameter through holes in a vertical line 9 in. from the end of each beam. This layout was used to facilitate girder lifting and because the pattern could be adapted for either full depth or partial depth end diaphragms. Typically in MnDOT detail B803 for partial depth diaphragms, the end diaphragm is connected to the girders with four reinforcing bars in a box-shaped pattern such that all reinforcement is contained in the transverse hoop reinforcement. Two additional through holes were needed to emulate this pattern in the laboratory bridge and to improve the flexural and torsional resistance of the partial depth diaphragm as it connected to the adjacent girders in the laboratory bridge. Drilling and adding a 1.25 in. diameter through hole in the top flange, located 6 in. away from the

existing holes, was completed. A smaller, 7/8 in. diameter hole (sized similar to the diameter of the reinforcement) shown in Figure 4-6, was relocated at a lower elevation through the girder web to avoid the draped strand. This hole was still within the transverse hoop stirrup. All through holes in the exterior girders were filled with Hilti HIT-RE 500-SD epoxy to secure the threaded rod reinforcement; the through holes were plugged from the exterior side of the girder such that only half of the web or top flange widths were grouted.

Concrete for the partial depth end diaphragm was placed simultaneously with the bridge deck on March 5, 2014. The end diaphragm was subjected to a seven-day moist cure using wet burlap that was periodically remoistened covered by polyethylene plastic.

4.3.5 Barrier Fabrication

The barrier was added to the superstructure on March 12, 2014, one week after the bridge deck was placed. Approximately 5 yd^3 of concrete were delivered at 7 am and pumped into the laboratory using a 2 in. diameter hose. Discussion of the barrier concrete mix appropriate for pumping in a 2 in. diameter hose is presented in Section 4.4.3. Placement and finishing of the concrete deck was completed by volunteers from Graham Construction while researchers from the University of Minnesota made cylinder test specimens. The barrier was subjected to a seven-day moist cure using wet burlap that was periodically remoistened covered by polyethylene plastic. Formwork was removed on March 13, 2014.

The barrier was left on the bridge for the duration of elastic live loading, after which, the barrier was saw cut off of the bridge by Langford Tool & Drill Co. / Mason-Cutters at the original longitudinal construction joint. Removal of the barrier was done so that the bridge transverse cross section was symmetric for ultimate testing of two corners of the structure.

4.4 Bridge Material Properties

4.4.1 Girders

4.4.1.1 Concrete Trial Mix Design and Properties

To achieve the target 28-day compressive strength of 7,500 psi, Cretex Concrete Products conducted two trial batch studies for this project. Mix information for the batches is given in Table 4-5. The first batch, designated "525 Cement," achieved the target compressive strength at 28 days. On June 25, 2013, during the first day of girder fabrication, slight modifications were made to the original non-air-entrained batch to confirm the early compressive strength properties of the concrete, designated "525 Cement Early Age." This batch was used to predict the amount of time needed to achieve the required minimum compressive strength to meet allowable stresses at release. The fresh and hardened concrete mix properties are shown in Table 4-6 for each trial batch.

4.4.1.2 Concrete Mix Properties

During girder fabrication, Cretex Concrete personnel made 12 Sure-Cure cylinder specimens that were primarily used to track early age compressive strengths of the concrete to determine if required compressive strengths were reached prior to release. The temperature of the Sure-Cure cylinders was controlled by a thermocouple probe attached to the girder formwork to mimic the girder temperature during curing. University of Minnesota personnel made 50 concrete cylinders in 4 x 8 in. plastic molds to determine the compressive strength, modulus of elasticity, and the splitting tensile strength of the concrete at different ages. Six modulus of rupture specimen were also made in 6 x 6 x 24 in. steel molds. All concrete test specimens were made in accordance with ASTM C31 (2012), but they were not cured in accordance with the standard. The cylinders and modulus of rupture beams were placed next to the girder formwork and covered with the same tarpaulins used to cover the formwork. All of the concrete samples were transported to the University of Minnesota after 48 hours when the tarpaulins were removed. The girder concrete mix properties and number of companion specimen per batch are given in Table 4-7.

4.4.1.3 Concrete Compressive Strength

The target girder concrete compressive strengths were 4,600 psi at release and 7,500 psi at 28 days. Three out of five cylinder compressive strengths measured at approximately 22 hours were slightly lower than the target release strength. These tests, performed to determine if the strands could be released, were based on a single cylinder compressive strength from each end of the casting bed, which is typical practice for Cretex Concrete Products. Initial concrete strengths of the UMN cylinders cured under the tarpaulin were lower than those obtained using the Sure-Cure system. After 48 hours of cure time, the concrete strength was found to be above the minimum required to release the girders.

The compressive strengths of the 4 x 8 in. UMN cylinders were determined in accordance with ASTM C39 (2012). The Sure-Cure cylinders were tested at Cretex Concrete Products using a neoprene end cap in accordance with ASTM C1231 (2012). The other cylinders, cured under the tarpaulins, were capped with a high-strength sulfur-based capping compound in accordance with ASTM C617 (2012) and tested at the University of Minnesota. The loading rate was approximately 475 lb/sec (approximately 38 psi/sec). Cylinder strength values over time are given in Table 4-8. Average measured compressive strength values for each age of interest (i.e., elastic testing and inelastic testing) were used for the respective analysis calculations.

4.4.1.4 Concrete Modulus of Elasticity

The concrete static modulus of elasticity, E_c, was determined for 4 x 8 in. cylinders using a compressometer in accordance with ASTM C469 (2010). Measured and predicted values for all five girders are given in Table 4-9 in association with the dates of structural testing (i.e., elastic testing and inelastic testing). Each tabulated modulus of elasticity value represents the average of three tests completed on an individual cylinder. Predicted values were calculated in accordance with AASHTO LRFD (2010) Eqn. 5.4.2.4-1 (shown in Table 4-9) considering the measured concrete unit weight given in Table 4-7 and measured compressive strengths given in Table 4-8. The change of concrete unit weight over time was not measured in this study. Average measured modulus of elasticity data for each age of interest (i.e., elastic testing and inelastic testing) were used for analysis calculations.

4.4.1.5 Concrete Tensile Strength

The tensile strength of the girder concrete was evaluated using both split cylinder and modulus of rupture tests. Splitting tensile strength tests were conducted on 4 x 8 in. cylinders in accordance with ASTM C496 (2011) at a loading rate of approximately 100 lb/sec (approximately 119 psi/min). Modulus of rupture tests were conducted on 6 x 6 x 24 in. beams at a loading rate of approximately 30 lb/sec (approximately 150 psi/min) under simple beam third-point flexural loading conditions in accordance with ASTM C78 (2010). Measured and predicted values for all five girders are given in Table 4-10 and Table 4-11 for the respective test types. Predicted values were calculated in accordance with AASHTO LRFD (2010) Sections 5.4.2.6 and 5.4.2.7 (equations shown in Table 4-10 and Table 4-11) considering the measured compressive strengths from Table 4-8. Average measured split cylinder tensile strength values and modulus of rupture values for each age of interest (i.e., elastic testing and inelastic testing) were used for analysis calculations. The modulus of rupture data were used for calculation of the flexural cracking moment.

4.4.1.6 Transverse Reinforcement Properties

All transverse reinforcement used in the girders was uncoated Grade 60 stirrups. Stress versus strain curves, shown in Figure 4-14, were measured using ten samples of No. 4 rebar taken from nine different stirrups. Each specimen was cut to a length of 18 in. and tested at a load rate of 0.125 in./min to determine the yield strength. The yield strength was determined during testing using an extensometer and a foil strain gage applied near the center of the 18 in. gage length. Tests and data analysis were completed in accordance with ASTM A370 (2012) and ASTM A615 (2012). ASTM A615 (2012) states that if steel specimens do not have a well-defined yield point, the yield strength shall be determined by the 0.2 percent offset method outlined in ASTM A370 (2012). This was the method used to obtain an average stirrup yield strength of 69 ksi, modulus of elasticity of 29,100 ksi, and yield strain of 0.0024, shown in Table 4-12, for analysis calculations. Because an extensometer was used, the yield strength data corresponding to the Extension Under Load (EUL) Method outlined in ASTM A370 (2012) was also used for comparison. This method specifies that when testing does not exhibit a distinct yield point and yield plateau, an

equivalent yield point value can be determined by recording the load producing a specified extension of 0.005 in./in. for steel with a known yield stress less than 80 ksi.

Figure 4-14, which shows the stress versus strain curves the No. 4 rebar, includes three distinct lines: the dotted line represents the 0.2 percent offset used to obtain the yield stress of the steel because no distinct yield point or plateau was visible; the dashed line represents the minimum stress corresponding to a minimum tensile strain of 0.0035; the solid vertical line represents the stress producing a specified extension of 0.005 in./in.

In the single companion girder, additional stirrups (i.e., No. 4 epoxy-coated stirrups) were placed near midspan to facilitate testing the second end of the girder; those stirrups were not tested to determine the material properties.

4.4.1.7 Prestressing Strand Properties

The 0.5 in. diameter, 270 ksi, 7-wire low relaxation prestressing strands used in this project were provided by Cretex Concrete Products and were manufactured by the Sumiden Wire Products Corporation in accordance with ASTM A416 (2012). Sumiden Wire Products Corporation provided material properties for the strand, including the diameter, area, elastic modulus, and ultimate stress. Nominal material properties from Nilson (1987) and manufacturer provided material properties are given in Table 4-13. The manufacturer provided material properties were used for all analysis calculations.

4.4.2 Deck and End Diaphragm Concrete

The concrete specified for the bridge deck and partial depth end diaphragm (cast simultaneously) was chosen to replicate 1970's era MnDOT mix designs. Bridge deck mixes from this time period typically had ¾ in. maximum aggregate and a 28-day nominal compressive strength of 4,000 psi. Engineers at Cemstone Concrete were able to provide a concrete mix (mix designation 4164P) that met the compressive strength and aggregate size requirements and was similar to what was used in the 1970's. The mix was modified to have a 6 in. slump so that the concrete could be pumped. Specified mix details and information for each 10 yd^3 batch are given in Table 4-14. The fresh and hardened concrete mix properties are given in Table 4-15.

4.4.3 Barrier Concrete

The concrete specified for the barrier was chosen to meet three criteria: a 28-day nominal compressive strength of 4,000 psi (similar to the bridge deck), a slump of 5 in. that could be pumped, and an aggregate size that allowed for pumping in a 2 in. diameter hose (for ease). Engineers at Cemstone Concrete were able to provide a concrete mix (mix designation 4594P) that met the compressive strength requirement and was easily pumped. Specified mix details and information for the 5 yd^3 batch are given in Table 4-16. The fresh and hardened concrete mix properties are given in Table 4-17.

4.5 Instrumentation and Data Acquisition

This section provides a summary of the data acquisition system and instrumentation that was used in the laboratory and field tests. Additional instrumentation details, including manufacturer, model number, gage length, and application techniques are provided in Appendix C.

4.5.1 Data Acquisition

In the laboratory tests, voltage sensor data were collected via the Civil Engineering Data Acquisition (CE DAQ) system, which consisted of a National Instruments SCXI high performance data acquisition system that simultaneously sampled up to 64 voltage channels (at ±10 V) and 128 channels of quarter bridge 120 ohm strain gage input at a rate of 1 Hz. Vibrating wire strain gages (VWG) were used in both the laboratory and field tests and were collected through a Campbell Scientific, Inc. CR1000 measurement and control datalogger (CR1000 DAQ). In both the laboratory and field tests, the terminal boards were connected to the datalogger using 70 ft, 100 ft, or 136 ft 24-pin military connector cables that carried five channels each (every VWG used one channel). To prevent dust particles in the laboratory or inclement weather in the field from affecting the CR1000 DAQ, the datalogger was covered in plastic sheeting or housed in a minivan, in the respective situations. The CR1000 DAQ was constantly powered using a wall outlet in the laboratory and a Honda EU1000i generator in the field.

The datalogger measured up to 80 vibrating wire sensor channels through five AM16/32 multiplexers, interfaced through two AVW4 vibrating wire interfaces. Specific batch factors, specified by Geokon, were utilized to correct for the method of wire clamping

used during vibrating wire strain gage fabrication which shortens the vibrating wire causing it to over-register the strain. Sample CR1000 programs can be found in Appendix C. The CR1000 program cycled through and saved data for each of the 80 channels five separate times for each measurement increment so that an average reading could be calculated during post-processing. Collecting a set of five cycles typically required seven to eight minutes. Because of this requirement, loading was always paused in the laboratory or trucks were left in place for field testing to complete the cycles. In the laboratory, the CE DAQ continuously collected data throughout the length of the tests. The laboratory test data collected by the two DAQ systems were always linked with the same time stamp, the force signals from all three actuators, and the actuator displacement signals from all three actuators. The output data files were annotated and saved off of the CR1000 using RTDAQ 1.1.1.8 software.

4.5.1.1 Data Acquisition Modifications for Foil Strain Gages

The data from the foil strain gages used in the laboratory tests were collected by means of a CR1000 data acquisition unit after making a significant change to the setup. Instead of wiring the multiplexers through a vibrating wire interface, each individual multiplexer was connected to the CR1000 using a single Campbell Scientific 4WFB120 terminal input module (TIM). The TIM module completed a full bridge for multiple quarter bridge strain gages connected to a single multiplexer. Data collected using this configuration was read sequentially at a rate of 0.05 scan intervals/sec. Modifications to the CR1000 programing can be found in Appendix C.

4.5.2 Girder Internal Instrumentation

Three separate types of instrumentation were installed prior to and during fabrication of the five girders. The instrumentation was used to measure the strain in the transverse reinforcement, the initial prestressing force in the 7-wire prestressing strands, and prestress losses due to elastic shortening and time-dependent creep and shrinkage effects.

4.5.2.1 Instrumentation for Stirrup Strains

Foil strain gages were installed at three vertical locations on one leg of five stirrups at each end of each girder to capture the stirrup strains during testing. The strain gages were installed so that they were evenly distributed through the web depth, as shown in Figure 4-15 using techniques described in Appendix C. The strain gage naming convention included the girder number in which the stirrup was placed (G1-G5, where G1 was the girder nearest the dead end of the bed and G5 was the girder nearest the live end of the bed); the location of the stirrup along the length of the girder (stirrup label A started at the dead end of a beam and stirrup label J ended at the live end of a beam); and whether the gage was the bottom (B), middle (M), or top (T) strain gage on the stirrup leg. For example, referencing Figure 4-15, G1-A-B was the name of the stirrup strain gage located at the bottom of the stirrup nearest the beam dead end in Girder 1. Girder orientation in the laboratory bridge in regards to cardinal directions, live versus dead end, and with respect to the end diaphragm was discussed in Section 4.3.2.

4.5.2.2 Instrumentation for Initial Prestressing Force

Foil strain gages were attached to a wire of the 7-wire prestressing strands to measure the initial prestressing force and the losses due to elastic shortening. The gages were installed using a similar procedure to that described in Appendix C. The foil strain gages were placed at various locations along the length of the prestressing bed, both inside and outside the girder formwork, on the strands indicated in Table 4-18 and Figure 4-16, which shows a cross-sectional view looking towards the live end of the prestressing bed. The midspan groups of four strain gages were installed so that they bracketed the vertical centroid of the prestressing strands. Groups of two or four strain gages were installed outside the formwork, either between the dead end bulkhead and the first beam end formwork or between the end formwork of two beams.

The first set of strain gages at the dead end between the bulkhead and end formwork was attached to the unstressed strands outside of the girder prior to tensioning. The remaining strain gages were attached at their respective locations after an initial prestress force of 4 kips was applied to the strands. The 4 kip preload was used to lift and straighten the strands off the prestressing bed. However, because of the length of the prestressing bed

and relaxation of the strands due to increasing temperatures, the 4 kip preload did not adequately lift and straighten the strands. It was deemed a preload of 6 kip would have been more appropriate and this level of preload was used by Mathys et al. (2014). Some strain gages were damaged or ripped off of the wire when the strands were stressed to higher levels.

4.5.2.3 Instrumentation for Prestress Losses

A single Model 4200 vibrating wire strain gage, manufactured by Geokon, was installed at midspan in each of the four laboratory bridge girders to measure prestress losses due to elastic shortening, creep, and shrinkage. The VWGs were placed near the vertical centroid of the prestressing strands, as shown in Figure 4-17, and secured to the strands with zip ties and additional pieces of rebar. The nominal distance between the VWG and the strand centroid was 0.25 in. Each VWG also contained a thermistor for recording temperature. Strain and temperature readings were read for each of the embedded VWGs using a Geokon GK-403 Vibrating Wire Readout Box.

A summary of the losses used for bridge girder capacity calculations are given in Table 4-19. The final prestress values include both theoretical prestress losses and average measured prestress losses (coefficient of variation of 2.6 percent for the four bridge girders). Theoretical losses for seating (obtained from Cretex Concrete) and strand relaxation were used where measured losses could not be obtained. Measured losses for elastic shortening, creep, and shrinkage were taken from the VWG data. Details regarding the measured prestressing strand force over time and losses for each individual girder are presented in Appendix D.

4.5.3 Girder Preparation for External Instrumentation and Crack Monitoring

Prior to external instrumentation, the entire exterior faces of each girder and approximately 3 in. of the girder-deck interfaces were white washed to facilitate observations of cracking during testing. The whitewash mixture, by weight, consisted of approximately 1.75 parts water and one part Mississippi Lime Co. hydrated lime. The location of externally mounted strain gages were covered with duct tape prior to white washing to preserve a pristine concrete surface. If the location of an externally mounted instrument was not known prior to white washing, the lime mixture was removed from the

concrete surface at the time of instrument application using a pneumatic sanding wheel. Stirrup locations and internal stirrup strain gage location grids were drawn on the web using permanent marker after white washing. An example grid is shown in Figure 4-18. The stirrup locations (noted by the reinforcement protruding from the top flange prior to deck placement) were marked along the girder top flange prior to placing deck concrete; the vertical stirrup grid line marks were transferred to the web after white washing. The strain gage grid marks were based on the nominal gage locations specified during construction.

4.5.4 Laboratory Bridge Elastic Testing Instrumentation

The laboratory bridge was tested in the elastic range in four quadrants with the following notation (in order of testing): Lab Bridge Elastic South East (LBESE), North East (LBENE), North West (LBENW), and South West (LBESW). The traffic barrier (denoted north barrier or NB) was included in tests conducted on the North side of the bridge (LBENE and LBENW) and the end diaphragm was included in tests conducted on the West end of the bridge (LBENW and LBESW). The actuators were designated as North (N), Middle (M), or South (S) in coordination with the cardinal directions in the laboratory. Load was applied to the bridge at two longitudinal locations in each quadrant: $2d_v$ and $4d_v$. Figure 4-19 shows an elevation view of the four quadrants, including actuators and secondary bridge parameters in each quadrant. Figure 4-20 shows a plan view of the four quadrants and indicates the longitudinal location of the actuators in relation to the critical section for shear, d_v.

The instrumentation used during elastic laboratory bridge testing evolved as testing progressed through each of the quadrants. Instrumentation used during tests on the LBESE quadrant varied from instrumentation required for other quadrants where a traffic barrier (LBENE and LBENW) or end diaphragm (LBENW and LBESW) was present. Generally, structural behavior was monitored with seven types of instrumentation during elastic testing. Instrumentation details for each bridge quadrant are given in Table 4-20 and shown in Figure 4-21 through Figure 4-25.

4.5.4.1 Shear Strain

Shear strain, γ_{xy}, was calculated using rosette strain data from foil and vibrating wire gages installed at multiple positions along the length of the girders measured relative

to the critical shear section, d_v from the interior edge of the sole plate. Vibrating wire strain data was collected from up to 80 Model 4000 gages. Typically, sets of four strain gages formed a box-type rosette, shown in Figure 4-26. The box-type rosette allowed for linear interpolation of strain between the two horizontal gages such that, when incorporated with the single vertical and diagonal gage, three directions of a 45 degree rosette strain measurement were captured at the center of the box configuration. This configuration assumed that the vertical strain did not vary significantly over a small longitudinal distance. The box-type rosette was configured on girder webs such that the diagonal strain gage was parallel to the principal compressive stress from the applied load to maximize the reading. Strain gages in the box-type rosette were applied in a repeatable fashion to the web of the prestressed concrete girders using the steps outlined in Appendix C. On each girder the bottom horizontal strain gage was 3.5 in. from the web-to-bottom flange interface, the centers of the diagonal and vertical strain gages were 7 in. from the web-to-bottom flange interface, and the top horizontal strain gage was 10.5 in. from the web-to-bottom flange interface. Data from trial tests, discussed in Chapter 5, indicated that VWGs and foil rosettes installed on the same side of the girder web at the same location ($1d_v$ on G3 and G4 during LBESE and at $1d_v$ on all girders during LBENE, LBENW, LBESW) gave similar results. This redundancy led to the use of VWGs on one side of the girder web and foil rosettes on the opposite side of the girder web in many locations to capture the effects of torsion and to facilitate determination of the vertical shear in the section. Vibrating wire strain gage rosette notation was defined in an XX-YY-ZZ manner, where XX stood for the longitudinal location ($0.5d_v$, $1.0d_v$, $2.0d_v$, or $4.0d_v$), YY stood for the structural element (G1, G2, G3, G4, or NB), and ZZ stood for the location of the individual gage within the rosette (Bottom, Top, Diagonal, or Vertical).

After ensuring the feasibility of using both types of gages, foil strain gage rosettes were installed at the same longitudinal positions as the VWG rosettes but were located on the opposite face of the web. Data collected from the VWG box-type rosettes and the foil rosettes were averaged to negate the torsional effects and to calculate shear strain due to the vertical shear strain resultant, γ_{xy_shear}. Foil rosette strain gage notation was defined in an AA_BB_CC_DD format, where AA was the structural element (G1, G2, G3, G4, or NB), BB was the cardinal direction related to the half of the span in which the gage was

installed (East or West), CC was the longitudinal location (0.5d_v, 1.0d_v, 2.0d_v, or 4.0d_v), and DD was the location of the individual gage within the rosette (Horizontal, Diagonal, or Vertical). Similar foil strain gage rosettes were also used in pairs in the end diaphragm to measure shear strain γ_{xy_shear} in LBENW and LBESW. Notation for the end diaphragm rosettes included the following, separated by underscores: location of the individual diaphragm designated by the girders it spanned between (G12DIA, G23DIA, or G34DIA), the location of the individual strain gage on the diaphragm using cardinal directions (NE, NW, SE, or SW), a letter designating the vertical location relative to the bottom of the end diaphragm (Bottom or Middle), and a letter denoting the location of the individual gage within the rosette (Bottom, Top, Diagonal, or Vertical). Foil strain gages were applied to concrete surfaces using application techniques outlined in Appendix C.

4.5.4.2 Vertical Deflection

Vertical girder deflection under the four girders at 2d_v from both ends and midspan was measured during elastic testing using linear variable differential transformers (LVDTs). Measurments from the LVDTs at 2d_v and midspan included the vertical bearing pad displacement as well as the girder flexural deflection. The vertical deflection of each girder was obtained by subtracting the bearing pad vertical deflection from the girder LVDT data. Notation for girder displacement LVDTs consisted of the following, separated by underscores: identification of girder (G1, G2, G3, or G4), the cardinal direction related to the half of the span in which the LVDT was installed (East, West, or nothing if located at 0.5L), and the longitudinal location (2.0d_v or 0.5L). The LVDT rod was fitted with a threaded aluminum Altigweld 4043 rod, manufactured by AlcoTec, which was attached to the girder using hot glue. The LVDT signal was conditioned and calibrated using a general purpose AC powered ATA-2001 LVDT analog conditioner manufactured by Measurement Specialties. LVDTs with a range of ±1.0 in. were used at each location to measure vertical displacements.

Vertical displacement of the girder bearing pads was measured using two or four ±0.5 in. LVDTs per pad. Two LVDTs were used for LBESE and LBENE, centered longitudinally on the 10 in. bearing pad length, and four LVDTs were used for LBENW and LBESW, located at each corner of the bearing pad. Bearing pad LVDT notation was defined in an XX_BP_YY manner, where XX stood for the girder number (G1, G2, G3, or

G4), BP stood for Bearing Pad, and YY stood for the location of the LVDT using cardinal directions (N or S when two LVDTs were used or NE, NW, SE, or SW when four LVDTs were used).

4.5.4.3 Girder Rotation

Rotation at the end of each girder nearest the applied load was measured using a single model 800 tiltmeter with a range of ±0.5 degrees manufactured by Jewell Instruments, formerly Applied Geomechanics. The centerline of each tiltmeter was longitudinally located approximately 2 ft from the girder end and centered vertically on the bottom flange. Notation for the tiltmeters consisted of the girder number (G1, G2, G3, or G4) followed by the word Tilt, separated by an underscore. The tiltmeters were attached to a 1/8 in. thick steel plate using magnets and each plate was fastened to the girder bottom flange with a pair of pipe clamps. Rotation at the end of each girder was also measured during LBESE and LBENE using a set of two LVDTs, one approximately 1 in. down from the top of the girder cross section and one approximately 1 in. up from the bottom of the girder cross section. Data from these LVDTs did not corroborate with rotation data from the tiltmeters or numerical models. Therefore, the data from the LVDTs were not used to measure rotation and the LVDTs were moved to the bearing pads to measure vertical displacement during LBENW, LBESW, and inelastic testing.

4.5.4.4 Flexural Strain Distribution through Cross-Sectional Depth

Flexural strain distribution through the depth of the barrier or end diaphragm was measured with groups of single horizontal foil strain gages. Data from gages distributed through the depth of the traffic barrier and end diaphragm at various locations were used to determine the approximate location of the neutral axis. Notation for gages through the depth of the barrier consisted of the following, separated underscores: NB for North Barrier, a letter for the cardinal direction related to the half of the span in which the gage was installed (East or West), the longitudinal location of the gage ($1.0d_v$ or $2.0d_v$), and a letter or set of letters representing the vertical location of the gage (Bottom, BVWG for a gage applied under and at the same location as the Bottom VWG in a rosette, TVWG for a gage applied under and at the same location as the Top VWG in a rosette, or Top). Notation for gages through the depth of the end diaphragm included the following, separated by

underscores: location of the individual diaphragm designated by the girders it spanned between (G12DIA, G23DIA, or G34DIA), the location of the strain gage at the centerline of the end diaphragm span denoted by ME for Middle and East side, the vertical location of the gage relative to the bottom of the end diaphragm (Bottom, Middle, or Tdeck for Top of the deck), and a letter denoting the location of the individual gage within the rosette (Bottom, Top, Diagonal, or Vertical).

4.5.4.5 Relative Horizontal Displacement between Girders

Relative horizontal displacement, in the transverse direction, between an exterior and interior girder bottom flange was measured at the bearing pad and at $4d_v$ using a single model P1010-10 analog cable extension linear position transducer (referred to as a string pot) with a range of 10 in. manufactured by UniMeasure. The centerline of each string pot was vertically located at half the bottom flange height. The string pots were attached to a base made of a 1/2 in. thick piece of plywood using screws; each base was attached to the girder bottom flange with a pair of pipe clamps. Notation for the String Pot instrumentation consisted of an SP followed by the longitudinal location (Bearing Pad or $4d_v$), separated by an underscore.

4.5.5 Laboratory Bridge Inelastic Testing Instrumentation

The laboratory bridge was tested to the inelastic range of behavior in two diagonally opposite quadrants, shown in Figure 4-27. Lab Bridge Ultimate West (LBUW) was the first test in the southwest quadrant with the end diaphragm and Lab Bridge Ultimate East (LBUE) was the second test in the northeast quadrant without an end diaphragm. The traffic barrier was saw cut off of the bridge at the original longitudinal construction joint prior to inelastic testing. Removal of the barrier ensured that the bridge transverse cross section was symmetric making the only change between the two tests the effect of the presence of the end diaphragm in LBUW.

Instrumentation used during inelastic testing on the West end of the bridge (LBUW) and during testing on the East end of the bridge (LBUE) was very similar to the instrumentation used for elastic testing on the final quadrant (LBESW). The six types of instrumentation and corresponding notation discussed for elastic bridge testing in Section 4.5.4 were used for inelastic testing with slight modification. Instrumentation details for

the end diaphragm during LBUW testing were shown in Figure 4-25. Instrumentation details for each inelastic bridge test are given in Table 4-21 and shown in Figure 4-28 through Figure 4-31.

No instrumentation was installed for the second inelastic test on a previously damaged section of the bridge (i.e., the West end of G3 during LBUE testing). Similar to LBESW testing, ±0.5 in. LVDTs were located at each corner of the bearing pads to measure their vertical displacement. Relative horizontal displacement between an exterior and interior girder was measured during LBUW on the bottom flange and on the web at $4d_v$ using string pots with a range of 10 in. The string pots were attached to the girder web using hot glue. During LBUE, the string pots were positioned at approximately $2d_v$ between both G1-G2 and G2-G3.

The distribution of strain over the length of a girder stirrup was measured with foil strain gages at three vertical locations oriented along the axis of the stirrup leg as described in Section 4.5.2.1. These gages had been attached to the stirrups prior to installation of the stirrups in the girder cross sections. Prior to testing, a baseline or zero measurement was obtained for each strain gage so that the change in strain due to applied live load could be calculated. For LBUW testing, which focused on Girder 3, strain in stirrups F, G, H, I, and J was monitored for G2, G3, and G4. For LBUE testing, which focused on Girder 2, strain in stirrups A, B, C, D, and E was monitored for G1, G2, and G3. Notation for the stirrup strain gages was discussed in Section 4.5.2. An additional CR1000 data acquisition unit, configured similar to the datalogger discussed in Section 4.5.1, was used during inelastic testing to monitor stirrup strain gages on three girders (up to 48 foil strain gage channels using three multiplexers). Stirrup strains were only measured during ultimate testing because the magnitude of the load applied during elastic testing was low and the readings from the strain gages would be very small, especially due to a lack of web-shear cracking during that phase of testing.

4.6 Experimental Test Setups

There were three main goals for testing the laboratory bridge in the elastic range: (1) obtain data for validation of the elastic finite element modeling technique to be used in the parametric study, (2) develop a better understanding of the effect of a traffic barrier on shear distribution, and (3) determine if the partial depth end diaphragm had an effect on

the shear distribution at elastic levels. There were three main goals for inelastic testing of the laboratory bridge: (1) quantify the amount of shear force shed by an interior girder to adjacent girders when web-shear cracking damaged the loaded girder and precipitated failure, (2) determine the effects of an end diaphragm on ultimate shear capacity and shear distribution in the inelastic range, and (3) compare the ultimate shear capacity of the loaded bridge to the capacity predicted by AASHTO Specifications. Within the third goal, data from the single girder companion test described in Appendix A were used to compare ultimate shear capacity of the same beam within a bridge system and as a single member.

4.6.1 Laboratory Bridge Elastic Testing Setup

During testing of all four quadrants, any combination of three point loads were applied to the specimen using 77 kip MTS Model 244.40S actuators. The hydraulic actuators were operated with three MTS Model 407 analog controllers that were in force control during testing. The actuators were designated as North (N), Middle (M), or South (S) in coordination with the cardinal directions in the Theodore V. Galambos Structural Engineering Laboratory at the University of Minnesota. Combinations of actuators applying load at the same time were designated with the following notation: NM for loading with both the North and Middle actuators, SM for loading with both the South and Middle actuators, and SMN for loading with all three actuators. When a combination of two or three actuators were used, the force feedback signal from the Middle actuator was used as the command signal to the North and/or South actuators.

The actuators were suspended from a transverse W36x150 steel load frame beam. The transverse loading beam was bolted to the underside of two longitudinal W36x150 steel load frame beams which were supported at the bridge abutments by four W12x120 columns as shown in Figure 4-32. The steel load frame beams (with an assumed yield strength of 36 ksi) were donated by MnDOT and fabricated by Lejeune Steel. The load frame was braced transversely by six L4x4x1/4 single angles and sat on top of the concrete abutments to form a self-reacting system with the bridge.

Boundary conditions at the point of applied load on the bridge deck consisted of a 2 in. thick steel plate attached to the bottom of the actuator that applied load to a 0.5 in. thick neoprene pad cut to be the same dimensions as the AASHTO tire contact area of a wheel, which is a single rectangle with a 20 in. width and 10 in. length. The neoprene pad

was aligned such that the 10 in. dimension was parallel to the length of the bridge girders. Alignment of the actuators, steel plates, and neoprene pads can be seen in Figure 4-33.

Load was applied to the bridge at two longitudinal locations in each quadrant: $2d_v$ and $4d_v$. Testing at $2d_v$ positioned the transverse line of actuators approximately 6 ft 7 in. from the centerline of the nearest girder supports and approximately 24 ft 2 in. from the centerline of the farthest girder supports. Testing at $4d_v$ positioned the transverse line of actuators approximately 12 ft 6 in. from the centerline of the nearest girder supports and approximately 18 ft 3 in. from the centerline of the farthest girder supports. In a simply supported beam with a span length of 30 ft 9 in. Applied load at $2d_v$ equated to a shear span-to-depth ratio (a/d) of approximately 1.7 and applied load at $4d_v$ equated to a shear span-to-depth ratio (a/d) of approximately 3.3.

4.6.2 Laboratory Bridge Inelastic Testing Setup

During both inelastic tests, a patch load was applied to the specimen using a combination of two MTS Model 244.41 110 kip actuators and one MTS Model 244.51 220 kip actuator suspended from the transverse steel load frame beam. The 110 kip actuators were designated as either North (N) or South (S), in coordination with the cardinal directions in the laboratory, and the 220 kip actuator was designated as Middle (M). The hydraulic actuators were operated with three MTS Model 407 analog controllers. The 110 kip actuators were operated in force control and slaved to one half of the 220 kip actuator force. The 220 kip actuator was operated in displacement control during testing.

The steel load frame was modified for inelastic testing to account for the maximum available load of 440 kips that could be applied by the actuators. Two additional W12x120 columns were placed in a horizontal position on top of and clamped to the longitudinal load frame beams to provide bracing. This modification to the load frame is shown in Figure 4-34. Two 2.5 in. all-thread Dywidag bars were used to tie each longitudinal steel load frame to the strong floor at midspan of the bridge. The Dywidag bars halved the unbraced length of the load frame beams and provided sufficient stability for ultimate testing. The force in the Dywidag bars was spread among multiple hole sets in the strong floor via two steel tie down assemblies under the bridge. Figure 4-34 shows the load frame above the bridge and Figure 4-35 shows the tie down assemblies below the bridge.

Boundary conditions at the point of applied load on the bridge deck were formed by making a bolted connection between the three actuators and a 5 ft long W14x159 steel load beam. A single concentrated patch load was formed by two 2 in. thick steel plates tack welded to the bottom flange of the load beam to concentrate the load to a rectangular area 14 in. wide longitudinally by 40 in. wide transversely. The load was further concentrated using 1 in. thick neoprene rubber pads aligned in a rectangular area 12 in. wide longitudinally by 36 in. wide transversely. The patch area was sized using engineering judgement to align with the transverse width of the three actuators and the size of available neoprene pads. Use of the AASHTO tire patch dimension, 10 in. by 20 in., was unnecessary because the loading configuration did not represent truck tires. Alignment of the actuators, load beam, tack welded plates, and neoprene pads can be seen in Figure 4-36.

The LBUW testing focused on the live end of the beams and the end of the span with the partial depth end diaphragm. During LBUW testing, the patch load was applied over interior Girder 3. The LBUE testing focused on the dead end of the girders and the end of the span without an end diaphragm. During LBUE testing, the patch load was applied over interior Girder 2. The point load was applied a distance of 9 ft 7 in. from the centerline of the nearest girder supports and 21 ft 2 in. from the centerline of the farthest girder supports in both inelastic test configurations. In a simply supported beam with a span length of 30 ft 9 in., this equated to a shear span-to-depth ratio (a/d) of 2.5. This was the same shear span-to-depth ratio used for testing the single companion girder.

Table 4-1. Design stresses vs. AASHTO Standard Allowable Limits

Behavior	End Stresses (ksi) †		Harping Point Stresses (ksi) †		
	Allowable	Design	Allowable		Design
Stresses at Release with f'_{ci} = 4,600 psi					
Compression	$-0.6f'_{ci}$ =	-2.76	-2.22	$-0.6f'_{ci}$ =	-2.76	-2.68
Tension	$3\sqrt{f'_{ci}}$ =	0.20	0.10	$3\sqrt{f'_{ci}}$ =	0.20	0.49
				$7.5\sqrt{f'_{ci}}$ ‡ =	0.51	0.49
Stresses at Service with f'_c = 7,500 psi					
Compression	$-0.4f'_c$ =	-3.00	-1.75	$-0.4f'_c$ =	-3.00	-1.63
Tension	$0\sqrt{f'_c}$ =	0.00	-0.05	$6\sqrt{f'_c}$ =	0.52	0.21

† The equations to calculate stress use concrete strength in psi, but the results are shown in ksi.

‡ This case required use of bonded reinforcement.

Table 4-2. Bridge Girder Design Properties

Property	Symbol [Units]	Value
Span Length	L_s [ft]	30.75
Relative Humidity	RH [%]	73
Girder Depth	h_g [in.]	36
Girder Area	A_g [in.^{2}]	384
Girder Web Width	b_v [in.]	6
Girder Centroid (from bottom)	y_{gb} [in.]	15.7
Composite Girder Centroid (from bottom)	y_{cb} [in.]	31.2
Girder Moment of Inertia	I_g [in.^{4}]	52,266
Girder Concrete Compressive Strength	f'_c [ksi]	7.5
Girder Concrete Release Compressive Strength	f'_{ci} [ksi]	4.6
Deck Concrete Compressive Strength	f'_{cd} [ksi]	4
Deck Effective Flange Width (interior girder)	b_{eff} [ft]	7.69
Deck Thickness	t_d [in.]	9
Haunch Depth	t_h *[in.]*	1
Stirrup Yield Strength	f_y [ksi]	60
Stirrup Modulus of Elasticity	E_s [ksi]	29,000
Stirrup Leg Area	A_v [in.^{2}]	0.2
Stirrup Spacing	s [in.]	24
Strand Specified Tensile Strength	f_{pu} [ksi]	270
Strand Modulus of Elasticity	E_{ps} [ksi]	28,500
Jacking Force per Strand	P_j [kip]	25
Strand Diameter	d_{ps} [in.]	0.5
Single Strand Area	A_{ps} [in.^{2}]	0.153
Total Draped Strand Area	A_{psd} [in.^{2}]	0.92
Total Straight Strand Area	A_{pss} [in.^{2}]	2.45
Draped Strand Centroid at Harping Point	y_{HPd} [in.]	9
Draped Strand Centroid at End	y_{Ed} [in.]	25
Straight Strand Centroid	y_s [in.]	3.75

Table 4-3. Review of Deck Design Details and Final Laboratory Deck Details

Bridge	Design Year	Deck Thickness (in.)	Girder Spacing (ft)	Transverse Reinforcement		Longitudinal Reinforcement		
				Top	Bottom	Top	Bottom	
							Center	Outer
09002*	1968	8.25	11.5	No. 6 at 5 in.	No. 6 at 5 in.	No. 3 at 9 in.	No. 5 at 5.5 in.	No. 5 at 14 in.
65006*	1978	9	11.0	No. 6 at 6.5 in.	No. 6 at 6.5 in.	No. 4 at 18 in.	No. 5 at 6.5 in.	No. 5 at 12 in.
46004	1978	9	8.9	No. 5 at 6 in.	No. 5 at 6 in.	No. 4 at 18 in.	No. 5 at 8 in.	No. 5 at 12 in.
19033	1973	9	9.5	No. 6 at 7.5 in.	No. 6 at 7.5 in.	No. 4 at 18 in.	No. 5 at 7 in.	No. 5 at 12 in.
83030	1973	8.25	9.5	No. 5 at 5 in.	No. 5 at 5 in.	No. 3 at 9 in.	No. 5 at 6.5 in.	No. 5 at 12 in.
14006	1983	9	9.8	No. 5 at 5 in.	No. 5 at 5 in.	No. 4 at 18 in.	No. 5 at 7 in.	No. 5 at 12 in.
MnDOT Design Table	1996	9	9.0	No. 5 at 5.5 in.	No. 5 at 5.5 in.	No. 4 at 18 in.	No. 5 at 8 in.	No. 5 at 16 in.
MnDOT Design Table	2013	9	9.0	No. 4 at 5 in.	No. 4 at 6 in.	No. 4 at 18 in.	No. 5 at 10 in.	No. 5 at 10 in.
Laboratory Bridge	----	9	9.0	No. 5 at 5.5 in.	No. 5 at 5.5 in.	No. 4 at 18 in.	No. 5 at 8 in.	No. 5 at 12 in.

* Field Tested Bridges

Table 4-4. Laboratory Girder Fabrication and Testing Timeline

Date	Time	Time since casting (days)	Event
June 25, 2013	11 am	----	Strands stressed and instrumented
	11 am - 8 pm		Rebar cage tied
June 26, 2013	11 am	----	Installation of vibrating wire strain gages
	11 am, 12pm, 6:30 pm		VWG readings
	2 pm		Bottom blockouts installed
	3 pm		Formwork installed
June 27, 2013	2 pm	----	Top blockouts installed
	2 pm - 3 pm		Beam concrete placed
	3:30 pm		VWG readings immediately before tarping
June 29, 2013	11 am	2	Formwork removed
	12 pm, 12:30 pm, 1 pm		VWG readings
	12 pm - 12:30 pm		Strands cut and prestress force transferred
	1 pm		Camber measurements
July 3, 2013	8:30 am, 10:30 am	6	VWG readings, camber measurements
	8:30 am - 10:30 am		Beams lifted and bunked
July 25, 2013	----	28	Beam 28 day strength
July 26, 2013	10:30 am	29	Beams shipped to UMN
Nov 5, 2013	10 am	131	Place single beam deck concrete
Jan 28, 2014	10 am	215	Test single beam 31.75 ft span (first end)
Feb 3, 2014	10 am	221	Test single beam 22.5 ft span (second end)
Mar 5, 2014	8 am - 10 am	251	Place bridge deck concrete
Mar 12, 2014	7 am	258	Place barrier concrete
May 8, 2014	7 am	315	Begin southeast quadrant elastic testing
Sept 9, 2014	7 am	439	Begin northeast quadrant elastic testing
Oct 7, 2014	7 am	467	Begin northwest quadrant elastic testing
Nov 4, 2014	7 am	495	Begin southwest quadrant elastic testing
Dec 8, 2014	7 am	529	West ultimate test
Dec 17, 2014	7 am	538	East ultimate test

Table 4-5. Laboratory Girder Trial Batch Mix Designs

	Trial Batch 1		Trial Batch 2	
	Batch Qty	**Qty / cy**	**Batch Qty**	**Qty / cy**
Mix Name	525 Cement		525 Cement Early Age	
Batch Date/Time	11/28/12 10:00 AM		6/25/13 11:00 AM	
Lehigh Mason City Type III Cement (lb)	778	516	798	545
Elk River Barton 3/4 in. Agg. (lb)	2,381	1,573	2,281	1,547
Elk River Barton Sand (lb)	2,472	1,567	2,408	1,579
Water (gal)	42.05	37	44.30	39
Air Entraining (oz)	----	----	----	----
Recover Grace Retarder (oz)	----	----	9	6.1
W.R. Grace Adva 575 HRWR (oz)	30	19.9	36	24.6

Table 4-6. Fresh and Hardened Trial Batch Concrete Properties

	Trial Batch 1	**Trial Batch 2**
Mix Name	525 Cement	525 Cement Early Age
Batch Date/Time	11/28/12 10:00 AM	6/25/13 11:00 AM
Air (%)	2.8	1.6
Slump (in.)	6	----
Spread (in.)	----	17.5
Temp. (°F)	70	80
W/C Ratio	0.602	0.595
Theoretical Unit Wt. (pcf)	146.91	147.98
Actual Unit Wt. (pcf)	148.2	148.2
Average Compressive Strength of Two Cylinders, f'_c (psi)		
22 Hour	----	4,182
1 Day	4,206	----
2 Day	----	----
7 Day	5,351	----
14 Day	5,706	----
28 Day	7,514	----
56 Day	7,529	----

Table 4-7. Laboratory Girder Batch Properties

Girder Batch No.	**1**	**2**	**3**	**4**	**5**	**6**
Batch Date/Time	6/27/13 1:52 PM	6/27/13 2:16 PM	6/27/13 2:32 PM	6/27/13 2:48 PM	6/27/13 3:06 PM	6/27/13 3:06 PM
Location of Batch in Girders (G1-G5)	G1	G1, G2	G2, G3	G3, G4	G4, G5	1/4 G5
Batch Material Quantities						
Lehigh Mason City Type III Cement (lb)	1,590	1,594	1,583	1,581	1,581	1,581
Elk River Barton 3/4 in. Agg. (lb)	4,761	4,674	4,730	4,790	4,757	4,790
Elk River Barton Sand (lb)	4,890	4,859	4,883	4,798	4,930	4,796
Metered Water (gal)	81.1	60.5	81.03	84.4	70	70.6
Air Entraining (oz)	----	----	----	----	----	----
Recover Grace Retarder (oz)	15	15	15	15	15	15
W.R. Grace Adva 575 HRWR (oz)	72	72	72	72	72	72
Fresh Concrete Properties and Specimen Count						
Air (%)	2.6	----	----	----	----	----
Quick Slump (in.)	9.5	8.5	9.75	9.5	9.25	9.0
Quick Spread (in.)	20.5	17.0	17.0	18.0	17.0	16.0
Temp. (°F)	80	82	80	79	81	----
Actual Unit Wt. (pcf)	144.6	144.6	144.6	144.6	144.6	144.6
Cretex Cylinder Count	3	3	3	1	2	0
UMN Cylinder Count	10	10	10	10	10	0
UMN Flexure Beam Count	1	1	1	1	1	1

Table 4-8. Laboratory Girder Batch Concrete Compressive Strengths (psi)

Girder Batch No.		1	2	3	4	5	Avg
Age (day)	Batch Date/Time	6/27/13 1:52 PM	6/27/13 2:16 PM	6/27/13 2:32 PM	6/27/13 2:48 PM	6/27/13 3:06 PM	
22 hr	Cretex	4,255	----	4,738	----	4,870	4,621
22 hr	UMN	3,925	----	----	----	4,350	4,138
2	Cretex	----	----	4,698	----	----	4,698
28	Cretex	----	----	6,618	----	----	6,618
28	UMN	5,390	7,126	6,416	6,513	6,576	6,404
56	Cretex	----	----	6,754	----	----	6,754
216	Companion Girder	----	----	----	----	6,893	6,893
329	Elastic Bridge East Testing	7,012	7,809	6,828	7,061	----	7,177
476	Elastic Bridge West Testing	6,398	7,145	6,516	6,355	----	6,604
533	Inelastic Bridge Testing	6,419	7,374	6,347	6,014	----	6,538

Table 4-9. Laboratory Girder Modulus of Elasticity

Girder Batch No.		1	2	3	4	5	Avg
Age (day)	Batch Date/Time	6/27/13 1:52 PM	6/27/13 2:16 PM	6/27/13 2:32 PM	6/27/13 2:48 PM	6/27/13 3:06 PM	
Modulus of Elasticity, E_c (ksi)							
216	Single Girder						
	Measured	----	----	----	----	4,331†	4,331
	$33w_c^{1.5}\sqrt{f'c}$ *	----	----	----	----	4,764	4,764
329	Elastic Bridge East Testing						
	Measured	----	5,313	4,663	5,025	----	5,000
	$33w_c^{1.5}\sqrt{f'c}$	4,805	5,071	4,741	4,822	----	4,860
476	Elastic Bridge West Testing						
	Measured	4,241	4,673	----	4,270	----	4,395
	$33w_c^{1.5}\sqrt{f'c}$	4,590	4,850	4,632	4,574	----	4,662
533	Inelastic Bridge Testing						
	Measured	----	4,118	4,830	4,769	----	4,572
	$33w_c^{1.5}\sqrt{f'c}$	4,597	4,928	4,571	4,450	----	4,637

† An average of three cylinders

* The equation $33w_c^{1.5}\sqrt{f'c}$ uses w_c in lb/ft^3 from Table 4-7 and $f'c$ in psi

Table 4-10. Laboratory Girder Split Tensile Strength

Girder Batch No.		1	2	3	4	5	Avg
Age (day)	Batch Date/Time	6/27/13 1:52 PM	6/27/13 2:16 PM	6/27/13 2:32 PM	6/27/13 2:48 PM	6/27/13 3:06 PM	
Splitting Tensile Strength, f_t (psi)							
216	Single Girder						
	Measured	----	----	----	----	546†	546
	$0.23\sqrt{f'c}$ *	----	----	----	----	604	604
329	Elastic Bridge East Testing						
	Measured	458	564	475	494	----	498
	$0.23\sqrt{f'c}$	609	643	601	611	----	616
	Inelastic Bridge Testing						
	Measured	576	555	552	565	----	562
	$0.23\sqrt{f'c}$	583	625	579	564	----	588

† An average of three cylinders

* The equation $0.23\sqrt{f'c}$ uses $f'c$ in ksi units

Table 4-11. Laboratory Girder Modulus of Rupture Strength

Girder Batch No.		1	2	3	4	5	Avg
Age (day)	Batch Date/Time	6/27/13 1:52 PM	6/27/13 2:16 PM	6/27/13 2:32 PM	6/27/13 2:48 PM	6/27/13 3:06 PM	
Modulus of Rupture Strength, f_r (psi)							
216	Single Girder						
	Measured	----	----	792	749	713	751
	$0.2\sqrt{f'c}$ *	----	----	----	----	525	525
	$0.37\sqrt{f'c}$ *	----	----	----	----	971	971
533	Inelastic Bridge Testing						
	Measured	735	767	----	----	----	751
	$0.2\sqrt{f'c}$	507	543	504	490	----	511
	$0.37\sqrt{f'c}$	937	1005	932	907	----	945

* The equations $0.2\sqrt{f'c}$ and $0.37\sqrt{f'c}$ use $f'c$ in ksi units

Table 4-12. Transverse Reinforcement Tensile Test Results

Bar No.	ASTM A615 §9.2.2					ASTM A370 §14.1.3
	σ_{min} @ $\varepsilon = 0.0035$	$\sigma_{min} > 60$ ksi	F_y (ksi) *	E_s (ksi)	ε_y	F_y (ksi)
1	62.2	Yes	67.7	29200	0.0023	67.7
2	68.5	Yes	72.4	31200	0.0023	72.6
3	60.3	Yes	64.6	29000	0.0022	64.6
4	60.3	Yes	67.2	26800	0.0025	66.5
5	59.1	No	----	----	----	62.8
6	64.6	Yes	71.7	29200	0.0025	71.3
7	58.8	No	----	----	----	63.2
8	64.8	Yes	70.8	29300	0.0024	70.8
9	60.8	Yes	68.7	29000	0.0024	68.7
10	59.7	No	----	----	----	65.7
		Avg:	69.0	29100	0.0024	67.4

* Obtained with the 0.2% offset

Table 4-13. Prestressing Strand Material Properties

Material Property	**Nominal**	**Manufacturer Provided**
Diameter (in.)	0.5	0.5
Area (in.)	0.153	0.1528
Modulus of Elasticity (ksi)	28,500	28,700
Yield Stress (ksi)	243	----
Ultimate Stress (ksi)	270	270

Table 4-14. Bridge Deck Concrete Mix Design

	Specified	Truck 1	Truck 2	Truck 3	Truck 4
	Qty / cy	Batch Qty	Batch Qty	Batch Qty	Batch Qty
Mix Name	4164P	4164P	4164P	4164P	4164P
Batch Date/Time	10/15/10	3/5/14 7:23 AM	3/5/14 8:00 AM	3/5/14 8:27 AM	3/5/14 8:55 AM
Lafarge at Davenport, IA Type I Cement (lb)	564	5495	5535	5525	5485
Aggregate Industries 3/4 in. Aggregate (lb)*	1820	18540	18200	17920	17920
Aggregate Industries Sand (lb)	1321	7820	7800	7840	7780
Water (gal)	30.5	296	296	293	294
BASF MB AE 90 Air Entrainer (oz)	3	37	35	35	35
BASF Polyheed 1020 MRWR (oz)	17	----	170	170	170
BASF Glenium 7500 HRWR (oz)	11	290	310	330	330
BASF Rheomac VMA 358 (oz)	----	162	165	165	165
Cylinder Count	----	18	18	18	18
Flexure Beam Count	----	0	0	0	0

* Aggregate designation on delivery sheets

Table 4-15. Fresh and Hardened Bridge Deck Concrete Properties

	Specified	Truck 1	Truck 2	Truck 3	Truck 4
Mix Name	4164P	4164P	4164P	4164P	4164P
Batch Date/Time	----	3/5/12 7:23 AM	3/5/12 8:00 AM	3/5/12 8:27 AM	3/5/12 8:55 AM
Air (%)	6 ± 1.5	3.25	----	----	----
Slump (in.)	6.0	5.0	6.5	5.5	4.5
W/C Ratio	0.45	0.449	0.446	0.442	0.447
Unit Wt. (pcf)	145	145.6	147	145.8	145.4
Average Compressive Strength of Three Cylinders, *f'c* (psi)					
28 day	4,000	5,509	4,293	6,252	5,611
Elastic Bridge East Testing	----	6,261	6,405	7,173	6,549
Elastic Bridge West Testing	----	6,062	6,052	7,357	6,994
Inelastic Bridge Testing	----	5,827	6,314	6,866	6,678

Table 4-16. Barrier Concrete Mix Design

	Specified	Truck 1
	Qty / cy	Batch Qty
Mix Name	4594P	4594P
Batch Date/Time	8/5/2010	3/12/14 6:21 AM
Lafarge at Davenport, IA Type I Cement (lb)	655	3,315
Aggregate Industries 3/8 in. Aggregate (lb)	1,393	7,160
Aggregate Industries Sand (lb)	1,470	6,420
Water (gal)	35.4	175
BASF MB AE 90 Air Entrainer (oz)	4	18
BASF Glenium 7500 HRWR (oz)	13	90
BASF Rheomac VMA 358 (oz)	20	102
Cylinder Count	----	12
Flexure Beam Count	----	0

Table 4-17. Fresh and Hardened Barrier Concrete Properties

	Specified	Truck 1
Mix Name	4594P	4594P
Batch Date/Time	----	3/12/14 6:21 AM
Air (%)	7.5 ± 1.5	----
Slump (in.)	6	6.5
W/C Ratio	0.45	0.44
Unit Wt. (pcf)	139.7	141.5
Average Compressive Strength of Three Cylinders, *f'c* (psi)		
28 day	4,000	4,657
Elastic Bridge West Testing	----	4,686

Table 4-18. Locations of Instrumented Prestressing Strand in Figure 4-16

Location	Strands Instrumented	Prestress at Install (k)
Dead end between bulkhead and end formwork	1, 6, 7, 12	0
Midspan Girder 1	9, 10, 14, 15	4
Between end forms of Girder 1 and Girder 2	1, 6, 7, 12	4
Midspan Girder 2	8, 11, 13, 16	4
Between end forms of Girder 2 and Girder 3	2, 4	4
Midspan Girder 3	7, 12, 14, 15	4
Midspan Girder 4	8, 11, 13, 16	4
Midspan Girder 5	9, 10, 14, 15	4

Table 4-19. Prestress Loss Summary

Time Step	Event	Prestress Loss (ksi)				Row Sum:	Remaining Stress (ksi)	% of f_{pj}	Notes
		ANC	ES	RE	CR+SH				
0	Prestressing Strand Jacking	6.6	--	--	--	6.6	158.6	100%	f_{pj} (after seating)
1	Tensioning to release	--	16.2	0.72	--	16.9	141.7	11%	f_{pi}
2	Release to single beam deck	--	--	0.24	19.2	19.5	122.3	12%	
3	Single beam deck to test single beam	--	--	0.03	2.7	2.8	119.5	2%	f_{pe} (single beam)
4	Test single beam to bridge deck	--	--	0.01	0.7	0.7	118.8	0%	
5	Bridge deck to elastic testing	--	--	0.01	1.0	1.0	117.8	1%	
6	Elastic testing to inelastic testing	--	--	0.03	1.6	1.6	116.1	1%	f_{pe} (bridge)
	Column Sum:	6.6	16.2	1.04	25.3	42.5		27%	

Table 4-20. Laboratory Bridge Elastic Testing Instrumentation Plan

Instrument Type	Purpose	Location*	Bridge Element	Quadrant
VWG box-type rosette	Calculation of shear strain	$0.5d_v$, d_v (both sides of web), $2d_v$	G1, G2, G3, G4	LBESE, LBENE, LBENW, LBESW
		$0.5d_v$, d_v, $2d_v$, $4d_v$	Barrier‡	LBESE, LBENE
		d_v, $2d_v$	Barrier	LBENW
Foil rosette gages on web, opposite VWGs		$0.5d_v$, d_v, $2d_v$	G1, G2, G3, G4	LBESE, LBENE, LBENW, LBESW
Foil rosette gages on end diaphragm		North and South of diaphragm CL, on both East and West face	† B/w G1-G2 and G2-G3	LBENW
			B/w G2-G3 and G3-G4	LBESW
Horizontal single strain gage on East side of end diaphragm	Measure the variation in strain through the diaphragm depth	Centerline of diaphragm span	B/w G1-G2 and G2-G3	LBENW
			B/w G2-G3 and G3-G4	LBESW
Four horizontal strain gages through barrier depth	Measure the variation in strain through the barrier depth	d_v, $2d_v$	Barrier	LBENE, LBENW
Horizontal strain gage on North face of girder		d_v, $2d_v$	G1 bottom and top flange	LBENW
Three LVDTs under girder	Calculation of girder vertical deflection	East $2d_v$, $0.5L$, West $2d_v$	G1, G2, G3, G4	LBESE, LBENE, LBENW, LBESW
Two LVDTs at bearing pad	Calculation of girder vertical deflection and measure bearing pad vertical deflection	N and S centerline	G1, G2, G3, G4	LBESE, LBENE
Four LVDTs at bearing pad		NW, NE, SW, SE corners	G1, G2, G3, G4	LBENW, LBESW
Tiltmeter	Measure girder rotation	End of girder bottom flange	G1, G2, G3, G4	LBESE, LBENE, LBENW, LBESW
Two rotation LVDTs on girder end		End of girder, top and bottom of cross section	G1, G2, G3, G4	LBESE, LBENE
String pots	Measure relative horizontal displacement between girders	Bearing pad and $4d_v$	B/w G3-G4	LBESE, LBESW
		Bearing pad and $4d_v$	B/w G1-G2	LBENE, LBENW

* All instruments, except girder displacement LVDTs, were located in the loaded half of the span for quadrant of interest (i.e., East half of bridge for LBESE ,West half of bridge for LBESW)

‡ The value of d_v from the composite girder was used to locate gages on the barrier (i.e., gages on the girder and barrier were at the same longitudinal location)

† B/w is short for between

Table 4-21. Laboratory Bridge Inelastic Testing Instrumentation Plan

Instrument Type	Purpose	Location*	Bridge Element	Quadrant
VWG box-type rosette on web	Calculation of shear strain	$0.5d_v$, d_v (both sides of web), $2d_v$	G1, G2, G3 (only LBUW), G4	LBUW, LBUE
		d_v on opposite side of span		
Foil rosette gages on web, opposite VWGs		$0.5d_v$, d_v, $2d_v$	G1, G2, G3 (only LBUW), G4	LBUW, LBUE
		d_v on opposite side of span		
Foil rosette gages on end diaphragm		North and South of diaphragm CL, on both East and West face	† B/w G2-G3 and G3-G4	LBUW
			B/w G1-G2 and G2-G3	LBUE
Horizontal single strain gage on East side of end diaphragm	Measure the variation in strain through the diaphragm depth	Centerline of diaphragm span	B/w G2-G3 and G3-G4	LBUW
			B/w G1-G2 and G2-G3	LBUE
Stirrup foil gages (3 on ea.)	Measure stirrup strain	Stirrup F, G, H, I, J	G2, G3, G4	LBUW
		Stirrup A, B, C, D, E	G1, G2, G3	LBUE
Three LVDTs	Calculation of girder vertical deflection	East $2d_v$, $0.5L$, West $2d_v$	G1, G2, G3, G4	LBUW, LBUE
Four LVDTs at bearing pad	Calculation of girder vertical deflection and measure bearing pad vertical deflection	NW, NE, SW, SE corners	G1, G2, G3, G4	LBUW, LBUE
Tiltmeter	Measure girder rotation	End of girder bottom flange	G1, G2, G3, G4	LBUW, LBUE
String pots	Measure relative horizontal displacement between girders	Bearing pad and $4d_v$	B/w G3-G4	LBUW
		Approximately $2d_v$	B/w G1-G2 and b/w G2-G3	LBUE

* All instruments, except girder displacement LVDTs, were located in the loaded half of the span (i.e., West half of span for LBUW, East half of span for LBUE)

† B/w is short for between

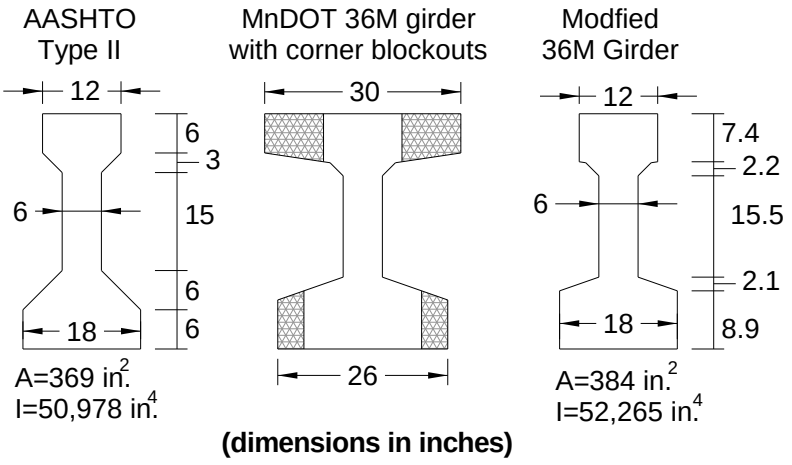

Figure 4-1. 36M Cross Section Modified to Represent AASHTO Type II Girders

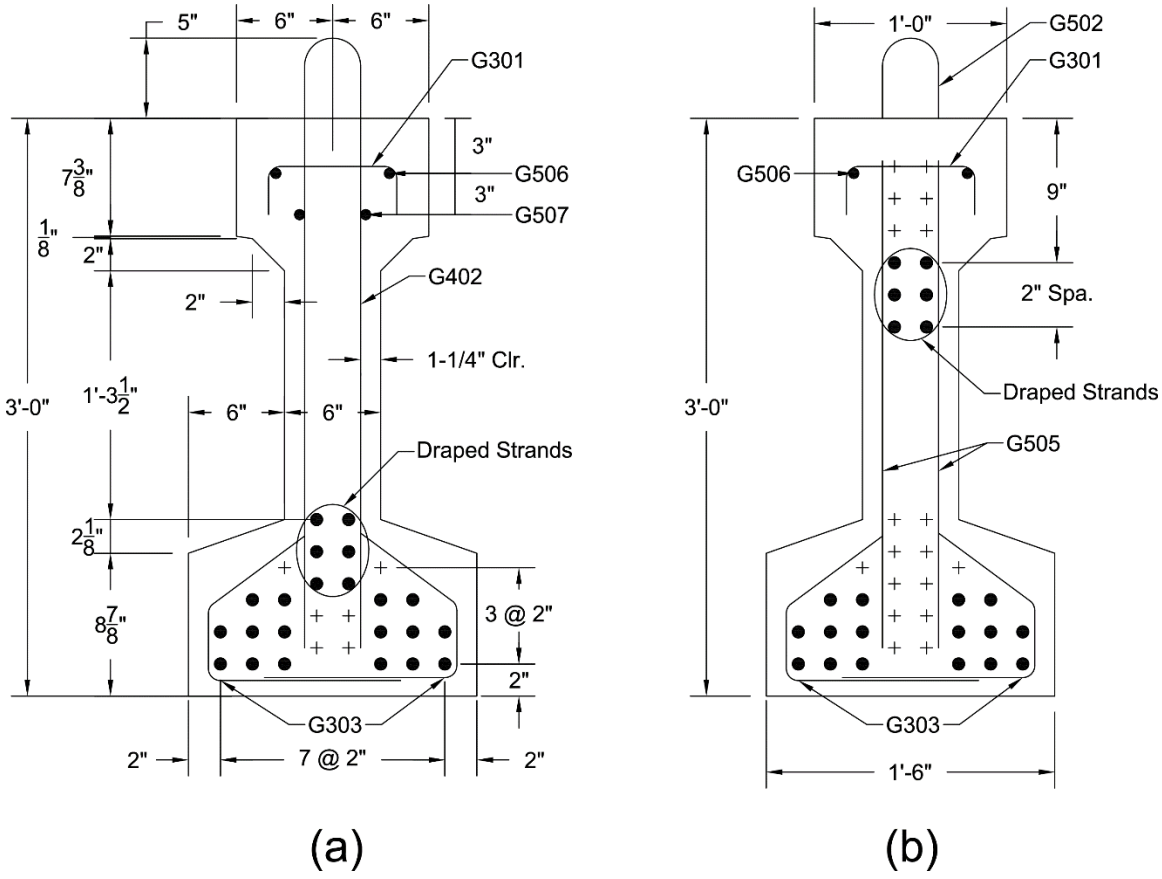

Figure 4-2. Laboratory Bridge Girder (a) Midspan and (b) End Cross Section Details

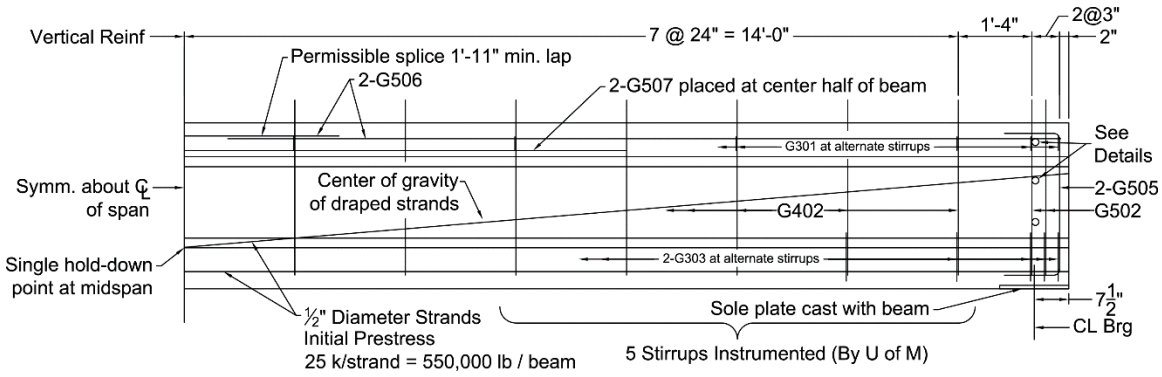

Figure 4-3. Half Laboratory Bridge Girder Elevation

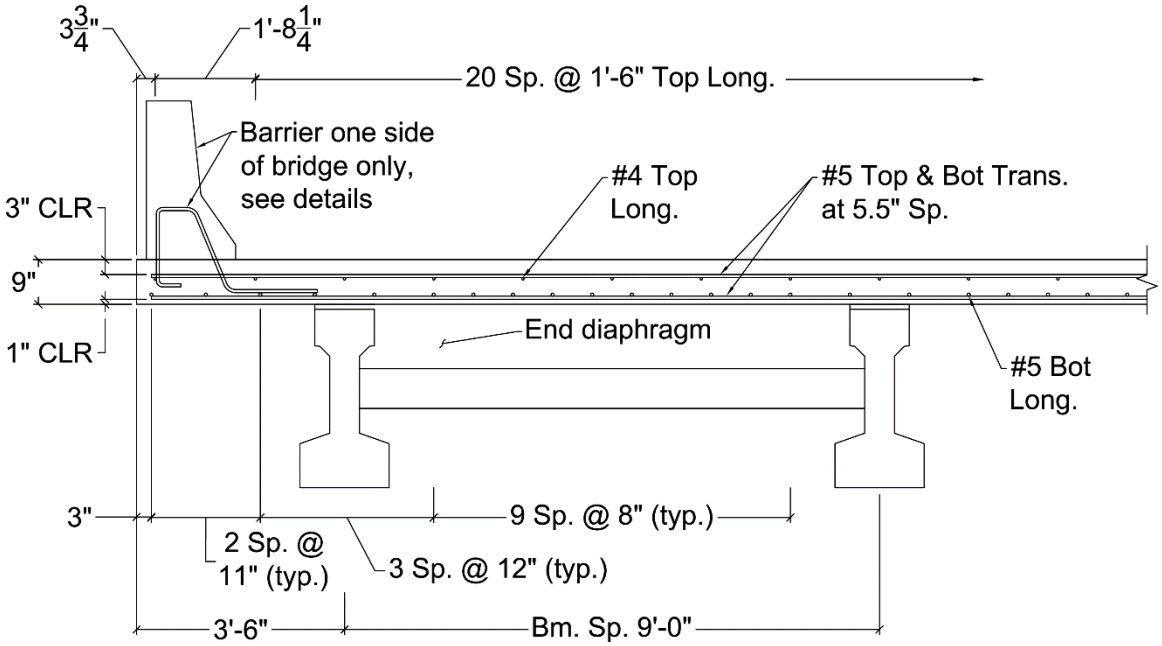

Figure 4-4. Half Laboratory Bridge Deck Transverse Cross Section

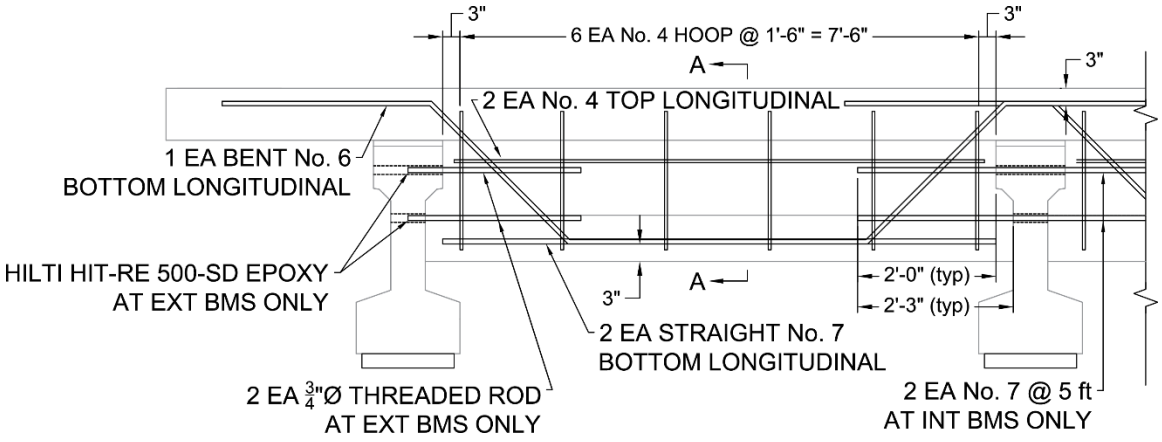

Figure 4-5. Partial End Diaphragm Transverse Cross Section

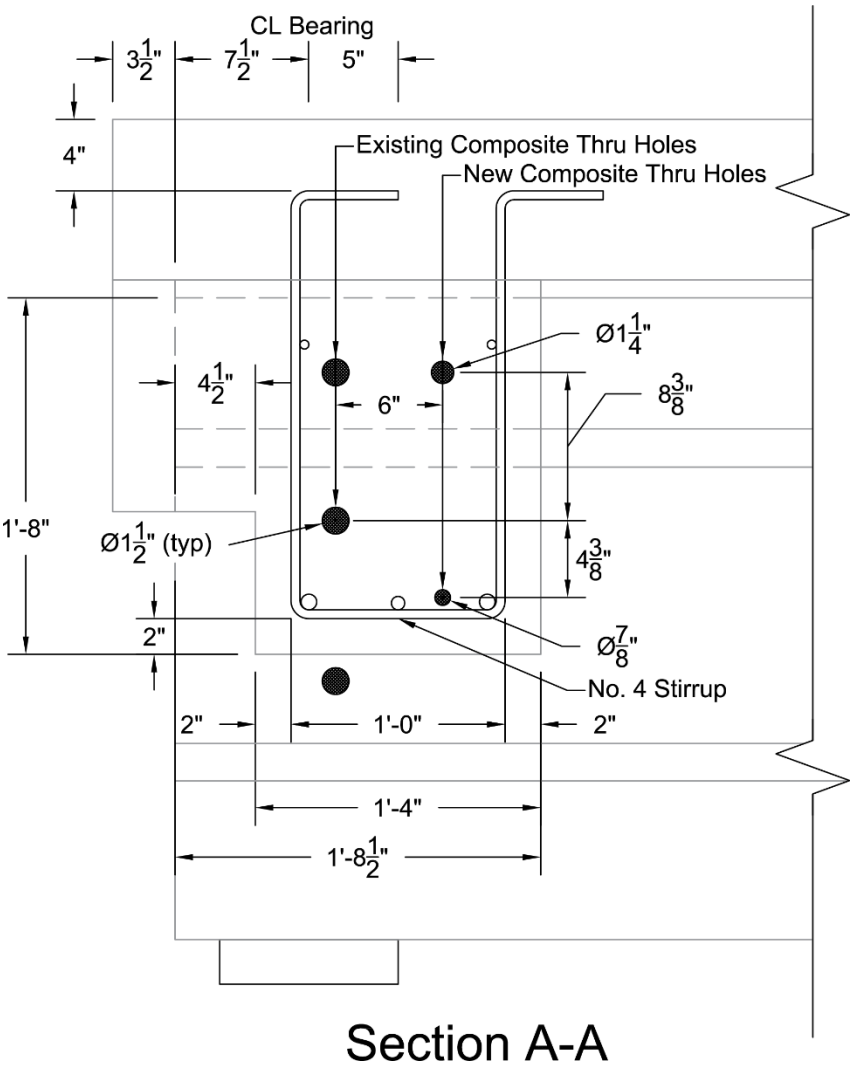

Figure 4-6. Cross Section of Partial End Diaphragm

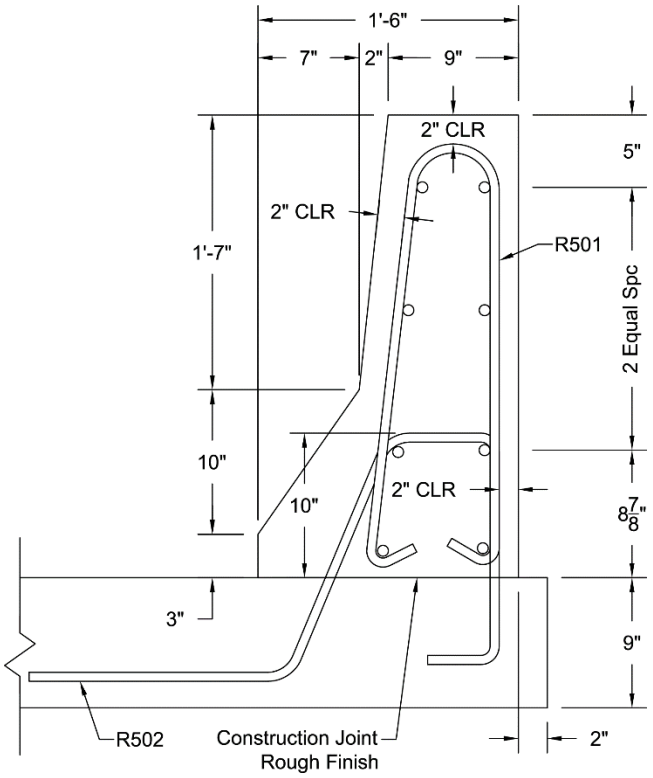

Figure 4-7. Barrier Transverse Cross Section

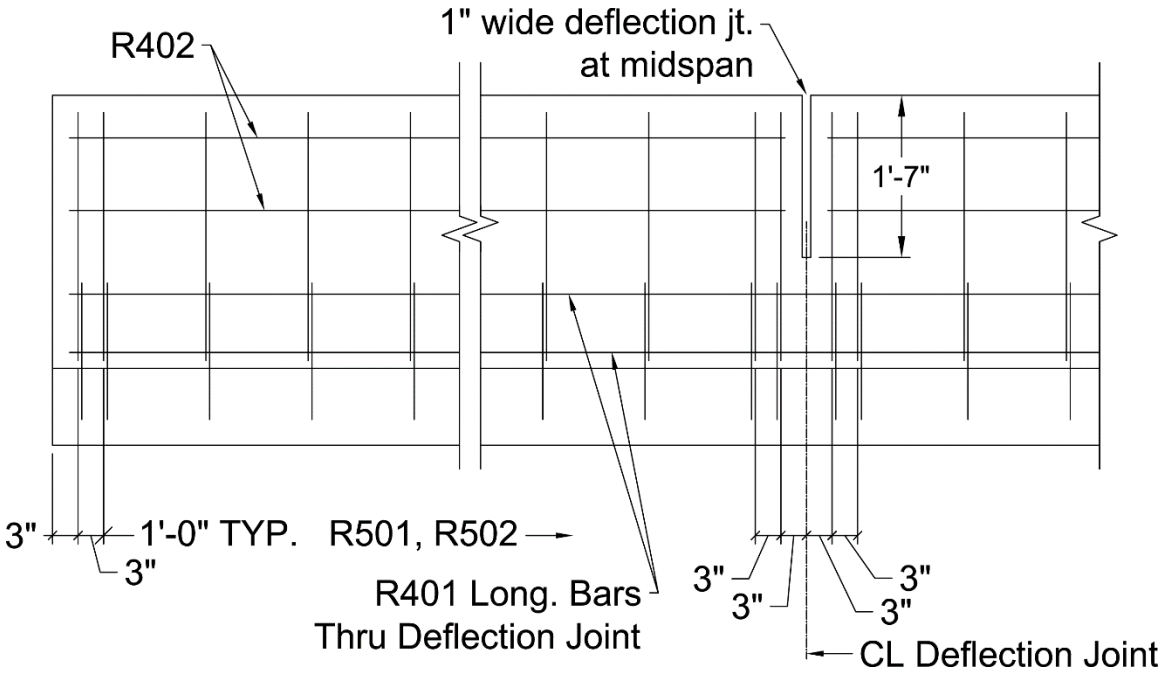

Figure 4-8. Barrier Partial Elevation

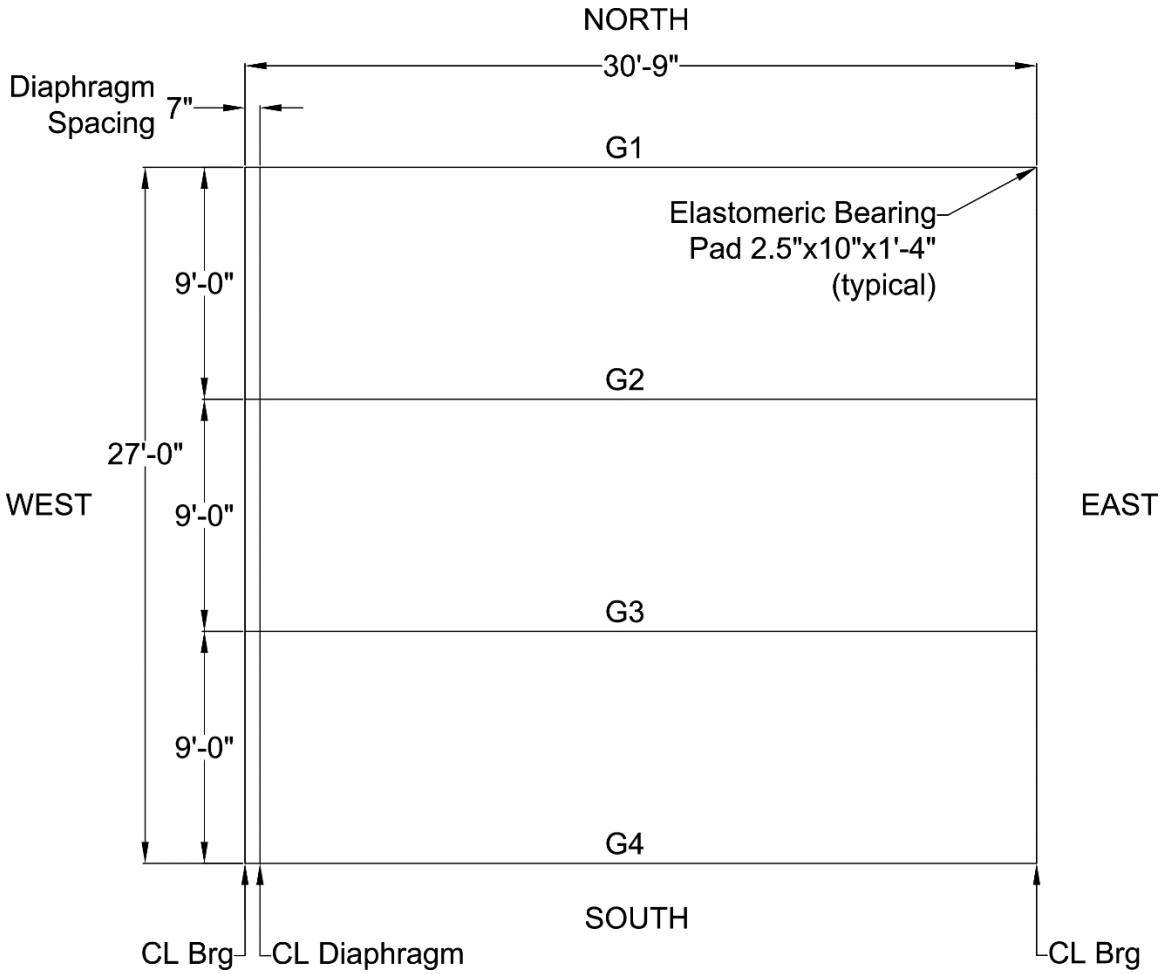

Figure 4-9. Laboratory Bridge Framing Plan

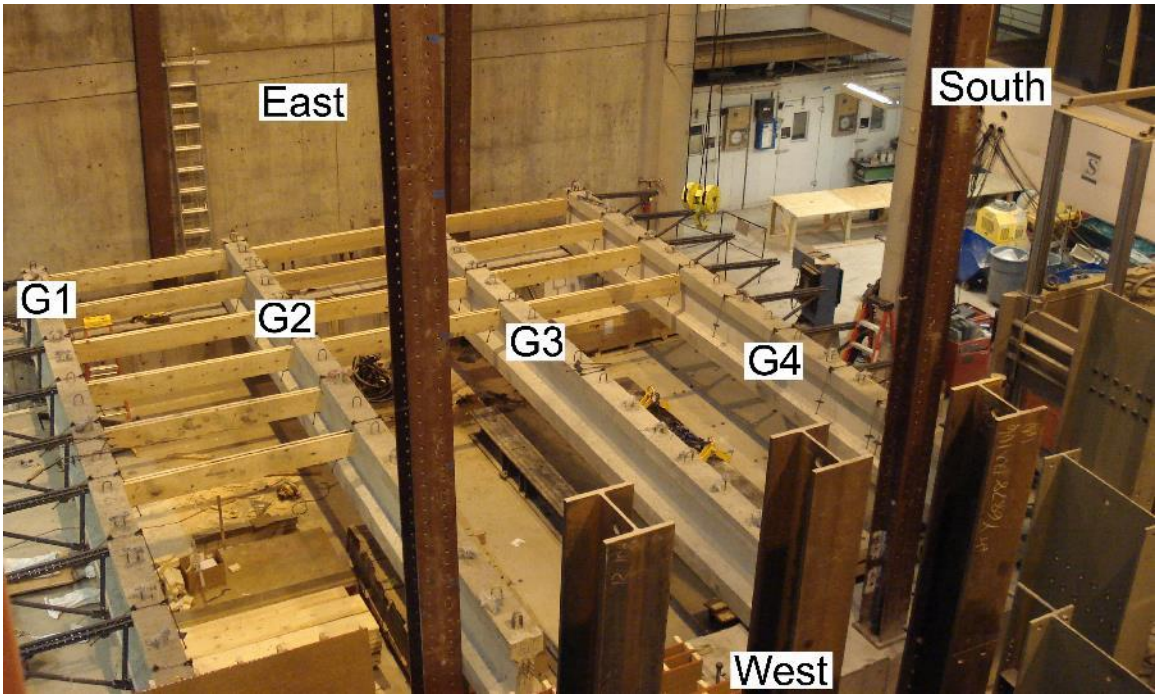

Figure 4-10. Laboratory Bridge Girder Orientation

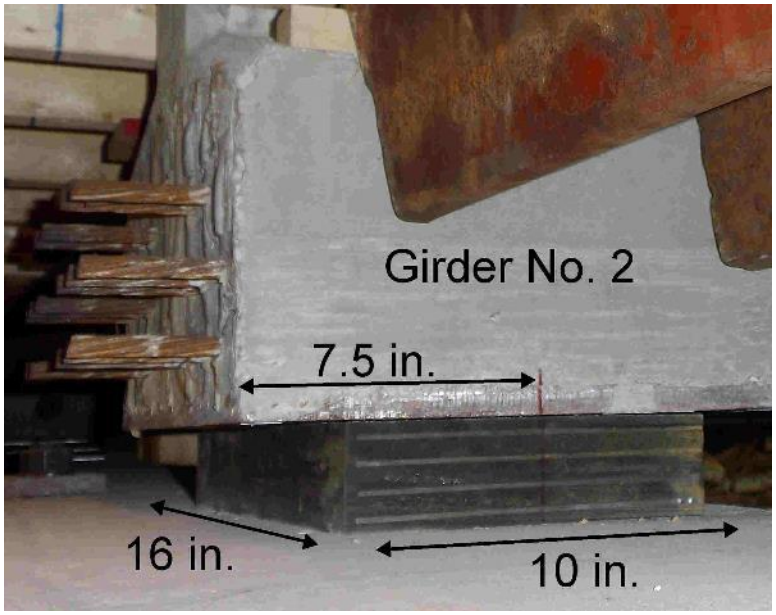

Figure 4-11. Laboratory Bridge Girder Bearing Pad Boundary Conditions

Figure 4-12. Bridge Deck Placement and Finishing

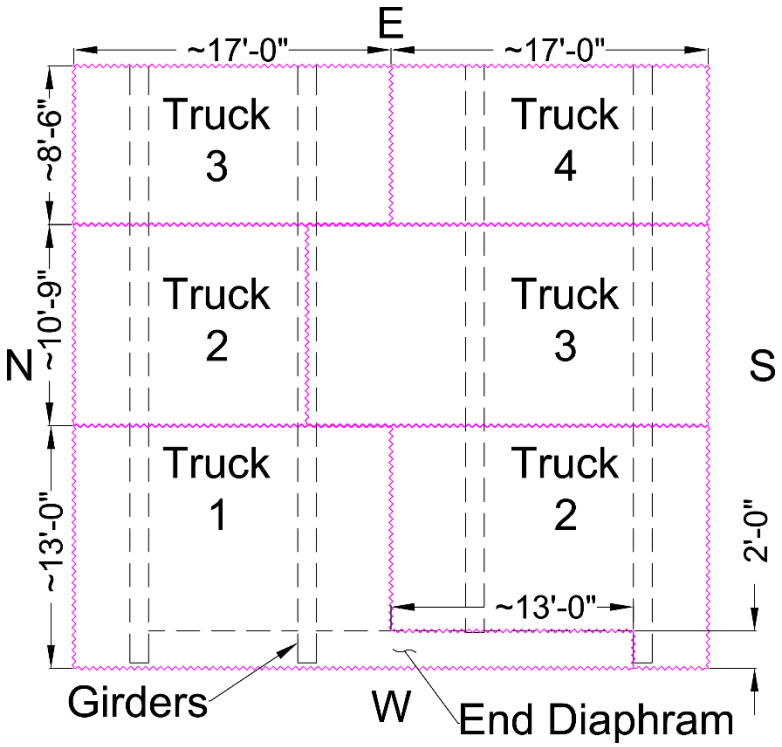

Figure 4-13. Bridge Deck Concrete Placement Diagram

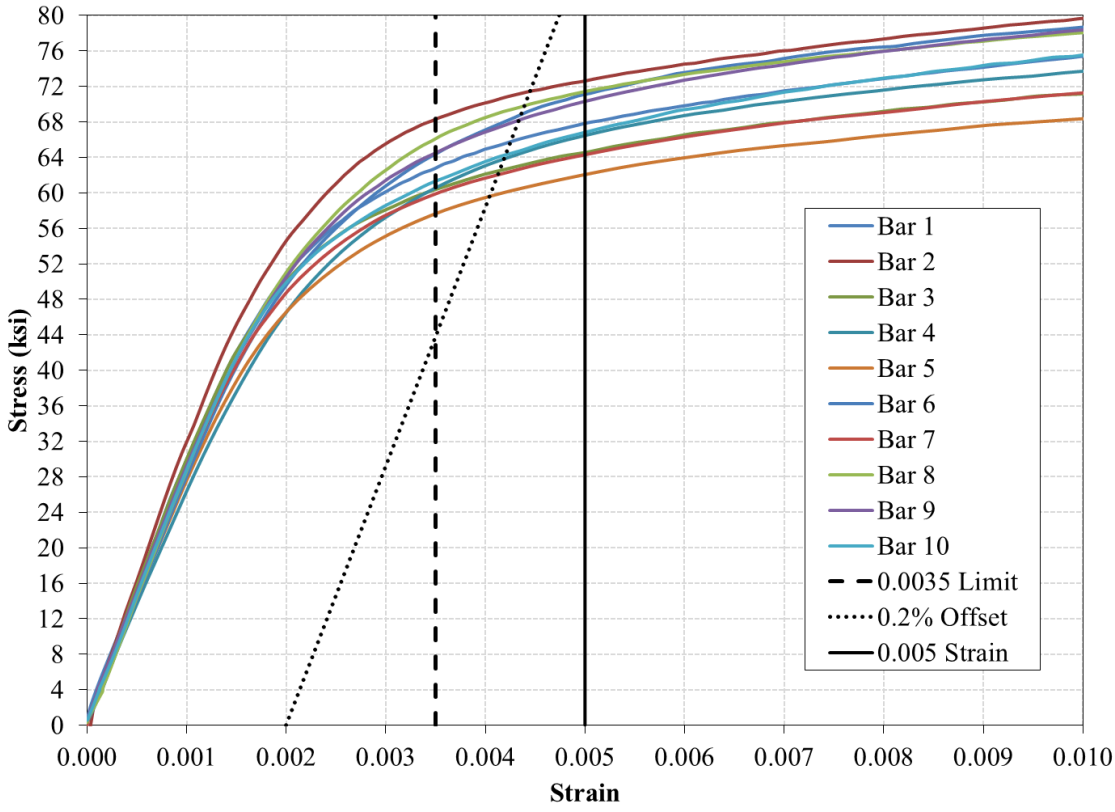

Figure 4-14. Stress-Strain Curves for Transverse Reinforcement

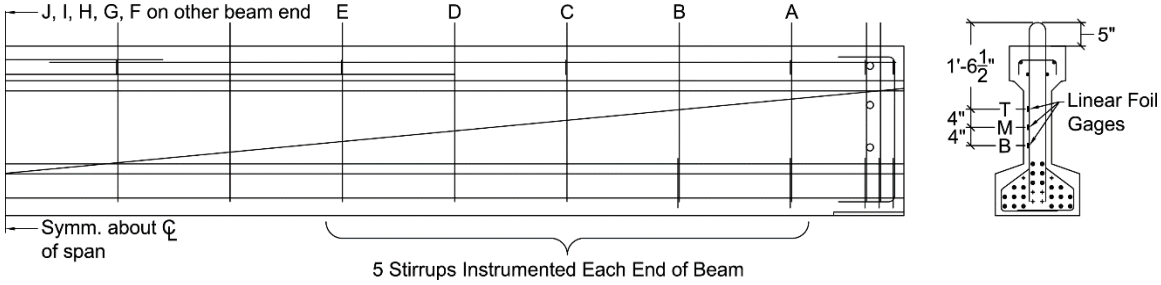

Figure 4-15. Transverse Reinforcement Strain Gages

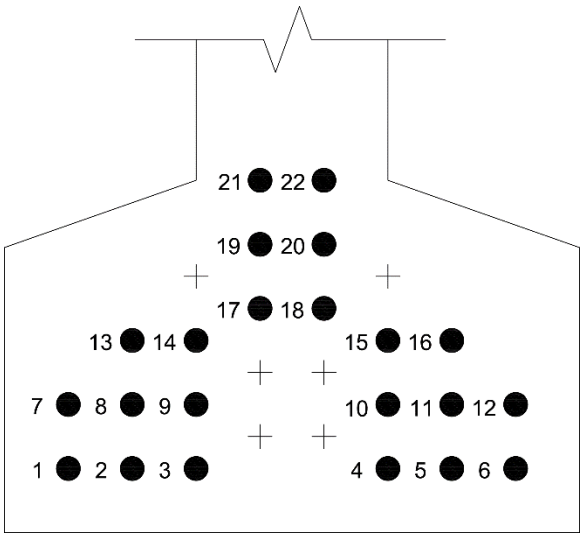

Figure 4-16. Prestressing Strand Numbering Looking Toward Live End

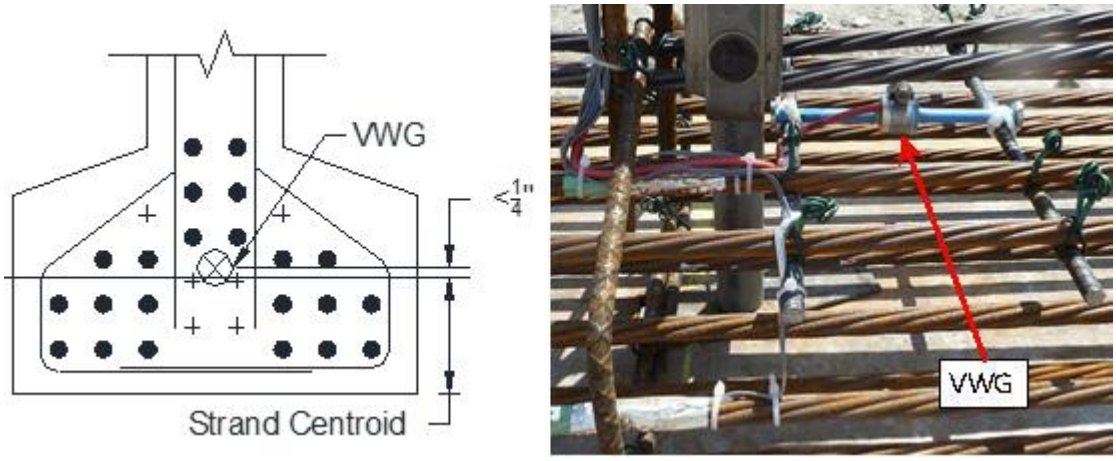

Figure 4-17. Location of Internal Vibrating Wire Strain Gages

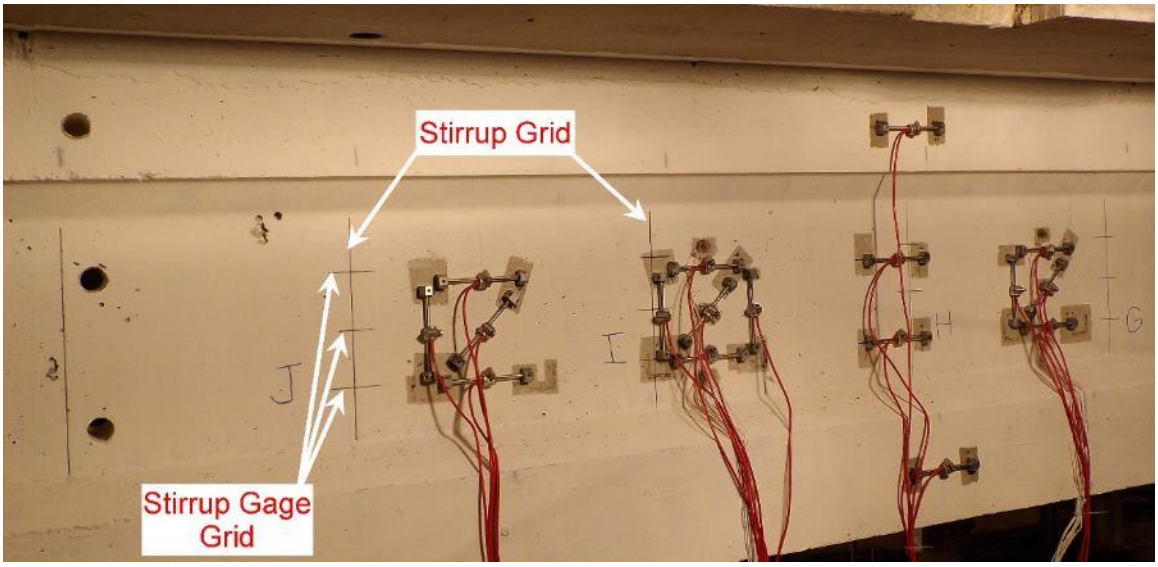

Figure 4-18. Stirrup and Stirrup Strain Gage Grid Lines

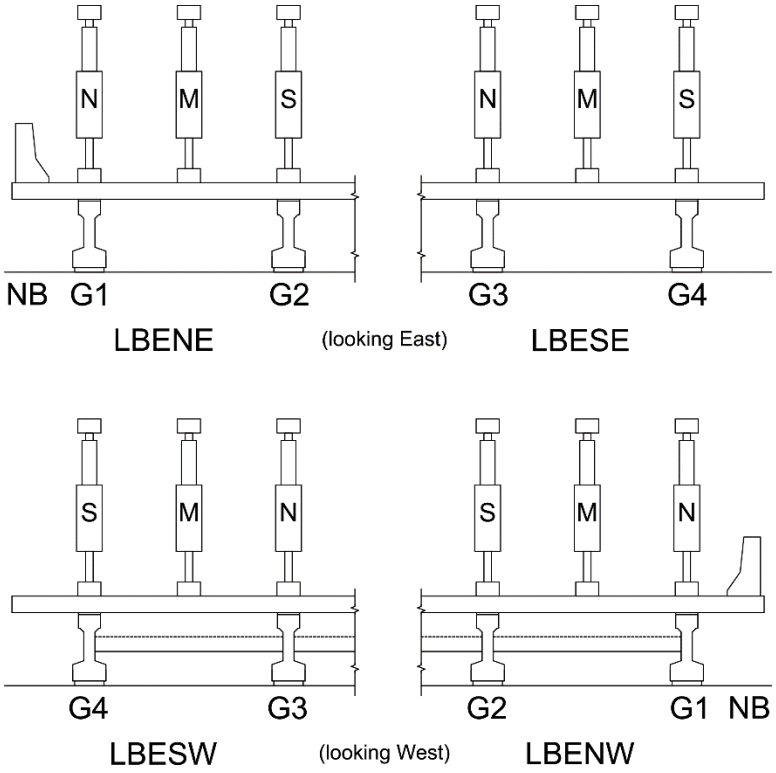

Figure 4-19. Elevation of Four Bridge Quadrants Tested Elastically

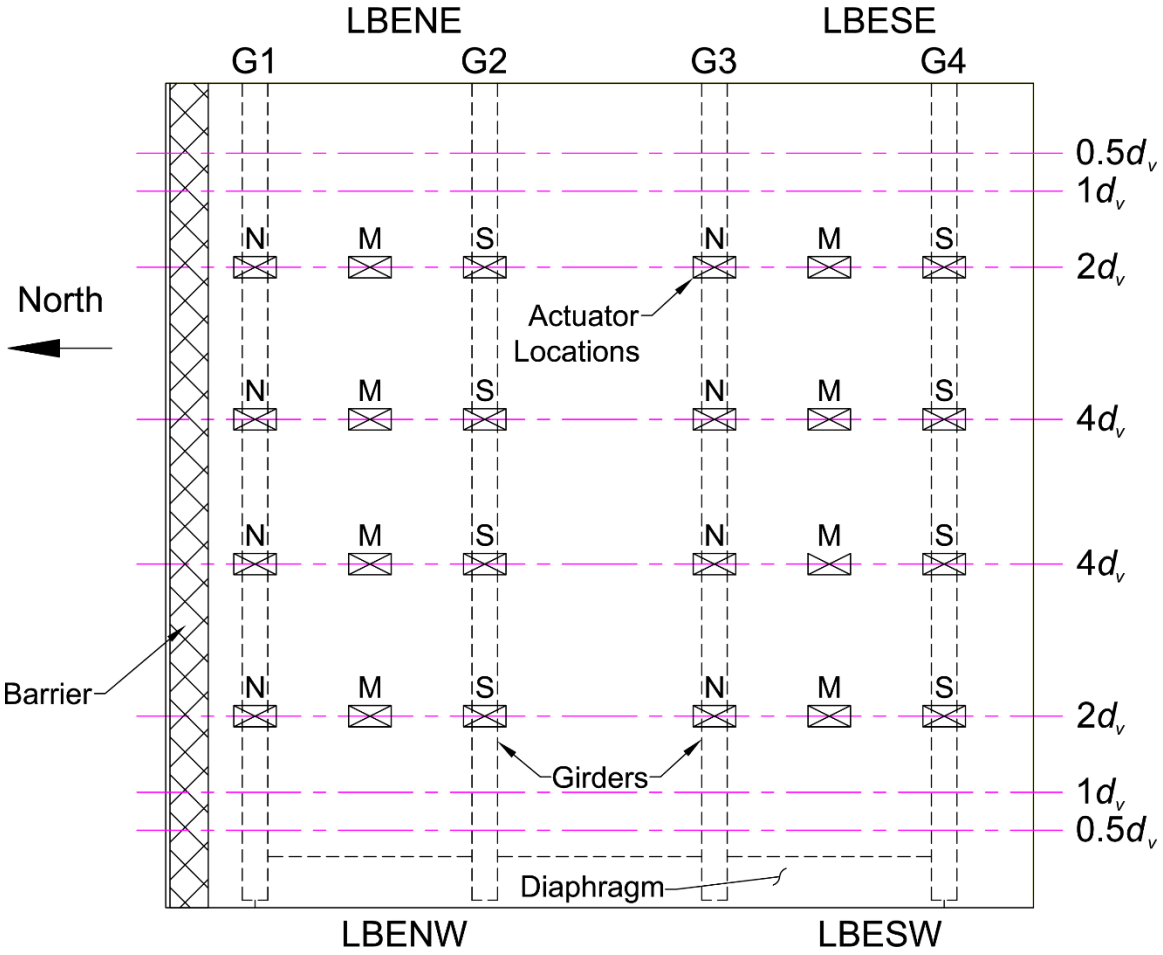

Figure 4-20. Plan of Four Bridge Quadrants Tested Elastically

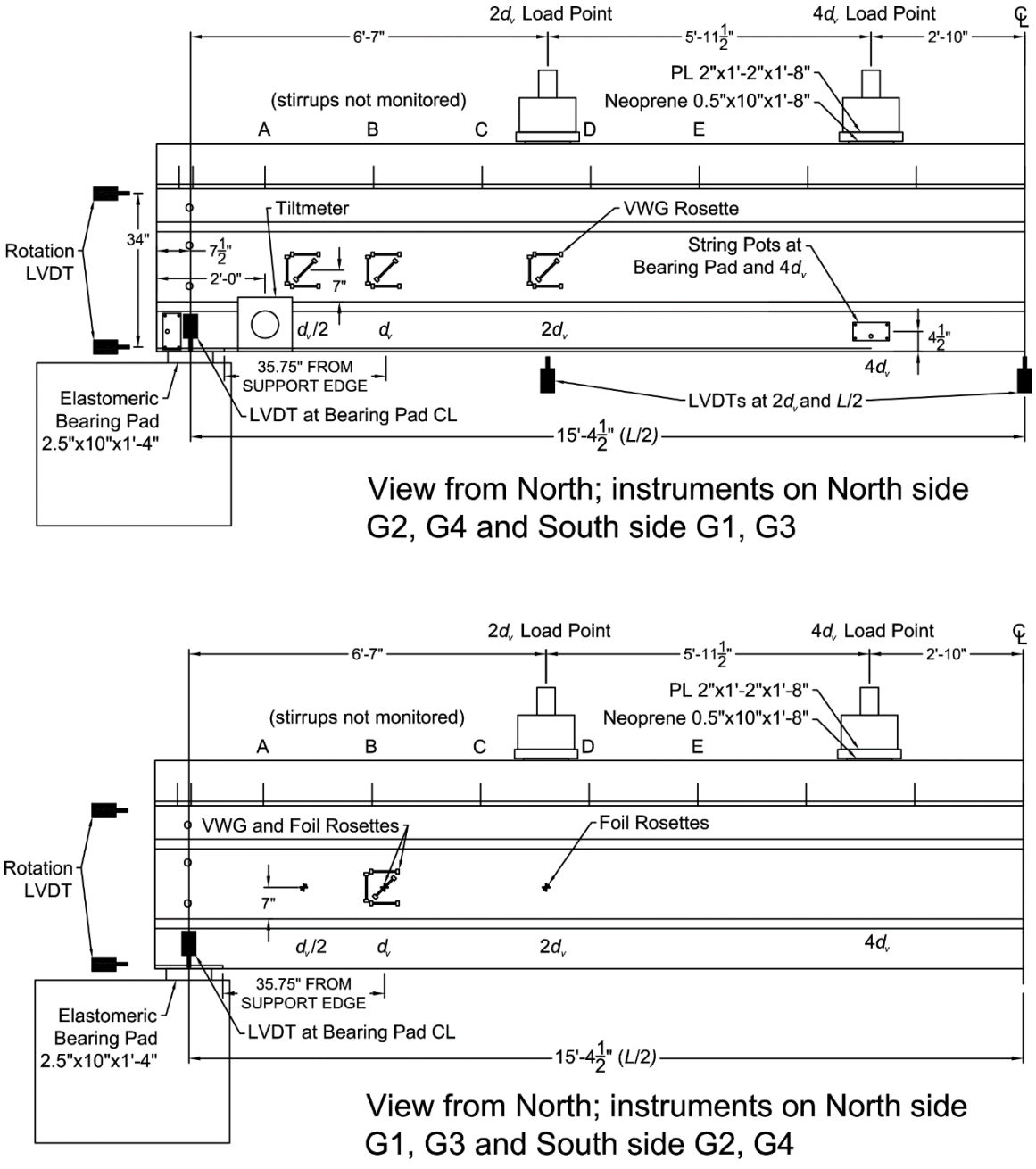

Figure 4-21. Instrumentation on East Half of Span for LBESE and LBENE

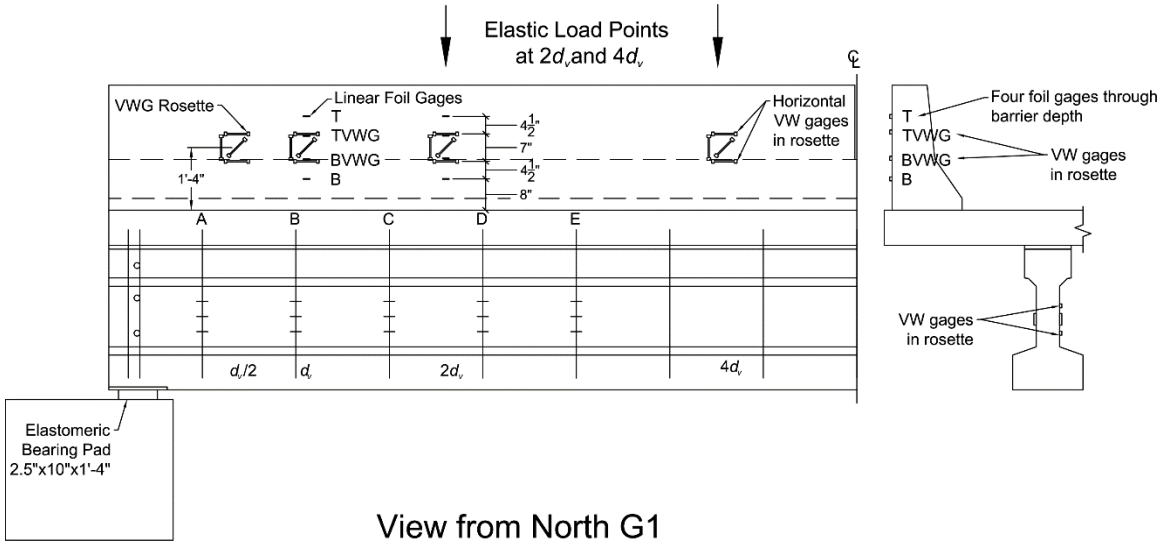

Figure 4-22. Instrumentation on East Half of Barrier for LBESE and LBENE

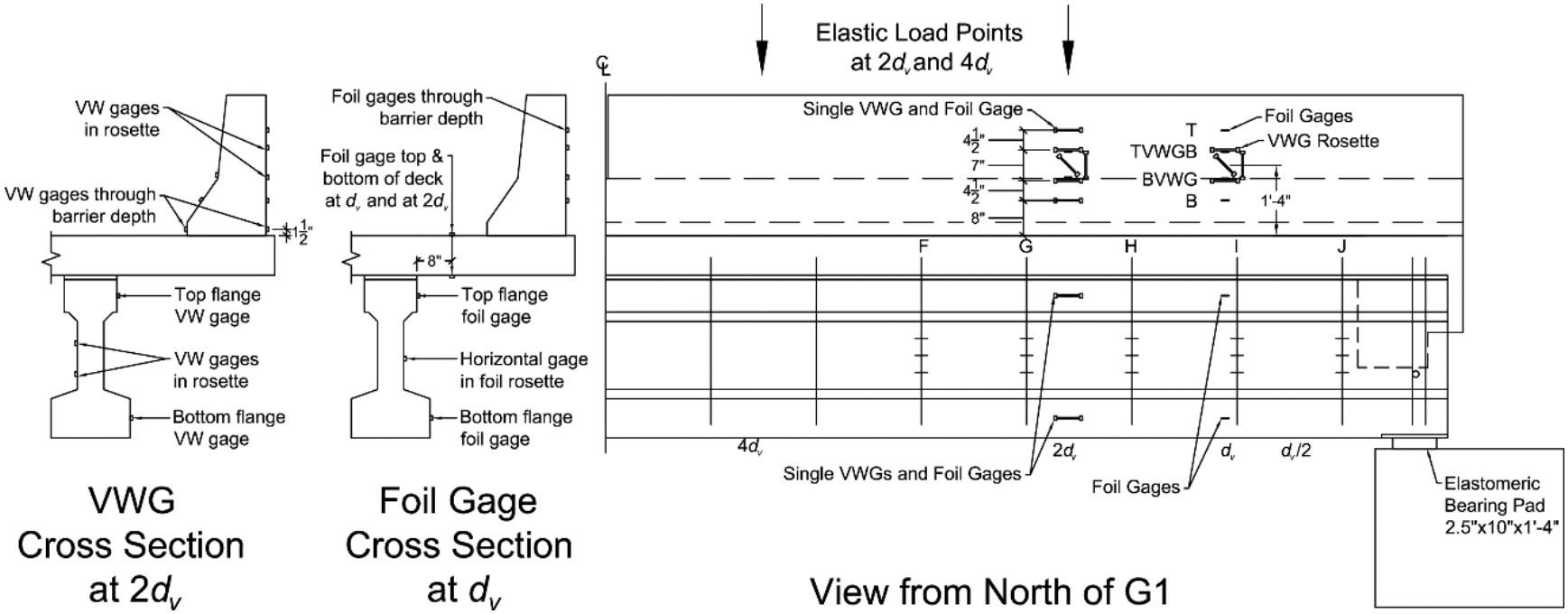

Figure 4-23. Instrumentation on West Half of Barrier for LBENW

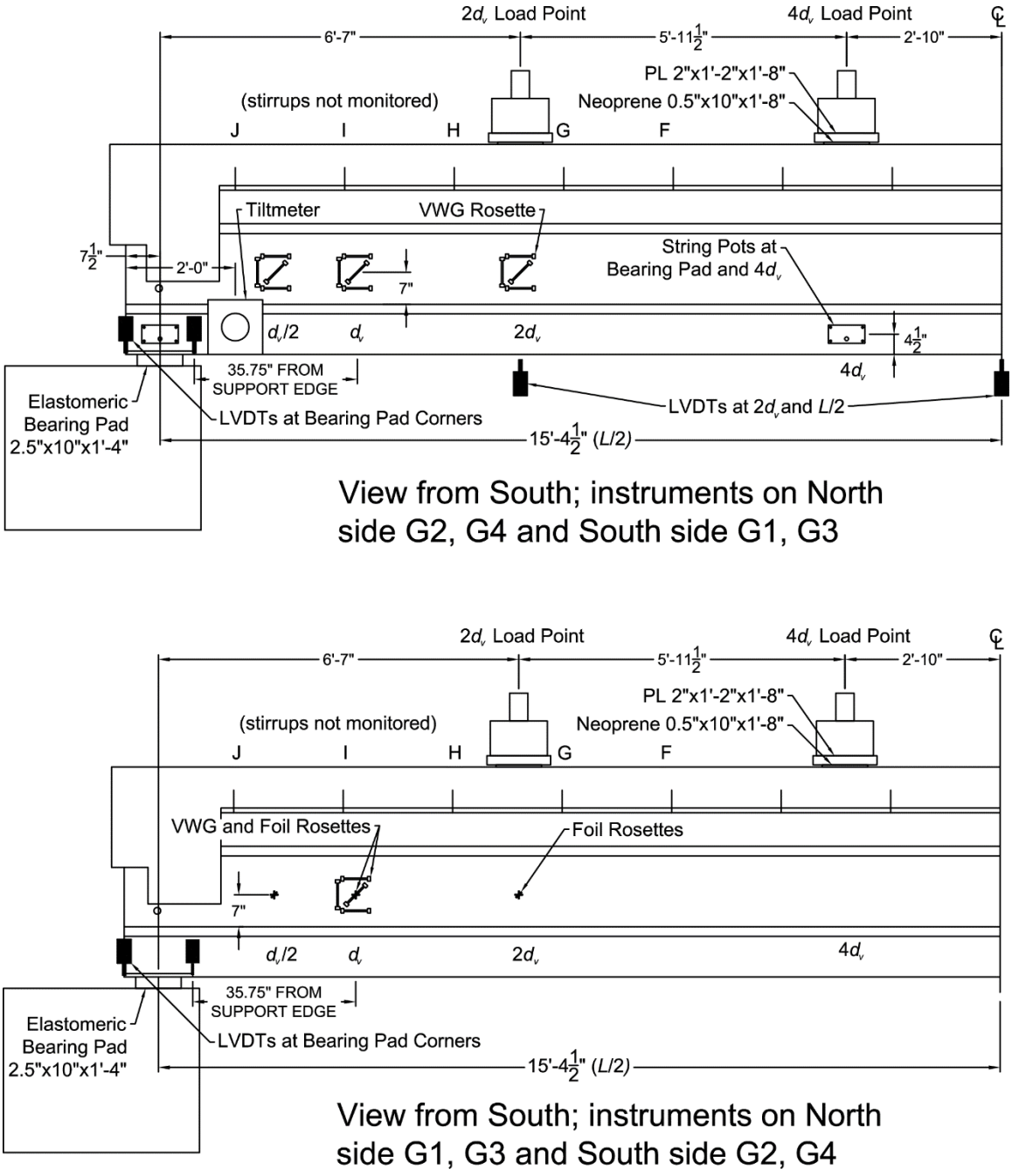

Figure 4-24. Instrumentation on West Half of Span for LBENW and LBESW

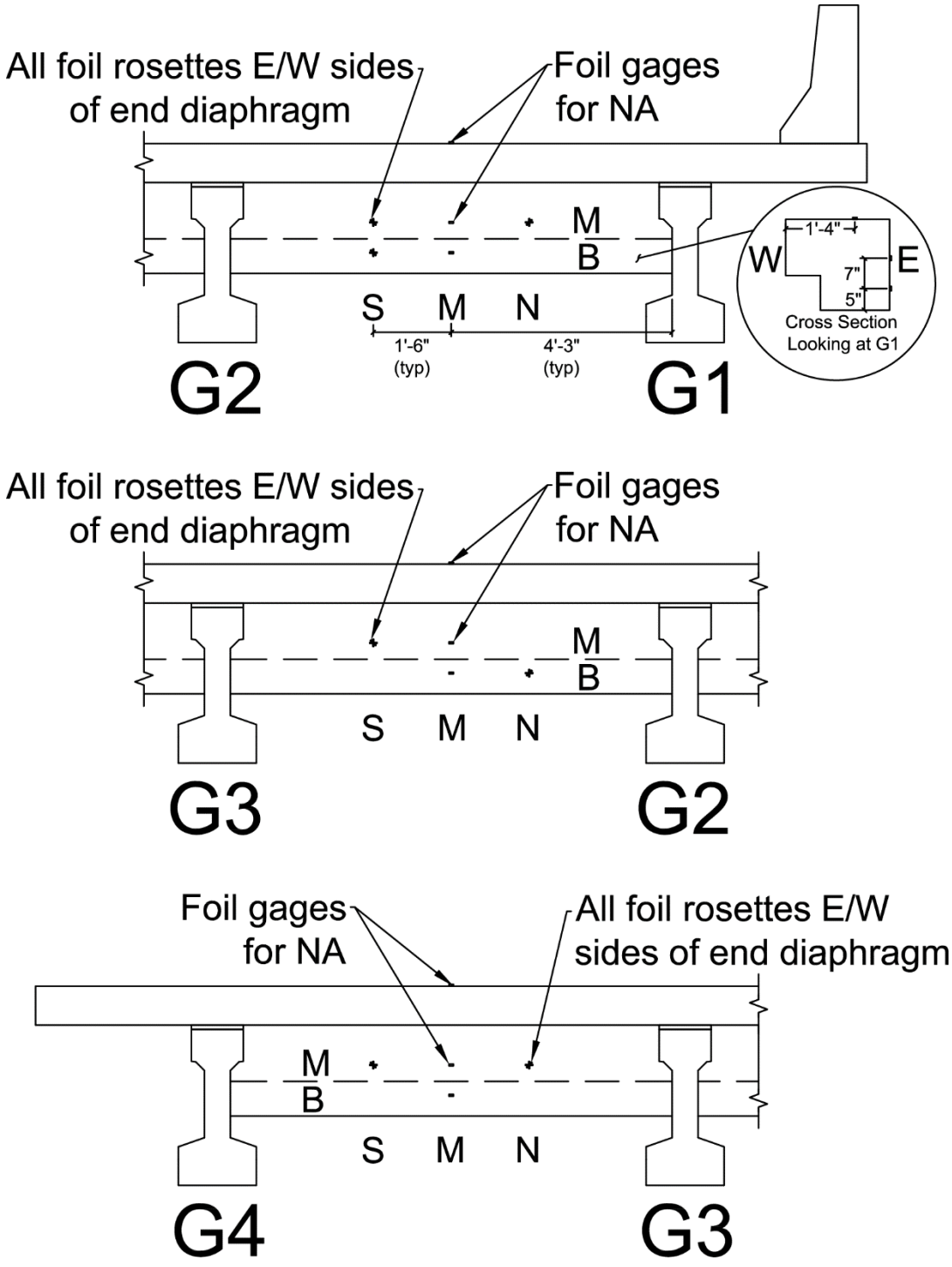

Figure 4-25. Instrumentation on End Diaphragm for LBENW, LBESW, and LBUW Looking West

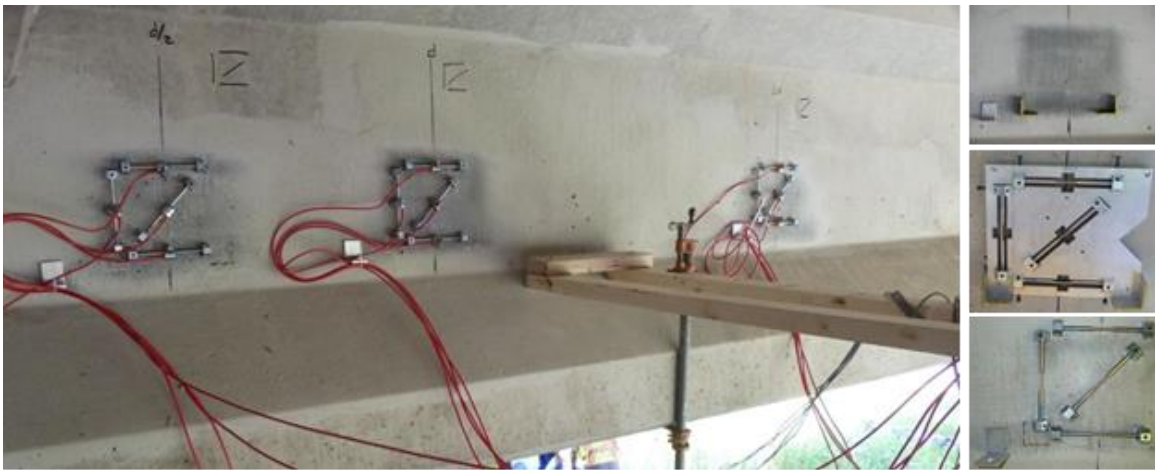

Figure 4-26. Example Box-Type Rosette VWGs

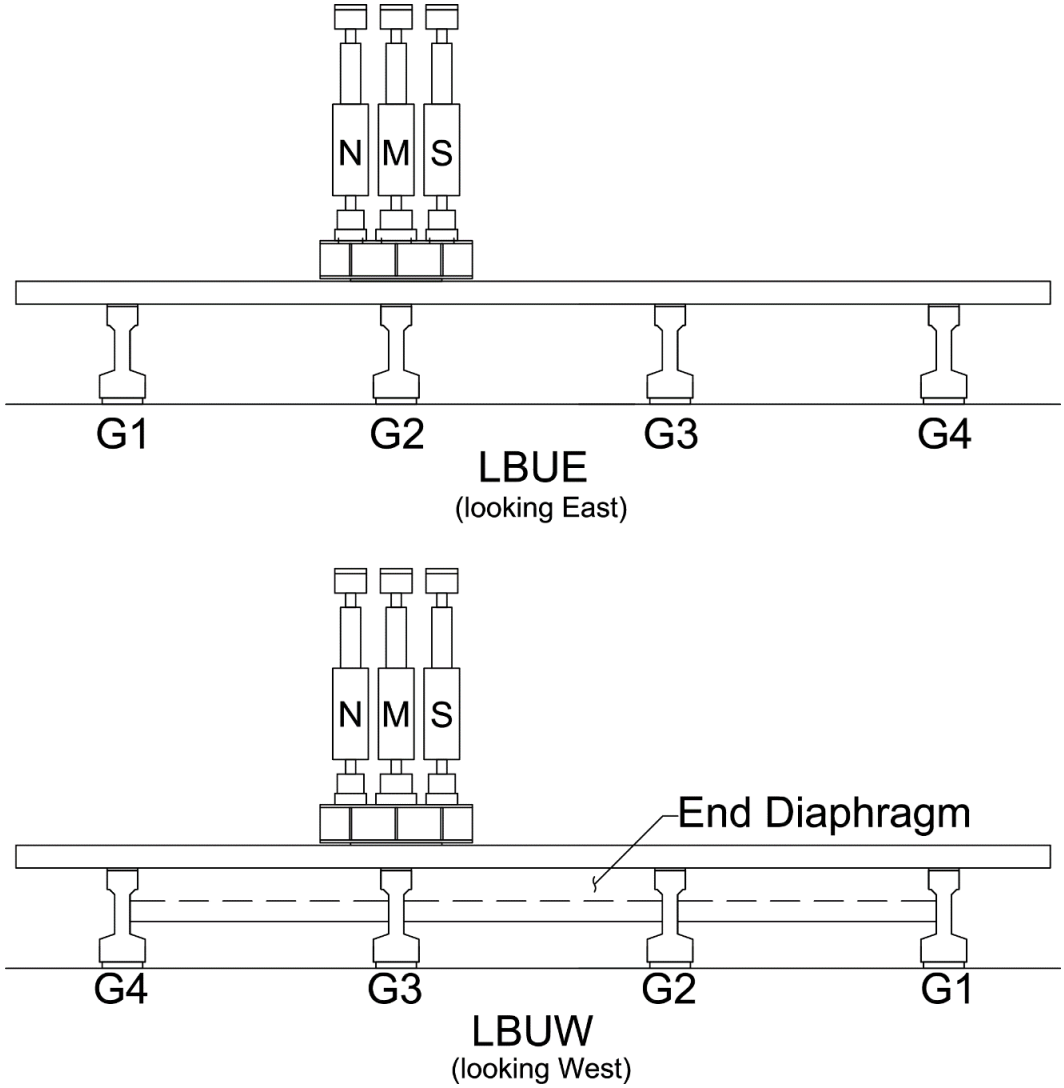

Figure 4-27. Diagonally Opposite Quadrants Tested Inelastically

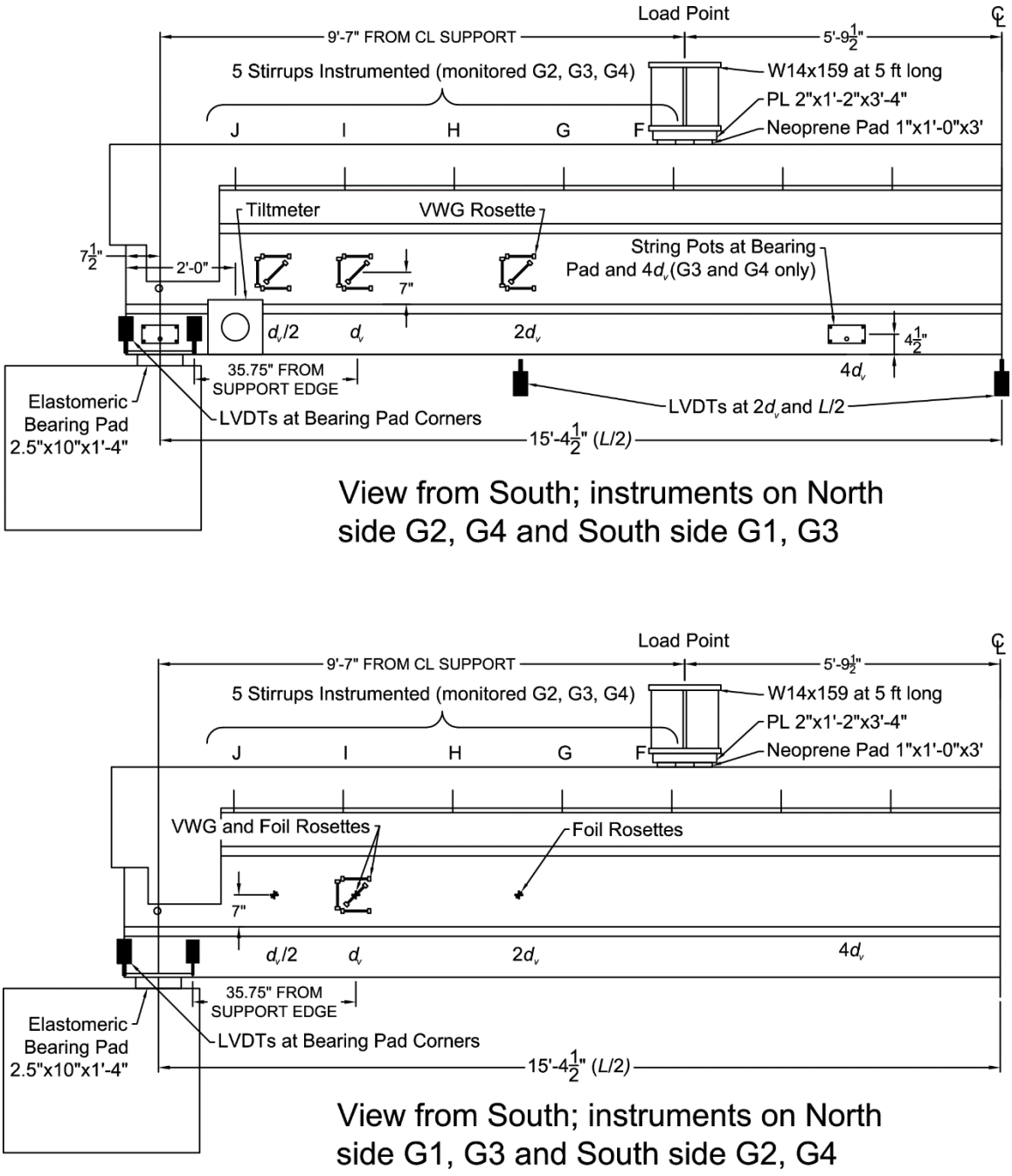

Figure 4-28. Instrumentation on West Half of Span for LBUW

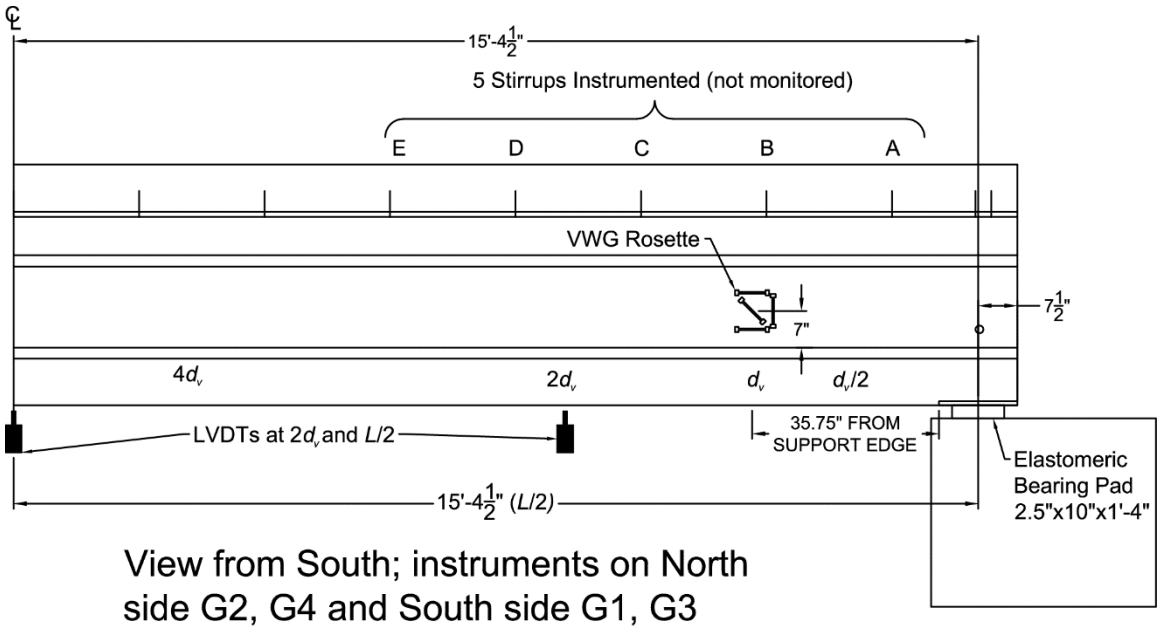

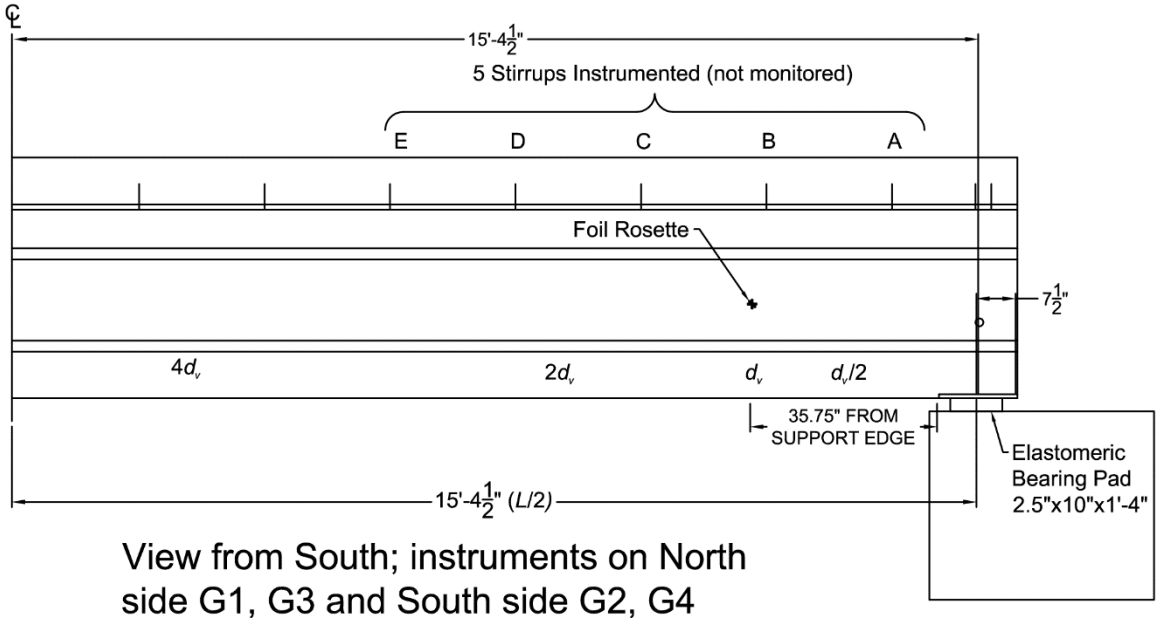

Figure 4-29. Instrumentation on East Half of Span for LBUW

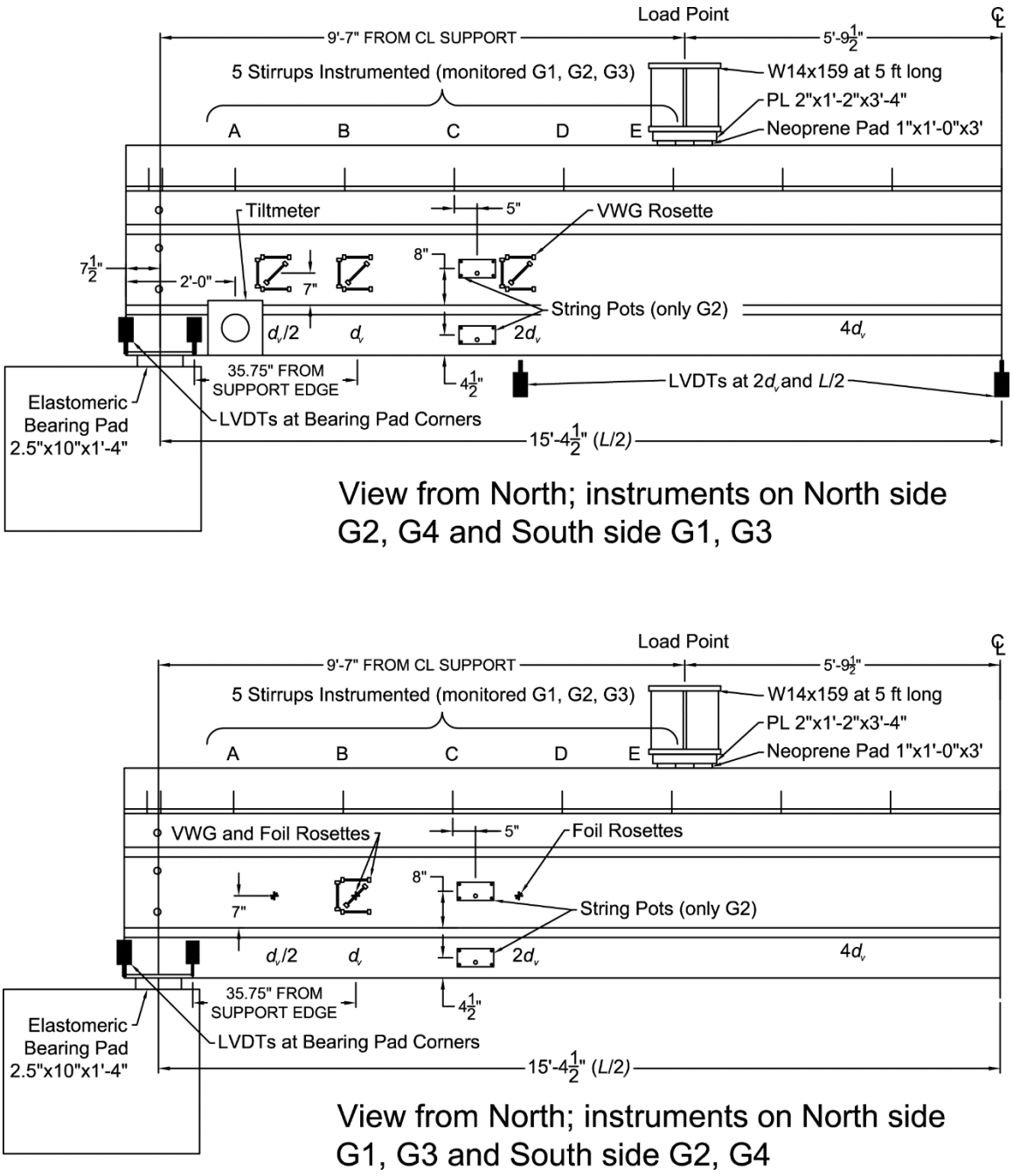

Figure 4-30. Instrumentation on East Half of Span for LBUE

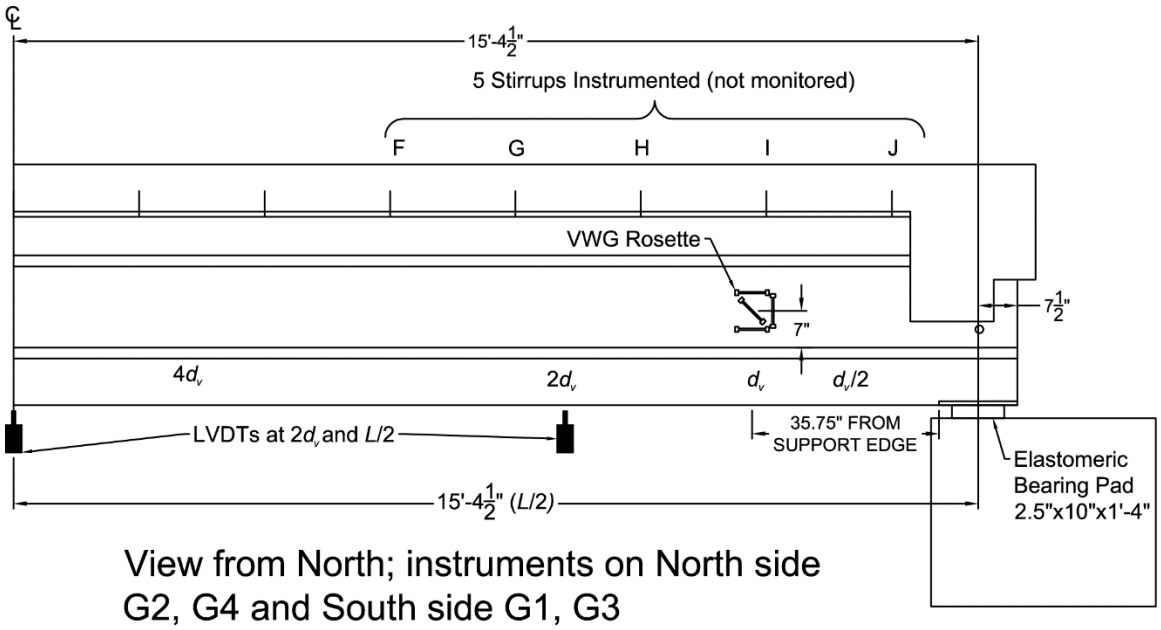

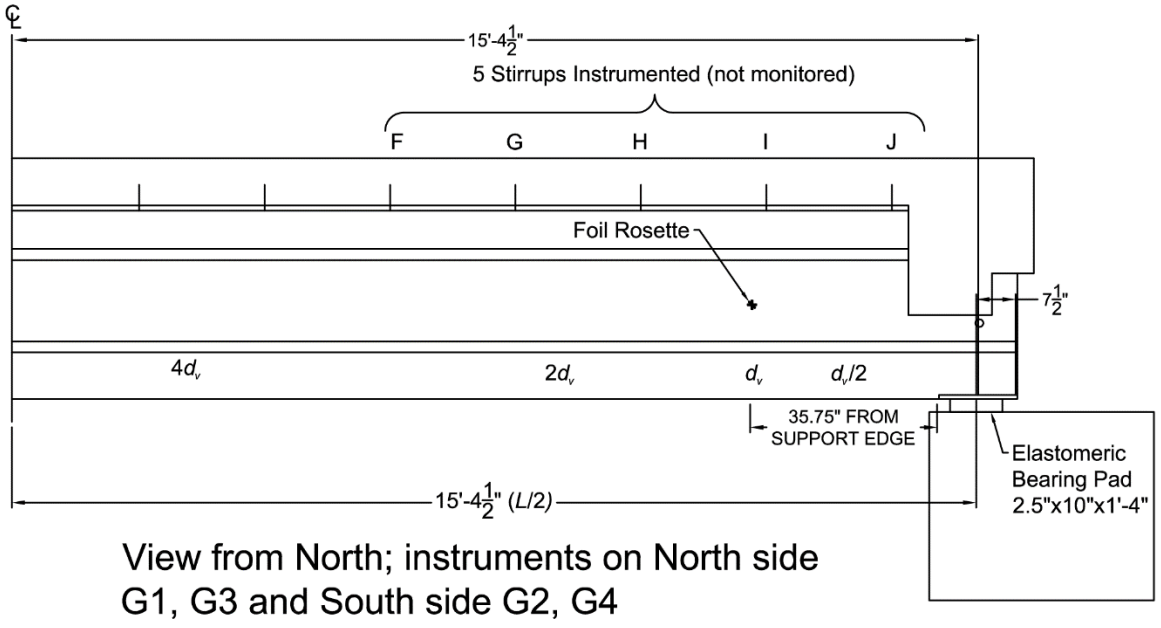

Figure 4-31. Instrumentation on West Half of Span for LBUE

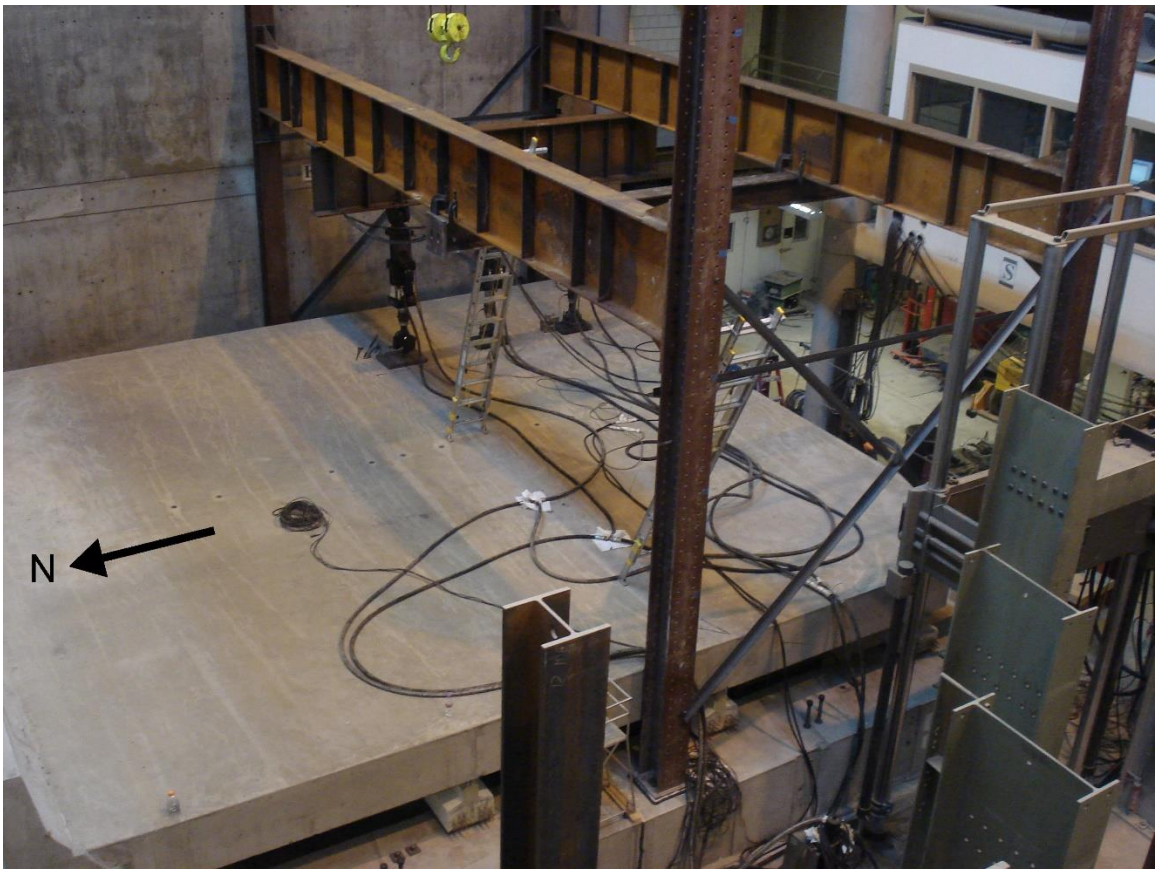

Figure 4-32. Steel Load Frame Configured for LBESE Testing

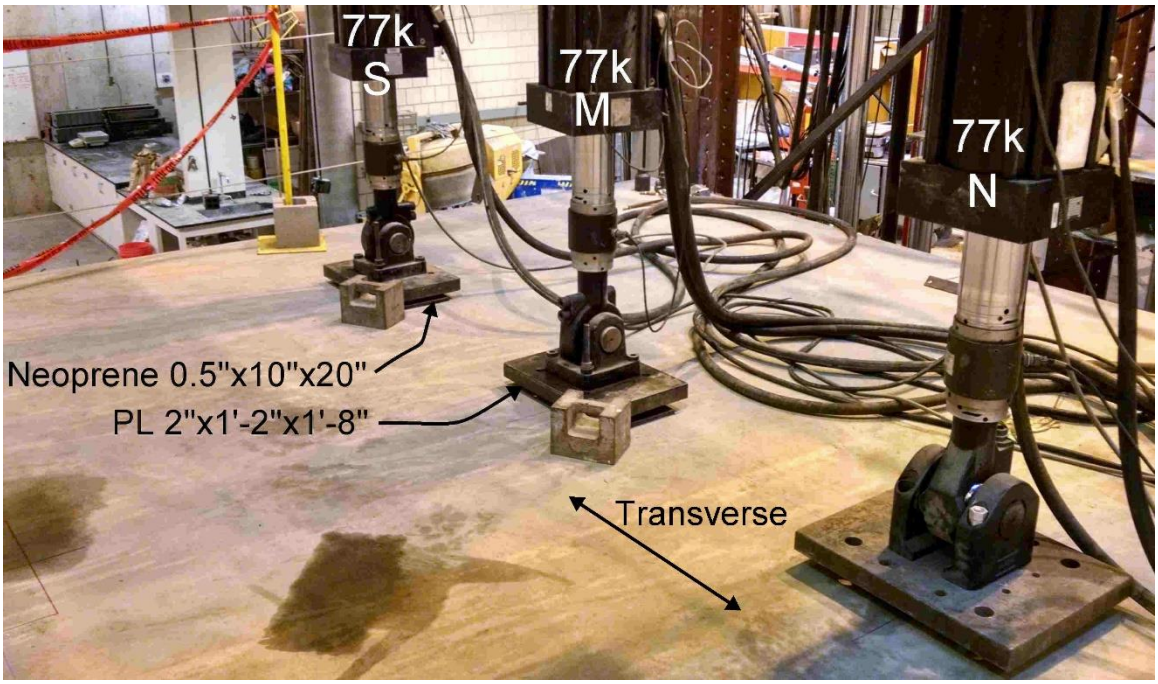

Figure 4-33. Applied Load Configuration for Elastic Tests during LBESW

Figure 4-34. Load Frame Tie-Down Systems above Bridge Deck during LBUE

Figure 4-35. Load Frame Tie-Down Systems at Midspan below Bridge Deck Looking West during LBUW

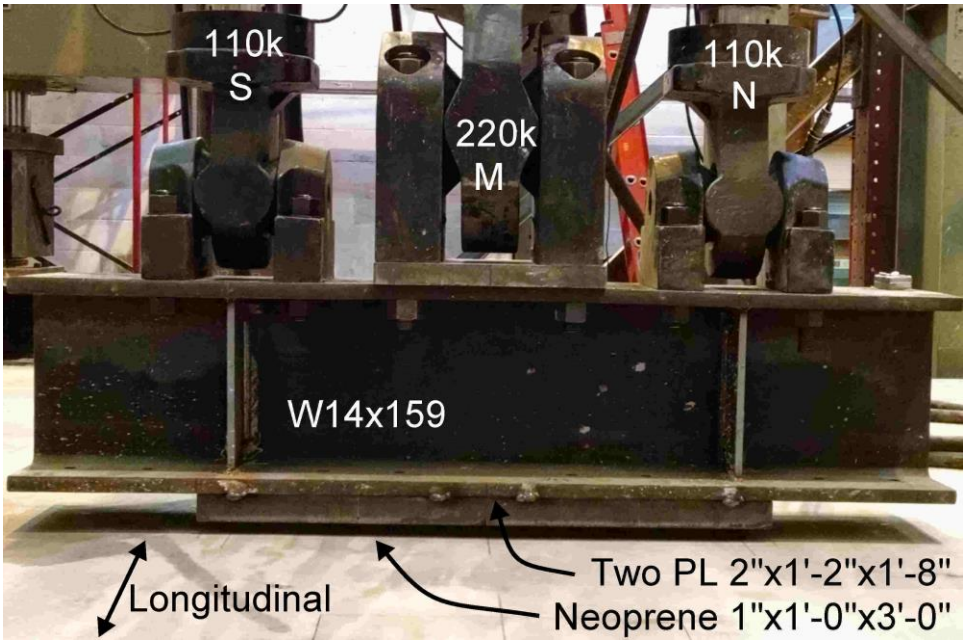

Figure 4-36. Applied Load Configuration for Inelastic Tests

CHAPTER 5. RESULTS OF LABORATORY BRIDGE TESTING AND FEM VALIDATION

5.1 Introduction

There were three main goals for testing the laboratory bridge in the elastic range. First, a rigorous elastic testing protocol was critical for validation of the elastic finite element modeling technique to be used in the parametric study. These tests and the corresponding models provided better understanding of the behavior related to shear distribution, boundary conditions, and interactions between structural elements in a controlled environment with known material properties and applied loads. The validated finite element modeling technique was used to broaden the results of the shear distribution study beyond the laboratory and field experimental results and was used to develop the final shear distribution recommendations. The second goal was to develop a better understanding of the effect of a traffic barrier on shear distribution, and the third goal was to determine if the partial depth end diaphragm had an effect on the shear distribution at elastic levels.

There were three main goals for inelastic testing of the laboratory bridge. The first was to quantify the amount of shear force shed by an interior girder to adjacent girders when web-shear cracking damaged the loaded girder and precipitated failure. The second goal was to quantify the effects of an end diaphragm on ultimate shear capacity and shear distribution in the inelastic range. The third goal was to compare the ultimate shear capacity of the loaded bridge girders to the capacity predicted by AASHTO Specifications. Within this goal, data from the single girder test were used to compare ultimate shear capacity of the same beam within a bridge system and as a single member.

Throughout this chapter, the term applied shear refers to the shear in the short shear span caused by application of the live load.

5.2 Conversion of Shear Strain to Force

Data collected from the VWG box-type rosettes included strain measured by four gages: a bottom horizontal gage, a top horizontal gage, a vertical gage, and a diagonal gage. The box-type rosette allowed for linear interpolation of bending strain between the two

horizontal gages such that, when incorporated with the single vertical and diagonal gage, three directions of a 45 degree rosette strain measurement were captured at the center of the configuration. Using strength of materials principles, the horizontal, diagonal, and vertical strains from the VWG and foil rosettes were used to calculate the shear strain, γ_{xy}.

The measured shear strain included effects from the combination of the vertical shear resultant and torsion at the section of measurement. In order to differentiate between the shear strain due to torsion and the shear strain due the vertical shear resultant, rosette strain gages were placed at the same location on both sides of a girder web. VWG box-type rosettes were installed on one side of the girder web and foil rosettes were installed on the opposite side of the girder web as discussed in Section 4.5.4. To check the quality of strain data between the two types of rosettes, an extra VWG box-type rosette was installed directly above the foil rosette at d_v such that a VWG box-type rosette was on each side of the web (at d_v on G3 and G4 during LBESE and at d_v on all girders during LBENE, LBENW, LBESW, and during inelastic testing). Individual values from the three legs of a foil rosette (Horizontal, Diagonal, and Vertical) were compared to equivalent VWG data. The horizontal VWG data was an average of the top and bottom VWGs in the rosette. Table 5-1 shows data at the same longitudinal location (d_v) and on the same side of the web for both a foil rosette and a VWG box-type rosette. The difference in the data ranged from 3 to 13 με with an average of 6 με. This variation was considered to be within the noise range of the foil rosettes. Furthermore, Table 5-1 shows that the variation in shear strain, γ_{xy}, calculated using rosette strains was between 2 and 22 με, with an average of 9 με. When available, data from two VWG box-type rosettes installed at the same longitudinal location, on opposite sides of the web, were used instead of the VWG and foil rosette combination to calculate the shear strain due to the higher signal-to-noise ratio for VWGs compared to foil rosettes.

The shear strain due to the vertical shear resultant was calculated by averaging the shear strain, γ_{xy}, from both sides of the girder web. The shear strain due to torsion was calculated as the the difference between the maximum or minimum shear strain and the average shear strain. The shear strain, γ_{xy}, was converted into a vertical shear force using common strength of materials relations:

$$\gamma_{xy} = \tau / G \text{ and } \tau = \frac{VQ}{It} \quad (5.1)$$

where γ_{xy} is the shear strain, τ is the shear stress, and G is the shear modulus which is related to the measured Young's modulus using the Poisson's ratio,v ($G = E_{meas} / (2+2v)$), V is the applied vertical shear force at the longitudinal location of interest, Q is the first moment, with respect to the neutral axis, of the area of the cross section located above or below the elevation being considered, I is the transformed centroidal moment of inertia of the entire composite cross-sectional area (the longitudinal deck steel, deck concrete, haunch, and prestressing strands were transformed to girder concrete), and t is the width of the cross section at the elevation being considered.

In this study, the composite section was assumed to contain an effective flange width equal to the girder spacing for interior beams and half of the girder spacing plus the overhang length for exterior beams (the barrier was not included in this composite section) per Section 4.6.2.6 of the 2010 AASHTO LRFD Specification. Use of the girder spacing for effective deck width is justified in the 2010 AASHTO LRFD Specifications through reference of Chen et al. (2005). Section 9.8.3 of the AASHTO Standard Specifications (2002) historically defined the effective flange width of the composite section as the minimum of (1) one-fourth of the girder span length, (2) six times the thickness of the slab on each side of the web width plus the web width, and (3) one-half the clear distance on each side of the web width plus the web width. For the laboratory bridge, these values would be 92 in., 114 in., and 108 in. (96 in. for exterior girder), respectively.

5.3 Bridge Elastic Testing

Four quadrants of the bridge were tested using three individual actuators or a combination of the actuators in force control. Testing of the laboratory bridge started in the southeast quadrant where no traffic barrier and no end diaphragm were present. Figure 4-20 presented a plan view of the bridge showing each quadrant and the actuator positions. The lack of additional bridge components allowed for a clearer picture of bridge girder shear behavior. Initial trial tests were completed to determine the appropriate loading rate, unloading rate, and elastic load steps. Selection of the loading rate and unloading rate was primarily done by investigating vertical displacement measured by LVDTs on the bridge

girders and bearing pads. A loading rate of 0.0375 k/sec and an unloading rate of 0.3 k/sec were selected for all elastic tests to limit the effects of viscoelastic creep behavior in the neoprene bearing pads during data collection. In other words, a slower loading rate was selected so that the results were more repeatable and more representative of a truck moving across a bridge (opposed to fast loading from a hydraulic actuator); a slower loading rate allowed the bearing pads to settle at each load step. After unloading, a pause of approximately 20 minutes was taken prior to conducting another test to allow the bearing pads to return to an unloaded position. A faster loading rate would have caused the bearing pad material to creep while data were collected during a pause in loading.

Elastic load steps with applied loads of 50 and 75 kips per actuator were selected for the majority of elastic tests because lower load steps (e.g., at 25 kips) did not provide large enough changes in strain for clear detection by the foil strain gage rosettes. When a single actuator was used (loading scenario S, M, or N), load steps were at 50 and 75 kips total load. When a combination of two actuators were used (loading scenarios SM and NM), load steps were at 100 and 150 kips total load (50 and 75 kips per actuator). When all three actuators were used in loading scenario SMN, a single load step was at 150 kips total load (50 kips per actuator). Application of a total load higher than 150 kips was excluded from the elastic testing plan to avoid potential damage to the structure.

Shear forces calculated with rosette data were checked to verify linear elastic behavior between the 50 and 75 kip load steps for single actuator testing completed in LBESE and LBENE. Data given in Table 5-2 shows the cross section shear force at d_v, obtained from summing the shear force in each girder for the 50 and 75 kip load steps. The linearity of the data is shown by scaling the data obtained from the 50 kip load step by 1.5 and comparing it to the measured data at the 75 kip load step. The data compared well, the average difference between the data scaled from the 50 kip load step and the measured 75 kip load step was approximately 1 percent or less (with a maximum of 6 to 7 percent).

Voltage and strain data (e.g., displacements from LVDTs and string pots, rotations from tiltmeters, and strain from rosettes) for all elastic tests were continuously collected, from the beginning of each test until load was no longer applied through the CE DAQ. Vibrating wire strain gage data were collected only at steps of constant load (0, 50 and/or 75 kips per actuator) with the CR1000 DAQ. Test data between the two DAQ systems were

always linked with the same date/time stamp, the force signal from all three actuators, and the displacement signal from all three actuators. Unless noted otherwise, all data presented from elastic testing were from the maximum load per actuator load level (75 kips total load for single actuators and 150 kips total load for combinations of actuators) to increase the signal-to-noise ratio in the instruments.

Test nomenclature for both the CE DAQ and the CR1000 DAQ included the quadrant name (LBESE, LBENE, LBENW, and LBESW as defined in Section 4.5.4) where the load was applied in the elastic range (LBE in the quadrant name designated Lab Bridge Elastic), the longitudinal loading location at $2d_v$ or $4d_v$ which were designated with 2d or 4d (d_v and d were used interchangeably in this study), the position of the actuator or actuator combination that was used (S, M, N, or combinations: NM, SM, SMN), and notation indicating repetitive tests during the same calendar day (1, 2, etc.). The calendar date was also included in the file naming scheme to keep track of tests repeated on different days throughout the project. For example, data collected from anywhere on the bridge with the loads applied in the LBESE quadrant with the north and middle actuators at $2d_v$ would be written as LBESE_2d_NM. Because VWG data were not continuously collected, the nomenclature from the CR1000 DAQ also included the magnitude of applied load in a single actuator: 0 for a zero reading with actuators not in contact with the bridge, 50k for 50 kips applied load per actuator, or 75k for 75 kips applied load per actuator. For example, data collected in association with 75 kips of load applied in both the north and middle actuators (i.e., 150 kips total load) at $2d_v$ in the LBESE quadrant would be written as LBESE_2d_NM_75k. Detailed loading histories for each of the four bridge quadrants can be found in Appendix E and include date tested, time tested, and any pertinent test description or notes.

5.3.1 Effects of Torsion on Shear Strain

An investigation related to the effects of torsion on shear strain was completed using the laboratory bridge specifically looking at load case LBESE_4d_M because it was the most likely to cause torsion in adjacent girder webs. The amount of shear strain due to torsion compared to the amount of shear strain due to the vertical shear resultant was of primary interest when investigating the effects of torsion in the laboratory bridge. The shear strain due to the vertical shear force resultant (γ_{xy_shear}) was calculated as the average of the

total shear strain, γ_{xy}, from each face of the girder web. The shear strain due to torsion (γ_{xy_tor}) was calculated as the difference between the total shear strain, γ_{xy}, from either face of the girder web and the absolute value of the shear strain due to the vertical shear force resultant, γ_{xy_shear}. The absolute value of the ratio of the shear strain due to torsion divided by the shear strain due to the vertical shear resultant ($|\gamma_{xy\_tor} / \gamma_{xy\_shear}|$) was calculated as a percentage for each location of interest to describe the difference in relative magnitudes of the torsional shear strain and the shear strain due to the vertical shear resultant. In other words, a value of 100 percent would indicate that the shear strain due to torsion was equal to the shear strain due to the vertical shear resultant.

Data in Table 5-3 show that the magnitude of the shear strain due to torsion was approximately 40 percent of the magnitude of shear strain due the vertical shear resultant for LBESE_4d_M. The middle actuator in load case LBESE_4d_M applied force between an interior and exterior girder which caused approximately equal torsional shear strain (16 to 18 με) in both girders. Applying load above a girder (load cases using S or N actuator only) caused less torsional shear strain in the girder below the actuator (3 to 6 με) when compared to the torsional shear strain in the girder adjacent the actuator (8 to 12 με). Data in Table 5-3 indicate that the ratio of $|\gamma_{xy\_tor} / \gamma_{xy\_shear}|$ is much larger (62 to 74 percent) for the girder adjacent to the actuator compared to the girder below the actuator (4 to 8 percent) when load is applied directly above a single girder. Table 5-3 also has a column for the absolute value of the ratio of the torsional shear strain divided by the total shear strain ($\gamma_{xy\_tor} / \gamma_{xy}$). This ratio is not discussed in Chapter 5, but it is referenced when comparing torsional effects present during field testing and laboratory testing in Chapter 6.

To determine if the effects of torsion could be negated, a steel prop was added to the bridge structure to simulate an intermediate diaphragm. Figure 5-1 shows the steel prop fabricated from a 7.5 ft long 3 ½ x 3 ½ x 3/8 HSS tube with 1 in. thick steel plates welded on each end. The prop was positioned under the girder bottom flanges at $4d_v$, which was also the location of applied load. A 1 in. diameter threaded rod, placed through the webs of G3 and G4, was attached to each of the exterior HSS braces to stabilize the steel prop diaphragm. Horizontal displacement between the bottom flanges of Girder 3 and Girder 4 was measured with a string pot at the bearing pad and at $4d_v$.

Figure 5-2 shows that the steel prop acting as an intermediate diaphragm did prevent relative horizontal displacement between Girder 3 and Girder 4 at the bearing pad and limited the horizontal displacement at $4d_v$. The horizontal displacement at $4d_v$ was not entirely eliminated because the axial stiffness of the steel prop was insufficient. An adequately stiff steel prop would have been too heavy to maneuver. The steel prop was sized such that it could be handled by laboratory research assistants under the bridge and between girders.

The fact that the steel prop limited horizontal displacement between G3 and G4 highlights the potential importance of intermediate diaphragms beyond providing stability during construction. Laboratory data indicated that well-connected intermediate diaphragms may provide bracing to limit shear strains due to torsion in the webs of prestressed concrete girders. However, the distance between intermediate diaphragms in as-built bridges may be equal to or longer than the unbraced span length of the laboratory bridge. The spacing, stiffness, and connectivity of intermediate diaphrams in the field were not investigated experimentally; consequently, it is not clear whether they are sufficient to eliminate torsion in the field. It should be noted that loading scenarios in the laboratory bridge (load applied with a single actuator or combination of three actuators in a small, concentrated footprint) are likely much different than those encountered on a field bridge (load applied with vehicles that typically contain many individual tires contacting the bridge deck in a large footprint), but the effects of torsion may still be present. Chapter 6 presents an additional study of torsion due to truck loading on field bridges and a discussion about the effects of intermediate diaphragms in field bridge finite element models.

5.3.2 Validation of the FEM Technique

One of the primary reasons for detailed elastic testing of the laboratory bridge was to validate the elastic FEM technique discussed in Section 3.3. The following subsections compare the results of the tests to the FEM analyses. This section describes the different load cases used for the comparisons. The FEM was elastic in both tension and compression. Elastic laboratory testing included twelve tests in each of the four quadrants (i.e., 48 total elastic tests). The twelve tests consisted of applying load with actuator configurations M, S, N, NM, SM, and SMN at both $2d_v$ and $4d_v$. Four standard load cases within each bridge quadrant (i.e., 16 total load cases) were selected to spot check and verify the FEM behavior.

Comparisons between FEM results and experimental data were made at the maximum applied load of 75 kips in each load case to maximize the signal-to-noise ratio of the experimental instrumentation. An exception to this comparison was made for the SMN load cases where a single actuator maximum load only reached 50 kips. Comparisons were made using both data from the CR1000 DAQ (VWGs) and from the CE DAQ (foil strain gages, displacements, etc.). A single VWG data point for each sensor was averaged from data collected over five cycles that took approximately eight minutes while the applied force was held constant. Data collected on the CE DAQ was condensed into a single data point at the maximum applied load using an average of data collected over the same eight minute time period used to collect VWG data.

The four standard load cases were selected to evaluate the structural response from maximum bending, shear, or torsional effects in each quadrant. Load cases at $4d_v$ were used for multiple reasons: the ability to maximize longitudinal bending and vertical displacement (SMN load case), the ability to maximize torsional bending behavior in the interior and exterior beams at a location away from the bearing pad supports (M load case), and the ability to increase sensor signal quality at more locations between the support and the applied load by locating the disturbed region at the concentrated load further into the span. Load cases at $2d_v$ were used to maximize individual girder shear effects at $1d_v$ and maximize displacement of girder bearing pads (to compare the largest LVDT signal to FEM results during validation). Table 5-4 highlights the four standard load cases of interest in each quadrant (i.e., 16 total standard load cases), the measured structural behavior for comparison, and the maximum load effect considered.

In addition to the 16 total standard load cases, specific load cases were selected to further validate structural behavior of the FEM related to the traffic barrier and end diaphragm. To investigate the north barrier (NB) behavior, load cases at $4d_v$ using the North actuator were used to maximize shear and bending in the barrier, minimize torsional effects due to loading between girders, and increase sensor signal quality by locating the disturbed region at the applied load further into the span. To investigate the end diaphragm, load cases at $2d_v$ were used to: maximize bending in the end diaphragm for neutral axis calculation (M load case), divide shear effects from the end diaphragm between two girders (M load case), and maximize shear in the end diaphragm by applying load over an interior

girder (S or N load cases). Table 5-5 lists the specific load cases, the measured structural behavior for comparison, and the maximum load effect considered. Figure 4-20 presents a plan view of the four bridge quadrants that is a useful reference for examining Table 5-5.

FEM displacement data was collected at individual nodes for comparison to LVDT data or for calculation of girder end rotation for comparison to tiltmeter data. FEM shear strain data was collected at the integration point on a specific element for shear strain comparisons at the center of a strain gage rosette. However, VWGs (6 in. gage length) measure shear strain in an average sense compared to a single integration point on an element and foil rosettes (gage length of approximately 1.25 in.). FEM element sizes were approximately 2 in. in the girder and end diaphragm and the shear strain varied by 3 to 5 με at integration points one element higher or lower in the girder web and end diaphragm, as shown in Figure 5-3 and Figure 5-4. Figure 5-3 was generated using FEM results from the LBENE quadrant, at the G2_0.5d_v strain gage location (VWG and foil rosettes), for three load cases (4d_M, 4d_SMN, and 2d_S). The shear strain behavior in Figure 5-3 was representative of that observed in the other three quadrants subjected to similar loading scenarios. Figure 5-4 was generated using FEM results from the LBESW quadrant, at the G34DIA_N foil rosette strain gage location (NW_B, NW_M, NE_B, and NE_M), for three load cases (2d_N, 2d_M, and 2d_S). In all cases, the vertical shear strain variation was approximately linear such that the average of strain from the integration point one element higher and lower in the girder web or end diaphragm averaged to equal the shear strain at the integration point of the element nearest the center of a strain gage rosette.

Laboratory data were compared to FEM results for the two girders located within the bridge quadrant of interest: LBESE and LBESW included G3 and G4 while LBENE and LBENW included G1 and G2. Shear strains from both sides of the girder web were compared to FEM results at various longitudinal locations: 0.5d_v, 1d_v, 2d_v for load applied at 4d_v, and at 0.5d_v and 1d_v for load applied at 2d_v. These locations were selected to avoid disturbed regions in the vicinity of the applied load (i.e., the applied load was at least d_v away from the section of interest in each case). The average of the north and south shear strains (i.e., the shear strain due to applied shear only) was computed and used for validation as discussed in Section 5.3.2.1. Vertical displacement data were compared with

the FEM results at $2d_v$ on both the east (E) and west (W) ends of the bridge along with displacement recorded at midspan as discussed in Section 5.3.2.2.

The LBENW and LBESW quadrants contained a partial depth concrete end diaphragm that was cast simultaneously with the bridge deck. Because the exact stiffness of the connection between the diaphragm and the girders could not be measured, three different FE models were constructed with variations in the end diaphragm fixity to the web of the girders.

The as-built conditions of the laboratory bridge end diaphragm were simualted in the FEM with an end diaphragm that was partitioned and meshed to have areas for surface-to-surface constraints that were approximately equal to the area of rebar acting as a dowel from the end diaphragm through the girder web and top flange. Figure 5-5 shows the girder to end diaphragm connection (with through holes in the laboratory bridge girders) and how the equivalent FEM dowel action areas were partitioned. For data comparison purposes, this type of fixity was referred to as pinned. No contact surface constraints were placed in other areas where the diaphragm and girder interacted; it is possible that the diaphragm concrete could inapporpriately penetrate the girder concrete in these locations. A rigid condition was modeled to simulate the upper bound of connectivity between the end diaphragm and girder web. In this case, the entire north or south face of the FEM end diaphragm was connected to an equivalent area on a girder web using surface-to-surface constraints. Figure 5-6 shows the girder web to end diaphragm connection and how the entire end of a diaphragm was affixed to the web.

A free condition was also modeled to simulate the lower bound of connectivity between the end diaphragm and girder web. In this case, there was no connection simulated between the end of a diaphragm and a girder web. The sole connection between an end diaphragm and the structure was made at the deck to end diaphragm interface. The bottom of deck to top of end diaphragm connection simulated the as-built condition of the structure in that the end diaphragm and bridge deck were cast monolithically.

In the rigid case, the surface-to-surface tie constraints between the end of the diaphragm and the girder web/top flange prevented penetration behavior. In the pinned and free cases, no contact surfaces were defined to prevent parts of the end diaphragm concrete from penetrating the girder concrete. This was assumed because the loading was elastic

and very low level (75 to 150 k). However, small magnitude penetration of end diaphragm concrete and girder concrete was observed in the pinned and free cases. This indicated that the pinned and free cases were lower bounds of the anticipated behavior and that the free cases more closely aligned with a case where no end diaphragm was present.

5.3.2.1 Girder Shear Strain

A positive or negative percent difference of 10 percent or less for the average shear strains in the web or a difference between individual strain readings of 8 με or less was deemed acceptable for girder shear strain validation purposes. Percent difference values may be exaggerated when comparing measured data that is the same order of magnitude as the noise or resolution of the signal. Comparisons of measured and FEM predicted girder shear strains from the four quadrants of the bridge for the four base load cases described in Table 5-4 are displayed in Table 5-6 through Table 5-9. Each of these tables shows the shear strain on each face of the girder web for both laboratory data and FEM results, the average of the shear strains which is the shear strain due to the vertical shear resultant (no effects of torsion), and the percent differences between laboratory data and FEM results.

Table 5-6 through Table 5-9 show that the majority of the averaged FEM results and averaged laboratory shear strain data compared favorably; percent difference values were typically less than 10 percent, even though the differences at each web face may be much larger. Table 5-7 show some differences between individual strain readings greater than 8 με. Outlier percent difference values associated with averaged data and differences in strains greater than 8 με were investigated and, generally, discrepancies could be attributed to a larger than normal noise-to-signal ratio for a single linear strain gage within a rosette (this was particularly evident for the foil rosette at G4_2d_S in Table 5-6). In the LBENW quadrant, averaged girder shear strains for Girder 2 in load case LBENW_4d_N did not match as well as data at other locations (Table 5-9). This was attributed to very low magnitude strains on the south side of Girder 2 (furthest from the applied load) that were not accurately measured by foil strain gages. In the LBESW quadrant (Table 5-8), averaged girder shear strain comparisons at $0.5d_v$ did not match as well as data at other locations. This was attributed to the proximty of $0.5d_v$ to the disturbed region at the end of the girder where the end diaphragm framed into the top flange and web as shown in Figure 5-7.

Data in Table 5-8 shows that the fixity of the end diaphragm in the LBESW finite element results had a negligible effect on the corresponding tabulated girder average shear strains. The laboratory shear strain due to the vertical shear resultant data were not bounded by the different types of end diaphragm fixity. However, concrete penetration was allowed in the pinned and free cases; the behavior in these cases served as a lower than anticipated bound (more similar to no end diaphragm). The rigid case represented an upper bound on the behavior. This indicated that, when considering shear distribution behavior, the connection between the top of the end diaphragm and the bridge deck was more significant than the connection between the end diaphragm and the girder web/top flange. Differences amongst the fixity types did not bound the shear strain readings on each side of the web, which included the effects of torsion. This may be due to the fact that the FEM model did not capture the torsional behavior as accurately as expected.

5.3.2.2 Girder Displacement, Girder Rotation, and Bearing Pad Displacement

Measured girder displacement, rotation, and bearing pad displacement were compared to FEM results in four quadrants at the 75 kip per actuator load level (except SMN load case which was 50 kip per actuator). Girder displacements were recorded at three locations along the span length (at $2d_v$ on both the east and west ends of the span and at midspan.). Girder rotations and bearing pad displacements were measured at the loaded end of the span. Bearing pad vertical displacement data were averaged from four values measured at each corner of the rectangular pad. Finite element models were linear elastic and did not contain bi-linear or nonlinear behavior for the neoprene bearing pad material. The bearing pad was assumed to have a Young's modulus of 17.9 ksi, a Poisson's ratio of 0.49995, and a density of 0.0813 lb /in.^{3} as discussed in Section 3.3.1.

Girder vertical displacement along the span length, rotation at the east or west end, and bearing pad vertical displacements are compared to FEM results in Table 5-10 through Table 5-21. The percent difference between measured laboratory data and FEM results are reported. Percent difference values may be exaggerated when comparing measured data that is the same order of magnitude as the noise or resolution of the signal. Other than the vertical displacement at G3_E_2d in Table 5-10, FEM results and laboratory data compared well for girder displacement, girder rotation, and bearing pad displacement. Percent differences of magnitude 20 to 30 percent may be attributed to comparing data that

was the same order of magnitude as the noise or resolution of the signal. However, in the case of the LVDT measurements for girder or bearing pad vertical displacement, this may not explain the large percent differences. Data in Table 5-16 through Table 5-18 show that the fixity of the end diaphragm in the LBESW finite element results had a negligible effect on the corresponding tabulated behaviors.

5.3.2.3 Traffic Barrier

Barrier shear strains calculated using measured data from a single VWG box-type rosette (including the effects of torsion) from the north side of the traffic barrier were compared to FEM results for model validation in the LBENE_4d_N load case at $0.5d_v$, $1d_v$, and $2d_v$ as shown in Table 5-7. Large percent differences were noticeable, but the results were within approximately 5 to 10 με. Exaggerated differences between FEM results and laboratory data were attributed to the flexural behavior of the barrier outlined in the following discussion.

Measured barrier longitudinal strains through the section due to flexure were compared to FEM results for model validation in the LBENE_4d_N load case at $0.5d_v$, $1d_v$, and $2d_v$ as shown in Table 5-22. This load case produced maximum longitudinal bending in the traffic barrier. The differences between the measured strains and the FEM predicted strains were always within 8 με, which was close to the accuracy of the foil strain gages. Extrapolating the linear trendlines from FEM results to the *y*-axis intercept in Figure 5-8 indicates that the neutral axis of the traffic barrier was approximately 6 to 7.5 in. below the barrier-to-deck interface. Data recorded from the bottom (B) strain gage at $1d_v$ and $2d_v$ did not follow the expected linear trend, shown in Figure 5-8, for use in finding the neutral axis of the composite barrier section. Due to these discrepencies, supplementary data were collected in the LBENW quadrant for barrier FEM validation.

Additional longitudinal VW gages were added to the exterior of the girder bottom flange, girder top flange, traffic barrier near the barrier-to-deck interface, and on the south side of the barrier at $2d_v$ in quadrant LBENW as shown in Figure 5-9. These gages were in addition to the longitudinal gages that made up the box-type rosette and the four longitudinal gages on the north side of the barrier (similar to those in Table 5-22). Data collected from the additional instrumentation was used to investigate the neutral axis (NA) because of the observed nonlinear relationship between longitudinal strain and height in

the barrier shown in Figure 5-8. Loading after the installation of the additional gages was primarily over the exterior girder at $4d_v$ in the LBENW_4d_N load case. This load case produced the least amount of torsion in the exterior girder, as shown in Table 5-3, and the maximum amount of shear and bending in the barrier.

Longitudinal strains from the VWGs through the section depth are shown in Figure 5-9. A linear trendline from FEM results and the single point at which both the lab data and FEM results cross the *y*-axis were used to estimate the neutral axis location to be between 38 and 41 in. above the bottom of the composite cross section. This was equivalent to approximately 5 to 8 in. below the barrier-to-deck interface. Data from the barrier in the LBENE quadrant also indicated that the barrier neutral axis was approximately 6 to 7.5 in. below the barrier-to-deck interface.

Figure 5-9 shows that the laboratory longitudinal strains exhibited a nonlinear behavior with height through the cross section in the barrier, near the change in cross section width. The vibrating wire strain gages added to the south side of the barrier were used to double check the unusual behavior. As expected, FEM results predicted the strains to vary linearly through the depth of the cross section. To further investigate the nonlinear relation between strain and depth, additional load cases using combinations of actuators were investigated with the increased barrier instrumentation. Data from loading with the north and middle actuator (LBENW_4d_NM) and from loading with the south, middle, and north actuators (LBENW_4d_SMN) are shown in Figure 5-10 (data are from the same instruments used to generate Figure 5-9). The north and south barrier data indicated that the neutral axis was in approximately the same vertical location, 36 in. above the bottom of the composite section. However, the nonplanar behavior was still visible in the barrier cross section near the thickness change. The reason for the nonplanar behavior was not determined. This behavior was likely not due to the precense of the end diaphragm and was observed throughout the experimental portion of the project (lab data and field data).

Discussion related to the effects of the traffic barrier on shear distribution, beyond FEM validation, are presented in Section 5.3.3.

5.3.2.4 Partial Depth End Diaphragm

Measured strains produced by longitudinal bending along the length of the end diaphragm when loading with the middle actuator at $2d_v$ and $4d_v$ were compared to FEM

results for model validation. Details regarding the end diaphragm instrumentation were shown in Figure 4-25. Three horizontal strain gages were applied through the depth of each end diaphragm (and composite bridge deck above the end diaphragm) at midspan of the diaphragm; the gages were referred to as bottom strain gage (B), middle strain gage (M), and strain gage on the top of the deck (Tdeck). The three strain gages were used to determine the neutral axis of the end diaphragm. Data in Table 5-23 for LBESW show that the partial depth end diaphragm behaved somewhere between the pinned and free FEM models for LBESW; data in Table 5-24 for LBENW are compared to FEM pinned results. The end diaphragm was modeled as contiguous with the deck, but the conditions adjacent to the girder web were modeled as free, pinned, or fixed. However, concrete penetration was allowed in the pinned and free cases; the behavior in these cases served as a lower than anticipated bound (more similar to no end diaphragm). The surface-to-surface tie constraints in the rigid case did not allow concrete penetration and represented an upper bound on the behavior. Figure 5-11 shows that the neutral axis of the end diaphragm was approximately 15 in. above the bottom of the cross section.

End diaphragm average shear strains produced when loading at $2d_v$ with any single actuator (S over G4, M between G3 and G4, or N over G3) were also compared to FEM results for model validation in the LBESW and LBENW quadrants. Similar to the girder instrumentation, data from two foil strain gage rosettes were averaged at various locations on the end diaphragm to negate torsional effects and calculate the shear strain due to the vertical shear resultant, γ_{xy_shear}. Average measured values in Table 5-25 and Table 5-26 compared well to the FEM results and differences between the measured data and the FEM results assuming a pin connection were never larger than 7 με. In general, the partial depth end diaphragm behaved somewhere between the pinned and free FEM models considering end diaphragm averaged shear strain behavior for the specific load cases discussed in Table 5-5.

Discussion related to the effects of the end diaphragm on shear distribution, beyond FEM validation, are presented in Section 5.3.4.

5.3.3 Effects of Traffic Barrier on Elastic Shear Distribution

Puckett et al. (2007) noted that secondary bridge elements such as traffic barriers can have a significant impact on lateral load distribution. However, Puckett et al. (2007)

stated that the literature shows conflicting results with respect to their degree of effectiveness. Previous work has been completed to characterize the effect of traffic barriers on flexural distribution (Eamon and Nowak 2002, Conner and Huo 2006, Akinci et al. 2008, Roddenberry et al. 2011) but a more detailed picture of how traffic barriers affect shear distribution was warranted. Validation of a FE modeling technique considering a traffic barrier was discussed in Section 5.3.2.3 and data from laboratory testing corroborated well with FEM results. The impact of a traffic barrier on lateral shear distribution was studied in depth using the FEM of the laboratory bridge and results are presented in this section. Finite element shear forces were calculated as outlined in Section 3.3 and the percent of applied shear was calculated by dividing the shear force in any single girder or the traffic barrier by the reaction calculated from statics for a beam line analysis subjected to the same amount of load; a beam line analysis refers to the bridge idealized as a 1D structure along its length to determine the shear across a section of the bridge. The force in the traffic barrier was taken as the sum of nodal forces in the barrier cross section only, the shear in the deck overhang was assigned to the exterior composite girder, not the barrier.

The effect of the north barrier (NB) on the percent of applied shear was studied with FEM results for a laboratory bridge quadrant that contained (LBENE) and did not contain a barrier (LBESE). The results were generated from loading at $4d_v$ and collected at transverse cross sections corresponding to $0.5d_v$, $1d_v$, $2d_v$. Results from loading at $2d_v$ were not included because fewer cross sections of interest were d away from the load to avoid disturbed regions. Specific cases for comparison are shown in Table 5-27 with highlighted cells, noting that the loading geometry and actuator naming was mirrored about the centerline of the bridge longitudinally. Of particular importance is the comparison between LBENE_4d_N and LBESE_4d_S (highlighted in blue), LBENE_4d_NM and LBESE_4d_SM (highlighted in gray), and LBENE_4d_SMN and LBESE_4d_SMN (highlighted in purple). The results indicate that the traffic barrier may carry up to 19 percent of the total shear force if load was applied directly above the exterior girder with a single actuator (N/S load case). Results in Table 5-27 indicate that the exterior composite girder, when the barrier was present, carried 70 percent of the total shear at d_v compared to 89 percent of the total shear when the barrier was not present. The traffic barrier carried

between 10 and 14 percent of the shear force when load was applied with multiple actuators between the exterior and interior girders in the SMN load case and NM/SM load case, respectively. Results in Table 5-27 indicate that the exterior composite girder, when the barrier was present, carried between 41 and 55 percent of the total shear at d_v (for the SMN and the NM/SM load cases, respectively) compared to 50 to 68 percent of the total shear when the barrier was not present (for the SMN and the NM/SM load cases, respectively).

The traffic barrier had a negligible effect on the interior girder shear distribution. This can be seen in Table 5-27 comparing FEM results from LBENE_4d_S and LBESE_4d_N (highlighted in green) and results from LBENE_4d_SM and LBESE_4d_NM (highlighted in yellow). While the percent of applied shear in the exterior girder slightly changed in these loading scenarios, the percent of applied shear in the interior girder did not change at all. The shear force load sharing benefits of a traffic barrier were limited to the exterior girder. Results in Table 5-27 also indicated that the sum of shear in the barrier and the exterior girder (LBENE) was equal to the shear carried by the exterior girder when no barrier was present (LBESE).

In summary, results from this study have shown that a traffic barrier carried up to 19 percent of the shear in a transverse cross section of the bridge when the force was applied above the exterior girder. However, the shear distribution effects from a traffic barrier diminish quickly when load was not applied near the barrier. It is conservative to ignore the effects of a traffic barrier on shear distribution; furthermore, the traffic barrier had no effect on the interior girder shear distribution.

5.3.4 Effects of Partial Depth End Diaphragm on Elastic Shear Distribution

One end of the laboratory bridge was constructed with a partial depth end diaphragm placed simultaneously with the bridge deck and connected to the girder with dowels placed transversely to the girder through the top flange and web. Validation of an FE modeling technique considering an end diaphragm was discussed in Section 5.3.2.4 and data from laboratory testing corroborated well with FEM results. The impact of the end diaphragm on lateral shear distribution was studied in depth using the FEM of the laboratory bridge and results are presented in this section. Results in the following discussion were generated with the rigid diaphragm-to-girder connection as discussed in

Section 5.3.2. This connectivity was selected to eliminate the concrete penetration that was allowed in the other FEM validation connectivity cases (free and pinned).

Previous research has been done to investigate the effects of end diaphragms and intermediate diaphragms on shear distribution. Bae and Oliva (2012) specifically considered the effect of end diaphragms on shear load distribution from overload trucks and reported that end diaphragms increased shear distribution factors by up to seven percent compared to bridges without an end diaphragm. Meaning, the most heavily loaded composite girder section (including the deck) may carry more shear and distribute less to adjacent girders. Furthermore, conflicting numerical analysis results were presented by Huo et al. (2003) and Puckett et al. (2007) in their studies of Bridge No. 24, which was a prestressed concrete girder bridge described by Huo et al. Results from Huo et al. (2003) indicated that abutment support diaphragms caused a decrease in the shear distribution factor in conflict with the study done by Puckett et al. (2007) that indicated abutment support diaphragms slightly increased the shear distribution factor.

To investigate the effect of the partial depth end diaphragm on shear distribution in this study, FEM results are compared for the end of the laboratory bridge with no end diaphragm (LBESE) and the end of the bridge with an end diaphragm (LBESW). The results were generated from two load cases at $4d_v$, utilizing either the north (N) actuator over interior girder G3 or the south (S) actuator over exterior girder G4. Shear forces in the composite section (including shear in the deck) were collected at transverse cross sections corresponding to $0.5d_v$, $1d_v$, $2d_v$. Shear forces were obtained from the FEM nodal forces using methods discussed in Section 3.3.2 and a composite deck width equal to the girder spacing as discussed in Section 5.2. The results shown in Table 5-28 from loading above both the interior and exterior composite girder indicated that the percent of applied shear would be larger if load was applied closer to the end of the bridge with the diaphragm compared to the end of the bridge without the diaphragm. Results indicated that approximately 4 percent more applied shear was carried in the exterior composite girder with an end diaphragm present and approximately 6 percent more applied shear was carried in the interior composite girder with an end diaphragm present. Each cross section along the length had similar percent increases. An increase of 4 to 6 percent applied shear is not

significant, but it does indicate that the end diaphragm acts to keep shear in the loaded composite girder rather than distributing it to adjacent composite girders.

To further examine the effect of the end diaphragm, shear force results from the validated FEM were tabulated separately for each bridge girder (no deck) and the corresponding composite deck section (no girder). However, to amplify the effect of the diaphragm and study the upper bound, the FE model was rerun using the fixed partial depth end diaphragm after increasing the modulus of elasticity of the diaphragm by a factor of 10. This modification also increased the shear modulus by a factor of 10 because an isotropic material model was used for the diaphragm concrete. Results are presented in Table 5-29 for the laboratory bridge quadrant that contained no end diaphragm and in Table 5-30 and Table 5-31 for the quadrant that contained an end diaphragm. Results in Table 5-30 were generated using the fixed partial depth end diaphragm; Table 5-31 shows the results generated using the stiffened end diaphragm. The left set of tables shows the percent of applied shear generated for the girder cross section only and the right set of tables shows the percent of applied shear for the bridge deck only. Addition of the girder shear and deck shear in Table 5-29 yields results from LBESE (without an end diaphragm) in the left half of Table 5-28; addition of the girder shear and deck shear in Table 5-30 yields results from LBESW (with an end diaphragm) in the right side of Table 5-28.

Comparison of the percent of applied shear for the exterior girder with no end diaphragm, with the as-built end diaphragm, and with the stiffened end diaphragm (highlighted in green in the left side of Table 5-29 through Table 5-31) indicate that as the end diaphragm stiffness was increased, the percent of applied shear at $0.5d_v$ near the end of the span decreased from 69 to 68 percent while the percent of applied shear at $2d_v$ near the loading point increased from 71 to 79 percent. Furthermore, the opposite trend was evident in the percent of applied shear calculated for the exterior girder composite deck as the stiffness of the end diaphragm changed (highlighted in orange in right side of Table 5-29 through Table 5-31). As the end diaphragm stiffness increased, the percentage of shear that the bridge deck carried increased from 21 to 30 percent at the end of the girder near the support. The same trend was revealed in a comparison of the percent of applied shear for the interior girder (highlighted in blue in the left side of Table 5-29 through Table 5-31). Results indicated that as the end diaphragm stiffness was increased, the percent of applied

shear carried by the girder at $0.5d_v$ near the end of the span decreased from 51 to 50 percent while the percent of applied shear carried by the girder at $2d_v$ near the loading point increased from 58 to 68 percent. Similar to the exterior girder, the opposite trend was evident in the percent of applied shear calculated for the interior girder composite deck (highlighted in gray in right side of Table 5-29 through Table 5-31). As the end diaphragm stiffness increased, the percentage of the applied shear carried by the bridge deck increased from 18 to 32 percent at the end of the girder near the support.

Results from the validated FEM indicated that the end diaphragm increased the amount of shear force in the girder near the point of applied load but slightly decreased the amount of shear force in the girder near the end of the span when load was applied over the girder. However, results in Table 5-28 indicated that the distribution of the percent of applied shear did not change significantly (6 percent or less) amongst composite girders; the amount of shear force carried in the deck and girder changed. For this length structure and loading scenario, the end diaphragm increased the amount of load carried to the end of the span through the bridge deck rather than through the girder. This behavior, observed with results from the upper bound, stiffened diaphragm case, indicated that more shear remained in the deck until the very end of the span, near the reaction, and transferred to the support through the end diaphragm or the girder web at the very end of the span. In this region, the girder has additional shear capacity because it experiences vertical compression due to the load and reaction. This conclusion assumed a fixed condition connecting the end diaphragm to the girder web and was also drawn from a single bridge with a specified length and an upper bound end diaphragm stiffness (10 times the measured Young's modulus).

Cai et al. (2002) and Cai and Shahawy (2004) indicated that the as-built diaphragm stiffness in bridges is uncertain due to possible concrete cracking and weakness of the diaphragm-to-girder connection. Cracking at the end diaphragm-to-girder connection was seen in this project during field testing, shown in Figure 5-12, and during inelastic laboratory testing as discussed in Section 5.4. End diaphragm cracking was also observed during field visual inspection conducted by Dereli et al. (2010). These issues create many unknowns related to the effect of end diaphragms on load distribution of in-service bridges.

In summary, the end diaphragm acted to increase the amount of shear carried to the end of the span via the deck rather than the girder; however, the shear force in the short shear span carried by the composite girder section increased by 4 to 6 percent when the end diaphragm was present. It was shown to be slightly inaccurate to ignore the effects of an end diaphragm when considering elastic bridge behavior in prestressed concrete girder structures, but neglecting the effects of an end diaphragm may still be warranted to increase the speed and ease of modeling a structure using FEM without sacrificing a significant amount of accuracy. Additional discussion related to the effects of an end diaphragm are presented in Section 5.4.3 related to testing of the laboratory bridge through the inelastic range.

5.3.5 Summary and Conclusions of Elastic Bridge Testing

Measured data indicated that the shear strain due to torsion was approximately 40 percent of the magnitude of shear strain due the vertical shear resultant for the laboratory loading scenario most likely to cause torsion in adjacent girder webs (a single point load applied between the interior and exterior girder). Loading scenarios that used a single actuator above a girder generated shear strains due to torsion that were approximately 62 to 74 percent of the shear strain due to the vertical shear resultant in the adjacent girders (without the actuator loading above); however, the magnitude of the shear strain due to the vertical shear resultant was lower in the adjacent girder in this loading scenario compared to the magnitude of shear strain due to the vertical shear resultant generated from loading between girders. Loading scenarios in the laboratory bridge (load applied with a single actuator or combination of three actuators in a small, concentrated footprint) were different than those that would be encountered on a field bridge (load applied with vehicles that typically contain many individual tires contacting the bridge deck in a large footprint), but the effects of torsion may still be present. Laboratory data indicated that well-connected, stiff intermediate diaphragms may provide bracing to limit torsion effects in the webs of prestressed concrete girders. Chapter 6 presents an additional study of torsion due to truck loading on FEM models of the field bridges and a discussion about the effects of intermediate diaphragms in field bridge finite element models.

A study was conducted using the validated FEM to better understand the effect of traffic barriers on shear distribution. Shear force results from the FEM indicated that the

traffic barrier carried up to 19 percent of the total shear force at d_v when the load was applied directly above the exterior girder in this bridge geometry with a specific girder spacing and overhang. The traffic barrier had a negligible effect on the percent of applied shear in the interior girder. This behavior supports AASHTO LRFD Section 4.6.3 which states that "A structurally continuous railing, barrier, or median, acting compositely with the supporting components, may be considered to be structurally active at service and fatigue limit states. This provision reflects the experimentally observed response of bridges. This source of stiffness has traditionally been neglected but exists and may be included, provided that full composite behavior is assured." Within the context of this study, if composite action between the barrier and deck is verified through the use of details similar to those shown in Figure 4-7 and visual inspection that does not indicate cracking, composite action between the barrier and exterior girder may be assumed to decrease the percent of applied shear in the exterior girder . The decrease in percent of applied shear is also dependent on the type of barrier and relative depth of the girder. However, it is conservative to ignore the effects of the traffic barrier when calculating live load distribution for shear.

A goal of elastic testing was to determine if the partial depth end diaphragm had an effect on the shear distribution at elastic levels. Three types of fixity between the girder web and end diaphragm were considred for FEM validation: rigid, pinned, and free. However, concrete penetration was allowed in the pinned and free cases; the behavior in these cases served as a lower bound (more similar to no end diaphragm). The rigid case represented an upper bound on the behavior. In general, the differences between the three types of fixity were minimal, but measured data indicated that the partial depth end diaphragm behaved somewhere between the pinned and free FEM models considering end diaphragm average shear strain behavior, torsional behavior, and flexural bending behavior.

The shear force in the short shear span carried by the most loaded composite girder section increased by 4 to 6 percent when the end diaphragm was present compared to results when no end diaphragm was present. Shear distribution results from finite element models of prestressed concrete girder bridges that ignore the effects of an end diaphragm on shear distribution may be inaccurate by 4 to 6 percent. However, neglecting the effects

of an end diaphragm may still be warranted to increase the speed and ease of modeling a bridge using FEM without sacrificing a significant amount of accuracy.

Results from the validated FEM with the girder and deck separate indicated that the end diaphragm increased the amount of shear force in the girder near the point of applied load but decreased the amount of shear force in the girder near the end of the span. The end diaphragm did not affect the amount of shear force in the deck near the point of applied load but increased the amount of shear force in the deck near the end of the span. This behavior occurred because the end diaphragm attracted shear force toward the support through the deck; shear remained in the deck until the very end of the span, near the reaction, and transferred to the support through the end diaphragm or the girder web at the very end of the span. In this region, the girder has additional shear capacity because it experiences vertical compression due to the load and reaction. The literature (Cai et al. 2002, Cai and Shahawy 2004) and previous research at the University of Minnesota (Dereli et al. 2010) indicated that the as-built diaphragm stiffness in bridges may be uncertain due to possible concrete cracking and weakness of the diaphragm-to-girder connection, as discussed in Section 5.3.4. This creates unknowns as to how well end diaphragms redistribute load compared to pristine laboratory conditions and FE models.

5.4 Bridge Inelastic Testing

Testing in the inelastic range provided the ability to investigate if an interior girder shed shear force to adjacent girders as that girder transitioned from uncracked to cracked to ultimate behavior. The ultimate shear capacities were compared to the capacities predicted by AASHTO Specifications, and data from testing a single companion girder to ultimate in shear were used to compare ultimate shear capacity of the same beam within a bridge system and as a single member.

To achieve the objectives, two inelastic tests were conducted on the laboratory bridge in diagonally opposite quadrants. Prior to inelastic testing, the traffic barrier was saw cut off of the bridge to create a symmetric transverse cross section. The two ends of the bridge still differed to investigate the effect of the end diaphragm as the bridge was taken to ultimate. The quadrant that included an end diaphragm, LBUW, was tested first and the quadrant with no end diaphragm, LBUE, was tested second. Any damage to the

bridge deck or to the west end of Girder 3 from LBUW testing were inherently present during LBUE testing.

5.4.1 Ultimate Testing Load Histories

During both inelastic tests, a patch load was applied to the specimen using a combination of two 110 kip actuators and one 220 kip actuator. The 110 kip actuators were operated in force control and slaved to one half of the 220 kip actuator force, with the 220 kip actuator operated in displacement control. Details of the test setup were discussed in Section 4.6.2. The LBUW testing focused on the end of the span with the partial depth end diaphragm. For this test, the patch load was applied over interior Girder 3. The LBUE testing focused on the end of the span without the end diaphragm with the patch load applied over interior Girder 2. During both tests, the patch load was applied a distance of 9 ft 7 in. from the centerline of the nearest girder bearing (a/d of 2.5) and 21 ft 2 in. from the centerline of the farthest girder bearing.

Test nomenclature for both the CE DAQ and the CR1000 DAQ during inelastic testing was very similar to, but simpler than, the nomenclature for elastic testing discussed in Section 5.3. Inelastic testing nomenclature only included the calendar date on which the test was performed and the test name (LBUW or LBUE for Lab Bridge Ultimate West or East).

5.4.1.1 Lab Bridge Ultimate West (LBUW)

The displacement controlled load history for LBUW is given in Table 5-32. The LBUW testing procedure, completed on December 8, 2014, is summarized in the following sequence. Load was applied in 25 kip increments up to 200 kips to record linear elastic strain and displacement behavior. The first web-shear crack was observed in the west end of Girder 3 at approximately 225 kips of applied load. After observing the first web-shear crack, testing was continued and cracks were marked with permanent marker and tagged with the current applied load. The initial flexural crack was observed under the point load at approximately 275 kips applied load. Web-shear cracking and damage increased as load was applied to 325 kips. After data collection at 325 kips, the applied load was reduced to 10 kips to determine if web-shear cracks remained visible with near zero applied load. The primary web-shear crack decreased in width from 0.023 in. at 325 kips applied load to

0.009 in. at 10 kips applied load and was still visible in the region of the girder with 24 in. stirrup spacing. Visibility of web-shear cracks is highly dependent on the level of applied load and the stirrup spacing. These results were consistent with web-shear crack behavior observed by Mathys et al. (2014); Mathys et al. found that web-shear cracks in areas with widely spaced stirrups (approximately 24 in.) were still visible upon unloading, and web-shear cracks in areas with closely spaced stirrups (approximately 8 in.) were not visible upon unloading. Data were collected during re-loading of the structure and additional cracks were marked as the applied load surpassed 325 kips.

Web-shear crushing and bridge deck punching occurred after reaching a peak load of approximately 444 kips applied load. Following the punching failure, the applied load dropped quickly due to a loss of girder stiffness and deck punching, and the structure was unloaded in displacement control. Bridge girder displacement, girder rotation, and bearing pad displacement behavior during LBUW are documented in Appendix E. The flexural capacity (approximately 2,860 kip-ft as discussed in Section 4.2.1) was not approached during testing. Crack patterns and web-shear deterioration observed in Girder 3 can be seen in Figure 5-13, where 12 of the 15 stirrup strain gages within the shear span (indicated by filled in dots in Figure 5-13) exceeded the predicted yield strain for LBUW as detailed in Appendix E. No web-shear or flexural cracking was observed in any other bridge girder. The lack of web-shear cracking in adjacent girders was confirmed with stirrup strain gage data that indicated near zero tensile strain in the stirrups throughout LBUW. Bridge deck punching and web-shear crushing led to ultimate failure in Girder 3 as shown in Figure 5-14 through Figure 5-16. However, the order in which deck punching and web-shear crushing occurred was not directly observed as the two events happened nearly simultaneously. Diagonal cracks in the end diaphragm between Girder 3 and Girder 4 and also between Girder 2 and Girder 3 as shown in Figure 5-17 and Figure 5-18 were observed at approximately 350 to 400 kips applied load (failure occurred at approximately 444 kips applied load).

5.4.1.2 Lab Bridge Ultimate East (LBUE)

The displacement controlled loading history for LBUE is given in Table 5-33. The testing procedure, completed on December 17, 2014, is summarized in the following sequence. Load was applied in 25 kip increments up to 225 kips to record linear elastic

strain and displacement behavior. The first web-shear crack was observed in the east end of Girder 2 at an applied load of approximately 232 kips. After observing the first web-shear crack, testing was continued and cracks were marked with permanent marker. Web-shear cracking and damage increased as load was applied to 250 kips. After data collection at 250 kips, the girder applied load was reduced to 10 kips to determine if web-shear cracks remained visible with near zero applied load. The primary web-shear crack decreased in width from 0.014 in. at 250 kips applied load to 0.004 in. at 10 kips applied load and was still visible in the region of the girder with 24 in. stirrup spacing. Data were collected during re-loading of the structure and additional cracks were marked as the applied load surpassed 250 kips. The initial flexural crack was observed under the point load at approximately 300 kips.

Web-shear crushing and bridge deck punching occurred after reaching a peak load of approximately 452 kips. Following failure, the applied load dropped quickly due to a loss of girder stiffness and deck punching, and the structure was unloaded in displacement control. Bridge girder displacement, girder rotation, and bearing pad displacement behavior during LBUE are documented in Appendix E. The flexural capacity (approximately 2,860 kip-ft as discussed in Section 4.2.1) was not approached during testing. Crack patterns and web-shear deterioration observed in Girder 2 can be seen in Figure 5-19, which indicated that that 8 of the 15 stirrup strain gages within the shear span (indicated by the filled in dots in Figure 5-19) exceeded the predicted yield strain for LBUE as detailed in Appendix E. No web-shear or flexural cracking was observed in any other bridge girder, and the lack of web-shear cracking in adjacent girders was confirmed with stirrup strain gage data that indicated near zero tensile strain in the stirrups throughout LBUE. Bridge deck punching and web-shear crushing both precipitated ultimate failure in Girder 2 as shown in Figure 5-15, Figure 5-16, and Figure 5-20. However, similar to LBUW, the order in which deck punching and web-shear crushing occurred was not directly observed.

5.4.2 Shear Distribution in the Inelastic Range

Shear distribution behavior in the inelastic range was characterized using shear forces calculated from measured rosette strain gage data obtained on the girder web. Vibrating wire strain gage box-type rosettes were installed on the girder web at $0.5d_v$, $1.0d_v$,

or 2.0d_v along the length of the beam. Foil strain gage rosettes were installed at the same longitudinal positions but were located on the opposite face of the web. Data collected from the VWG box-type rosettes and the foil rosettes were averaged to negate torsional effects and were used to calculate shear strain due to the vertical shear resultant, γ_{xy_shear}. Linear elastic shear forces in the short shear span due to live load for each girder were calculated using γ_{xy_shear} as discussed in Section 5.2. The effects of dead load are not included in this analysis and discussion. Material and cross-sectional properties used for calculation of elastic shear force in the short shear span are given in Table 5-34 and previously in Table 4-2. The sum of elastic shear force from each of the four girders in the short shear span was within 5 percent of the live load reaction calculated with statics. Differences were likely due to the assumption of effective slab width equal to the girder spacing and error in the measured material properties. When the loaded girder (Girder 3 in LBUW and Girder 2 in LBUE) developed web-shear cracking in the web, the rosette strain gage instrumentation was no longer used to calculate shear force in the short shear span on the cracked girder. However, the shear force in the short shear span of the damaged girder was calculated by subtracting the sum of shear forces in the short shear span in the remaining undamaged girders from the total shear force in the short shear span calculated using statics and a beam line analysis with a single applied patch load, where in the bridge was idealized as a 1D structure along its length to determine the shear across a section of the bridge. This technique of calculating shear forces to characterize shear distribution was used to near ultimate failure, prior to deck punching; this methodology would become unreliable if multiple girders developed web-shear cracking.

The total applied load versus the shear force in the short shear span calculated using data from rosette strain gages is shown in Figure 5-21 through Figure 5-23 for LBUW and in Figure 5-24 through Figure 5-26 for LBUE. In both sets of figures, the calculated interior girder response was plotted from the initial loading step to the final loading step (just prior to ultimate failure). Comparison between this calculated shear force in the interior girder and the shear force derived in the elastic range using the strain rosette on the interior girder shows that the two methods of determining shear force produce similar results, with the largest difference observed at 0.5d_v during LBUW. Changes in the slope of the response for each girder (which indicates changes in transverse shear distribution) occurred

approximately when web-shear cracking was observed in the loaded girder. The presence of disturbed regions near the support and applied load may have affected the data at $0.5d_v$ and $2d_v$.

At the critical section, d_v, Figure 5-22 and Figure 5-25 show that approximately 20 and 22 kips of shear force in the short shear span (out of approximately 290 kips total shear) were redistributed to each girder adjacent to G3 and G2 as the loaded beam cracked and failed for LBUW and LBUE, respectively. The linear elastic response of the loaded girder was extrapolated beyond cracking using a best fit line of the linear elastic data (from 50 to 150 kips applied load) to highlight the loaded girder loss of stiffness and shear redistribution when the slope of the applied load versus shear force data changed after web-shear cracking. When web-shear cracks were observed, the live load shear demand calculated using measured data from the loaded girder was approximately 121 and 126 kips for LBUW and LBUE, respectively. Furthermore, an assumption of bilinear behavior in the loaded girder data (linear elastic until web-shear cracking and linear at a different slope after cracking until failure) was used to calculate the shear force at ultimate failure. Strain at failure could not be measured by the VWGs or recorded by the CR1000 DAQ due to the prolonged time needed to collect five cycles of VWG data. Figure 5-22 and Figure 5-25 show the best fit line used to extrapolate the data after cracking until failure (fit to calculated data after web-shear cracking until approximately 425 kips applied load, which was the last load step before failure). The shear force in the girder at failure was calculated using the measured applied load and the slope and *y*-intercept of the best fit line. The calculated shear force in the short shear span at the critical section of Girder 3 was approximately 206 kips at LBUW failure (using an applied load of 444 kips) and at the critical section of Girder 2 was approximately 211 kips at LBUE failure (using an applied load of 452 kips). The LBUW test (conducted first chronologically) was stopped immediately after deck punching to avoid further damaging the structure prior to LBUE testing (conducted second). This may be the reason for the slight difference between calculated shear forces in the short shear span at failure.

Data in Figure 5-22 and Figure 5-25 indicate that the shear in the loaded girder redistributed transversely after observation of web-shear and flexural cracks and before

ultimate failure. The redistribution of shear continued to increase as the damaged girder stiffness decreased.

5.4.3 Effects of Partial Depth End Diaphragm on Inelastic Behavior

LBUW testing focused on the end of the bridge with a diaphragm. Quantitatively, the ratio of LBUE live load shear demand to LBUW live load shear demand shown in Table 5-35 indicated that the end diaphragm had a minimal effect on the cracking loads and the ultimate failure loads; the ratio was 1.03 for web-shear cracking, 1.09 for flexural cracking, and 1.02 for ultimate capacity. The live load shear demand at observed web-shear cracking, observed flexural cracking, and ultimate failure were slightly lower for LBUW (with the end diaphragm). Data indicated that near ultimate failure, load had been redistributed in tests with and without an end diaphragm to approximately the same shear force at the critical section of the loaded girder (hence the similar peak loads at failure). This behavior indicated that, while an interior girder may carry more load when an end diaphragm is present, the shear force redistributed such that near ultimate failure the behavior was similar with and without an end diaphragm.

Qualitatively, Figure 5-27 and Figure 5-28 show that the web-shear cracking pattern was different for the LBUW test with the diaphragm when compared to the LBUE test without the diaphragm. Figure 5-27 shows that the end diaphragm present during LBUW testing focused shear cracking higher in the web and toward the support centerline rather than toward the face of the support. The web-shear cracking pattern shown in Figure 5-27 extensively penetrated the top flange and engaged more of the bridge deck above the web along the shear span where three of the four stirrups are highlighted. However, the web-shear cracking pattern in Figure 5-28 only penetrated the top flange and engaged the bridge deck above the web near the applied load where two of the four stirrups are highlighted. Furthermore, Figure 5-28 shows bottom flange section loss during LBUE at ultimate failure where the concrete spalled off near the bottom layer of prestressing strands at the interior face of the support (sole plate). The bottom flange section loss in LBUE testing may have occurred because load continued to be applied after deck punching during LBUE and not during LBUW, which was stopped to preserve the structure for future testing.

5.4.4 Comparison of Predicted and Measured Bridge Response

A goal of inelastic testing was to compare the ultimate shear capacity of the loaded bridge girders to the capacity predicted by AASHTO Specifications. To achieve this goal, the predicted and measured capacity was considered in terms of the live load shear demand (and thus applied load) required to achieve shear failure. The applied live load and the shear demand in bridge girders in the elastic range (and indirectly in the inelastic range) were measured in the laboratory during LBUW and LBUE. The following discussion presents the predicted and measured response at ultimate behavior followed by a similar discussion for web-shear cracking; the behavior at ultimate failure was of primary interest due to the shear redistribution that occurred after cracking.

The predicted ultimate shear capacity of the interior composite bridge girder was calculated at $h_c/2$ from the face of the support using Section 9.20 of the AASHTO Standard Specification (2002), measured material properties for inelastic bridge testing discussed in Section 4.4, cross-sectional properties given in Table 5-34 and Table 4-2, and shear distribution factors calculated in accordance with Section 3.23.1 of the 2002 AASHTO Standard; however, use of the AASHTO distribution factors to distribute the total cross-sectional live load (LL) shear demand due to a single patch load to an individual girder in the laboratory bridge is not the intention of the AASHTO Specifications. The AASHTO Standard distribution factors are meant to be used in conjunction with the HS20 design truck or lane load and not an individual patch load. Furthermore, as discussed in Section 4.2.1, it has been shown that a girder shear capacity at ultimate may be approximately 30 percent greater than would be predicted using the nominal shear capacity from the AASHTO Standard Specifications (Hawkins et al. 2005, Runzel et al. 2007).A factor of $1.3V_n$ was not used in the following discussion because it is not included in the AASHTO Specifications. However, the methods used to compare the predicted and measured interior girder live load shear demand are discussed herein.

The predicted shear capacity of the interior composite girder, V_n, was 160 kips. The shear demand ($V_{DL}+DF_{shear}*V_{LL}$) was composed of both dead and live loads. The dead load shear due to the bridge deck was proportioned to the interior girder as a distributed load using tributary areas equal to the girder spacing. The interior girder shear demand due to

dead load was calculated using statics and the girder span length (V_{DL} equal to approximately 18 kips from the girder and composite deck).

The predicted interior girder live load shear demand (DF_{shear}*V_{LL}) was estimated using the AASHTO Standard shear distribution factor multiplied by the total shear demand in the bridge cross section (V_{LL}) in the short shear span. The bridge cross-sectional live load shear demand required to cause shear failure in the short shear span (V_{LL} equal to approximately 176 kips) was calculated from an applied live load of 255 kips located 9 ft 7 in. from the centerline of bearing (a/d of 2.5) using statics and a beam line analysis (the bridge is idealized as a 1D structure along its length to determine the shear across a section of the bridge). The bridge cross-sectional live load shear was distributed to the interior girder using the AASHTO Standard shear distribution factor calculated with the "S-over" equation for two lanes loaded (equal to 0.82 lanes per beam using S divided by 5.5 for this bridge type and lane loading) because the two lanes loaded case would maximize the interior girder shear demand in accordance with the AASHTO Standard. The AASHTO distribution factor for a single lane loaded, which represents one HS20 truck, may be related to an applied load geometry more similar to that used in the laboratory (a single truck has fewer tire patch loads and is thus more representative of a single patch load). Use of the distribution factor for a single lane loaded (equal to 0.64 lanes per beam using S divided by 7 for this bridge type and lane loading) would have indicated more shear distribution due to a smaller distribution factor.

The measured interior girder live load shear demand (in addition to the inherent dead load shear demand) may not have been the force that was required to cause girder ultimate shear failure because deck punching and web-shear crushing happened nearly simultaneously as described in Section 5.4.1. If the deck had not punched, the most heavily loaded interior girder may have been able to carry more shear or the bridge system may have re-distributed more shear prior to ultimate failure. However, the measured interior girder live load shear demand at ultimate failure for LBUW and LBUE testing was estimated using the applied live load at failure (444 and 452 kips for LBUW and LBUE, respectively) and a linear approximation for the post-cracking behavior as discussed in Section 5.4.2. Figure 5-22 and Figure 5-25 show that the shear force at d_v in the loaded girder at failure was 206 and 211 kips for LBUW and LBUE, respectively.

The predicted behavior at web-shear cracking was calculated similarly to the behavior at ultimate capacity. The predicted web-shear concrete capacity, V_{cw}, was approximately 113 kips; this value was calculated using the 2002 AASHTO Standard Specifications. To initiate web-shear cracking, the dead load shear demand (V_{DL}) and the interior girder live load shear demand ($DF_{shear}*V_{LL}$) must exceed V_{cw} (i.e., $V_{DL}+ DF_{shear}*V_{LL} > V_{cw}$). The dead load shear demand (equal to approximately 18 kips) was included in the calculations because it was applied to the laboratory structure prior to live loading and contributed to the formation of observed web-shear cracks. The predicted interior girder live load shear demand ($DF_{shear}*V_{LL}$) was estimated using the two lanes loaded AASHTO Standard shear distribution factor multiplied by the shear demand in the bridge cross section (V_{LL}). The predicted bridge cross-sectional live load shear demand required to cause web-shear cracking in the short shear span (V_{LL} equal to approximately 117 kips) was calculated using statics and a beam line analysis with an applied live load of 170 kips. The measured interior girder live load shear demand at d_v when web-shear cracking was observed during LBUW and LBUE testing is shown in Figure 5-22 (121 kips shear force at cracking) and Figure 5-25 (126 kips shear force at cracking), respectively.

Table 5-36 shows the predicted and measured applied live load and interior girder live load shear demand at web-shear cracking and at failure for LBUW and LBUE. Data in Table 5-36 show that, during LBUW, the loaded interior girder (Girder 3) was observed to carry 26 to 43 percent more live load shear before web-shear cracking and ultimate failure compared to that predicted by the AASHTO Standard Specifications. During LBUE, the loaded interior girder (Girder 2) was observed to carry 31 to 47 percent more live load shear before web-shear cracking and ultimate failure compared to predicted AASHTO Standard values. To generate the comparisons in Table 5-36, the two lane loaded AASHTO shear distribution factor was used, even though their intended use is for distributing multi-axle truck loads, not single patch loads; use of the distribution factor for a single lane loaded would have decreased the predicted interior girder live load shear demand and exacerbated the comparison to experimental values. Differences in the predicted and measured interior girder live load shear demand at ultimate failure (43 to 47 percent) may be attributed to the amount of shear re-distribution occuring in the laboratory bridge system during inelastic behavior. Furthermore, differences in the predicted and

measured shear demand at ultimate failure may also be attributed to using the AASHTO distribution factors for a single patch load and the fact that the AASHTO Standard shear capacity equations have been shown to under predict girder capacity by approximately 30 percent (Hawkins et al. 2005, Runzel et al. 2007). Table 5-36 also shows the percent of applied shear for both LBUW and LBUE. The percent of applied shear values were calculated by dividing the experimental interior girder live load shear demand by the bridge cross-sectional live load shear demand. The AASHTO Standard distribution factor predicted that 82 percent of the live load would go to the loaded girder during both elastic behavior and inelastic behavior. The experimental percent of applied shear values indicated that approximately 79 percent of the live load would go to the interior girder at d_v during elastic behavior and approximately 68 percent of the live load would go to the interior girder at d_v during inelastic behavior.

Within the goal of comparing the ultimate shear capacity, data from the companion girder tests were compared to data from the bridge inelastic testing. Appendix A describes the companion girder testing where a single point load was applied to the girder during testing of both ends at a shear span-to-depth ratio of 2.5. For the first test, the companion girder was configured to have a simply supported span of 30 ft 9 in. with the single point load applied at a distance of 9 ft 7 in. from the west support centerline (a/d = 2.5). For the second test, the companion girder was rotated 180^o and was configured to have a simply supported span of 22 ft 6 in. with the single point load again applied at a distance of 9 ft 7 in. from the west support centerline (a/d = 2.5). The live load shear demand in the companion girder during testing of the 30.75 ft span and the 22.5 ft span were calculated using statics. In each of the four tests (LBUW, LBUE, 30.75 ft span companion girder, and 22.5 ft span companion girder) the shear span to depth ratio was 2.5. The measured laboratory bridge cross-sectional live load shear demand in the short shear span (which includes all four girders) was calculated using a beam line analysis and the applied live load.

Table 5-35 facilitates comparison of the live load shear demand at observed web-shear cracking, observed flexural cracking, and at ultimate capacity for the companion girder and the laboratory bridge. The data show that the laboratory bridge cross section carried approximately 25 to 29 percent more shear compared to 30.75 ft span companion

girder and approximately 8 to 11 percent more shear compared to the 22.5 ft span companion girder before web-shear cracks were observed. Furthermore, the laboratory bridge cross section carried approximately 30 to 33 percent more shear compared to 30.75 ft span companion girder and approximately 17 to 19 percent more shear compared to the 22.5 ft span companion girder before ultimate failure. However, because the bridge deck punched prior to shear failure of the interior girder, the interior bridge girder may have had additional shear capacity. A comparison of the experimental interior girder live load shear demand at failure during bridge testing, shown in Table 5-36 as 206 and 211 kips, to the live load shear demand at failure of the single companion girder tests, shown in Table 5-35 as 234 and 262 kips, indicated that the bridge interior girders may have been able to carry more applied load if the deck had not punched. The comparison between the laboratory bridge and companion girder is dependent on d_v, which may not be exactly the same because it depends on the effective slab width engaged during inelastic behavior. The effective slab width for the laboratory bridge was assumed to be the 9 ft girder spacing while the effective slab width for the companion girder was assumed to be 4.5 ft in this comparison. It should be noted that in the companion girder tests, the effective flange width that best correlated with the measured neutral axis depth was equal to 3 ft and the effective flange width that best correlated with the composite moment of inertia calculated from the elastic displacement profile was equal to the width of the girder top flange as discussed in Appendix A.

5.4.5 Summary and Conclusions from Inelastic Testing

The ability of an interior girder to shed shear demand to adjacent girders during inelastic loading, particularly after individual girder failure was of interest; however, deck puching precluded further load redistribution after failure of the interior girder. Data in Figure 5-22 and Figure 5-25 showed that approximately 20 kips were shed to each adjacent beam (at d_v) just prior to ultimate failure compared to the projected linear elastic behavior. These figures indicated that the shear in the loaded girder redistributed transversely after observation of initial web-shear and flexural cracks and before ultimate failure. The redistribution of shear continued to increase as the damaged girder stiffness decreased. Use of linear elastic load distribution factors was shown to be conservative when considering shear distribution at ultimate capacity for this structure.

The effects of an end diaphragm on shear distribution were studied during testing of the laboratory bridge in the inelastic range. Data in Table 5-35 show that the observed web-shear cracking load, observed flexural cracking load, and peak applied load at ultimate failure were larger by 2 to 9 percent for LBUE (no diaphragm) than LBUW (diaphragm). This indicated that the end diaphragm acted to slightly increase the amount of shear in the loaded beam (less distribution and therefore less load needed to cause cracking and failure in the girder). Qualitatively, the end diaphragm focused shear cracking higher in the web and toward the support centerline (LBUW) rather than toward the face of the support (LBUE). Figure 5-27 and Figure 5-28 show the differences in the web-shear cracking patterns. This cracking pattern corroborated with elastic FEM results which indicated that the end diaphragm may cause more shear to be carried to the end of the span via the deck rather than the girder.

A comparison was made between the measured and predicted interior girder live load shear demand at web-shear cracking and ultimate failure for the laboratory bridge. To complete the comparison, the AASHTO shear distribution factors were used, but their intended use is not for distributing the bridge cross-sectional live load shear demand due to a single patch load to an individual girder; furthermore, the live load applied when the bridge deck punched may not have been the load that was required to cause ultimate shear failure in the interior girder because the interior girder may have carried more shear demand or the bridge system may have re-distributed more shear demand if the deck had not punched. Data in Table 5-36 show that during LBUW the loaded interior girder (Girder 3) was observed to carry 26 to 43 percent more live load shear demand at observed web-shear cracking and ultimate failure compared to that predicted by the AASHTO Standard Specifications, respectively. During LBUE, the loaded interior girder (Girder 2) was observed to carry 31 to 47 percent more live load shear demand at observed web-shear cracking and ultimate failure compared to predicted AASHTO Standard values, respectively. The larger differences at ultimate failure (43 and 47 percent) compared to those at observed web-shear cracking (26 and 31 percent) may indicate that the shear in the loaded girder redistributed transversely after observation of web-shear cracks and before ultimate failure. The redistribution of shear continued to increase as the damaged girder stiffness decreased.

The laboratory bridge cross section carried more live load shear demand compared to the shear demand from both the 30.75 and 22.5 ft span companion girder tests when web-shear cracks were observed and at ultimate failure. The comparison between the laboratory bridge and companion girder was dependent on d_v and the effective slab width of each structure engaged during inelastic behavior.

Table 5-1. Comparison of Foil and VWG Strains (με) at d_v for LBESE and LBENE

	Foil Rosette Microstrain at d_v								VWG Rosette Microstrain at d_v								Rosette Leg Max |Foil - VWG|	γ_{xy} Max |Foil - VWG|
LBESE	**Girder 3**				**Girder 4**				**Girder 3**				**Girder 4**					
	H*	**D**	**V**	γ_{xy}	**H**	**D**	**V**	γ_{xy}	**H**	**D**	**V**	γ_{xy}	**H**	**D**	**V**	γ_{xy}		
2d S	3	-3	0	-8	17	-56	-20	-110	2	-2	0	-7	15	-59	-17	-115	2	5
2d M	24	-12	16	-64	14	-14	17	-59	17	-12	12	-53	14	-14	17	-58	7	11
2d N	28	-40	8	-115	2	-1	2	-7	15	-44	1	-104	2	-1	2	-7	13	11
4d S	4	-3	-2	-8	14	-38	-8	-83	2	-3	-2	-5	14	-41	-8	-88	3	5
4d M	12	-15	-4	-38	7	-17	-14	-26	6	-10	-11	-16	4	-17	-13	-26	7	22
4d N	21	-25	4	-74	3	-3	0	-8	12	-23	0	-58	2	-2	-2	-4	8	16
LBENE	**Girder 3**				**Girder 4**				**Girder 3**				**Girder 4**					
	H	**D**	**V**	γ_{xy}	**H**	**D**	**V**	γ_{xy}	**H**	**D**	**V**	γ_{xy}	**H**	**D**	**V**	γ_{xy}		
2d S	2	1	2	-4	12	-36	0	-83	2	-2	1	-6	13	-39	-7	-85	7	2
2d M	13	-12	10	-46	14	-10	9	-42	17	-15	9	-57	18	-11	8	-49	4	11
2d N	8	-43	-12	-82	2	-1	0	-5	14	-48	-20	-90	1	-3	-2	-4	8	8
4d S	1	-4	-2	-8	10	-21	2	-53	2	-3	-3	-4	12	-22	-3	-53	5	4
4d M	4	-11	-13	-14	9	-12	-7	-26	4	-16	-17	-18	5	-14	-12	-21	5	5
4d N	10	-26	-12	-50	4	1	-5	4	16	-28	-17	-56	6	-1	-1	-6	5	10
																Avg:	6	9

X = indicates leg of rosette with max |Foil-VWG|

X = indicates γ_{xy} with max |Foil-VWG|

* Horizontal (H), Diagonal (D), or Vertical (V) rosette legs. VWG H is average of top and bottom gages.

Table 5-2. Linearity of Laboratory Shear Force Data for LBESE and LBENE

		Shear Force at d_v (k)						
LBESE		**G1**	**G2**	**G3**	**G4**	**Sum**	**50 k Sum Scaled by 1.5**	**Sum / Scaled Sum**
2dS	**50 k**	-1	2	3	35	38		
	75 k	-1	2	5	52	58	58	1.00
2dM	**50 k**	-1	1	19	19	38		
	75 k	-1	0	29	26	54	57	0.94
2dN	**50 k**	0	-2	36	5	39		
	75 k	0	-3	55	7	59	58	1.01
4dS	**50 k**	0	0	5	26	32		
	75 k	0	0	8	38	46	47	0.97
4dM	**50 k**	-1	0	18	17	34		
	75 k	0	0	27	24	50	51	0.98
4dN	**50 k**	0	-1	23	8	30		
	75 k	-1	-1	35	9	43	45	0.96
LBENE		**G1**	**G2**	**G3**	**G4**	**Sum**	**50 k Sum Scaled by 1.5**	**Sum / Scaled Sum**
2dS	**50 k**	2	28	4	-1	33		
	75 k	4	42	6	-3	49	50	0.98
2dM	**50 k**	15	16	0	1	32		
	75 k	24	22	0	1	47	48	0.99
2dN	**50 k**	29	2	-1	0	30		
	75 k	43	4	-1	0	46	45	1.02
4dS	**50 k**	4	18	6	0	28		
	75 k	7	27	9	0	42	42	1.02
4dM	**50 k**	12	15	1	1	29		
	75 k	18	22	2	0	42	43	0.98
4dN	**50 k**	18	2	0	0	20		
	75 k	27	5	0	0	32	30	1.07
							Avg	0.99

Table 5-3. Magnitude of Torsional Strain (με) Induced during LBESE_4d Testing

Location	γ_{xy}	γ_{xy_shear}	γ_{xy_tor}	$\lvert\gamma_{xy\_tor}\rvert$ / $\lvert\gamma_{xy}\rvert$ (%)	$\lvert\gamma_{xy\_tor}\rvert$ / $\lvert\gamma_{xy\_shear}\rvert$ (%)
LBESE_4d_M_75k					
G3_1d_N	-26	-44	18	67	40
G3_1d_S	-61	-44	-18	29	
Avg:	-44				
G4_1d_N	-57	-42	-16	27	37
G4_1d_S	-26	-42	16	60	
Avg:	-42				
LBESE_4d_S_75k					
G3_1d_N	-5	-14	8	---	62
G3_1d_S	-22	-14	-8	38	
Avg:	-14				
G4_1d_N	-67	-73	6	9	8
G4_1d_S	-78	-73	-6	7	
Avg:	-73				
LBESE_4d_N_75k					
G3_1d_N	-58	-61	3	5	4
G3_1d_S	-63	-61	-3	4	
Avg:	-61				
G4_1d_N	-29	-17	-12	42	74
G4_1d_S	-4	-17	12	---	
Avg:	-17				

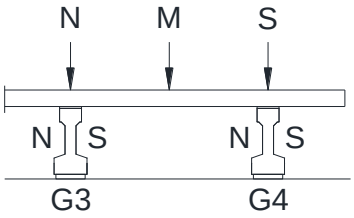

γ_{xy_shear} = Avg. of N and S γ_{xy}

γ_{xy_tor} = (Individual N or S γ_{xy}) - γ_{xy_shear}

Table 5-4. Load Cases for Standard FEM Validation

Load Case	Structural Behavior for Comparison	Load Effects
XX indicates use in quadrants: SE, NE, SW, NW		
LBEXX_4d_M	Girder shear strain	Maximum torsion in girders with single point load
LBEXX_4d_SMN	Vertical girder displacement; girder end rotation; girder shear strains	Simultaneous maximum interior and exterior girder displacement
LBEXX_2d_S	Girder shear strain; vertical bearing pad displacement	Maximum individual girder shear and lowest girder torsion, maximum bearing pad displacement
LBEXX_2d_N	Girder shear strain; vertical bearing pad displacement	Maximum individual girder shear and lowest girder torsion, maximum bearing pad displacement
Total Standard Load Cases Selected for FEM Validation: 16		

Table 5-5. Specific Load Cases for Barrier and End Diaphragm FEM Validation

Load Case	Structural Behavior for Comparison	Load Effects
LBENE_4d_N LBENW_4d_N	Barrier shear strains; barrier longitudinal strains	Minimal girder torsion; maximum barrier shear and bending
LBESW_2d_M LBESW_4d_M	End diaphragm longitudinal strains	Maximum end diaphragm bending
LBESW_2d_N LBESW_2d_S	End diaphragm shear strains	Maximum end diaphragm shear
Additional Specific Load Cases (not duplicated in standard list): 3		

Table 5-6. Comparison of Girder Shear Strain, γ_{xy}, (με) for LBESE (No Barrier or Diaphragm)

		LBESE_4d_M_75k			LBESE_4d_SMN_50k			LBESE_2d_S_75k			LBESE_2d_N_75k		
Location	**Gage Type**	**FEM**	**Lab**	**% Diff**	**FEM**	**Lab**	**% Diff**	**FEM**	**Lab**	**% Diff**	**FEM**	**Lab**	**% Diff**
G3_05d_N	Foil	37	36	-2	72	69	-4				99	95	-3
G3_05d_S	VWG	60	59	0	95	95	0				99	80	-18
	Avg:	***48***	***48***	***0***	***83***	***82***	***-1***				***99***	***88***	***-10***
G3_1d_N	VWG	35	38	8	70	77	9				99	115	15
G3_1d_S	VWG	59	68	14	94	98	4				99	101	1
	Avg:	***47***	***53***	***11***	***82***	***88***	***6***				***99***	***108***	***8***
G3_2d_N	Foil	38	33	-11	76	64	-15						
G3_2d_S	VWG	62	64	4	100	95	-4						
	Avg:	***50***	***49***	***-2***	***88***	***80***	***-9***						
G4_05d_N	VWG	56	69	24	101	110	8	114	114	0			
G4_05d_S	Foil	34	30	-10	89	98	9	123	143	16			
	Avg:	***45***	***50***	***10***	***95***	***104***	***8***	***119***	***129***	***8***			
G4_1d_N	VWG	57	67	19	100	92	-7	112	94	-15			
G4_1d_S	VWG	34	26	-21	88	73	-16	120	110	-8			
	Avg:	***45***	***47***	***3***	***94***	***83***	***-12***	***116***	***102***	***-11***			
G4_2d_N	VWG	59	57	-3	104	94	-9						
G4_2d_S	Foil	38	24	-36	93	60	-35						
	Avg:	***49***	***41***	***-16***	***98***	***77***	***-21***						

% difference calculated as (LAB-FEM)/FEM*100

Table 5-7. Comparison of Girder and Barrier Shear Strain, γ_{xy}, (με) for LBENE

		LBENE_4d_M_75k			LBENE_4d_SMN_50k			LBENE_4d_N_75k			LBENE_2d_S_75k			LBENE_2d_N_75k		
Location	**Gage Type**	**FEM**	**Lab**	**% Diff**	**FEM**	**Lab**	**% Diff**	**FEM**	**Lab**	**% Diff**	**FEM**	**Lab**	**% Diff**	**FEM**	**Lab**	**% Diff**
G1_05d_N	VWG	23	15	-33	61	67	9	62	49	-20				90	104	16
G1_05d_S	Foil	48	50	4	88	89	1	66	58	-11				96	84	-12
	Avg:	***35***	***33***	***-7***	***75***	***78***	***4***	***64***	***54***	***-15***				***93***	***94***	***1***
G1_1d_N	VWG	22	14	-36	56	53	-5	55	56	1				85	82	-4
G1_1d_S	VWG	49	56	15	85	93	9	60	57	-4				91	87	-3
	Avg:	***36***	***35***	***0***	***70***	***73***	***3***	***57***	***57***	***-1***				***88***	***85***	***-3***
G1_2d_N	VWG	30	17	-45	64	63	-2	60	55	-7						
G1_2d_S	Foil	56	57	2	92	92	0	65	60	-7						
	Avg:	***43***	***37***	***-14***	***78***	***77***	***0***	***62***	***58***	***-7***						
G2_05d_N	VWG	57	61	6	91	100	10	19	20	5	98	88	-9			
G2_05d_S	Foil	36	25	-30	70	61	-12	8	7	-6	99	88	-10			
	Avg:	***47***	***43***	***-8***	***81***	***81***	***0***	***13***	***14***	***1***	***98***	***88***	***-10***			
G2_1d_N	VWG	57	61	7	91	91	0	19	22	16	98	81	-16			
G2_1d_S	VWG	34	26	-23	69	57	-16	8	6	-21	99	83	-15			
	Avg:	***46***	***44***	***-4***	***80***	***74***	***-7***	***13***	***14***	***5***	***99***	***82***	***-16***			
G2_2d_N	VWG	60	54	-10	97	94	-3	18	13	-24						
G2_2d_S	Foil	37	27	-26	75	81	8	6	2	-68						
	Avg:	***48***	***40***	***-16***	***86***	***88***	***1***	***12***	***8***	***-36***						
NB_05d_N	VWG	9	9	8	11	19	81	4	19	395						
NB_1d_N	VWG	12	14	19	15	18	20	5	11	102						
NB_2d_N	VWG	13	15	10	16	11	-32	6	11	79						

% difference calculated as (LAB-FEM)/FEM*100

NB = North Barrier

Table 5-8. Comparison of Girder Shear Strain, γ_{xy}, (με) for LBESW (Diaphragm)

Location	Gage Type	LBESW_4d_M_75k					LBESW_4d_SMN_50k				
		FEM			Lab	% Diff	FEM			Lab	% Diff
		Fix	Pin	Free			Fix	Pin	Free		
G3_05d_N	Foil	-31	-29	-30	-29	0	-67	-63	-64	-74	15
G3_05d_S	VWG	-54	-57	-57	-82	44	-87	-90	-91	-104	16
	Avg:	***-43***	***-43***	***-43***	***-55***	***27***	***-77***	***-77***	***-77***	***-89***	***16***
G3_1d_N	VWG	-30	-30	-33	-16	-47	-66	-66	-68	-64	-2
G3_1d_S	VWG	-65	-64	-61	-74	15	-100	-100	-96	-102	2
	Avg:	***-47***	***-47***	***-47***	***-45***	***-4***	***-83***	***-83***	***-82***	***-83***	***0***
G3_2d_N	Foil	-34	-35	-37	-24	-31	-73	-75	-76	-62	-16
G3_2d_S	VWG	-70	-69	-66	-79	14	-109	-107	-105	-96	-10
	Avg:	***-52***	***-52***	***-52***	***-52***	***0***	***-91***	***-91***	***-91***	***-79***	***-13***
G4_05d_N	VWG	-56	-59	-57	-70	19	-96	-100	-101	-96	-3
G4_05d_S	Foil	-31	-28	-30	-6	-77	-87	-85	-86	-60	-29
	Avg:	***-43***	***-43***	***-44***	***-38***	***-12***	***-92***	***-92***	***-93***	***-78***	***-15***
G4_1d_N	VWG	-63	-63	-60	-83	32	-103	-103	-102	-113	9
G4_1d_S	VWG	-27	-27	-30	-3	-87	-84	-84	-86	-68	-18
	Avg:	***-45***	***-45***	***-45***	***-43***	***-3***	***-94***	***-94***	***-94***	***-91***	***-3***
G4_2d_N	VWG	-68	-66	-64	-76	14	-110	-110	-109	-103	-6
G4_2d_S	Foil	-30	-31	-34	-21	-32	-89	-90	-91	-75	-16
	Avg:	***-49***	***-49***	***-49***	***-49***	***-1***	***-100***	***-100***	***-100***	***-89***	***-11***

Location	Gage Type	LBESW_2d_S_75k					LBESW_2d_N_75k				
		FEM			Lab	% Diff	FEM			Lab	% Diff
		Fix	Pin	Free			Fix	Pin	Free		
G3_05d_N	Foil						-93	-92	-91	-106	14
G3_05d_S	VWG						-93	-92	-91	-99	6
	Avg:						***-93***	***-92***	***-91***	***-102***	***10***
G3_1d_N	VWG						-103	-102	-100	-103	1
G3_1d_S	VWG						-103	-102	-101	-100	-2
	Avg:						***-103***	***-102***	***-100***	***-102***	***0***
G3_2d_N	Foil										
G3_2d_S	VWG										
	Avg:										
G4_05d_N	VWG	-105	-105	-109	-94	-10					
G4_05d_S	Foil	-121	-122	-120	-106	-13					
	Avg:	***-113***	***-114***	***-115***	***-100***	***-12***					
G4_1d_N	VWG	-107	-107	-111	-113	5					
G4_1d_S	VWG	-127	-126	-123	-119	-5					
	Avg:	***-117***	***-117***	***-117***	***-116***	***0***					
G4_2d_N	VWG										
G4_2d_S	Foil										
	Avg:										

% difference calculated as (LAB-FEM Pin)/FEM Pin*100

Table 5-9. Comparison of Girder and Barrier Shear Strain, γ_{xy}, (με) for LBENW (Barrier, Diaphragm)

		LBENW_4d_M_75k			LBENW_4d_SMN_50k			LBENW_4d_N_75k			LBENW_2d_S_75k			LBENW_2d_N_75k		
Location	Gage Type	FEM	Lab	% Diff	FEM	Lab	% Diff	FEM	Lab	% Diff	FEM	Lab	% Diff	FEM	Lab	% Diff
G1_05d_N	VWG	19	13	-29	63	67	6	68	78	14				98	104	6
G1_05d_S	Foil	54	60	10	91	98	7	59	61	3				92	96	3
	Avg:	***37***	***37***	***0***	***77***	***82***	***7***	***64***	***69***	***9***				***95***	***100***	***5***
G1_1d_N	VWG	18	3	-83	58	50	-13	69	70	0				100	82	-18
G1_1d_S	VWG	59	82	38	92	113	23	55	61	10				90	104	15
	Avg:	***38***	***43***	***10***	***75***	***82***	***9***	***62***	***65***	***5***				***95***	***93***	***-2***
G1_2d_N	VWG	27	15	-44	68	46	-32	74	59	-20						
G1_2d_S	Foil	67	83	24	103	115	12	65	67	2						
	Avg:	***47***	***49***	***4***	***85***	***81***	***-5***	***70***	***63***	***-9***						
G2_05d_N	VWG	54	72	34	85	100	17	21	16	-21	92	97	5			
G2_05d_S	Foil	28	18	-34	61	49	-19	11	3	-68	92	69	-24			
	Avg:	***41***	***45***	***10***	***73***	***75***	***1***	***16***	***10***	***-37***	***92***	***83***	***-9***			
G2_1d_N	VWG	62	76	23	96	110	14	19	17	-11	102	107	5			
G2_1d_S	VWG	30	18	-41	66	51	-22	6	0	-94	102	94	-8			
	Avg:	***46***	***47***	***1***	***81***	***81***	***0***	***12***	***9***	***-31***	***102***	***100***	***-1***			
G2_2d_N	VWG	67	72	7	105	103	-1	16	14	-16						
G2_2d_S	Foil	35	20	-44	76	55	-27	4	1	-87						
	Avg:	***51***	***46***	***-10***	***90***	***79***	***-12***	***10***	***7***	***-31***						
NB_1d_N	VWG	19	19	0	18	18	0	2	3	84						
NB_2d_N	VWG	21	30	39	20	28	41	2	6	138						

% difference calculated as (Lab-FEM)/FEM*100

NB = North Barrier

Table 5-10. Comparison of Girder Vertical Displacement for LBESE (No Barrier or Diaphragm)

	LBESE_4d_SMN_50k		
Location	**FEM**	**Lab**	**% Diff**
G3_E_2d	-0.057	-0.040	-30
G3_0.5L	-0.078	-0.073	-7
G3_W_2d	-0.047	-0.044	-6
G4_E_2d	-0.067	-0.067	1
G4_0.5L	-0.093	-0.090	-2
G4_W_2d	-0.057	-0.061	7

All values in inches

% Diff = (Lab-FEM)/FEM*100

Table 5-11. Comparison of Girder End Rotation for LBESE (No Barrier or Diaphragm)

	LBESE_4d_SMN_50k		
Location	**FEM**	**Lab**	**% Diff**
G3_East	0.028	0.034	20
G4_East	0.034	0.036	5

All values in degrees

% Diff = (Lab-FEM)/FEM*100

Table 5-12. Comparison of Bearing Pad Vertical Displacement for LBESE (No Barrier or Diaphragm)

Location	Load Case	FEM	Lab	% Diff
G3_East	LBESE_2d_N_75k	-0.019	-0.020	3
G4_East	LBESE_2d_S_75k	-0.023	-0.025	13

All values in inches
% Diff = (Lab-FEM)/FEM*100

Table 5-13. Comparison of Girder Vertical Displacement for LBENE (Barrier)

	LBENE_4d_SMN_50k		
Location	**FEM**	**Lab**	**% Diff**
G1_E_2d	-0.054	-0.057	6
G1_0.5L	-0.073	-0.073	0
G1_W_2d	-0.046	-0.046	0
G2_E_2d	-0.055	-0.053	-4
G2_0.5L	-0.075	-0.071	-5
G2_W_2d	-0.045	-0.043	-5

All values in inches
% Diff = (Lab-FEM)/FEM*100

Table 5-14. Comparison of Girder End Rotation for LBENE (Barrier)

	LBENE_4d_SMN_50k		
Location	**FEM**	**Lab**	**% Diff**
G1_East	0.025	0.029	17
G2_East	0.027	0.029	8

All values in degrees
% Diff = (Lab-FEM)/FEM*100

Table 5-15. Comparison of Bearing Pad Vertical Displacement for LBENE (Barrier)

Location	Load Case	FEM	Lab	% Diff
G1_East	LBENE_2d_N_75k	-0.033	-0.035	7
G2_East	LBENE_2d_S_75k	-0.019	-0.016	-13

All values in inches
% Diff = (Lab-FEM)/FEM*100

Table 5-16. Comparison of Girder Vertical Displacement for LBESW (Diaphragm)

Location	LBESW_4d_SMN_50k				
	FEM			Lab	% Diff
	Fix	Pin	Free		
G3_W_2d	-0.055	-0.055	-0.056	-0.053	-4
G3_0.5L	-0.077	-0.077	-0.078	-0.074	-4
G3_E_2d	-0.047	-0.047	-0.048	-0.044	-6
G4_W_2d	-0.067	-0.067	-0.067	-0.064	-5
G4_0.5L	-0.093	-0.093	-0.093	-0.090	-3
G4_E_2d	-0.057	-0.057	-0.057	-0.057	0

All values in inches

% Diff = (Lab-FEM Pin)/FEM Pin*100

Table 5-17. Comparison of Girder End Rotation for LBESW (Diaphragm)

Location	LBESW_4d_SMN_50k				
	FEM			Lab	% Diff
	Fix	Pin	Free		
G3_West	-0.027	-0.028	-0.028	-0.030	10
G4_West	-0.033	-0.033	-0.033	-0.028	-15

All values in degrees

% Diff = (Lab-FEM Pin)/FEM Pin*100

Table 5-18. Comparison of Bearing Pad Vertical Displacement for LBESW (Diaphragm)

Location	Load Case	FEM			Lab	% Diff
		Fix	Pin	Free		
G3_West	LBESW_2d_N_75k	-0.015	-0.016	-0.017	-0.014	-9
G4_West	LBESW_2d_S_75k	-0.022	-0.022	-0.022	-0.029	31

All values in inches

% Diff = (Lab-FEM Pin)/FEM Pin*100

Table 5-19. Comparison of Girder Vertical Displacement for LBENW (Barrier, Diaphragm)

	LBENW_4d_SMN_50k		
Location	FEM Pin	Lab	% Diff
G1_W_2d	-0.059	-0.059	0
G1_0.5L	-0.079	-0.077	-2
G1_E_2d	-0.050	-0.050	0
G2_W_2d	-0.054	-0.053	-1
G2_0.5L	-0.075	-0.073	-2
G2_E_2d	-0.046	-0.046	0

All values in inches

% Diff = (Lab-FEM Pin)/FEM Pin*100

Table 5-20. Comparison of Girder End Rotation for LBENW (Barrier, Diaphragm)

	LBENW_4d_SMN_50k		
Location	**FEM Pin**	**Lab**	**% Diff**
G1_West	0.024	0.029	19
G2_West	0.026	0.027	3

All values in degrees

% Diff = (Lab-FEM Pin)/FEM Pin*100

Table 5-21. Comparison of Bearing Pad Vertical Displacement for LBENW (Barrier, Diaphragm)

Location	Load Case	FEM Pin	Lab	% Diff
G1_West	LBENW_2d_N_75k	-0.024	-0.030	29
G2_West	LBENW_2d_S_75k	-0.016	-0.016	4

All values in inches

% Diff = (Lab-FEM Pin)/FEM Pin*100

Table 5-22. Comparison of North Barrier (NB) Longitudinal Strains for LBENE

	LBENE_4d_N_75k			
Location	**FEM**	**Lab**	**% Diff**	**Gage Placement**
NB_05d_TVWG	-3	0	-101	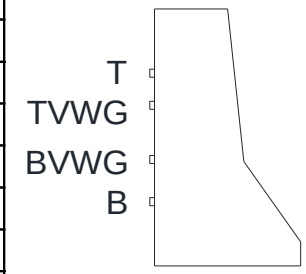
NB_05d_BVWG	-2	-3	25	
NB_1d_T	-15	-15	1	
NB_1d_TVWG	-13	-12	-6	
NB_1d_BVWG	-9	-8	-11	
NB_1d_B	-7	-12	66	
NB_2d_T	-38	-30	-20	
NB_2d_TVWG	-31	-25	-22	
NB_2d_BVWG	-24	-16	-32	
NB_2d_B	-18	-24	29	

% Diff = (Lab-FEM)/FEM*100

Table 5-23. Comparison of End Diaphragm Longitudinal Strains for LBESW

Location	Load Case	FEM			Lab	% Diff
		Fix	Pin	Free		
G34DIA_B	LBESW_2d_M_75k	23.7	22.0	14.6	15.2	-31
	LBESW_4d_M_75k	12.6	10.0	6.6	10.2	2
G34DIA_M	LBESW_2d_M_75k	8.3	7.1	3.5	5.0	-30
	LBESW_4d_M_75k	4.8	3.1	1.5	2.5	-20
G34DIA_Tdeck	LBESW_2d_M_75k	-25.9	-25.7	-22.0	-11.2	-56
	LBESW_4d_M_75k	-10.4	-10.0	-8.0	-9.8	-1

% Diff = (Lab-FEM Pin)/FEM Pin*100

Table 5-24. Comparison of End Diaphragm Longitudinal Strains for LBENW

Location	Load Case	FEM Pin	Lab	% Diff
G12DIA_B	LBENW_2d_M_75k	19.5	14.4	-26
	LBENW_4d_M_75k	10.6	11.3	6
G12DIA_M	LBENW_2d_M_75k	5.3	6.9	31
	LBENW_4d_M_75k	2.9	5.4	88
G12DIA_Tdeck	LBENW_2d_M_75k	-26.6	-17.5	-34
	LBENW_4d_M_75k	-12.5	-10.4	-17

% Diff = (Lab-FEM Pin)/FEM Pin*100

Table 5-25. Comparison of End Diaphragm Shear Strains (με) for LBESW

		LBESW_2d_S_75k				
Location	Gage Type	FEM			Lab	% Diff
		Fix	Pin	Free		
G34DIA_NE_M	Foil	43	37	26	35	
G34DIA_NW_M	Foil	-20	-18	-13	-14	
Avg:		***11***	***9***	***6***	***11***	***13***
G34DIA_SE_M	Foil	44	38	32	31	
G34DIA_SW_M	Foil	-21	-19	-16	-24	
Avg:		***11***	***10***	***8***	***3***	***-65***

		LBESW_2d_N_75k				
Location	Gage Type	FEM			Lab	% Diff
		Fix	Pin	Free		
G23DIA_NE_B	Foil	25	23	17	18	
G23DIA_NW_B	Foil	-14	-13	-12	-19	
Avg:		***6***	***5***	***3***	***0***	***-104***
G23DIA_SE_M	Foil	35	30	20	33	
G23DIA_SW_M	Foil	-11	-9	-7	-15	
Avg:		***12***	***10***	***7***	***9***	***-13***
G34DIA_NE_M	Foil	-33	-27	-16	-29	
G34DIA_NW_M	Foil	12	10	7	10	
Avg:		***-10***	***-8***	***-5***	***-9***	***12***
G34DIA_SE_M	Foil	-36	-33	-26	-29	
G34DIA_SW_M	Foil	12	12	10	21	
Avg:		***-12***	***-10***	***-8***	***-4***	***-65***

% difference calculated as (LAB-FEM Pin)/FEM Pin*100

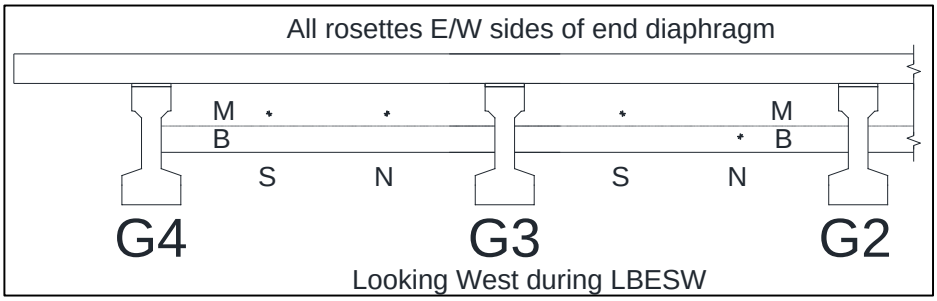

Table 5-26. Comparison of End Diaphragm Shear Strains (με) for LBENW

		LBENW_2d_N_75k		
Location	**Gage Type**	**FEM Pin**	**Lab**	**% Diff**
G12DIA_NE_M	Foil	-24	-45	
G12DIA_NW_M	Foil	11	15	
Avg:		***-6***	***-15***	***140***
G12DIA_SE_B	Foil	17	19	
G12DIA_SW_B	Foil	-15	-10	
Avg:		***1***	***4***	***420***
G12DIA_SE_M	Foil	25	17	
G12DIA_SW_M	Foil	-11	-10	
Avg:		***7***	***4***	***-45***

		LBENW_2d_S_75k		
Location	**Gage Type**	**FEM Pin**	**Lab**	**% Diff**
G12DIA_NE_M	Foil	34	48	
G12DIA_NW_M	Foil	-13	-8	
Avg:		***11***	***20***	***87***
G12DIA_SE_B	Foil	-19	-22	
G12DIA_SW_B	Foil	13	10	
Avg:		***-3***	***-6***	***71***
G12DIA_SE_M	Foil	-28	-16	
G12DIA_SW_M	Foil	10	6	
Avg:		***-9***	***-5***	***-43***
G23DIA_NE_B	Foil	-20	-21	
G23DIA_NW_B	Foil	10	5	
Avg:		***-5***	***-8***	***53***

% difference calculated as (Lab-FEM)/FEM*100

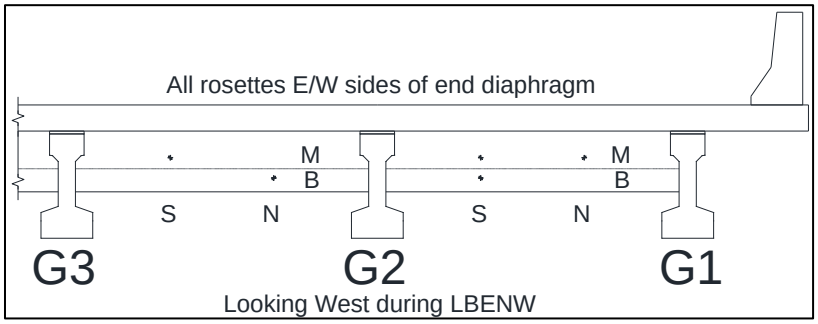

Table 5-27. Effects of the Traffic Barrier on Percent Applied Shear with Load at $4d_v$

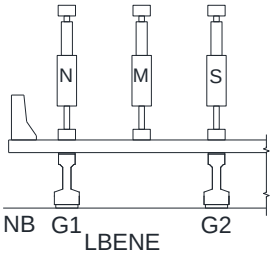

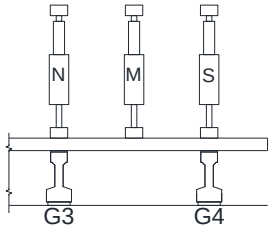

Test	Loc.	NB	G1	G2	G3	G4
LBENE 4d N 75k	**0.5d**	17%	73%	12%	-2%	0%
LBENE 4d N 75k	**1.0d**	19%	70%	12%	-2%	0%
LBENE 4d N 75k	**2.0d**	18%	72%	11%	-1%	0%

Test	Loc.	NB	G1	G2	G3	G4
LBESE 4d S 75k	**0.5d**	0%	0%	-2%	13%	89%
LBESE 4d S 75k	**1.0d**	0%	0%	-2%	13%	89%
LBESE 4d S 75k	**2.0d**	0%	0%	-1%	12%	90%

Test	Loc.	NB	G1	G2	G3	G4
LBENE 4d S 75k	**0.5d**	2%	12%	69%	19%	-2%
LBENE 4d S 75k	**1.0d**	2%	12%	70%	18%	-2%
LBENE 4d S 75k	**2.0d**	1%	11%	74%	15%	-1%

Test	Loc.	NB	G1	G2	G3	G4
LBESE 4d N 75k	**0.5d**	0%	-2%	19%	69%	14%
LBESE 4d N 75k	**1.0d**	-1%	-1%	18%	70%	14%
LBESE 4d N 75k	**2.0d**	-1%	-1%	15%	75%	12%

Test	Loc.	NB	G1	G2	G3	G4
LBENE 4d M 75k	**0.5d**	9%	40%	50%	2%	-1%
LBENE 4d M 75k	**1.0d**	9%	40%	50%	2%	-1%
LBENE 4d M 75k	**2.0d**	5%	45%	49%	2%	-1%

Test	Loc.	NB	G1	G2	G3	G4
LBESE 4d M 75k	**0.5d**	0%	-1%	2%	52%	47%
LBESE 4d M 75k	**1.0d**	-1%	-1%	2%	51%	48%
LBESE 4d M 75k	**2.0d**	0%	0%	2%	51%	49%

Test	Loc.	NB	G1	G2	G3	G4
LBENE 4d NM 75k	**0.5d**	13%	57%	31%	0%	-1%
LBENE 4d NM 75k	**1.0d**	14%	55%	31%	0%	-1%
LBENE 4d NM 75k	**2.0d**	12%	58%	30%	0%	-1%

Test	Loc.	NB	G1	G2	G3	G4
LBESE 4d SM 75k	**0.5d**	0%	-1%	0%	33%	68%
LBESE 4d SM 75k	**1.0d**	0%	0%	0%	32%	68%
LBESE 4d SM 75k	**2.0d**	0%	0%	0%	31%	69%

Test	Loc.	NB	G1	G2	G3	G4
LBENE 4d SM 75k	**0.5d**	6%	26%	60%	11%	-2%
LBENE 4d SM 75k	**1.0d**	5%	26%	60%	10%	-2%
LBENE 4d SM 75k	**2.0d**	3%	28%	62%	8%	-1%

Test	Loc.	NB	G1	G2	G3	G4
LBESE 4d NM 75k	**0.5d**	0%	-1%	11%	61%	31%
LBESE 4d NM 75k	**1.0d**	-1%	-1%	10%	61%	31%
LBESE 4d NM 75k	**2.0d**	-1%	-1%	8%	63%	30%

Test	Loc.	NB	G1	G2	G3	G4
LBENE 4d SMN 50k	**0.5d**	9%	42%	44%	7%	-1%
LBENE 4d SMN 50k	**1.0d**	10%	41%	44%	6%	-1%
LBENE 4d SMN 50k	**2.0d**	8%	43%	45%	5%	-1%

Test	Loc.	NB	G1	G2	G3	G4
LBESE 4d SMN 50k	**0.5d**	0%	-1%	6%	45%	50%
LBESE 4d SMN 50k	**1.0d**	-1%	-1%	6%	45%	50%
LBESE 4d SMN 50k	**2.0d**	0%	0%	5%	46%	50%

Note: All results from finite element analysis

Table 5-28. Percent of Applied Shear for Girder Composite Sections with and without End Diaphragm

LBESE

No Diaphragm

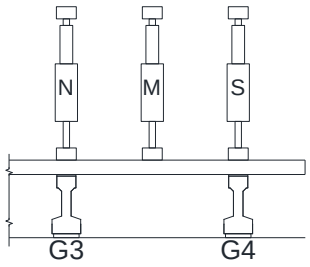

LBESE

Test	Loc.	G1	G2	G3	G4
LBESE 4d S 75k	**0.5d**	0%	-2%	13%	89%
LBESE 4d S 75k	**1.0d**	0%	-2%	13%	89%
LBESE 4d S 75k	**2.0d**	0%	-1%	12%	90%

Test	Loc.	G1	G2	G3	G4
LBESE 4d N 75k	**0.5d**	-2%	19%	69%	14%
LBESE 4d N 75k	**1.0d**	-1%	18%	70%	14%
LBESE 4d N 75k	**2.0d**	-1%	15%	75%	12%

LBESW

Fixed Diaphragm

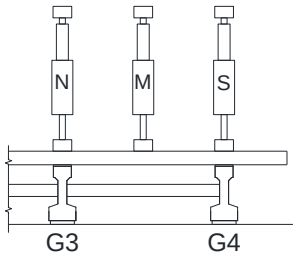

LBESW

Test	Loc.	G1	G2	G3	G4
LBESW 4d S 75k	**0.5d**	0%	-2%	11%	93%
LBESW 4d S 75k	**1.0d**	0%	-2%	10%	93%
LBESW 4d S 75k	**2.0d**	0%	-2%	9%	94%

Test	Loc.	G1	G2	G3	G4
LBESW 4d N 75k	**0.5d**	-2%	16%	76%	12%
LBESW 4d N 75k	**1.0d**	-2%	15%	76%	11%
LBESW 4d N 75k	**2.0d**	-2%	13%	80%	9%

Note: All results from finite element analysis

Table 5-29. Percent Applied Shear for Girder and Deck without an End Diaphragm

Girder Shear Only

No Diaphragm

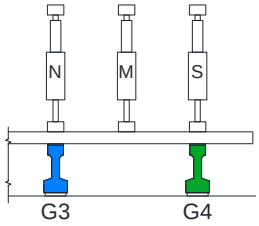

LBESE

Test	Loc.	G1	G2	G3	G4	Sum
LBESE 4d S 75k	**0.5d**	0%	-1%	13%	69%	80%
LBESE 4d S 75k	**1.0d**	0%	-1%	12%	69%	80%
LBESE 4d S 75k	**2.0d**	0%	-1%	11%	71%	82%

Test	Loc.	G1	G2	G3	G4	Sum
LBESE 4d N 75k	**0.5d**	-1%	16%	51%	12%	79%
LBESE 4d N 75k	**1.0d**	0%	15%	52%	12%	79%
LBESE 4d N 75k	**2.0d**	0%	13%	58%	11%	81%

Deck Shear Only

No Diaphragm

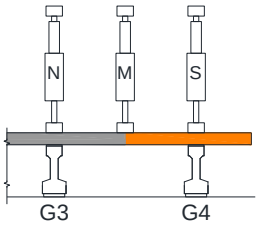

LBESE

Test	Loc.	G1	G2	G3	G4	Sum
LBESE 4d S 75k	**0.5d**	0%	-1%	1%	21%	20%
LBESE 4d S 75k	**1.0d**	0%	-1%	1%	21%	20%
LBESE 4d S 75k	**2.0d**	0%	-1%	1%	19%	19%

Test	Loc.	G1	G2	G3	G4	Sum
LBESE 4d N 75k	**0.5d**	-1%	3%	18%	2%	22%
LBESE 4d N 75k	**1.0d**	-1%	3%	18%	1%	21%
LBESE 4d N 75k	**2.0d**	-1%	2%	17%	1%	19%

All results from finite element analysis

Table 5-30. Percent of Applied Shear for Girder and Deck with Fixed End Diaphragm

Girder Shear Only
Fixed End Diaphragm

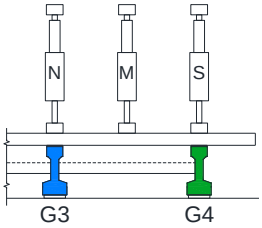

LBESW

Test	Loc.	G1	G2	G3	G4	Sum
LBESW 4d S 75k	**0.5d**	0%	0%	12%	68%	80%
LBESW 4d S 75k	**1.0d**	0%	-1%	10%	71%	80%
LBESW 4d S 75k	**2.0d**	0%	-1%	8%	75%	82%

Test	Loc.	G1	G2	G3	G4	Sum
LBESW 4d N 75k	**0.5d**	0%	14%	50%	11%	74%
LBESW 4d N 75k	**1.0d**	-1%	13%	55%	10%	78%
LBESW 4d N 75k	**2.0d**	-1%	11%	62%	9%	81%

Deck Shear Only
Fixed End Diaphragm

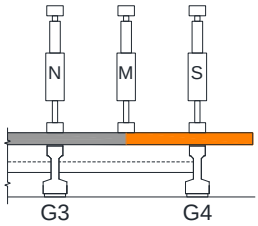

LBESW

Test	Loc.	G1	G2	G3	G4	Sum
LBESW 4d S 75k	**0.5d**	0%	-2%	-1%	25%	21%
LBESW 4d S 75k	**1.0d**	0%	-1%	0%	22%	20%
LBESW 4d S 75k	**2.0d**	0%	-1%	0%	19%	19%

Test	Loc.	G1	G2	G3	G4	Sum
LBESW 4d N 75k	**0.5d**	-2%	2%	26%	0%	27%
LBESW 4d N 75k	**1.0d**	-1%	2%	21%	1%	23%
LBESW 4d N 75k	**2.0d**	-1%	2%	18%	1%	19%

Note: All results from finite element analysis

Table 5-31. Percent Applied Shear for Girder and Deck with a Stiffened End Diaphragm

Girder Shear Only
10*End Diaphragm *E*

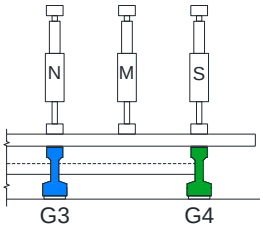

LBESW

Test	Loc.	G1	G2	G3	G4	Sum
LBESW 4d S 75k	**0.5d**	0%	0%	12%	68%	80%
LBESW 4d S 75k	**1.0d**	-1%	-2%	7%	75%	80%
LBESW 4d S 75k	**2.0d**	-1%	-3%	5%	79%	82%

Test	Loc.	G1	G2	G3	G4	Sum
LBESW 4d N 75k	**0.5d**	-1%	12%	50%	8%	69%
LBESW 4d N 75k	**1.0d**	-2%	11%	61%	7%	77%
LBESW 4d N 75k	**2.0d**	-2%	9%	68%	6%	81%

Deck Shear Only
10*End Diaphragm *E*

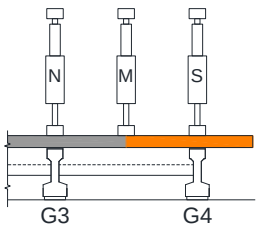

LBESW

Test	Loc.	G1	G2	G3	G4	Sum
LBESW 4d S 75k	**0.5d**	-1%	-4%	-3%	30%	22%
LBESW 4d S 75k	**1.0d**	-1%	-2%	-1%	24%	20%
LBESW 4d S 75k	**2.0d**	0%	-1%	0%	20%	19%

Test	Loc.	G1	G2	G3	G4	Sum
LBESW 4d N 75k	**0.5d**	-1%	1%	32%	-1%	31%
LBESW 4d N 75k	**1.0d**	-1%	2%	23%	0%	24%
LBESW 4d N 75k	**2.0d**	-1%	1%	19%	0%	19%

Note: All results from finite element analysis

Table 5-32. LBUW Loading Protocol

Applied Load (k)	West Reaction Sum from Statics (k)	Load Rate (in. / min)	Notes:
25	17	0.02	Linear elastic data points
50	34		
75	52		
50	34		
75	52		
100	69		
125	86		
150	103		
175	120		
200	138		
225	155	0.02	Web-shear cracking observed
250	172		
275	189		Flexural cracking observed
300	207		
325	224		
10	7	0.04	Unload
50	34	0.02	Reload
150	103		Reload
325	224		Reload
350	241		
375	258	0.04	No crack marking this step
400	275		
425	293		No crack marking this step or beyond for safety reasons
444	305		Peak load, web crushing and deck punching, no VWG data collection

Table 5-33. LBUE Loading Protocol

Applied Load (k)	East Reaction Sum from Statics (k)	Load Rate (in. / min)	Notes:
25	17	0.02	Linear elastic data points
50	34		
75	52		
50	34		
75	52		
100	69		
125	86		
150	103		
175	120		
200	138		
225	155		
232	160	0.02	Web-shear cracking observed
250	172		
10	7	0.04	Unload
50	34	0.02	Reload
150	103		Reload
250	172		Reload
275	189		
300	207		Flexural cracking observed
325	224		
350	241		
375	258	0.04	No crack marking this step
400	275		
425	293		No crack marking this step or beyond
452	311		Peak load, web crushing and deck punching, no VWG data collection

Table 5-34. Material Properties used to Calculate Elastic Shear Forces

Property	Symbol [Units]	Value
Girder Concrete Compressive Strength (measured)	f'_c [ksi]	7.177
Girder Modulus of Elasticity (measured)	E_c [ksi]	5,000
Girder Shear Modulus (calculated with v = 0.2)	G [ksi]	2,083
Deck Concrete Compressive Strength (measured)	f'_{cd} [ksi]	6.597
Deck Modulus of Elasticity (measured)	E_{cd} [ksi]	4,520
Rebar Modulus of Elasticity	E_s [ksi]	29,000
Strand Modulus of Elasticity	E_{ps} [ksi]	28,700
Interior Girder		
Deck Effective Flange Width	b_{eff} [ft]	9
Composite Deck Longitudinal Area of Steel (top)	A_s [in.^{2}]	1.20
Composite Deck Longitudinal Area of Steel (bottom)	A_s [in.^{2}]	3.72
Transformed Composite Centroid (from bottom)	y_{cb} [in.]	33.5
Transformed Moment of Inertia	I_t [in.^{4}]	250,280
First Moment of Area at Rosette Elevation	Q [in.^{3}]	6,118
Exterior Girder		
Deck Effective Flange Width	b_{eff} [ft]	8
Composite Deck Longitudinal Area of Steel (top)	A_s [in.^{2}]	1.00
Composite Deck Longitudinal Area of Steel (bottom)	A_s [in.^{2}]	3.10
Transformed Composite Centroid (from bottom)	y_{cb} [in.]	32.8
Transformed Moment of Inertia	I_t [in.^{4}]	242,524
First Moment of Area at Rosette Elevation	Q [in.^{3}]	5,996

Table 5-35. Comparison of Bridge Cross-Sectional Live Load Shear Demand during LBUW and LBUE to the Live Load Shear Demand in the Companion Girder

Behavior	Bridge Cross-Sectional LL Shear Demand (k)		LBUE / LBUW	Companion Girder LL Shear Demand (k)		LBUW / 30.75 ft Span	LBUE / 30.75 ft Span	LBUW / 20.5 ft Span	LBUE / 20.5 ft Span
	LBUW	LBUE		30.75 ft Span	22.5 ft Span				
Observed web-shear cracking	155	160	1.03	124	144	1.25	1.29	1.08	1.11
Observed flexural cracking	189	207	1.09	162	165	1.17	1.27	1.15	1.25
Ultimate capacity	305	311	1.02	234	262	1.30	1.33	1.17	1.19

All tests had a/d = 2.5

Table 5-36. Comparison of Measured and Predicted Applied Live Load and Interior Girder Live Load Shear Demand at Web-Shear Cracking and Ultimate Capacity for LBUW and LBUE

Behavior	Experimental Values[1]					Predicted AASHTO Standard Values[1]				Measured / Predicted Interior Gider LL Shear Demand
	Test	Applied LL (k)	Bridge Cross-Sectional LL Shear Demand from Statics (k)	% Shear in Interior Girder[2]	Interior Girder LL Shear Demand (k)[3]	Applied LL (k)	Bridge Cross-Sectional LL Shear Demand from Statics (k)	Shear DF for Interior Girder[4]	Interior Girder LL Shear Demand (k)	
Web-shear cracking	LBUW	225	155	78	121	170	117	0.82	96	1.26
	LBUE	232	160	79	126					1.31
Ultimate shear failure	LBUW	444	305	67	206	255	176		144	1.43
	LBUE	452	311	68	211					1.47

[1] The dead load shear demand was inherently present in the laboratory structure and was accounted for in predicted values.

[2] Calculated as (Interior Girder LL Shear Demand / Bridge Cross-Sectional LL Shear Demand from Statics)

[3] Taken from figures discussed in Section 5.4.2 for data at d_v

[4] From the "S-over" equation for two lanes loaded. Using the AASHTO shear DF to distribute the bridge cross-sectional LL shear demand due to a single patch load to an individual girder was not the intention of the AASHTO Specification.

Figure 5-1. Steel Prop Simulating Potential Effect of Intermediate Diaphragm below Girders

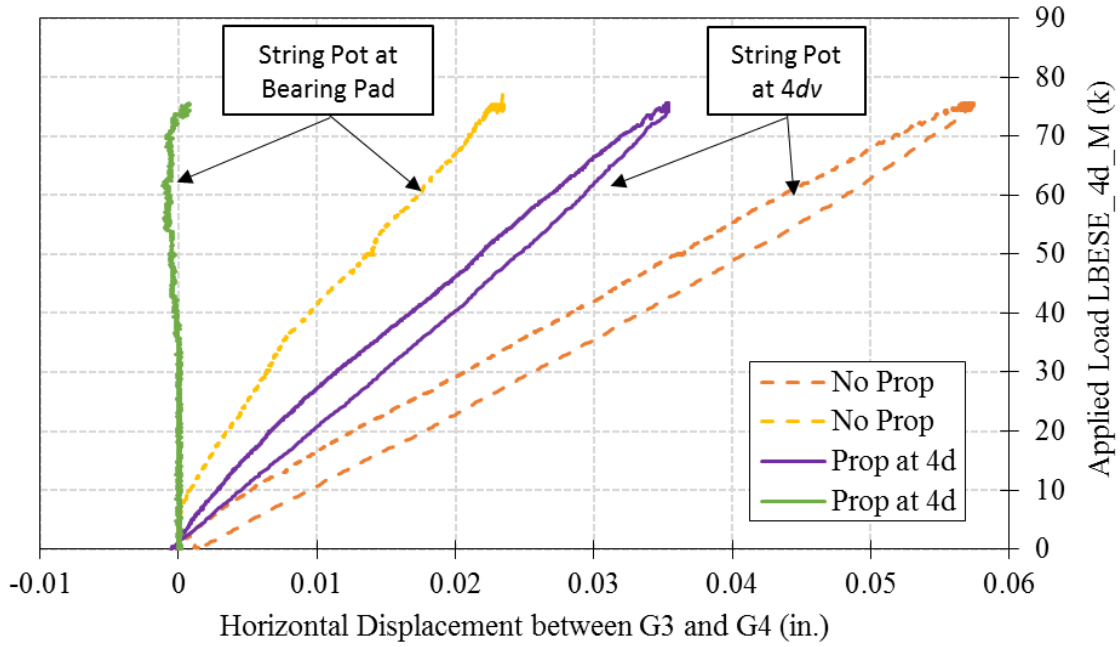

Figure 5-2. Influence of Steel Prop on Girder Horizontal Displacement

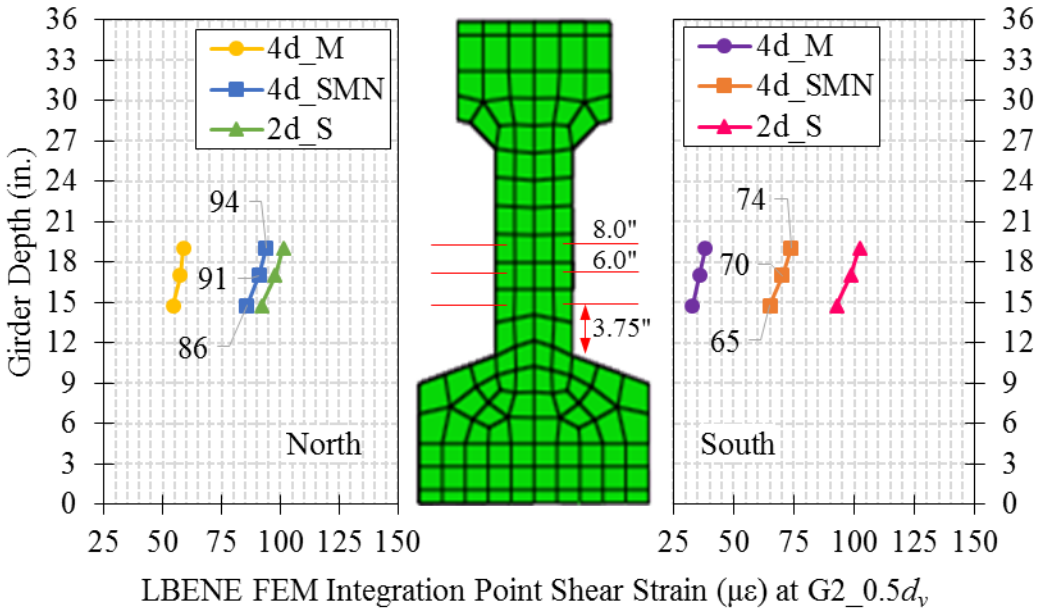

Figure 5-3. Shear Strain Variation through Girder Web Depth for LBENE

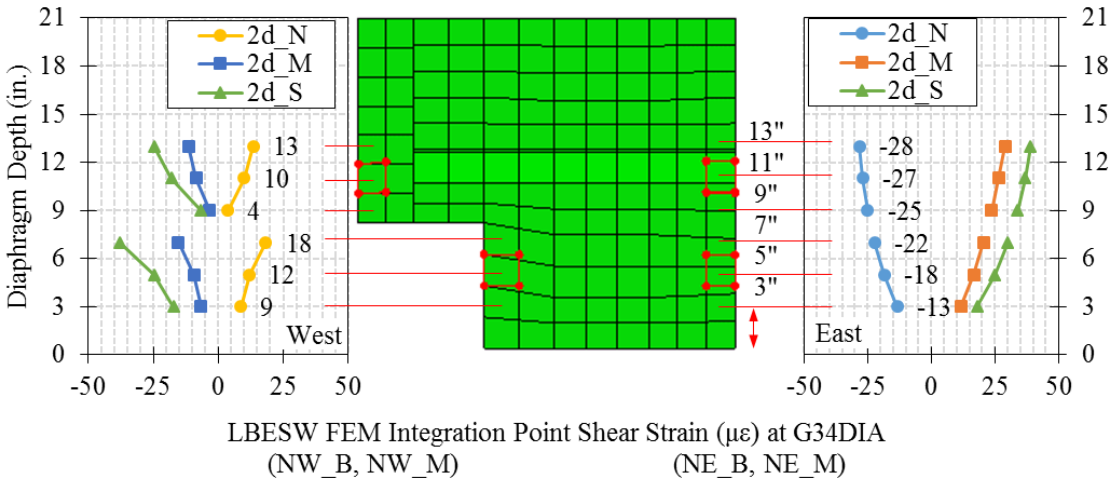

Figure 5-4. Shear Strain Variation through End Diaphragm Depth for LBESW

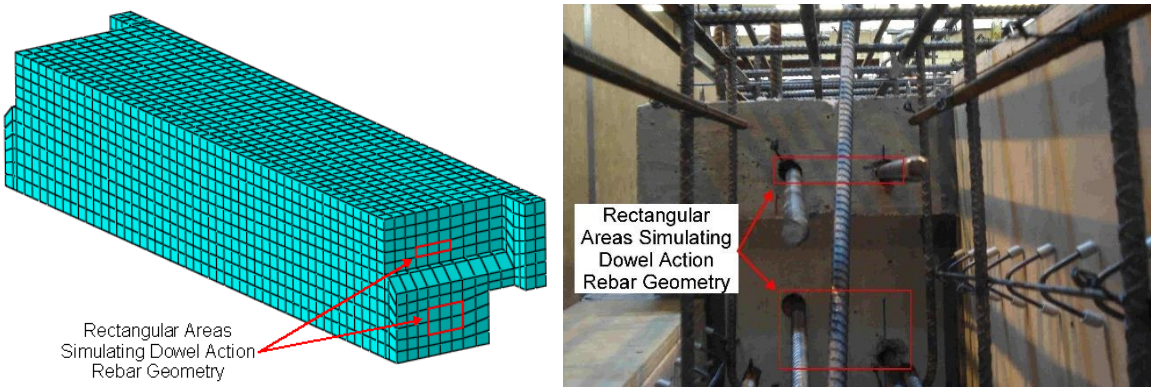

Figure 5-5. End Diaphragm Pinned Fixity Simulating As-Built Connectivity

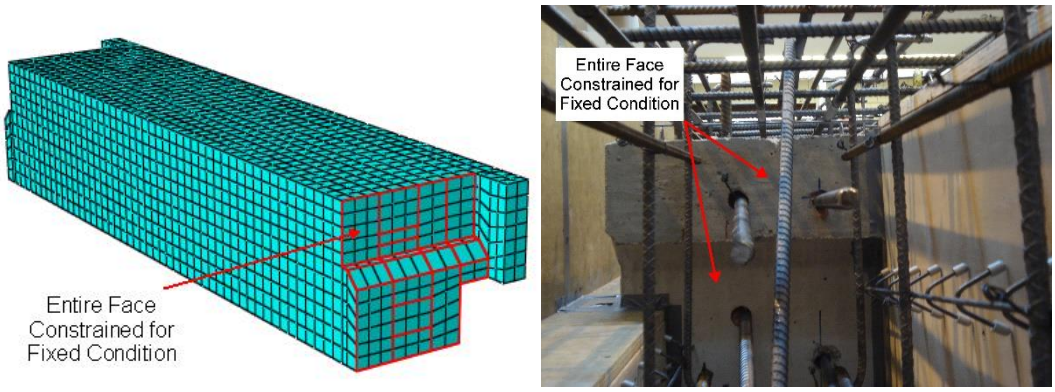

Figure 5-6. End Diaphragm Rigid Fixity Simulating As-Built Connectivity

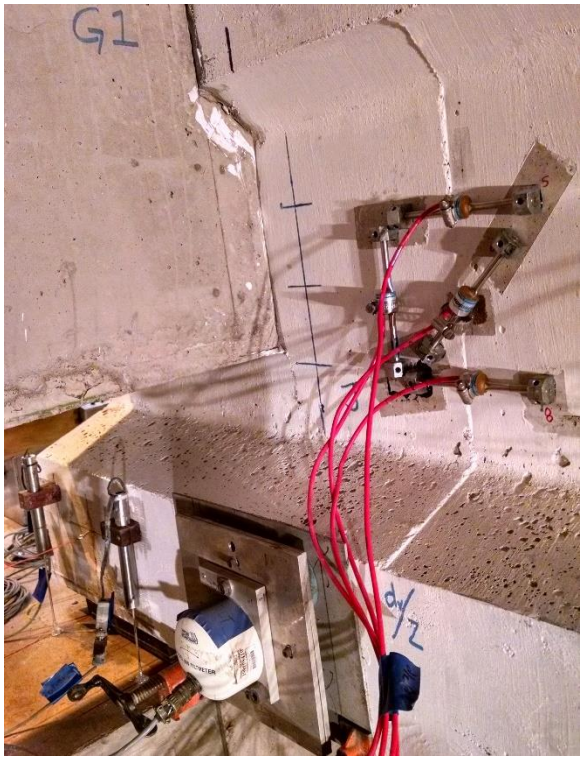

Figure 5-7. Instrumentation at 0.5d_v near End Diaphragm

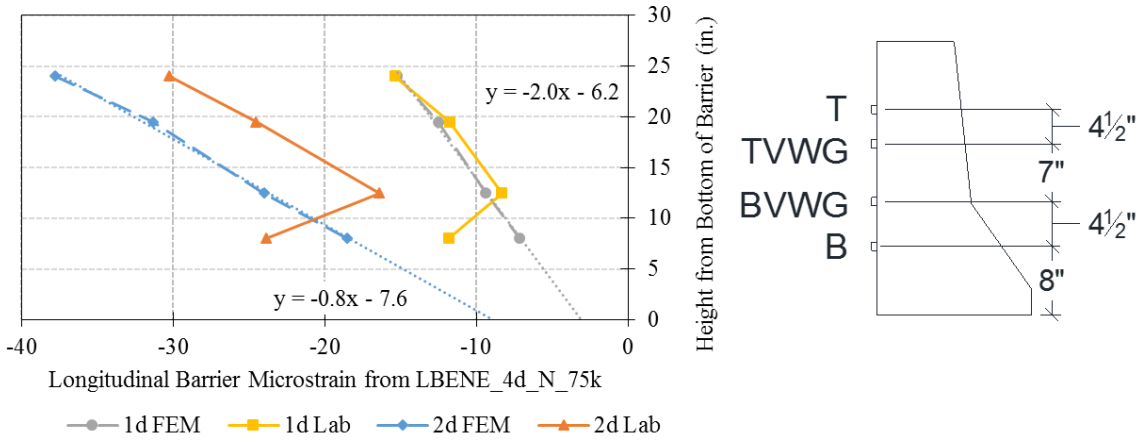

Figure 5-8. Barrier Longitudinal Strain through Section at 1d_v and 2d_v for LBENE

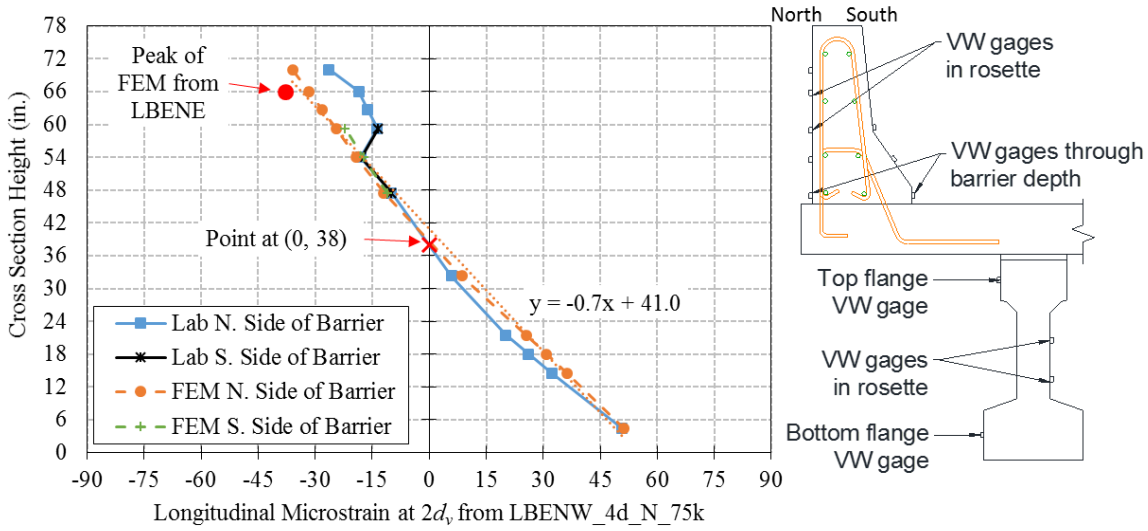

Figure 5-9. Exterior Girder and Barrier Neutral Axis from LBENW_4d_N_75k

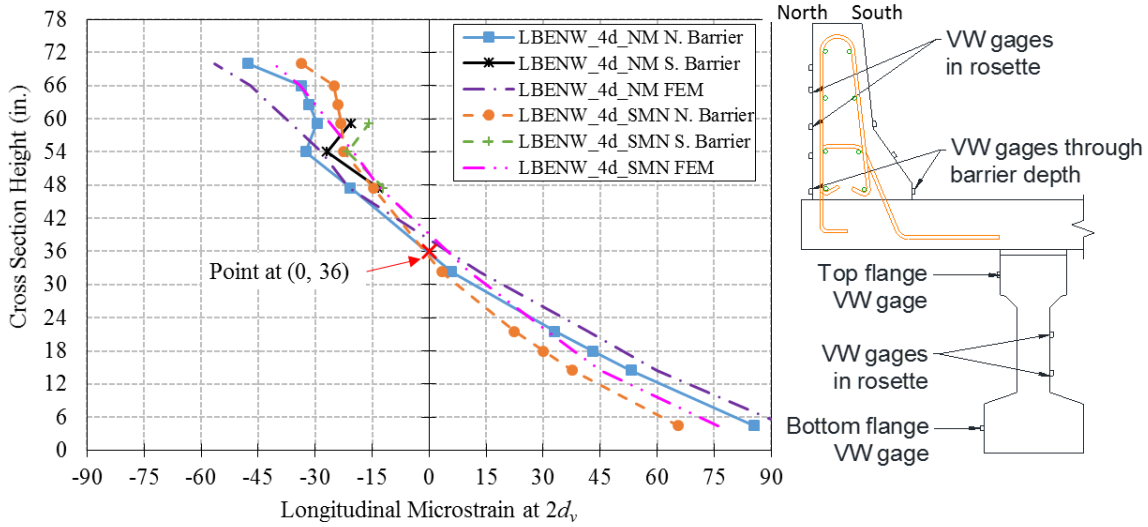

Figure 5-10. Exterior Girder and Barrier Neutral Axis from LBENW_4d_NM_75k and SMN_50k

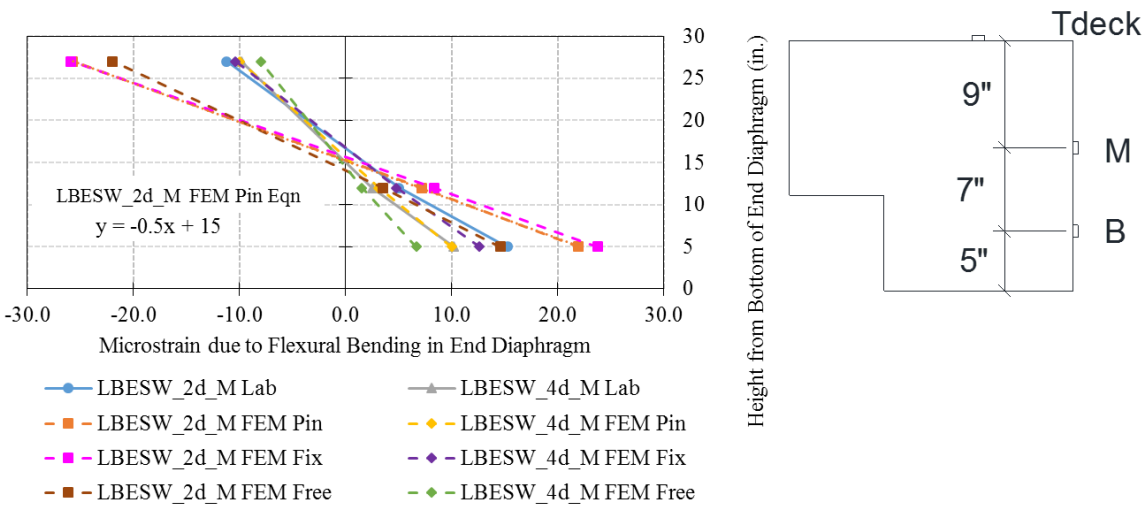

Figure 5-11. Comparison of End Diaphragm Neutral Axis for LBESW

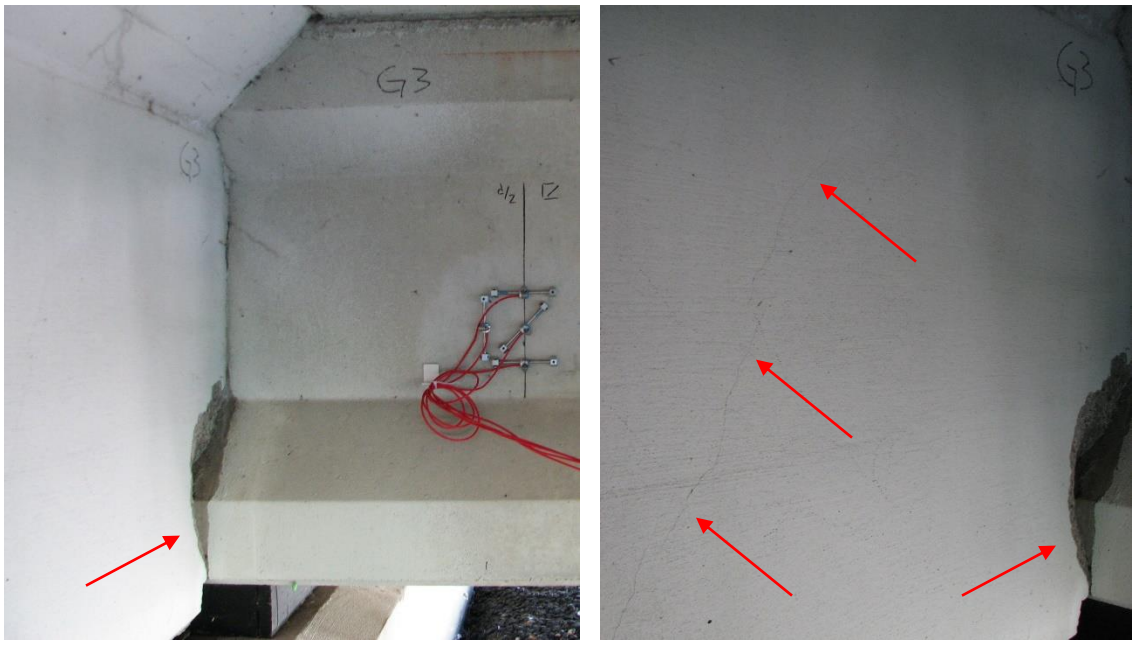

Figure 5-12. End Diaphragm Cracking Observed in Field Bridge 73872

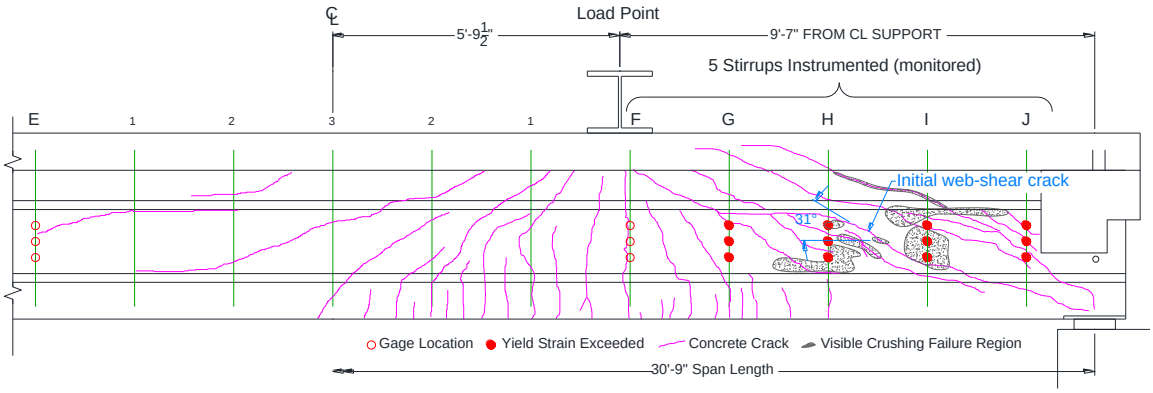

Figure 5-13. Girder 3 Northwest Cracking and Failure from LBUW Looking South

Figure 5-14. Web-Shear Crushing and Deck Punching in G3 during LBUW Looking South

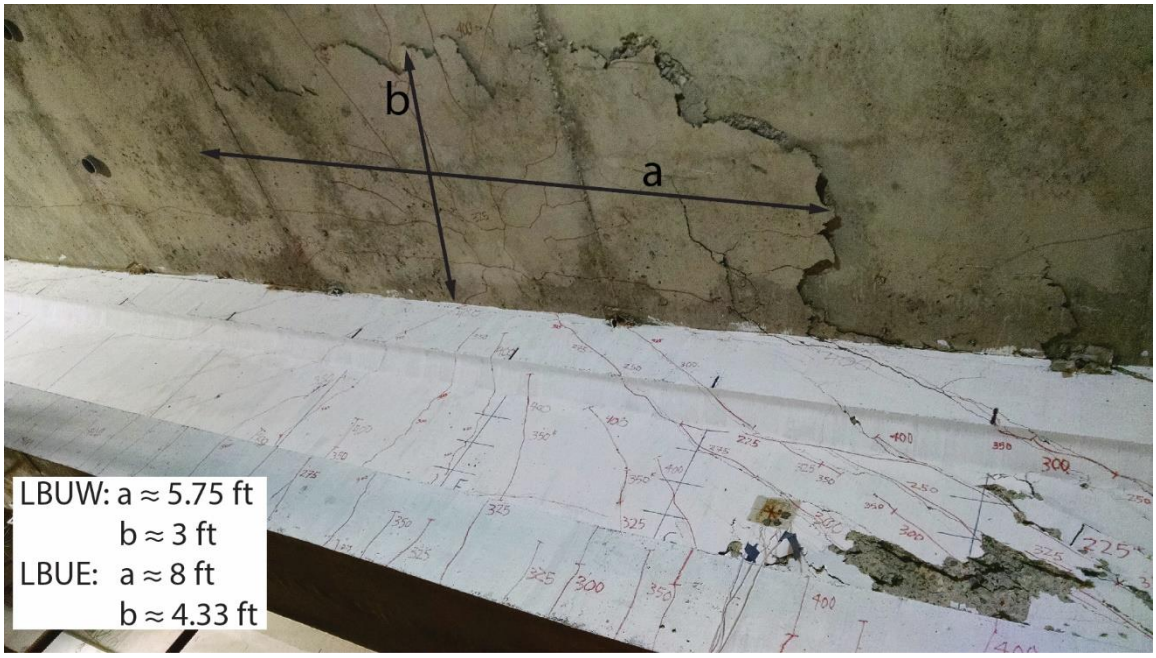

Figure 5-15. Typical Deck Punching Surface below Slab

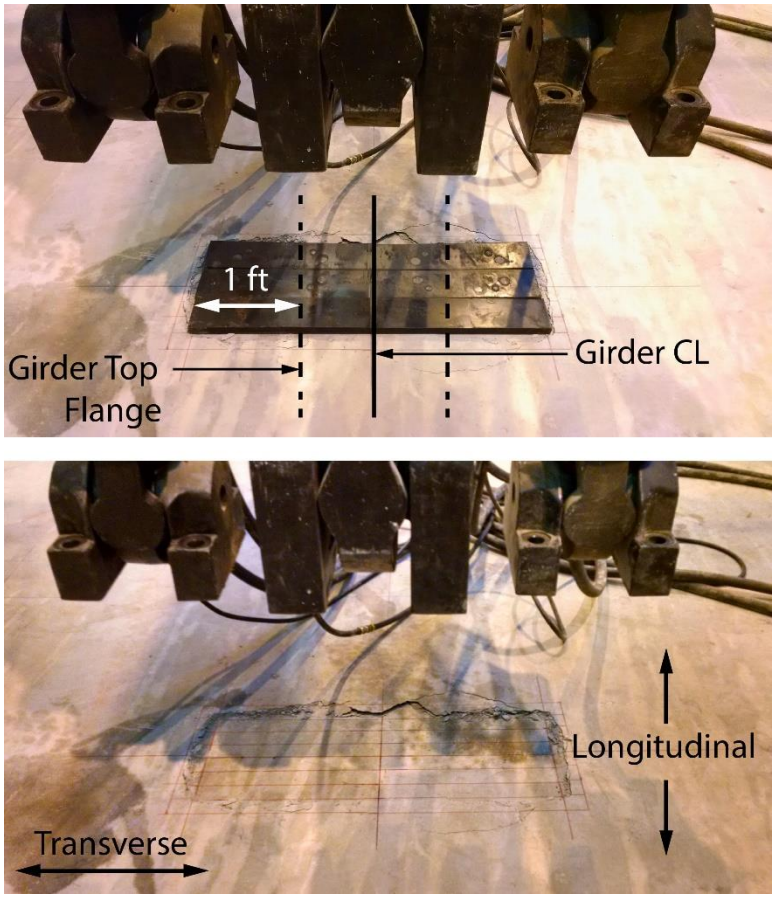

Figure 5-16. Typical Deck Punching Surface above Slab

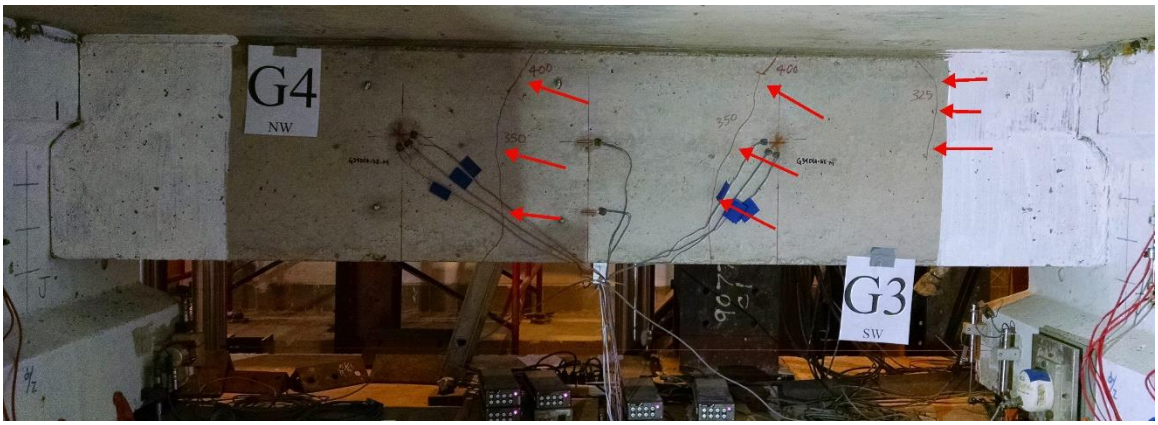

Figure 5-17. Diagonal Cracks on End Diaphragm between G3 and G4 during LBUW

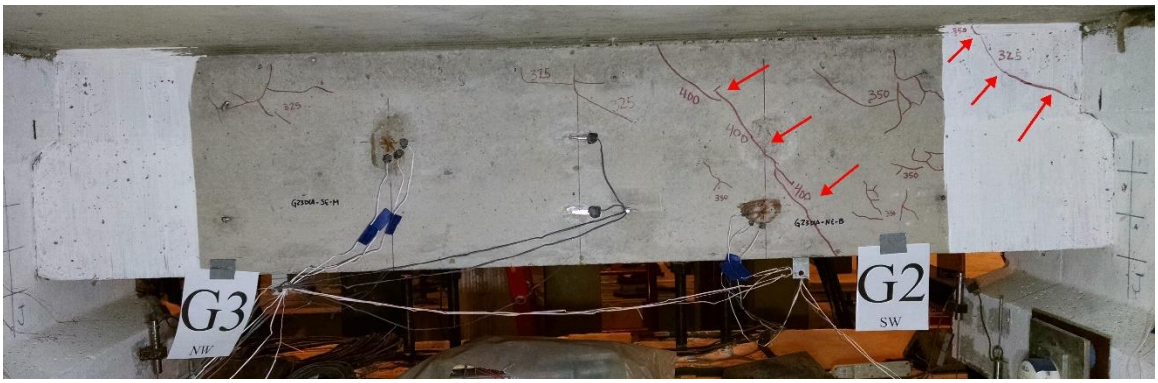

Figure 5-18. Diagonal Cracks on End Diaphragm between G2 and G3 during LBUW

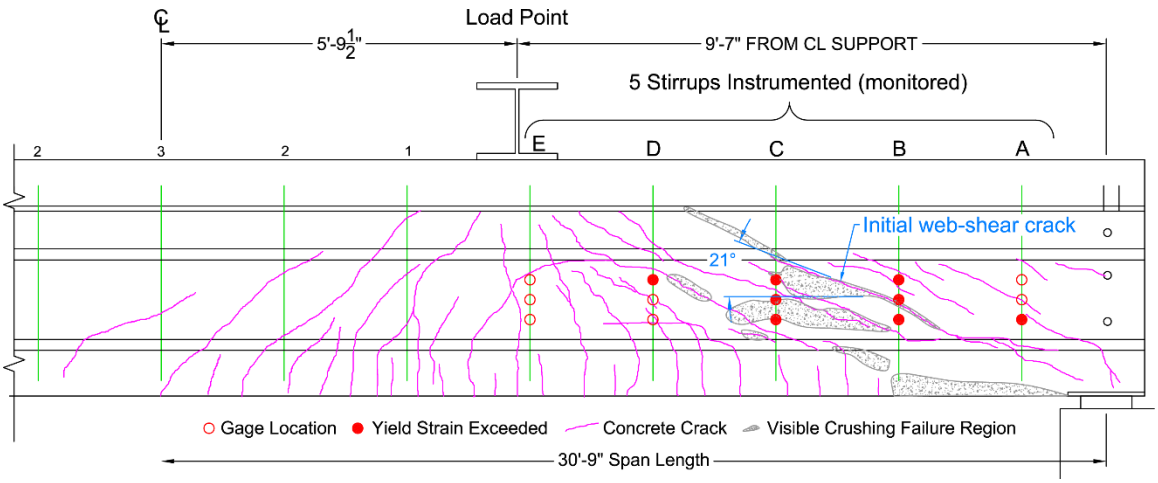

Figure 5-19. Girder 2 Southeast Cracking and Failure from LBUE Looking North

Figure 5-20. Web-Shear Crushing and Deck Punching in G2 during LBUE Looking North

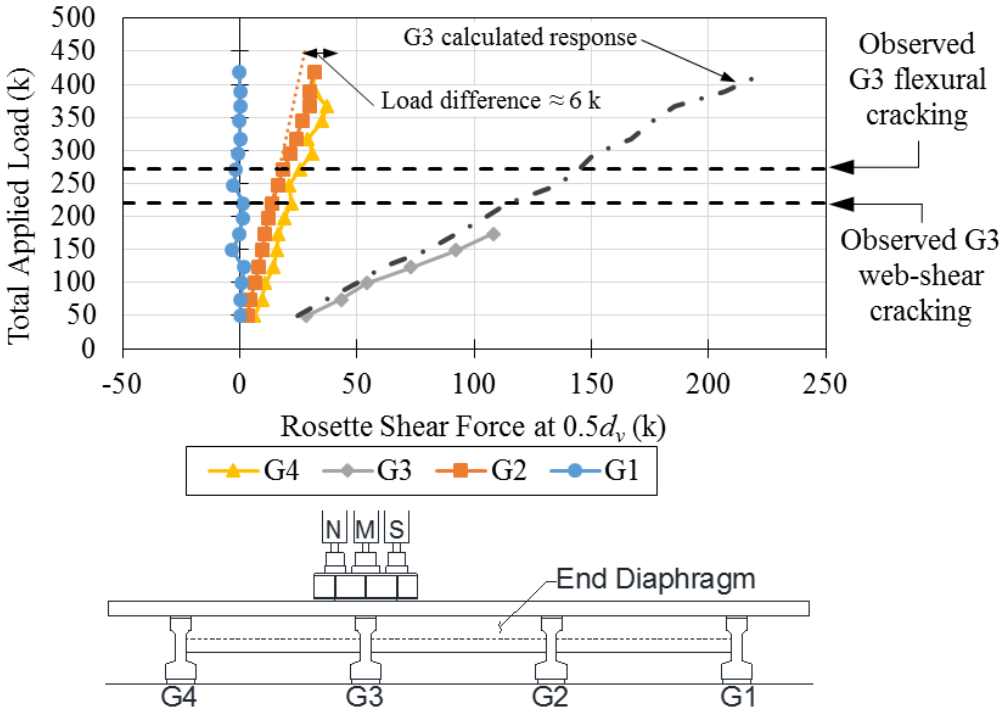

Figure 5-21. Shear Redistribution at 0.5d_v during LBUW

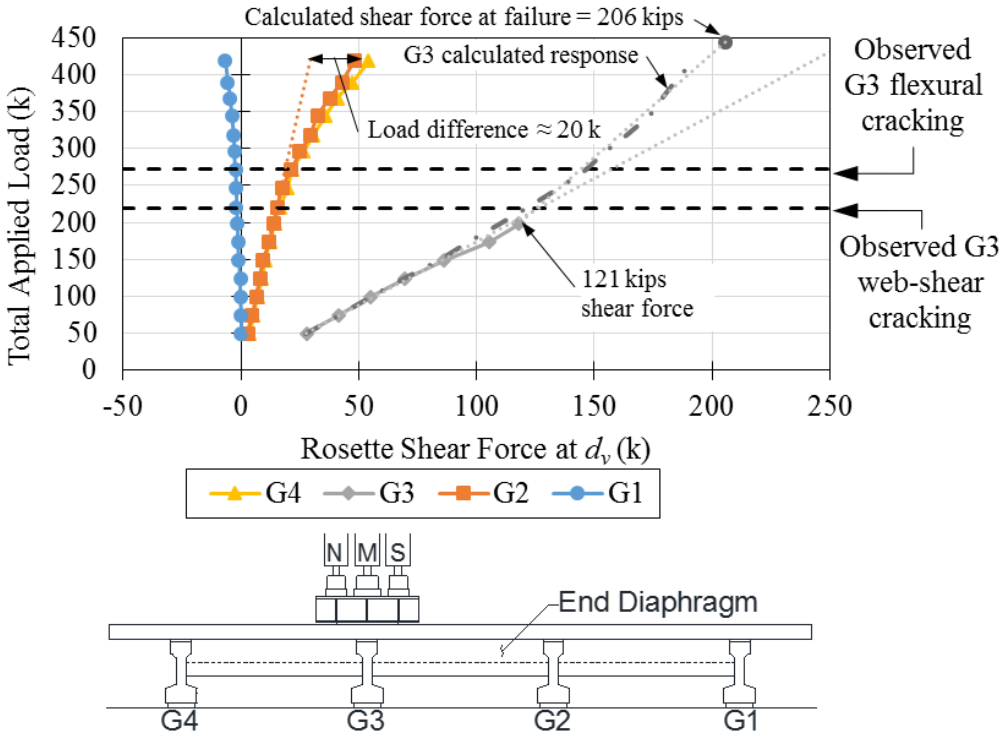

Figure 5-22. Shear Redistribution at d_v during LBUW

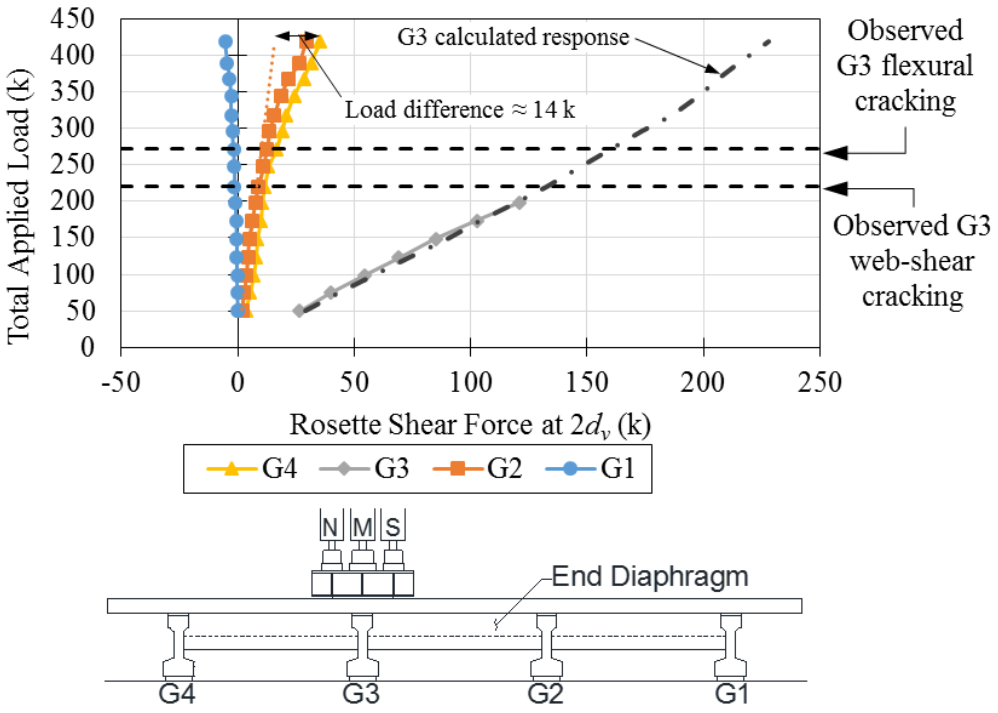

Figure 5-23. Shear Redistribution at $2d_v$ during LBUW

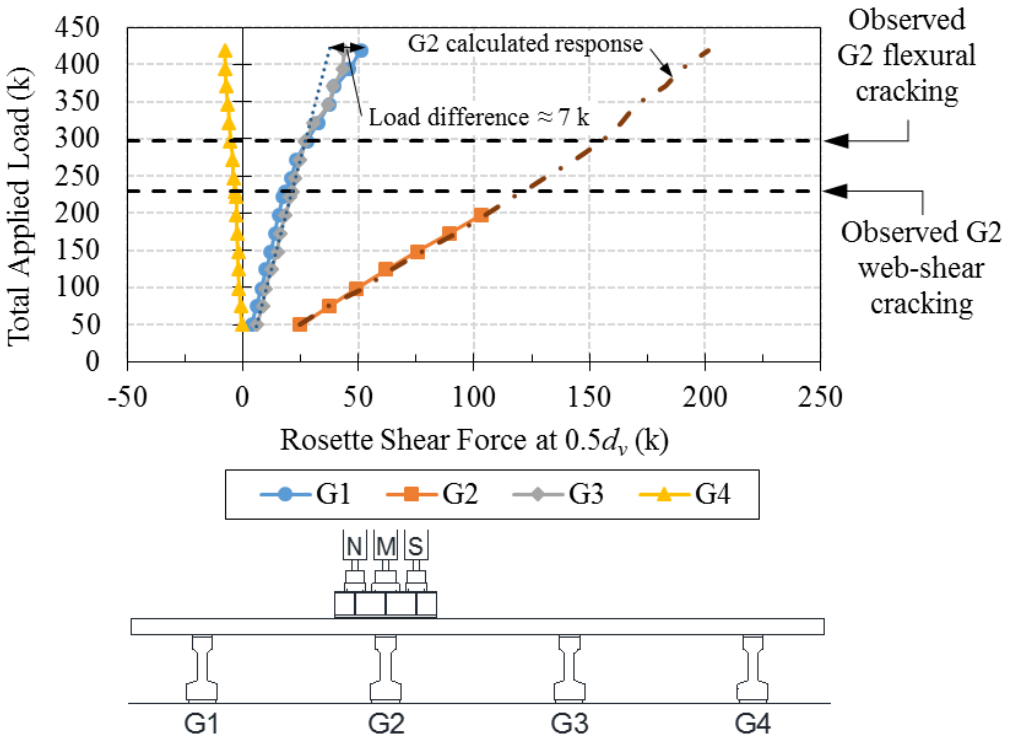

Figure 5-24. Shear Redistribution at 0.5d_v during LBUE

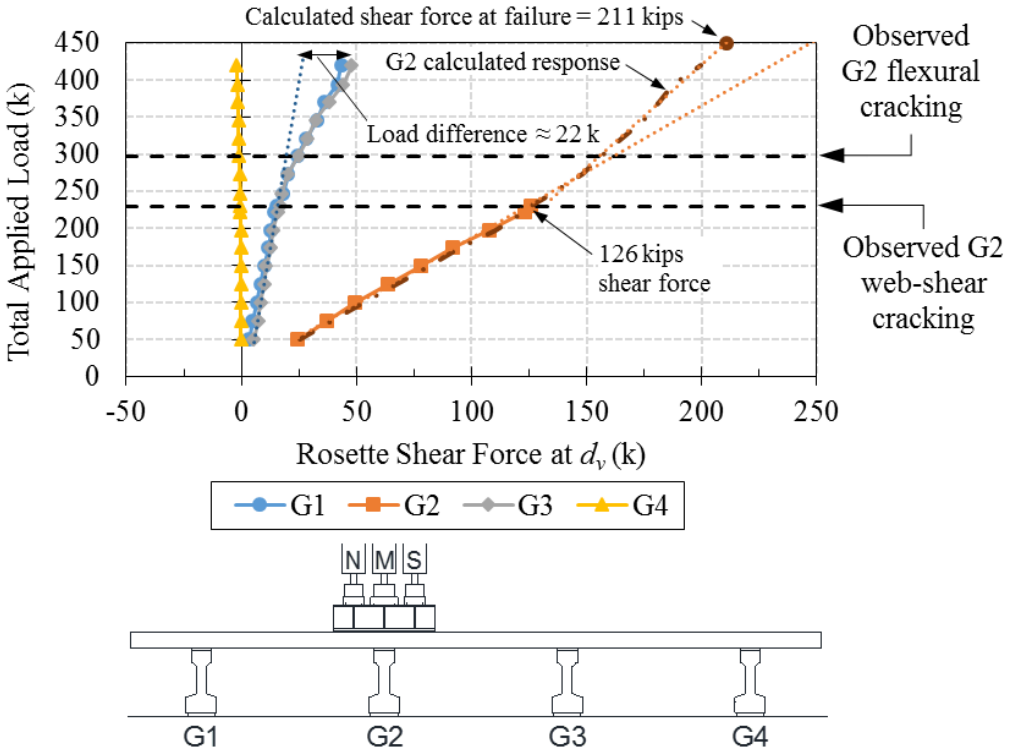

Figure 5-25. Shear Redistribution at d_v during LBUE

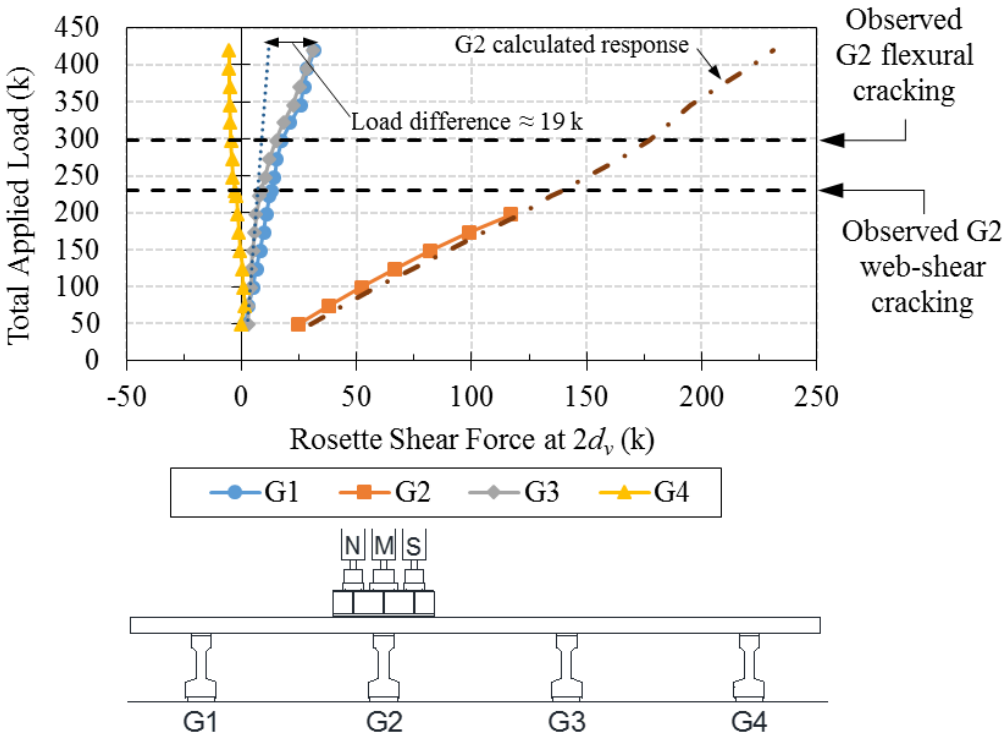

Figure 5-26. Shear Redistribution at 2d_v during LBUE

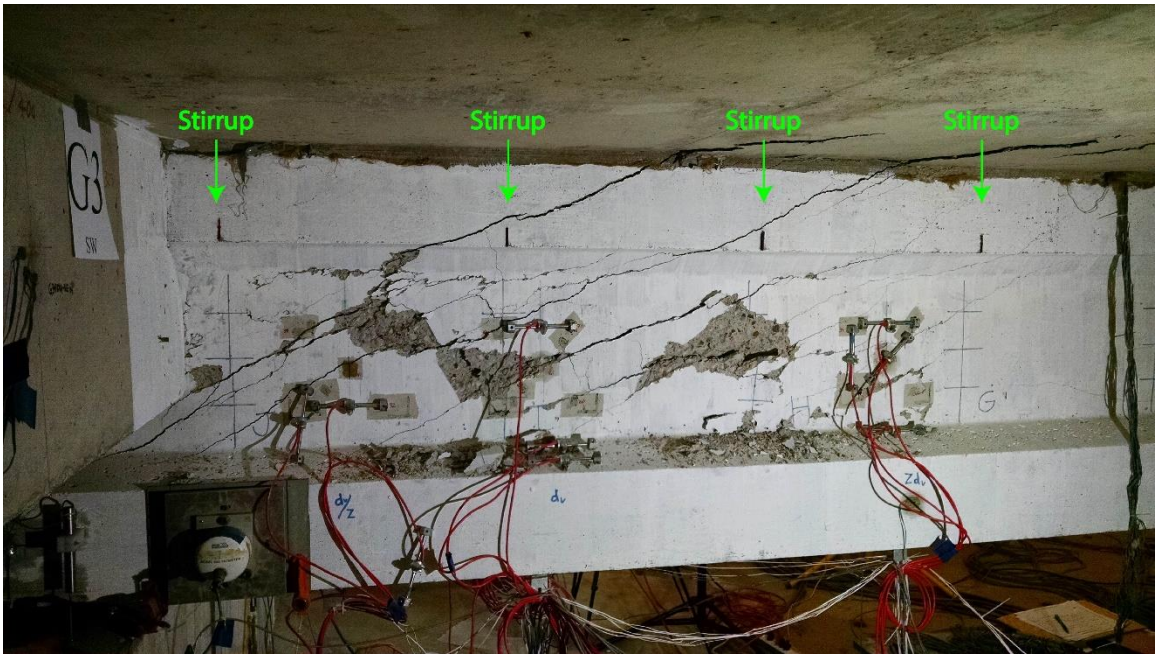

Figure 5-27. Web-Shear Cracking Pattern in G3 during LBUW (end diaphragm)

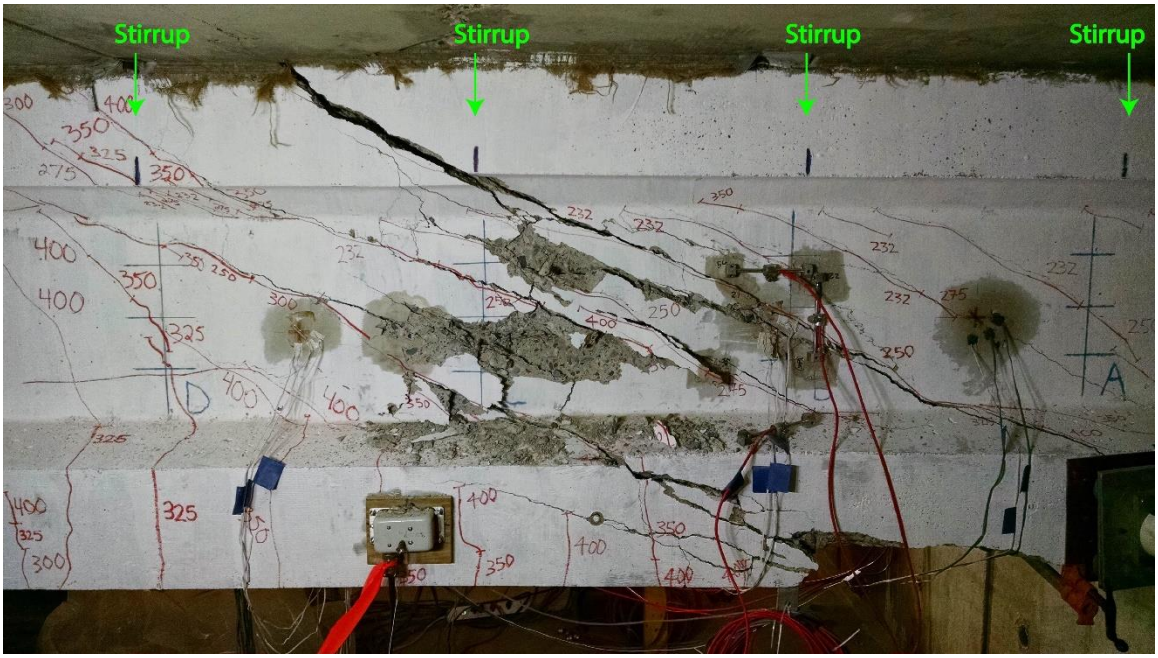

Figure 5-28. Web-Shear Cracking Pattern in G2 during LBUE (no end diaphragm)

CHAPTER 6. FIELD BRIDGE TESTING METHODS AND RESULTS

6.1 Introduction

The original goal of live load testing field bridges was to evaluate the distribution of shear forces in as-built prestressed concrete bridges at service load levels to more accurately assess load carrying capacity. Load tests with weighted sand dump trucks were completed on six prestressed concrete girder bridges from the MnDOT inventory during the summers of 2012 and 2013. Furthermore, single interior girders were salvaged from two field bridges (not part of the six field tested) when the structures were removed from service. Test setup information and the load at which shear cracking, flexural cracking, and ultimate failure occurred during the single girder tests are discussed in Appendix F.

6.1.1 Bridge Selection

Selection of the bridges for live load testing accounted for bridge characteristics that were considered to affect shear distribution, including:

- girder depth
- girder type/shape
- girder spacing
- number of girders in end span
- span length and aspect ratio
- skew
- end diaphragm type
- support fixity and continuity

Bridges were selected on the basis of trying to vary a single parameter from bridge to bridge to isolate the effect of the parameter on behavior. Additionally, bridges that rated low for shear were preferred in the selection of field bridges for study.

A database outlined by Dereli et al. (2010) in MnDOT Report 2010-03 indicated that the majority of MnDOT bridges with inventory shear rating factors below unity were designed according to AASHTO Specifications prevalent in 1965 through 1983 and were constructed with 36, 45, or 54 in. deep girders. Using this information and the identified

important bridge characteristics, six bridges were selected for field investigation. Table 6-1 highlights these structures.

The first two bridges tested were very similar structures built with 54 in. AASHTO Type IV girders. The main difference between the two bridges was the type of end diaphragm. The first bridge tested had a partial depth end diaphragm that had no visible cracking. The second bridge tested had a full depth end diaphragm that exhibited cracking at the girder to diaphragm interface, as shown in Figure 6-1. Results from testing these two bridges were expected to provide insight as to how the type of end diaphragm affected the shear distribution near the critical section of the girder.

The third field tested bridge was constructed with 45 in. AASHTO Type III girders, and the fourth field tested bridge was constructed with MnDOT 45M girders. Field testing a bridge constructed with 45M girders was expected to provide insight as to how the wider top flange, shown in Figure 6-2, interacted with the bridge deck and affected the distribution of live load shear.

The fifth and sixth bridges investigated were very similar structures built with 36 in. AASHTO Type II girders. The main difference between the two bridges was the angle of skew. The fifth bridge had no skew and the sixth bridge had a 30 degree skew angle. The effect of skew on shear distribution was not comprehensively studied using experimental methods due to a limited number of field specimen. However, field testing both a skewed and non-skewed structure built with 36 in. AASHTO Type II girders and testing a non-skewed laboratory bridge built with girders of approximately the same shape was expected to provide data that linked the shear distribution behavior of skewed prestressed girder field bridges to behavior observed under controlled conditions in the laboratory.

6.2 Determination of Applied Load and Instrument Type

A three-dimensional grillage model was prepared for Bridge 73852 to aid in the determination of the loading and instrumentation plans for this bridge. Shear strain through the depth of the composite girder section was calculated using linear elastic principles and mechanics of materials approaches. The resulting low magnitudes of the calculated shear strain, $\gamma_{xy,}$ (approximately 30-40 με calculated from strain gages in a rosette that have

resolution on the order of 1-2 με) obtained using load applied by a single dump truck with geometry and weight information described by Altay et al. (2003), dictated the need to apply as large a truck load as possible. Maximum applied load required two tri-axle MnDOT sand dump trucks parked back-to-back, as shown in Figure 6-3, so that the rear tandem axles were as close as possible. Truck loads used in field testing consisted of approximately one 15.4 kip front axle and two 17.3 kip rear axles spaced 4.5 ft longitudinally. Individual truck weights, approximately 50 kips each, and axle weights were recorded at certified truck scales before and after testing. More detail on the individual truck dimensions and weights for each field test can be found in Appendix G. Each front tire had a contact patch that was approximately 8 in. long by 12 in. wide, and each rear tire set had a contact patch that was approximately 8 in. long by 22 in. wide (considering adjacent tires). Placed appropriately on the bridge, the back-to-back truck loading produced more shear strain and shear force in any single girder when compared to loading the bridge with a single truck or two side-by-side trucks.

The targeted minimum strain to be picked up on the horizontal, vertical, or diagonal legs of a strain gage rosette was approximately 5 με. Furthermore, fine resolution vibrating wire strain gages capable of detecting changes on the order of 1-2 με due to static loading were required to capture small magnitude strains on the prestressed concrete bridge girders. Research has shown that capturing small magnitude rosette strain was possible during load testing of field bridges (Milam and Ma 2005, Cross et al. 2010).

Results from the three-dimensional grillage model were used to select VWG box-type rosette locations on the girders of each field bridge. The neutral axis of the composite girder sections (where shear strain readings would be maximized) was not in the web and was typically in the girder top flange or at an elevation where the box-type rosette could not be adhered to a vertical face (e.g., chamfer of the girder top flange). To select an appropriate location for the box-type rosettes, the relationship between composite section depth and strain was investigated to determine the amount of strain variation in each leg of the rosette (horizontal, diagonal, and vertical) in the girder web for Bridge 73852. The predicted variation of strain in the vertical strain gage was zero, and the predicted strain in the horizontal strain gage varied linearly with the web depth as the gage moved from the neutral axis (horizontally oriented strain gages captured the largest magnitude bending

strain near the bottom of the section depth). The predicted variation of strain in the diagonal strain gage was less than 2 με through the depth of the web. Because the box-type rosette could not be placed near the neutral axis, it was determined that placing the rosette near the bottom of the web (the center of the rosette was approximately 7 in. above the bottom flange-to-web interface) would maximize both the horizontal and diagonal strain gage signal. This allowed for both calculation of a large magnitude shear strain and potential use of the horizontal strain gages to calculate the neutral axis of the cross section.

Box-type rosettes, outlined for laboratory testing in Section 4.5.4, were applied to one side of the girder web during field testing using the following criteria: instrument all bridge girders at each specific longitudinal section of interest to collect data related to shear distribution across the entire bridge section, instrument as many bridge cross sections as possible to collect data related to shear distribution along the length of the span, and maximize use of the data acquisition system which was limited to data collection from 80 Model 4000 vibrating wire strain gages per bridge. During field testing, the effects of torsion on the measured shear strains was not well understood and instruments were not placed on both sides of the girder web.

6.3 Field Location of Vibrating Wire Gages

Each field bridge had either four or five beams. Vibrating wire strain gages were installed on each girder (i.e., G1 through G4 or G5, depending on whether it was a four or five girder bridge). Table 6-2 shows the location of instrumentation for each field bridge. Within this table, box-type rosettes are indicated by the letter R, longitudinal VW gages installed on the bottom flange or web are indicated by the letter L, and individual diagonal or top VW strain gages in the box-type rosette (when the entire box-type rosette was not installed) are indicated by the letter D or T, respectively. A location that contained only two longitudinal gages was instrumented such that one gage was centered vertically on the bottom flange and the second gage was placed directly above on the web. At select locations, an additional longitudinal gage was placed on the exterior face of the bottom flange directly below a box-type rosette as shown in Figure 6-4. The extra longitudinal strain measurement through the section depth assisted with determination of the girder neutral axis depth. Additionally, a box-type rosette, sometimes with a supplemental

longitudinal strain gage, was installed on the barrier (B) of the first four bridges. More detail on individual field bridge instrumentation plans can be found in Appendix G.

The box-type rosettes were typically placed on one side of the girder web on all girders in the end span of each field bridge to measure the transverse distribution of shear strain. For all testing scenarios, strain gages were placed at various longitudinal locations on each girder to determine the shear strain distribution along the length of the span. Typically, the longitudinal gage locations were related to the critical section for shear, taken as d_v from the support face (edge of sole plate or edge of bearing, whichever was closer to midspan), but instrumentation was also installed relative to the span length, L, for some field bridges. This type of rosette instrumentation grid allowed for interpretation of strain at many cross sections longitudinally and also allowed for investigation of transverse symmetry (e.g., if the response caused by loading one exterior girder in a cross section was similar to the response caused by similarly loading the other exterior girder in the same cross section).

The majority of the live load testing and instrumentation focused on the abutment end of each end span. Specifically, one corner of the end span, at the intersection of an exterior girder and abutment, was selected to be the focus corner for the instrumentation and live load testing. The focus corner was located using cardinal directions. Instrumentation was also installed near the pier on the last two field bridges to obtain data at d_v from both ends of the span, but the live load testing was still focused on the abutment end of the span. Obtaining data from both ends of the span allowed for investigation of longitudinal symmetry (e.g., if the response at d_v near the abutment and d_v near the pier were similar when back-to-back trucks were centered at midspan longitudinally) and comparison of the girder response considering differences in the type of diaphragm and deck continuity at the abutment versus at the pier. Furthermore, the last bridge tested had a 30 degree skew and installing gages at the pier end of the span allowed for collection of data at both acute and both obtuse corners. The pier side of the end span was tested separately on the first two bridges to investigate the effect of no end diaphragm directly above the bearing pad at the pier. Diaphragms at the pier were similar to the intermediate diaphragms, not the abutment end diaphragms, and were located approximately 2 to 5 ft toward midspan. Because of the limited number of VW strain gages, instrumenting the pier

end of the end span involved removal of the abutment end instrumentation and re-installation of vibrating wire strain gages near the pier using a bucket truck.

6.4 Field Location of Live Load Trucks

Strain measurements were gathered after the trucks were parked at predetermined locations on the bridge deck. Truck locations were chosen to study the influence of loading over interior versus exterior girders, longitudinal position of loading, and loading over girders versus in between girders. The majority of the live load testing occurred near the focus corner, designated using cardinal directions, on the abutment side of an end span. Live load was applied with two tri-axle MnDOT sand dump trucks parked in various configurations: back-to-back (BB) so that the rear tandem axles were as close as possible, a single truck (ST) unmoved from a previous back-to-back configuration (enabling a superposition analysis), and two trucks facing the same direction parked side-by-side (SS) such that their rear axles aligned. More detail on the individual truck dimensions and weights for each field test can be found in Appendix G.

MnDOT sand trucks were transversely positioned across the bridge in relation to the bridge girders (G1-G4 or G1-G5) and longitudinally positioned in relation to a line of strain gage rosettes. Care was taken to avoid placing truck axles directly over a line of strain gages because of the disturbed region associated with the wheel loads. The strain profile through the depth of the cross section in the disturbed region may not be linear, as conventional Bernoulli beam theory is not applicable. Over the exterior girder, trucks were transversely positioned so that the exterior wheel line was directly over the centerline of the beam or as close as possible if the bridge deck width or barrier did not allow for the wheel to be placed over the girder. Over an interior girder, trucks were positioned so that each wheel line was an equal distance away from the centerline of the beam (straddling the beam). Trucks were also transversely located between girders (exterior-interior or interior-interior) so that the centerline of the trucks aligned with the centerline of the beam spacing.

Longitudinal truck positions (denoted with Loc for location and a number), given in Table 6-3, were chosen such that sets of axles in a back-to-back (BB), side-by-side (SS), or a single truck (ST) configuration were further into the span than a section of interest corresponding to a transverse line of rosette strain gages or centered at a location of interest (which was only the case for Loc 11 position, where two back-to-back trucks were centered

longitudinally at $L/2$ regardless of gage position so that the reaction due to live load at each end of the span was approximately equal). Typically, the longitudinal location of back-to-back trucks was selected to keep axles at least one girder depth away from a transverse line of gages; however, this was not always possible due to the length and number of axles in the back-to-back truck configuration compared to the length of the span and location of gages longitudinally. The order of longitudinal truck locations listed in Table 6-3 generally corresponded to the order of truck positioning used to investigate each transverse location of interest along the span length (i.e., Loc 3 always preceded Loc 0, Loc 5 always preceded Loc 1, and Loc 3/Loc 5 preceded Loc 7 or Loc 9). The numbering scheme used in Table 6-3 was a remnant of initial planning stages when there were more than 12 total load cases, which involved moving the back-to-back trucks in 2 ft intervals along the length of the structure; the number of load cases (and their corresponding position) was selectively reduced to those shown in Table 6-3 so that live load testing could be completed in one business day to reduce the bridge closure time that was required during testing.

Trucks were manually directed into position during testing using chalk lines as a guide on the bridge deck that corresponded to transverse locations measured from the inside of the barrier and longitudinal locations measured from the deck side of the expansion joint between the approach slab and bridge deck, as annotated in Figure 6-3. The centerline of the rear-most axle of the lead vehicle was aligned with the transverse chalk lines. For the skewed structure, Bridge 65006, locations of transverse chalk lines were always measured from the obtuse skew corner of the bridge. Longitudinal chalk lines aligned with the centerline of the driver's side front tire. Figure 6-5 shows a representative back-to-back truck configuration from testing of Bridge 73872 (no-skew) and the ensuing single truck position. The trucks shown in Figure 6-5 are transversely splitting Girder 1 and Girder 2 and longitudinally placed at test Location 3 such that all tandem axles are beyond the d_v section of interest.

The position of back-to-back trucks for each live load test were set by first parking the lead truck in the appropriate location at the intersection of a transverse and longitudinal chalk line, and second, parking the rear truck as close as possible to the lead truck (touching tailgates) along the same longitudinal line. Single truck testing positions were obtained from the preceding back-to-back test. Following a back-to-back configuration, the lead

vehicle was driven forward off the bridge and approach slab such that the single rear truck was left in the same position, as shown in Figure 6-5. To utilize other back-to-back testing locations along the same longitudinal line, the lead truck either returned to the span in reverse and was parked at the appropriate transverse line (after a single truck test) or was moved forward to the appropriate transverse line (after a back-to-back truck test). The red horizontal lines in Figure 6-5 indicate where the transverse lines of instrumentation were applied to the superstructure and the blue transverse lines define the location of the truck testing positions. Side-by-side truck configurations were also obtained from the preceding back-to-back test positioning. Following a back-to-back test, the rear truck was turned around and parked next to the lead vehicle (as close as possible) such that the rear-most axles aligned on the same transverse chalk line.

Table 6-4 and Table 6-5 show the live load testing protocol for each field bridge. A back-to-back truck configuration is abbreviated BB, a single truck configuration is abbreviated with an ST, and a side-by-side truck configuration is abbreviated SS. All tests were completed once and some were completed two or three times to check for repeatability. Superscript values on the truck configuration indicate the number of times the test location was repeated throughout a testing day. Each field bridge live load testing protocol also included periodic zero-readings, not shown in Table 6-4 and Table 6-5. Zero-reading strain gage data was collected when no trucks or live traffic were on the bridge. Zero-reading measurements were always taken prior to positioning the first trucks on the bridge and at the end of testing after all the trucks were removed from the bridge. Zero-reading measurements were also taken periodically throughout the course of a testing day. Typically, a block of four or five live load tests were performed between zero-readings, which were taken approximately once per hour. The zero-readings were used eliminate the effects of temperature change on the measured strains. The bridge naturally changes shape as the temperature gradients in the deck change over time. The strain gages were sensitive to both the thermally induced deformations as well as the truck load induced deformations. Data collection, filtering, and processing details are discussed in Section 6.5.

The pier side of the end span was also investigated on the first two bridges tested, as shown in Table 6-5. This involved removal of the abutment end instrumentation and re-installation of instrumentation near the pier. The truck testing protocol from the abutment

end of the span was duplicated on the pier end of the span. Specific trucks and their positions were mirrored longitudinally about the centerline of the span. The lead truck from the abutment end testing (driving onto the end span from the approach slab) was also used as the lead truck on the pier end testing (driving onto the end span from the second span of the structure). More detail on individual field bridge testing protocol can be found in Appendix G.

Longitudinal test Location 1 for Bridge 08011, marked by an asterisk (*) in Table 6-4, at G1, G2, G2-G3, and G3 was different than other test Location 1 configurations. The single truck left from the previous back-to-back configuration was flipped longitudinally so the rear tandem tires were in the same four locations as a normal Location 1 test, but the front axle was further into the span under investigation rather than located in the adjacent span. This configuration, shown in Figure 6-6, was achieved by chalking a box around the four outside tandem wheels of the lead truck during the previous back-to-back configuration. When back-to-back testing was completed, the rear vehicle was driven off the bridge and approach slab and the lead vehicle backed into the chalked wheel boxes. This method of truck placement was different than the case of the single truck at the abutment where the lead vehicle was driven off the bridge.

6.5 Vibrating Wire Gage Data Processing

6.5.1 Averaged Strain Readings

Field bridge data for each live load truck configuration or zero-reading was collected as a set of five readings, corresponding to five separate cycles through all of the strain gages. Abnormally large strain variation within a five cycle data set was minimized by discarding a maximum of two data points if they deviated from the five cycle average by plus or minus 50 με. Average data points for each gage within each test were calculated from remaining data. During laboratory testing, it was found that keeping dust off of the Campbell Scientific multiplexers and the terminal boards where strain gages were wired was critical to preventing large strain deviations. Typically, in a dust-free laboratory environment, the variation in vibrating wire strain readings was approximately 2 με or less within the five cycle period. However, laboratory data indicated that dust buildup on the wiring can cause strain variations on the order of hundreds of microstrain in one five cycle

period. Collecting vibrating wire strain gage data during field testing inherently had more noise due to uncontrollable variables, however an effort was made to keep wiring as clean as possible by placing the data acquisition system inside a minivan.

6.5.2 Temperature Correction

Apparent strain readings obtained from the datalogger after live load testing were based on the resonant frequency of the vibrating steel wire. The apparent strain readings were converted to mechanical strain using the following equation:

$$\varepsilon_M = (G_1 - G_0)B + (T_1 - T_0)\ (CF_s - CF_c) \tag{6.1}$$

where ε_M is the mechanical strain, G_1 is the VWG strain reading at any time after the initial reading, G_0 is the initial VWG strain reading, B is the batch factor (0.96 for gages used), T_1 is the VWG thermistor temperature coincident in time with G_1, T_0 is the initial VWG thermistor temperature reading coincident with G_0, CF_s is the thermal coefficient of expansion of steel (assumed to be 12.2 με/°C), CF_c is the thermal coefficient of expansion of concrete (assumed to be 10.4 με/°C). Values assumed for the steel and concrete thermal coefficients were provided by the VWG manufacturer.

The first term of Eqn. (6.1) is the apparent strain reading, which accounts for the shortening/lengthening of the vibrating wire gage and is related to strain by the batch factor specified by the VWG manufacturer. The second term of Eqn. (6.1) represents an adjustment for the difference between the coefficients of thermal expansion of the steel VWG and the concrete on which the gage is installed. The resulting concrete mechanical strain includes both temperature-induced mechanical strain, from restrained movement due to temperature variation over the course of testing, and load-induced mechanical strain, from truck live loading. Separation of the temperature-induced mechanical strain from the load-induced mechanical strain was done by subtracting an unloaded temperature-induced mechanical strain reading from the total mechanical strain. The unloaded temperature-induced mechanical strain readings were calculated using a time-based linear interpolation between the zero-readings immediately before and after any given live load test. Positive strains were defined to be tensile and negative strains compressive.

An example of the temperature-induced mechanical strain correction is shown in Figure 6-7 through Figure 6-9 for two diagonal strain gages on Girder 1 of Bridge 09002 at d_v and $2d_v$. Figure 6-7 shows the VWG data including both temperature- and load-induced mechanical strains. Zero-readings were taken eight times over the course of testing Bridge 09002, and the times of the zero-readings are indicated by the solid vertical green lines. Zero-reading data in Figure 6-7 generally did not align with a value of zero microstrain over the course of the day due to temperature-induced mechanical strains. Figure 6-8 shows the unloaded temperature-induced mechanical strain data interpolated for the entire day. Data points in Figure 6-8 were subtracted from data points at the same time of day in Figure 6-7 to generate Figure 6-9. Figure 6-9 shows the resulting load-induced mechanical strain for each data point collected over the course of testing. Zero-reading data in Figure 6-9 now align with a value of zero microstrain over the course of the day. With this correction method, it is assumed that the temperature-induced mechanical strains vary linearly between zero-readings, which may not always be the case.

6.6 Validation of the FEM Technique

Simply-supported, three-dimensional solid finite element models of the end span tested for three field bridges were constructed in accordance with Section 3.3 to further validate the finite element modeling technique. Bridge 09002 (five 36 in. deep beams in a non-skewed, 39 ft span) and Bridge 65006 (five 36 in. deep beams in a 45 ft span with 30 degree skew) were the most similar to the laboratory bridge which contained five 36 in. deep beams in a non-skewed, 30.75 ft span. Bridge 08011 (five 45 in. deep M-shape beams in a non-skewed, 76 ft span) was investigated to represent a dissimilar case to the other bridges in terms of girder shape, span length, and ratio of longitudinal to transverse stiffness.

Assumptions used for each of the three FE models in regards to material properties, section properties, and bridge characteristics are given in Table 6-1 and Table 6-6. Concrete compressive strengths given on the bridge plans were adjusted to account for concrete strength variability and concrete strength gain over time. Adjustment for differences between specified 28-day strengths and measured 28-day strengths were accounted for by multiplying the specified 28-day strenth by the statisitical bias factor, λ, discussed by Nowak and Szerszen (2003). An additional concrete strength gain factor of 1.2 accounted

for a minimum 20 percent strength gain over time as observed by Wood (1991) and Dereli (2010). Use of both values was verified for MnDOT specified concretes by Dereli et al. (2010) and was also verified in this project as discussed in Appendix H. It was assumed that the concrete compressive strengths of the bridge deck, barrier, and diaphragms were the same as each other (but different than the girder) due to a lack of documentation indicating otherwise. The concrete modulus of elasticity was calculated using the equation presented by Pauw (1960) and was dependent on the nominal concrete unit weight and the adjusted concrete compressive strength. The geometries for all primary bridge elements (bearing pads, girders, haunch, and bridge deck) and secondary bridge elements (end diaphragms, intermediate diaphragms, traffic barriers, and pedestrian sidewalks) in the finite element bridge models were obtained from the plans for each bridge. FEM meshing techniques aligned with those discussed in Section 3.3.1.

Boundary conditions at the bearing pad supports and the connectivity between different parts of the field bridge FE models were modeled using the same method as the laboratory bridge FEM, discussed in Section 3.3. However, a fixed connection between diaphragms and girders, as described for the laboratory bridge FEM in Section 5.3.2, was used for all field bridge FE models. A fixed connection was selected because variation of the fixity type (free, pinned, and fixed) while investigating the laboratory bridge FEM had little effect on laboratory FEM results. Construction of 3D finite element models in Abaqus was more efficient when diaphragm-to-girder connections were defined using the fixed connection. Load was applied to the field bridge FE models using the tire patch geometry discussed in Section 6.4 and truck axle weights tabulated in Appendix G. Figure 6-10 through Figure 6-12 show cutaway views of finite element models that were constructed with the end diaphragms, intermediate diaphragms, traffic barriers, and pedestrian sidewalks specified in the bridge plans for each of the three field tested structures (referred to as secondary elements in the figure titles).

Specific load cases, shown in Table 6-7, were selected to evaluate the structural response from multiple axle truck loading that produced maximum shear or torsional response. In each case, the field data used for validation were averaged from repeat loadings as discussed in Section 6.4. The location (Loc) 11 load cases were considered for Bridge 09002 and Loc 9 load cases were selected for Bridge 08011 because these truck

locations placed the rear axles furthest into the span length and as far from a transverse line of interest as possible (where strain gages were located). The Loc 3 load cases were considerd for Bridge 65006 because this truck location was repeated at all transverse locations across the width of the skewed structure during field testing. Investigation of data from the Loc 3 load cases allowed for comparison of measured shear strains to FEM shear strains in all five girders (on individual sides of the web), which were each located different distances from the acute and obtuse skewed corners of the span.

Similar to validation of the FEM using laboratory data discussed in Section 5.3.2, comparisons were made between FEM results and measured field data from select loading cases. Strain measured by individual legs of a rosette in the field were transformed to a total shear strain, γ_{xy}, (that included the effects of torsion and shear) as discussed in Section 5.2. Because VWG box-type rosettes were only installed on one side of the girder web in the field, it was not possible to average the total shear strain, γ_{xy}, on both sides of the girder web to negate the effects of torsion. Therefore, validation of the FEM technique using field data was completed by using the total shear strain on individual sides of the girder web from both FEM results and measured field data (the side of the web where field data were recorded).

6.6.1 Straight Field Bridges 09002 and 08011

This section shows a comparison of FEM results and measured field data for the two straight field bridges modeled (i.e., 09002 and 08011). The total shear strain, γ_{xy}, calculated using rosette field data from individual sides of the girder web (using notation Field γ_{xy}) are compared to the FEM total shear strain results (using notation FEM γ_{xy}) from the same side of the girder web in Table 6-8 for the three back-to-back truck load cases shown in Figure 6-13. Comparisons of measured data and FEM results are shown for individual strain gages at $1d_v$, $2d_v$, and $4d_v$ near the eastern abutment end of the span and at $1d_v$ near the western pier end of the span. For Bridge 08011, the Field γ_{xy} data from each side of the girder web are compared to the FEM γ_{xy} results in Table 6-9 for the three back-to-back truck load cases shown in Figure 6-14. Comparisons of measured data and FEM results are shown for individual strain gages at $0.5d_v$, $1d_v$, $2d_v$, $4d_v$, and $0.25L$ near the northern abutment end of the span. In the case of both straight bridges, strain gages were located on just one side of the girder webs as identified with an abbreviated cardinal

direction (N, S, E, or W) in Table 6-8 and Table 6-9, depending on the test setup and instrumentation configuration. FEM results are tabulated for both sides of the girder webs. The percent difference between FEM γ_{xy} and Field γ_{xy} values are shown in the tables for locations where field data were measured.

Validation of the FEM results with the laboratory bridge data was described in Section 5.3.1. In the comparisons between the averaged laboratory bridge shear strain data and the FEM results, a positive or negative 10 percent difference or less in the results was considered acceptable. The percent difference between the field data and FEM results of the two straight bridges (i.e., 09002 and 08011), given in Table 6-8 and Table 6-9, were higher for these two structures compared to values for the laboratory bridge. The majority of the field data were within approximately 20 percent of the FEM results. Data in Table 6-8 and Table 6-9 indicated that there were five cases with percent difference values greater than 30 percent. In all five of these cases, the difference in Field γ_{xy} and FEM γ_{xy} values was 9 με or less. Inspection of the field data indicated that the larger percent differences were typically affiliated with larger than expected variation in strain data (noise) from an individual rosette gage over the five cycles used to collect data. The larger percent difference values affiliated with the straight field bridge data were attributed to a low signal-to-noise ratio in the VWGs during field testing and lower magnitude applied live load from trucks compared to laboratory actuator load levels. Furthermore, the exact magnitude and location of each wheel load is not captured to the same degree of accuracy during field testing compared to laboratory testing.

6.6.2 Skewed Field Bridge 65006

One of the field bridges, Bridge 65006, had a significant skew of 30 degrees. The total shear strain obtained from field data (including the effects of torsion and shear), Field γ_{xy}, is compared to the FEM γ_{xy} results from the same side of the girder web and the same loading position in Table 6-10 through Table 6-14 for the five back-to-back truck load cases shown in Figure 6-15. Comparisons of measured data and FEM results are shown for individual strain gages at $1d_v$, $2d_v$, and $4d_v$ near the western abutment end of the span and at $1d_v$ near the eastern pier end of the span. The strain gages were located on either the north (N) or south (S) side of the web depending on the test setup and instrumentation configuration, but gages were not placed on both sides of the web. The FEM γ_{xy} results are

provided in the tables for both sides of the webs. The percent difference between FEM γ_{xy} and Field γ_{xy} data are shown in the tables for locations where field data were measured.

The percent difference between the FEM γ_{xy} results and Field γ_{xy} data for the skewed bridge (i.e., 65006), given in Table 6-10 through Table 6-14, were higher compared to values for the straight field bridges and the laboratory bridge. The majority of the skewed bridge field data were within approximately 15 to 30 percent of the FEM results, but some outliers are shown in Table 6-10 through Table 6-14. The larger percent difference values for the focus girders in each loading scenario (trucks positioned to maximize shear response in the girder), marked by a thick black border in each table, were typically on the pier (east) end of the span where the signal was lower in the field. Collection of field data at locations furthest from the applied live load had a lower signal-to-noise ratio due to a lower magnitude applied live load when compared to gages near the load. The lower shear strain results were also observable in the FE model, but the percent differences indicate that the shear strain, γ_{xy}, was not captured as accurately for the skewed field bridge compared to the straight field bridges. The largest percent difference values given in Table 6-10 through Table 6-14 are shown for girders adjacent to the focus girders in each loading scenario. The girders adjacent to the focus girders had maximum FEM γ_{xy} results in the 10 to 20 με range. Field γ_{xy} data from strain gages on the adjacent girders were smaller magnitude shear strains compared to FEM results. In some cases, when FEM γ_{xy} results were also low magnitude, comparison of small magnitude strains may create deceivingly large percent difference values.

When placing trucks in the field, care was taken to avoid locating axle and tire patch loads near strain gage locations. This was not always possible in the skewed bridge due to the complex geometry as shown in Figure 6-15. However, FEM results indicated that disturbed regions from truck wheel loads did not cause significant change in FEM γ_{xy} strains collected at integration points through the depth of the girder web (approximately 3 to 4 με variation). The disturbed regions should not have had an effect on Field γ_{xy} data, but the percent differences indicate that the shear strain, γ_{xy}, was not captured as accurately for the skewed field bridge compared to the straight field bridges.

6.7 Effects of Torsion on Field Bridge Shear Strain Data

Two ratios were used to investigate the effects of torsion on the field bridge FEM results only (because measured field data were not obtained from both sides of the girder webs). Both ratios involved use of the following shear strains affiliated with the vertical shear stresses: (1) the total shear strain, γ_{xy}, on either face of the girder web (using the notation Field γ_{xy} or FEM γ_{xy}) which included the effects of both vertical shear stress due to the vertical shear resultant and vertical shear stress due to torsion as depicted in Figure 6-16, (2) the shear strain due to the vertical shear force resultant (using the notation γ_{xy_shear}) which was calculated from FEM results as the average of the total shear strain, γ_{xy}, from each face of the girder web, and (3) the shear strain due to torsion (using the notation γ_{xy_tor}) which was calculated from FEM results as the difference between the total shear strain, γ_{xy}, from either face of the girder web and the absolute value of the shear strain due to the vertical shear force resultant, γ_{xy_shear}.

The absolute value of the ratio of the torsional shear strain from FEM results divided by the total FEM shear strain ($|\gamma_{xy\_tor}$ / FEM $\gamma_{xy}|$) is given as percentage for each face of the girder web at each location of interest and indicates two behaviors. First, it indicates the amount of torsional shear strain of the total shear strain on either face of the girder web. In other words, a value of 50 percent would indicate that torsional shear strain was 50 percent of the total shear strain on one face of the girder web. These values give an indication of the error associated with trying to quantify shear distribution by measuring shear on only one side of the girder webs. Values over approximately 10 percent are likely to yield highly inaccurate shear distributions. Second, the smaller ratio of the torsional shear strain divided by the total shear strain at any location of interest (e.g., at d_v on an interior girder) indicates the side of the web where the effects of torsion and the effects due to the vertical shear resultant were additive, similar to the shear stresses in same direction on the girder web in the foreground of Figure 6-16.

The absolute value of the ratio of the shear strain due to torsion divided by the shear strain due to the vertical shear resultant ($|\gamma_{xy\_tor}$ / $\gamma_{xy\_shear}|$) from FEM results is given as a percentage for each location of interest. This ratio indicates the difference in relative magnitudes of the torsional shear strain and the shear strain due to the vertical shear resultant. In other words, a value of 100 percent (which stems from the value of 50 percent

for the ratio of torsional shear strain divided by total shear strain in the previous example) would indicate that the shear strain due to torsion was equal to the shear strain due to the vertical shear resultant.

Discussion is provided in the following sections related to the straight and skewed field bridges modeled. In each section, a discussion is provided in the following order to highlight the effects of torsion from back-to-back truck load cases: (1) load cases where axles were transversely oriented so that one wheel line was directly above the exterior girder (the other wheel line was approximately 6 ft from the girder centerline), (2) load cases where trucks were transversely positioned equidistant from the centerline of two adjacent girders, and (3) load case where axles were transversely oriented to straddle an interior girder (tire patch loads approximately 3 ft on either side of the girder centerline). Within each discussion, consideration is first given to the girder primarily carrying the truck load (thus generating the maximum response) and discussion regarding the response of adjacent girders follows.

6.7.1 Straight Field Bridges 09002 and 08011

Table 6-8 and Table 6-9 show the two aforementioned ratios, generated with FEM results, involving the torsional shear strain for Bridges 09002 and 08011, respectively. The loading scenarios are similar for both structures (as shown in Figure 6-13 and Figure 6-14), but the trucks were longitudinally positioned further into the span of Bridge 09002 because it was a shorter span.

Exterior Girder 1 (considering load case G1 BB Loc 11 and Loc 9 for Bridges 09002 and 08011, respectively) had a range of torsional shear strain which was approximately 5 to 14 percent of the total shear strain on the face of the web where the strain due to torsion and the strain due to shear were additive (minimum ratio of $|\gamma_{xy\_tor}$ / FEM $\gamma_{xy}|$). The torsional shear strains ranged from 2 to 5 με in these cases. The ratio of $|\gamma_{xy\_tor} / \gamma_{xy\_shear}|$ indicated that torsional shear strain was approximately 5 to 17 percent of the shear strain from the vertical shear resultant in the girder with the maximum response. Interior Girder 2, adjacent to exterior Girder 1, exhibited more torsional response with shear strains due to torsion equal to approximately 45 percent of the shear strains due to the vertical shear resultant (torsional shear strain of magnitude 9 με). This was the largest magnitude shear strain due to torsion obtained from FEM results for Bridges 09002 and

08011. This behavior was not unexpected, based on laboratory FEM results, considering the load case geometry presented in Figure 6-13 and Figure 6-14, which indicate that the 6 ft truck axle would have a wheel line near the adjacent interior girder. A general discussion of field bridge results compared to results from the laboratory bridge are presented in Section 6.7.3.

Interior Girders 2 and 3 (considering load case G2-G3 BB Loc 11 and Loc 9 for Bridges 09002 and 08011, respectively) had a range of torsional shear strain which was approximately 3 to 22 percent of the total shear strain on the face of the web where the strain due to torsion and the strain due to shear were additive (minimum ratio of $|\gamma_{xy\_tor}$ / FEM $\gamma_{xy}|$). The torsional shear strains ranged from 1 to 7 με in these cases. This magnitude torsional shear strain was approximately equal to the torsional shear strain obtained from FEM results for the exterior girder G1 BB Loc 11 and Loc 9 load cases. This behavior was expected from the load case, when trucks were placed between two interior girders, based on laboratory FEM results because of the distance between the centerline of the interior girders and the nearest tire load patch. The ratio of $|\gamma_{xy\_tor} / \gamma_{xy\_shear}|$ indicated that torsional shear strain was, on average, 22 percent of the shear strain from the vertical shear resultant in the two interior girders. As expected, due to the geometry of the loading case, the difference in response when comparing the two interior girders was minimal; the effect of torsion was approximately equal in both girders.

Interior Girder 2 (considering load case G2 BB Loc 11 and Loc 9 for Bridges 09002 and 08011, respectively) had torsional strains which were approximately 2 percent or less of the total shear strain on the face of the web where the strain due to torsion and the strain due to shear were additive (minimum ratio of $|\gamma_{xy\_tor}$ / FEM $\gamma_{xy}|$). The torsional shear strains were approximately 0.5 με or less. Furthermore, the ratio of $|\gamma_{xy\_tor} / \gamma_{xy\_shear}|$ indicated that torsional shear strain was a very small percentage of the shear strain from the vertical shear resultant (2 percent or less). FEM results indicated that this loading scenario, with truck axles straddling an interior girder, had the lowest shear strain in the straddled girder due to torsion compared to the other truck locations shown in Figure 6-13 and Figure 6-14 (and compared to all the other truck locations investigated in this study). Girders adjacent to interior Girder 2 had total shear strains from FEM results on one face of the web (including the effects of torsion and shear) of approximately 20 με magnitude. Adjacent girders

experienced significantly more torsion (torsional shear strains of magnitude 2 to 7 με) during the straddled load case when compared to the loaded interior girder; this magnitude torsional strain was similar to the two loading cases where a wheel line was above the exterior girder or where trucks were placed to equidistant between two adjacent girders. The ratio of $|\gamma_{xy\_tor} / \gamma_{xy\_shear}|$ indicated that torsional shear strain made up, on average, approximately 23 to 34percent of the shear strain from the vertical shear resultant in girders adjacent to Girder 2.

The largest shear strain in Girder 2, on the face of the girder web where the torsional shear strain and the shear strain due to vertical shear were additive, was approximately equal for the case when the load was applied straddling Girder 2 and for the case when the load was centered between Girders 2 and 3. For Bridge 09002, data in Table 6-8 show that FEM shear strains in Girder 2 at d_v, $2d_v$, and $4d_v$ were either equal to or 1 με higher when the load was straddling Girder 2 compared to when the load was centered between Girders 2 and 3. For Bridge 08011, data in Table 6-9 show that FEM shear strains in Girder 2 were between 0 and 2 με larger when the load was straddling Girder 2 compared to when the load was centered between Girders 2 and 3.

6.7.2 Skewed Field Bridge 65006

Table 6-10 through Table 6-14 show the two aforementioned ratios involving the torsional shear strain for Bridge 65006. The FEM results were generated from loading scenarios shown in Figure 6-15.

Exterior Girder 1 and interior Girder 2 located near the obtuse corner of the abutment (considering load case G1-G2 BB Loc 3 in Table 6-10) had a range of torsional shear strain which was approximately 9 to 28 percent of the total shear strain on the face of the web where the strain due to torsion and the strain due to shear were additive (minimum ratio of $|\gamma_{xy\_tor}$ / FEM $\gamma_{xy}|$). The torsional shear strains ranged from 2 to 8 με in these cases. Exterior Girder 5 and interior Girder 4 located near the acute corner of the abutment (considering load case G4-G5 BB Loc 3 in Table 6-14) had a range of torsional shear strain which was approximately 5 to 31 percent of the total shear strain on the face of the web where the strain due to torsion and the strain due to shear were additive. The torsional shear strains ranged from 2 to 8 με in these cases. The influence of torsion, considering the magnitude of torsional shear strain from FEM results, was similar for

girders nearest both the acute and obtuse corners of the abutment. The ratio of $|\gamma_{xy\_tor} / \gamma_{xy\_shear}|$ also indicated that, on average, torsional shear strain was approximately 21 to 32 percent of the shear strain due to the vertical resultant shear in the obtuse corner and 16 to 35 percent of the shear strain due to the vertical resultant shear in the acute corner. Girders adjacent to the focus girders in these loading scenarios did not have large magnitude total shear strains, γ_{xy}, from FEM results. This behavior was expected based on FEM results from the straight bridge.

Interior Girders 2 (obtuse corner), 3 (center girder), and 4 (acute corner) (considering load cases G2 BB, G3 BB, and G4 BB at Loc 3 in Table 6-11 through Table 6-13) had similar ranges of torsional shear strain which were approximately 2 to 30 percent of the total shear strain on the face of the web where the strain due to torsion and the strain due to shear were additive (minimum ratio of $|\gamma_{xy\_tor}$ / FEM $\gamma_{xy}|$). The torsional shear strains ranged from 2 to 7 με in these cases. Furthermore, interior Girders 2, 3, and 4 had a ratio of $|\gamma_{xy\_tor} / \gamma_{xy\_shear}|$ that was similar on average (14 to 18 percent considering all gaged locations) but ranged between 2 and 44 percent. Typically, the ratio of $|\gamma_{xy\_tor} / \gamma_{xy\_shear}|$ was smaller at $1d_v$ and $2d_v$ near the abutment (ranged between 2 and 7 percent) compared to values at $4d_v$ (ranged between 25 and 44 percent). FEM results indicated that this loading scenario, with truck axles straddling an interior girder, had the lowest shear strain due to torsion compared to the other truck locations used to test the skewed bridge. However, for this type of loading scenario, the magnitude of $|\gamma_{xy\_tor} / \gamma_{xy\_shear}|$ from FEM results for the skewed bridge was larger at all locations of interest when compared to FEM results from the straight field bridges subjected to similar loading scenarios with truck axles straddling an interior girder. This observation indicated that the geometry of the skewed bridge was more prone to torsion than the geometry of the straight field bridges investigated in this FEM study. Torsion in skewed bridges has been studied by Fu and Chun (2013) and more torsional effects have been observed in skewed bridges, particularly the obtuse corner, when compared to straight bridges by Dhar et al. (2013). Similar to the straight field bridge FEM results, girders adjacent to interior Girder 2, 3 and 4 in this loading scenario experienced large torsional shear strains (maximum magnitude of 11 με) compared to the magnitude of total shear strain on either face of the adjacent girder web (maximum magnitude of approximately 26 με). The ratio of $|\gamma_{xy\_tor} / \gamma_{xy\_shear}|$ was significant in the

adjacent girders with average results that ranged between 28 and 94 percent (considering all gaged locations).

6.7.3 Comparison of Torsional Effects in Field Bridges and Laboratory Bridge

Bridges 09002 (girder spacing of 11.5 ft, span length of 39 ft, and no skew) and 65006 (girder spacing of 11 ft and span length of 45 ft, and 30 degrees skew) were very similar structures built with 36 in. AASHTO Type II girders and were the field bridges most similar to the laboratory bridge (girder spacing of 9 ft, span length of 30.75 ft, and no skew) in terms of girder shape, girder spacing, and span length. As a consequence, these bridges provided an opportunity to compare the effects of torsion on shear strain results for laboratory (controlled environment with concentrated patch load) versus field bridges, and non-skew versus skew bridge. An overview of the magnitude of shear strain due to torsion and the vertical shear resultant for the laboratory bridge loading scenarios that involved use of a single, high magnitude patch load were discussed in Section 5.3.1 and presented in Table 5-3.

Considering laboratory bridge results, data in Table 5-3 indicate that the ratio of $|\gamma_{xy\_tor} / \gamma_{xy\_shear}|$ was approximately 4 to 8 percent in the loaded girder when force was applied above the girder. The ratio of $|\gamma_{xy\_tor} / \gamma_{xy\_shear}|$ was 62 to 74 percent in the girder adjacent to the loaded girder, but the magnitude of shear strain due to the vertical shear resultant was smaller. The ratio of $|\gamma_{xy\_tor} / \gamma_{xy\_shear}|$ was approximately 40 percent in both girders when load was applied between the interior and exterior girder. The ratios of $|\gamma_{xy\_tor} / \gamma_{xy\_shear}|$ from the laboratory bridge were larger compared to similar ratios from the straight field bridges. This was because loading scenarios in the laboratory bridge (load applied with a single actuator or combination of three actuators in a small, concentrated footprint) were different than those used to test the straight field bridges (load applied with vehicles that had ten individual tires contacting the bridge deck in a large footprint). However, the effects of torsion were still observed in the straight field bridge FEM results because, even though truck axles provide more load distribution via the gage width and longitudinal spacing, the trucks still tended to twist the girders when one or more wheel lines was located between girders. This behavior was especially evident in the skewed field bridge which did not always have less torsional behavior compared to the laboratory bridge.

Specifically, the ratio of $|\gamma_{xy\_tor} / \gamma_{xy\_shear}|$ was often the same magnitude or higher in the skewed field bridge FEM results compared to the laboratory FEM results.

In the field bridge FE models, the largest shear strains due to the combination of vertical shear and torsion in the interior girder were similar when the load was applied directly above the interior girder (truck axles straddling a girder) and when the load was applied between two interior girders (truck axles centered between two girders). This effect was also evident in the measured shear strains in the laboratory bridge. Table 5-3 shows maximum measured shear strains of 63 and 61 με at d_v in Girder 3 when the 75 kip load was placed directly above Girder 3 and centered between Girders 3 and 4, respectively. These two loading cases generated similar maximum shear stresses in the bridge girders. The field bridges were modeled with intermediate diaphragms, which were not present in the laboratory bridge. The intermediate diaphragms, modeled with a fixed connection between the end of the diaphragm and the girder web as discussed in Section 6.6, did not eliminate the effects of torsion on shear strain. Similarly, the presence of end diaphragms in both the field bridge FE models and the laboratory bridge did not eliminate the effects of torsion.

6.7.4 Summary and Conclusions of Torsional Behavior in Field Bridges

The magnitude of torsional shear strains were confirmed with finite element models of the laboratory bridge and three of the field bridges. Loading scenarios in the laboratory bridge were different than those applied to field bridges, but the effects of torsion were still present. The total shear strain, γ_{xy}, on one face of the girder web would be higher than that on the other face due to the additive/subtractive nature of shear stress due to torsion and due to the vertical shear resultant as shown in Figure 6-16. The presence of intermediate diaphragms in the field bridge FE models, which were not part of the laboratory bridge, and the presence of end diaphragms in all FE models did not eliminate the effects of torsion on shear strain.

It was not possible to determine the shear strain due to the vertical resultant shear using the VWG rosettes in the field bridges because the rosettes were only placed on one side of the girder webs. In order to differentiate between torsion and vertical shear, gages need to be placed on both sides of the girder webs. This finding likely applies to other studies in the literature that have characterized shear distribution through the use of rosette

strain gages on one side of a prestressed concrete girder web. The literature has a dearth of information regarding the effects of torsion in the webs of precast concrete I- and bulb-tee beam bridges. Cross et al. (2006 and 2009) was the only study to note the potential effects of torsion after completing field tests and data processing. Ignoring the effect of torsion results in an unconservatism related to the combined effect of vertical shear stresses due to both torsion and the vertical shear force resultant; structural response due to the combined effect may govern compared to the response generated by vertical shear stress solely due to the vertical shear force resultant.

The largest total shear strain, γ_{xy}, in an interior girder was similar for the case when the load was centered over an interior girder and the case when the load was centered between two interior girders. Torsion is typically ignored in the design of girders in straight prestressed concrete bridges. These results indicate that for the specific cases examined, this is a reasonable assumption; however, there may be locations in the girder that were not examined in this study where the shear strains are larger for the case with significant torsion (when the load is centered between the girders) than for the case with little torsion (when the load is centered above the girder). In the case with significant torsion, the larger shear strain may contribute to larger principal tensile stresses in the girder web that may lead to premature diagonal cracking of the girder web under service loads. The onset of diagonal web-shear cracking is affiliated with the maximum principal tensile strain (and stress) in the girder web, not just the maximum shear strain, γ_{xy}.

However, the externally mounted rosette strain gages and FE models did not account for the effects of prestressing or dead load and how they affected the maximum principal tensile stress. The dead load and prestressing were not included in the FE models so that FEM results could be compared to the measured laboratory and field live load strain data. Therefore, discussion related to the magnitude of the principal tensile stress as it related to the load that causes diagonal web-shear cracking was not possible. Results from inspection of field bridges for diagonal web-shear cracks suggested that the amount of live load, dead load, and prestressing present during testing of the bridges did not approach the principal tensile stress associated with diagonal web-shear cracking, even when considering torsion in the loading cases. Additional discussion related to inspection of field bridges for diagonal web-shear cracks is presented in Section 6.8.

6.8 Visual Inspection of Field Tested Bridges that Rate Poorly for Shear

Field testing of six bridges that rated low for shear provided an opportunity to inspect the girders for diagonal web-shear cracks that may not be visible when the structures are subjected to regular traffic loads. Each field bridge was subjected to live load from weighted dump trucks arranged such that large magnitude shear forces were applied to individual girders near the abutment supports. If diagonal shear cracking had previously developed under the presence of overload, the cracks may not be visible in the absence of the overload. Mathys et al. (2014) observed that web-shear cracks were not visible upon unloading during laboratory testing of girders with stirrups spaced at 8 in.; however, web-shear cracks were visible upon unloading during laboratory testing of girders with stirrups spaced at 24 in. as discussed in Section 5.4.1.1.

Detailed visual inspections of loaded girders in each field bridge were completed while back-to-back truck load was applied on the bridge deck. No web-shear cracks were observed when girders were subjected to shear forces larger than those produced by the annual average daily traffic (AADT) for each bridge. This was in addition to findings reported by Dereli et al. (2010) who inspected six bridges from the MnDOT inventory during routine traffic loading and noted that none of the structures showed evidence of diagonal web-shear cracks.

6.9 Challenges and Suggested Methods for Shear Distribution Field Testing

6.9.1 Challenges of Field Testing to Measure Shear Distribution

Many challenges are associated with conducting live load field testing. This section describes some of the challenges that were encountered in the field when trying to quantify shear distribution during this project, and Section 6.9.2 suggests methods that can be used to overcome the challenges experienced.

A significant amount of torsion (shear strains due to torsion equal to 10 με compared to maximum total shear strain data in the 50 με range) was believed to be generated in the girders in the field based on results obtained from detailed FE models of select field bridges (discussed in Section 6.7). Accurate measurement of shear strains due to torsion and vertical shear in the field required instrumentation on both sides of the girder webs to differentiate between the shear strains due to these two actions. This critical

requirement was unknown prior to the field testing completed within this project and was discovered during the controlled laboratory testing discussed in Chapter 5. Without sufficient instrumentation, it is not possible to determine the average shear strain in the girders and the vertical shear force resultants generated from applying live load to the bridge from field measurements.

The total shear strain, γ_{xy}, generated in the prestressed concrete bridge girders in the field were generally low magnitude (i.e., less than |50| με) even with the application of two back-to-back 50 kip trucks because of the large stiffness of the bridges and the distribution of the load amongst the truck axles and wheels. The low magnitude shear strains created challenges in interpreting the data because of the low signal-to-noise ratios. Maximizing the signal-to-noise ratio requires one or more heavily loaded trucks positioned to maximize the bridge shear response and positioned to minimize the effects of disturbed regions due to location of loads relative to gages.

Environmental effects caused significant mechanical strains due to temperature during field testing. The bridge naturally changes shape as the temperature gradients in the deck change over time. Separation of the temperature-induced mechanical strain and the load-induced mechanical strain was completed by periodically taking readings throughout the day with the live load removed from the bridges. Data was obtained with no load on the bridge prior to testing, periodically throughout the course of a testing day, and after testing was complete. The frequency of data collected with no load on the bridge was highly dependent on the temperature gradient present while testing and the effects of cloud cover (partly cloudy, completely cloudy, or not cloudy). Variations in the readings due to environmental effects can be more significant on cloudy days.

6.9.2 Suggested Methods for Field Testing to Measure Shear Distribution

During this project, field installation of strain gages and live load testing each took an extended business day to complete. If an expedited process is desired to determine the distribution of shear at a specific longitudinal location (e.g., at d_v only), the number and locations of vibrating wire strain gages could be reduced. It is suggested that a full transverse line of box-type rosette strain gages, one on each side of each girder web, be applied at the longitudinal location(s) of interest. Instrumenting all girders in a transverse cross section alleviates the need to make assumptions as to how much shear force a girder

away from the loading location carries. However, data from laboratory testing and finite element modeling indicated that the majority of the applied shear force was carried by the individual girders nearest the load points (for axle loads with multiple tire patch loads) and one adjacent girder on each side. For structures with many girders, it may not be necessary to instrument all of the beams. However, consideration must be given to the loading scenarios. For example, if a two lane loaded scenario is desired, axles and tire patches will likely affect a wider cross section of girders.

Generally, analysis of both laboratory data and field bridge data indicated that the measured values at $1d_v$ and $2d_v$ provided the most insight into shear distribution and were often located away from disturbed regions created under load points and near support reactions. Specifically, data used to study the effects of shear distribution at d_v were the most useful for comparison to the critical section in AASHTO Specifications. However, data collected from transversely instrumented girders at a single longitudinal location of interest (e.g., at d_v only) will not describe the behavior of both transverse and longitudinal shear distribution from the applied load to the support. If a detailed picture of shear distribution is desired and an expedited process is not necessary, installation of a grid of VWG box-type rosettes similar to those installed in this project, including many longitudinal positions, is suggested. This grid of sensors will provide both transverse and longitudinal data related to shear distribution, which was the objective of this research project.

The ideal position for trucks is highly dependent on the span length and location of strain gages. If possible, the best back-to-back truck location would have the clustered set of rear axles further into the span length than the last line of transverse strain gages and the front axle of the rear truck would remain on the approach span. This loading scenario is shown in Figure 6-13. To address challenges related to the signal-to-noise ratio present during field testing, it is suggested that trucks carry as much weight as possible (keeping in mind legal limits and potential damage to the structure) to maximize the bridge response.

If the interior girder is of primary interest, back-to-back trucks positioned with axles straddling an interior girder (tire patch loads approximately 3 ft on either side of the girder centerline) likely produces the largest shear force in the girder for one lane loaded. If traffic closure allows, a loading scenario focused on the interior girder with two trucks side-by-

side (with the front axles oriented toward midspan), located to maximize the live load shear demand on the girder based on the lever rule as discussed in Section 7.2, is also suggested to collect data related to a two lane loaded scenario. However, truck positions that maximize both the torsion in the girder web and the principal tensile stress should be considered to record data related to the true behavior of the structure (i.e., no bridge is subjected to only torsional shear strains or only shear strains from the vertical shear resultant). Data collected from these truck positions will yield insight in regards to shear distribution including the effects of torsion and potential web-shear cracking.

It is recommended that extreme care be taken to not place trucks used for live loading near locations of instrumentation applied to the girder webs. Proximity of axle and tire patch loads to strain gage locations creates a disturbed region where the strain profile through the depth of the cross section will not be linear, as conventional Bernoulli beam theory is not applicable. Furthermore, placing axles near box-type rosettes may produce large strain readings in the vertical rosette strain gage which may create misleading shear strain data. Truck locations in this project carefully accounted for the locations of strain gages and still collected data that was likely affected by the proximity of tire patches. However, FEM results indicated that disturbed regions from truck wheel loads did not cause significant change in total shear strains, γ_{xy}, collected at integration points through the depth of the girder web (approximately 3 to 4 με variation).

The frequency of collecting strain gage data with no load on the bridge (zero-readings) was highly dependent on the cloud cover and varied from bridge to bridge during this project. Typically, a block of four or five live load tests were performed between zero-readings, which were taken approximately once per hour. If the cloud cover is consistent (completely cloudy or not cloudy) and temperature variation is approximately linear, the time between zero-readings may be increased, but if variation in cloud cover is anticipated throughout the course of a testing day, the frequency of zero-readings should be increased. Engineering judgement should be used when deciding the frequency of zero-readings compared to the natural lag between changes in cloud cover and bridge response (i.e., it takes time for changes in cloud cover to affect the bridge response). It is recommended that field testing be completed after dark to avoid unpredictability related to solar radiation.

However, zero-readings must still be taken on a frequent interval as the bridge deck cools after sunset.

Data from live load tests conducted to study shear distribution can be post-processed to resemble Figure 6-17. Figure 6-17 was created using data from loading scenario G2 BB Loc 3 on Bridge 09002. The figure was generated using data from VWG rosettes installed on one side of the girder web and so it is not accurate in regards to the distribution of shear due to the effects of torsion on the total shear strain, γ_{xy}, collected on either face of the girder web. Figure 6-17 is just meant to provide a representative example of a plot that could be created to show information obtained from live load testing of field bridges for shear distribution. The vertical axis shows the potential magnitude of shear distribution factors that sum to 1.0 transversely across the bridge. These shear distribution factors can be obtained by dividing the shear force carried by each individual girder by the sum of girder shear forces across a transverse cross section at each longitudinal location. Shear forces were derived from the VWG box-type rosettes using methods discussed in Section 5.2, transformed section properties, and nominal material properties from the bridge plans. The horizontal axis shows the location of transverse strain gage lines to scale, as a function of the critical section for shear (d_v), along the span length from the abutment (on the right) to the pier (on the left). Below the horizontal axis, data related to the back-to-back trucks is displayed. The truck axle locations and corresponding weights are shown to scale along the span length. The third axis, into the page, shows the location of each girder in a transverse cross section. A representative truck is displayed next to the third axis to annotate the transverse location of the truck axles on the bridge. Within the 3D space, data from both a 3D grillage analysis and field testing are compared. Information presented as the sample shown in Figure 6-17 can provide insight about shear distribution in both the transverse and longitudinal directions of a bridge structure.

Table 6-1. Live Load Tested Field Bridges

Bridge Characteristic	Bridge Number					
	73852	**73872**	**62826**	**08011**	**09002**	**65006**
Order Tested	1	2	3	4	5	6
Date Tested	June 2012	Aug. 2012	Oct. 2012	July 2013	Aug. 2013	Aug. 2013
Year Built	1976	1976	1969	1988	1970	1983
Design Spec Year	1973	1973	1965	1983	1969	1977
ADT	1,550	3,600	----	3,150	4,100	2,600
Main Span Crossing	Traffic	Traffic	Traffic	Water	Water	Water
Girder Type	54 in. Type IV	54 in. Type IV	45 in. Type III	45M	36 in. Type II	36 in. Type II
Girder Web Thickness (in.)	8	8	7	6	6	6
No. Girders	4	4	4	5	5	5
Girder Spacing (ft)	11	14.67	12.5	11	11.5	11
Span Length (ft)	63	58	38	76	39	45
Aspect Ratio (*L/W*)	1.58	1.15	0.85	1.51	0.73	0.9
Skew (deg)	2	0	2	0	0	30
Min. Deck Thickness (in.)	8	8.25	8.75	9	8.25	9
Abutment End Diaphragm Depth	partial	full	full	partial	full	partial
Inv. Rating	< 1	< 1	< 1	< 1	< 1	< 1
Abutment Bearing Type	Steel PL	Elastomeric	Steel PL	Elastomeric	Elastomeric	Elastomeric
Pier Bearing Type	Elastomeric	Elastomeric	Steel PL	Elastomeric	Steel PL	Elastomeric

shading indicates varied characteristic within girder depth range for selected bridges

Table 6-2. Field Location of VWGs

Bridge No. (corner)	Instrument Location	Abutment Focused Live Loading						Pier Focused Live Loading			
		B	G1	G2	G3	G4	G5	G1	G2	G3	G4
73852 (NW)	d_v / 2		R	R	R	R		R	R	R	R
	d_v= 50 in.		R	R	R	R		R	R	R	R
	$2d_v$	R	R	R	R	R		R	R	R	R
	$4d_v$		R	R	R	R					
	L/4										
	L/2 = 31.5 ft		2L	2L	2L	2L		2L	2L	2L	2L
73872 (NW)	d_v / 2		R	R	R	R		R	R	R	R
	d_v= 50 in.	R,L	R	R	R	R		R	R	R	R
	$2d_v$	R,L	R	R	R	R		R	R	R	R
	$4d_v$		R	R	D	D					
	L/4										
	L/2 = 29 ft		2L	2L	2L	2L		2L	2L	2L	2L
62826 (SW)	d_v / 2	R	R	R	R	R					
	d_v= 40 in.	R,L	R	R	R	R					
	$2d_v$	R,L	R	R	R	R					
	$4d_v$		R,L	R,L	R,L	T,D,L					
	L/4										
	L/2 = 19 ft										
08011 (NW)	d_v / 2		R	R	R						
	d_v= 40 in.	R,L	R	R	R	R	R				
	$2d_v$		R	R	R						
	$4d_v$		R	R	R						
	L/4		R,L	R,L	R,L						
	L/2 = 38 ft										
09002 (NE)	d_v / 2										
	d_v= 34 in.		R	R	R	R	R				
	$2d_v$		R	R	R	R	R				
	$4d_v$		R,L	R,L	R	R	R				
	L/4										
	L/2 = 19.5 ft										
Pier	d_v		R	R	R	R					
65006 (NW)	*Skew*	*Obtuse*			*Acute*						
	d_v= 34 in.		R	R	R	R	R				
	$2d_v$		R	R	R	R	R				
	$4d_v$		R	R	R,L	R,L					
	L/4										
	L/2 = 22.5 ft										
Pier	d_v		R	R	R	R	R				

Table Notes:

B = Barrier

R = Rosette VWGs

L = Longitudinal VWG

T = Top Rosette VWG

D = Diagonal Rosette VWG

Table 6-3. Longitudinal Truck Location and Corresponding Section of Interest

Test Location	Section of Interest
Loc 3	BB rear tandems beyond d_v
Loc 0	Rear ST from Loc 3
Loc 5	BB rear tandems beyond $2d_v$
Loc 1	Rear ST from Loc 5
Loc 7	BB rear tandems beyond $4d_v$
Loc 9	BB rear tandems beyond $L/4$
Loc 11	Center of BB rear tandems at L / 2
Loc 8	SS rear tandems on interior span

Table Notes:
BB = Back-to-Back Trucks
SS = Side-by-Side Trucks
ST = Single Truck

Table 6-4. Abutment Focused Live Load Testing Protocols

Bridge No. (corner)	Longitudinal Location (from exp. jt.)	Abutment Focused Live Loading Transverse Testing Location								
		G1	**G1-G2**	**G2**	**G2-G3**	**G3**	**G3-G4**	**G4**	**G4-G5**	**G5**
73852 (NW)	Loc 3 (21 ft)	BB[3]	BB[2]	BB[3]		BB	BB	BB		
	Loc 0	ST	ST	ST						
	Loc 5 (25 ft)	BB	BB	BB		BB	BB	BB		
	Loc 1	ST	ST	ST						
	Loc 7 (37.5 ft)	BB,SS	BB,SS	BB						
	Loc 8 (95 ft)		SS							
73872 (NW)	Loc 3 (21 ft)	BB[3]	BB[2]	BB[3]		BB	BB	BB		
	Loc 0	ST	ST	ST						
	Loc 5 (25 ft)	BB	BB	BB		BB	BB	BB		
	Loc 1	ST	ST	ST						
	Loc 7 (37.5 ft)	BB,SS	BB,SS	BB						
	Loc 8 (68 ft)		SS							
62826 (SW)	Loc 3 (18.5 ft)	BB[3]	BB[2]	BB[3]		BB	BB	BB		
	Loc 0	ST	ST	ST						
	Loc 5 (22 ft)	BB	BB	BB		BB	BB	BB		
	Loc 1	ST	ST	ST						
	Loc 7 (29.5 ft)	BB	BB	BB						
08011 (NW)	Loc 5 (22 ft)	BB[2]	BB[2]	BB[2]	BB	BB[2]		BB[2]		
	Loc 0	ST		ST	ST	ST				
	Loc 9 (38 ft)	BB[2]	BB[2]	BB[2]	BB	BB[2]		BB[2]		
	Loc 1*	ST		ST	ST	ST				
09002 (NE)	Loc 3 (18.5 ft)	BB[2]	BB[2]	BB[2]	BB[2]	BB[2]				
	Loc 0	ST[2]	ST[2]	ST[2]	ST[2]	ST[2]				
	Loc 7 (29.5 ft)	BB								
	Loc 11 (25.5 ft)	BB	BB	BB	BB	BB				
65006 (NW)	*Skew*	*Obtuse*						*Acute*		
	Loc 3 (18.33 ft)	BB[2]	BB[2]	BB[2]	BB[2]	BB[2]	BB[2]	BB[2]	BB[2]	BB[2]
	Loc 0		ST[2]			ST[2]			ST[2]	
	Loc 11 (24 ft)		BB[2]			BB[3]			BB[2]	

Table Notes:
BB = Back-to-Back Trucks
SS = Side-by-Side Trucks
ST = Single Truck with front axle on approach span (from superposition of BB trucks)
* = Single Truck flipped longitudinally so rear axle is still at superposition location
[2 or 3] = Total repetitions for testing location

Table 6-5. Pier Focused Live Load Testing Protocols

Bridge No. (corner)	Longitudinal Location (from exp. jt.)	Pier Focused Live Loading Transverse Testing Location								
		G1	G1-G2	G2	G2-G3	G3	G3-G4	G4	G4-G5	G5
73852 (NW)	Loc 3 (21 ft)	BB[3]	BB[3]	BB[2]						
	Loc 0	ST	ST	ST						
	Loc 5 (25 ft)	BB	BB	BB		BB	BB	BB		
	Loc 1	ST	ST	ST						
	Loc 7 (37.5 ft)	BB	BB,SS	BB						
	Loc 8 (95 ft)		SS							
73872 (NW)	Loc 3 (21 ft)	BB[3]	BB[2]	BB[3]						
	Loc 0	ST	ST	ST						
	Loc 5 (25 ft)	BB	BB	BB		BB	BB	BB		
	Loc 1	ST	ST	ST						
	Loc 7 (37.5 ft)	BB	BB,SS	BB						
	Loc 8 (68 ft)		SS							

Table Notes:
BB = Back-to-Back Trucks
SS = Side-by-Side Trucks
ST = Single Truck with front axle on approach span (from superposition of BB trucks)
[2 or 3] = Total repetitions for testing location

Table 6-6. Material Properties of Bridges 09002, 08011, and 65006 used for FEM

Property	Symbol [Units]	Br. 09002	Br. 08011	Br. 65006
Unit Weight of Concrete	w_c [pcf]	150		
Nominal Girder Concrete Compressive Strength	f'_c [ksi]	5	6.5	5
Adjusted Girder Concrete Compressive Strength (λ = 1.38 for f'_c = 5 ksi or 1.14 for f'_c = 6.5 ksi)	f'_c [ksi]	8.3	8.9	8.3
Adjusted Girder Modulus of Elasticity	E_c [ksi]	5,520	5,720	5,520
Adjusted Girder Shear Modulus (calculated with ν = 0.2)	G [ksi]	2,300	2,380	2,300
Adjusted Deck and Haunch Concrete Compressive Strength (λ = 1.235 for nominal f'_c = 4 ksi)	f'_{cd} [ksi]	5.9		
Adjusted Deck and Haunch Modulus of Elasticity	E_{cd} [ksi]	4,657		
Adjusted Barrier Modulus of Elasticity	E_{bar} [ksi]			
Adjusted End Diaphragm Modulus of Elasticity	E_{dia} [ksi]			
Intermediate Diaphragm Modulus of Elasticity	E_{int} [ksi]	4,660	29,000	4,660
Neoprene Bearing Pad Modulus of Elasticity	E_{bp} [psi]	17,900		

Table 6-7. Load Cases for Field Bridge FEM Validation

Bridge	Load Case	Structural Behavior for Comparison	Load Effects
09002	G1 BB Loc 11	Exterior girder shear strain	Maximum shear in exterior girder
	G2 BB Loc 11	Interior girder shear strain	Maximum shear in interior girder
	G2-G3 BB Loc 11		Maximum torsion in interior girders
08011	G1 BB Loc 9	Exterior girder shear strain	Maximum shear in exterior girder
	G2 BB Loc 9	Interior girder shear strain	Maximum shear in interior girder
	G2-G3 BB Loc 9		Maximum torsion in interior girders
65006	G1-G2 BB Loc 3	Obtuse exterior and interior girder shear strain	Maximum torsion in exterior and interior girders
	G2 BB Loc 3	Obtuse interior girder shear strain	Maximum shear in interior girder
	G3 BB Loc 3	Center girder shear strain	
	G4 BB Loc 3	Acute interior girder shear strain	
	G4-G5 BB Loc 3	Acute exterior and interior girder shear strain	Maximum torsion in exterior and interior girders

Table 6-8. Comparison of Measured and FEM Girder Shear Strain (με) for Bridge 09002 with Ratios from FEM Results Indicating the Effects of Torsion

	G1 BB Loc 11						**G2 BB Loc 11**						**G2-G3 BB Loc 11**					
				FEM						**FEM**						**FEM**		
Gage Location	**Field** γ_{xy}	**FEM** γ_{xy}	**% Diff**	γ_{xy_tor}	γ_{xy_tor} / γ_{xy} **(%)**	γ_{xy_tor} / γ_{xy_shear} **(%)**	**Field** γ_{xy}	**FEM** γ_{xy}	**% Diff**	γ_{xy_tor}	γ_{xy_tor} / γ_{xy} **(%)**	γ_{xy_tor} / γ_{xy_shear} **(%)**	**Field** γ_{xy}	**FEM** γ_{xy}	**% Diff**	γ_{xy_tor}	γ_{xy_tor} / γ_{xy} **(%)**	γ_{xy_tor} / γ_{xy_shear} **(%)**
G1_E_1d_N	n/a	39		2	5	6	n/a	8		-5	63	38						
G1_E_1d_S	29	34	-15	-2	6		19	18	3	5	28							
γ_{xy_shear}:		***36***						***13***										
G1_E_2d_N	n/a	41		2	5	5	n/a	9		-5	56	33						
G1_E_2d_S	29	37	-21	-2	5		16	20	-16	5	25							
γ_{xy_shear}:		***39***						***15***										
G1_E_4d_N	n/a	35		5	14	17	n/a	11		-2	18	14						
G1_E_4d_S	25	26	-2	-5	19		12	16	-26	2	13							
γ_{xy_shear}:		***30***						***14***										
G1_W_1d_N	n/a	37		2	5	6	n/a	9		-5	56	36						
G1_W_1d_S	31	32	-3	-2	6		19	19	-1	5	26							
γ_{xy_shear}:		***34***						***14***										
G2_E_1d_N	26	28	-9	9	32	45	36	32	13	0.5	2	2	11	19	-40	-6	32	24
G2_E_1d_S	n/a	11		-9	82		n/a	31		-0.5	2		n/a	32		6	19	
γ_{xy_shear}:		***20***						***31***						***25***				
G2_E_2d_N	26	29	-12	9	31	45	40	34	18	0.5	1	2	15	20	-22	-7	35	27
G2_E_2d_S	n/a	11		-9	82		n/a	33		-0.5	2		n/a	33		7	21	
γ_{xy_shear}:		***20***						***33***						***26***				
G2_E_4d_N	16	18	-14	4	22	29	24	20	22	0.3	2	2	17	16	8	-2	13	12
G2_E_4d_S	n/a	10		-4	40		n/a	20		-0.3	2		n/a	19		2	11	
γ_{xy_shear}:		***14***						***20***						***17***				
G2_W_1d_N	24	28	-16	8	29	40	22	29	-25	0.5	2	2	9	18	-52	-6	33	25
G2_W_1d_S	n/a	11		-8	73		n/a	28		-0.5	2		n/a	30		6	20	
γ_{xy_shear}:		***20***						***29***						***24***				
G3_E_1d_N							21	20	6	6	29	43	33	32	3	7	22	28
G3_E_1d_S							n/a	8		-6	67		n/a	18		-7	39	
γ_{xy_shear}:								***14***						***25***				
G3_E_2d_N							21	20	4	6	29	43	34	33	3	7	21	27
G3_E_2d_S							n/a	9		-6	67		n/a	19		-7	37	
γ_{xy_shear}:								***14***						***26***				
G3_E_4d_N							12	15	-21	3	20	25	27	19	38	2	11	12
G3_E_4d_S							n/a	9		-3	34		n/a	15		-2	13	
γ_{xy_shear}:								***12***						***17***				
G3_W_1d_N							21	20	5	5	27	36	32	30	7	6	20	25
G3_W_1d_S							n/a	9		-5	61		n/a	17		-6	35	
γ_{xy_shear}:								***14***						***24***				
										Avg G1 and G3:		34					***Avg:***	22

γ_{xy_shear} = Avg. of N and S FEM γ_{xy}

% difference = (FIELD-FEM)/FEM*100

γ_{xy_tor} = (Individual N or S FEM γ_{xy} Results) - $|\gamma_{xy\_shear}|$

X = minimum (γ_{xy_tor} / FEM γ_{xy}) value comparing both sides of web at each location

Table 6-9. Comparison of Measured and FEM Girder Shear Strain (με) for Bridge 08011 with Ratios from FEM Results Indicating the Effects of Torsion

Gage Location	G1 BB Loc 9						G2 BB Loc 9						G2-G3 BB Loc 9					
				FEM						FEM						FEM		
	Field γ_{xy}	FEM γ_{xy}	% Diff	γ_{xy_tor}	γ_{xy_tor} / γ_{xy} (%)	γ_{xy_tor} / γ_{xy_shear} (%)	Field γ_{xy}	FEM γ_{xy}	% Diff	γ_{xy_tor}	γ_{xy_tor} / γ_{xy} (%)	γ_{xy_tor} / γ_{xy_shear} (%)	Field γ_{xy}	FEM γ_{xy}	% Diff	γ_{xy_tor}	γ_{xy_tor} / γ_{xy} (%)	γ_{xy_tor} / γ_{xy_shear} (%)
G1_N_05d_E	31	39	-19	-2	5	5	28	29	-5	3	10	12						
G1_N_05d_W	n/a	43		2	5		n/a	23		-3	13							
γ_{xy_shear}:		***41***						***26***										
G1_N_1d_E	31	31	-2	-4	13	11	30	29	2	7	24	32						
G1_N_1d_W	n/a	40		4	10		n/a	16		-7	44							
γ_{xy_shear}:		***36***						***22***										
G1_N_2d_E	38	34	13	-4	12	11	31	29	6	7	24	32						
G1_N_2d_W	n/a	42		4	10		n/a	16		-7	44							
γ_{xy_shear}:		***38***						***22***										
G1_N_4d_E	32	25	30	-3	12	11	32	24	35	5	21	28						
G1_N_4d_W	n/a	31		3	10		n/a	13		-5	38							
γ_{xy_shear}:		***28***						***18***										
G1_N_025L_E	21	26	-18	-4	15	14	18	18	2	2	11	13						
G1_N_025L_W	n/a	33		4	12		n/a	13		-2	15							
γ_{xy_shear}:		***29***						***15***										
G2_N_05d_E	13	13	-3	-2	15	13	37	36	3	0.2	1	1	41	34	18	3	9	10
G2_N_05d_W	n/a	18		2	11		n/a	36		-0.2	1		n/a	28		-3	11	
γ_{xy_shear}:		***15***						***36***						***31***				
G2_N_1d_E	7	10	-32	-4	40	27	41	38	8	0.1	0	0	43	38	15	6	16	19
G2_N_1d_W	n/a	19		4	21		n/a	38		-0.1	0		n/a	26		-6	23	
γ_{xy_shear}:		***15***						***38***						***32***				
G2_N_2d_E	10	11	-4	-5	45	33	37	42	-13	0.1	0	0	43	40	5	6	15	17
G2_N_2d_W	n/a	20		5	25		n/a	42		-0.1	0		n/a	29		-6	21	
γ_{xy_shear}:		***15***						***42***						***35***				
G2_N_4d_E	9	8	17	-4	50	33	28	26	8	0.2	1	1	32	26	24	3	12	14
G2_N_4d_W	n/a	16		4	25		n/a	25		-0.2	1		n/a	19		-3	16	
γ_{xy_shear}:		***12***						***26***						***22***				
G2_N_025L_E	7	9	-30	-2	22	17	31	33	-6	0.2	1	1	34	28	20	2	7	7
G2_N_025L_W	n/a	14		2	14		n/a	32		-0.2	1		n/a	25		-2	8	
γ_{xy_shear}:		***12***						***33***						***27***				
G3_N_05d_E							n/a	21		-3	14	13	n/a	29		-3	10	9
G3_N_05d_W							23	27	-14	3	11		35	35	1	3	9	
γ_{xy_shear}:								***24***						***32***				
G3_N_1d_E							n/a	15		-7	47	32	n/a	27		-5	19	16
G3_N_1d_W							29	29	-2	7	24		42	38	12	5	13	
γ_{xy_shear}:								***22***						***32***				
G3_N_2d_E							n/a	16		-7	44	30	n/a	31		-5	16	14
G3_N_2d_W							29	30	-5	7	23		40	41	-1	5	12	
γ_{xy_shear}:								***23***						***36***				
G3_N_4d_E							n/a	15		-5	33	25	n/a	21		-4	19	16
G3_N_4d_W							19	25	-22	5	20		22	29	-22	4	14	
γ_{xy_shear}:								***20***						***25***				
G3_N_025L_E							n/a	15		-2	13	12	n/a	27		-1	4	4
G3_N_025L_W							20	19	5	2	11		31	28	9	1	4	
γ_{xy_shear}:								***17***						***27***				
											Avg G1 and G3:	23					***Avg:***	12

γ_{xy_shear} = Avg. of N and S FEM γ_{xy}

% difference = (FIELD-FEM)/FEM*100

γ_{xy_tor} = (Individual N or S FEM γ_{xy} Results) - $|\gamma_{xy\_shear}|$

X = minimum (γ_{xy_tor} / FEM γ_{xy}) value comparing both sides of web at each location

Table 6-10. Comparison of Measured and FEM Girder Shear Strain (με) for G1-G2 BB Loc 3 on Bridge 65006 with Ratios from FEM Results Indicating the Effects of Torsion

Gage Location	Field γ_{xy}	FEM γ_{xy}	% Diff	FEM γ_{xy_tor}	FEM γ_{xy_tor} / γ_{xy} (%)	FEM γ_{xy_tor} / γ_{xy_shear} (%)
G3_W_1d_N	7	10	-32	4	40	67
G3_W_1d_S	n/a	2		-4	100	
γ_{xy_shear}:		*6*				
G3_W_2d_N	9	10	-15	5	50	100
G3_W_2d_S	n/a	1		-5	100	
γ_{xy_shear}:		*5*				
G3_W_4d_N	6	9	-33	4	44	80
G3_W_4d_S	n/a	1		-4	100	
γ_{xy_shear}:		*5*				
G3_E_1d_N	5	10	-48	-1	10	9
G3_E_1d_S	n/a	13		1	8	
γ_{xy_shear}:		*11*				
					Avg:	64

Gage Location	Field γ_{xy}	FEM γ_{xy}	% Diff	FEM γ_{xy_tor}	FEM γ_{xy_tor} / γ_{xy} (%)	FEM γ_{xy_tor} / γ_{xy_shear} (%)
G2_W_1d_N	40	37	10	9	24	33
G2_W_1d_S	n/a	18		-9	50	
γ_{xy_shear}:		*27*				
G2_W_2d_N	40	43	-7	11	26	34
G2_W_2d_S	n/a	21		-11	52	
γ_{xy_shear}:		*32*				
G2_W_4d_N	27	29	-6	8	28	38
G2_W_4d_S	n/a	12		-8	67	
γ_{xy_shear}:		*21*				
G2_E_1d_N	27	27	-1	5	19	22
G2_E_1d_S	n/a	18		-5	28	
γ_{xy_shear}:		*23*				
					Avg:	32

Gage Location (obtuse cor.)	Field γ_{xy}	FEM γ_{xy}	% Diff	FEM γ_{xy_tor}	FEM γ_{xy_tor} / γ_{xy} (%)	FEM γ_{xy_tor} / γ_{xy_shear} (%)
G1_W_1d_N	n/a	26		-9	35	26
G1_W_1d_S	40	43	-5	9	21	
γ_{xy_shear}:		*34*				
G1_W_2d_N	n/a	16		-7	44	30
G1_W_2d_S	23	31	-25	7	23	
γ_{xy_shear}:		*23*				
G1_W_4d_N	n/a	13		2	15	18
G1_W_4d_S	1	9	-87	-2	22	
γ_{xy_shear}:		*11*				
G1_E_1d_N	n/a	19		-2	11	10
G1_E_1d_S	10	22	-57	2	9	
γ_{xy_shear}:		*21*				
					Avg:	21

Notes:

γ_{xy_shear} = Avg. of N and S FEM γ_{xy}

% difference = (FIELD-FEM)/FEM*100

γ_{xy_tor} = (Individual N or S FEM γ_{xy} Results) - $|\gamma_{xy\_shear}|$

X = minimum (γ_{xy_tor} / FEM γ_{xy}) value comparing both sides of web at each location

Table 6-11. Comparison of Measured and FEM Girder Shear Strain (με) for G2 BB Loc 3 on Bridge 65006 with Ratios from FEM Results Indicating the Effects of Torsion

Gage Location	Field γ_{xy}	FEM γ_{xy}	% Diff	FEM γ_{xy_tor}	FEM γ_{xy_tor} / γ_{xy} (%)	FEM γ_{xy_tor} / γ_{xy_shear} (%)
G3_W_1d_N	16	19	-15	7	37	58
G3_W_1d_S	n/a	5		-7	100	
γ_{xy_shear}:		*12*				
G3_W_2d_N	15	22	-30	8	36	57
G3_W_2d_S	n/a	5		-8	100	
γ_{xy_shear}:		*14*				
G3_W_4d_N	18	21	-15	7	33	54
G3_W_4d_S	n/a	6		-7	100	
γ_{xy_shear}:		*13*				
G3_E_1d_N	19	23	-17	4	17	20
G3_E_1d_S	n/a	16		-4	25	
γ_{xy_shear}:		*20*				
					Avg:	47

Gage Location	Field γ_{xy}	FEM γ_{xy}	% Diff	FEM γ_{xy_tor}	FEM γ_{xy_tor} / γ_{xy} (%)	FEM γ_{xy_tor} / γ_{xy_shear} (%)
G2_W_1d_N	44	47	-6	2	4	4
G2_W_1d_S	n/a	44		-2	5	
γ_{xy_shear}:		*46*				
G2_W_2d_N	36	46	-21	3	7	7
G2_W_2d_S	n/a	41		-3	7	
γ_{xy_shear}:		*43*				
G2_W_4d_N	20	26	-22	5	19	25
G2_W_4d_S	n/a	15		-5	33	
γ_{xy_shear}:		*20*				
G2_E_1d_N	20	38	-47	6	16	18
G2_E_1d_S	n/a	27		-6	22	
γ_{xy_shear}:		*33*				
					Avg:	14

Gage Location (obtuse cor.)	Field γ_{xy}	FEM γ_{xy}	% Diff	FEM γ_{xy_tor}	FEM γ_{xy_tor} / γ_{xy} (%)	FEM γ_{xy_tor} / γ_{xy_shear} (%)
G1_W_1d_N	n/a	4		-11	100	73
G1_W_1d_S	22	26	-16	11	42	
γ_{xy_shear}:		*15*				
G1_W_2d_N	n/a	1		-10	100	91
G1_W_2d_S	11	20	-46	10	50	
γ_{xy_shear}:		*11*				
G1_W_4d_N	n/a	5		-1	20	20
G1_W_4d_S	0	6	-99	1	17	
γ_{xy_shear}:		*5*				
G1_E_1d_N	n/a	5		-2	40	25
G1_E_1d_S	2	10	-75	2	20	
γ_{xy_shear}:		*8*				
					Avg:	52

Notes:

γ_{xy_shear} = Avg. of N and S FEM γ_{xy}

% difference = (FIELD-FEM)/FEM*100

γ_{xy_tor} = (Individual N or S FEM γ_{xy} Results) - $|\gamma_{xy\_shear}|$

X = minimum (γ_{xy_tor} / FEM γ_{xy}) value comparing both sides of web at each location

Table 6-12 Comparison of Measured and FEM Girder Shear Strain (με) for G3 BB Loc 3 on Bridge 65006 with Ratios from FEM Results Indicating the Effects of Torsion

Gage Location	Field γ_{xy}	FEM γ_{xy}	% Diff	FEM γ_{xy_tor}	FEM γ_{xy_tor} / γ_{xy} (%)	FEM γ_{xy_tor} / γ_{xy_shear} (%)
G4_W_1d_N	15	21	-27	8	38	62
G4_W_1d_S	n/a	5		-8	100	
γ_{xy_shear}:		***13***				
G4_W_2d_N	21	24	-12	9	38	64
G4_W_2d_S	n/a	5		-9	100	
γ_{xy_shear}:		***14***				
G4_W_4d_N	18	22	-19	8	36	57
G4_W_4d_S	n/a	6		-8	100	
γ_{xy_shear}:		***14***				
G4_E_1d_N	23	24	-6	4	17	20
G4_E_1d_S	n/a	16		-4	25	
γ_{xy_shear}:		***20***				
Notes:					***Avg:***	51

Gage Location	Field γ_{xy}	FEM γ_{xy}	% Diff	FEM γ_{xy_tor}	FEM γ_{xy_tor} / γ_{xy} (%)	FEM γ_{xy_tor} / γ_{xy_shear} (%)
G3_W_1d_N	38	50	-23	1	2	2
G3_W_1d_S	n/a	47		-1	2	
γ_{xy_shear}:		***49***				
G3_W_2d_N	48	47	3	3	6	7
G3_W_2d_S	n/a	41		-3	7	
γ_{xy_shear}:		***44***				
G3_W_4d_N	25	23	7	6	26	35
G3_W_4d_S	n/a	10		-6	60	
γ_{xy_shear}:		***17***				
G3_E_1d_N	30	40	-26	6	15	18
G3_E_1d_S	n/a	29		-6	21	
γ_{xy_shear}:		***34***				
					Avg:	15

Gage Location	Field γ_{xy}	FEM γ_{xy}	% Diff	FEM γ_{xy_tor}	FEM γ_{xy_tor} / γ_{xy} (%)	FEM γ_{xy_tor} / γ_{xy_shear} (%)
G2_W_1d_N	3	14	-78	-8	57	38
G2_W_1d_S	n/a	29		8	28	
γ_{xy_shear}:		***21***				
G2_W_2d_N	3	9	-66	-8	89	50
G2_W_2d_S	n/a	24		8	33	
γ_{xy_shear}:		***16***				
G2_W_4d_N	7	7	4	-1	14	13
G2_W_4d_S	n/a	9		1	11	
γ_{xy_shear}:		***8***				
G2_E_1d_N	7	10	-29	1	10	11
G2_E_1d_S	n/a	9		-1	11	
γ_{xy_shear}:		***9***				
					Avg:	28

γ_{xy_shear} = Avg. of N and S FEM γ_{xy}

% difference = (FIELD-FEM)/FEM*100

γ_{xy_tor} = (Individual N or S FEM γ_{xy} Results) - $|\gamma_{xy\_shear}|$

X = minimum (γ_{xy_tor} / FEM γ_{xy}) value comparing both sides of web at each location

Table 6-13. Comparison of Measured and FEM Girder Shear Strain (με) for G4 BB Loc 3 on Bridge 65006 with Ratios from FEM Results Indicating the Effects of Torsion

Gage Location (acute cor.)	Field γ_{xy}	FEM γ_{xy}	% Diff	FEM γ_{xy_tor}	FEM γ_{xy_tor} / γ_{xy} (%)	FEM γ_{xy_tor} / γ_{xy_shear} (%)
G5_W_1d_N	22	18	20	9	50	100
G5_W_1d_S	n/a	0		-9	100	
γ_{xy_shear}:		***9***				
G5_W_2d_N	22	21	6	10	48	100
G5_W_2d_S	n/a	0		-10	100	
γ_{xy_shear}:		***10***				
G5_W_4d_N	n/a	20		9	45	90
G5_W_4d_S	n/a	1		-9	100	
γ_{xy_shear}:		***10***				
G5_E_1d_N	15	23	-36	11	48	85
G5_E_1d_S	n/a	2		-11	100	
γ_{xy_shear}:		***13***				
Notes:					***Avg:***	94

Gage Location	Field γ_{xy}	FEM γ_{xy}	% Diff	FEM γ_{xy_tor}	FEM γ_{xy_tor} / γ_{xy} (%)	FEM γ_{xy_tor} / γ_{xy_shear} (%)
G4_W_1d_N	30	49	-38	2	4	4
G4_W_1d_S	n/a	45		-2	4	
γ_{xy_shear}:		***47***				
G4_W_2d_N	43	46	-7	3	7	7
G4_W_2d_S	n/a	39		-3	8	
γ_{xy_shear}:		***43***				
G4_W_4d_N	26	23	16	7	30	44
G4_W_4d_S	n/a	9		-7	78	
γ_{xy_shear}:		***16***				
G4_E_1d_N	41	41	1	6	15	17
G4_E_1d_S	n/a	28		-6	21	
γ_{xy_shear}:		***35***				
					Avg:	18

Gage Location	Field γ_{xy}	FEM γ_{xy}	% Diff	FEM γ_{xy_tor}	FEM γ_{xy_tor} / γ_{xy} (%)	FEM γ_{xy_tor} / γ_{xy_shear} (%)
G3_W_1d_N	0	13	-96	-7	54	33
G3_W_1d_S	n/a	28		7	25	
γ_{xy_shear}:		***21***				
G3_W_2d_N	0	9	-100	-7	78	44
G3_W_2d_S	n/a	23		7	30	
γ_{xy_shear}:		***16***				
G3_W_4d_N	3	7	-62	-1	14	13
G3_W_4d_S	n/a	9		1	11	
γ_{xy_shear}:		***8***				
G3_E_1d_N	3	9	-72	0	0	0
G3_E_1d_S	n/a	9		0	0	
γ_{xy_shear}:		***9***				
					Avg:	22

γ_{xy_shear} = Avg. of N and S FEM γ_{xy}

% difference = (FIELD-FEM)/FEM*100

γ_{xy_tor} = (Individual N or S FEM γ_{xy} Results) - $|\gamma_{xy\_shear}|$

X = minimum (γ_{xy_tor} / FEM γ_{xy}) value comparing both sides of web at each location

Table 6-14. Comparison of Measured and FEM Girder Shear Strain (με) for G4-G5 BB Loc 3 on Bridge 65006 with Ratios from FEM Results Indicating the Effects of Torsion

Gage Location (acute cor.)	Field γ_{xy}	FEM γ_{xy}	% Diff	FEM γ_{xy_tor}	FEM γ_{xy_tor} / γ_{xy} (%)	FEM γ_{xy_tor} / γ_{xy_shear} (%)
G5_W_1d_N	37	34	10	-9	26	35
G5_W_1d_S	n/a	16		9	53	
γ_{xy_shear}:		***25***				
G5_W_2d_N	41	39	6	-10	27	36
G5_W_2d_S	n/a	18		10	57	
γ_{xy_shear}:		***29***				
G5_W_4d_N	n/a	27		-8	31	45
G5_W_4d_S	n/a	10		8	82	
γ_{xy_shear}:		***19***				
G5_E_1d_N	21	29	-28	-6	20	25
G5_E_1d_S	n/a	17		6	34	
γ_{xy_shear}:		***23***				
Notes:					***Avg:***	35

Gage Location	Field γ_{xy}	FEM γ_{xy}	% Diff	FEM γ_{xy_tor}	FEM γ_{xy_tor} / γ_{xy} (%)	FEM γ_{xy_tor} / γ_{xy_shear} (%)
G4_W_1d_N	17	30	-44	8	26	20
G4_W_1d_S	n/a	46		-8	17	
γ_{xy_shear}:		***38***				
G4_W_2d_N	17	22	-22	6	26	21
G4_W_2d_S	n/a	34		-6	17	
γ_{xy_shear}:		***28***				
G4_W_4d_N	17	16	8	-2	15	18
G4_W_4d_S	n/a	11		2	22	
γ_{xy_shear}:		***13***				
G4_E_1d_N	19	20	-5	-1	5	5
G4_E_1d_S	n/a	18		1	5	
γ_{xy_shear}:		***19***				
					Avg:	16

Gage Location	Field γ_{xy}	FEM γ_{xy}	% Diff	FEM γ_{xy_tor}	FEM γ_{xy_tor} / γ_{xy} (%)	FEM γ_{xy_tor} / γ_{xy_shear} (%)
G3_W_1d_N	1	4	-85	4	99	50
G3_W_1d_S	n/a	13		-4	33	
γ_{xy_shear}:		***8***				
G3_W_2d_N	2	2	-13	4	100	67
G3_W_2d_S	n/a	11		-4	40	
γ_{xy_shear}:		***7***				
G3_W_4d_N	1	2	-39	2	95	49
G3_W_4d_S	n/a	6		-2	33	
γ_{xy_shear}:		***4***				
G3_E_1d_N	0	4	-93	0	5	5
G3_E_1d_S	n/a	4		0	5	
γ_{xy_shear}:		***4***				
					Avg:	43

γ_{xy_shear} = Avg. of N and S FEM γ_{xy}

% difference = (FIELD-FEM)/FEM*100

γ_{xy_tor} = (Individual N or S FEM γ_{xy} Results) - $|\gamma_{xy\_shear}|$

X = minimum (γ_{xy_tor} / FEM γ_{xy}) value comparing both sides of web at each location

Figure 6-1. (a) Partial Depth and (b) Full Depth Diaphragm with Interface Cracking

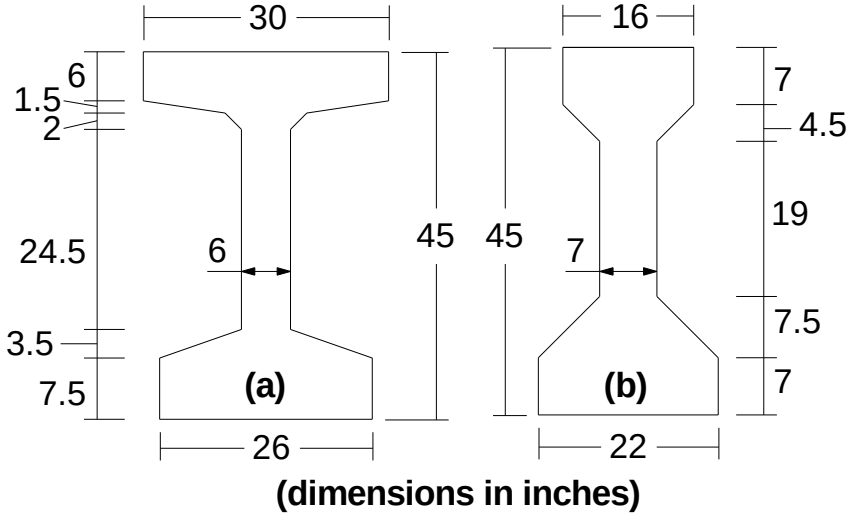

Figure 6-2. (a) MnDOT 45M Shape and (b) AASHTO Type III Shape

Figure 6-3. Back-to-Back Truck Position

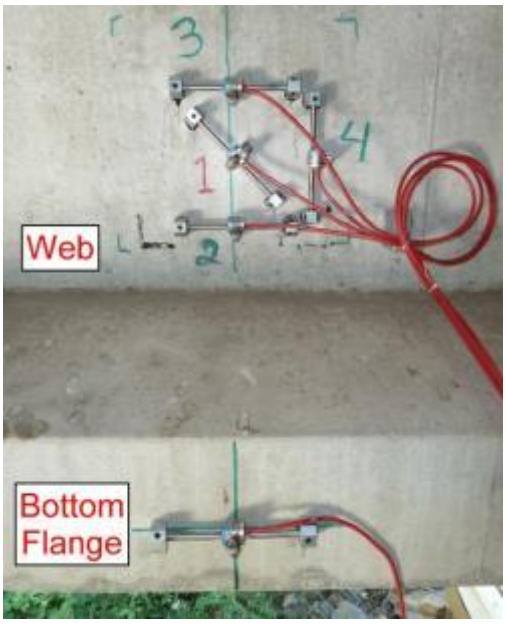

Figure 6-4. Horizontal Strain Gage on Bottom Flange

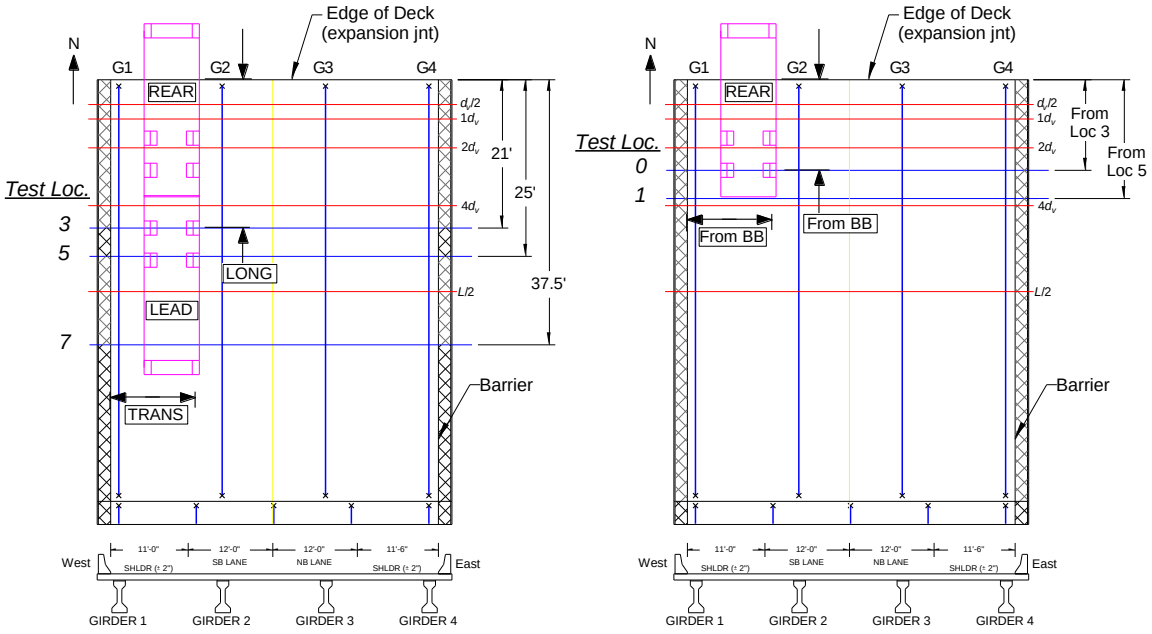

Figure 6-5. Representative Transverse and Longitudinal Locations for BB and ST from Bridge 73872

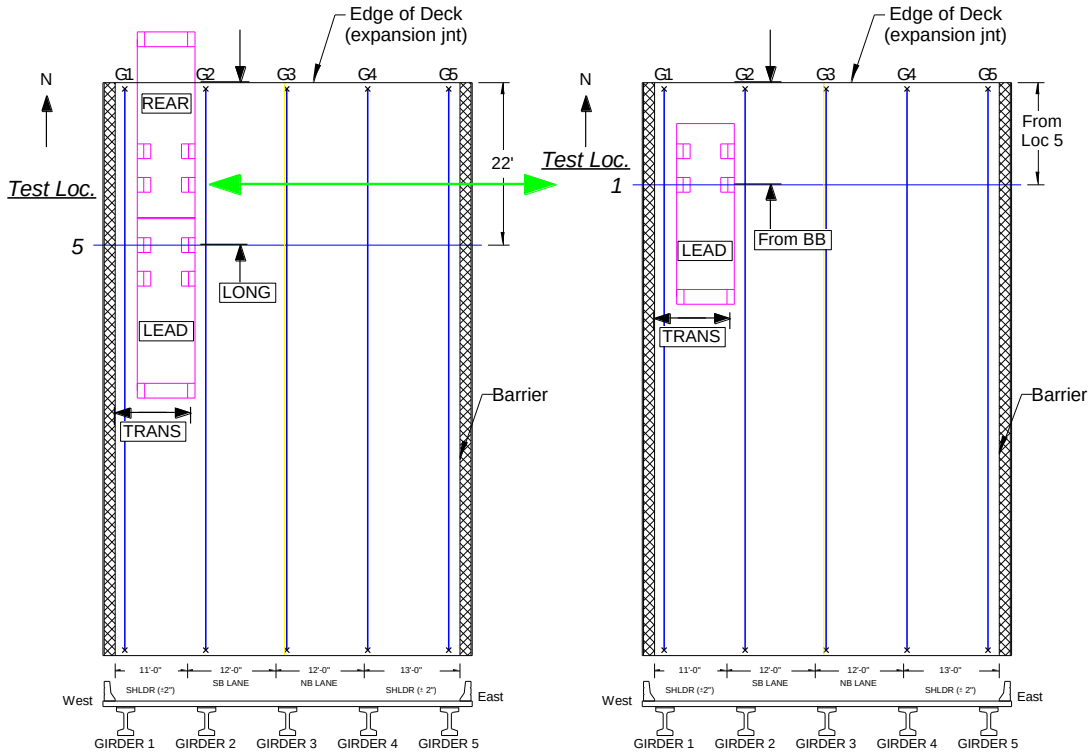

Figure 6-6. Longitudinally Flipped Testing Location 1 from Bridge 08011

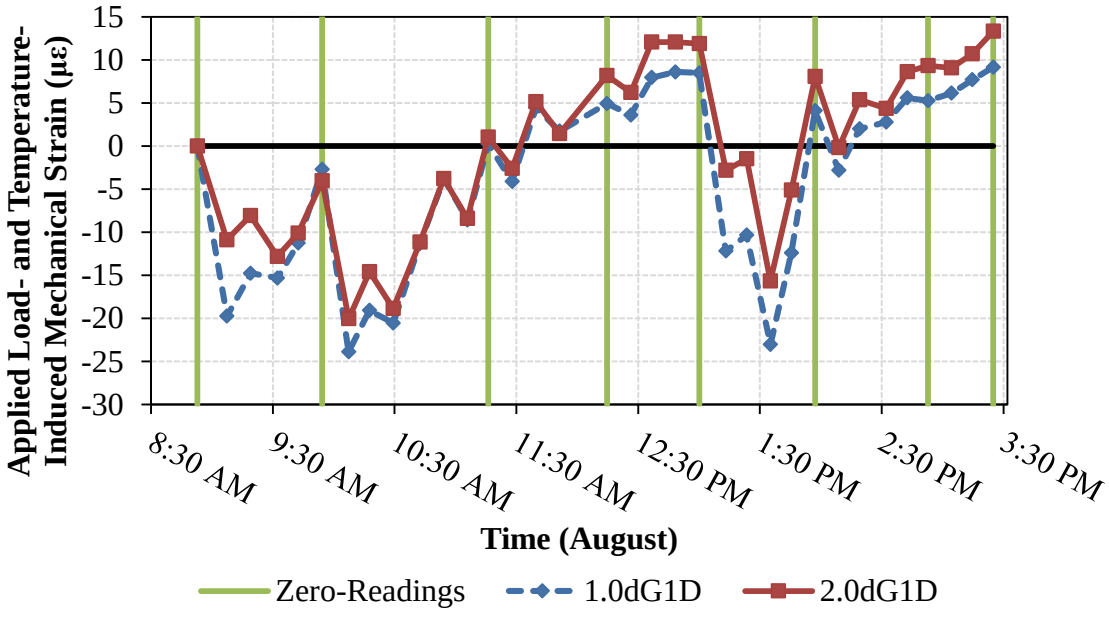

Figure 6-7. Applied Load- and Temperature-Induced Mechanical Strain from Bridge 09002

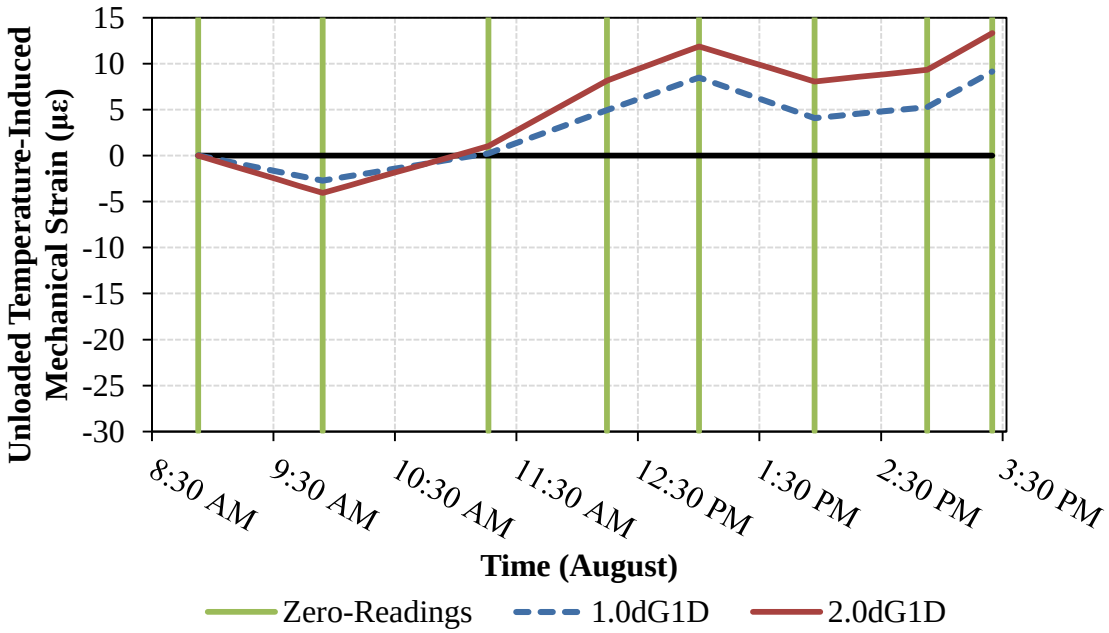

Figure 6-8. Unloaded Temperature-Induced Mechanical Strain from Bridge 09002

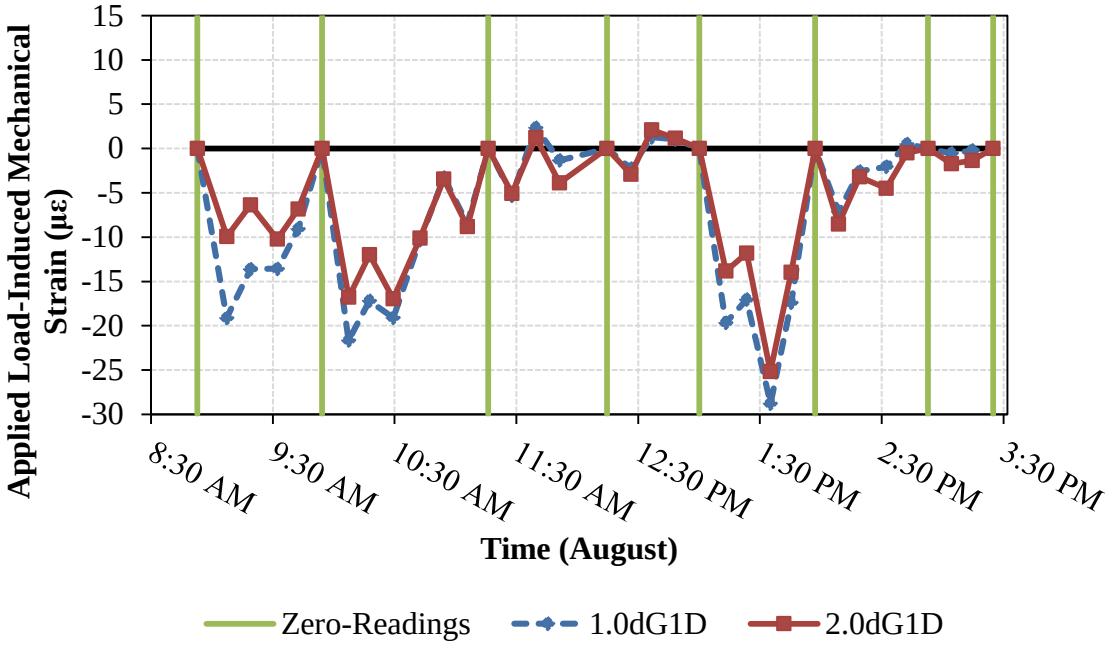

Figure 6-9. Applied Load-Induced Mechanical Strain Only from Bridge 09002

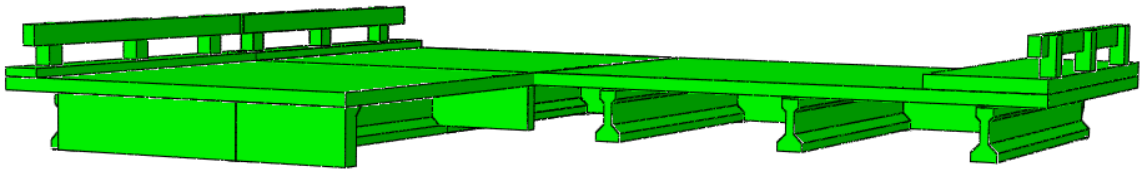

Figure 6-10. FEM Cutaway View of Straight Bridge 09002 with Secondary Elements

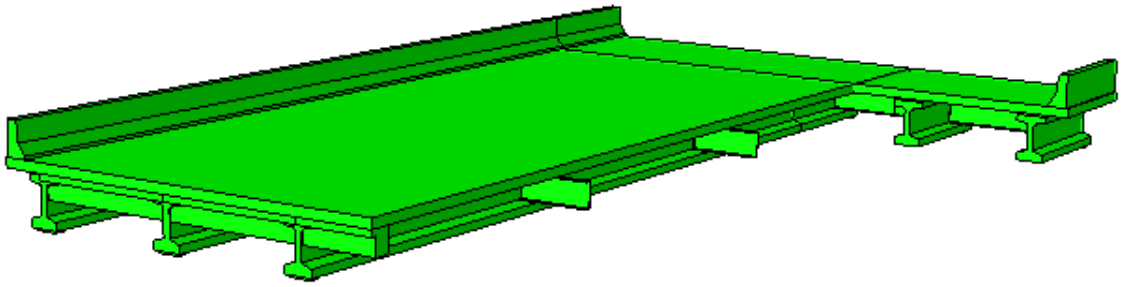

Figure 6-11. FEM Cutaway View of Straight Bridge 08011 with Secondary Elements

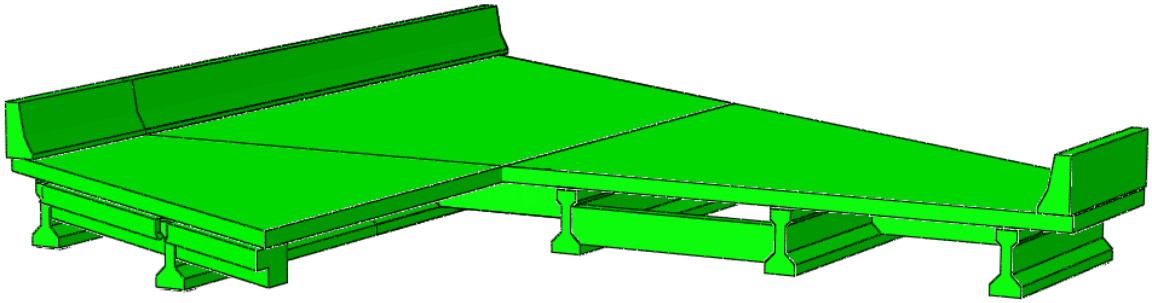

Figure 6-12. FEM Cutaway View of Skewed Bridge 65006 with Secondary Elements

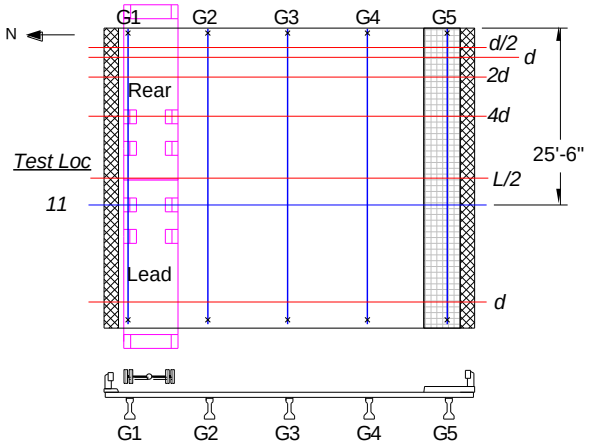

G1 BB Loc 11

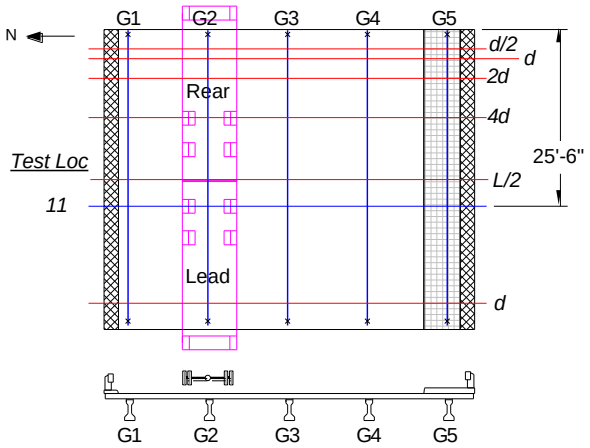

G2 BB Loc 11

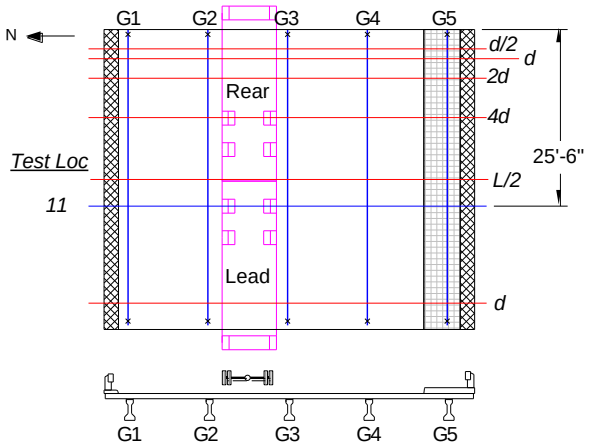

G2-G3 BB Loc 11

Figure 6-13. Loading Cases for Straight Bridge 09002 FEM Validation

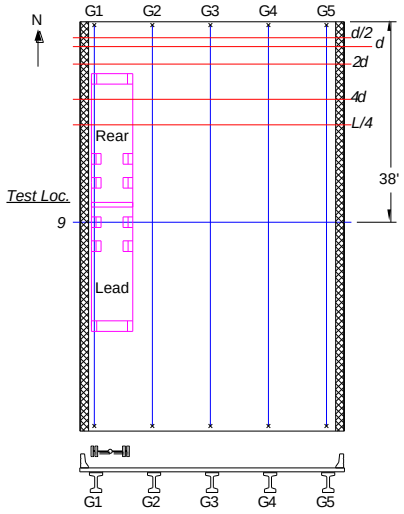

G1 BB Loc 9

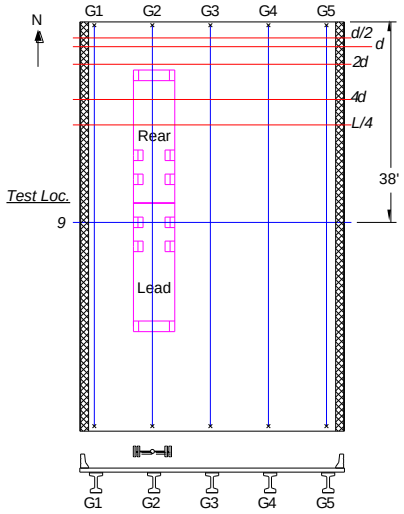

G2 BB Loc 9

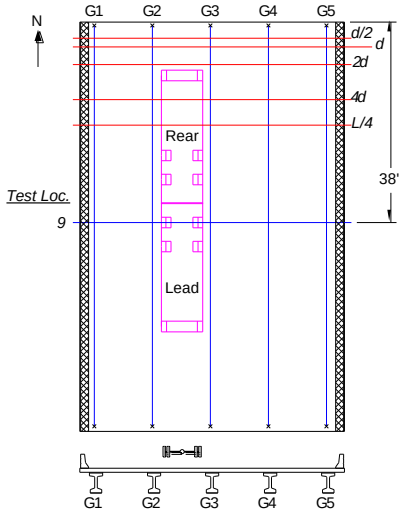

Figure 6-14. Loading Cases for Straight Bridge 08011 FEM Validation

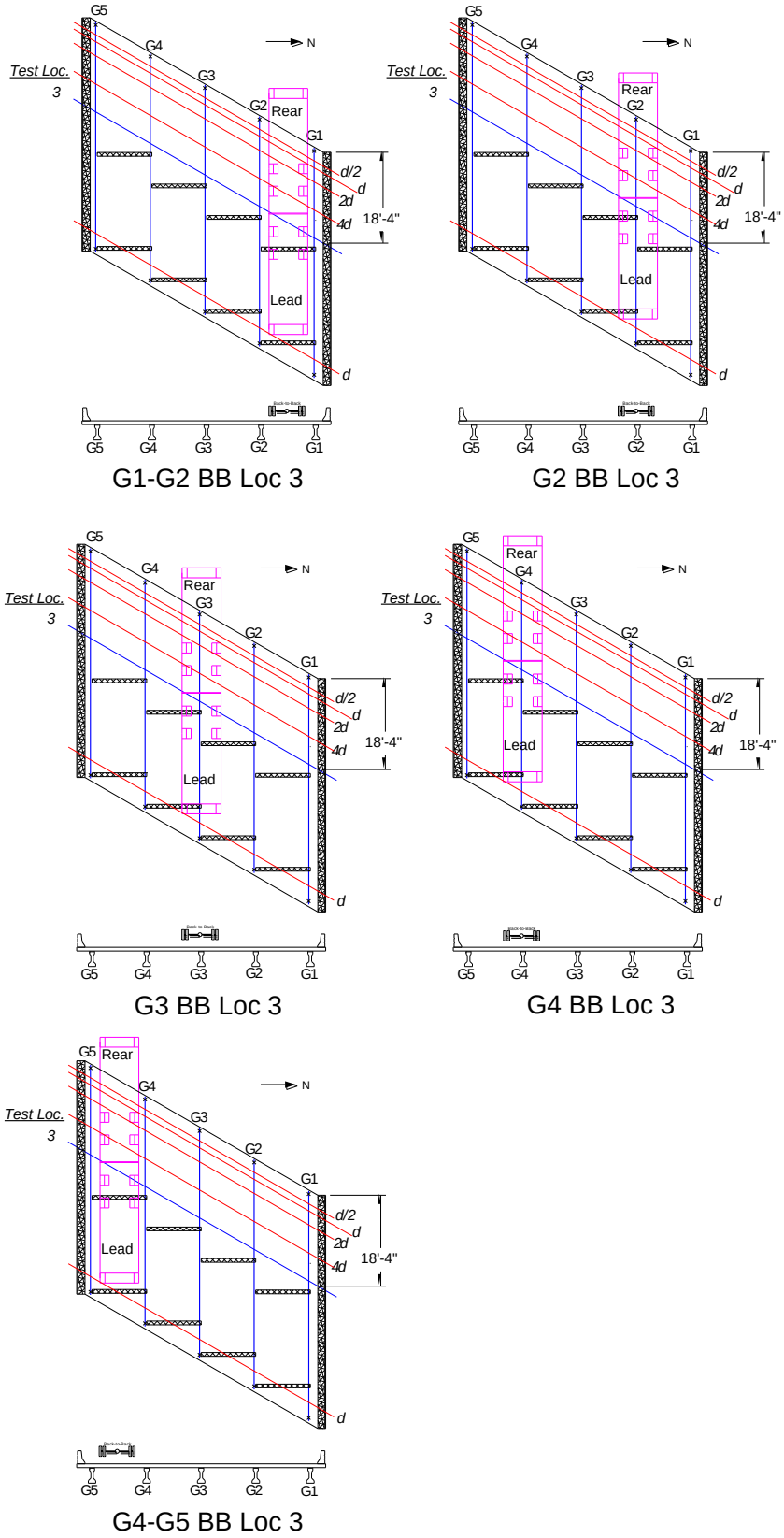

Figure 6-15. Loading Cases for Skewed Bridge 65006 FEM Validation

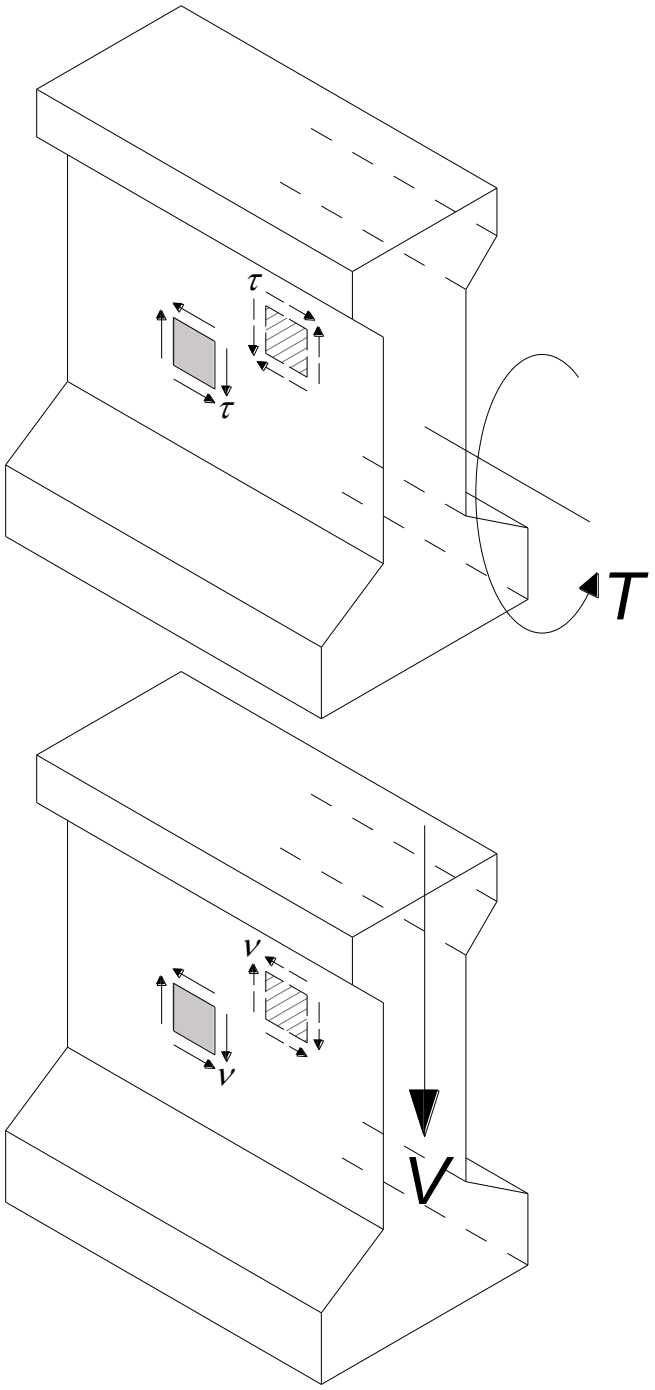

Figure 6-16. Shear Stresses due to Torsion (top) and the Vertical Shear Resultant (bottom) on both Sides of the Girder Web

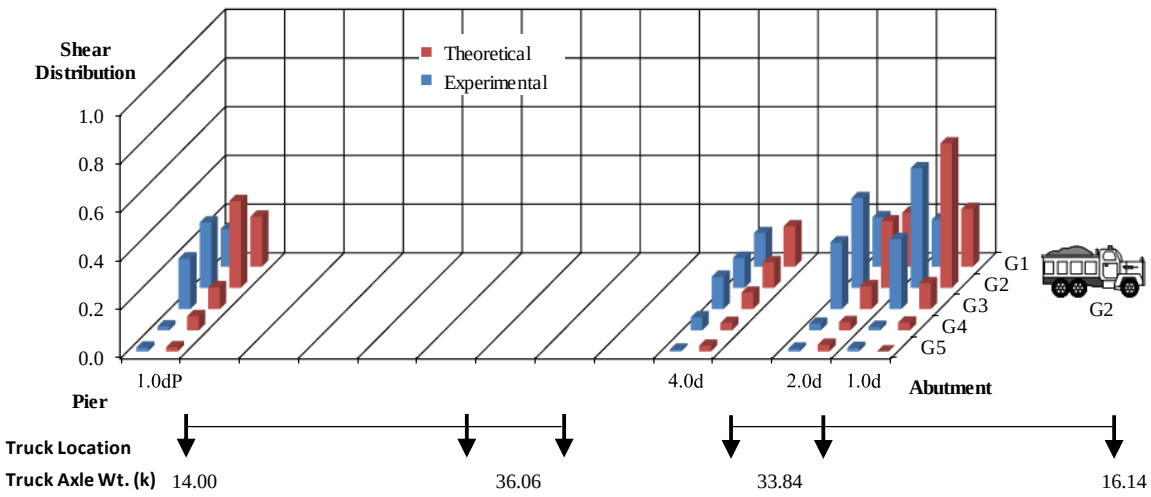

Figure 6-17. 3D Shear Distribution for Loading Case G2 BB Loc 3 on Bridge 09002

CHAPTER 7. SHEAR DISTRIBUTION PARAMETRIC STUDY AND PROPOSED METHOD FOR RATING

7.1 Introduction

This chapter discusses the parametric study of prestressed concrete girder bridges that was used to broaden the applicability of the results and develop the proposed methodology for shear rating and truck permitting. The parametric study examined how shear forces distribute in prestressed concrete girder bridge structures when core parameters (e.g., girder spacing and depth, span length, and deck thickness) were varied from a base configuration. The proposed methodology for rating and truck permitting was based on a comparison of live load shear demand from the parametric study to the live load shear demand generated using AASHTO shear distribution factor methods.

7.2 Parametric Study

A parametric study was conducted using the validated three-dimensional finite element modeling technique to develop shear distribution recommendations for prestressed concrete girder bridges. Parameters varied included girder depth and spacing, deck thickness, and span length. The full-scale laboratory bridge served as the base configuration for the parametric study. Models of six additional structures summarized in Table 7-1 were created for the study, where a single bridge parameter was varied in each model. The goal was to decouple the core bridge parameters to provide a clear picture of how each affected shear distribution. Each bridge studied contained four girders; when the girder spacing varied, the bridge width also varied.

The laboratory bridge base case included details discussed in Sections 3.3 and 4.1 and had the following specifications:

- Four 36 in. deep girders, 32 ft long, and nearly identical to AASHTO Type II girders with a Young's modulus of 5,000 ksi in the longitudinal direction of the bottom flange (to account for the stiffness of the prestressing strand) and 4,674 ksi in all other parts and directions.
- Girders spaced at 9 ft center-to-center.

- Simply supported span length of 30.75 ft.
- Zero degrees skew.
- Deck thickness of 9 in. with a transversely isotropic Young's modulus of 4,530 ksi, which accounted for the reinforcement.
- Elastomeric bearing pads, 2.5 in. thick, with a transversely isotropic Young's modulus of 17,857 psi, density of 0.0813 lb/in.^{3}, and Poisson's ratio of 0.49995.

There were two main goals to the parametric study. First, it was important to investigate the effect of any single variable on shear distribution by creating models with reasonable upper and lower bounds for important parameters. The following bounds were investigated: deck thickness of 6 in. minimum and 12 in. maximum, girder depth of 36 in. minimum and 72 in. maximum, span length of 30.75 ft minimum and 62.75 ft maximum, girder spacing of 6.5 ft minimum and 16 ft maximum. These limits were indicative of structures found in the MnDOT inventory. The second goal of the parametric study was to determine if the AASHTO Standard or AASHTO LRFD shear distribution factors provided an accurate estimate of live load shear demand compared to shear demand determined from the parametric study finite element models that had been validated with the laboratory bridge data. If the AASHTO shear distribution factors proved to be overly conservative for certain types of bridge structures, development of a screening tool to identify the these structures and a simple refined analysis methodology to calculate a more accurate live load shear demand was desired.

Seven simplifications were utilized when investigating shear distribution results within the parametric study to narrow the scope. First, based on the full-scale laboratory bridge test results discussed in Section 5.3.5, the effects of end diaphragms, intermediate diaphragms, and traffic barriers were ignored in developing the shear distribution recommendations. Ignoring the effects of an end diaphragm may be slightly inaccurate (by 4 to 6 percent), but this assumption was warranted for simplicity.

Second, it was assumed that interior girders controlled load rating. This was assumed for structures that rate poorly for shear in the MnDOT inventory after correspondence with the MnDOT Technical Liaison (Gao 2015). Parametric study analysis focussed on shear distribution in the first interior girder adjacent to the exterior girder

where the load distribution factors are generally the largest (Tabsh and Tabatabai 2001). Furthermore, load distribution to exterior girders is highly dependent on the length of the roadway overhang.

Third, the truck axle gage width was taken as 6 ft and a 4 ft transverse spacing was used between axles of multiple vehicles. For increased gage widths, the distribution factor is generally lower and therefore conservative (Zokaie et al. 1991b, Zokaie 2000, AASHTO MBE 2011).

Fourth, FEM results generated with a single axle rather than an entire HS20 truck indicated that the shear per unit load in the interior girder from two lanes loaded (with two single axles side-by-side) controlled compared to a single lane loaded. Puckett et al. (2007) confirmed that, when the multiple presence factors are included in the DF values, the two lane loaded DF typically controls when compared to three or four lane loaded DFs for concrete slab on precast concrete I-sections. When the three lane DF did control in the Puckett et al. study, the two lane loaded DF values were generally 90 percent or more of the three lane loaded value.

Fifth, the transverse truck position that maximized the live load shear demand in an interior girder was selected based on the lever rule. The lever rule transverse loading positions for one and two lanes loaded considering girder spacing between 6.5 and 16 ft are given in Table 7-2. Distributed lane loads were not used within this study.

Sixth, multiple presence factors in the AASHTO Standard Specifications were not used for comparison to results from the parametric study. Multiple presence factors are included in the distribution factor equations in the AASHTO LRFD Specifications; for comparison to results from the parametric study, AASHTO LRFD DFs were divided by the appropriate multiple presence factor. This approach was corroborated by Cross et al. (2009) who stated that "the multiple presence factor of 1.2 in LRFD [for one lane loaded] is not related to the shear distribution for a single truck, but is rather an increase in the loading to account for the probability of higher individual truck loadings than the HL-93 loading when one lane is loaded."

Seventh, shear forces collected from finite element models were determined assuming a composite section composed of the girder and the portion of the deck width equal to the girder spacing. This provided some inherent conservatism because not all of

the shear force carried to the end of the span by a composite section is carried through the girder. The shear force that is carried to the end of the span in the bridge deck is transferred to the support through the girder web near the reaction. In this region, the girder has additional shear capacity because it experiences vertical compression due to the load and reaction.

7.2.1 Shear Distribution of One and Two Lanes Loaded

To address the first goal of the parametric study, the FEM models were loaded with single axles configured transversely according to the lever rule to maximize the interior beam shear for both one and two lanes loaded as shown in Table 7-2. This loading scenario represented a single axle of an HS20 truck. Axle loads were applied to the bridge deck using the AASHTO tire contact area assumed to be a single rectangle, 20 in. wide (transversely) and 10 in. long (longitudinally). Interior girder shear forces were collected from the solid element three-dimensional finite element models that had been validated with data from both the laboratory bridge and bridges that were field tested. The axle loads were applied at each 10^{th} point of the span length. The shear per unit load in the interior girder was calculated using the following:

$$\text{Shear per Unit Load in Interior Girder} = \frac{V_{interior}}{\textit{Single Axle Load Magnitude}} \tag{7.1}$$

where $V_{interior}$ is the interior girder shear force at the location of interest for shear along the span length in a composite section assuming an effective deck width equal to the girder spacing, and *Single Axle Load Magnitude* is the total load applied by a single axle.

Plots of the shear per unit load in the interior girder versus the location of shear along the span length for each structure were generated for each loading case (one lane and two lanes) and loading location (10^{th} points along span). Example plots are shown in Figure 7-1 and Figure 7-2 for one lane and two lane loading, respectively. Additional plots for each of the structures in the parametric study are given in Appendix I. Each curve in Figure 7-1 and Figure 7-2 represents the shear per unit load (*y*-axis) in the interior girder at different longitudinal locations (*x*-axis) when axle loads were located at a specific point along the span length. The different curves in the graph are for different locations of the

axle loads. Each curve was generated with a single axle (one lane loaded) or two axles side-by-side (two lanes loaded) placed at each longitudinal location denoted in the legend. The individual points on each curve were generated with Eqn. (7.1) using interior girder shear force results collected at each 10^{th} point of the span length for structures spanning 30.75 ft or collected at each 20^{th} point of the span length for structures spanning 62.75 ft or more.

Shear force results for each curve were collected using nodal forces at least one girder depth away from the patch load because of the disturbed region immediately surrounding the patch load. The length of the disturbed region is generally associated with the composite depth instead of the girder depth, but the girder depth was used in this study for consistency amongst structures. For example, the series represented by the gray diamond line named "1 Lane at 0.3*L*" in Figure 7-1 contains results collected when an axle load was applied at 0.3*L*. In this series, results were collected from 0.0*L* to 0.25*L* but not directly under the load at 0.3*L* (in this case, 0.05*L* was approximately equal to the girder depth, *d*). Depending on the span length, the value of 0.05*L* or 0.1*L* were typically assumed to be approximately equal to *d* as shown in Table 7-1. In the case of the deep beam (72 in. depth), data were collected at a values of 0.1*L* (36.9 in.) which was approximately equal to half of the girder depth; disturbed region effects caused by the patch load were not noticed in shear force results collected using nodal forces at half the girder depth for this case. Furthermore, results collected at 0.0*L* were not obtained from the centerline of the finite element bearing pad due to the disturbed region immediately above the FEM boundary conditions. In all cases, the shear force results shown at 0.0*L* were collected 10.5 in. toward midspan, measured from the support centerline; this location was within a girder depth from the support, but no effects of the support boundary conditions were observed in shear force results collected using nodal forces. Each point in the series represented by the gray diamond line named "1 Lane at 0.3*L*" in Figure 7-1 shows the shear per unit load in the interior girder as a function of girder section of interest. With the axle applied at 0.3*L* (i.e., a particular position along the span), the shear distributed transversely to the adjacent girders at sections of interest closer to the support. Consequently, cross sections of interest located further toward the support from the point of load application had lower shear per unit load in the interior girder.

The overall behavior of the shear per unit load in the interior girder was similar for one and two lanes loaded shown in Figure 7-1 and Figure 7-2, respectively. In both figures, the shear per unit load is relative to one axle as shown in Eqn. (7.1), because the data in Figure 7-2 has already accounted for the presence of two axles transversely. The data in Figure 7-1 and Figure 7-2 would be used to distribute the live load shear demand from one axle to one or two lanes loaded, respectively. For two lanes loaded, with individual axles placed relative to the interior girder as shown in Table 7-2, results in Figure 7-2 indicated that the shear per unit load carried by the interior girder increased due to the additional applied load. However, data presented in Figure 7-1 cannot be multiplied by a factor of two to generate the data presented in Figure 7-2 because additional axles engage more of the transverse cross section and load is carried by adjacent girders in the bridge system. The only location in Figure 7-1 and Figure 7-2 where the shear per unit load curve for two lanes loaded was slightly lower than the one lane loaded case was when load was applied at 0.9L. The peak value of 0.15 in Figure 7-2 was slightly lower than the peak value of 0.16 in Figure 7-1. This may be due to differences in the type of loading specified by the lever rule in Table 7-2 for S = 9 ft and the proximity to the far support. Two wheel loads were within 3 ft of the interior girder for the case of one lane loaded (both less than one half the girder spacing away from the interior girder), but in the case of two lanes loaded one wheel was over the interior girder while one wheel was 4 ft from the girder (almost one half of the girder spacing away from the interior girder).

The double curvature behavior exhibited by the dashed lines connecting the peak of each individual shear per unit load curve in Figure 7-1, Figure 7-2, and Appendix I was more prominent in longer span bridges where more shear distributed amongst adjacent girders near the middle of the span. At the end of the span, the supports were closer to the applied load and may have led to less transverse shear distribution. A less pronounced double curvature in the base case parametric study bridge, shown in Figure 7-3 and Figure 7-4, indicated that the shear per unit load in the interior girder was similar near the point of applied load and the support (especially with two lanes loaded in Figure 7-4). In most cases, the double curvature shown in Figure 7-1, Figure 7-2, and Appendix I indicated that the shear per unit load in the interior girder was highest near the point of applied load and dropped as shear distributed to adjacent girders in sections of interest closer to the support.

The trend of decreasing shear per unit load in the interior girder sections of interest closer to the support was slightly reversed in Figure 7-2 for the case of two lanes loaded. This may be due to the nature of the loading specified by the lever rule. Two lanes loaded, with individual axles placed relative to the interior girder as shown in Table 7-2, provides more opportunity for shear to be carried by the deck near the end of the span when more than two wheel loads apply load near the interior girder. The shear carried by the deck travels to the support at the end of the span and may lead to increased shear force in the composite section at the end of the span.

7.2.2 Live Load Shear Demand using an Axle-Based Approach

Figure 7-1 and Figure 7-2 show the shear distribution behavior in the interior composite girder as the sections of interest are examined closer to the support than the point of load application; as load was applied further into the span length (e.g., at 0.8*L*) the shear force effects at a location of interest near the support were quite small (the shear per unit load near the end of the interior girder was about 0.06 considering the brown line marked with "+" symbols in Figure 7-1). Shear per unit load near the support from truck axles located away from the support was lower than the shear per unit load at the location of applied load.

For the specific structures investigated in the parametric study, results shown in Figure 7-1, Figure 7-2, and Appendix I could be used to calculate the live load shear demand at any location along the span length for a specific truck when information is known about the individual axle weights and spacing. The live load shear demand would be calculated using an axle-based approach that considers shear distribution along the span length rather than assigning a single shear distribution factor to all axles of a truck. Use of an axle-based method to determine live load shear demand would correctly account for the influence of load placement along the span length for the specific bridge and truck being considered.

For example, Figure 7-5 illustrates the effects of each axle from an HS20 truck configured on the long span parametric study bridge with the rear axle at 0.1*L*, the middle axle at approximately 0.325*L*, and the front axle at approximately 0.55*L*. The shear per unit load at 0.1*L* due to each axle is highlighted with an individual red circle at values of approximately 0.58 (rear axle), 0.31 (middle axle), and 0.13 (front axle). Thus, the live load

shear demand for this axle-based approach would be calculated by multiplying the weight of each axle by the appropriate shear per unit load in the interior girder. For the current example, the axle-based live load shear demand would be equal to approximately 30 kips (0.58*32 kips + 0.31*32 kips + 0.13*8 kips). The shear per unit load values accounted for the axle (and therefore truck) position along the span length and, in this example, were positioned transversely on the bridge in accordance with the lever rule to maximize the shear in the interior girder due to loading in a single lane. The live load shear demand from this method can be compared to the live load shear demand calculated using AASHTO distribution factor methodologies, which would involve finding the shear demand on the bridge cross section and multiplying that value by a shear distribution factor due to one lane loading to find the shear demand for the interior girder.

For the sake of comparison, consider an HS20 truck positioned at 0.1*L* as described. The reaction nearest the rear 32 kip axle in Figure 7-5 is approximately equal to 54 kips (0.9*32 kips + 0.675*32 kips + 0.45*8 kips). For one lane loaded and a girder spacing of 9 ft, the AASHTO LRFD shear distribution factor is equal to 0.6 (without the multiple presence factor of 1.2 as discussed in Section 7.2); the AASHTO Standard distribution factor is equal to 0.67 near the ends of the beam (using the lever rule) and 0.64 at other locations (using the *S*/D equation where D is equal to 7 for one lane loaded). For calculation of the AASHTO Standard live load shear demand, it was assumed that the location of 0.1*L* is near the beam end (hence variation of the distribution factor). The live load shear demand for the AASHTO LRFD method is approximately 32 kips (54 kip reaction*0.6) and the live load shear demand for the AASHTO Standard method is approximately 35 kips (0.67*0.9*32 kips + 0.64*0.675*32 kips + 0.64*0.45*8 kips). The live load shear demand from both AASHTO methods are larger than the live load shear demand from the axle based method by approximately 7 to 17 percent for the AASHTO LRFD and Standard, respectively.

If the section of interest is not near the support and is further into the span, the benefits increase considering shear distribution along the span length with an axle-based approach. This would be of interest if there was a problem with the stirrup spacing further into the span. If initial girder design was completed with the 1970 edition of the AASHTO Standard Specifications, when it was permissible to use the stirrup spacing required at the

quarter point of the span length for all locations in the girder between the support and the quarter point, the stirrup spacing may not provide adequate capacity using current AASHTO Specifications because of the conservatism in the distribution factor.

Figure 7-6 illustrates the effects of each axle from an HS20 configured on the long span parametric study bridge with the rear axle at 0.3*L*, the middle axle at approximately 0.525*L*, and the front axle at approximately 0.75*L*. The shear per unit load at 0.3*L* (where the shear demand will be the largest) due to each axle is highlighted with an individual red circle at values of approximately 0.41 (rear axle), 0.22 (middle axle), and 0.09 (front axle). In this situation, the axle-based live load shear demand will be lower than the previous example (lower shear per unit load values). The axle-based live load shear demand would be equal to approximately 21 kips (0.41*32 kips + 0.22*32 kips + 0.09*8 kips). The reaction nearest the rear 32 kip axle in Figure 7-6 is approximately equal to 40 kips (0.7*32 kips + 0.475*32 kips + 0.25*8 kips). The AASHTO LRFD shear distribution factor would still be equal to 0.6, and the AASHTO Standard distribution factor would be equal to 0.64 assuming all axle positions are not near beam ends. The live load shear demand for the AASHTO LRFD method is approximately 24 kips (40 kip reaction*0.6) and the live load shear demand for the AASHTO Standard method is approximately 26 kips (40 kip reaction*0.64). Similar to the previous example, the live load shear demand from both AASHTO methods are larger than the live load shear demand from the axle based method by approximately 14 to 24 percent for the AASHTO LRFD and Standard, respectively.

7.2.3 Comparison of Shear per Unit Load to AASHTO Distribution Factors

The shear per unit load in the girder near 0.0*L* was compared to AASHTO Specification shear distribution factors at the support for one lane and two lanes loaded, respectively. The calculation of shear distribution factors using AASHTO Standard (2002) or AASHTO LRFD (2010) Specifications is only based on the girder spacing. Distribution factors in the AASHTO LRFD (2010) Specifications were developed using HS20 trucks rather than sets of individual axles, which means that an “average” shear distribution factor is assigned for each axle. In other words, the same AASHTO LRFD shear distribution factor is used to calculate the shear force effects from a truck axle placed near the support and the shear force effects from a truck axle placed at other locations along the span length.

The AASHTO Standard (2002) specifies use of the lever rule for transverse shear distribution when wheel loads are "at ends of the beams" and use of the S-over equations (expressed in an *S*/D format, where *S* is the girder spacing and D is a constant based on superstructure type and the type of lane loading) for wheels or axles in other positions on the span. This may be because, historically, authors of the AASHTO Standard Specifications felt that the lever rule provided a better estimation of shear distribution near the support where the live load shear demand is maximized and the cross section is stiffened by its proximity to the supports. Therefore, the shear distribution from the applied load of a truck axle near the end of the beam is calculated with the lever rule while the shear distribution from the applied load of the remaining truck axles is calculated with the appropriate *S*-over equation. Similar to the AASHTO LRFD, the *S*-over equation does not vary based on where the truck is located along the span length. However, the AASHTO Standard states that the lever rule should be used instead of the *S*/D formulas if the girder spacing exceeds 10 or 14 ft for one lane loaded or two lanes loaded, respectively. In the case of the wide girder spacing parametric study case (S = 16 ft), the lever rule was used to calculate the AASHTO distribution factor at all locations. In the parametric study, the "ends of the beams" was defined as any location between $0.0L$ and $0.1L$ (including at $0.1L$).

The dashed line connecting the peak of each individual shear per unit load curve in Figure 7-1 through Figure 7-4 and all parametric study bridges in Appendix I were collected into Figure 7-7 and Figure 7-8 for the one and two lanes loaded cases, respectively. Figure 7-7 and Figure 7-8 combine all of the results for each case in the parametric study to show how the shear per unit load in the most heavily loaded interior composite girder at the location of applied load changes along the span length with respect to the parametric study variables. In Figure 7-7 and Figure 7-8, the curve associated with the long span case extends to $0.85L$ because data were collected at each 20^{th} point along the span. Furthermore, the double curvature behavior of the long span curve, which is present for other curves, is exacerbated in Figure 7-7 and Figure 7-8 because the length of the span is twice that of the other structures and the *x*-axis is plotted with respect to a percent of the span length.

Three sets (S = 6.5, 9, and 16 ft) of two lines (AASHTO Standard and AASHTO LRFD) are plotted in Figure 7-7 and Figure 7-8 to indicate changes in the AASHTO shear

distribution factor as the girder spacing varied. Figure 7-7 and Figure 7-8 show the AASHTO LRFD distribution factors that would be used for an axle near the support. As discussed in Section 2.3.1, the AASHTO LRFD distribution factors were generated by Zokaie et al. (1991b) by placing HS20 trucks on the bridge rather than individual axles. The lines representing the AASHTO Standard distribution factors change at 0.1*L* due to use of the S-over equations rather than the lever rule.

Results in Figure 7-7 show some difference between AASHTO distribution factors and the shear per unit load in the interior girder for S = 9 ft near 0.0*L* for one lane loaded related to the following parametric study cases: the 6 in. deck, the base case, and the 72 in. beam. Differences related to the AASHTO LRFD distribution factors is likely related to the discussion about an "average" shear distribution factor due to the applied load from an HS20 truck rather than sets of individual axles. However, both Specifications were different than the shear per unit load in the case of the 6 in. deck. The AASHTO Standard distribution factor was calculated with the lever rule near 0.0*L*. Thin bridge decks (e.g., 6 or 7 in.) may have historically been part of the MnDOT inventory, but since approximately the 1980's a 9 in. deck thickness has been typically specified in new design. Furthermore, almost all bridge decks constructed prior to this time period have since had a structural overlay to increase the deck thickness to at least 9 in. (Gao 2015). However, bridges with a thin deck should be investigated because bridge deck thickness was shown to have an effect on shear distribution as discussed in Section 7.3 and this behavior may not be adequately captured using AASHTO distribution factors for rating. Results in Figure 7-8 show that the AASHTO LRFD distribution factors were greater than the shear per unit load near 0.0*L* for two lanes loaded in all parametric study cases except the 16 ft spacing. The slight difference in the 16 ft spacing case was attributed to the "average" distribution factors generated with HS20 trucks. Results in Figure 7-8 show that the AASHTO Standard distribution factors calculated with the lever rule at the ends of beams were greater than the shear per unit load near 0.0*L* for two lanes loaded in all parametric study cases.

7.3 Parametric Study Results and Screening Tool Ratio Definition

Results from the parametric study indicated that the girder spacing and depth, deck thickness, and span length affected the amount of shear per unit load in the interior girder. Smaller girder spacing (less transverse flexibility), a thicker deck (less transverse

flexibility), and a longer span length (more longitudinal flexibility) had the most effect on reducing the shear per unit load in the interior girder. Results indicated that the girder depth had a slight effect on the shear per unit load in the interior girder, but this was likely more related to the longitudinal stiffness/flexibility rather than the girder depth alone (because longitudinal stiffness/flexibility is related to the composite section and span length). This observation is also true of deck thickness as a function of transverse span length (i.e., the girder spacing plays a large role in the transverse stiffness).

It was determined that a dimensionless ratio of longitudinal bending stiffness to transverse bending stiffness, given in Eqn. (7.2), corresponded with the trend in shear per unit load in the interior girder near 0.0*L*, as shown in Table 7-3 with data from Figure 7-7 and Figure 7-8 (i.e., in most cases, as the value of the stiffness term decreased, the shear per unit load near 0.0*L* was observed to decrease).

$$\text{Stiffness Ratio} = \frac{I_{long}}{L^3}\frac{S^3}{I_{trans}} \tag{7.2}$$

where I_{long} is the gross composite moment of inertia including both the girder and composite deck with a width equal to the girder spacing (in.^{4}), L is the span length (ft), S is the girder spacing (ft), and I_{trans} is the gross moment of inertia of a 12 in. wide transverse section of bridge deck (in.^{4}).

Table 7-4 shows each of the non-skewed parametric study bridges with the corresponding ratio of stiffness values from Eqn. (7.2). Furthermore, Table 7-4 shows the interior girder live load shear demand due to HS20 trucks at 0.1*L* with two lanes loaded for each structure in the parametric study calculated using distribution factors from AASHTO LRFD Specifications, distribution factors from AASHTO Standard (STD) Specifications, and 3D finite element analysis. The location of 0.1*L* was chosen for consistency across all of the structures because the cross section depths varied. The value of 0.1*L* was approximately equal to the girder depth, *d*, for most cases investigated in the parametric study, but differences in the relationship between 0.1*L* and *d* were given in Table 7-1.

Table 7-4 shows that the AASHTO LRFD specifies one shear distribution factor in an interior girder regardless of where the live load is positioned longitudinally. The

AASHTO Standard specifies use of the lever rule for transverse shear distribution when wheel loads are "at ends of the beams" and use of the S-over equations for wheels or axles at other positions on the span. Therefore, using the AASHTO Standard, the shear distribution from the applied load of a truck axle near the end of the beam was calculated with the lever rule while the shear distribution from the applied load of the remaining truck axles was calculated with the appropriate S-over equation. The trend in the stiffness ratio does not always align with the trend in AASHTO distribution factors (e.g., 62.75 ft span length bridge and 6.5 ft girder spacing bridge) because the AASHTO distribution factors are only dependent on S and the stiffness ratio is equally dependent on L. Therefore, the longer span length made the stiffness ratio lower for the 62.75 ft span bridge whereas the narrow girder spacing made the AASHTO distribution factor smaller for the 6.5 ft girder spacing bridge. The FEM analysis results presented in Table 7-4 are the interior girder live load shear demand values generated by placing the entire HS20 design truck, with 14 ft longitudinal axle spacing, on the structure. The truck was oriented on the 3D finite element model such that the rear axle was at $0.1L$ and the remaining axles were toward midspan. The FEM live load shear demand for the interior girder was collected using nodal forces at $0.05L$ to avoid the disturbed region associated with the applied patch loads.

Information in Table 7-4 shows that Eqn. (7.2) can be used as a screening tool to select which structures have a lower live load shear demand at $0.1L$ from two lanes loaded using a 3D FEM compared to AASHTO distribution factor based analyses. The benefit of applying the HS20 truck load further into the span (e.g., at $0.3L$ compared to $0.1L$) was discussed in Section 7.2.1 with an example. Bridges with a screening tool ratio based on Eqn. (7.2) less than 1.5 had a slightly lower live load shear demand due to HS20 trucks from FEM analysis compared to live load shear demand values calculated using AASHTO distribution factors. Structures with a screening tool ratio based on Eqn. (7.2) greater than 1.5 and less than 5.0 had approximately the same live load shear demand value from either an AASHTO distribution factor analysis or a FEM analysis. Structures with a screening tool ratio based on Eqn. (7.2) larger than 5.0 had a lower live load shear demand generated from AASHTO DF methodologies.

7.3.1 Verification of the Screening Tool Ratio with MnDOT Bridges

Five additional structures were selected from the database of bridges in MnDOT Report 2010-03 (Dereli et al. 2010) to verify that bridges with a screening tool ratio less than 1.5 have a lower live load shear demand using a finite element analysis. Several assumptions were used to construct and apply load to the FEM for each bridge; the first group of assumptions were the simplifications listed in Section 7.2 related to the parametric study:

1. Ignore the effects of diaphragms and barriers, interior beams controlled shear rating, standard 6 ft axle gage width, two lanes loaded truck configuration, lever rule used to select the transverse truck position, no multiple presence factors, and a composite section used to collect FEM results composed of the girder and the portion of the deck width equal to the girder spacing.
2. Live load was applied using the HS20 truck with axles spaced 14 ft longitudinally. For consistency with the parametric study, the rear axle was positioned at $0.1L$ and the remaining axles were oriented toward midspan.
3. A standard deck thickness of 9 in. was used for each of the bridges from MnDOT Report 2010-03. After email correspondence with the MnDOT Technical Liaison, it was assumed that structures built later than 1980 have a 9 in. thick deck and structures built before that time have since had a structural overlay to increase the deck thickness to 9 in. (Gao 2015). This assumption was made because MnDOT bridge plans list the minimum bridge deck thickness required at the time of design (which may be less than 9 in.) and this value may not be representative of the current deck thickness.
4. The framing geometry, span length, number of girders, and girder spacing were obtained from the plans for each structure. However, for simplicity, the skew angle of each structure was assumed to be zero.
5. Nominal concrete material properties were obtained from MnDOT Report 2010-03 and were adjusted to account for concrete variability and concrete strength gain over time by multiplying the nominal concrete compressive strengths by a factor of $1.2*\lambda$ as discussed in Section 6.6 and Appendix H. The material properties for each bridge are given in Table 7-5.

Information in Table 7-6 shows that screening tool ratios generated using Eqn. (7.2) aligned with results from the parametric study. Bridges with a screening tool value less than 1.5 had a lower live load shear demand due to HS20 trucks from FEM analysis compared to the live load shear demand determined using methodologies from AASHTO Specifications. Each of the five bridges from MnDOT Report 2010-03 were also modeled using a simple 2D grillage analysis in SAP2000 (discussed in Section 3.4 and shown in Figure 3-4) to compare live load shear demand results from a simple modeling technique to results obtained from 3D FEM. In the simplified grillage models, all grillage elements were constructed using gross section properties. Longitudinal grillage members were constructed to represent a single beam, the haunch, and a section of composite bridge deck with width equal to the girder spacing. The geometry of the longitudinal composite cross section was defined in the SAP2000 Section Designer (Computers and Structures, Inc. 2009) and gross composite section properties were automatically determined. The modulus of elasticity of the bridge deck and girder were defined separately and were the same values used in the 3D FEM.

Transverse grillage members were constructed to represent 12 in. wide rectangular sections of bridge deck that spanned the girder spacing. The modulus of elasticity of these sections was equal to the deck modulus of elasticity (i.e., E of the longitudinal composite system was different than E of the transverse deck system). Two-dimensional grillage models only considered the simply-supported span of interest and did not contain rebar, end diaphragms, intermediate diaphragms, or traffic barriers to maintain simplicity. Furthermore, because the grillage models were based on the 3D FEM models, the five assumptions listed at the beginning of this section for the FEM of each bridge also applied to the grillage models. Information in Table 7-6 shows that results from simple refined analysis using grillage models were within approximately three percent of detailed solid element FEM results on average. Grillage analysis results were conservative and similar to results generated using a solid element FEM; grillage analysis was appropriate for calculating live load shear demand for structures with a screening tool ratio less than 1.5.

7.3.2 Effects of Skew on Shear Distribution

The results presented in Table 7-4 and Table 7-6 are for straight, non-skewed bridges. It has been shown in the literature (Zokaie et al. 1991b, Modjeski and Masters, Inc. 2002, Huo et al. 2005, Puckett et al. 2007) that skew has an effect on shear distribution. In the case of a skewed support, load is transferred to the supports in the shortest path which is generally toward the obtuse corners. Typically, skew increases shear force effects in the end of an exterior girder at the obtuse corner compared to a non-skewed bridge of the same length and size. The AASHTO LRFD Specifications present a skew correction factor for shear, shown in Table 2-3 and in AASHTO LRFD Table 4.6.2.2.3c-1, which was derived by Zokaie et al. (1991b) for exterior beams at obtuse corners of skewed, simple span bridges. The effects of skew on shear distribution for the exterior beam are pronounced because of the short distance to the exterior girder support for load placed in the vicinity of the obtuse corner. The effects of skew on shear distribution may be less prominent for an interior girder because the distance to the support of the adjacent girder near the obtuse corner is shorter (more load will travel there) while the distance to the support of the adjacent girder near the acute corner is further (less load will travel there) when load is placed in the vicinity of the interior girder. Thus, the effects of the acute corner geometry and the obtuse corner geometry may effectively cancel each other out for an interior girder.

The skew effect was determined by Zokaie et al. (1991b) by taking the ratio of skewed to non-skewed load distribution factors for bridges with the same parameters and loading. Load distribution factor results were generated from computer models using plate elements for the deck and beam elements for the girder that were offset from the centroid of the deck to account for differences in centroid elevation of the two elements. The skew correction factor is greater than or equal to unity depending on the angle of skew and is applied to the distribution factor used to obtain live load shear demand.

The AASHTO LRFD Specification stipulates that the skew correction factor be applied to the end of all girders in the bridge cross section, both interior and exterior. However, during the development of the skew correction factors Zokaie et al. (1991b) noted that “shear in interior girders need not be corrected for skew effects; that is, the shear distribution to interior girders and the girder at the acute corner is similar to that of the

straight bridge." Furthermore, Puckett et al. (2007) noted that "generally, skew angles below 30° had a small effect on live load distribution. As the skew angle increased from 30° to 60°…the live load shear distribution factor increased." Huo et al. (2005) confirmed that skew angles between 0 and 33.5 degrees did not show a significant effect on shear distribution factors for interior beams in precast concrete I-beam bridges.

Amplification of shear distribution for skewed bridges could be accomplished using the AASHTO LRFD skew correction factors in conjunction with results from either the AASHTO distribution factors or a simple 2D grillage analysis of the equivalent straight bridge. Construction of a 2D grillage model for a skewed bridge presents challenges related to the orientation and connectivity of the transverse deck elements to the longitudinal composite elements (Zokaie et al. 1991b, Hambly 1991). For example, in a skewed bridge grillage model, Zokaie et al. stated "the longitudinal members should still be placed coincidental with the girder lines, but the transverse members must be placed perpendicular to the longitudinal members, not parallel to the [skewed] support. Otherwise, higher than actual wheel load distribution factors will result. An exception to this transverse layout would be when the main transverse [deck] reinforcement runs parallel to the skew supports and cracking of the [deck] concrete is expected." Considering the added complexity of modeling a skewed structure, the equivalent straight bridge would contain no skew angle but the same girder spacing, girder length, and span length. In the case of a span with different skew angles at each end (or skew at only one end), it is conservative to define the length of the equivalent straight bridge as the length of the shortest beam because it has been shown in this project that longer span lengths act to increase shear distribution.

To obtain the live load shear demand for a skewed bridge, the shear demand from the equivalent straight bridge may be multiplied by the appropriate skew correction factor. The skew correction factor, described in Section 4.6.2.2.3c of the AASHTO LRFD Specifications (2010), for precast concrete I- and bulb-tee beam bridges is:

$$1.0+0.2\left(\frac{12Lt_s^3}{K_g}\right)^{0.3}\tan\theta \qquad (7.3)$$

where θ is the skew angle (degrees), L is the span length (ft), t_s is the thickness of the deck (in.), K_g is the longitudinal stiffness parameter (in.^{4}) and is equal to $n(I+Ae_g^2)$; within K_g, n is the modular ratio of beam to deck concrete, I is the noncomposite beam moment of inertia (in.^{4}), A is the noncomposite beam area (in.^{2}), and e_g is the distance between the centers of gravity of the beam and deck (in.).

Huo et al. (2005) and Puckett et al. (2007) showed that the AASHTO LRFD skew correction factor can be simplified to the following expression for concrete and steel beam and slab bridges (AASHTO superstructure types a, e, h, i, and j):

$$1.0+0.2\tan\theta \tag{7.4}$$

Puckett et al. (2007) also presented a skew correction factor, simplified from Eqn. (7.3), specifically for AASHTO superstructure type k which is precast concrete I- and bulb-tee beam bridges:

$$1.0+0.09\tan\theta \tag{7.5}$$

Eqn. (7.5) was derived by calculating the average of the $0.2(12Lt_s/K_g)^{0.3}$ term in Eqn. (7.3) for all type k superstructures in the bridge set given by Zokaie et al. (1991b) and then replacing the $0.2(12Lt_s/K_g)^{0.3}$ term with the average value (0.09). The effect of skew in this simplified, specific formula was reduced because of different stiffness characteristics for this type of superstructure. Puckett et al. (2007) noted that Eqn. (7.5) is applicable for skew angles between 0 and 60 degrees. Use of this equation would increase the live load shear demand by approximately five percent for bridges with a 30 degree skew and by approximately 16 percent for bridges with a 60 degree skew compared to bridges with no skew.

The effects of skew were investigated in this project using the FEM of Bridge 65006 from the field bridge testing portion of the project. Bridge 65006 had a 30 degree skew and was used for validation of the FEM as discussed in Section 6.6.2. A duplicate FEM of Bridge 65006 was constructed without the skew angle to serve as the equivalent straight bridge. In both models, the traffic barrier and diaphragms (end or intermediate) were removed to be consistent with both the parametric study and how the skew correction

factor was derived by Zokaie et al. (1991b). All other parameters and assumptions within the FEM were unchanged. The ratio of skewed to non-skewed live load shear demand for interior Girder 2 (adjacent to the exterior girder in the obtuse corner) was compared with load applied from an HS20 truck at $0.1L$ for consistency with other loading scenarios completed in the parametric study. The truck was oriented on the 3D finite element models such that the rear axle was at $0.1L$ and the remaining axles (spaced at 14ft longitudinally) were toward midspan. The FEM live load shear demand for the interior girder was collected using nodal forces at $0.05L$ to avoid the disturbed region associated with the applied patch loads. In both FE models, the live load shear demand was obtained using the composite cross section assuming a width of bridge deck equal to the girder spacing and perpendicular to the girder. In the skewed bridge, the composite cross section was assumed to be perpendicular to the girder because this was the direction of the transverse deck reinforcement given in the bridge plans. The ratio of skewed to non-skewed live load shear demand was calculated to be 1.01, which was smaller than the values of 1.12 and 1.05 calculated with Eqn. (7.4) and Eqn. (7.5), respectively.

7.4 Summary and Proposed Shear Distribution Methodology for Load Rating

A detailed study was completed to examine shear distribution and address two goals: (1) investigate and bound the effects of various bridge characteristics on shear distribution, (2) determine if AASHTO shear distribution factors provide an accurate estimate of live load shear demand compared to the live load shear demand determined from FEM results. If the AASHTO shear distribution factors proved to be overly conservative for certain types of bridge structures, it was desired to develop a screening tool to identify the structures for which the AASHTO shear distribution factors were found to be conservative. For those structures, a simple refined analysis methodology to calculate a more accurate live load shear demand was desired.

Several assumptions outlined in Sections 7.2 and 7.3.1 were used in the FEM study to simplify analysis. The main assumptions included: effects of diaphragms and barriers were ignored, interior beams controlled shear load rating, trucks had a standard 6 ft axle gage width and were configured transversely using the lever rule to maximize shear demand for the case of two lanes loaded, and the composite section used to collect FEM results was composed of the girder and the portion of the deck width equal to the girder

spacing. This study only compared the live load shear demand from HS20 trucks and did not include the effects of the distributed lane load from the AASHTO LRFD Specifications.

Results from the parametric study indicated that a narrow girder spacing, a thicker deck, and a longer span length more effectively distributed the shear (i.e., resulted in the lowest shear distribution factors for the most heavily loaded girder). Figure 7-7 shows that AASHTO distribution factors may not adequately capture shear distribution behavior at 0.0L in thin bridge decks (e.g., 6 in.) for one lane loaded and a girder spacing of 9 ft. Thin bridge decks may have historically been part of the MnDOT inventory, but most have had a structural overlay to increase the deck thickness to at least 9 in. (Gao 2015). However, bridges with a thin deck should be investigated because bridge deck thickness was shown to have an effect on shear distribution.

It was determined from parametric study results that the dimensionless ratio of longitudinal bending stiffness to transverse bending stiffness presented in Eqn. (7.2) corresponded with the trend in shear per unit load in the interior girder near 0.0L as shown in Table 7-3. Results from the seven parametric study bridges and five additional bridges from MnDOT Report 2010-03 (Dereli et al. 2010) verified that Eqn. (7.2) could be used as a screening tool to indicate which structures may have a lower live load shear demand from refined analysis compared to live load shear demand generated using AASHTO distribution factor methods. The live load shear demand due to HS20 trucks from both 3D FEM and simplified 2D grillage models were lower than the live load shear demand predicted by AASHTO for bridges with a screening tool ratio less than 1.5.

A simplified 2D grillage analysis is recommended for determining the live load shear demand for interior girders of MnDOT structures that rate poorly for shear and have a screening tool ratio, calculated with Eqn. (7.2), lower than 1.5. For bridges with skew greater than 30 degrees, the live load shear demand for interior girders could be amplified by a factor calculated with Eqn. (7.5) to account for the effects of skew. This skew correction formula was presented by Puckett et al. (2007). The ratio of skewed to non-skewed live load shear demand for the first interior girder adjacent to the obtuse corner of the deck was investigated using FE models of Bridge 65006 in this study. Results from the FEM indicated that the ratio of skewed to non-skewed live load shear demand from an

HS20 truck was 1.01, which was less than the value generated using Eqn. (7.5). However, there was not enough experimental data in the current study to fully evaluate the factor.

The benefits of considering shear distribution along the span length by determining the live load shear demand with a simple 2D grillage analysis are gained because AASHTO uses an "average" distribution factor for each axle as discussed in Section 7.2.3. A simple 2D grillage model used to determine live load shear demand of an interior girder correctly accounted for the influence of load placement along the span length. The benefits of considering shear distribution along the span length were especially evident if the section of interest was not near the support and was further into the span as discussed in Section 7.2.2. This would be of interest if there was a problem with the stirrup spacing further into the span; if the initial girder design specified use of the same stirrup spacing between $0.25L$ and the end of the beam, the stirrup spacing may not provide adequate capacity using current AASHTO Specifications. Furthermore, the benefits of considering shear distribution along the span length are applicable to permitting of trucks as discussed in the following section.

7.4.1 Application of Shear Distribution Methodology to Permitting

Shear distribution as function of longitudinal load placement on the bridge and use of a simple 2D grillage analysis is likely useful for permitting trucks to cross bridges. The maximum shear demand generated in an interior girder from permit trucks that are longer or have more axles than an HS20 design truck may be lower because many of the axles will be far from the critical section for shear near the support. Live load shear demand due to permit trucks calculated with a simplified 2D grillage model may be lower than the live load shear demand calculated with AASHTO distribution factor methodologies and may have an effect on truck permitting, even for bridges that do not have a screening tool ratio less than 1.5. In regard to the use of grillage analyses for permitting trucks, Zokaie (2000) also noted that "the live load analysis for permit trucks (by applying one lane of the truck to a beam model and adjusting that by the distribution factor) may be too conservative, since it assumed that all lanes are loaded by similar trucks. A simple grillage analysis can, in most cases, be performed to calculate more accurate distribution factors than the formula results if needed."

Table 7-1. Parametric Study Bridge Structures

Case	Girder d (in.)	Deck t (in.)	Girder Spacing S (ft)	Bridge Width (ft)	Span L (ft)	d_{girder} / L	$d_{composite}$ / L
Base	36	9	9	34	30.75	0.1	0.12
Deep Beam	72	9	9	34	30.75	0.2	0.22
Long Span	36	9	9	34	62.75	0.05	0.06
Thin Deck	36	6	9	34	30.75	0.1	0.12
Thick Deck	36	12	9	34	30.75	0.1	0.13
Narrow Spacing	36	9	6.5	26.5	30.75	0.1	0.12
Wide Spacing	36	9	16	55	30.75	0.1	0.12

shaded indicates single parameter varied from base case

* In all cases: haunch thickness = 1 in., number of girders = 4

Table 7-2. Axle Positions to Maximize Shear in Interior Beams According to the Lever Rule

Number of Lanes Loaded	Resultant Load on Interior Girder at Cross Section where Loads are Applied (indicated by arrow under girder in diagram)	Application Range	Loading Diagram
1	1 - 3/S	S > 6 ft	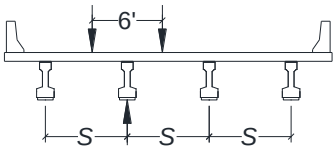
2	3/2 - 5/S	6 < S ≤ 10 ft	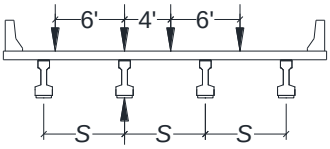
2	2 - 10/S	10 < S ≤ 16 ft	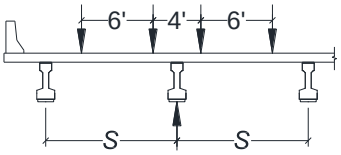

Table 7-3. Parametric Study Bridge Stiffness Ratios and Shear per Unit Load Near 0.0L for One and Two Lanes Loaded with Single Axles

Parametric Study Bridge	Girder d (in.)	Span L (ft)	Bridge Width (ft)	Spacing S (ft)	Deck t (in.)	Deck Transverse I_g (in.^{4})	Composite Longitudinal I_g (in.^{4})	$\frac{I_{long}S^3}{I_{trans}L^3}$ (Eqn. 7.2)	Shear per Unit Load near 0.0L	
									One Lane Loaded	Two Lanes Loaded
62.75 ft Span	36	62.75	34	9	9	729	241,772	1.0	0.58	0.80
6.5 ft Spacing	36	30.75	26.5	6.5	9	729	222,118	2.9	0.45	0.61
12 in. Deck	36	30.75	34	9	12	1728	288,222	4.2	0.61	0.81
Base	36	30.75	34	9	9	729	241,772	8.3	0.66	0.84
72 in. Beam	72	30.75	34	9	9	729	1,618,247	55.7	0.67	0.86
6 in. Deck	36	30.75	34	9	6	216	196,658	22.8	0.70	0.87
16 ft Spacing	36	30.75	55	16	9	729	272,689	52.7	0.82	1.37

Table 7-4 Parametric Study Bridge Stiffness Ratios and Live Load Shear Demand at 0.1L due to an HS20 Configured for Two Lanes Loaded

Parametric Study Bridge	Girder d (in.)	Span L (ft)	Bridge Width (ft)	Spacing S (ft)	Deck t (in.)	Deck Transverse I_g (in.^{4})	Composite Longitudinal I_g (in.^{4})	$\frac{I_{long}S^3}{I_{trans}L^3}$ (Eqn. 7.2)	LRFD Shear DF	STD Shear DF		Beam Line Shear at 0.1L from HS20 Axles (k)				Interior Beam V_{LL} at 0.1L (k)			Method with Lower V_{LL} at 0.1L for 2 Lane Loading
										Bm End*	Non-Bm End	Rear (Bm End)	Middle	Front	Total	LRFD	STD	FEM	
62.75 ft Span	36	62.75	34	9	9	729	241,772	1.0	0.88	0.94	0.82	29	22	4	54	48	49	44	Refined
6.5 ft Spacing	36	30.75	26.5	6.5	9	729	222,118	2.9	0.71	0.73	0.59	29	14	0	43	31	29	29	Same
12 in. Deck	36	30.75	34	9	12	1728	288,222	4.2	0.88	0.94	0.82	29	14	0	43	38	39	38	Same
Base	36	30.75	34	9	9	729	241,772	8.3	0.88	0.94	0.82	29	14	0	43	38	39	40	AASHTO
72 in. Beam	72	30.75	34	9	9	729	1,618,247	55.7	0.88	0.94	0.82	29	14	0	43	38	39	42	AASHTO
6 in. Deck	36	30.75	34	9	6	216	196,658	22.8	0.88	0.94	0.82	29	14	0	43	38	39	42	AASHTO
16 ft Spacing	36	30.75	55	16	9	729	272,689	52.7	1.32	1.38	1.38	29	14	0	43	57	59	63	AASHTO

* STD uses lever rule at "ends of the beams"

x.x = stiffness ratio lower than 1.5

x.x = stiffness ratio lower than 5.0

Table 7-5. Material Properties of MnDOT Bridges used for Screening Tool Verification

Property	Symbol [Units]	Br. 27942	Br. 49016-2	Br. 46004	Br. 24825-5	Br. 73872-2_3
Unit Weight of Concrete	w_c [pcf]	150				
Girder Gross Area	A_g [in.^{2}]	789	560	560	560	789
Girder Gross Centroid (from bottom)	y_{cb} [in.]	24.7	20.3	20.3	20.3	24.7
Haunch Thickness	t_h [in.]	1				
Nominal Girder Concrete Compressive Strength	f'_c [ksi]	5.8	5.1	6.0	5.8	5.0
Statistical bias factor from Nowak and Szerszen (2003)	λ	1.16	1.38	1.16	1.16	1.38
Adjusted Girder Concrete Compressive Strength	f'_c [ksi]	8.1	8.5	8.3	8.1	8.3
Adjusted Girder Modulus of Elasticity	E_c [ksi]	5,460	5,590	5,520	5,460	5,520
Adjusted Girder Shear Modulus (calculated with $\nu = 0.2$)	G [ksi]	2,280	2,330	2,300	2,280	2,300
Adjusted Deck and Haunch Concrete Compressive Strength (λ = 1.235 for nominal f'_c = 4 ksi)	f'_{cd} [ksi]	5.9				
Adjusted Deck and Haunch Modulus of Elasticity	E_{cd} [ksi]	4,660				
Modular ratio (E_{cd}/E_c)	n	0.85	0.83	0.84	0.85	0.84
Adjusted Girder Bottom Flange Modulus of Elasticity (FEM only)	E_{bf} [ksi]	5,780	5,910	5,900	5,780	5,840

Table 7-6. MnDOT Verification Bridge Stiffness Ratios and Live Load Shear Demand at 0.1*L* due to an HS20 Configured for Two Lanes Loaded

MnDOT Bridge No.	Girder d (in.)	Span L (ft)	Bridge Width (ft)	Spacing S (ft)	Deck t (in.)	Deck Transverse I_g (in.^{4})	Composite Longitudinal I_g (in.^{4})	$\frac{I_{long}S^3}{I_{trans}L^3}$ (Eqn. 7.2)	LRFD Shear DF	STD Shear DF		Beam Line Shear at 0.1L from HS20 Axles (k)				Interior Beam V_{LL} at 0.1L (k)				Grillage / FEM	Method with Lower V_{LL} at 0.1L for 2 Lane Loading
										Bm End*	Non-Bm End	Rear (Bm End)	Middle	Front	Total	LRFD	STD	FEM	Grillage		
27942	54	97	29.6	7.5	9	729	703,293	0.4	0.78	0.83	0.68	29	23	4	58	45	43	39	40	1.02	Refined
49016-2	45	76	37	7.5	9	729	407,985	0.5	0.78	0.83	0.68	29	23	4	56	44	43	38	39	1.03	Refined
46004	45	76	34	9	9	729	431,520	1.0	0.88	0.94	0.82	29	22	4	56	49	49	44	46	1.04	Refined
24825-5	45	67	40	11	9	729	456,862	2.8	1.02	1.09	1.00	29	24	5	55	56	61	55	56	1.03	Same
73872-2_3	54	79	40	11	9	729	795,114	2.9	1.02	1.09	1.00	29	23	4	56	57	59	57	58	1.03	Same

* STD uses lever rule at "ends of the beams"

x.x = stiffness ratio lower than 1.5

x.x = stiffness ratio lower than 5.0

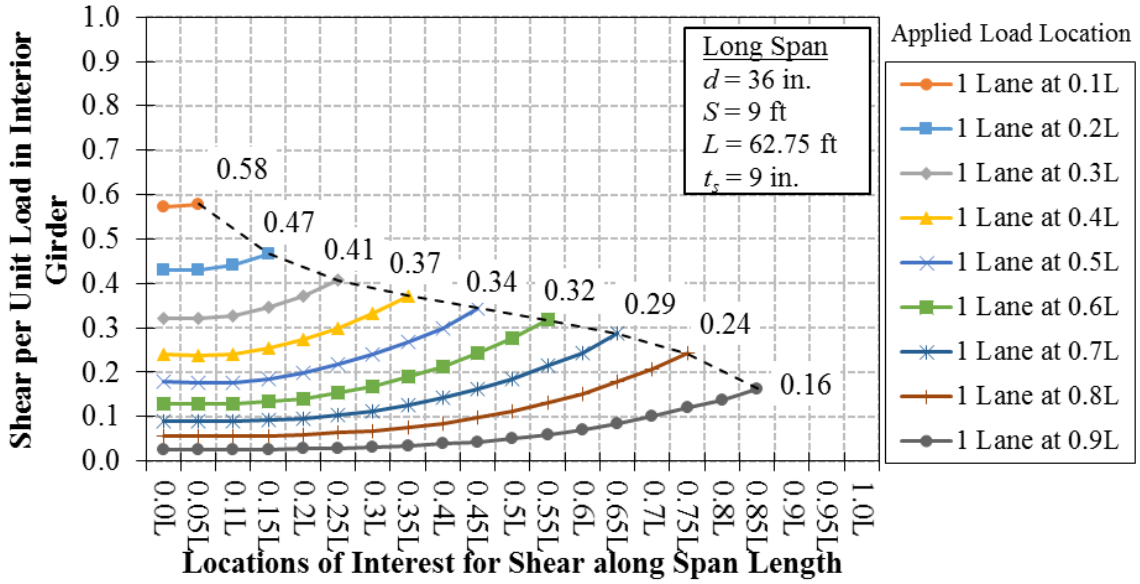

Figure 7-1. Shear per Unit Load in Interior Girder vs. Span Length for One Lane Loaded on 62.75 ft Span from Parametric Study

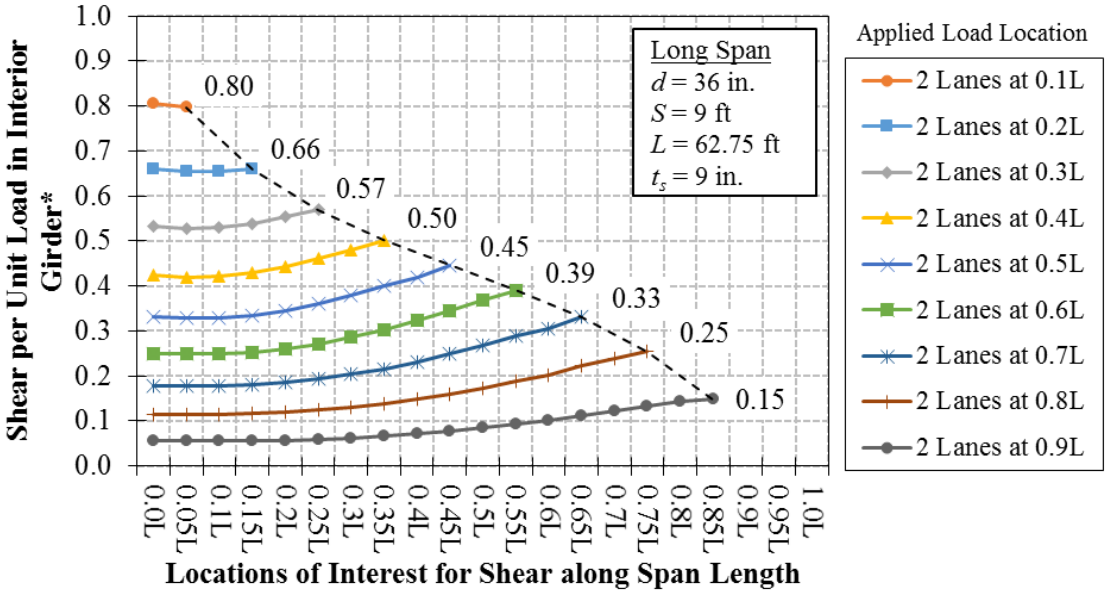

*The Shear per Unit Load in Interior Girder values already account for the presence of two axles.

Figure 7-2. Shear per Unit Load in Interior Girder vs. Span Length for Two Lanes Loaded on 62.75 ft Span from Parametric Study

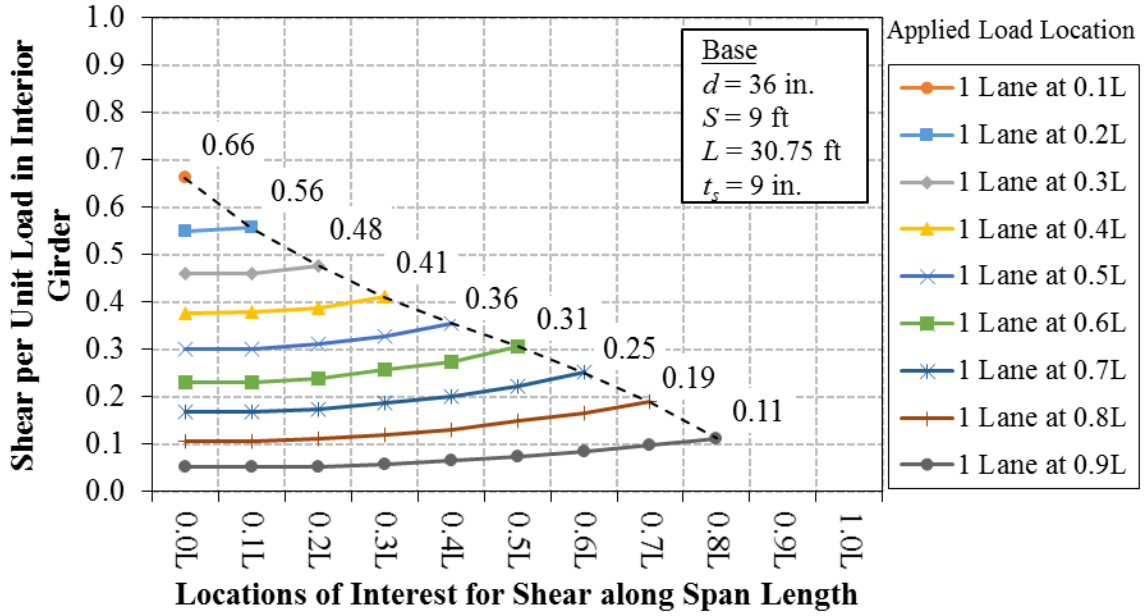

Figure 7-3. Shear per Unit Load in Interior Girder vs. Span Length for One Lane Loaded on Base Case Bridge from Parametric Study

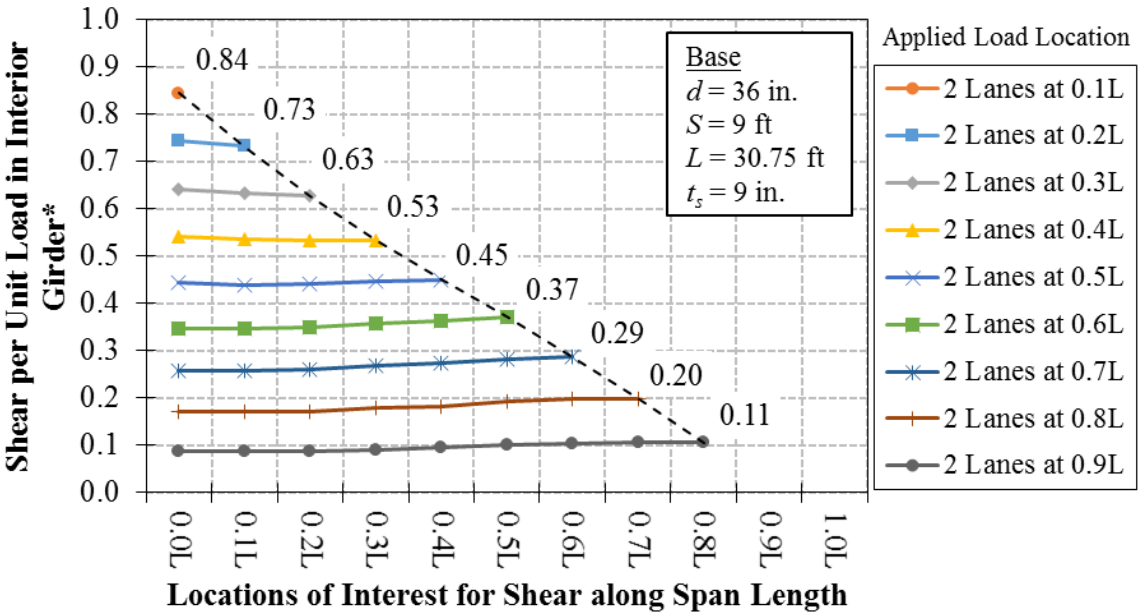

*The Shear per Unit Load in Interior Girder values already account for the presence of two axles.

Figure 7-4. Shear per Unit Load in Interior Girder vs. Span Length for Two Lanes Loaded on Base Case Bridge from Parametric Study

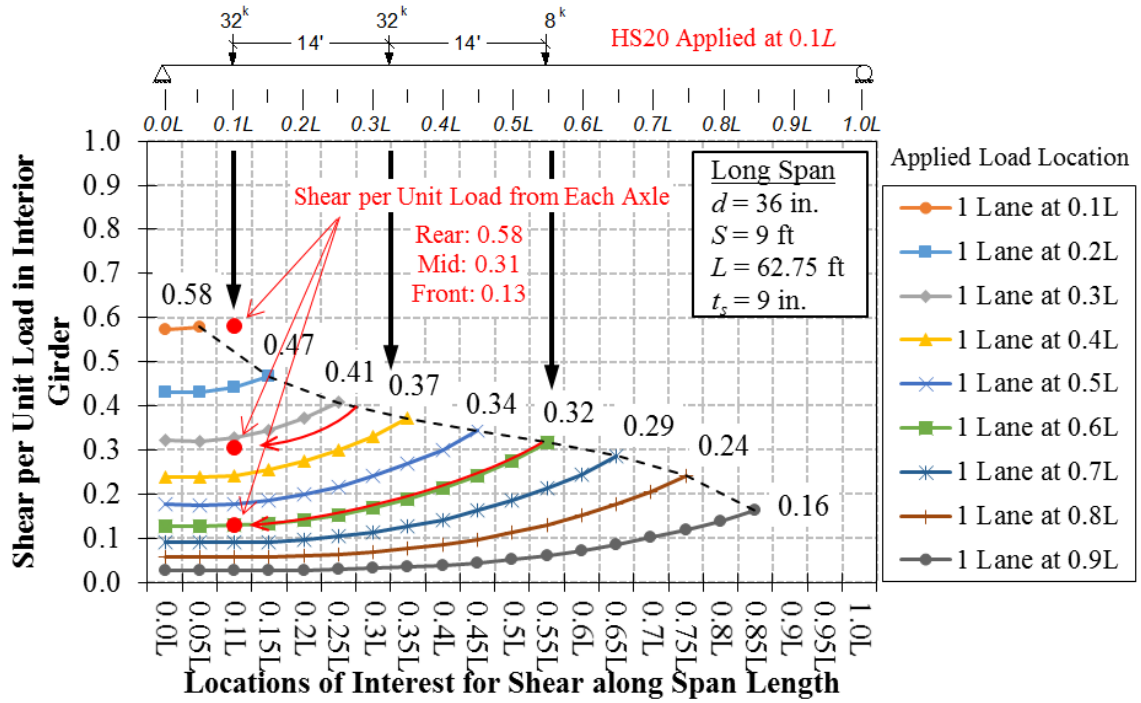

Figure 7-5. Shear per Unit Load for each HS20 Axle Location with 1 Lane Loaded at 0.1*L* on Parametric Study Long Span Bridge

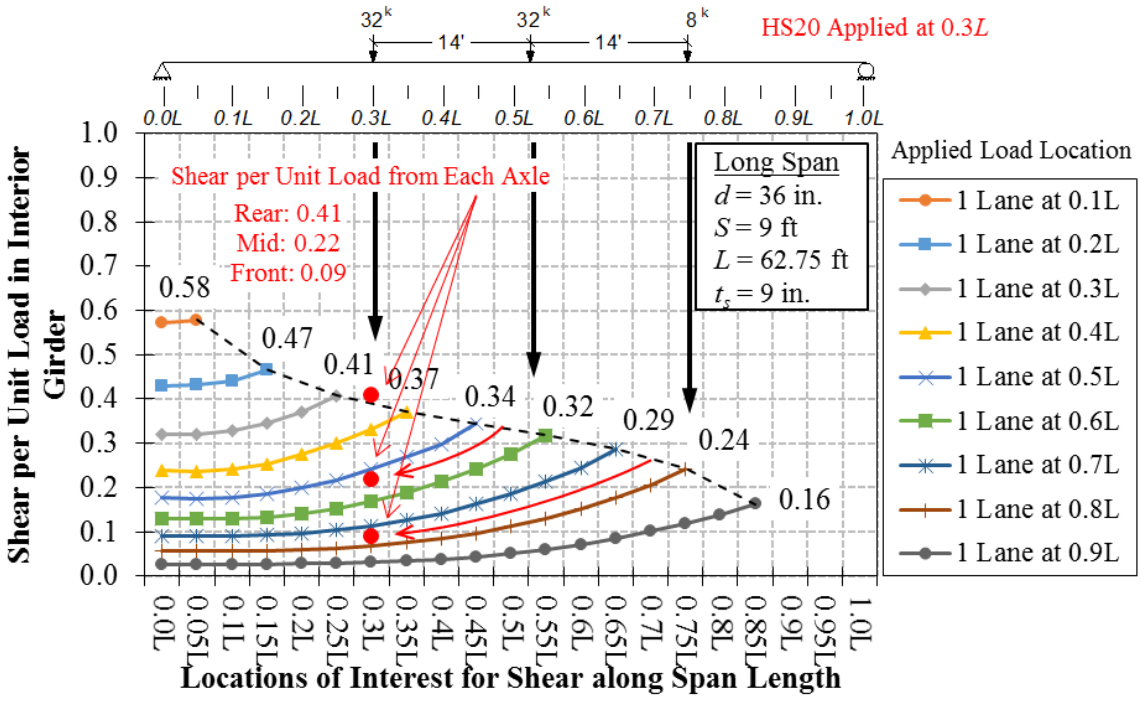

Figure 7-6. Shear per Unit Load for each HS20 Axle Location with 1 Lane Loaded at 0.3*L* on Parametric Study Long Span Bridge

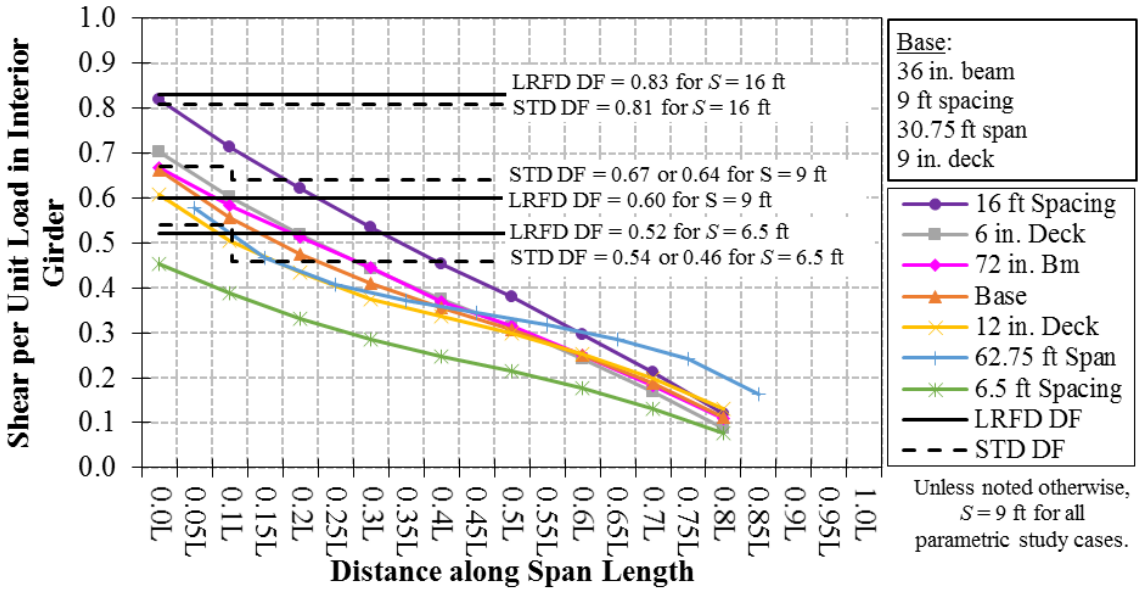

Figure 7-7. Variation in Shear per Unit Load near Applied Load for 1 Lane Loaded in Parametric Study and Appropriate AASHTO Distribution Factors without Multiple Presence

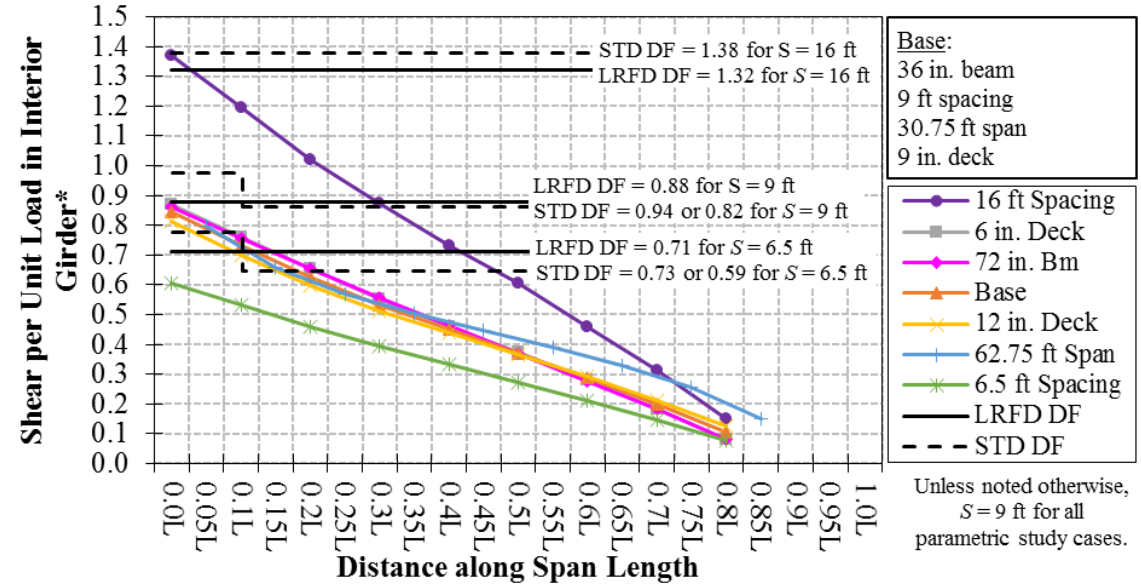

*The Shear per Unit Load in Interior Girder values already account for the presence of two axles.

Figure 7-8. Variation in Shear per Unit Load near Applied Load for 2 Lanes Loaded in Parametric Study and Appropriate AASHTO Distribution Factors without Multiple Presence

CHAPTER 8. SYNTHESIS OF STUDY AND RECOMMENDATIONS FOR RATING AND PERMITTING

8.1 Introduction

Shear distribution factors have been used in bridge design and evaluation since the early 20th century as a method to estimate bridge system live load effects on individual girders. Although few shear problems have been observed in the field, many current prestressed concrete girder bridges rate low for shear with current techniques in the MBE (2011), particularly those designed using the 1970 edition of the AASHTO Standard Specifications. As a consequence, a better understanding of shear distribution was needed to more accurately assess *in situ* capacity of prestressed concrete girder bridges and to provide recommendations on shear distribution to be used by MnDOT for rating and permitting. The limited and conflicting information in the literature related to shear distribution, particularly with respect to the effects of end diaphragms (Dereli et al. 2010), led to this study.

This investigation consisted of three primary components to numerically and experimentally investigate live load shear distribution in prestressed concrete girder bridges: (1) full-scale laboratory bridge tests to validate numerical models in the elastic range of behavior and to investigate if an interior girder shed shear force to adjacent girders as that girder transitioned from uncracked to cracked to ultimate failure both with and without an end diaphragm present, (2) a parametric study using validated numerical modeling techniques to understand shear distribution behavior and determine if AASHTO shear distribution factors provide an accurate estimate of live load shear demand, and (3) field live load testing to evaluate the distribution of shear forces in as-built prestressed concrete bridges at service load levels. This chapter synthesizes the information gained through this study with that found in the literature and provides final recommendations related to a proposed shear distribution methodology for load rating prestressed concrete girder bridges.

8.2 Elastic versus Inelastic Shear Distribution

Codified live load shear distribution factors are based on linear elastic results and are used to evaluate response with the nominal member resistance at the ultimate limit state. The first load distribution principles published in the AASHTO Standard Specifications (1931), for concrete slabs and beams, were developed by Westergaard (1930) and Newmark et al. (1946) and were based on elastic plate theory. The AASHTO Standard Specifications (2002) required use of the lever rule to calculate shear distribution factors, which assumes that the bridge deck acts as a simple span between beams, or use of "S-over" equations (expressed in an *S* / D format, where *S* is the girder spacing and D is a constant based on superstructure type and the type of lane loading). Equations developed by Zokaie et al. (1991b) were adopted for shear distribution factors in the AASHTO LRFD Specifications. These equations are dependent on the girder spacing and were developed using linear elastic frame and shell element finite element models loaded with the HS20 notional design truck.

Full-scale destructive tests of non-prestressed concrete girder bridges performed since 1970 were discussed by Bechtel et al. (2011) who also investigated the ultimate flexural capacity of a steel girder bridge. The results, which were all related to flexural load distribution and capacity, indicated that bridges (and inherently individual girders within the system) generally had greater capacity than those predicted with AASHTO design and rating techniques applicable during the time period of each test. This concept was further reinforced by Araujo and Cai (2006) who found that current bridge rating methods considerably underestimated the predicted flexural capacity of a prestressed concrete girder bridge using 3D FEM results validated in the elastic range.

The observed reserve strength relative to predicted capacity may be attributed to the fact that current design and rating procedures use elastic distribution and consider the resistance of individual members at the component level rather than at the system level, where load redistribution occurs during inelastic behavior (Bechtel et al. 2011). There is a dearth of both experimental and analytical research on shear live load distribution in prestressed concrete girder bridges in the inelastic range and near ultimate failure. During inelastic laboratory testing in this project, data collected prior to failure indicated that the shear demand caused by application of the live load in the loaded interior girder

redistributed after observation of initial web-shear and flexural cracks and before ultimate failure. The redistribution of shear continued to increase as the damaged girder stiffness decreased. Therefore, an inherent factor of safety existed in the laboratory bridge for the shear demand caused by application of the live load carried by the interior girder between elastic and inelastic behavior. This factor of safety for inelastic redistribution may not apply to all bridge geometries, especially in a structure with a wide girder spacing where the shear force must distribute over a longer transverse distance. However, use of linear elastic load distribution factors is conservative when considering shear distribution at ultimate capacity.

8.3 Effects of Torsion

The primary concern of this study was to address shear distribution in terms of the vertical shear resultant, but throughout the course of the project torsional shear strains were found to have an effect on the total shear strain, γ_{xy}, on either face of the girder web. The shear strain calculated from rosette strain gage data and the shear strain results from FEM both included the effects of vertical shear stress due to torsion (γ_{xy_tor}) and due to the vertical shear resultant (γ_{xy_shear}) as depicted in Figure 6-16. The magnitudes of torsional shear strains were confirmed with a validated FEM, especially during elastic laboratory testing which chronologically occurred after field testing. Laboratory data and FEM results indicated that torsional shear strains were a significant percent of the shear strain due to the vertical shear resultant.

In the laboratory, the ratio of torsional shear strain to shear strain from the vertical shear resultant ($|\gamma_{xy\_tor} / \gamma_{xy\_shear}|$) was approximately 4 to 8 percent in the loaded girder when force was applied above a girder (62 to 74 percent in the girder adjacent to the loaded girder, but the magnitude of shear strain due to the vertical shear resultant was smaller). The ratio of $|\gamma_{xy\_tor} / \gamma_{xy\_shear}|$ was approximately 40 percent in both girders when load was applied between the interior and exterior girder.

Loading scenarios used to test the laboratory bridge (load applied with a single actuator or combination of three actuators in a small, concentrated footprint) were different than those used to test the field bridges (load applied with trucks that had ten individual tires contacting the bridge deck in a large footprint). However, as discussed in Chapter 6, the effects of torsion were still observed in the field bridge FE model results; although truck

axles provide more load distribution via the gage width and longitudinal spacing, the trucks still tended to twist the girders when one or more wheel lines was located between girders. This behavior was especially evident in the skewed field bridge FEM results which did not always have less torsional behavior compared to the laboratory bridge. Specifically, the ratio of $|\gamma_{xy\_tor} / \gamma_{xy\_shear}|$ was often the same magnitude or higher in the skewed field bridge FEM results compared to the laboratory data. The field bridges were modeled with intermediate diaphragms, which were not present in the laboratory bridge. The intermediate diaphragms, modeled with a fixed connection between the end of the diaphragm and the girder web, did not eliminate the effects of torsion on shear strain. Similarly, the presence of end diaphragms with a fixed connection in both the field bridge FE models and the laboratory bridge FEM did not negate the effects of torsion.

Challenges of the live load field testing were discussed in Chapter 6 and a methodology was suggested for future live load tests to assess shear distribution for *in situ* structures. Calculation of the shear strain due to the vertical resultant shear only was not possible using data collected during live load field testing because rosettes were only placed on one side of the girder webs. In order to differentiate between torsion and vertical shear, gages needed to be placed on both sides of the girder webs. This finding likely applies to other studies in the literature that have characterized shear distribution through the use of rosette strain gages on one side of a prestressed concrete girder web. The literature has a dearth of information regarding the effects of torsion in the webs of precast concrete I- and bulb-tee beam bridges. Cross et al. (2006 and 2009) was the only study to note the potential effects of torsion (amongst many other variables) on field data after completing testing and data processing.

Ignoring the effect of torsion can result in an unconservatism related to the combined effect of vertical shear stresses due to both torsion and the vertical shear force resultant (depending on which side of the girder web is being considered). Structural response due to the combined effect may govern compared to the response generated by vertical shear stress solely due to the vertical shear force resultant.

8.4 Effects of Primary Bridge Parameters on Shear Distribution

The effects of primary bridge parameters and secondary bridge elements on shear distribution were investigated using the vertical shear force resultant obtained from validated FE models and are discussed in the following sections.

8.4.1 Girder Spacing and Depth, Deck Thickness, and Span Length

Historically, girder spacing has been the only parameter in the shear distribution factor equations in both the AASHTO Standard Specifications (2002) and the AASHTO LRFD Specifications (2010). Furthermore, other methods described in Chapter 2 (Huo et al. 2005, Puckett et al. 2007, Suksawang et al. 2013) reinforced the importance of girder spacing as it relates to shear distribution factors. Huo et al. (2005) discussed use of Henry's equal distribution factor method which was developed within the Tennessee Department of Transportation and was based on equal distribution of live load in all girders, exterior and interior. This equal distribution inherently involved the bridge width and number of girders which are directly related to the girder spacing. Puckett et al. (2007) advocated for use of a calibrated lever rule where results from the lever rule, which is dependent on the girder spacing, were calibrated with the mean of 2D grillage model results using affine transformations.

Results from the parametric study discussed in Chapter 7, which did not include the effects of barriers, diaphragms, or skew, indicated that the girder spacing, deck thickness, and span length had the greatest effect on elastic shear distribution. Thin bridge decks (e.g., 6 or 7 in.) may have historically been part of the MnDOT inventory, but since approximately the 1980's a 9 in. deck thickness has been typically specified in new design. Furthermore, almost all bridge decks constructed prior to this time period have since had a structural overlay to increase the deck thickness to at least 9 in. (Gao 2015). Bridges with a thin deck should be investigated because thinner bridge decks were shown to decrease the amount of shear distribution.

More distribution of shear was observed when the ratio of transverse bending stiffness to longitudinal bending stiffness was high. This happened for combinations of narrower girder spacing, thicker deck, and longer span lengths. It was determined that a dimensionless ratio of longitudinal bending stiffness to transverse bending stiffness,

discussed in Section 7.3, corresponded with the trend in shear per unit load in the interior girder near the end of the span length; in other words, as the value of the stiffness ratio decreased, the shear per unit load in an interior girder near the end of the span length was observed to decrease in most cases.

Results from the seven parametric study bridges and five additional bridges from MnDOT Report 2010-03 (Dereli et al. 2010) verified that the dimensionless ratio of longitudinal bending stiffness to transverse bending stiffness could be used as a screening tool to identify which bridges may have a lower live load shear demand from HS20 trucks using a refined analysis when compared to an AASHTO distribution factor-based analysis. The distributed lane load discussed in the AASHTO LRFD Specifications was not used in this study. This assumption was also used in the literature by Zokaie et al. (1991b) and Puckett et al. (2007). Bridges with a screening tool ratio, calculated using Eqn. (7.2), less than 1.5 had a lower live load shear demand from HS20 trucks for rating from both 3D FEM and simplified 2D grillage models compared to the live load shear demand calculated using AASHTO Standard and AASHTO LRFD distribution factor methodologies Live load shear demand results from simplified 2D grillage analyses were conservative and within three percent of those generated using a solid element FEM; use of an efficient 2D grillage analysis was appropriate for calculating live load shear demand from HS20 trucks for bridges with a screening tool ratio less than 1.5. Bridges with a screening tool ratio between 1.5 and 5.0 had approximately the same live load shear demand value when calculations were performed with AASHTO distribution factors or a refined analysis (3D FEM or 2D grillage models). Bridges with a screening tool ratio greater than 5.0 had a lower live load shear demand generated from AASHTO distribution factor methodologies.

Zokaie et al. (1991b) noted that the AASHTO Standard "S-over" formulas for shear distribution can produce unconservative (up to 6 percent) or conservative (up to 17 percent) shear distribution factors compared to FEM results and that the AASHTO LRFD formulas for shear distribution generally produce results within five percent of those from FEM. In this study, for straight parametric study and MnDOT verification bridges with a screening tool ratio less than 1.5, the 3D FEM results for interior girder live load shear demand at $0.1L$ due to two lanes loaded with HS20 trucks were approximately 7 to 13 percent lower than results generated with the AASHTO LRFD shear distribution factors and 8 to 11

percent lower than results generated with the AASHTO Standard shear distribution factors. For the parametric study and MnDOT verification bridges with a screening tool ratio between 1.5 and 5.0, the 3D FEM live load shear demand results were typically less than 5 percent different compared to results calculated using either AASHTO Specification. For parametric study bridges with a screening tool ratio greater than 5.0, the live load shear demand was lower by approximately 5 to 10 percent using AASHTO LRFD Specifications and 3 to 8 percent using AASHTO Standard Specifications compared to 3D FEM results.

Additional benefit related to lower live load shear demand can be realized if consideration is given to the longitudinal distribution of shear forces. AASHTO specifies use of an "average" distribution factor for each axle as discussed in Section 7.2.3. Results from a simple 2D grillage analysis used in the parametric study correctly accounted for the influence of individual axle load placement along the span length when determining live load shear demand at specific cross sections. The limitations discussed by Sotelino et al. (2004) related to 2D grillage (e.g., not accounting for interaction between girders and deck slab, support location, or shear lag) did not significantly affect results in this study. Use of 2D grillage analyses in this study likely provided results similar to 3D FEM because of the small transverse element spacing (12 in.) and the use of composite sections with the deck width equal to the girder spacing. The location or elevation of the support in 2D grillage models may affect the distribution of support reactions, especially when end diaphragm members frame into the same node as the support. However, end diaphragms were not included in the 2D grillage analyses in this study. Results of the simple 2D grillage analysis could be emulated by calculating and summing the live load shear demand from each individual axle as discussed in Section 7.2.2. Furthermore, if the section of interest was not near the support and was further into the span, the benefits of considering shear distribution along the span length increase.

The maximum shear demand generated in an interior girder from permit trucks that are longer or have more axles than an HS20 design truck may be lower because many of the axles will be far from the critical section for shear near the support. However, the AASHTO shear distribution factor method assumes these axles have the same average influence on shear at the section of interest as the axles located near the section of interest, leading to overly conservative estimates of the shear demand. Live load shear demand due

to permit trucks calculated with a simplified 2D grillage model may be lower than the live load shear demand calculated with AASHTO distribution factor methodologies and may have an effect on truck permitting, even for bridges that do not have a screening tool ratio less than 1.5.

Results from this project that highlighted the importance of span length on live load shear distribution corroborate with concepts from the literature for flexural distribution. Similar to flexural distribution, shear distribution behavior was found to be dependent on factors other than girder spacing. The AASHTO LRFD Specifications account for the ratio of longitudinal to transverse stiffness by including a ratio of girder spacing to span length (S/L) in the calculation of flexural distribution factors. Zokaie et al. (1991b) stated that, in general, beam spacing was the most significant bridge parameter affecting load distribution, but that the span length, longitudinal stiffness, and transverse stiffness "also affect the wheel load distribution factors." Additionally, Puckett et al. (2007) sought simplified methods to describe live load flexural distribution that did not include the span length. However, for flexural distribution, the researchers recognized that inclusion of a parameter that represents the longitudinal to transverse stiffness was necessary.

The complexities independently associated with both elastic load distribution and shear behavior of prestressed concrete bridge girders are well documented in the literature. Findings from the parametric study in Chapter 7 of this report suggested that refined analyses using simplified 2D grillage techniques are more accurate for shear distribution than AASHTO distribution factor methods for certain bridge geometries that are included in the MnDOT inventory. Increased accuracy of the 2D grillage analysis compared to the linear equations presented in the AASHTO Standard Specifications or the exponential curve-fitting equations presented in the AASHTO LRFD Specifications was not unforeseen. The AASHTO Loads and Load Distribution (T-5) Technical Committee recognized that the future of load distribution was influence surfaces, that is, grillage or shell modeling as opposed to girder-line analysis (Hida 2010).

8.4.2 Skew

When the support of a bridge is skewed, the load is transferred to the reaction along the shortest path which is generally toward the obtuse corners. Skew typically increases shear force effects in the end of an exterior girder at the obtuse corner when compared to

an identical non-skewed bridge (Zokaie et al. 1991b, Modjeski and Masters, Inc. 2002, Huo et al. 2005, Puckett et al. 2007). The shear distribution factors in the AASHTO Standard Specifications (2002) did not account for skew, but a formula introduced by Zokaie et al. (1991b), which was adopted in the AASHTO LRFD Specifications, accounts for skew effects by increasing the shear distribution factor using a correction factor greater than or equal to unity that was dependent on the skew angle. Zokaie et al. developed the skew correction formula by taking the ratio of skewed to non-skewed load distribution factors for bridges with the same parameters and loading. The skewed and non-skewed structures were modeled using 3D FEM with frame elements for the girders and plate elements for the deck.

The AASHTO LRFD Specification stipulates that the skew correction factor be applied to the end of all girders in the bridge cross section, both interior and exterior. However, Zokaie et al. (1991b) found that the shear in interior girders was not affected by skew. Huo et al. (2005), using 3D FEM, and Puckett et al. (2007), using 2D grillage models, found skew angles below 30 degrees have a small effect on live load shear distribution factors for interior beams in precast concrete I-beam bridges. The angle at which skew affects shear distribution in exterior girder was not explicitly stated. However, data from Zokaie et al. (1991b) indicated that, on average, skew increased the shear in obtuse corner girders by approximately 5 percent for 15 degrees of skew, 10 percent for 30 degrees of skew, 20 percent for 45 degrees of skew, and 32 percent for 60 degrees of skew. As discussed in Section 7.3.2, the amplification of shear distribution factors for skewed bridges can be accomplished using the AASHTO LRFD skew correction factor or a simplified version of the AASHTO LRFD skew correction factor presented by Puckett et al. (2007) specifically for AASHTO superstructure type k which is precast concrete I- and bulb-tee beam bridges. Use of Eqn. (7.5) would increase the live load shear demand by approximately five percent for bridges with a 30 degree skew and by approximately 16 percent for bridges with a 60 degree skew.

The ratio of skewed to non-skewed live load shear demand for the first interior girder adjacent to the obtuse corner of the deck was investigated using FE models of Bridge 65006 in this study. Results from the FEM indicated that the ratio of skewed to non-skewed

live load shear demand from an HS20 truck was 1.01 for an interior girder, which was less than the value generated using Eqn. (7.5).

8.5 Effects of Secondary Bridge Elements on Shear Distribution

Secondary bridge elements including traffic barriers and end diaphragms were considered in this study. The laboratory bridge included a partial depth end diaphragm on one end and a traffic barrier along one side of the bridge to both experimentally and numerically investigate the effects of these elements and validate the FEM technique. Puckett et al. (2007) noted that that secondary bridge elements such as diaphragms and traffic barriers can have a significant impact on lateral load distribution, but their degree of effectiveness has been characterized by conflicting results in the literature.

8.5.1 End Diaphragms

The effects of a partial depth end diaphragm were investigated while testing the laboratory bridge from low level elastic loads through inelastic behavior. In the case of low level elastic loads, the strains obtained from the webs of an interior and exterior girder (at all locations along the length between the point load and support) were not found to be noticeably different in magnitude or behavior at the opposite ends of the bridge (i.e., with and without end diaphragms) for similar loading conditions. However, small differences in the percent of shear caused by application of the live load (approximately 3 to 4 percent) from data measured on the girder webs warranted a detailed FEM investigation to better understand the behavior. Effects from the end diaphragm were investigated using FEM results related to how the bridge deck carried and distributed shear forces because the end diaphragm and bridge deck were cast together and formed a full composite connection. Observations from the elastic portion of the ultimate tests, with higher magnitude elastic loads, indicated that the end diaphragm slightly increased the amount of shear strain carried by the loaded interior composite girder at the critical section, d_v, compared to results without an end diaphragm.

The effect of a partial depth end diaphragm on elastic shear distribution was studied with the validated finite element model of the laboratory bridge. The connectivity between the end diaphragm and the girder was assumed to be fixed in both tension and compression, which served as an upper bound. The FEM results generated with load applied at $4d_v$

indicated that the end diaphragm increased the amount of shear force carried by the loaded girder composite section (i.e., girder section assuming the effective deck width equal to the girder spacing) between $2d_v$ and $0.5d_v$ by approximately 4 to 6 percent compared to the results without an end diaphragm. Furthermore, FEM results indicated that the end diaphragm increased the amount of shear force carried by the loaded girder near the point of applied load but slightly decreased the amount of shear force carried by the loaded girder near the end of the span. The end diaphragm did not affect the amount of shear force in the deck near the point of applied load but increased the amount of shear force in the deck near the end of the span. For the length of structure and loading scenario in the laboratory, the FEM results indicated that the end diaphragm increased the amount of load carried to the end of the span through the 9 in. bridge deck rather than through the girder. When load was applied directly above a girder in the FEM, this behavior indicated that more shear remained in the deck until the very end of the span, near the reaction, and transferred to the support through the end diaphragm or the girder web at the very end of the span. In this region the girder has additional shear capacity because it experiences vertical compression due to the load and reaction.

Observations were made regarding the effect of the end diaphragm on inelastic behavior and ultimate failure. The partial depth end diaphragm was present during one of two tests that incorporated inelastic behavior. Quantitatively, for this laboratory bridge geometry and loading scenario, it was shown that the end diaphragm had a small effect on the cracking loads and the ultimate failure loads. The live load shear demand at observed web-shear cracking, observed flexural cracking, and at ultimate failure were slightly lower, by approximately 2 to 9 percent, during inelastic testing with an end diaphragm. Data indicated that near ultimate failure, load had been redistributed in tests with and without an end diaphragm to approximately the same shear demand caused by application of the live load (i.e., similar peak applied loads at failure). This indicated that the shear force redistribution that occurred near ultimate failure was similar with and without an end diaphragm. Qualitatively, the end diaphragm focused diagonal shear cracking higher in the web and toward the support centerline rather than toward the face of the support during inelastic testing and failure. The web-shear cracking pattern between the support and the location of applied load at failure extensively penetrated the top flange and engaged more

of the bridge deck above the web when the end diaphragm was present whereas the web-shear cracking pattern was mainly in the girder web between the support and the location of applied load when the end diaphragm was not present.

Various researchers have categorized how end diaphragms affect shear distribution. Bae and Oliva (2012) specifically considered the effect of end diaphragms on shear load distribution from overload trucks using 3D FEM, with shell elements representing the deck and frame elements representing the girders. The researchers reported that end diaphragms increased shear live load distribution factors by up to seven percent when compared to bridges without an end diaphragm. To calculate shear distribution, Bae and Oliva (2012) maximized shear response in an interior girder using oversize, overweight vehicles configured in longitudinal and transverse positions for one lane and two lanes loaded. Thus, the vehicular live load often consisted of more than three axles longitudinally and transverse axle gage widths of 8 to 18 ft (greater than the standard 6 ft). The shear distribution factor was calculated by dividing the shear in the interior girder by the sum of the shear in all of the girders.

Furthermore, Huo et al. (2003) and Puckett et al. (2007) obtained conflicting numerical analysis results in their studies of Bridge No. 24, which was a prestressed concrete girder bridge described by Huo et al. Huo et al. (2003) used 3D FEM with frame elements for the girders and shell elements for the deck, and Puckett et al. (2007) used 2D grillage models. Both research groups used the following: one or more HS20 design trucks (depending on the number of lanes loaded) configured transversely and longitudinally to maximize shear response in the girder, an effective deck width equal to the girder spacing, and distribution factors on a per lane basis calculated by dividing the maximum live load shear demand from an interior girder in the bridge system by the shear generated from a beam-line analysis (the bridge is idealized as a 1D structure along its length to determine the shear across a section of the bridge) with the load at the same longitudinal location on the span. Results from Huo et al. (2003) indicated that abutment support diaphragms caused a decrease in the shear distribution factor in conflict with the study done by Puckett et al. (2007) that indicated abutment support diaphragms slightly increased the shear distribution factor. The biggest difference between the two studies was the type of modeling used to generate the shear distribution results. Furthermore, the boundary conditions related to how

the end diaphragm was connected to the support may have varied between the two studies. Huo et al. (2003) indicated that use of "line supports…instead of individual point support under beams" were used to consider diaphragm effects. This type of connectivity was not mentioned by Puckett et al. (2007) and a picture displaying a representative grillage model only showed supports under girder elements. Differences in the modeling techniques may be responsible for the discrepancies related to the effects of the end diaphragm. Specifically, if the end diaphragm was constrained to the support between girders it may have caused more shear distribution amongst adjacent girders.

Results from the present study corroborated the findings from Bae and Oliva (2012) and Puckett et al. (2007) and indicated that the loaded composite girder section carried 4 to 6 percent more shear force when an end diaphragm was present. Shear forces collected from finite element models in this project were always determined from shear stresses assuming a composite section composed of the girder and deck width equal to the girder spacing. This provided some inherent conservatism because not all of the shear force carried to the end of the span by the composite section was carried through the girder. The shear force that is carried to the end of the span in the bridge deck is transferred to the support through the girder web near the reaction.

Cai et al. (2002) and Cai and Shahawy (2004) indicated that the as-built diaphragm stiffness in bridges was uncertain due to possible concrete cracking and weakness of the diaphragm-to-girder connection. Cracking at the end diaphragm-to-girder connection was observed in this project during field testing as discussed in Section 5.3.4 and during visual inspection of field bridges conducted by Dereli et al. (2010). These issues create many unknowns related to the effect of end diaphragms on load distribution of in-service bridges. The effects of end diaphragms were not considered throughout Chapter 7 for the parametric study numerical modeling in both three-dimensional finite element models and in simplified two-dimensional grillage models. Ignoring the effects of an end diaphragm may be slightly inaccurate by 4 to 6 percent, but this assumption was warranted for simplicity.

8.5.2 Traffic Barrier

Cross et al. (2009) noted that "nonstructural" concrete items on a bridge such as a parapet were quite stiff and tended to attract shear away from girders at a distance *d* from the reaction. Finite element modeling results discussed in Chapter 5 indicated that a

composite traffic barrier carried shear force as near as $0.5d_v$ away from the face of the support (interior edge of the sole plate) when the load was applied directly above the exterior girder. This behavior indicated that shear forces may not transfer from the barrier to the girder web until near the end of the span, between the critical section and the face of the support. In this region the girder has additional shear capacity because it is experiencing vertical compression due to the load and reaction. However, the traffic barrier had a negligible effect on the shear distribution when the load was applied mainly over an interior girder.

These findings agreed with statements in Section 4.6.3.1 of the AASHTO LRFD Specifications (2010) which declared that additional stiffness provided by barriers exists and has been experimentally observed in bridges. However, the additional stiffness has traditionally been conservatively neglected in design and analysis. In this study, composite action between the barrier and exterior girder was shown to decrease the percent of shear caused by application of the live load in an exterior girder at the critical section by up to 19 percent based on FEM results with a point load applied directly above the exterior girder at either $2d_v$ or $4d_v$ along the span length.

Because it is conservative to ignore the effects of the traffic barrier when calculating live load distribution for shear, this assumption was used throughout the parametric study numerical modeling discussed in Chapter 7. The AASHTO MBE (2011) supports this assumption when noting that the level of structural participation from barriers could vary from bridge to bridge. Field testing procedures described in Chapter 6 may be utilized to verify the shear distribution behavior of exterior girders in the presence of a traffic barrier if additional investigation is warranted.

8.6 Synthesis Summary

The synthesis interwove discussion and results from the four primary components of this study used to investigate live load shear distribution in prestressed concrete girder bridges: (1) a comprehensive literature review of shear distribution in prestressed concrete bridges, (2) a laboratory investigation of shear distribution on a full-scale prestressed girder bridge subjected to loading that produced elastic and inelastic behavior, (3) a parametric study conducted to understand shear distribution behavior and determine if AASHTO shear distribution factors provide an accurate estimate of live load shear demand, and (4) field

live load testing to evaluate the distribution of shear in as-built prestressed concrete bridges at service load levels. Specifically, the effects of elastic versus inelastic shear distribution, torsion, primary bridge parameters, and secondary bridge elements on shear distribution in prestressed concrete girder bridges was discussed. Section 8.7 provides final recommendations related to a proposed shear distribution methodology for load rating prestressed concrete girder bridges.

8.7 Recommendations for Rating and Permitting

The following recommendations are provided for bridge rating and permitting trucks for prestressed concrete girder bridges in the MnDOT inventory that currently rate low for shear. The recommendations are a culmination of results from the integrated aspects of the experimental and numerical research components used to determine how live load shear forces distribute in prestressed concrete girder bridges.

1. For shear rating, if the rating for a structure in the MnDOT inventory is currently ignored, the longitudinal to transverse stiffness ratio defined in Eqn. (7.2) as $(I_{long}/L^3)/(I_{trans}/S^3)$ should be calculated for use as a screening tool to determine if refined analysis provides benefit in regard to the controlling live load shear demand from AASHTO HS20 design trucks for an interior girder. The effects of the lane load discussed in the AASHTO LRFD Specifications was not considered in this study. It was assumed that interior girders controlled load rating for bridges that rate poorly for shear in the MnDOT inventory after email correspondence with the MnDOT Technical Liaison (Gao 2015).
2. If the screening tool ratio is greater than a value of 1.5, an analysis using AASHTO Standard or AASHTO LRFD shear distribution factors for interior girders will likely provide a suitable method to calculate the controlling live load shear demand from the AASHTO HS20 design truck.
3. If the screening tool ratio is less than a value of 1.5, determination of the live load shear demand from AASHTO HS20 design trucks for an interior girder in the span under consideration may be more accurate and provide lower girder shear demands if calculated from a simple 2D grillage analysis than the live load shear demand computed using AASHTO shear distribution factor methods.

a. To simplify the 2D grillage analysis, ignoring the effects of the traffic barrier end diaphragms was shown to be acceptable.
b. The grillage model should be constructed using longitudinal composite beam members (one for each girder) and transverse deck members spaced at 12 in. on center in the longitudinal direction as described in Sections 3.4 and 7.3.1.

4. For bridges with skew angles greater than 30 degrees and a screening tool ratio less than 1.5, the calculated live load shear demand for the interior girder from AASHTO distribution factor methods or from simple grillage analysis of the equivalent straight bridge could be amplified with a skew correction factor calculated using Eqn. (7.5).
    a. The equivalent straight bridge should contain no skew angle but the same girder spacing, girder length, and span length.
    b. In the case of a span with different skew angles at each end (or skew at only one end), the length of the equivalent straight bridge should be defined as the length of the shortest beam.
5. For permitting, a simplified 2D grillage analysis may be used to determine the controlling live load shear demand due to permit trucks for girders of MnDOT prestressed concrete girder bridges that rate low for shear. The live load shear demand due to permit trucks calculated with a simplified 2D grillage model may be lower than the live load shear demand calculated with AASHTO distribution factor methodologies and may have an effect on truck permitting, even for bridges that do not have a screening tool ratio lower than 1.5.
6. If further investigation of shear distribution for a particular *in situ* prestressed concrete girder bridge is warranted through nondestructive load testing, it is recommended that the guidelines discussed in Chapter 6 be followed.

REFERENCES

Akinci, N. O., Liu, J., and Bowman, M. D. (2008). "Parapet Strength and Contribution to Live Load Response for Superload Passages." *Journal of Bridge Engineering*, 13(1), 55-63.

Al-Omaishi, N., Tadros, M. K., and Seguirant, S. J. (2009). "Estimating Prestress Loss in Pretensioned, High-Strength Concrete Members." *PCI Journal*, 54(4), 132-159.

Altay, A. K., Arabbo, D. S., Corwin, E. B., Dexter, R. J., and French, C. E. (2003). "Effects of Increasing Truck Weight on Steel and Prestressed Bridges." *Report No. MN/RC 2003-16*. Department of Civil Engineering, University of Minnesota, Minneapolis, MN, pp. 129.

American Association of State and Highway Transportation Officials (AASHTO). (1931). *Standard Specifications for Highway Bridges and Incidental Structures*, 1st Edition, Washington, D.C.

American Association of State and Highway Transportation Officials (AASHTO). (1989). *Standard Specifications for Highway Bridges*, 14th Edition with 1991 Interim Specifications, Washington, D.C.

American Association of State and Highway Transportation Officials (AASHTO). (2002). *Standard Specifications for Highway Bridges*, 17th Edition, Washington, D.C.

American Association of State and Highway Transportation Officials (AASHTO). (2003). *Manual for Condition Evaluation of Bridges*, 2nd Edition, Washington, D.C.

American Association of State Highway and Transportation Officials (AASHTO) (2010). *AASHTO LRFD Bridge Design Specifications*, 5th Edition, Washington, DC.

American Association of State Highway and Transportation Officials (AASHTO) (2011). *The Manual for Bridge Evaluation*, 2nd Edition, Washington, DC.

American Concrete Institute (ACI) (2011). *Building Code Requirements for Structural Concrete (ACI 318-11)*, 2nd printing, Farmington Hills, MI.

Araujo, M. and Cai, C. S. (2006). "Performance of Prestressed Concrete Bridges – Evolution from Elastic to Failure Stages." *Structures Congress: Structural Engineering and Public Safety*, St. Louis, MO.

Arockiasamy, M. and Amer, A. (1998). "Load Distribution on Highway Bridges Based on Field Test Data." *Final Report Florida DOT Contract No. BA489, WPI 0510668, Job No. 99500-3512-119*, Center for Infrastructure and Constructed Facilities, Florida Atlantic University, Boca Raton, FL, pp.169.

ASCE-ACI Committee 426. (1973). "The Shear Strength of Reinforced Concrete Members." *Journal of the Structural Division*, 99(6), 1091-1187.

ASCE-ACI Committee 445. (1998). "Recent Approaches to Shear Design of Structural Concrete." *Journal of Structural Engineering*, 124(12), 1375-1417.

ASTM A370/A370M-12a. (2012) "Standard Test Methods and Definitions for Mechanical Testing of Steel Products." American Society for Testing and Materials (ASTM), West Conshohocken, Pennsylvania.

ASTM A416/A416M-12a. (2012). "Standard Specification for Steel Strand, Uncoated Seven-Wire for Prestressed Concrete." American Society for Testing and Materials (ASTM), West Conshohocken, Pennsylvania.

ASTM A615/A615M-12. (2012). “Standard Specification for Deformed and Plain Carbon-Steel Bars for Concrete Reinforcement.” American Society for Testing and Materials (ASTM), West Conshohocken, Pennsylvania.

ASTM A1061-09. (2009). “Standard Test Methods for Testing Multi-Wire Steel Strand.” American Society for Testing and Materials (ASTM), West Conshohocken, Pennsylvania.

ASTM C31/C31M-12. (2012). “Standard Practice for Making and Curing Concrete Test Specimens in the Field.” American Society for Testing and Materials (ASTM), West Conshohocken, Pennsylvania.

ASTM C39/C39M-12. (2012). “Standard Test Method for Compressive Strength of Cylindrical Concrete Specimens.” American Society for Testing and Materials (ASTM), West Conshohocken, Pennsylvania.

ASTM C42/C42M-13. (2013). “Standard Test Method for Obtaining and Testing Drilled Cores and Sawed Beams of Concrete.” American Society for Testing and Materials (ASTM), West Conshohocken, Pennsylvania.

ASTM C78/C78M-10. (2010). “Standard Test Method for Flexural Strength of Concrete (Using Simple Beam with Third-Point Loading).” American Society for Testing and Materials (ASTM), West Conshohocken, Pennsylvania.

ASTM C192/C192M-13. (2013). “Standard Practice for Making and Curing Concrete Test Specimens in the Laboratory.” American Society for Testing and Materials (ASTM), West Conshohocken, Pennsylvania.

ASTM C469/C469M-10. (2010). “Standard Test Method for Static Modulus of Elasticity and Poisson’s Ratio of Concrete in Compression.” American Society for Testing and Materials (ASTM), West Conshohocken, Pennsylvania.

ASTM C496/C496M-11. (2011). “Standard Test Method for Splitting Tensile Strength of Cylindrical Concrete Specimens.” American Society for Testing and Materials (ASTM), West Conshohocken, Pennsylvania.

ASTM C617/C617M-12. (2012). “Standard Practice for Capping Cylindrical Concrete Specimens.” American Society for Testing and Materials (ASTM), West Conshohocken, Pennsylvania.

ASTM C1231/C1231M-12. (2012). “Standard Practice for Use of Unbonded Caps in Determination of Compressive Strength of Hardened Concrete Cylinders.” American Society for Testing and Materials (ASTM), West Conshohocken, Pennsylvania.

ASTM D4014-12. (2012). “Standard Specification for Plain and Steel-Laminated Elastomeric Bearings for Bridges.” American Society for Testing and Materials (ASTM), West Conshohocken, Pennsylvania.

Bae, H. U. and Oliva, M. G. (2012). “Moment and Shear Load Distribution Factors for Multigirder Bridges Subjected to Overloads.” *Journal of Bridge Engineering*, 17(3), 519-527.

Bakht, B. and Jaeger, L.G. (1992). “Simplified Methods of Bridge Analysis for the Third Edition of OHBDC.” *Canadian Journal of Civil Engineering*, 19(4), 551-559.

Barnes, R. W., Stallings, J. M., and Porter, P. W. (2003). “Live-Load Response of Alabama’s High-Performance Concrete Bridge.” *Transportation Research Record 1945*, 115-124.

Barr, P. J., and Amin, MD. N. (2006). "Shear Live-Load Distribution Factors for I-Girder Bridges." *Journal of Bridge Engineering*, 11(2), 197-204.

Barr, P. J., Eberhard, M. O., and Stanton, J. F. (2001). "Live-Load Distribution Factors in Prestressed Concrete Girder Bridges." *Journal of Bridge Engineering*, 6(5), 298-306.

Bechtel, A., McConnell, J., and Chajes, M. (2011). "Ultimate Capacity Destructive Testing and Finite-Element Analysis of Steel I-Girder Bridges." *Journal of Bridge Engineering*, 16(2), 197-206.

Bradberry, T. E. (2015). Summary of Shear Rating Concrete Bridges in Texas. Personal communication.

Bentz, E. C., F. J. Vecchio, and M. P. Collins. (2006). "The Simplified MCFT for Calculating the Shear Strength of Reinforced Concrete Elements." *ACI Structural Journal*, 103(4), 614–624.

Cai, C. S. and Shahawy, M. (2004). "Predicted and Measured Performance of Prestressed Concrete Bridges." *Journal of Bridge Engineering*, 9(1), 4-13.

Cai, C. S., Shahawy, M., and Peterman, R. J. (2002). "Effect of Diaphragms on Load Distribution of Prestressed Concrete Bridges." *Transportation Research Record 1814*, 47-54.

Chen, S. S., A. J. Aref, I.-S. Ahn, M. Chiewanichakorn, J. A. Carpenter, A. Nottis, and I. Kalpakidis. (2005). "Effective Slab Width for Composite Steel Bridge Members." National Cooperative Highway Research Program Report 543, Transportation Research Board, National Research Council, Washington, D.C.

Collins, M. P., Mitchell, D., Adebar, P., and Vecchio, F. J. (1996). "A General Shear Design Method." *ACI Structural Journal*, 93(1), 36-45.

Collins, M. P., and Mitchell, D. (1997). *Prestressed Concrete Structures*, Response Publications, Canada.

Computers and Structures, Inc. (2009). "SAP2000 v14.0.0," Berkeley, CA.

Conner, S. and Huo, X. S. (2006). "Influence of Parapets and Aspect Ratio on Live-Load Distribution." *Journal of Bridge Engineering*, 11(2), 188-196.

Cross, B., Vaughn, B., Panahshahi, N., Petermeier, D., Siow, Y. S., and Domagalski, T. (2009). "Analytical and Experimental Investigation of Bridge Girder Shear Distribution Factors." *Journal of Bridge Engineering*, 14(3), 154-163.

Cross, B., Panahshahi, N., Vaughn, B., Petermeier, D., and Siow, Y. (2006). "Investigation of Select LRFD Design Factors through Instrumentation of Bridge Bearings." *Physical Research Report No. 152*, Southern Illinois University Edwardsville, Edwardsville, IL, pp. 349.

Dassault Systèmes (2011). "Abaqus," *SIMULIA*. Providence, RI.

Densmore, D. (2000). "Load and resistance factor design." Federal Highway Administration Policy Memorandums, Washington, D.C.,

Dereli, O., Shield, C., and French, C. (2010). "Discrepancies in Shear Strength of Prestressed Beams with Different Specifications." *Report No. MN/RC 2010-03*, Department of Civil Engineering, University of Minnesota, Minneapolis, MN, pp. 242.

Devalapura, R.K. and Tadros, M.K. (1992). "Stress-Strain Modeling of 270 ksi Low-Relaxation Prestressing Strands," *PCI Journal*, 37(2), 100-105.

Dhar, A., Mazumder, M., Chowdhury, M., and Karmakar, S. (2013). "Effect of Skew Angle on Longitudinal Girder (support shear, moment, torsion) and Deck Slab of an IRC Skew Bridge." *Indian Concrete Journal*, 87(12), 46-52.

Eamon, C. D. and Nowak, A. S. (2002). "Effects of Edge-Stiffening Elements and Diaphragms on Bridge Resistance and Load Distribution." *Journal of Bridge Engineering*, 7(5), 258-266.

Ebeido, T. and Kennedy, J. B. (1995). "Shear Distribution in Simply Supported Skew Composite Bridges." *Canadian Journal of Civil Engineering*, 22(6), 1143-1154.

Ebeido, T. and Kennedy, J. B. (1996). "Shear and Reaction Distributions in Continuous Skew Composite Bridges." *Journal of Bridge Engineering*, 1(4), 155-165.

Federal Highway Administration (FHWA). (2011). National Bridge Inventory Data 2011. www.fhwa.dot.gov/bridge/deficient.htm. Accessed April, 2012.

Fink, J. E. (2013). Personal Email Communication. January 14 through April 1, Minneapolis, MN.

Fu, G. and Chun, P. (2013). "Skewed Highway Bridges." *Report No. RC-1541*, Department of Civil and Environmental Engineering, Wayne State University, Detroit, MI, pp. 193.

Gao, Y. (2015). Personal Email Communication. May 8 through June 12, Minneapolis, MN.

Goodrich, B. L. and Puckett, J. A. (2002). "Comparison of LFR and LRFR for Concrete Bridges." *Concrete Bridge Conference*, Nashville, TN.

Green, T., Yazdani, Y., and Spainhour, L., (2004). "Contribution of Intermediate Diaphragms in Enhancing Precast Bridge Girder Performance." *Journal of Performance of Constructed Facilities*, 18(3), 142-46.

Hambly, E. C. (1991). *Bridge Deck Behaviour*. Taylor & Francis, New York, NY.

Hawkins, N. M., Kuchma, D. A., Mast, R. F., Marsh, M. L., and Reineck, K-H. (2005). "Simplified Shear Design of Structural Concrete Members." National Cooperative Highway Research Program (NCHRP) Report 549, Transportation Research Board, Washington, D.C.

Hida, S. (2010). Summary of 2007 AASHTO Loads and Load Distribution (T-5) Technical Committee meeting minutes from the Committee Chair. Personal communication.

Huo, X.S., Conner, S.O., and Iqbal, R. (2003). "Re-examination of the Simplified Method (Henry's Method) of Distribution Factors for Live Load Moment and Shear." *Report No. TNSPR-RES 1218*, Center for Electric Power, Tennessee Technological University, Cookeville, TN, pp. 254.

Huo, X. S., Wasserman, E. P., and Iqbal, R. A. (2005). "Simplified Method for Calculating Lateral Distribution Factors for Live Load Shear." *Journal of Bridge Engineering* 10(5), 544-554.

Idriss, R. L. and Liang, Z. (2010). "In-Service Shear and Moment Girder Distribution Factors in Simple-Span Prestressed Concrete Girder Bridge." *Transportation Research Record 2172*, 142-150.

Kuchma, D. A., Hawkins, N. M., Kim, S., Sun, S., and Kim, K. S. (2008). "Simplified shear provisions of the AASHTO LRFD Bridge Design Specifications." *PCI Journal*, 53(3), 53-73.

Lichtenstein Consulting Engineers (2001). "Manual for Condition Evaluation and Load Rating of Highway Bridges Using Load and Resistance Factor Philosophy."

National Cooperative Highway Research Program (NCHRP) Project C12-46 Web Document 28, Transportation Research Board, Washington, D.C.

Mathys, B., Shield, C., and French, C. (2014). "Anchorage of Shear Reinforcement in Prestressed Concrete Bridge Girders." *Report No. MN/RC 2014-36*, Department of Civil Engineering, University of Minnesota, Minneapolis, MN, pp. 256.

Mertz, D. R. (2005). "Load Rating by Load and Resistance Factor Evaluation Method." National Cooperative Highway Research Program (NCHRP) Project 20-07/Task 122 Final Report, Transportation Research Board, Washington, D.C.

Minervino, C., Sivakumar, B., Moses, F., Mertz, D., and Edberg, W. (2004). "New AASHTO Guide Manual for Load and Resistance Factor Rating of Highway Bridges." *Journal of Bridge Engineering*, 9(1), 43–54.

Millam, J. L. and Ma, Z. (2005). "Single-Lane Live Load Distribution Factor for Decked Precast, Prestressed Concrete Girder Bridges." *Transportation Research Record 1928*, 142-152.

Minnesota Department of Transportation (MnDOT). (1996). *Bridge Design Manual 5-392.501(1)*, St. Paul, MN.

Minnesota Department of Transportation (MnDOT). (2013). *LRFD Bridge Design Manual 5-392*, St. Paul, MN.

Modjeski and Masters, Inc. (2002). "Shear in Skewed Multi-Beam Bridges." National Cooperative Highway Research Program Final Report for Project 20-7/Task 107, Transportation Research Board, National Research Council, Washington, D.C.

Moen, C. D. and Fernandez, L. (2009). "A Comparison of AASHTO Bridge Load Rating Methods." *Structures Congress: Don't Mess with Structural Engineers*, Austin, TX.

Moses, F. (2001). "Calibration of Load Factors for LRFR Bridge Evaluation." National Cooperative Highway Research Program (NCHRP) Report 454, Transportation Research Board, Washington, D.C.

Newmark, N. M., Siess, C. P., and Peckham, R. R. (1946). "Studies of Slab and Beam Highway Bridges. Part I: Tests of Simple-Span Right I-Beam Bridges." Bulletin Series No. 363, Engineering Experiment Station, University of Illinois, Urbana, IL, pp. 132.

Nilson, A. H. (1987). *Design of Prestressed Concrete*, Second Edition, John Wiley & Sons, New York.

Nowak, A. S. (1999). "Calibration of LRFD Bridge Design Code." National Cooperative Highway Research Program Report 368, Transportation Research Board, National Research Council, Washington, D.C.

Nowak, A. S. and Szerszen, M. M. (2003). "Calibration of Design Code for Buildings (ACI 318): Part 1 – Statistical Models for Resistance." *ACI Structural Journal*, 100(3), 377-382.

Pauw, A. (1960). "Static Modulus of Elasticity of Concrete as Affected by Density." *ACI Journal*, 32(6), 679-687.

Pei, J. S., Martin, R. D., Sandburg, C. J., Kang, T. H.-K. (2008). "Rating Precast Prestressed Concrete Bridges for Shear." *Report No. FHWA-OK-08-08*, School of Civil Engineering and Environmental Science, University of Oklahoma, Norman, OK, pp. 118.

Potisuk, T. and Higgins, C. (2007). "Field Testing and Analysis of CRC Deck Girder Bridges." *Journal of Bridge Engineering*, 12(1), 53-63.

Precast Prestressed Concrete Institute (PCI) (1997). *PCI Bridge Design Manual*, 1st Edition, Chicago, IL.

Preston, H. Kent. (1975). "Recommendations for Estimating Prestress Losses." *Journal of the Prestressed Concrete Institute*, 20(4), 44-75.

Puckett, J.A., Mertz, D., Huo, X.S., Jablin, M.C., Peavy, M.D, and Patrick, M.D. (2007). "Simplified Live Load Distribution Factor Equations." National Cooperative Highway Research Program Report 592, Transportation Research Board, National Research Council, Washington, D.C.

Roddenberry, M. R., Chipperfield, J. and Tawfiq, K. S. (2011). "Effect of Secondary Elements on Load Distribution in Prestressed Bridge Girders." *Don't Gamble on your Future - Come to the Structures 2011 Congress*, Las Vegas, NV.

Roeder, C. W., Stanton, J. F., and Taylor, A. W. (1987). "Performance of Elastomeric Bearings." National Cooperative Highway Research Program Report 298, Transportation Research Board, Washington, D.C.

Rogers, B. J. and Jáuregui, D. V. (2005). "Load Rating of Prestressed Concrete Girder Bridges: Comparative Analysis of Load Factor Rating and Load and Resistance Factor Rating." *Transportation Research Record 1928*, Transportation Research Board, Washington, D.C., 53-63.

Runzel, B., Shield, C.K., and French, C.W. (2007). "Shear Capacity of Prestressed Concrete Beams." *Report No. MN/RC 2007-47*, Department of Civil Engineering, University of Minnesota, Minneapolis, MN, pp. 237.

Sanders, W. W. Jr., and Elleby, H. A. (1970). "Distribution of Wheel Loads on Highway Bridges." National Cooperative Highway Research Program Report No. 83, Transportation Research Board, Washington, D.C.

Schwarz, M. and Laman, J. A. (2001). "Response of Prestressed Concrete I-Girder Bridges to Live Load." *Journal of Bridge Engineering*, 6(1), 1-8.

Sengupta, S. and Breen, J. E. (1973). "The Effect of Diaphragms in Prestressed Concrete Girder and Slab Bridges." *Research Report No. 158-1F*, Center for Highway Research, University of Texas, Austin, TX, pp. 256.

Shah, D. M. (2007). Effective Flange Width Evaluation for Prestressed Concrete Bulb-Tee Girder Bridges. M.S. Thesis, The State University of New York at Buffalo, Buffalo, New York.

Sotelino, E. D., Liu, J. Chung, W. Phuvoravan, K. (2004). "Simplified Load Distribution Factor for Use in LRFD Design." *Report No. FHWA/IN/JTRP-2004/20*, Joint Transportation Research Program, Purdue University, West Lafayette, IN, pp. 203.

Suksawang, N., Nassif, H., and Su, D. (2013). "Verification of Shear Live-load Distribution Factor Equations for I-Girder Bridges." *Korean Society of Civil Engineer (KSCE) Journal of Civil Engineering*, 17(3), 550-555.

Tabsh, S. W. and Tabatabai, M. (2001). "Live load distribution in girder bridges subject to oversized trucks." *Journal of Bridge Engineering*, 6(1), 9-16.

Tjhin, T. and Kuchma, D. (2004) CAST - Computer Aided Strut-and-Tie Software Version 0.9.11, University of Illinois, Urbana-Champagne, IL.

Tobias, D. H. (2011). "Perspectives on AASHTO Load and Resistance Factor Design." *Journal of Bridge Engineering*, 15(6), 684-692.

Vecchio, F. J., and M. P. Collins. (1986). “The Modified Compression Field Theory for Reinforced Concrete Elements Subjected to Shear.” *Journal of the American Concrete Institute*, 83(2), 219–231.

Weisstein, Eric W. (2015) “Affine Transformation.” From *MathWorld* – A Wolfram Web Resource. http://mathworld.wolfram.com/AffineTransformation.html.

Westergaard, H. M. (1930). “Computations of Stresses in Bridge Slabs Due to Wheel Loads.” *Public Roads*, 11(1), 1-23.

Wood, S.L. (1991). “Evaluation of the Long-Term Properties of Concrete.” *Research and Development Bulletin RD102*, Portland Cement Association, Skokie, IL.

Zheng, L., Huo, X. S., and Hayworth, R. P. (2007). “Comparison of Load Factor Rating (LFR) to Load and Resistance Factor Rating (LRFR) of Prestressed Concrete I-Beam Bridges.” *Structures Congress: New Horizons and Better Practices*, Long Beach, CA.

Zokaie, T. (2000). “AASHTO-LRFD Live Load Distribution Specifications.” *Journal of Bridge Engineering*, 5(2), 131-138.

Zokaie, T., Osterkamp, T. A., and Imbsen, R. A. (1991a). “Distribution of Wheel Loads on Highway Bridges.” *Transportation Research Record 1290, Volume 1*, Transportation Research Board, Washington, D.C., 119-126.

Zokaie, T., Osterkamp, T. A., and Imbsen, R. A. (1991b). “Distribution of Wheel Loads on Highway Bridges.” National Cooperative Highway Research Program Final Report 12-26/1, Transportation Research Board, Washington, D.C.

APPENDIX A. LABORATORY COMPANION GIRDER DESIGN, FABRICATION, TESTING, AND RESULTS

A.1 Design, Fabrication, Material Properties, Instrumentation, and Test Setup

Composite Girder Design and Fabrication

A single girder, referred to as Girder 5 or G5, was fabricated at the same time as the four laboratory bridge girders. The specifications for the single girder were the same as that of the other four girders, but more transverse reinforcement was added near midspan as shown in Figure A-1 to minimize the width of cracks incurred during testing near midspan. The additional transverse reinforcement consisted of No. 4 epoxy-coated U-shaped stirrups spaced at 8 in. for approximately 4.67 ft on either side of the beam centerline. This enabled testing of the second end of the girder. Epoxy-coated stirrups were used in this section of the beam because Cretex Concrete did not have additional uncoated stirrups for this portion of the beam due to an error when ordering supplies.

The composite single girder deck was designed to simulate the effective shear depth, d_v, of the composite beams in the full laboratory bridge deck; however, the deck width was limited to 5 ft to fit within the 600 kip MTS testing frame limits. A 9 in. deck thickness was chosen to be consistent with that of the laboratory bridge. To match the effective shear depth of the bridge composite girders, which had effective deck widths of 9 ft cast with 4,000 psi concrete, a 7,000 psi concrete deck (5 ft wide) was required for the single girder. Transformed sections were considered for comparison of the effective shear depths. Uncoated black rebar was used for the deck reinforcement. The 9 in. deck thickness and reinforcement for the single girder bridge deck, shown in Figure A-2, was representative of an interior girder from the full bridge. Ultimately, the deck width had to be reduced to 4.5 ft as discussed in the next paragraph due to lifting weight restrictions.

Fabrication of the single prestressed concrete girder occurred simultaneously with fabrication of the four laboratory bridge girders. Details regarding girder fabrication are discussed in Section 4.3.1. A composite cast-in-place concrete deck was placed on the single girder on November 5, 2013 in the loading dock of the Civil Engineering Building. Approximately 5.25 yd^3 of concrete was delivered at 10 am and placed in the formwork using the concrete truck chute. Concrete deck placement, concrete deck finishing, and companion cylinder test specimen fabrication was completed by researchers from the University of Minnesota. The concrete cured outdoors and was covered with insulated blankets, on loan from Graham Construction, for 14 days. Overnight temperatures were

below freezing, but no additional heat was provided and the concrete achieved the specified compressive strength at 28-days.

The single girder deck width was modified prior to placing the specimen in the 600 kip MTS testing frame. The combined weight of the composite concrete cross section, steel spreader beam used for lifting, and rigging equipment was more than the capacity of the overhead crane. The weight of the composite concrete section was reduced by cutting 3 in. off of each side of the deck, reducing the width from 5 ft to 4.5 ft. Reduction of the deck width to 4.5 ft did not have a significant effect (less than 1 percent) on the effective shear depth when compared that of the original 5 ft deck width.

Girder and Deck Measured Material Properties

Single girder material properties are shown simultaneously with laboratory bridge girder results in Section 4.4.1. The concrete specified for the single girder deck was chosen to have ¾ in. maximum aggregate and a 28-day nominal compressive strength of 7,000 psi. Engineers at Cemstone Concrete were able to provide a concrete mix (mix designation 7054P) that met the compressive strength and aggregate size requirements and typically gained 90 percent of the 28-day compressive strength in two weeks. This was advantageous to facilitate a fast cure in cold temperatures because the single girder deck concrete was placed on the beam in the open-air loading dock of the Civil Engineering building. The mix was modified to have a 7 in. slump for ease of placement. Specified mix details and information for the 5.25 yd^3 batch are given in Table A-1. The fresh and hardened concrete mix properties are given in Table A-2.

Instrumentation

During testing of the single girder, structural behavior was monitored using six separate types of instruments. The strain distribution along the length of the girder stirrups was monitored using the foil strain gages installed at three vertical locations on a stirrup leg described in Section 4.5.2.1. Shear strain on a vertical face, γ_{xy}, was determined using strains collected with vibrating wire gage box-type rosettes and rosette foil strain gages installed along the length of the girder. The foil rosettes were installed at three vertical locations on the web of the girder to investigate the distribution of shear strains on the web

section. Strain readings from the internally mounted foil strain gages on the stirrups were compared to data collected by a single vertical Model 4000 vibrating wire strain gage that was mounted externally to the girder web as shown in Figure A-3 in an attempt to correlate the strain in the concrete to the strain in the rebar at the onset of web-shear cracking. The VWG was centered vertically on the web of the girder and attached in an upright position at the same location along the beam length as the internally instrumented stirrups. The flexural strain distribution through the girder depth, used to calculate the location of the neutral axis, was measured with four single horizontal Model 4000 vibrating wire strain gages that were vertically spaced and installed at multiple positions along the length of the beam. The four gages were installed on the bottom flange (one), web (two), and top flange (one), as shown in Figure A-4. Vertical girder deflections were measured along the span length during testing using LVDTs.

Shear tests were conducted on both ends of the single girder to investigate the variability in web-shear cracking behavior and maximum shear capacity. In the first test, the entire 30.75 ft. span was loaded to near failure at one end. The second end of the girder was tested with the support moved in (shorter span length) to avoid loading the damaged end, resulting in a span length of 22.5 ft. During each test, the single point load was applied at a distance of 9 ft 7 in. from the west support centerline. This equated to a shear span to depth ratio (a/d) of 2.5.

The specific instrumentation monitored during testing of the 30.75 ft span and test setup details are highlighted in Table A-3, Figure A-5, and Figure A-6. The three strain gages on all instrumented stirrups (A, B, C, D, E, F, G, H, I, and J) were monitored to investigate occurrence of yielding during the test. VWG box-type rosettes were applied at $0.5d_v$, d_v, and $2d_v$ on both ends of the beam, while a fourth box-type rosette was applied on the 21 ft 2 in. shear span at $4d_v$. Strains from these VWG box-type rosettes were used to calculate the vertical shear strain at the instrumented locations along the length of the girder. Three additional foil strain gage rosettes were evenly spaced through the web depth at two locations, d_v and $2d_v$, on ends of the girder to evaluate how the vertical shear strain varied through the depth of the girder web. The results of the foil strain gage rosettes were compared to those of the VWG box-type rosettes to investigate the accuracy of the two means of calculating shear strains. Girder deflections were measured at every sixth point

of the span length (L/6 points). The LVDTs were symmetric about midspan (location naming nomenclature shown in parentheses), utilizing a ±0.5 in. LVDT at the supports (E, W), ±1.0 in. LVDTs at L/6 (E1, W1), ±1.0 in. LVDTs at L/3 (E2, W2), and a ±3 in. LVDT at midspan (M). LVDTs placed at the support were used to measure the deflection of the elastomeric bearing pads. Four horizontal VWGs through the depth of the girder were installed at the same locations as the LVDTs, excluding the supports (E1, E2, M, W2, W1). Data from these horizontal VWGs were used to evaluate the neutral axis of the composite section during elastic loading.

Specific instrumentation monitored during testing of the 22.5 ft span and test setup details are highlighted in Table A-4, Figure A-7, and Figure A-8. Strain gages on stirrups A, B, C, D, and E were monitored. VWG box-type rosettes remained on the girder from the previous test at $0.5d_v$, d_v, $2d_v$, and $4d_v$. Three additional foil strain gage rosettes, evenly spaced through the web depth, remained on the girder from the previous test at d_v and $2d_v$. Girder deflection was not measured during testing of the 22.5 ft span length. Four horizontal VWGs through the depth of the girder remained on the beam from the previous test at the original L/6, L/3, and L/2 locations (where L = 30.75 ft).

Test Setup

There were two main objectives of the single girder testing. First, it was important to see how various types of instrumentation performed in a laboratory setting, particularly as the structure cracked and approached ultimate capacity. Second, it was important to observe the behavior of a girder similar to those in the laboratory bridge. Specifically, care was taken to record the lower bound values of applied load for initial observed web-shear cracking, initial observed flexural cracking, and ultimate shear failure in a single beam with no ability for load distribution to adjacent girders.

The single girder was tested in two separate configurations such that both ends of the girder failed in web-shear. The applied load and boundary conditions were similar for each test while variations were made in the instrumentation and in the simply-supported span length. During both tests, a single point load was applied to the specimen using the 600 kip MTS Model 311 Material Test Frame. The hydraulic actuator was controlled with an MTS FlexTest IIM Digital Controller that was operated in displacement control during

each test. Point load boundary conditions consisted of a clevis load pin attached to the MTS piston which allowed in-plane rotation along the length of the beam. A 5 ft long W14x159 was bolted to the clevis load pin and grouted to the girder deck to create a uniform loading surface across the entire flange. Girder boundary conditions at the ends of the span consisted of one W14x120 support beam perpendicular to the girder that was clamped to two steel beams, made of built-up channel and plate sections, that sat on the laboratory strong floor and were oriented parallel to the span length as shown in Figure A-9. The girder sole plates rested on ½ in. x 12 in. x 22 in. elastomeric bearing pads which were supported by 1 in. x 14 in. x 24 in. steel plates that were grouted to the W14x120 support beams to ensure a level bearing surface. All grout used to create the boundary conditions was USG Ultracal 30 gypsum cement mixed by weight at a ratio of 38 parts water to 100 parts gypsum cement.

The first single girder test was focused on the end of the girder that was oriented toward the live end in the prestressing bed during construction. The girder was configured in the 600 kip MTS test frame to have a simply-supported span of 30 ft 9 in. and the single point load was applied at a distance of 9 ft 7 in. from the west support centerline. This equated to a shear span to depth ratio (a/d) of 2.5. This shear span to depth ratio was the same as that studied during inelastic bridge testing. The remaining 21 ft 2 in. formed a larger, secondary shear span. Test setup details are shown in Figure A-5 and Figure A-6.

The second test on the single girder was focused on the opposite end of the girder. Two holes were cored through the composite deck and Girder 5 was rotated with chain slings such that the end of the girder that had been oriented toward the dead end, in the prestressing bed during construction, was placed to the west of the 600 kip MTS test frame. The girder was configured in the 600 kip MTS test frame to have a simply supported span length of 22.5 ft and the single point load was applied at a distance of 9 ft 7 in. from the west support centerline. This equated to a shear span to depth ratio (a/d) of 2.5. The remaining 12 ft 11 in. span formed a larger, secondary shear span. Test setup details are shown in Figure A-7 and Figure A-8.

A.2 Elastic and Inelastic Testing Results

The single girder was tested to investigate the behavior where there was no opportunity for load distribution to other members as was the case for the laboratory bridge structure. Both ends of the girder were tested as described in the following sections. Shear loads associated with initial observed web-shear cracking, initial observed flexural cracking, and ultimate shear failure were recorded.

Single Girder Loading Histories

The displacement controlled loading history for testing of the 30.75 ft span is given in Table A-5. The vertical end reaction was calculated from statics assuming the distance between the support and the point load was 9 ft 7 in. (a/d = 2.5). The testing procedure, completed on January 28, 2014, is summarized as follows. Load was applied in 25 kip increments up to 175 kips to record strain and displacement behavior while the beam was in the uncracked elastic range. There were pauses in the loading at each increment to record VWG strains, but the voltage data were collected continuously through the loading history. The first crack observed in the girder was a web-shear crack that occurred at approximately 180 kips of applied load.

After the initial web-shear crack was detected, but not traced with permanent marker, the girder applied load was reduced to 10 kips to determine if the web-shear crack remained visible with near zero applied load. The width of web-shear cracks decreased but were still observable at an unloaded state; this corroborated with results from the laboratory bridge discussed in Section 5.4.1.1. Because bridge superstructures are unlikely to be inspected during possible overload events, it is important to determine if existing web-shear cracks are visible after removing the load that caused the distress. This is particularly important to consider for prestressed concrete girder bridges that have a low inventory or operating rating factor for shear. If the structure shows no sign of shear distress under normal traffic loads during inspection, they are often deemed to be in good condition, and in accordance with the AASHTO Manual for Bridge Evaluation (2011), the resulting shear rating may be neglected by the bridge owner. The MBE states that "in-service concrete bridges that show no visible signs of shear distress need not be checked for shear when rating for the design load or legal loads." Web-shear cracks remained visible after

unloading in the region with a large stirrup spacing of 24 in. These results were consistent with web-shear crack behavior observed by Mathys et al. (2014); Mathys et al. found that web-shear cracks in areas with widely spaced stirrups (approximately 24 in.) were still visible upon unloading, and web-shear cracks in areas with closely spaced stirrups (approximately 8 in.) were not visible upon unloading.

After observing the first web-shear crack, testing was continued and cracks were marked with permanent marker to indicate the current applied load at each load pause. The initial flexural crack was observed under the point load at approximately 235 kips. Web-shear cracking and damage increased as load was applied beyond 300 kips applied load. Web-shear crushing occurred after reaching a peak load of approximately 340 kips (234 kips shear in the short shear span). Following web-shear failure, the applied load dropped quickly due to a loss of girder stiffness and the beam was unloaded in displacement control. The flexural capacity of 2,860 kip-ft was not approached during testing. Crack patterns and web-shear deterioration can be seen in Figure A-10 which includes open circles on stirrups F through J that designate strain gage locations on a single leg of the vertical reinforcement. Solid circles in Figure A-10 indicate measured strain values in excess of the measured yield strain. Cracks observed during testing of the 30.75 ft span are shown in Figure A-10 as sketched lines. The region of the girder that crushed at ultimate failure is outlined with the hatched regions.

The displacement controlled loading history for testing of the 22.5 ft span is given in Table A-6. The vertical end reaction was calculated from statics assuming the distance between the support and the point load was 9 ft 7 in. (a/d = 2.5). The testing procedure, completed on February 3, 2014, is summarized in the following sequence. Load was applied in 25 kip increments up to 175 kips to record linear elastic strain and displacement behavior. The first crack observed in the girder was a web-shear crack that occurred at an applied load of approximately 250 kips. After the initial web-shear crack was detected, testing was continued (no unload, reload sequence) and cracks were marked with permanent marker to indicate the current applied load at all subsequent points of interest. The initial flexural crack was observed under the point load at approximately 288 kips applied load (165 kips shear in the short shear span). Web-shear cracking and damage increased as load was applied beyond 400 kips. Web-shear crushing occurred after reaching

a peak load of approximately 456 kips. Following web-shear failure, the applied load dropped quickly due to a loss of girder stiffness and the beam was unloaded in displacement control. Crack patterns and web-shear deterioration is shown in Figure A-11. Cracks from testing the 30.75 ft span are not shown in Figure A-11; no web-shear cracks formed in the girder web at the opposite end of the beam during testing of the 30.75 ft span, but some flexural cracks formed on the opposite side of midspan during testing of the 30.75 ft span.

Shear Capacity and Measured Demand

Nominal shear capacity of the 30.75 ft span was calculated with measured material properties using Section 9.20 of the AASHTO Standard Specifications (1989) with 1991 Interim Revisions at various locations along half of the symmetric girder length. The effects of the reduced stirrup spacing at midspan was taken into account. The ultimate shear force, consisting of unfactored dead and peak live load, was plotted with respect to the predicted shear capacity and the individual components of capacity in Figure A-12. Figure A-12 also indicates the shear capacity with an over-strength factor of 1.3 as discussed in section 4.2.

Figure A-12 shows that the ultimate applied shear force (including an estimate of dead load as discussed in Section 5.4.4 for the laboratory bridge) exceeded the predicted shear capacity between 2 and 10 ft from the end of the girder. Figure A-13 and Figure A-14 highlight the ultimate web-shear cracking pattern prior to and after web-shear crushing failure, respectively. The applied shear force (with an estimate of the dead load) exceeded the calculated web-shear cracking component of shear, V_{cw}, along all of the 9 ft 7 in. shear span. Figure A-12 shows that the applied shear force also slightly exceeded the calculated web-shear cracking capacity in the 21 ft 2 in. shear span, however, no web-shear cracking was noted in that shear span during the testing procedure. During testing, flexural cracks close to the load point turned into flexure-shear cracks as shown in Figure A-10 and Figure A-11.

Table A-7 summarizes the observed web-shear crack angle, web-shear cracking capacity, and ultimate shear capacity at the critical section compared to the values predicted using the AASHTO Standard Specifications (1989), nominal design material properties, and transformed section properties with a deck width equal to 4.5 ft. The critical section

for shear was calculated at half the composite height, $h_c/2$, away from the face of the support. The ratio of observed web-shear cracking to predicted web-shear cracking was 1.13. The ratio of applied shear force to nominal shear capacity was 1.60.

Shear strains were measured during testing with VWG box-type rosettes at $0.5d_v$, d_v, and $2d_v$ on both shear spans and a fourth box-type rosette at $4d_v$ on the 21 ft 2 in. shear span. Three additional foil strain gage rosettes were evenly spaced through the web depth at d_v and $2d_v$ on both shear spans. Figure A-15 shows the VWG and foil rosettes installed at various locations.

Shear forces due to the applied loads were calculated from rosette shear strains using a measured girder concrete modulus of elasticity of 4,300 ksi and measured girder compressive strength of 6,900 psi. The measured compressive strength of the deck (8,400 psi) was used to calculate the modulus of elasticity of the deck (5,600 ksi) using the equation developed by Pauw (1930). A transformed composite moment of inertia of 228,000 $in.^4$ (based on an effective deck width of 4.5 ft) was calculated by converting the deck concrete and prestressing strands to girder concrete. Details regarding the amount of prestressing steel are shown in Figure 4-2. Figure A-16 and Figure A-17 highlight the shear force calculated from the VWG box-type rosettes strain data (as described in Section 5.2) in the 9 ft 7 in. and 21 ft 2 in. shear spans, respectively. The figures show that shear forces calculated from VWG box-type rosette measurements matched the shear due to the applied load calculated as the reaction based on statics during elastic loading. Matching the calculated shear force and reaction based on statics indicated that it would be possible to calculate the shear force in the laboratory bridge or field bridges from the box-type rosettes. The data shown in Figure A-16 and Figure A-17 do not contain information about the dead load shear; the external VWG instrumentation was applied to the girder after casting the deck and the theoretical shear was calculated as the reaction due to live load only. The VWG data was not used after the first web-shear crack was observed in the beam, at approximately 124 kips of shear force, and cracking propagated through the strain gage areas.

Figure A-18 and Figure A-19 show that the shear force calculated from the foil rosettes did not match the theoretical applied shear calculated as the reaction based on statics. The foil rosette data was unreliable for elastic loading and became more scattered

during inelastic loading. This indicated that the FRA-6-11-5LT foil strain gage rosettes, with a 0.25 in. gage length, were not a reliable source for capture of shear strain measurements on a specimen with ¾" maximum aggregate size. This was not unexpected as many strain gage manufacturers suggest using a gage with a gage length of at least four times the maximum aggregate size. However, gages of that length are extremely difficult to install with constant pressure on a vertical face. To collect quality data during testing of the laboratory bridge, foil rosette gages with a gage length of approximately 1-1/8 in. were used. These gages were straightforward to install and provided quality data, but their gage length was not four times the ¾ in. aggregate size (3 in.) which was recommended by the manufacturer.

Stirrup Yielding

Figure A-10 shows that eight of the 15 stirrup strain gages within the shear span exceeded the predicted yield strain during the 30.75 ft span test and Figure A-11 shows that seven of the 15 stirrup strain gages within the shear span exceeded the yield strain during the 20.5 ft span test. The predicted yield strain, ε_y, of 0.0024 was calculated based on the measured stirrup yield strain as provided in Table 4-12. Figure A-20 through Figure A-22 show the shear in short shear span due to applied load versus stirrup strain for stirrups I, H, and G during testing of the 30.75 ft span. Figure A-23 through Figure A-25 show the shear in short shear span due to applied load versus stirrup strain for stirrups B, C, and D. Data in each figure indicated the onset of yielding from most of the strain gages on these six stirrups. Prior to observation of web-shear cracking, the strain gages indicated near zero tensile strain in the stirrups. Variation from approximately zero tensile strain in the gages did not always occur simultaneously with the observed web-shear cracking during testing of the 20.5 ft span. There could have been some permanent strain in the stirrups during the 20.5 ft span test that was generated during the initial 30.75 ft span test, but no web-shear cracks were observed in the opposite end of the span during the initial 30.75 ft span test. However, most of the strain gages recorded yield strain prior to the peak applied shear.

The data in Figure A-20 through Figure A-25 show that the maximum strains measured in many of the stirrups during testing exceeded both the yield strain and the specified strain offset value of 5,000 με, discussed in Section 4.4.1.6. Generally, stirrups

that recorded the smallest strain readings were located in disturbed regions of the girders (as shown in Figure A-10 and Figure A-11). These locations of discontinuity are located near the abutment reactions and the applied load where effects of local compressive stress do not promote formation of cracks and large tensile strains in the vertical reinforcement. Figure A-10 and Figure A-11 reinforce this concept by indicating that gages typically did not reach the yield strain unless a web-shear crack crossed a stirrup near a gage. The initial test on the single girder (30.75 ft span) was ended after web-shear failure to preserve the girder for the second test. No web-shear cracks formed in the girder web at the opposite end of the beam during testing of the 30.75 ft span; any permanent strain locked into the stirrups from the initial test was not accounted for when analyzing data from the second test (20.5 ft span).

Girder Neutral Axis

The neutral axis (NA) was determined experimentally for the 30.75 ft span single girder test using the four horizontal VWGs through the beam depth at the same locations as the LVDTs. The neutral axis was determined experimentally for the 22.5 ft span single girder test at the E1, E2, and M locations remaining from the 30.75 ft span test. The neutral axis height, measured from the bottom of the girder, was calculated by determining the y-intercept of a line plotted with four data points from each of the four VWGs on the girder bottom flange (BF), bottom web (BW), top web (TW), and top flange (TF). Figure A-26 through Figure A-30 show how the neutral axis varied at each of the instrumented locations for the 30.75 ft span, and Figure A-31 through Figure A-33 show how the neutral axis varied at each of the instrumented locations for the 22.5 ft span test. Data from each test were compared to the theoretical neutral axis for three different effective deck widths (b_{eff} = 4.5 ft, 3.5 ft, and 2.5 ft). The theoretical neutral axis height values were calculated using transformed composite section properties at mid-length of the girder based on measured modulus of elasticity at the time of testing. The composite section at service load levels included transformation of the strands to girder concrete (n = 6.63), the deck steel to deck concrete (n = 5.23), and the deck and haunch to girder concrete (n = 1.28).

Table A-8 and Table A-9 summarize the variation of experimentally determined neutral axis values for each longitudinal VWG location at each elastic load point for the

30.75 ft span and the 22.5 ft span, respectively. Table A-10 shows the theoretical neutral axis height and transformed composite moment of inertias for different effective deck widths (applicable to both tests). The average neutral axis height from the bottom of the girder, in the middle of the 9 ft 7 in. shear span, was 28.8 in. for the 30.75 ft span (at W1) and 25.6 in. for the 22.5 ft span (at E1). These values corresponded with an approximate composite deck width of 3 ft (for the 30.75 ft span) and 2 ft (for the 22.5 ft span) instead of the 4.5 ft deck width as constructed.

Girder Vertical Displacement

Seven LVDTs were placed symmetrically about midspan of the girder for the 30.75 ft span test, but no LVDTs were used during testing of the 22.5 ft span to expedite the testing process. Two of the seven LVDTs (E, W), placed at the supports, were used to measure the deflection of the elastomeric bearing pads. Displacement data for the remaining five LVDTs (E1, E2, M, W2, W1) were calculated by eliminating both rigid body displacement (using an average of both E and W bearing pad data) and rigid body rotation (using the span length and difference between E and W bearing pad data). Figure A-34 illustrates the applied shear in the 9 ft 7 in. shear span versus the displacement measured by the LVDTs.

Figure A-34 shows that testing of the 30.75 ft span ended when a maximum shear of 243 kips was applied. The maximum live load displacement measured prior to a significant load drop was approximately 1.17 in. at location W2. Displacements shown in Figure A-34 remained linear with respect to load to the point where the initial web-shear crack was observed (applied shear of 124 kips) and then began to exhibit non-linear behavior, particularly after the first flexural crack was observed, at an applied shear of 162 kips. This behavior indicated a trilinear response which included: uncracked elastic, cracked elastic after web shear cracking, and cracked inelastic after flexural cracking.

Figure A-35 shows the displacement profile for five applied shear load steps in the linear elastic range of behavior for the 30.75 ft span. A composite moment of inertia equal to 127,000 in.^{4} was calculated using the known displacement profile, the standard equations for displacement at any position due to a single point load, and a modulus of elasticity of 4331 ksi measured at the time of single girder testing. The effects of dead load were not

considered in this calculation. This moment of inertia value corresponded to a deck width of approximately 1 ft (calculated with transformed sections), which was also the width of the top flange of the beam.

Conclusions and Comparison to Code Predictions

The main objective of the single girder testing was to capture the load and applied shear for the following events: initial observed web-shear cracking, initial observed flexural cracking, and ultimate failure (including observation of the failure mode). These values were compared to the predicted values using the AASHTO Standard Specifications (1989) with 1991 Interim Revisions to determine the over-strength factor. Results from testing of the single girder also served as a baseline for behavior of the laboratory bridge assuming a shear distribution factor of 1.0 because the single girder was unable to distribute the applied load in a bridge system. Table A-11 shows both the applied load and applied shear at which web-shear cracking, initial flexural cracking, and ultimate failure were observed. For comparison to values predicted using the AASHTO Standard Specifications, the following were predicted: web-shear cracking would begin at an applied shear due to both dead and live load of approximately 114 kips (when $V_{LL}+V_{DL} > V_{cw}$), flexural cracking would begin at an applied shear of approximately 158 kips (when $M_{LL} > M_{cr}$), and ultimate shear failure would occur at an applied shear due to both dead load and live load of 200 kips ($V_{LL}+V_{DL} > 1.3V_n$ using $V_s = A_v f_y * d/s$). For comparison, ultimate shear failure was predicted to occur at an applied shear due to both dead and live load of approximately 255 kips using $V_{LL}+V_{DL} > 1.3V_n$ and $V_s = A_v f_y * 2d/s$. Using a multiplier of two on the d/s term indicates that the primary web-shear crack will cross more stirrups and that the crack angle was more shallow than the implicit 45 degrees (e.g., cotangent of 26.5 degrees equals 2.0). The value of two was selected using engineering judgement to investigate an upper bound. A value of 1.8 may also have been appropriate based on the upper limit of the cotθ term using in the AASHTO LRFD Specifications (2010).

Table A-1. Single Girder Deck Concrete Mix Design

	Specified	Truck 1
	Qty / cy	Batch Qty
Mix Name	7054P	7054P
Batch Date/Time	10/10/2005	11/5/12 8:28 AM
Lafarge at Davenport, IA Type I Cement (lb)	750	3930
Aggregate Industries 3/4 in. Aggregate (lb)	1740	9200
Aggregate Industries Larson Plant Sand (lb)	1162	6860
Water (gal)	33.4	165
BASF MB AE 90 Air Entrainer (oz)	3.2	32
BASF Glenium 7500 HRWR (oz)	45	240
BASF Polyheed 1020 MRWR (oz)	11	50
Cylinder Count	----	20
Flexure Beam Count	----	0

Table A-2. Fresh and Hardened Single Girder Deck Concrete Properties Measured at the Time of the Initial Single Girder Test (30.75 ft Span)

	Specified	Truck 1
Mix Name	7054P	7054P
Batch Date/Time	----	11/5/12 8:28 AM
Air (%)	6.0 ± 1.5	----
Slump (in.)	7.0	8.5
W/C Ratio	0.37	0.35
Unit Wt. (pcf)	144.5	141.5
Average Compressive Strength of Three Cylinders, f'_c (psi)		
28 day	7,000	7,504
Single Girder Test	----	8,414
Average Split Tensile Strength of Three Cylinders, f'_t (psi)		
Single Girder Test	----	657

Table A-3. Single Girder 30.75 ft Span Instrumentation Plan

Instrument Type	Instrument Location	Shear Span / Length
Stirrup foil gages (3 on ea.)	A, B, C, D, E, F, G, H, I, J	West / 9 ft 7 in.
VWG box-type rosette	$0.5d_v$, d_v, $2d_v$	West / 9 ft 7 in.
	$0.5d_v$, d_v, $2d_v$, $4d_v$	East / 21 ft 2 in.
Vertical single VWG at instrumented stirrup	Stirrup F, G, H, I, J	West / 9 ft 7 in.
	Stirrup A, B, C, D, E	East / 21 ft 2 in.
Four single horizontal VWGs through girder depth	$L/6$, $L/3$, $L/2$	West / 9 ft 7 in.
	$L/6$, $L/3$	East / 21 ft 2 in.
Three foil strain gage rosettes on web	d_v, $2d_v$	West / 9 ft 7 in.
	d_v, $2d_v$	East / 21 ft 2 in.
Seven LVDTs	Supports and every $L/6$	----

Table A-4. Single Girder 22.5 ft Span Instrumentation Plan

Instrument Type	Instrument Location	Shear Span / Length
Stirrup foil gages (3 on ea.)	Stirrup A, B, C, D, E	West / 9 ft 7 in.
VWG box-type rosette	$0.5d_v$, d_v, $2d_v$, $4d_v$	West / 9 ft 7 in.
Vertical single VWG at instrumented stirrup	Stirrup A, B, C, D, E	West / 9 ft 7 in.
Four horizontal VWGs through girder depth	$L/6$, $L/3$, $L/2$	West / 9 ft 7 in.
Three foil strain gage rosettes on web	d_v, $2d_v$	West / 9 ft 7 in.

Table A-5. Single Girder 30.75 ft Span Loading History

Applied Load (k)	Shear due to Applied Load (k)	Load Rate (in. / min)	Notes:
25	17	0.01	Linear elastic data points
50	34		
75	52		
100	69		
125	86		
150	103		
175	120		
180	124	0.005	Web-shear cracking observed
10	7	0.04	Unload
180	124	0.04	Reload
200	138	0.01	
225	155		
235	162		Flexural cracking observed
250	172		
275	189		
300	207	0.02	
340	234	0.04	Web crushing

Table A-6. Single Girder 22.5 ft Span Loading History

Applied Load (k)	Shear due to Applied Load (k)	Load Rate (in. / min)	Notes:
25	14	0.01	Linear elastic data points
50	29		
75	43		
100	57		
125	72		
150	86		
175	100		
200	115		
225	129		
250	144		Web-shear cracking observed
275	158		
288	165		Flexural cracking observed
300	172		
325	187		
350	201	0.02	
375	215		
400	230	0.04	
456	262		Web crushing

Table A-7. Observed versus Predicted Shear Capacity for 30.75 ft Span

Behavior	Observed	Predicted	Observed / Predicted
Critical section from face of support (in.)	----	23	----
Web-shear crack angle (deg)	35	45	----
Web-shear cracking, V_{cw} (k)	124	110	1.13
Steel shear capacity, V_s (k)	----	43	----
Ultimate shear capacity (k)	245	153	1.6

Table A-8. Experimentally Measured Neutral Axis Height for 30.75 ft Span

Applied Shear (k)	W1 NA (in.)	W2 NA (in.)	M NA (in.)	E2 NA (in.)	E1 NA (in.)	Row Avg:
51	28.5	30.0	28.9	27.4	32.3	29.4
68	28.6	30.1	29.0	27.8	31.8	29.5
85	28.7	30.1	28.8	27.9	31.4	29.4
102	28.9	30.0	29.0	28.1	29.9	29.2
119	29.4	30.2	29.1	28.3	30.8	29.6
Column Avg:	28.8	30.1	29.0	27.9	31.2	29.4

Table A-9. Experimentally Measured Neutral Axis Height for 22.5 ft Span

Applied Shear (k)	M NA (in.)	E2 NA (in.)	E1 NA (in.)	Row Avg:
42	24.9	30.8	26.1	27.3
57	24.5	30.0	25.4	26.6
71	24.4	29.8	25.3	26.5
85	24.4	30.0	25.6	26.7
100	24.5	30.1	25.7	26.8
Column Avg:	24.5	30.2	25.6	26.8

Table A-10. Theoretical Neutral Axis Heights for 30.75 and 22.5 ft Span Length Tests

Effective Width (ft)	NA Height (in.)	$I_{trans\text{-}comp}$ (in.^{4})
b_{eff} = 4.5	31.5	228,651
b_{eff} = 4.0	30.8	220,791
b_{eff} = 3.5	29.9	211,810
b_{eff} = 3.25	29.5	206,817
b_{eff} = 3.0	29.0	201,434
b_{eff} = 2.5	27.9	189,296
b_{eff} = 2.0	26.6	174,884
b_{eff} = 1.5	25.0	157,470
b_{eff} = 1.0	23.0	135,977

Table A-11. Observed Cracking and Failure Loads for Single Girder Tests

Behavior	30.75 ft Span		22.5 ft Span		AASHTO Std.
	Applied Load	Applied Shear	Applied Load	Applied Shear	Applied Shear
Web-shear cracking (k)	180	124	250	144	114
Flexural cracking (k)	235	162	288	165	158
Ultimate shear failure (k)	340	234	456	262	200

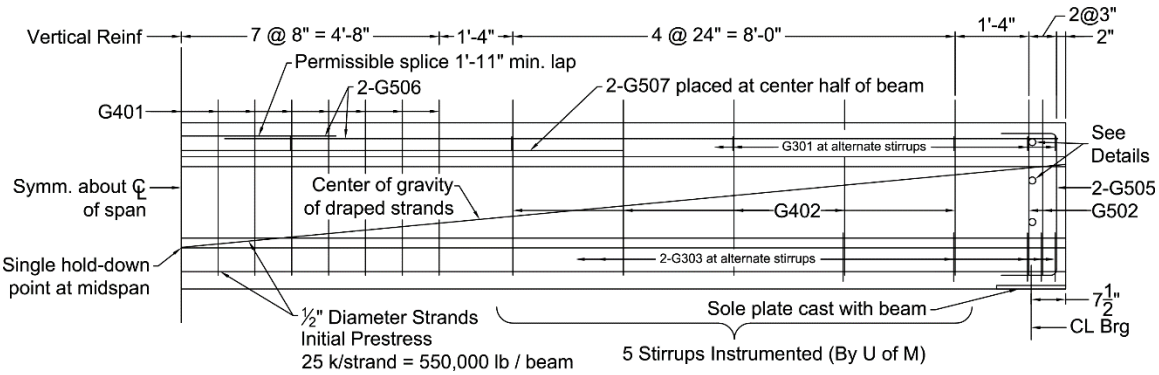

Figure A-1. Single Girder Half Elevation

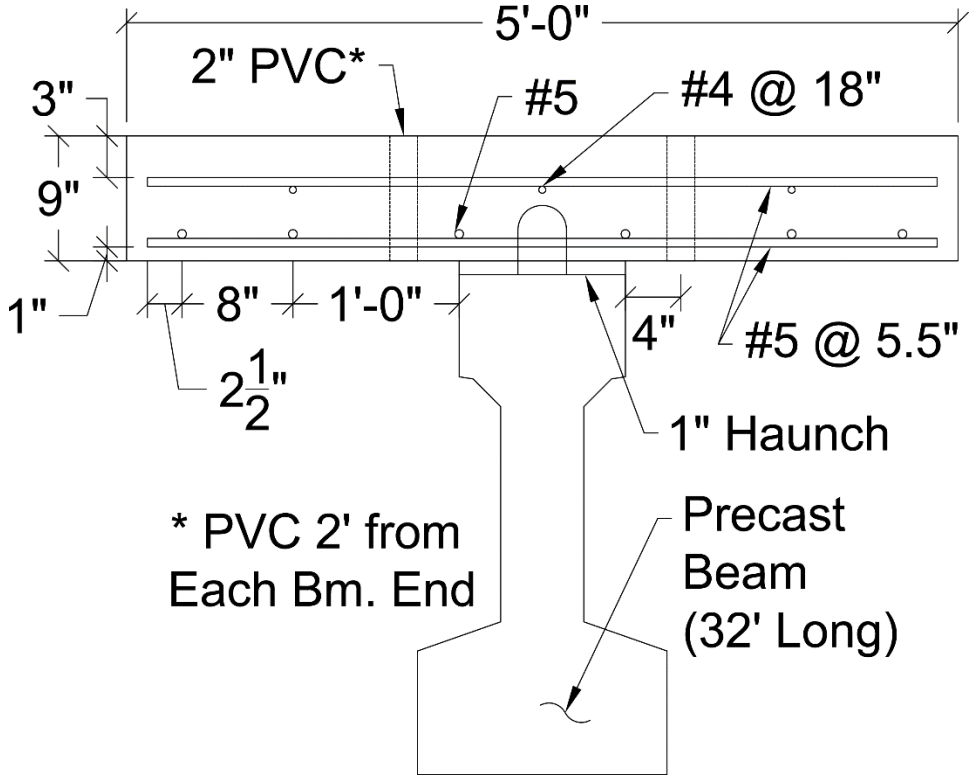

Figure A-2. Single Girder Deck Transverse Cross Section

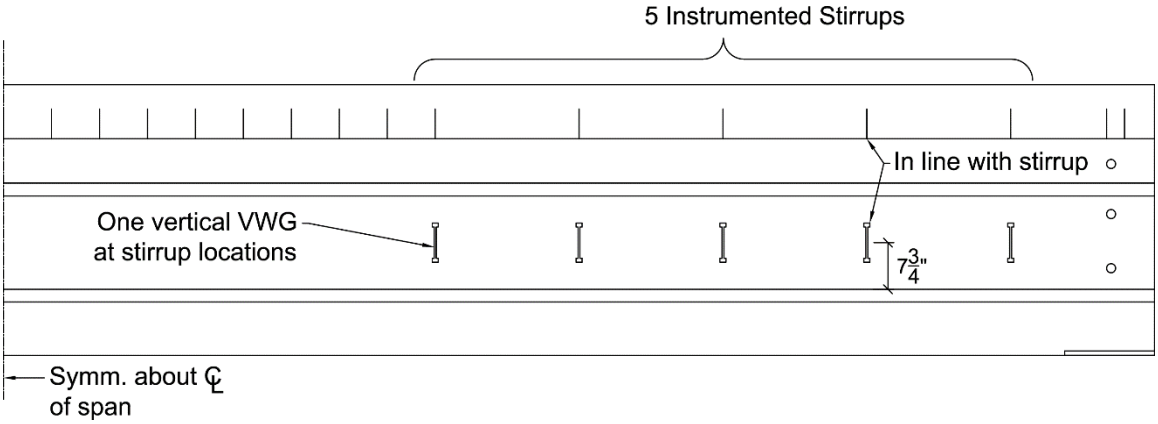

Figure A-3. Half Elevation with Vertical Single VWG Positions

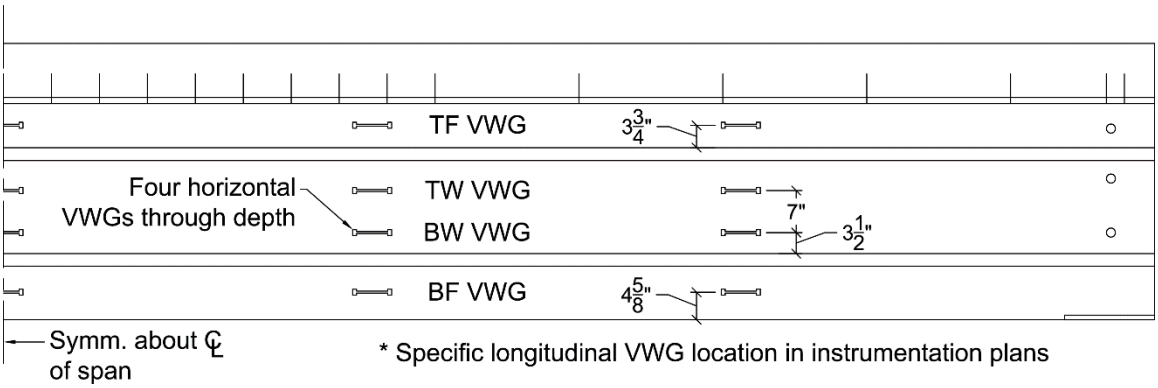

Figure A-4. Half Elevation with Four Horizontal VWG Positions

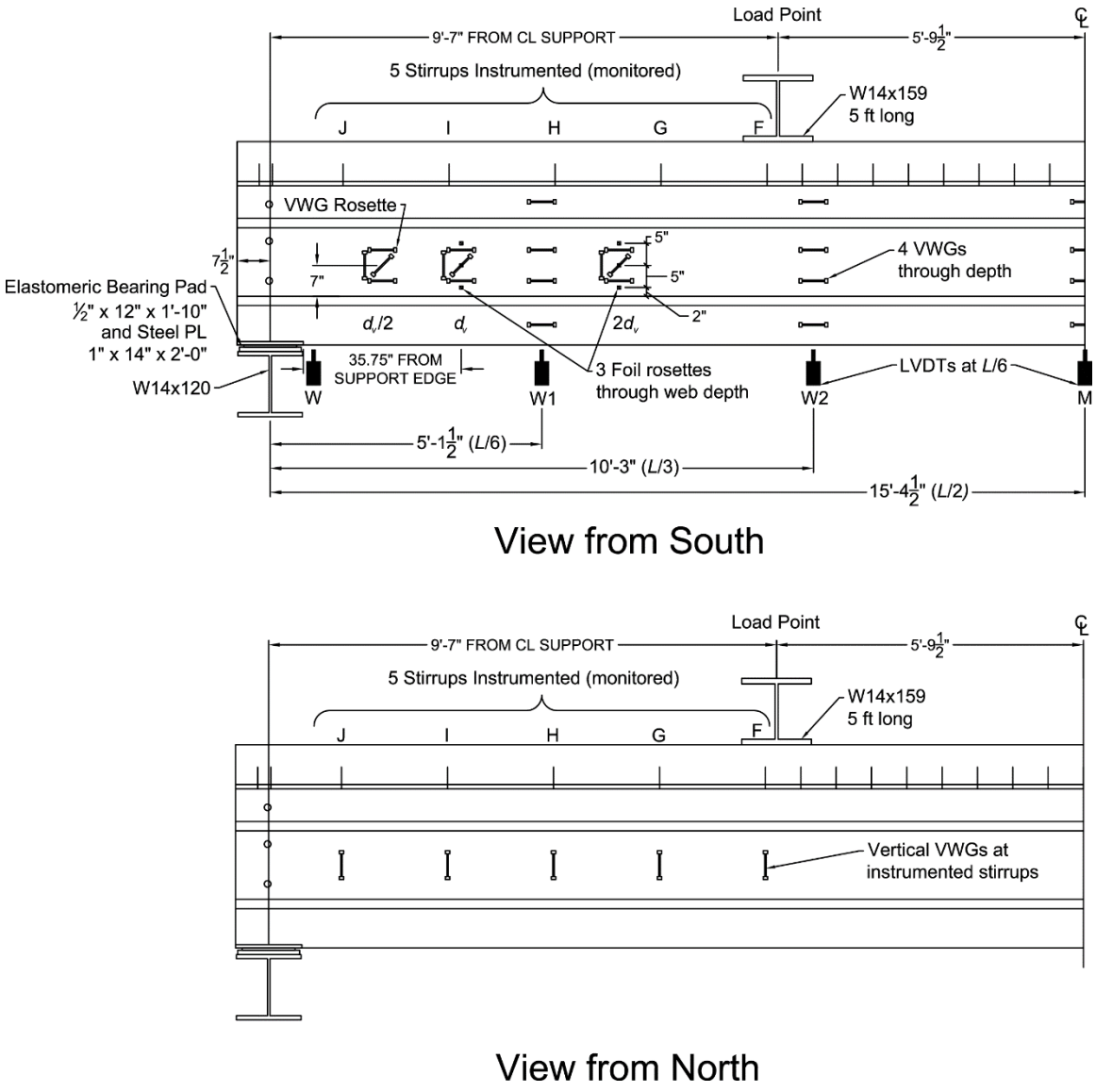

Figure A-5. Single Girder 30.75 ft Span West Shear Span Instrumentation

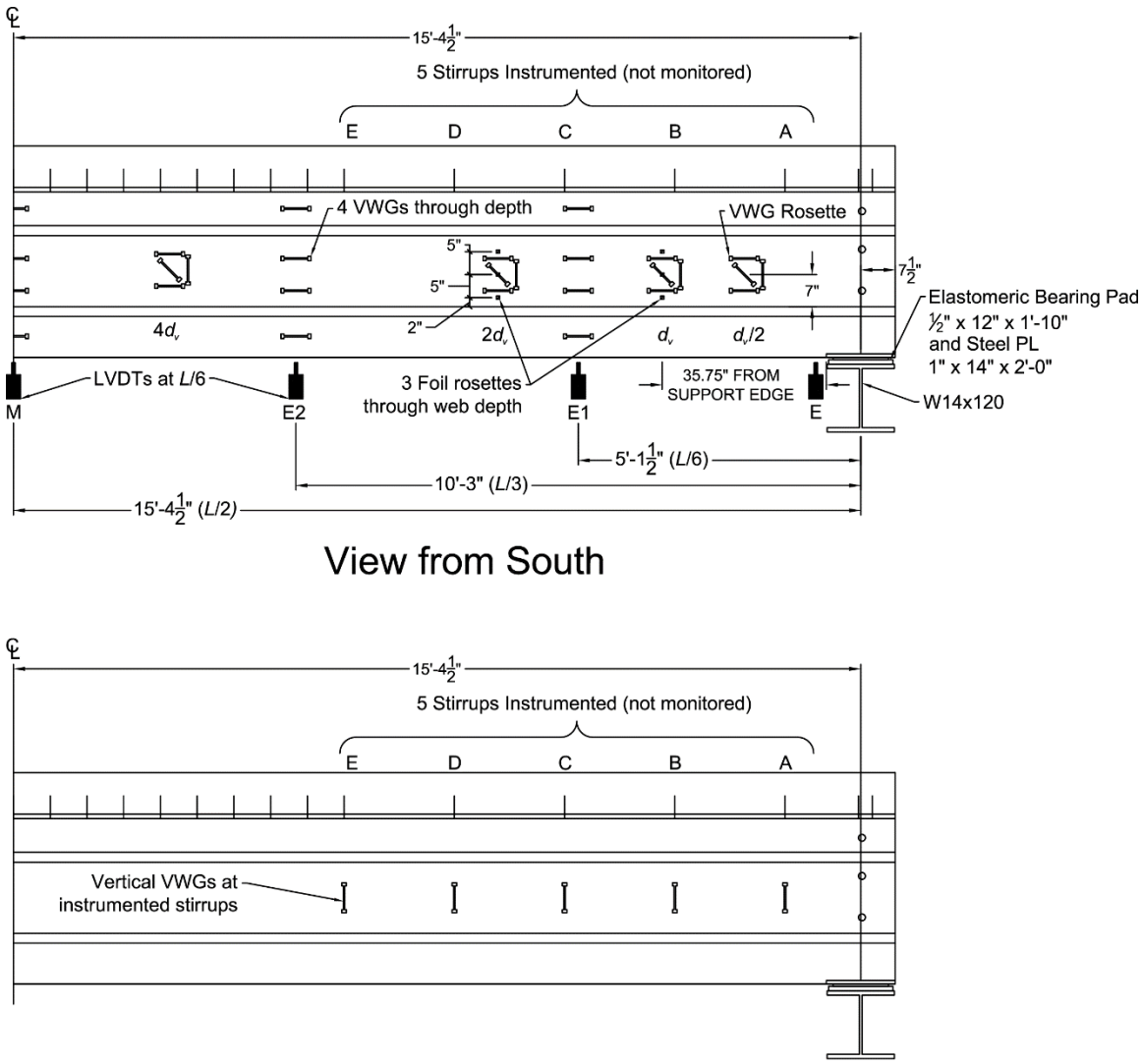

Figure A-6. Single Girder 30.75 ft Span East Shear Span Instrumentation

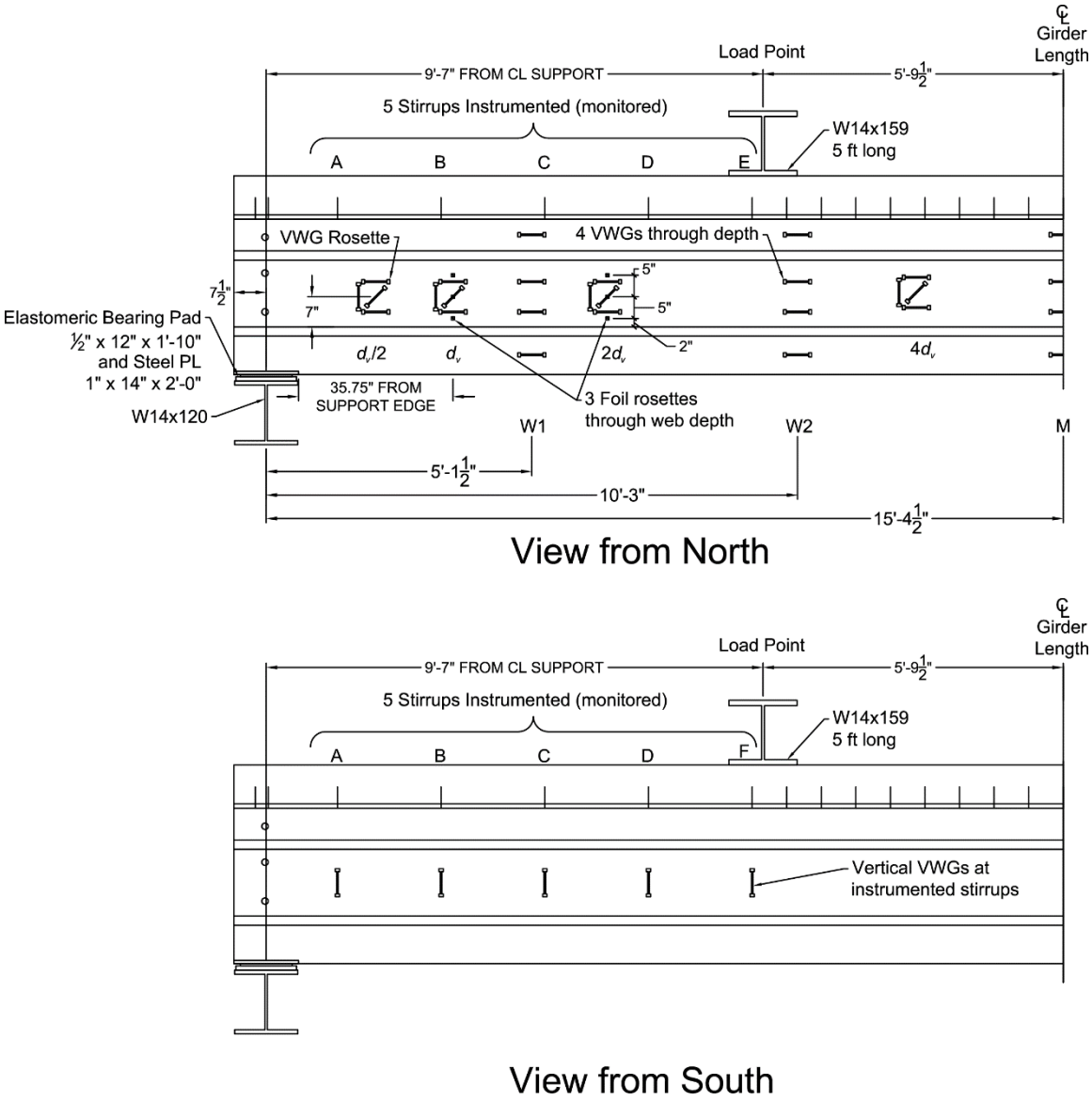

Figure A-7. Single Girder 22.5 ft Span West Shear Span Instrumentation

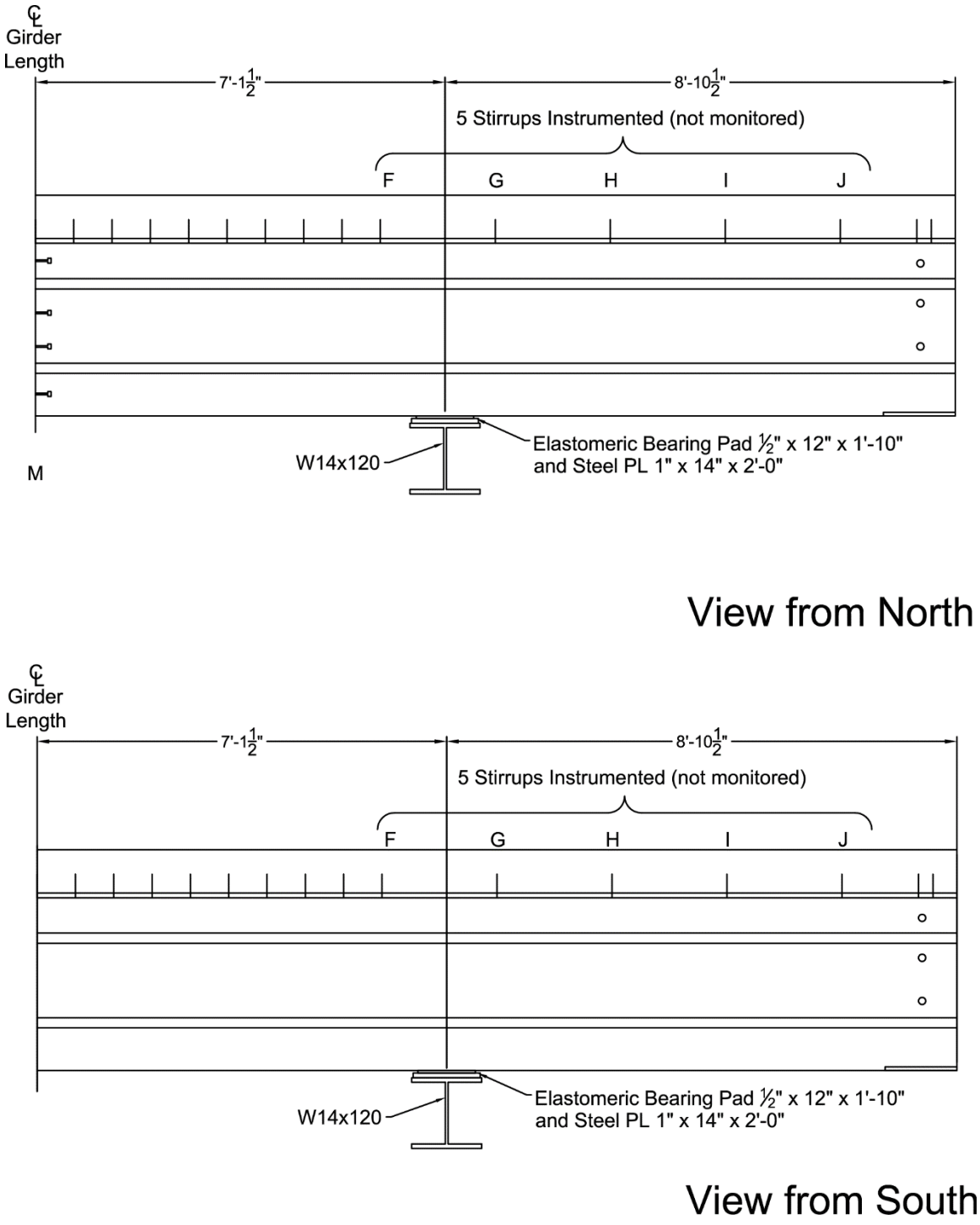

Figure A-8. Single Girder 22.5 ft Span East Shear Span Instrumentation

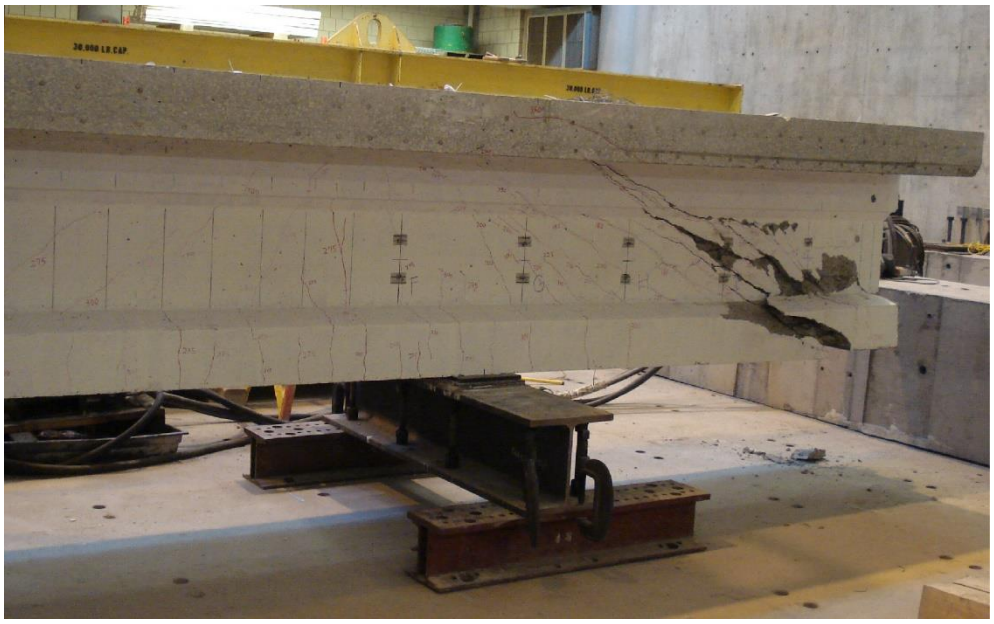

Figure A-9. Single Girder Support Configuration

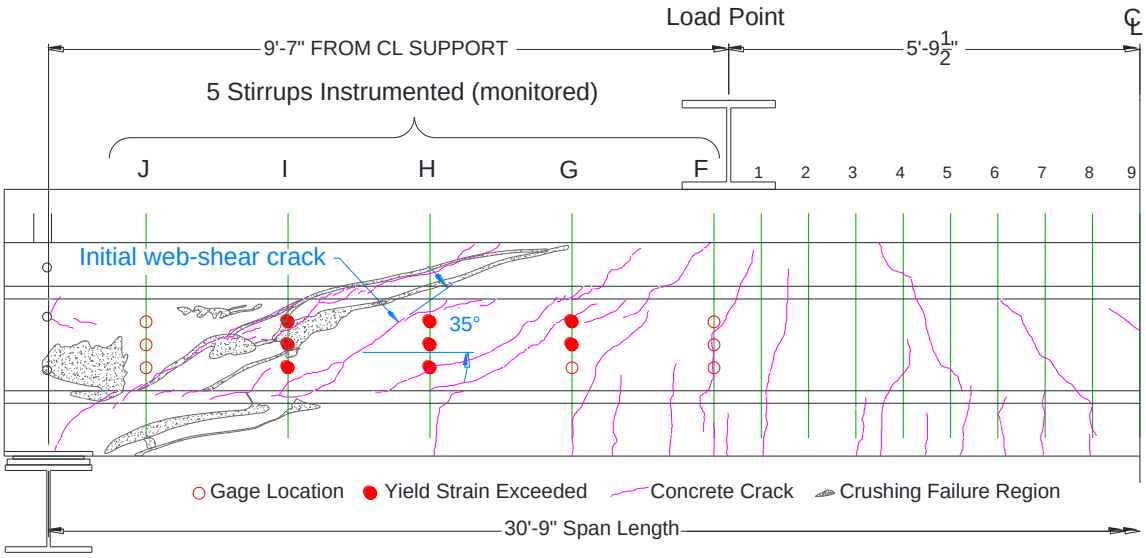

Figure A-10. Single Girder 30.75 ft Span West Shear Span Cracking and Failure

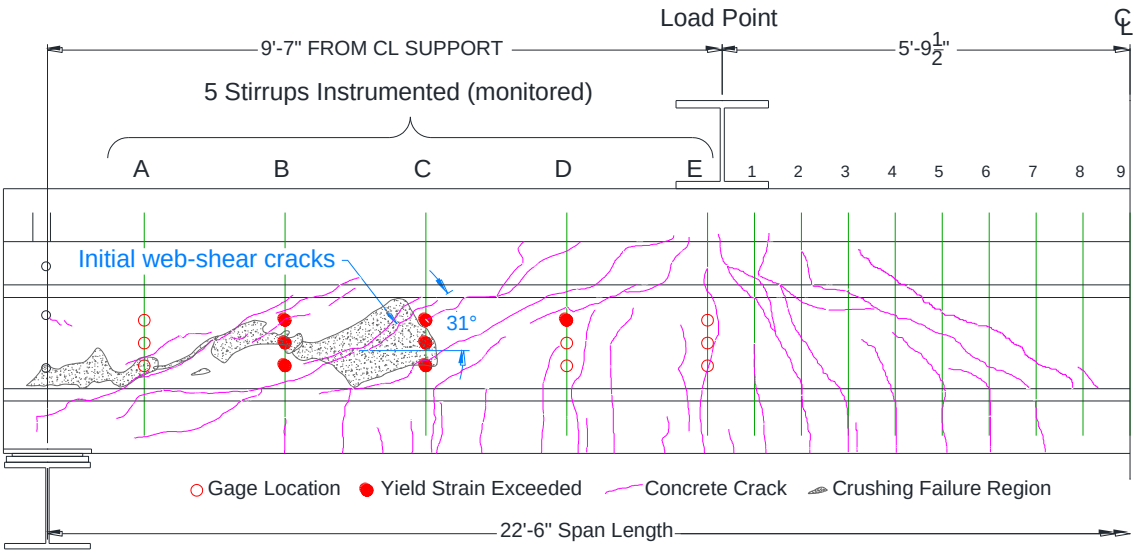

Figure A-11. Single Girder 22.5 ft Span West Shear Span Cracking and Failure

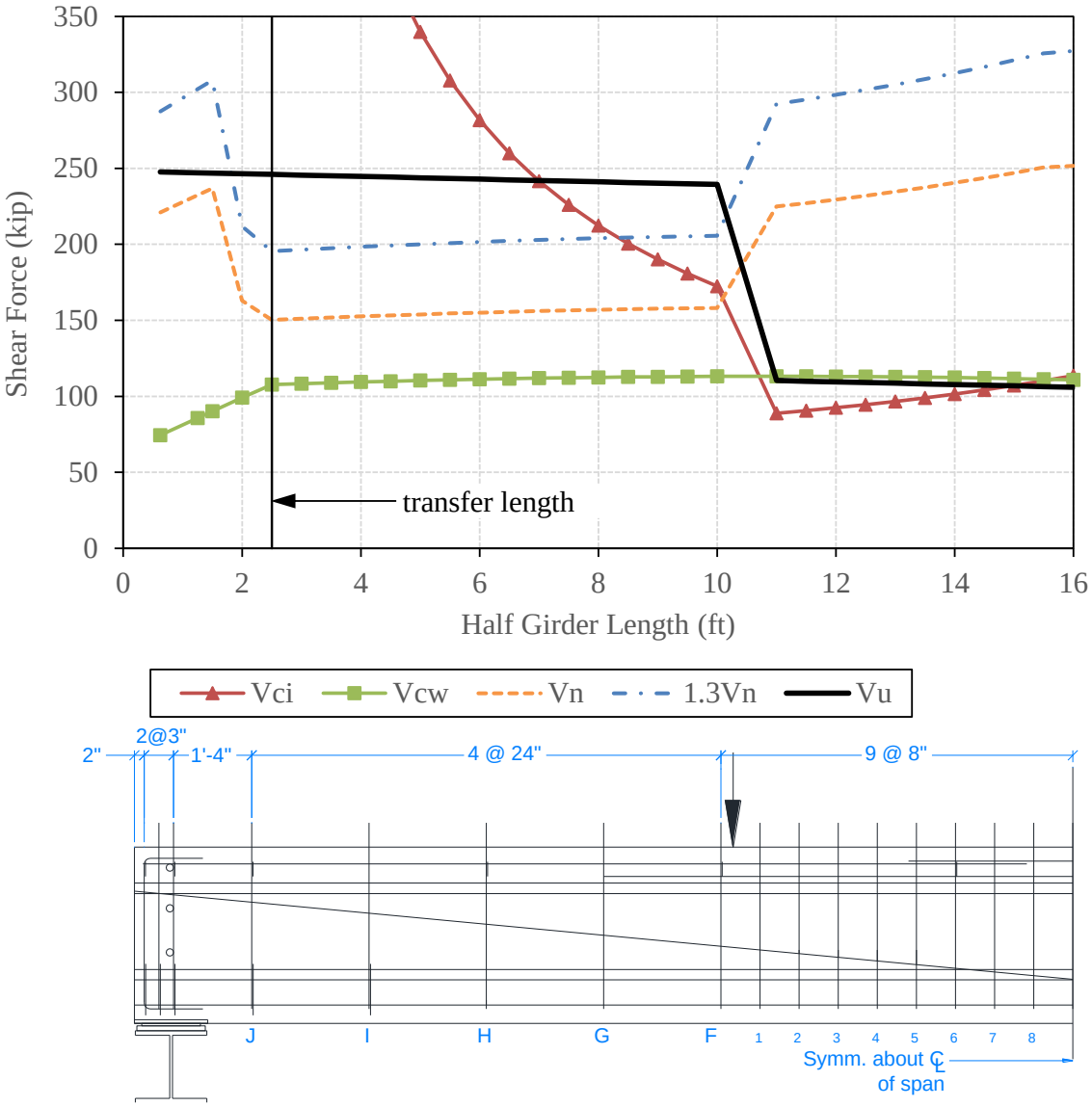

Figure A-12. Shear Force Diagram for 30.75 ft Span (*a*/*d* = 2.5)

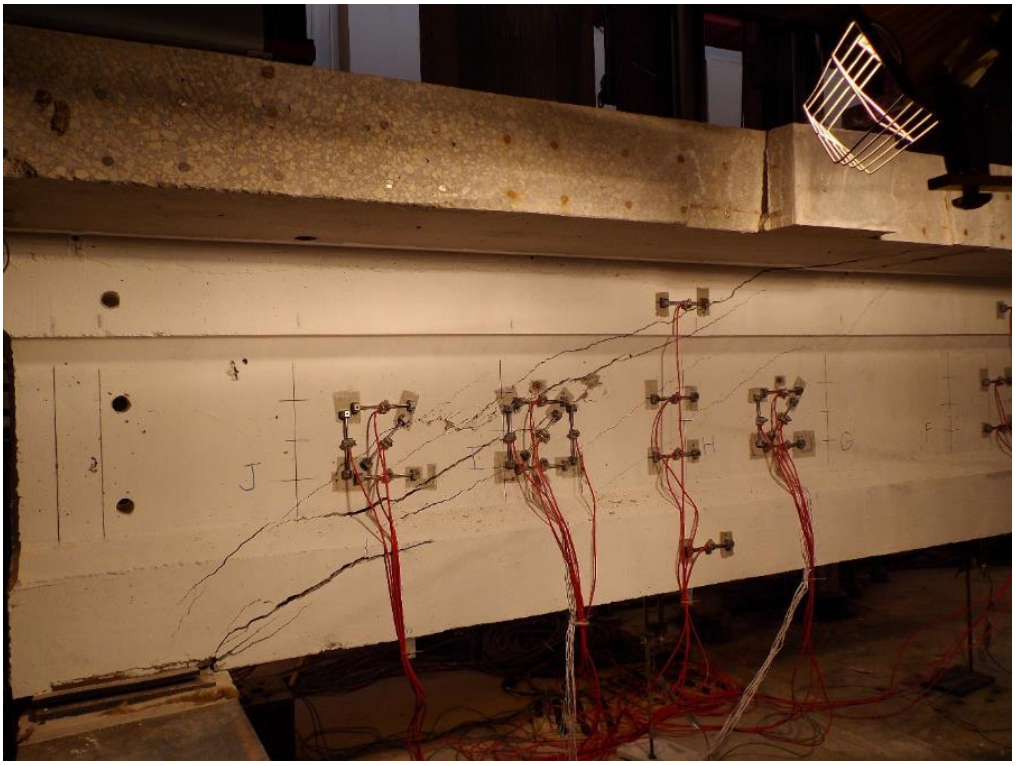

Figure A-13. Web-Shear Cracking Pattern before Failure for 30.75 ft Span

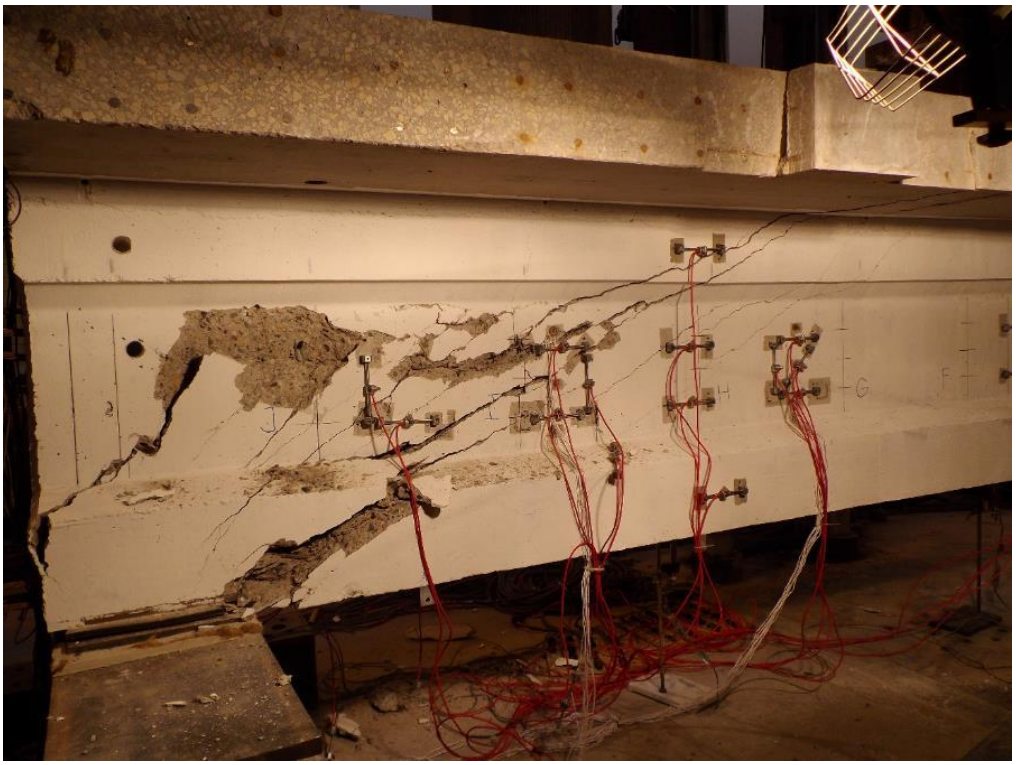

Figure A-14. Web-Shear Crushing Failure in 30.75 ft Span

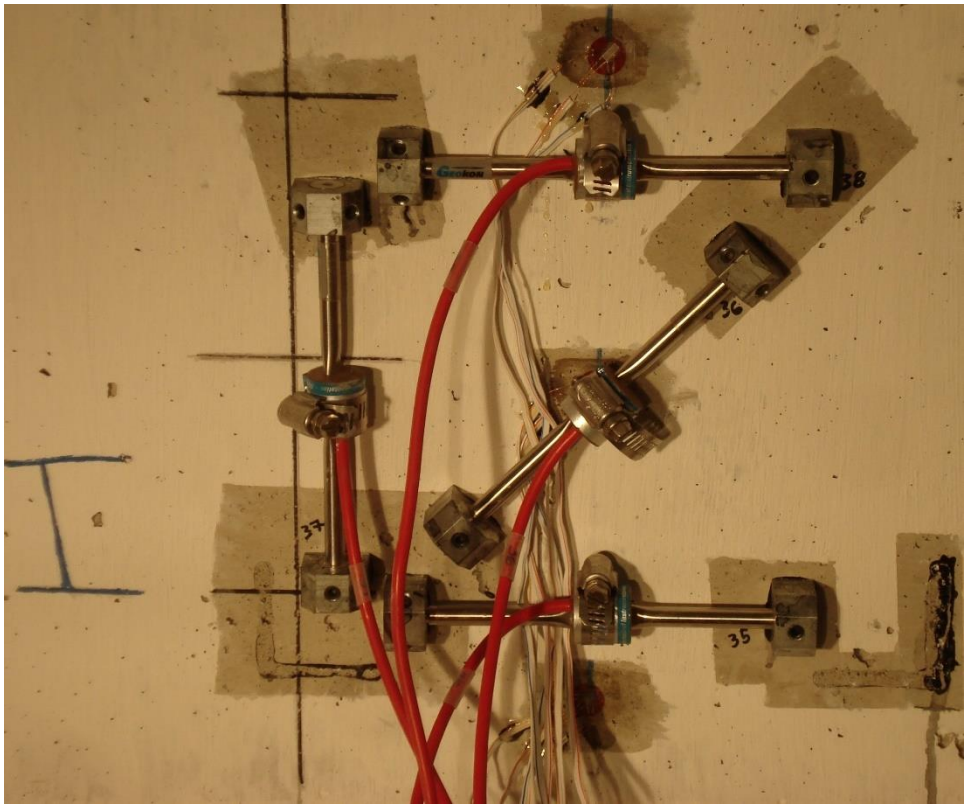

Figure A-15. VWG Box-Type Rosette with Three Foil Rosettes

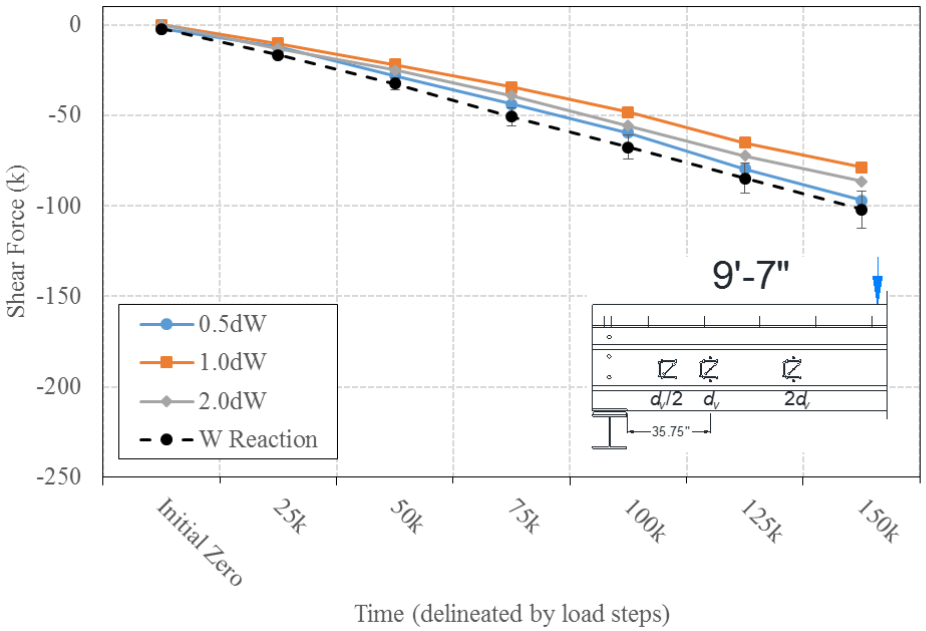

Figure A-16. Elastic Force Derived from VWG Rosette Strains in 9 ft 7 in. Shear Span for 30.75 ft Span (*a*/*d* = 2.5)

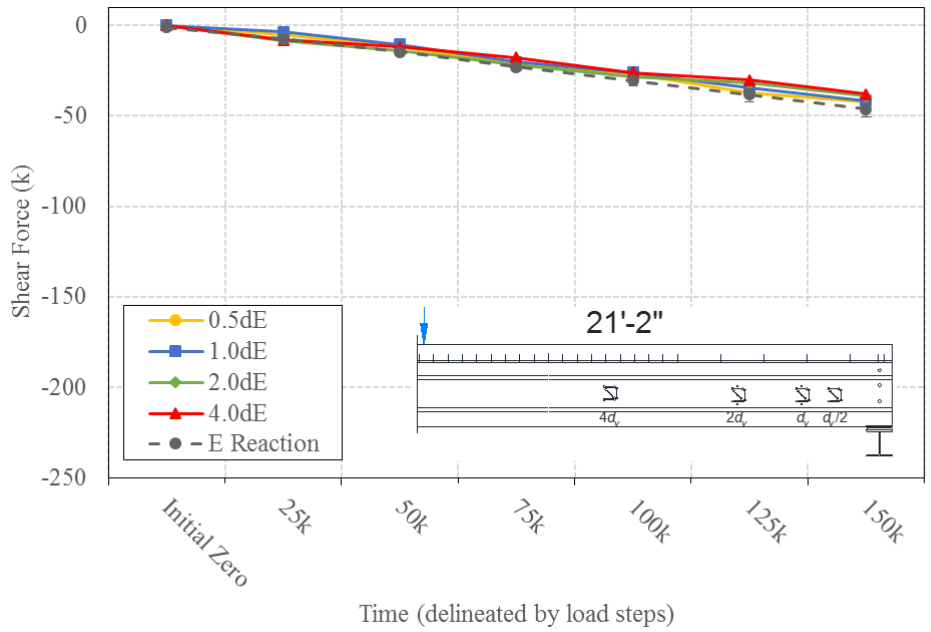

Figure A-17. Elastic Force Derived from VWG Rosette Strains in 21 ft 2 in. Shear Span for 30.75 ft Span (*a*/*d* = 2.5)

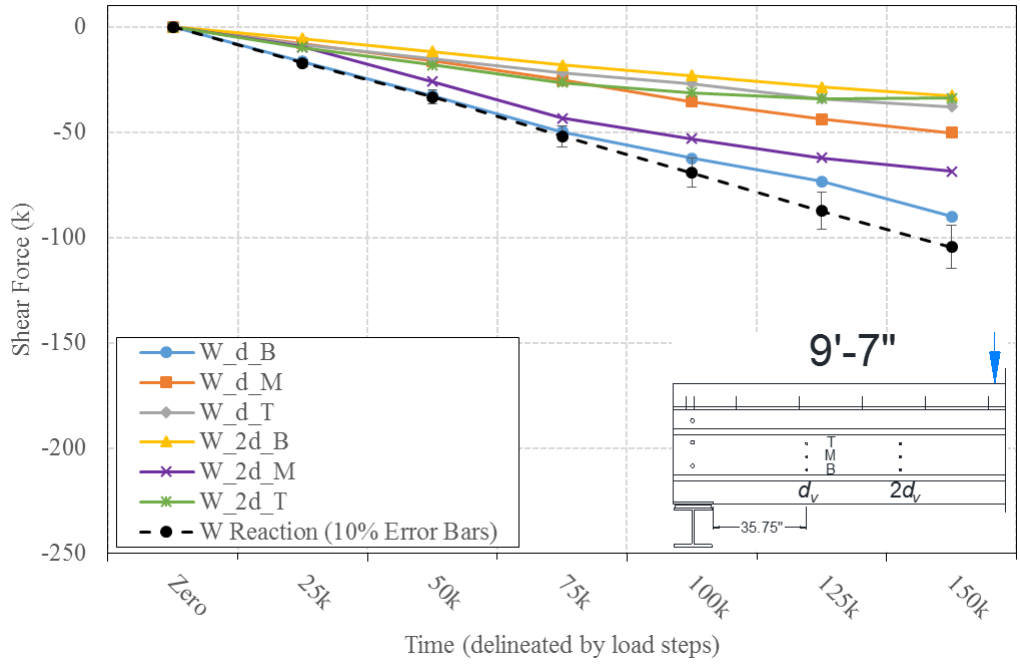

Figure A-18. Elastic Force Derived from Foil Rosette Strains in 9 ft 7 in. Shear Span for 30.75 ft Span (*a*/*d* = 2.5)

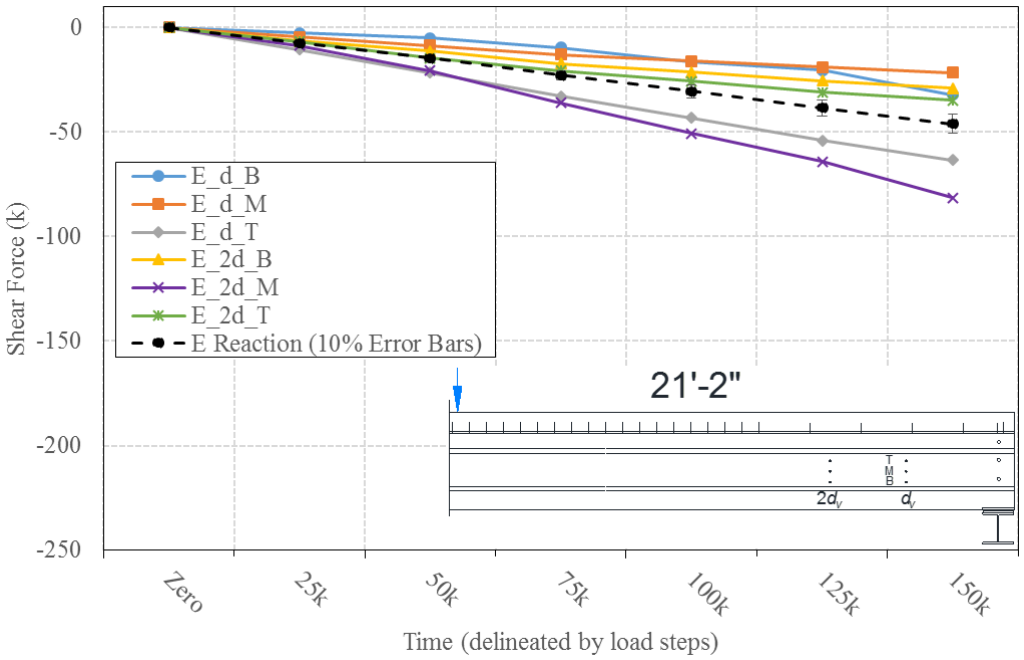

Figure A-19. Elastic Force Derived from Foil Rosette Strains in 21 ft 2 in. Shear Span for 30.75 ft Span (*a*/*d* = 2.5)

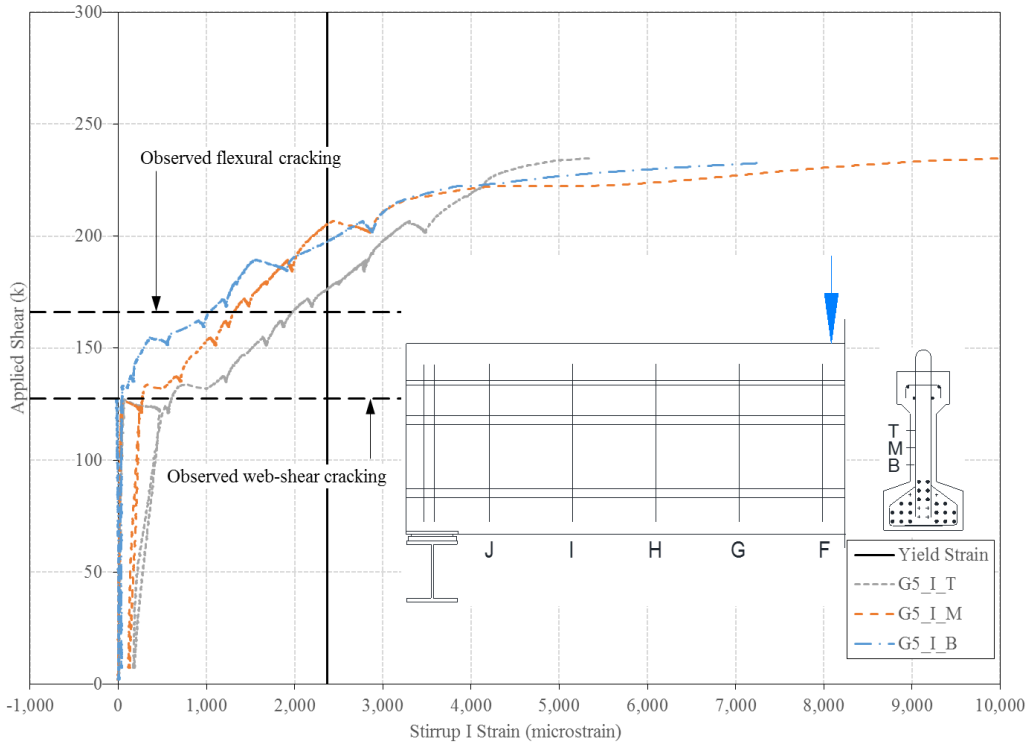

Figure A-20. Applied Shear vs. Stirrup I Strain for 30.75 ft Span (*a*/*d* = 2.5)

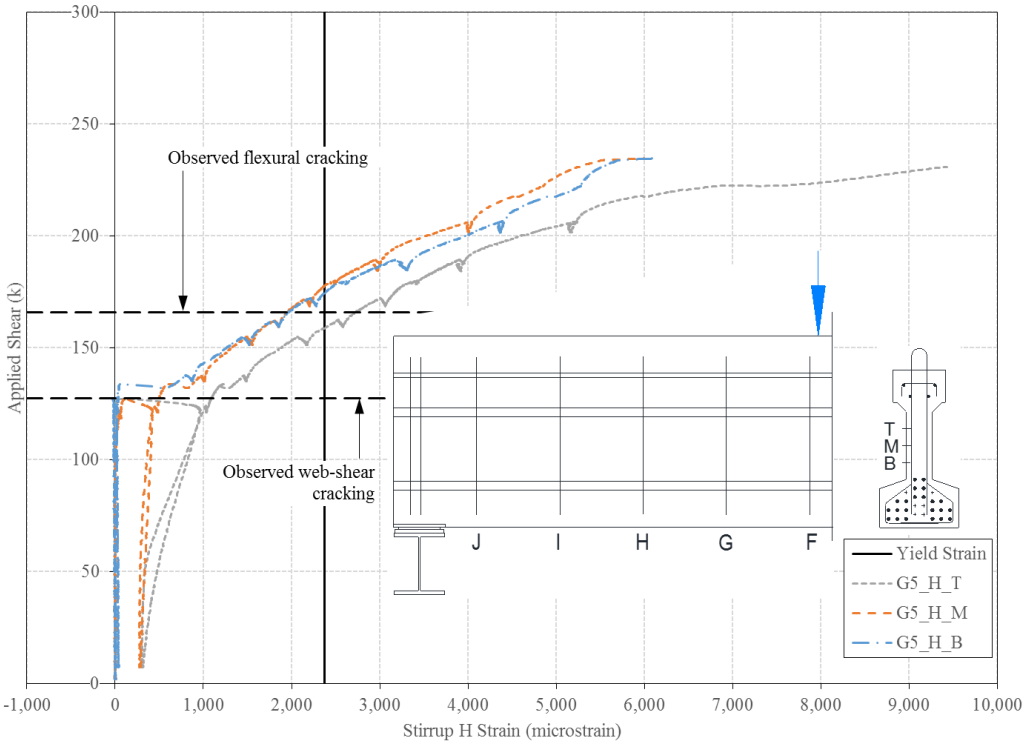

Figure A-21. Applied Shear vs. Stirrup H Strain for 30.75 ft Span (*a*/*d* = 2.5)

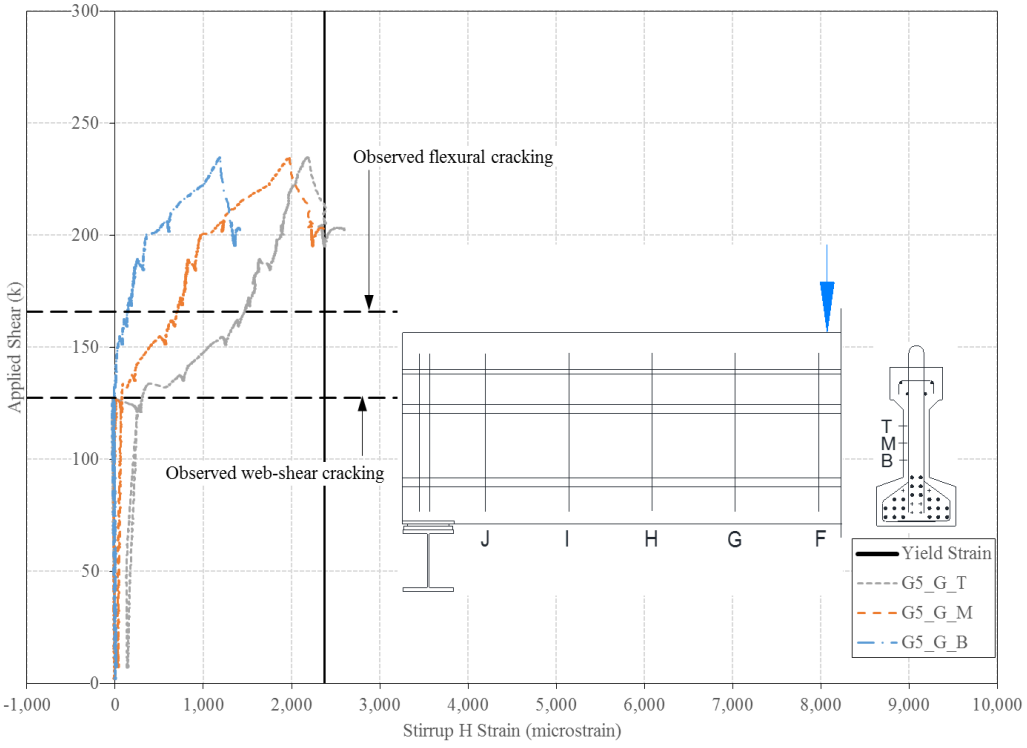

Figure A-22. Applied Shear vs. Stirrup G Strain for 30.75 ft Span (*a*/*d* = 2.5)

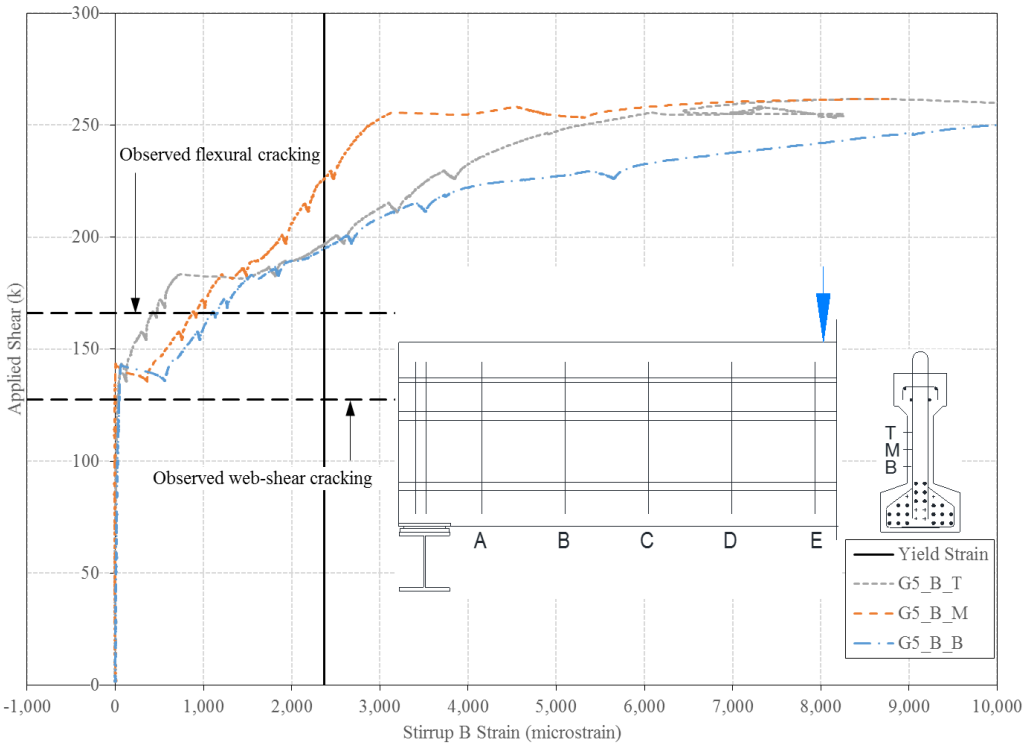

Figure A-23. Applied Shear vs. Stirrup B Strain for 22.5 ft Span (*a*/*d* = 2.5)

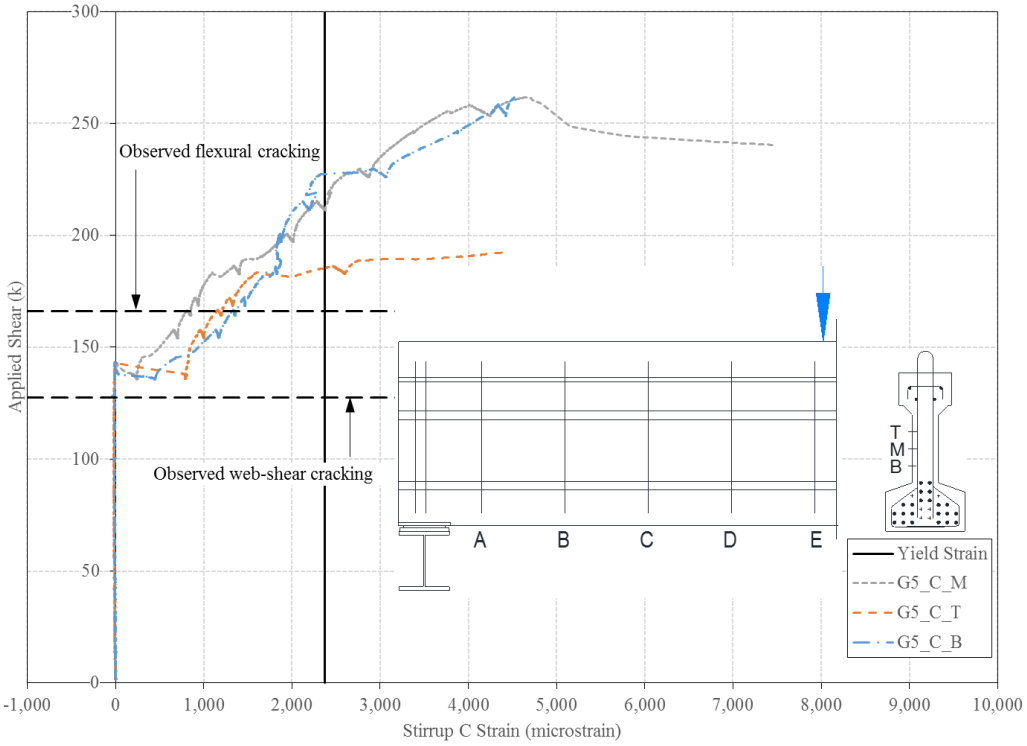

Figure A-24. Applied Shear vs. Stirrup C Strain for 22.5 ft Span (*a*/*d* = 2.5)

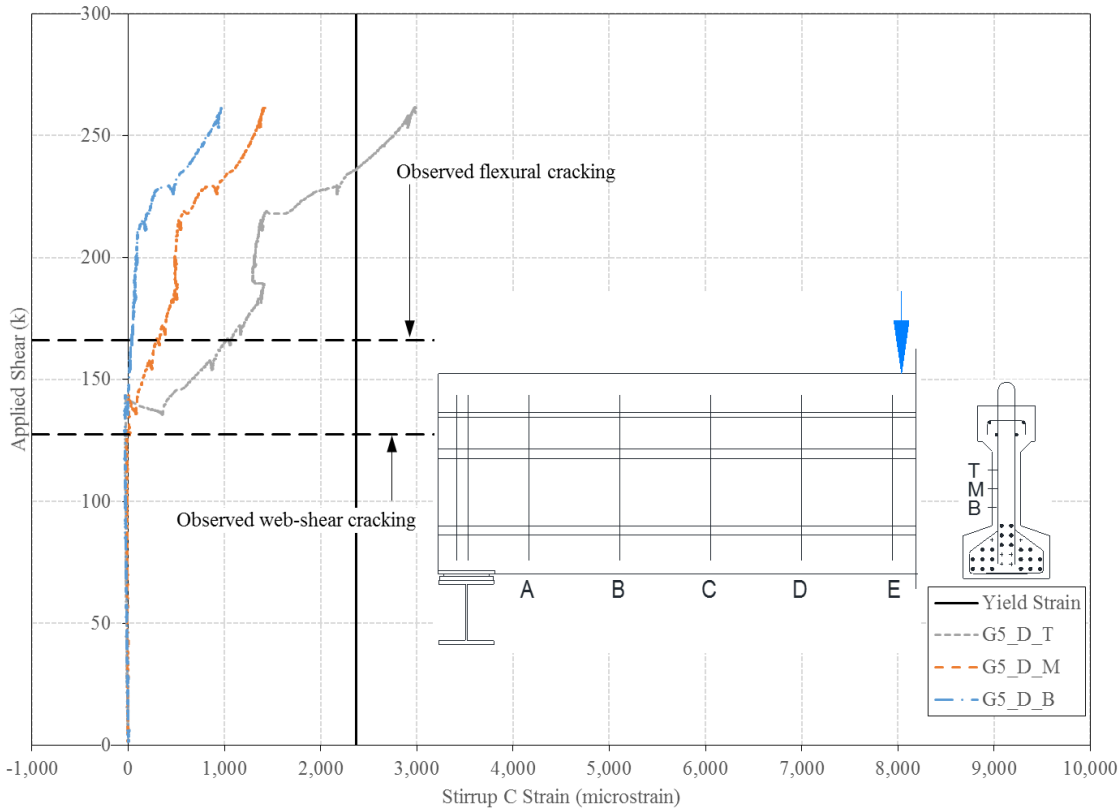

Figure A-25. Applied Shear vs. Stirrup D Strain for 22.5 ft Span (*a*/*d* = 2.5)

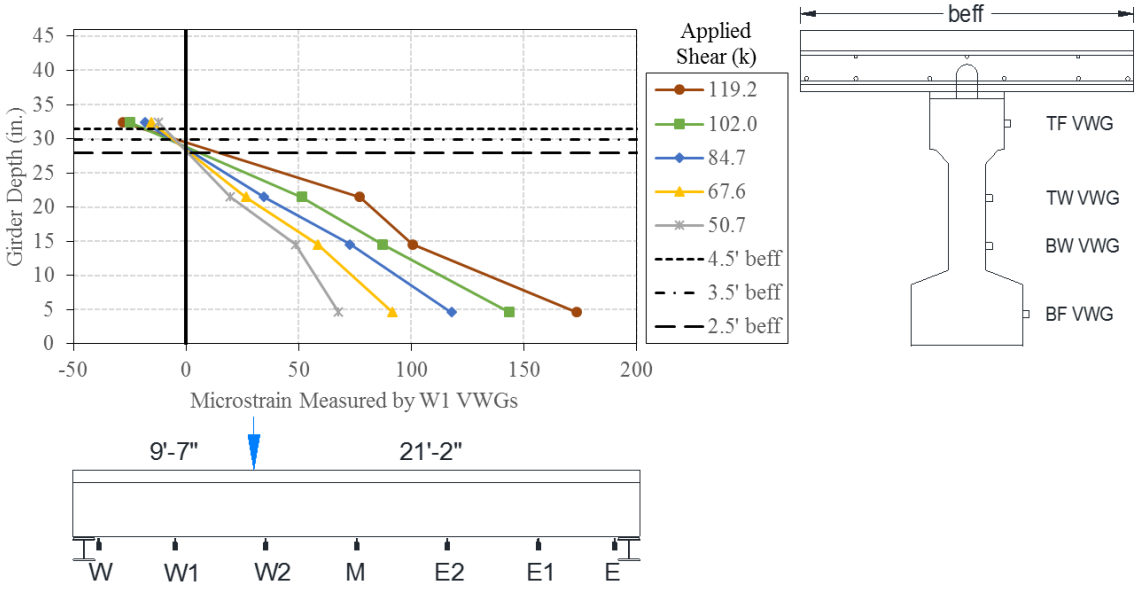

Figure A-26. Neutral Axis Height at W1 Location for 30.75 ft Span (*a*/*d* = 2.5)

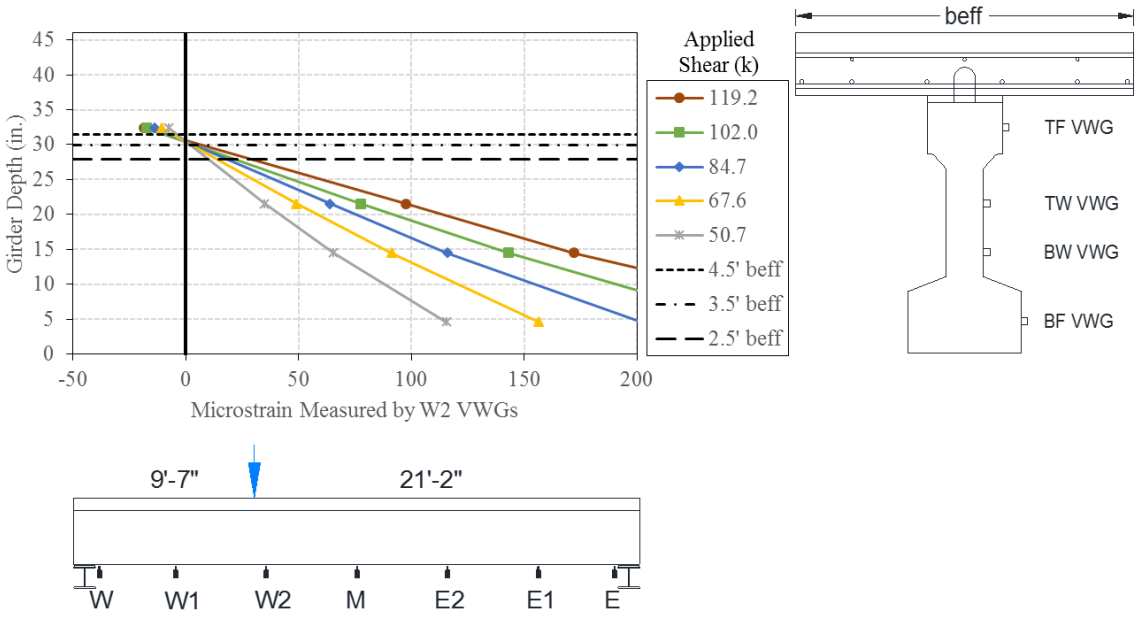

Figure A-27. Neutral Axis Height at W2 Location for 30.75 ft Span (*a*/*d* = 2.5)

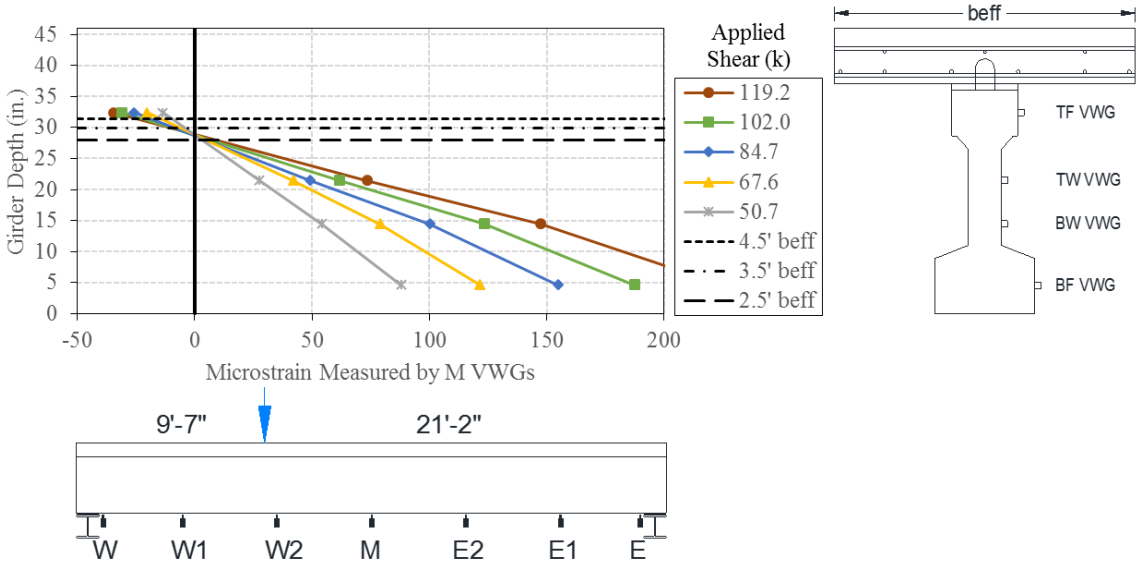

Figure A-28. Neutral Axis Height at M Location for 30.75 ft Span (*a*/*d* = 2.5)

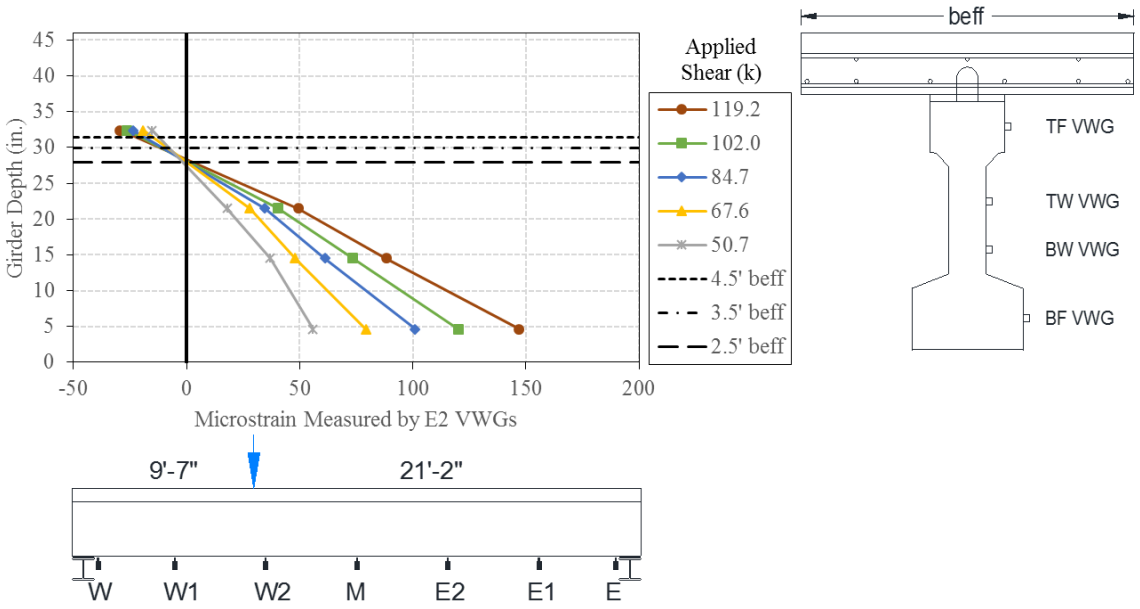

Figure A-29. Neutral Axis Height at E2 Location for 30.75 ft Span (*a*/*d* = 2.5)

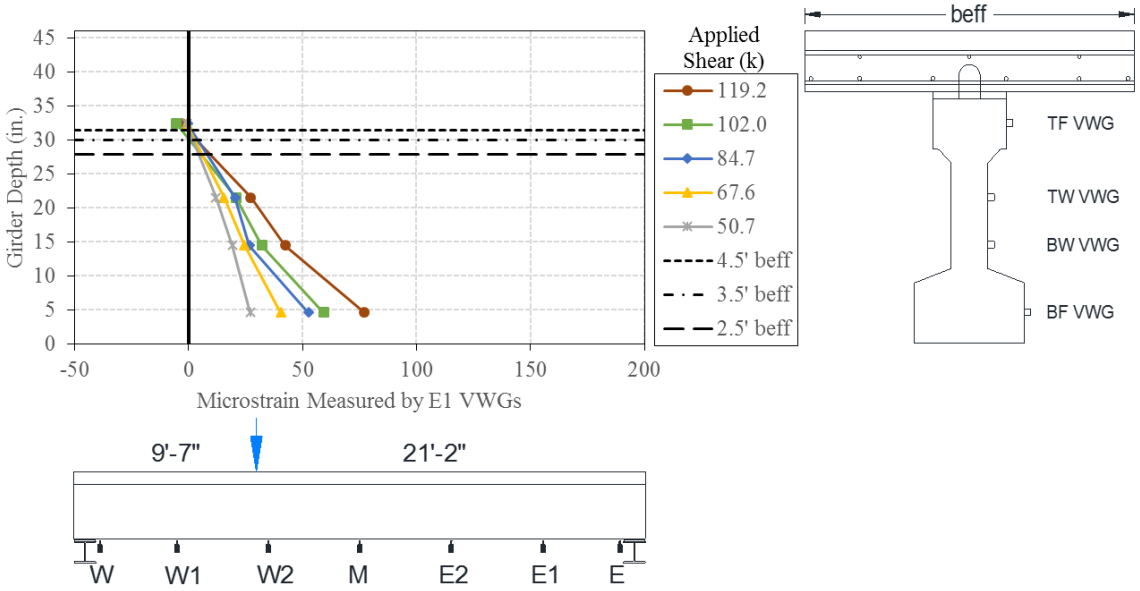

Figure A-30. Neutral Axis Height at E1 Location for 30.75 ft Span (*a*/*d* = 2.5)

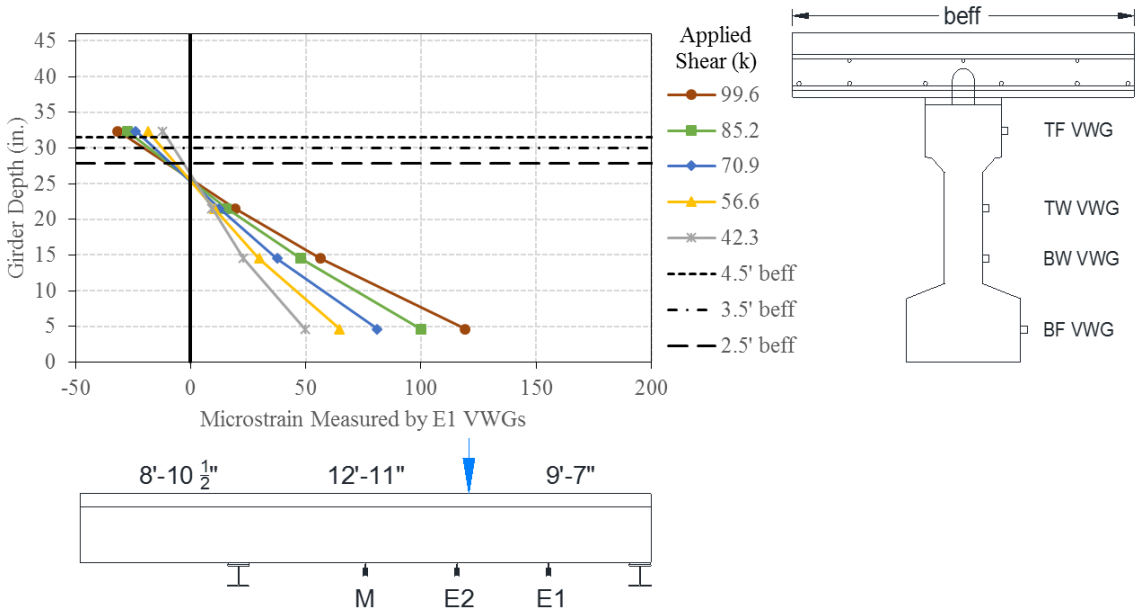

Figure A-31. Neutral Axis Height at E1 Location for 22.5 ft Span (*a*/*d* = 2.5)

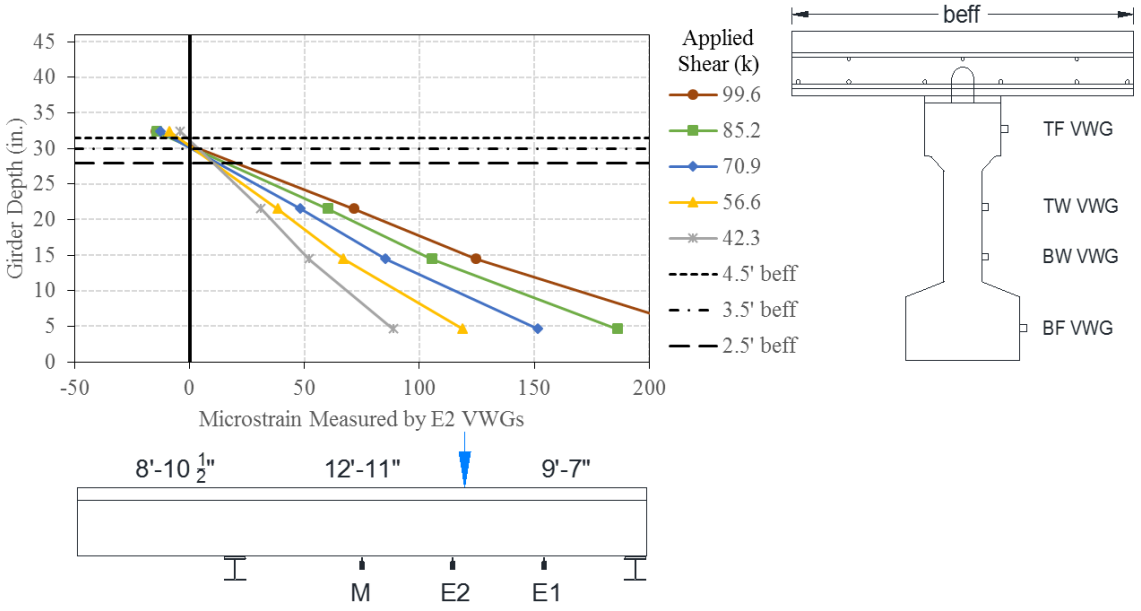

Figure A-32. Neutral Axis Height at E2 Location for 22.5 ft Span (*a*/*d* = 2.5)

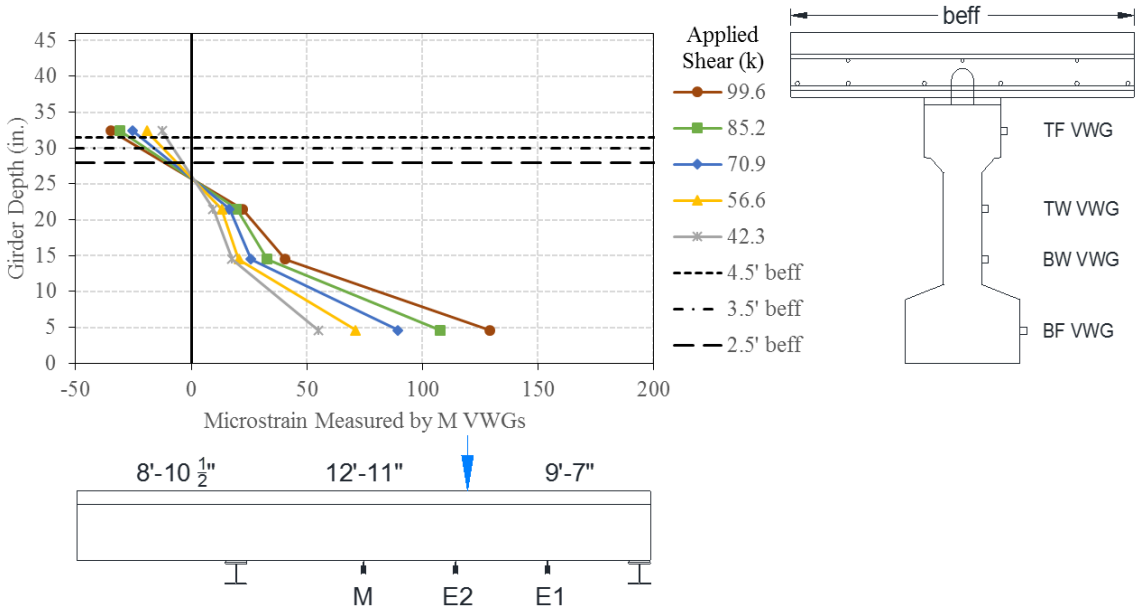

Figure A-33. Neutral Axis Height at M Location for 22.5 ft Span (*a*/*d* = 2.5)

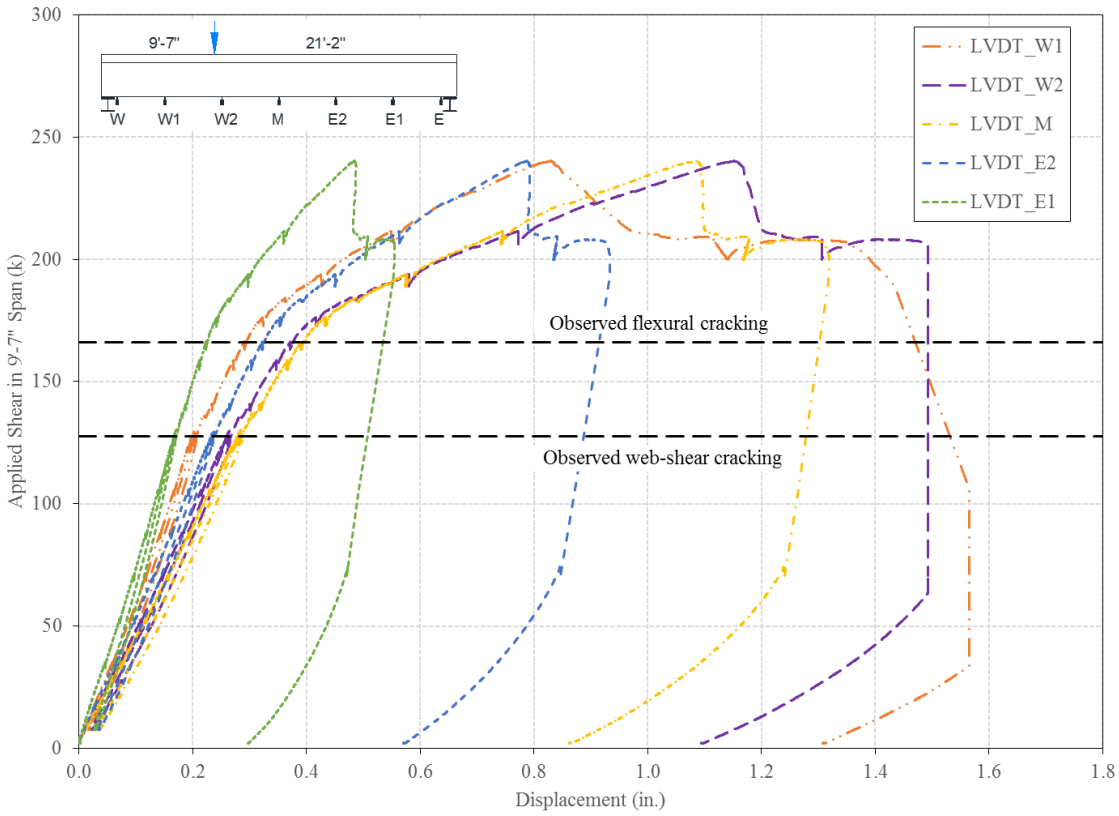

Figure A-34. Applied Shear vs. Displacement for 30.75 ft Span (*a*/*d* = 2.5)

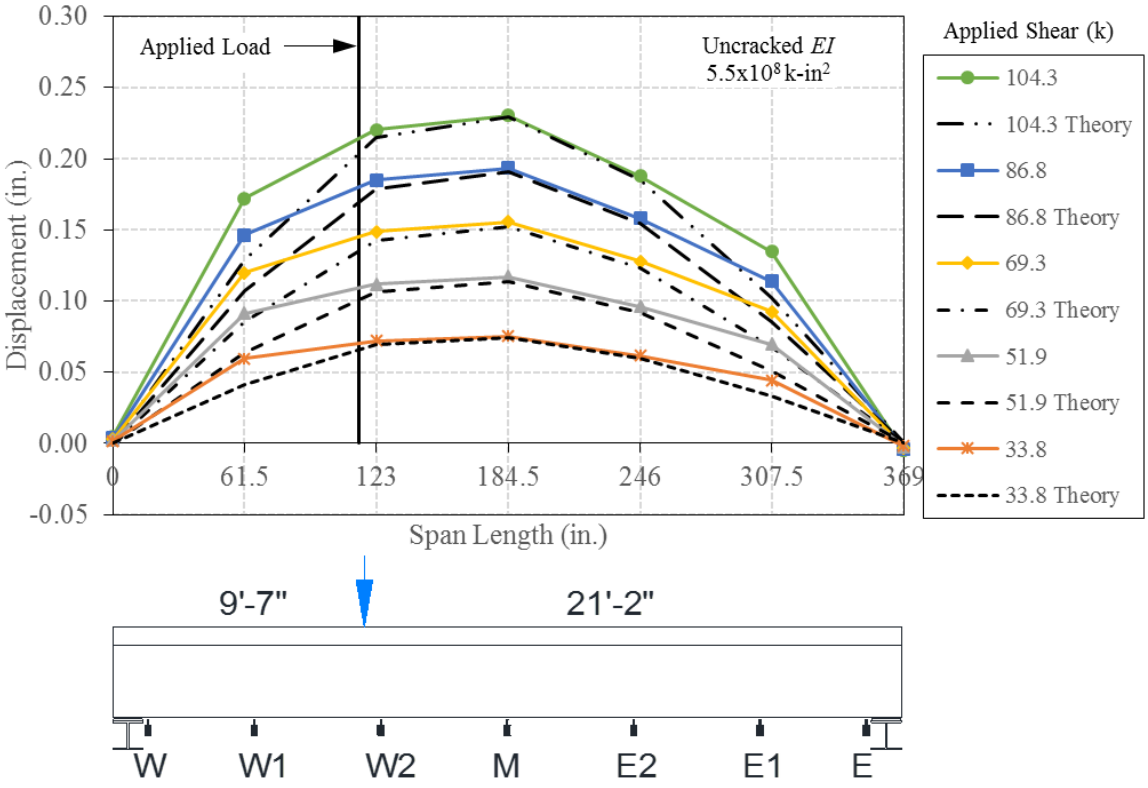

Figure A-35. Elastic Displacement Profile with Varying Live Load for 30.75 ft Span (*a*/*d* = 2.5)

APPENDIX B. LABORATORY BRIDGE DESIGN AND CONSTRUCTION DETAILS

Appendix B includes details related to the laboratory bridge design and construction. Section B.1 and B.2 contain the laboratory bridge girder design calculations using loads expected in the laboratory and a comparison to loads expected from an HS20-44 truck. Section B.3 includes details related to the design, construction, and material properties of the laboratory bridge abutments. Section B.4 contains formwork details for the bridge deck, companion single girder bridge deck, end diaphragm, and traffic barrier.

B.1 Laboratory Bridge Girder Design Calculations

This section contains the design calculations for the laboratory bridge. The AASHTO Standard Specifications (1989) with 1991 Interim Revisions and the Precast/Prestressed Concrete Institute (PCI) Bridge Design Manual (1997) were used as guidelines. Additional live load and factored loads are presented in Section B.2 based on HS20-44 shear and moment envelopes for comparison to design loads in the laboratory. The HS20-44 shear and moment envelopes and the corresponding factored loads were lower than those expected in the laboratory.

Design of Lab Bridge Girders

References: 1989 AASHTO STD w/ 1991 Interims
PCI Bridge Design Manual 3rd Ed.

yellow denotes input variables & assumptions
blue denotes checks
red denotes sections of interest (SOI)

ORIGIN := 1

Bridge Geometry:

BeamType := "interior" use "interior" or "exterior" for BeamType

$L_g := 32ft$ $L_{span} := 30.75ft$ $brng := (L_g - L_{span}) \div 2 = 7.50 \cdot in$ $x_{HP} := 0.5L_g = 16.00\,ft$

$N_g := 4$ $S := 9ft$ $width_{oh} := 3.5ft$ from CL beam $width_{deck} := (N_g - 1) \cdot S + 2 \cdot width_{oh} = 34.00\,ft$

$L_{soleplate} := 15in$ $skew := 0deg$ $RH := 73$ relative humidity

Girder Properties:

$h_g := 36in$ $tf_h := 7.35in$ $tf_{ch} := 2.15in$ $tf_w := 12in$

$bf_h := 8.9in$ $bf_{ch} := 2.1in$ $bf_w := 18$

$b_v := 6in$ $h_{web} := 15.5in$ $h_{webbf} := bf_h + bf_{ch} + h_{web} = 26.50 \cdot in$

$y_{gb} := 15.73in$

$A_g := 384.25in^2$

$I_g := 52265.72in^4$

Girder Concrete Properties:

$w_{cg} := 155pcf$ $\lambda := 1.0$ $w_g := w_{cg} \cdot A_g = 413.60 \cdot plf$

$f'_{ci} := 4.6ksi$ $E_{ci} := \left[33000 \cdot \left[(w_{cg} - 5pcf) \cdot \frac{ft^3}{kip}\right]^{1.5} \cdot \lambda \sqrt{f'_{ci}}\right] \cdot ksi^{0.5} = 4112 \cdot ksi$

$f'_{cg} := 7.5ksi$ $E_{cg} := \left[33000 \cdot \left[(w_{cg} - 5pcf) \cdot \frac{ft^3}{kip}\right]^{1.5} \cdot \lambda \sqrt{f'_{cg}}\right] \cdot ksi^{0.5} = 5250 \cdot ksi$

$\beta_{1g} := if\left[f'_{cg} \le 4ksi, 0.85, \max\left[0.65, 0.85 - \frac{0.2}{4ksi} \cdot (f'_{cg} - 4ksi)\right]\right] = 0.675$

Deck & Haunch Geometry:

$t_d := 9in$

$t_h := 1in$ $w_h := tf_w = 12.00 \cdot in$ total composite height $h_c := h_g + t_d + t_h = 46.0 \cdot in$

Deck & Haunch Concrete Properties:

$w_{cd} := 150pcf$ $w_d := w_{cd} \cdot (S \cdot t_d) + t_h \cdot tf_w \cdot w_{cd} = 1025 \cdot plf$ (use c-c spacing for weight only and include haunch)

$f'_{cd} := 4ksi$ $E_{cd} := \left[33000 \cdot \left[(w_{cd} - 5pcf) \cdot \frac{ft^3}{kip}\right]^{1.5} \cdot \sqrt{f'_{cd}}\right] \cdot ksi^{0.5} = 3644.15 \cdot ksi$

$\beta_{1d} := if\left[f'_{cd} \le 4ksi, 0.85, \max\left[0.65, 0.85 - \frac{0.2}{4ksi} \cdot (f'_{cd} - 4ksi)\right]\right] = 0.85$

Rebar Properties:

$f_y := 60ksi$ $E_s := 29000ksi$ $A_3 := 0.11in^2$ $A_4 := 0.2in^2$ $A_5 := 0.31in^2$ $A_8 := 0.79in^2$

$d_3 := 0.375in$ $d_4 := 0.5in$ $d_5 := 0.625in$ $d_8 := 1in$

Strand Properties & Layout:

StrandType := "LR" LR = low-relaxation, SR = stress relieved

$A_{strand} := 0.153in^2$ $d_{ps} := 0.5in$ $E_{ps} := 29000ksi$

$f_{pu} := 270ksi$ $f_{py} := if(StrandType = "LR", 0.9 \cdot f_{pu}, 0.85 \cdot f_{pu}) = 243.00 \cdot ksi$ $k := 2 \cdot \left(1.04 - \frac{f_{py}}{f_{pu}}\right) = 0.28$

$P_{jstrand} := 25kip$ $f_{pj} := if(StrandType = "LR", 0.75 \cdot f_{pu}, 0.7 \cdot f_{pu}) = \blacksquare \cdot ksi$ (disabled eval to specify f_{pj} < code max)

Strand Layout at End

Straight Strands

$y_{st} := \begin{pmatrix} 24 \\ 22 \\ 20 \\ 18 \\ 16 \\ 14 \\ 12 \\ 10 \\ 8 \\ 6 \\ 4 \\ 2 \end{pmatrix} in$ $E_{st} := \begin{pmatrix} 0 \\ 0 \\ 0 \\ 0 \\ 0 \\ 0 \\ 0 \\ 0 \\ 0 \\ 4 \\ 6 \\ 6 \end{pmatrix}$

Draped Strands

$y_d := \begin{pmatrix} 3 \\ 5 \\ 7 \\ 9 \\ 11 \\ 13 \\ 15 \\ 17 \\ 19 \\ 21 \\ 23 \\ 25 \end{pmatrix} in$ $E_d := \begin{pmatrix} 0 \\ 0 \\ 0 \\ 2 \\ 2 \\ 2 \\ 0 \\ 0 \\ 0 \\ 0 \\ 0 \\ 0 \end{pmatrix}$

$n_{Es} := \sum E_{st} = 16.00$ $n_{Ed} := \sum E_d = 6.00$

$y_{Es} := \frac{y_{st} \cdot E_{st}}{n_{Es}}$ $y_{Es} = 3.75 \cdot in$ $e_{Es} := y_{gb} - y_{Es}$ $e_{Es} = 11.98 \cdot in$

$y_{Ed} := h_g - \frac{y_d \cdot E_d}{n_{Ed}}$ $y_{Ed} = 25.00 \cdot in$ $e_{Ed} := y_{gb} - y_{Ed}$ $e_{Ed} = -9.27 \cdot in$

$n_{Etot} := n_{Es} + n_{Ed} = 22.00$

Strand Layout at HP

Straight Strands

$HP_{st} := \begin{pmatrix} 0 \\ 0 \\ 0 \\ 0 \\ 0 \\ 0 \\ 0 \\ 0 \\ 0 \\ 4 \\ 6 \\ 6 \end{pmatrix}$

Draped Strands

$y_{HP\_d} := \begin{pmatrix} 25 \\ 23 \\ 21 \\ 19 \\ 17 \\ 15 \\ 13 \\ 11 \\ 9 \\ 7 \\ 5 \\ 3 \end{pmatrix} in$ $HP_d := \begin{pmatrix} 0 \\ 0 \\ 0 \\ 0 \\ 0 \\ 0 \\ 0 \\ 2 \\ 2 \\ 2 \\ 0 \\ 0 \end{pmatrix}$

$n_{HPs} := \sum HP_{st} = 16.00$ $n_{HPd} := \sum HP_d = 6.00$

$y_{HPs} := \frac{y_{st} \cdot HP_{st}}{n_{HPs}}$ $y_{HPs} = 3.75 \cdot in$ $e_{HPs} := y_{gb} - y_{HPs}$ $e_{HPs} = 11.98 \cdot in$

$y_{HPd} := \frac{y_{HP\_d} \cdot HP_d}{n_{HPd}}$ $y_{HPd} = 9.00 \cdot in$ $e_{HPd} := y_{gb} - y_{HPd}$ $e_{HPd} = 6.73 \cdot in$

$n_{HPtot} := n_{HPs} + n_{HPd} = 22.00$

No_Strands_Check := if($n_{Etot} = n_{HPtot}$, "OK", "NG") = "OK"

$y_{end} := \frac{(n_{Es} \cdot y_{Es}) + (n_{Ed} \cdot y_{Ed})}{n_{Etot}} = 9.55 \cdot in$ $e_{end} := y_{gb} - y_{end} = 6.18 \cdot in$

$y_{HP} := \frac{(n_{HPs} \cdot y_{HPs}) + (n_{HPd} \cdot y_{HPd})}{n_{HPtot}} = 5.18 \cdot in$ $e_{HP} := y_{gb} - y_{HP} = 10.55 \cdot in$

$I_{ps} := A_{strand} \cdot \left[E_{st} \cdot (y_{st} - y_{Es})^2 + E_d \cdot \left[y_d - (h_g - y_{Ed}) \right]^2 \right] = 8.41 \cdot in^4$

$A_{ps} := n_{Etot} \cdot A_{strand} = 3.37 \cdot in^2$ $A_{pss} := n_{Es} \cdot A_{strand} = 2.45 \cdot in^2$ $A_{psd} := n_{Ed} \cdot A_{strand} = 0.92 \cdot in^2$

Section Properties:

Non-composite Section Properties:

$y_{gt} := h_g - y_{gb} = 20.27 \cdot in$ $S_{gb} := \frac{I_g}{y_{gb}} = 3322.68 \cdot in^3$ $S_{gt} := \frac{I_g}{y_{gt}} = 2578.48 \cdot in^3$

Composite Section Properties:

Effective Flange Width: (STD 8.10.1)

Interior Beam $b_{eff\_int} := \min(0.25 \cdot L_{span}, 12 \cdot t_d + b_v, S) = 92.25 \cdot in$

Exterior Beam $b_{eff\_ext} := 0.5 b_{eff\_int} + \min[(1 \div 12) \cdot L_{span}, 6 \cdot t_d, width_{oh}] = 76.88 \cdot in$

$b_{eff} := if(BeamType = "interior", b_{eff\_int}, b_{eff\_ext}) = 92.25 \cdot in$

Transform Deck & Haunch Concrete to Beam Concrete (at Harping Point):

$A_h := t_h \cdot w_h = 12.00 \cdot in^2$ $I_h := \frac{1}{12} \cdot w_h \cdot t_h^3 = 1.00 \cdot in^4$ $y_h := t_h \div 2 = 0.50 \cdot in$

$A_d := b_{eff} \cdot t_d = 830.25 \cdot in^2$ $I_d := \frac{1}{12} \cdot b_{eff} \cdot t_d^3 = 5604.19 \cdot in^4$ $y_d := t_d \div 2 = 4.50 \cdot in$

$n_{dg} := \frac{E_{cd}}{E_{cg}} = 0.69$ $A_c := A_g + n_{dg} \cdot (A_d + A_h) = 968.85 \cdot in^2$

$y_{cb} := \frac{A_g \cdot y_{gb} + n_{dg} \cdot A_d \cdot (h_g + t_h + y_d) + n_{dg} \cdot A_h \cdot (h_g + t_h \div 2)}{A_c} = 31.24 \cdot in$

$y_{ct} := h_c - y_{cb} = 14.76 \cdot in$

$y_{ctg} := h_g - y_{cb} = 4.76 \cdot in$

$I_c := I_g + A_g \cdot (y_{cb} - y_{gb})^2 \ldots = 211199 \cdot in^4$
$+ I_d + n_{dg} \cdot A_d \cdot (h_g + t_h + y_d - y_{cb})^2 \ldots$
$+ I_h + n_{dg} \cdot A_h \cdot (h_g + y_h - y_{cb})^2$

$S_{cb} := \frac{I_c}{y_{cb}} = 6761 \cdot in^3$ $S_{ct} := \frac{I_c}{y_{ct}} = 14305 \cdot in^3$ $S_{ctg} := \frac{I_c}{y_{ctg}} = 44337 \cdot in^3$

Section Property Summary

Noncomposite Gross:	$A_g = 384 \cdot in^2$	$S_{gt} = 2578 \cdot in^3$
	$I_g = 52266 \cdot in^4$	$S_{gb} = 3323 \cdot in^3$
	$y_{gb} = 15.73 \cdot in$	$y_{gt} = 20.27 \cdot in$
Composite: (at Harping Point)	$A_c = 969 \cdot in^2$	$S_{ctg} = 44337 \cdot in^3$
	$I_c = 211199 \cdot in^4$	$S_{ct} = 14305 \cdot in^3$
	$y_{cb} = 31.24 \cdot in$	$S_{cb} = 6761 \cdot in^3$
	$y_{ct} = 14.76 \cdot in$	

Section of Interest:

At Section of Interest (from end of girder): $x := 10.208\text{ft}$ $h_c \cdot 2.5 = 9.583\,\text{ft}$

max load applied $a/h_c > 2.5$ for shear failure = 9.583' + 7.5" bearing = 10.208' from end of beam (~9.38' from support
critical section $h_c / 2$ from support face = 23" + 7.5" for 1/2 $L_{soleplate}$ + 7.5" bearing = ~3' from beam end (2.38' from support)

Angle of draped strands:

$$\alpha := \operatorname{atan}\left[\frac{(y_{Ed} - y_{HPd})}{x_{HP}}\right] = 4.76\cdot\text{deg}$$

$y_{xd} := \tan(\alpha)\cdot(x_{HP} - x) + y_{HPd} = 14.79\cdot\text{in}$

$$y_{xtot} := \frac{(n_{Es}\cdot y_{Es}) + (n_{Ed}\cdot y_{xd})}{n_{Etot}} = 6.76\cdot\text{in}$$

$e_{xtot} := y_{gb} - y_{xtot} = 8.97\cdot\text{in}$

Compression block depth at section of interest:

$d_{px} := h_c - y_{xtot} = 39.24\cdot\text{in}$

$$c_{vx} := \frac{A_{ps}\cdot f_{pu}}{0.85\cdot f'_{cd}\cdot\beta_{1d}\cdot b_{eff} + k\cdot A_{ps}\cdot\frac{f_{pu}}{d_{px}}} = 3.33\cdot\text{in}$$

$a_{vx} := \beta_{1d}\cdot c_{vx} = 2.83\cdot\text{in}$

Effective shear depth at section of interest:

$$d_{vx} := \max\left(h_c - y_{xtot} - \frac{a_{vx}}{2}, 0.9d_{px}, 0.72\cdot h_c\right) = 37.82\cdot\text{in}$$

Moments and Shears:

Design Locations of Interest:

From end of girder

$x_i :=$ (0in; brng; 15in; 2ft; $60\cdot d_{ps}$; 3ft; 4ft; 5ft; 6ft; 7ft; 8ft; 9ft; 10ft; 11ft; 12ft; 13ft; $L_g \div 2$)

center line of support
transfer length of strands
approx $h_c / 2$
approx d_v
approx $2d_v$
approx L_d
approx $3d_v$
approx $4d_v$

$x_{itot} := \text{rows}(x_i) = 17$

$x_e := \text{submatrix}(x_i, 2, x_{itot}, 1, 1) - \text{brng}$

From center line of support

Sections of Interest

spot 5

spot 12

$x_e =$ (0.00; 0.62; 1.37; 1.87; 2.38; 3.37; 4.37; 5.38; 6.37; 7.38; 8.38; 9.38; 10.38; 11.38; 12.38; 15.38) ft

center line of support
transfer length of strands
approx $h_c / 2$
approx d_v
approx $2d_v$
approx L_d
approx $3d_v$
approx $4d_v$

$zi := 1 .. x_{itot}$ (only used for initial calcs)

$x_{etot} := \text{rows}(x_e) = 16$

$z := 1 .. x_{etot}$

A subscript zi (release) or z (service) will be used throughout the calculations to tabulate each position of interest

Centroid, eccentricity, and depth of strands at locations of interest:

$y_{xi_{zi}} := y_{end} - \left(x_{i_{zi}} + x_{HP}\right) \cdot \left(y_{end} - y_{HP}\right)$ $\quad y_x := \text{submatrix}\left(y_{xi}, 2, x_{itot}, 1, 1\right)$ (y_x not taken from composite props)

$y_{xi}^T = (9.55\ \ 9.38\ \ 9.20\ \ 9.00\ \ 8.86\ \ 8.73\ \ 8.45\ \ 8.18\ \ 7.91\ \ 7.64\ \ 7.36\ \ 7.09\ \ 6.82\ \ 6.55\ \ 6.27\ \ 6.00\ \ 5.18)\cdot in$

$y_x^T = (9.38\ \ 9.20\ \ 9.00\ \ 8.86\ \ 8.73\ \ 8.45\ \ 8.18\ \ 7.91\ \ 7.64\ \ 7.36\ \ 7.09\ \ 6.82\ \ 6.55\ \ 6.27\ \ 6.00\ \ 5.18)\cdot in$

$e_{xi_{zi}} := y_{gb} - y_{xi_{zi}}$ $\quad e_x := \text{submatrix}\left(e_{xi}, 2, x_{itot}, 1, 1\right)$

$e_{xi}^T = (6.18\ \ 6.36\ \ 6.53\ \ 6.73\ \ 6.87\ \ 7.00\ \ 7.28\ \ 7.55\ \ 7.82\ \ 8.09\ \ 8.37\ \ 8.64\ \ 8.91\ \ 9.18\ \ 9.46\ \ 9.73\ \ 10.55)\cdot in$

$e_x^T = (6.36\ \ 6.53\ \ 6.73\ \ 6.87\ \ 7.00\ \ 7.28\ \ 7.55\ \ 7.82\ \ 8.09\ \ 8.37\ \ 8.64\ \ 8.91\ \ 9.18\ \ 9.46\ \ 9.73\ \ 10.55)\cdot in$

$d_{p_z} := h_c - y_{x_z}$

$d_p^T = (36.6\ \ 36.8\ \ 37\ \ 37.1\ \ 37.3\ \ 37.5\ \ 37.8\ \ 38.1\ \ 38.4\ \ 38.6\ \ 38.9\ \ 39.2\ \ 39.5\ \ 39.7\ \ 40\ \ 40.8)\cdot in$

Dead Load:

Self-weight of Girder at Release (full girder length) $w_g = 413.60\cdot plf$

$M_{gi_{zi}} := \frac{w_g \cdot x_{i_{zi}}}{2} \cdot \left(L_g - x_{i_{zi}}\right)$

$M_{gi}^T = (0\ \ 4.1\ \ 7.9\ \ 12.4\ \ 15.3\ \ 18\ \ 23.2\ \ 27.9\ \ 32.3\ \ 36.2\ \ 39.7\ \ 42.8\ \ 45.5\ \ 47.8\ \ 49.6\ \ 51.1\ \ 52.9)\cdot kip\cdot ft$

Self-weight of Girder at Service (includes bearing overhang effects)

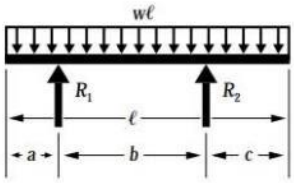

$R_g := w_g \cdot L_g \div 2 = 6.62\cdot kip$

$M_{ge_z} := R_g \cdot x_{e_z} - \frac{w_g \cdot \left(x_{e_z} + brng\right)^2}{2}$

$M_{ge}^T = (-0.1\ \ 3.8\ \ 8.3\ \ 11.1\ \ 13.9\ \ 19\ \ 23.8\ \ 28.1\ \ 32.1\ \ 35.6\ \ 38.7\ \ 41.4\ \ 43.6\ \ 45.5\ \ 46.9\ \ 48.8)\cdot kip\cdot ft$

$f_{d_z} := \frac{M_{ge_z}}{S_{gb}}$ stress at extreme tension fiber due to dead load only

$f_d^T = (-0.00\ \ 0.01\ \ 0.03\ \ 0.04\ \ 0.05\ \ 0.07\ \ 0.09\ \ 0.10\ \ 0.12\ \ 0.13\ \ 0.14\ \ 0.15\ \ 0.16\ \ 0.16\ \ 0.17\ \ 0.18)\cdot ksi$

$V_{ge_z} := w_g \cdot \left(\frac{L_{span}}{2} - x_{e_z}\right)$

$V_{ge}^T = (6.4\ \ 6.1\ \ 5.8\ \ 5.6\ \ 5.4\ \ 5\ \ 4.5\ \ 4.1\ \ 3.7\ \ 3.3\ \ 2.9\ \ 2.5\ \ 2.1\ \ 1.7\ \ 1.2\ \ 0)\cdot kip$

Self-weight of Deck at Service (center-to-center bearing length)

$R_d := w_d \cdot L_g \div 2 = 16.40\cdot kip$

$M_{de_z} := R_d \cdot x_{e_z} - \frac{w_d \cdot \left(x_{e_z} + brng\right)^2}{2}$

$M_{de}^T = (-0.2\ \ 9.4\ \ 20.5\ \ 27.5\ \ 34.3\ \ 47.1\ \ 58.9\ \ 69.7\ \ 79.4\ \ 88.1\ \ 95.8\ \ 102.5\ \ 108.1\ \ 112.7\ \ 116.3\ \ 120.9)\cdot kip\cdot ft$

$V_{de_z} := w_d \cdot \left(\frac{L_{span}}{2} - x_{e_z}\right)$

$V_{de}^T = (15.8\ \ 15.1\ \ 14.3\ \ 13.8\ \ 13.3\ \ 12.3\ \ 11.3\ \ 10.2\ \ 9.2\ \ 8.2\ \ 7.2\ \ 6.2\ \ 5.1\ \ 4.1\ \ 3.1\ \ 0)\cdot kip$

Live Load:

$P := 440kip$ applied at a point $x = 10.208\,ft$ from the end of the beam.

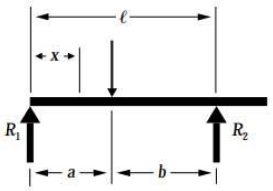

6/20

$a_{LL} := (x - brng) = 9.583\,ft$

$b_{LL} := L_{span} - (x - brng) = 21.167\,ft$

$R_1 := \frac{P \cdot b_{LL}}{L_{span}} = 302.9 \cdot kip$

$R_2 := \frac{P \cdot a_{LL}}{L_{span}} = 137.1 \cdot kip$

$V_{LL_z} := if\left(x_{e_z} < a_{LL}, R_1, R_1 - P\right)$

$V_{LL}^T = (303\ \ 303\ \ 303\ \ 303\ \ 303\ \ 303\ \ 303\ \ 303\ \ 303\ \ 303\ \ 303\ \ 303\ \ -137\ \ -137\ \ -137\ \ -137) \cdot kip$

$M_{LL_z} := if\left[x_{e_z} < a_{LL}, V_{LL_z}\left(x_{e_z}\right), R_1 \cdot a_{LL} + V_{LL_z}\left(x_{e_z} - a_{LL}\right)\right]$ $\qquad M_{LL\_max} := \frac{P \cdot a_{LL} \cdot b_{LL}}{L_{span}} = 2902.47 \cdot kip \cdot ft$

$M_{LL}^T = (0\ \ 189\ \ 416\ \ 568\ \ 719\ \ 1022\ \ 1325\ \ 1628\ \ 1931\ \ 2234\ \ 2537\ \ 2839\ \ 2794\ \ 2657\ \ 2520\ \ 2108) \cdot kip \cdot ft$

Live Load Distribution Factors:

Flexural Distribution Factors (STD 3.23.2)

$d_e := 1ft$ distance from center of exterior girder to the location of the centroid of the outermost wheel group

$N_L := floor\left[\left(width_{deck} - 2 \cdot 1.67ft\right) \div 12ft\right] = 2.00$ number of lanes that can be loaded

Exterior Beam

$$DF_{extf_{1,1}} := \begin{cases} \frac{S}{7ft} & \text{if } S \le 10ft \\ 1 + \frac{d_e}{S} - \frac{3ft}{S} & \text{otherwise} \end{cases} = 1.286$$

wheels/beam, for 1 lane loaded, but:

$DF_{extf_{1,1}} := 0.5 \cdot DF_{extf_{1,1}} = 0.64$ lanes/beam

$$DF_{extf_{1,2}} := \begin{cases} \frac{S}{5.5ft} & \text{if } S \le 14ft \\ 1 + \frac{d_e}{S} - \frac{3ft}{S} & \text{otherwise} \end{cases} = 1.636$$

wheels/beam, for 2+ lanes loaded, but:

$DF_{extf_{1,2}} := 0.5 \cdot DF_{extf_{1,2}} = 0.82$ lanes/beam

Interior Beam

$$DF_{intf_{1,1}} := \begin{cases} \frac{S}{7ft} & \text{if } S \le 10ft \\ 1 - \frac{3ft}{S} & \text{otherwise} \end{cases} = 1.286$$

wheels/beam, for 1 lane loaded, but:

$DF_{intf_{1,1}} := 0.5 \cdot DF_{intf_{1,1}} = 0.64$ lanes/beam

$$DF_{intf_{1,2}} := \begin{cases} \frac{S}{5.5ft} & \text{if } S \le 14ft \\ \frac{3}{2} - \frac{5ft}{S} & \text{otherwise} \end{cases} = 1.636$$

wheels/beam, for 2+ lanes loaded, but:

$DF_{intf_{1,2}} := 0.5\, DF_{intf_{1,2}} = 0.82$ lanes/beam

Shear Distribution Factors (STD 3.23.1)

$d_e := 1ft$ distance from center of exterior girder to the location of the centroid of the outermost wheel group

Exterior Beam

$$DF_{extv_{1,1}} := \begin{cases} \frac{S}{7ft} & \text{if } S \le 10ft \\ 1 + \frac{d_e}{S} - \frac{3ft}{S} & \text{otherwise} \end{cases} = 1.286$$

wheels/beam, for 1 lane loaded, but:

$DF_{extv_{1,1}} := 0.5 \cdot DF_{extv_{1,1}} = 0.64$ lanes/beam

$$DF_{extv_{1,2}} := \begin{cases} \frac{S}{5.5ft} & \text{if } S \le 14ft \\ 1 + \frac{d_e}{S} - \frac{3ft}{S} & \text{otherwise} \end{cases} = 1.636$$

wheels/beam, for 2+ lanes loaded, but:

$DF_{extv_{1,2}} := 0.5 \cdot DF_{extv_{1,2}} = 0.82$ lanes/beam

Interior Beam

$$DF_{intv_{1,1}} := \begin{cases} \frac{S}{7ft} & \text{if } S \le 10ft \\ 1 - \frac{3ft}{S} & \text{otherwise} \end{cases} = 1.286$$

wheels/beam, for 1 lane loaded, but:

$DF_{intv_{1,1}} := 0.5 \cdot DF_{intv_{1,1}} = 0.64$ lanes/beam

$$DF_{intv_{1,2}} := \begin{cases} \frac{S}{5.5ft} & \text{if } S \le 14ft \\ \frac{3}{2} - \frac{5ft}{S} & \text{otherwise} \end{cases} = 1.636$$

wheels/beam, for 2+ lanes loaded, but:

$DF_{intv_{1,2}} := 0.5\, DF_{intv_{1,2}} = 0.82$ lanes/beam

Summary

Lanes: 1 2+

$DF_{intf} = (0.64 \quad 0.82)$

$DF_{extf} = (0.64 \quad 0.82)$

Moment DF

$DF_f := if(BeamType = "interior", max(DF_{intf}), max(DF_{extf})) = 0.82$

use max DF to be conservative

$DF_{intv} = (0.64 \quad 0.82)$

$DF_{extv} = (0.64 \quad 0.82)$

Shear DF

$DF_v := if(BeamType = "interior", min(DF_{intv}), max(DF_{extv})) = 0.64$

use min DF to be conservative

Prestress Losses & Transfer Stresses:

Prestress Losses at Release:

$f_{pj} := P_{jstrand} \cdot n_{Etot} \div A_{ps} = 163.40 \cdot ksi$ $\quad f_{pj} \div f_{pu} = 0.61$ (STD 9.16.2.1.2)

$P_j := A_{ps} \cdot f_{pj} = 550.00 \cdot kip$

Initial Prestress Loss due to Elastic Shortening:

Estimate Elastic Shortening: $ES := 15.69ksi$ and iterate until actual ES matches

$P_i := A_{ps} \cdot (f_{pj} - ES) = 497 \cdot kip$

$$f_{cir} := \frac{P_i}{A_g} + \frac{P_i \cdot e_{HP}^2}{I_g} - \frac{M_{gi_{x_{itot}}} \cdot e_{HP}}{I_g} = 2.22 \cdot ksi$$

$$ES := \frac{E_{ps}}{E_{ci}} \cdot f_{cir} = 15.69 \cdot ksi$$

$f_{pi} := f_{pj} - ES = 147.71 \cdot ksi$ $\quad P_i := A_{ps} \cdot f_{pi} = 497 \cdot kip$

Stresses due to Prestress at Release:

Bottom Stresses at End

$$f_{pib\_E} := -\frac{P_i}{A_g} - \frac{P_i \cdot e_{end} \cdot y_{gb}}{I_g} = -2.22 \cdot ksi$$

Top Stresses at End

$$f_{pit\_E} := -\frac{P_i}{A_g} + \frac{P_i \cdot e_{end} \cdot y_{gt}}{I_g} = -0.10 \cdot ksi$$

Bottom Stresses at HP

$$f_{pib\_HP} := -\frac{P_i}{A_g} - \frac{P_i \cdot e_{HP} \cdot y_{gb}}{I_g} + \frac{M_{gi_{x_{itot}}} \cdot y_{gb}}{I_g} = -2.68 \cdot ksi$$

Top Stresses at HP

$$f_{pit\_HP} := -\frac{P_i}{A_g} + \frac{P_i \cdot e_{HP} \cdot y_{gt}}{I_g} - \frac{M_{gi_{x_{itot}}} \cdot y_{gt}}{I_g} = 0.49 \cdot ksi$$

Check Stresses at Release: (STD 9.15.2.1)

End

Allowable	*Actual*	
$f_{endi\_t} := 3 \cdot \sqrt{f'_{ci}} \cdot \sqrt{psi} = 0.203 \cdot ksi$	$f_{pit\_E} = -0.10 \cdot ksi$	$end\_T\_check := if(f_{endi\_t} \geq f_{pit\_E}, "OK", "NG") = "OK"$
$f_{endi\_c} := -0.6 \cdot f'_{ci} = -2.76 \cdot ksi$	$f_{pib\_E} = -2.22 \cdot ksi$	$end\_C\_check := if(f_{endi\_c} \leq f_{pib\_E}, "OK", "NG") = "OK"$

Harping Point

Allowable *Actual*

$f_{HPi\_t} := 7.5 \cdot \sqrt{f'_{ci}} \cdot \sqrt{psi} = 0.509 \cdot ksi$ $f_{pit\_HP} = 0.494 \cdot ksi$ $HP\_T\_check := if\left(f_{HPi\_t} \geq f_{pit\_HP}, "OK", "NG"\right) = "OK"$

using this limit requires that the tensile force be carried by additional steel in the tensile region

$$x_{ic} := \frac{f_{pit\_HP} \cdot h_g}{\left(f_{pit\_HP} - f_{pib\_HP}\right)} = 5.60 \cdot in$$

$T_i := 0.5 f_{pit\_HP} \cdot tf_w \cdot x_{ic} = 16.58 \cdot kip$

$f_s := \min\left(0.5 \cdot f_y, 30ksi\right) = 30.00 \cdot ksi$

$A_{st} := T_i \div f_s = 0.55 \cdot in^2$

$n_{5t} := ceil\left(A_{st} \div A_5\right) = 2$ use #5 bars in the top, tensile region

$f_{HPi\_c} := -0.6 \cdot f'_{ci} = -2.76 \cdot ksi$ $f_{pib\_HP} = -2.681 \cdot ksi$ $HP\_C\_check := if\left(f_{HPi\_c} \leq f_{pib\_HP}, "OK", "NG"\right) = "OK"$

Prestress Losses at Service: (STD 9.16.2.1)

Shrinkage Losses:

$SH := 17000psi - 150psi \cdot RH = 6.05 \cdot ksi$

Concrete Creep Losses:

$$f_{cir} := \frac{P_i}{A_g} + \frac{P_i \cdot e_{HP}^2}{I_g} - \frac{M_{gi_{x_{itot}}} \cdot e_{HP}}{I_g} = 2.22 \cdot ksi$$

$$f_{cds} := \frac{M_{de_{x_{etot}}} \cdot e_{HP}}{I_g} = 0.29 \cdot ksi$$

$CR_c := 12 \cdot f_{cir} - 7 \cdot f_{cds} = 24.64 \cdot ksi$

Prestressing Relaxation Losses:

$$CR_s := \begin{cases} 5000psi - 0.1ES - 0.05 \cdot \left(SH + CR_c\right) & \text{if } StrandType = "LR" \\ 20000psi - 0.4ES - 0.2 \cdot \left(SH + CR_c\right) & \text{otherwise} \end{cases} = 1.90 \cdot ksi$$

Determine Total Prestress Losses & Check Steel Stress:

$\Delta f_s := ES + SH + CR_c + CR_s = 48.27 \cdot ksi$ $\%Loss := \frac{\Delta f_s}{f_{pj}} \cdot 100 = 29.54$

$f_{pe} := f_{pj} - \Delta f_s = 115.13 \cdot ksi$ $P_e := f_{pe} \cdot A_{ps} = 387.51 \cdot kip$

$f_{all} := 0.8 \cdot f_{py} = 194.40 \cdot ksi$ $stress\_check := if\left(f_{pe} \leq f_{all}, "OK", "NG"\right) = "OK"$

Stresses due to Prestress at Service: (NO LL INCLUDED)

Bottom Stresses

$$f_{peb_z} := -\frac{P_e}{A_g} - \frac{P_e \cdot e_{x_z}}{S_{gb}} + \frac{M_{ge_z} + M_{de_z}}{S_{gb}}$$

Top Stresses

$$f_{pet_z} := -\frac{P_e}{A_g} + \frac{P_e \cdot e_{x_z}}{S_{gt}} - \frac{M_{ge_z} + M_{de_z}}{S_{gt}}$$

$$f_{peb} = \begin{pmatrix} -1.75 \\ -1.72 \\ -1.69 \\ -1.67 \\ -1.65 \\ -1.62 \\ -1.59 \\ -1.57 \\ -1.55 \\ -1.54 \\ -1.53 \\ -1.53 \\ -1.53 \\ -1.54 \\ -1.55 \\ -1.63 \end{pmatrix} \cdot ksi \qquad f_{pet} = \begin{pmatrix} -0.05 \\ -0.09 \\ -0.13 \\ -0.16 \\ -0.18 \\ -0.22 \\ -0.26 \\ -0.29 \\ -0.31 \\ -0.33 \\ -0.34 \\ -0.34 \\ -0.33 \\ -0.32 \\ -0.31 \\ -0.21 \end{pmatrix} \cdot ksi$$

Check Stresses at Service: (STD 9.15.2.2)

End

Allowable

$f_{end\_t} := 0 \cdot \sqrt{f'_{cg}} \cdot \sqrt{psi} = 0 \cdot ksi$

$f_{end\_c} := -0.4 \cdot f'_{cg} = -3 \cdot ksi$

Actual

$f_{pet_1} = -0.05 \cdot ksi$

$f_{peb_1} = -1.75 \cdot ksi$

$T\_check := if\left(f_{end\_t} \geq f_{pet_1}, "OK", "NG"\right) = "OK"$

$C\_check := if\left(f_{end\_c} \leq f_{peb_1}, "OK", "NG"\right) = "OK"$

Harping Point

Allowable

$f_{HP\_t} := 6 \cdot \sqrt{f'_{cg}} \cdot \sqrt{psi} = 0.52 \cdot ksi$

$f_{HP\_c} := -0.4 \cdot f'_{cg} = -3 \cdot ksi$

Actual

$f_{pet_{x_{etot}}} = -0.21 \cdot ksi$

$f_{peb_{x_{etot}}} = -1.63 \cdot ksi$

$T\_check := if\left(f_{HP\_t} \geq f_{pet_{x_{etot}}}, "OK", "NG"\right) = "OK"$

$C\_check := if\left(f_{HP\_c} \leq f_{peb_{x_{etot}}}, "OK", "NG"\right) = "OK"$

Anchor Zone Reinforcement: (STD 9.21.3)

$P_r := 0.04 \cdot P_i = 19.89 \cdot kip$

$f_s := 20 \cdot ksi$

$A_{s\_anchor} := \frac{P_r}{f_s}$ $A_{s\_anchor} = 1.0 \cdot in^2$

Number of bars which must be placed within $d/4$ of the end of the beam: $\frac{d_{p_1}}{4} = 9.2 \cdot in$ $n_{reqd} := ceil\left(\frac{A_{s\_anchor}}{2 \cdot A_5}\right) = 2.00$

use 2-#5 bars in the first 9 inches of the beam

Confinement Reinforcement: (STD 9.21.3)

For the distance of d from the end of the beam, reinforcement shall be placed to confine the prestressing steel in the bottom flange.

$d := h_c - y_{end} = 36.45 \cdot in$ Provide #3 bars enclosing the bottom flange strands at least 34 in. from beam end.

Flexural Limit State: (STD 9.17.1)

At each section the following must be satisfied for flexure:

$M_u \le \phi M_n$ with $\phi_f := 1.0$ for the lab

and $\phi M_n = \phi A_{ps} \cdot f_{ps} \cdot d_p \cdot \left(1 - 0.6 \cdot \frac{\rho_{ps} \cdot f_{ps}}{f'_c}\right)$ if $f_{pe} > 0.5 f_{pu}$ (STD 9.17.2)

$stress\_check := if\left(f_{pe} \ge 0.5 \cdot f_{pu}, "OK", "NG"\right) = "NG"$ If NG, use strain compatibility (STD 9.17.4.1)

Transfer and Development Length:

Assume f_{ps} and check later $f_{ps} := 270ksi$

$L_d := d_{ps} \cdot \left(f_{ps} - \frac{2}{3} \cdot f_{pe}\right) \cdot ksi^{-1} = 8.05 ft$ $L_d = 96.62 \cdot in$ (STD 9.27.1)

$L_t := 60 \cdot d_{ps} = 30.00 \cdot in$ (LRFD 5.11.4.1)

Fraction of Strands Developed:

$$Ld_{df_z} := if\left[\left(x_{e_z} + brng\right) \ge L_d, 1, if\left[x_{e_z} < L_t, \frac{\left(x_{e_z} + brng\right)}{L_t} \cdot \frac{f_{pe}}{f_{pu}}, \frac{f_{pe}}{f_{pu}} + \frac{\left(x_{e_z} + brng\right) - L_t}{L_d - L_t} \cdot \left(1 - \frac{f_{pe}}{f_{pu}}\right)\right]\right]$$

$Ld_{df}^T = (0.11 \ 0.21 \ 0.34 \ 0.43 \ 0.51 \ 0.58 \ 0.68 \ 0.79 \ 0.89 \ 0.99 \ 1.00 \ 1.00 \ 1.00 \ 1.00 \ 1.00 \ 1.00)$

$x_e^T = (0.00 \ 0.62 \ 1.37 \ 1.87 \ 2.38 \ 3.37 \ 4.37 \ 5.38 \ 6.37 \ 7.38 \ 8.38 \ 9.38 \ 10.38 \ 11.38 \ 12.38 \ 15.38)\ ft$

Fraction of Strands in Transfer Length:

$$Lt_{df_z} := if\left[\left(x_{e_z} + brng\right) \ge L_t, 1, \frac{\left(x_{e_z} + brng\right)}{L_t}\right]$$

$Lt_{df}^T = (0.3 \ 0.5 \ 0.8 \ 1.0 \ 1.0 \ 1.0 \ 1.0 \ 1.0 \ 1.0 \ 1.0 \ 1.0 \ 1.0 \ 1.0 \ 1.0 \ 1.0 \ 1.0)$

$x_e^T = (0.0 \ 0.6 \ 1.4 \ 1.9 \ 2.4 \ 3.4 \ 4.4 \ 5.4 \ 6.4 \ 7.4 \ 8.4 \ 9.4 \ 10.4 \ 11.4 \ 12.4 \ 15.4)\ ft$

Strain Compatibility Approach for Beam Flexural Strength (PCI 8.2.2.5)

stress_check := if($f_{pe} \geq 0.5 \cdot f_{pu}$, "OK", "NG") = "NG" $f_{pe} = 115.13 \cdot ksi$ $0.5 \cdot f_{pu} = 135.00 \cdot ksi$

Input estimated N.A. location and revise until total steel force = total concrete force:

$c := 0.01$

Slot #

$$c_{sc} := \begin{pmatrix} 0.35 + c \\ 0.72 + c \\ 1.15 + c \\ 1.44 + c \\ 1.73 + c \\ 1.97 + c \\ 2.32 + c \\ 2.68 + c \\ 3.03 + c \\ 3.38 + c \\ 3.40 + c \\ 3.40 + c \\ 3.40 + c \\ 3.40 + c \\ 3.40 + c \\ 3.40 + c \end{pmatrix} in \qquad \begin{pmatrix} 1 \\ 2 \\ 3 \\ 4 \\ 5 \\ 6 \\ 7 \\ 8 \\ 9 \\ 10 \\ 11 \\ 12 \\ 13 \\ 14 \\ 15 \\ 16 \end{pmatrix}$$

$a_{sc_z} := \beta_{1d} \cdot c_{sc_z}$

$$a_{sc} = \begin{pmatrix} 0.31 \\ 0.62 \\ 0.99 \\ 1.23 \\ 1.48 \\ 1.68 \\ 1.98 \\ 2.29 \\ 2.58 \\ 2.88 \\ 2.90 \\ 2.90 \\ 2.90 \\ 2.90 \\ 2.90 \\ 2.90 \end{pmatrix} \cdot in$$

Consider draped strands and straight strands separately:

Draped:

$y_{xid_{zi}} := y_{Ed} - \left(x_{i_{zi}} + x_{HP}\right) \cdot \left(y_{Ed} - y_{HPd}\right)$ $y_{xd} := \text{submatrix}\left(y_{xid}, 2, x_{itot}, 1, 1\right)$

$y_{xd}^{T} = (24.38 \;\; 23.75 \;\; 23.00 \;\; 22.50 \;\; 22.00 \;\; 21.00 \;\; 20.00 \;\; 19.00 \;\; 18.00 \;\; 17.00 \;\; 16.00 \;\; 15.00 \;\; 14.00 \;\; 13.00 \;\; 12.00 \;\; 9.00) \cdot in$

Straight:

$y_{xis_{zi}} := y_{Es} - \left(x_{i_{zi}} + x_{HP}\right) \cdot \left(y_{Es} - y_{HPs}\right)$ $y_{xs} := \text{submatrix}\left(y_{xis}, 2, x_{itot}, 1, 1\right)$

$y_{xs}^{T} = (3.75 \;\; 3.75 \;\; 3.75 \;\; 3.75 \;\; 3.75 \;\; 3.75 \;\; 3.75 \;\; 3.75 \;\; 3.75 \;\; 3.75 \;\; 3.75 \;\; 3.75 \;\; 3.75 \;\; 3.75 \;\; 3.75 \;\; 3.75) \cdot in$

Distance from top of compression section to strand center of gravity:

Draped:

$d_{scd_z} := h_c - y_{xd_z}$

$d_{scd}^{T} = (21.63 \;\; 22.25 \;\; 23.00 \;\; 23.50 \;\; 24.00 \;\; 25.00 \;\; 26.00 \;\; 27.00 \;\; 28.00 \;\; 29.00 \;\; 30.00 \;\; 31.00 \;\; 32.00 \;\; 33.00 \;\; 34.00 \;\; 37.00) \cdot in$

Straight:

$d_{scs_z} := h_c - y_{xs_z}$

$d_{scs}^{T} = (42.25 \;\; 42.25 \;\; 42.25 \;\; 42.25 \;\; 42.25 \;\; 42.25 \;\; 42.25 \;\; 42.25 \;\; 42.25 \;\; 42.25 \;\; 42.25 \;\; 42.25 \;\; 42.25 \;\; 42.25 \;\; 42.25 \;\; 42.25) \cdot in$

Compute strain in each layer of steel: (PCI 8.2.2.5)

Draped:

$$\varepsilon_{scd_z} := 0.003 \cdot \left(\frac{d_{scd_z}}{c_{sc_z}} - 1 \right) + \frac{f_{pe}}{E_{ps}}$$

$$\varepsilon_{scd}^{T} = (0.181 \quad 0.092 \quad 0.060 \quad 0.050 \quad 0.042 \quad 0.039 \quad 0.034 \quad 0.031 \quad 0.029 \quad 0.027 \quad 0.027 \quad 0.028 \quad 0.029 \quad 0.030 \quad 0.031 \quad 0.034)$$

Straight:

$$\varepsilon_{scs_z} := 0.003 \cdot \left(\frac{d_{scs_z}}{c_{sc_z}} - 1 \right) + \frac{f_{pe}}{E_{ps}} \qquad 0.003 \cdot \left(\frac{d_{scs_1}}{c_{sc_1}} - 1 \right) = 0.35$$

$$d_{scs_1} = 42.25 \cdot in \qquad c_{sc_1} = 0.36 \cdot in$$

$$\varepsilon_{scs}^{T} = (0.353 \quad 0.175 \quad 0.110 \quad 0.088 \quad 0.074 \quad 0.065 \quad 0.055 \quad 0.048 \quad 0.043 \quad 0.038 \quad 0.038 \quad 0.038 \quad 0.038 \quad 0.038 \quad 0.038 \quad 0.038)$$

Use formula developed by Devalapura and Tadros (1992) that defines the stress-strain relationship for 270 ksi low-relaxation strands to determine the stress in the strands. (PCI 8.2.2.5)

Draped:

$$f_{scd_z} := \min\left[\varepsilon_{scd_z} \cdot \left[887 + \frac{27613}{\left[1 + \left(112.4 \cdot \varepsilon_{scd_z} \right)^{7.36} \right]^{\frac{1}{7.36}}} \right] \cdot ksi, f_{pu} \right]$$

$$f_{scd}^{T} = (270 \quad 270 \quad 270 \quad 270 \quad 270 \quad 270 \quad 270 \quad 270 \quad 270 \quad 269 \quad 270 \quad 270 \quad 270 \quad 270 \quad 270 \quad 270) \cdot ksi$$

Straight:

$$f_{scs_z} := \min\left[\varepsilon_{scs_z} \cdot \left[887 + \frac{27613}{\left[1 + \left(112.4 \cdot \varepsilon_{scs_z} \right)^{7.36} \right]^{\frac{1}{7.36}}} \right] \cdot ksi, f_{pu} \right]$$

$$f_{scs}^{T} = (270 \quad 270 \quad 270 \quad 270 \quad 270 \quad 270 \quad 270 \quad 270 \quad 270 \quad 270 \quad 270 \quad 270 \quad 270 \quad 270 \quad 270 \quad 270) \cdot ksi$$

Steel and concrete areas:

Draped: $A_{psd} = 0.92 \cdot in^2$

Straight: $A_{pss} = 2.45 \cdot in^2$

Concrete:

$$rect\_check_z := if\left(a_{sc_z} < t_d, "OK", "NG" \right)$$

$$rect\_check^{T} = ("OK" \quad "OK" \quad "OK" \quad "OK" \quad "OK" \quad "OK" \quad "OK" \quad "OK" \quad "OK" \quad "OK" \quad "OK" \quad "OK" \quad "OK" \quad "OK" \quad "OK" \quad "OK")$$

$$A_{beffsc_z} := if\left(a_{sc_z} < t_d, b_{eff} \cdot a_{sc_z}, b_{eff} \cdot t_d \right)$$

$$A_{beffsc}^{T} = (28 \quad 57 \quad 91 \quad 114 \quad 136 \quad 155 \quad 183 \quad 211 \quad 238 \quad 266 \quad 267 \quad 267 \quad 267 \quad 267 \quad 267 \quad 267) \cdot in^2$$

Steel and concrete forces:

$total\_Fsteel_z := Ld_{df_z} \cdot \left(A_{psd} \cdot f_{scd_z} + A_{pss} \cdot f_{scs_z} \right)$

$total\_Fsteel^T = (97 \ 194 \ 310 \ 388 \ 465 \ 528 \ 622 \ 716 \ 810 \ 903 \ 909 \ 909 \ 909 \ 909 \ 909 \ 909) \cdot kip$

$total\_Fconc_z := 0.85 \cdot f'_{cd} \cdot A_{beffsc_z}$

$total\_Fconc^T = (96 \ 195 \ 309 \ 387 \ 464 \ 528 \ 621 \ 717 \ 810 \ 904 \ 909 \ 909 \ 909 \ 909 \ 909 \ 909) \cdot kip$

$(total\_Fsteel - total\_Fconc)^T = (1 \ -1 \ 1 \ 1 \ 1 \ 0 \ 1 \ -1 \ -0 \ -1 \ -0 \ -0 \ -0 \ -0 \ -0 \ -0) \cdot kip$

Slot # (1 2 3 4 5 6 7 8 9 10 11 12 13 14 15 16)

$sc\_check_z := if(|total\_Fsteel_z - total\_Fconc_z| \le 2kip, "OK", "NG")$

$sc\_check^T = ("OK" \ "OK" \ "OK" \ "OK" \ "OK" \ "OK" \ "OK" \ "OK" \ "OK" \ "OK" \ "OK" \ "OK" \ "OK" \ "OK" \ "OK" \ "OK")$

Sum moments about top of composite section for nominal capacity:

$\phi M_{n_z} := Ld_{df_z} \cdot \phi_f \cdot \left[\left(A_{psd} \cdot f_{scd_z} \cdot d_{scd_z} \right) + \left(A_{pss} \cdot f_{scs_z} \cdot d_{scs_z} \right) \right] - \left[0.85 \cdot f'_{cd} \cdot A_{beffsc_z} \cdot \left(a_{sc_z} \div 2 \right) \right]$

$\phi M_n^T = (294 \ 589 \ 943 \ 1179 \ 1416 \ 1616 \ 1910 \ 2205 \ 2502 \ 2800 \ 2837 \ 2858 \ 2878 \ 2899 \ 2920 \ 2982) \cdot kip \cdot ft$

$M_{u_z} := 1.10 \left[\left(M_{ge_z} + M_{de_z} \right) + \left(DF_f \cdot M_{LL_z} \right) \right]$ no load factors for laboratory, use 10% extra M_u to be conservative

$M_u^T = (-0 \ 185 \ 406 \ 554 \ 700 \ 993 \ 1284 \ 1573 \ 1860 \ 2146 \ 2431 \ 2714 \ 2681 \ 2565 \ 2447 \ 2084) \cdot kip \cdot ft$

$\left(\phi M_n - M_u \right)^T = (295 \ 404 \ 537 \ 626 \ 715 \ 623 \ 626 \ 632 \ 642 \ 654 \ 406 \ 144 \ 197 \ 334 \ 472 \ 897) \cdot kip \cdot ft$

$Mn\_check_z := if \left[M_{u_z} \le \left(\phi M_n \right)_z, "OK", "NG" \right]$

$Mn\_check^T = ("OK" \ "OK" \ "OK" \ "OK" \ "OK" \ "OK" \ "OK" \ "OK" \ "OK" \ "OK" \ "OK" \ "OK" \ "OK" \ "OK" \ "OK" \ "OK")$

1 2 3 4 5 6 7 8 9 10 11 12 13 14 15 16

Minimum Steel Check: (STD 9.18.2.1)

$f_r := 7.5 \cdot \sqrt{f'_{cg}} \cdot \sqrt{psi} = 0.65 \cdot ksi$

$f_{cpe_z} := \frac{P_e}{A_g} + \frac{P_e \cdot e_{x_z}}{S_{gb}}$

$M_{cr_z} := S_{cb} \cdot \left(f_r + f_{cpe_z} \right) - M_{ge_z} \cdot \left(\frac{S_{cb}}{S_{gb}} - 1 \right)$

$M_{n\_limit_z} := 1.2 \cdot M_{cr_z}$

$M_{n\_limit}^T = (1622 \ 1631 \ 1641 \ 1649 \ 1656 \ 1671 \ 1687 \ 1703 \ 1719 \ 1737 \ 1754 \ 1772 \ 1791 \ 1810 \ 1830 \ 1892) \cdot kip \cdot ft$

$Mnlimit\_check_z := if \left(\phi M_{n_z} \ge M_{n\_limit_z}, "OK", "NG" \right)$

$Mnlimit\_check^T = ("NG" \ "NG" \ "NG" \ "NG" \ "NG" \ "NG" \ "OK" \ "OK" \ "OK" \ "OK" \ "OK" \ "OK" \ "OK" \ "OK" \ "OK" \ "OK")$

1 2 3 4 5 6 7 8 9 10 11 12 13 14 15 16

Consider only the critical section per STD 9.18.2.1:

$crit\_section\_check := if \left(\phi M_{n_{12}} \ge M_{n\_limit_{12}}, "OK", "NG" \right) = "OK"$

Shear Limit State:

At each section the following must be satisfied for shear:

$V_u \le \phi V_n$ with $\phi_v := 1.0$ for the lab

and $V_n = V_c + V_s$ (STD 9.20.1.3)

and $V_c = \min(V_{ci}, V_{cw})$ (STD 9.20.2.1)

Critical Section for Shear: (STD 9.20.1.4)

$$d_{vcrit} := \frac{h_c}{2} = 23.00 \cdot in$$

$d_{vcrit} \div 2 = 11.50 \cdot in$ $d_{vcrit} = 23.00 \cdot in$ $2 \cdot d_{vcrit} = 46.00 \cdot in$ $3 \cdot d_{vcrit} = 69.00 \cdot in$ $4 \cdot d_{vcrit} = 92.00 \cdot in$

$d_{vcrit} \div 2 = 0.96 \cdot ft$ $d_{vcrit} = 1.92 ft$ $2 \cdot d_{vcrit} = 3.83 \cdot ft$ $3 \cdot d_{vcrit} = 5.75 \cdot ft$ $4 \cdot d_{vcrit} = 7.67 \cdot ft$

Critical section for shear from beam end: $x_{crit} := d_{vcrit} + \frac{L_{soleplate}}{2} + brng = 3.2 \cdot ft$

Critical section for shear from CL support: $x_{crit} := d_{vcrit} + \frac{L_{soleplate}}{2} = 2.54 \cdot ft$

Calculate effective shear depths: (STD 9.20.2)

$$d_{v_z} := \max\left(d_{p_z}, 0.8 \cdot h_c\right)$$

$$d_v^T = (36.8 \;\; 36.8 \;\; 37 \;\; 37.1 \;\; 37.3 \;\; 37.5 \;\; 37.8 \;\; 38.1 \;\; 38.4 \;\; 38.6 \;\; 38.9 \;\; 39.2 \;\; 39.5 \;\; 39.7 \;\; 40 \;\; 40.8) \cdot in$$

Concrete Contribution to Shear: (STD 9.20.2)

Calculate V_{ci}: (STD 9.20.2.2)

$$V_{i_z} := \left|1.6 V_{LL_z}\right|$$

$$M_{max_z} := \left|1.6 \cdot M_{LL_z}\right| \qquad M_{max_1} := 10^{-2} kip \cdot ft \quad \text{(prevent division by zero)}$$

$$f_r := 6 \cdot \sqrt{f'_{cg}} \cdot \sqrt{psi} = 0.52 \cdot ksi$$

$$M_{cre_z} := S_{cb} \cdot \left(f_r + f_{cpe_z} - \frac{M_{ge_z}}{S_{gb}}\right)$$

$$M_{cre}^T = (1279 \;\; 1282 \;\; 1286 \;\; 1290 \;\; 1293 \;\; 1300 \;\; 1309 \;\; 1318 \;\; 1328 \;\; 1338 \;\; 1350 \;\; 1362 \;\; 1376 \;\; 1390 \;\; 1405 \;\; 1455) \cdot kip \cdot ft$$

$$V_{ci_z} := \max\left[0.6 \cdot \sqrt{f'_{cg}} \cdot \sqrt{psi} \cdot b_v \cdot d_{v_z} + \left(V_{ge_z} + V_{de_z}\right) + \frac{V_{i_z} \cdot M_{cre_z}}{M_{max_z}}, 1.7 \cdot \sqrt{f'_{cg}} \cdot \sqrt{psi} \cdot b_v \cdot d_{v_z}\right]$$

$$V_{ci}^T = (61969337 \;\; 2084 \;\; 967 \;\; 719 \;\; 575 \;\; 414 \;\; 327 \;\; 271 \;\; 233 \;\; 205 \;\; 183 \;\; 166 \;\; 87 \;\; 90 \;\; 93 \;\; 107) \cdot kip$$

Calculate V_{cw}: (STD 9.20.2.3)

16/20

$$f_{pc_z} := \left[\frac{Lt_{df_z} \cdot P_e}{A_g} - \frac{Lt_{df_z} \cdot P_e \cdot e_{x_z} \cdot (h_{webbf} - y_{gb})}{I_g} + \frac{(M_{ge_z} + M_{de_z}) \cdot (h_{webbf} - y_{gb})}{I_g} \right]$$

$f_{pc}^T = (0.125 \;\; 0.277 \;\; 0.448 \;\; 0.556 \;\; 0.568 \;\; 0.591 \;\; 0.61 \;\; 0.626 \;\; 0.638 \;\; 0.646 \;\; 0.651 \;\; 0.653 \;\; 0.65 \;\; 0.645 \;\; 0.635 \;\; 0.586) \cdot ksi$

$V_{p_z} := if(x_{e_z} \le x_{HP}, Lt_{df_z} \cdot f_{pe} \cdot A_{psd} \cdot \sin(\alpha), 0)$

$V_p^T = (2.2 \;\; 4.4 \;\; 7 \;\; 8.8 \;\; 8.8 \;\; 8.8 \;\; 8.8 \;\; 8.8 \;\; 8.8 \;\; 8.8 \;\; 8.8 \;\; 8.8 \;\; 8.8 \;\; 8.8 \;\; 8.8 \;\; 8.8) \cdot kip$

$V_{cw_z} := \left(3.5 \cdot \sqrt{f'_{cg}} \cdot \sqrt{psi} + 0.3 \cdot f_{pc_z}\right) \cdot b_v \cdot d_{v_z} + V_{p_z}$

$V_{cw}^T = (77 \;\; 90 \;\; 104 \;\; 113 \;\; 115 \;\; 117 \;\; 119 \;\; 121 \;\; 123 \;\; 124 \;\; 125 \;\; 126 \;\; 127 \;\; 127 \;\; 127 \;\; 126) \cdot kip$

Calculate V_c:

$V_{c_z} := if(V_{cw_z} < V_{ci_z}, V_{cw_z}, V_{ci_z})$

$V_c^T = (77 \;\; 90 \;\; 104 \;\; 113 \;\; 115 \;\; 117 \;\; 119 \;\; 121 \;\; 123 \;\; 124 \;\; 125 \;\; 126 \;\; 87 \;\; 90 \;\; 93 \;\; 107) \cdot kip$

Steel Contribution to Shear: (STD 9.20.3)

Stirrup Spacing $s_{max} := 24$

$$s := \begin{pmatrix} 3 \\ 4 \\ 16 \\ s_{max} \\ s_{max} \\ s_{max} \\ s_{max} \\ s_{max} \\ s_{max} \\ s_{max} \\ s_{max} \\ s_{max} \\ s_{max} \\ s_{max} \\ s_{max} \\ s_{max} \end{pmatrix} in$$

3 center line of support
4
16
s_{max} transfer length of strands
s_{max} approx h_c / 2
s_{max} approx d_v
s_{max}
s_{max}
s_{max}
s_{max}
s_{max} approx $2d_v$
s_{max}
s_{max}
s_{max}
s_{max} approx L_d
s_{max} approx $3d_v$
s_{max}
s_{max} approx $4d_v$

Area of Transverse Reinforcement $A_s := A_4$

$$A_v := 2 \begin{pmatrix} A_5 \\ A_s \\ A_s \\ A_s \\ A_s \\ A_s \\ A_s \\ A_s \\ A_s \\ A_s \\ A_s \\ A_s \\ A_s \\ A_s \\ A_s \\ A_s \end{pmatrix}$$

A_5 center line of support
A_s
A_s
A_s transfer length of strands
A_s approx h_c / 2
A_s approx d_v
A_s
A_s
A_s
A_s approx $2d_v$
A_s
A_s
A_s
A_s approx L_d
A_s approx $3d_v$
A_s
A_s approx $4d_v$

$$A_v = \begin{pmatrix} 0.62 \\ 0.40 \\ 0.40 \\ 0.40 \\ 0.40 \\ 0.40 \\ 0.40 \\ 0.40 \\ 0.40 \\ 0.40 \\ 0.40 \\ 0.40 \\ 0.40 \\ 0.40 \\ 0.40 \\ 0.40 \end{pmatrix} \cdot in^2$$

$$V_{s_z} := \min\left(\frac{A_{v_z}\cdot f_y\cdot d_{v_z}}{s_z}, 8\sqrt{f'_{cg}}\cdot\sqrt{psi}\cdot b_v\cdot d_{v_z}\right)$$ (STD 9.20.3.1)

$V_s^T = (153\ \ 153\ \ 56\ \ 37\ \ 37\ \ 38\ \ 38\ \ 38\ \ 38\ \ 39\ \ 39\ \ 39\ \ 39\ \ 40\ \ 40\ \ 41)\cdot kip$

$$V_{scheck_z} := 4\cdot\sqrt{f'_{cg}}\cdot\sqrt{psi}\cdot b_v\cdot d_{v_z}$$ (STD 9.20.3.2)

$V_{scheck}^T = (76\ \ 76\ \ 77\ \ 77\ \ 77\ \ 78\ \ 79\ \ 79\ \ 80\ \ 80\ \ 81\ \ 81\ \ 82\ \ 83\ \ 83\ \ 85)\cdot kip$

Nominal Shear Resistance:

$$V_{n_z} := \left(V_{c_z} + V_{s_z}\right)\cdot 1.3$$ use additional strength factor (1.3*V_n) from Hawkins et al. (2005) and Runzel et al. (2007) (STD 9.20.1.3)

$V_n^T = (299\ \ 315\ \ 208\ \ 196\ \ 198\ \ 201\ \ 204\ \ 207\ \ 209\ \ 211\ \ 213\ \ 215\ \ 164\ \ 168\ \ 173\ \ 193)\cdot kip$

$$V_{u_z} := \left(Vge_z + Vde_z\right) + \left(DF_v\cdot\left|VLL_z\right|\right)$$ no load factors for lab, use DF to estimate LL shear on one girder

$V_u^T = (217\ \ 216\ \ 215\ \ 214\ \ 213\ \ 212\ \ 211\ \ 209\ \ 208\ \ 206\ \ 205\ \ 203\ \ 95\ \ 94\ \ 92\ \ 88)\cdot kip$

$(\phi_v\cdot V_n - V_u)^T = (83\ \ 99\ \ -7\ \ -18\ \ -16\ \ -11\ \ -7\ \ -2\ \ 2\ \ 5\ \ 8\ \ 11\ \ 69\ \ 75\ \ 81\ \ 104)\cdot kip$

$Vn\_check_z := if\left(V_{u_z} \le \phi_v\cdot V_{n_z}, "OK", "NG"\right)$

$Vn\_check^T = ("OK"\ \ "OK"\ \ "NG"\ \ "NG"\ \ "NG"\ \ "NG"\ \ "NG"\ \ "NG"\ \ "OK"\ \ "OK"\ \ "OK"\ \ "OK"\ \ "OK"\ \ "OK"\ \ "OK"\ \ "OK")$

1 2 3 4 5 6 7 8 9 10 11 12 13 14 15 16

Check Minimum Transverse Reinforcement: (STD 9.20.3.3)

$$A_{v\_min} := \frac{50psi\, b_v}{f_y} = 0.06\cdot\frac{in^2}{ft}$$

$$s_{min} := \frac{2A_s}{A_{v\_min}} = 80.00\cdot in$$

$smin\_check_z := if\left(s_z \le s_{min}, "OK", "NG"\right)$

$smin\_check^T = ("OK"\ \ "OK"\ \ "OK"\ \ "OK"\ \ "OK"\ \ "OK"\ \ "OK"\ \ "OK"\ \ "OK"\ \ "OK"\ \ "OK"\ \ "OK"\ \ "OK"\ \ "OK"\ \ "OK"\ \ "OK")$

Check Maximum Stirrup Spacing: (STD 9.20.3.2)

$$s_{max_z} := if\left(V_{s_z} > 4\sqrt{f'_{cg}}\cdot\sqrt{psi}\cdot b_v\cdot d_{v_z}, 0.5\cdot\min\left(0.75\cdot h_c, 24\cdot in\right), \min\left(0.75\cdot h_c, 24\cdot in\right)\right)$$

$s_{max}^T = (12\ \ 12\ \ 24\ \ 24\ \ 24\ \ 24\ \ 24\ \ 24\ \ 24\ \ 24\ \ 24\ \ 24\ \ 24\ \ 24\ \ 24\ \ 24)\cdot in$

$smax\_check_z := if\left(s_z \le s_{max_z}, "OK", "NG"\right)$

$smax\_check^T = ("OK"\ \ "OK"\ \ "OK"\ \ "OK"\ \ "OK"\ \ "OK"\ \ "OK"\ \ "OK"\ \ "OK"\ \ "OK"\ \ "OK"\ \ "OK"\ \ "OK"\ \ "OK"\ \ "OK"\ \ "OK")$

Interface Shear: (STD 9.20.4.3)

Calculate Interface Shear Demand:

$b_{vi} := tf_w = 12.00 \cdot in$

$V_{nh_z} := (350psi) \cdot b_{vi} \cdot d_{p_z}$

$V_u^T = (199 \ 198 \ 197 \ 196 \ 196 \ 194 \ 193 \ 191 \ 190 \ 189 \ 187 \ 186 \ 87 \ 86 \ 84 \ 80) \cdot kip$

$V_{nh}^T = (154 \ 155 \ 155 \ 156 \ 157 \ 158 \ 159 \ 160 \ 161 \ 162 \ 163 \ 165 \ 166 \ 167 \ 168 \ 171) \cdot kip$

$Vi\_check_z := if\left(\phi_v \cdot V_{nh_z} \geq V_{u_z}, "OK", "NG"\right)$

$Vi\_check^T = ("NG" \ "NG" \ "NG" \ "NG" \ "NG" \ "NG" \ "NG" \ "NG" \ "NG" \ "NG" \ "NG" \ "NG" \ "OK" \ "OK" \ "OK" \ "OK")$

Consider Percent of Reinforcement Beyond Minimum: (STD 9.20.4.3)

$Avbys := \frac{A_v}{s}$

$Avbys^T = (2.48 \ 1.20 \ 0.30 \ 0.20 \ 0.20 \ 0.20 \ 0.20 \ 0.20 \ 0.20 \ 0.20 \ 0.20 \ 0.20 \ 0.20 \ 0.20 \ 0.20 \ 0.20) \cdot \frac{in^2}{ft}$

$Avbys_{min} := \frac{(50psi) \cdot b_{vi}}{f_y} = 0.12 \cdot \frac{in^2}{ft}$ (STD 9.20.4.5)

$Percent\_diff_z := \left(\frac{Avbys_z - Avbys_{min}}{Avbys_{min}}\right) \cdot 100$

$Percent\_diff^T = (1967 \ 900 \ 150 \ 67 \ 67 \ 67 \ 67 \ 67 \ 67 \ 67 \ 67 \ 67 \ 67 \ 67 \ 67 \ 67)$

For each percent of tie reinforcement in excess of minimum, increase V_{nh} by: (STD 9.20.4.3)

$Percent\_add_z := \frac{160 \cdot f_y}{40000} \cdot b_v \cdot d_{p_z}$

$Percent\_add^T = (53 \ 53 \ 53 \ 53 \ 54 \ 54 \ 54 \ 55 \ 55 \ 56 \ 56 \ 56 \ 57 \ 57 \ 58 \ 59) \cdot kip$

Calculate Interface Shear Demand:

$\phi V_{nh_z} := \phi_v \cdot \left[V_{nh_z} + \left(Percent\_diff_z \cdot Percent\_add_z\right)\right]$

$\phi V_{nh}^T = (103876 \ 47841 \ 8147 \ 3721 \ 3735 \ 3762 \ 3789 \ 3817 \ 3844 \ 3871 \ 3899 \ 3926 \ 3953 \ 3981 \ 4008 \ 4090) \cdot kip$

$Vi\_check_z := if\left(\phi V_{nh_z} \geq V_{u_z}, "OK", "NG"\right)$

$Vi\_check^T = ("OK" \ "OK" \ "OK" \ "OK" \ "OK" \ "OK" \ "OK" \ "OK" \ "OK" \ "OK" \ "OK" \ "OK" \ "OK" \ "OK" \ "OK" \ "OK")$

Maximum Interface Shear Stirrup Spacing:

$spacing\_check_z := if\left[s_z \leq \min\left[4 \cdot \left(b_v\right), 24in\right], "OK", "NG"\right]$

$spacing\_check^T = ("OK" \ "OK" \ "OK" \ "OK" \ "OK" \ "OK" \ "OK" \ "OK" \ "OK" \ "OK" \ "OK" \ "OK" \ "OK" \ "OK" \ "OK" \ "OK")$

1989 AASHTO STD LFR

at location $x_{crit} = 2.54\,ft$ or use $x_{e_5} = 2.38\,ft$ for ease

Estimate dead loads on an interior girder of in situ lab bridge:

girder $w_g = 413.60\cdot plf$

deck & haunch $w_d = 1025.00\cdot plf$

barrier $w_b := \frac{(2)\cdot(456in^2)\cdot(150pcf)}{N_g} = 237.50\cdot plf$

diaphragm $w_{dia} := \frac{(3)\cdot(158in^2)\cdot(150pcf)}{N_g} = 123.44\cdot plf$

wearing surface $w_{wc} := \frac{(2in)\cdot(150pcf)\cdot width_{deck}}{N_g} = 212.50\cdot plf$

Shear forces and moments from dead loads:

$V_g := w_g\cdot(0.5\cdot L_{span} - x_{e_5}) = 5.38\cdot kip$ $M_g := 0.5\cdot w_g\cdot x_{e_5}\cdot(L_{span} - x_{e_5}) = 13.94\cdot kip\cdot ft$

$V_d := w_d\cdot(0.5\cdot L_{span} - x_{e_5}) = 13.32\cdot kip$ $M_d := 0.5\cdot w_d\cdot x_{e_5}\cdot(L_{span} - x_{e_5}) = 34.54\cdot kip\cdot ft$

$V_b := w_b\cdot(0.5\cdot L_{span} - x_{e_5}) = 3.09\cdot kip$ $M_b := 0.5\cdot w_b\cdot x_{e_5}\cdot(L_{span} - x_{e_5}) = 8.00\cdot kip\cdot ft$

$V_{dia} := w_{dia}\cdot(0.5\cdot L_{span} - x_{e_5}) = 1.60\cdot kip$ $M_{dia} := 0.5\cdot w_{dia}\cdot x_{e_5}\cdot(L_{span} - x_{e_5}) = 4.16\cdot kip\cdot ft$

$V_{wc} := w_{wc}\cdot(0.5\cdot L_{span} - x_{e_5}) = 2.76\cdot kip$ $M_{wc} := 0.5\cdot w_{wc}\cdot x_{e_5}\cdot(L_{span} - x_{e_5}) = 7.16\cdot kip\cdot ft$

$V_{dc} := V_g + V_d + V_b + V_{dia} = 23.39\cdot kip$

$V_{dw} := V_{wc} = 2.76\cdot kip$

Estimate live loads on an interior girder of in situ lab bridge:

$DF_v := if(BeamType = "interior", max(DF_{intv}), max(DF_{extv})) = 0.82$

LL shear of $V_{ll} := DF_v\cdot 50kip$ from SAP2000 for HS20-44 loading in AASHTO STD

Inventory Rating Factor $\phi_v := 0.9$

$\gamma_D := 1.3$ $\gamma_L := 2.17$ $I := \min\left(0.30, \frac{50ft}{b_{LL} + 125ft}\right) = 0.30$ (STD 3.8.2.1)

$V_{ll} = 40.91\cdot kip$ $V_{nr} := V_{n_5} \div 1.3 = 151.98\cdot kip$ $V_{dl} := V_{dc} + V_{dw} = 26.16\cdot kip$

$RF_{inv} := \frac{\phi_v\cdot V_{nr} - \gamma_D\cdot V_{dl}}{\gamma_L\cdot V_{ll}\cdot(1 + I)} = 0.89$ (MCE 6.5.1)

Operating Rating Factor $\phi_v = 0.90$

$\gamma_D := 1.3$ $\gamma_L := 1.3$ $I = 0.30$

$V_{ll} = 40.91\cdot kip$ $V_{nr} = 151.98\cdot kip$ $V_{dl} := V_{dc} + V_{dw} = 26.16\cdot kip$

$RF_{op} := \frac{\phi_v\cdot V_{nr} - \gamma_D\cdot V_{dl}}{\gamma_L\cdot V_{ll}\cdot(1 + I)} = 1.49$ (MCE 6.5.1)

Results on this page still uses an applied load of 440 kips. Shear failure would occur prior to the flexural failure indicated.

Single Girder Check no distribution factors on M_{LL} or V_{LL}

20/20

Flexural Capacity

$\phi M_n^T = (294\ 589\ 943\ 1179\ 1416\ 1616\ 1910\ 2205\ 2502\ 2800\ 2837\ 2858\ 2878\ 2899\ 2920\ 2982)\cdot kip\cdot ft$

$M_{u_z} := \left[\left(Mge_z + Mde_z\right) + \left(MLL_z\right)\right]$

$M_u^T = (-0\ 203\ 445\ 607\ 768\ 1088\ 1408\ 1726\ 2042\ 2357\ 2671\ 2983\ 2946\ 2815\ 2683\ 2278)\cdot kip\cdot ft$

$\left(\phi M_n - M_u\right)^T = (295\ 387\ 498\ 573\ 648\ 528\ 502\ 479\ 460\ 443\ 166\ -126\ -67\ 84\ 237\ 704)\cdot kip\cdot ft$

$Mn\_check_z := if\left(M_{u_z} \le \phi M_{n_z}, "OK", "NG"\right)$

$Mn\_check^T = ("OK"\ "OK"\ "OK"\ "OK"\ "OK"\ "OK"\ "OK"\ "OK"\ "OK"\ "OK"\ "NG"\ "NG"\ "OK"\ "OK"\ "OK")$

Shear Capacity

$V_n^T = (299\ 315\ 208\ 196\ 198\ 201\ 204\ 207\ 209\ 211\ 213\ 215\ 164\ 168\ 173\ 193)\cdot kip$

$V_{u_z} := \left[\left(Vge_z + Vde_z\right) + \left|VLL_z\right|\right]$

$V_u^T = (325\ 324\ 323\ 322\ 322\ 320\ 319\ 317\ 316\ 314\ 313\ 312\ 144\ 143\ 141\ 137)\cdot kip$

$\left(V_n - V_u\right)^T = (-26\ -9\ -115\ -127\ -124\ -119\ -115\ -110\ -107\ -103\ -100\ -97\ 20\ 26\ 32\ 55)\cdot kip$

$Vn\_check_z := if\left(V_{u_z} \le V_{n_z}, "OK", "NG"\right)$

$Vn\_check^T = ("NG"\ "NG"\ "NG"\ "NG"\ "NG"\ "NG"\ "NG"\ "NG"\ "NG"\ "NG"\ "NG"\ "NG"\ "OK"\ "OK"\ "OK"\ "OK")$

B.2 HS20-44 Shear and Moment Design Live Load Envelopes

Live Load:

HS20-44 Truck Shear and Moment Envelope (max magnitude): (PCI 8.11.1)

$$V_{LL_z} := \text{if}\left[\frac{x_{e_z}}{L_{span}} \le 0.5, \frac{72kip\cdot\left[\left(L_{span} - x_{e_z}\right) - 9.33ft\right]}{L_{span}}, \text{"NG"}\right]$$

$V_{LL}^{T} = (50\ \ 49\ \ 47\ \ 46\ \ 45\ \ 42\ \ 40\ \ 38\ \ 35\ \ 33\ \ 31\ \ 28\ \ 26\ \ 24\ \ 21\ \ 14)\cdot kip$

$$M_{LL_z} := \text{if}\left[\frac{x_{e_z}}{L_{span}} < 0.333, \frac{72kip\cdot x_{e_z}\cdot\left[\left(L_{span} - x_{e_z}\right) - 9.33ft\right]}{L_{span}}, \frac{72kip\cdot x_{e_z}\cdot\left[\left(L_{span} - x_{e_z}\right) - 4.67ft\right]}{L_{span}} - 112kip\cdot ft\right]$$

$M_{LL}^{T} = (0\ \ 18\ \ 65\ \ 86\ \ 106\ \ 143\ \ 175\ \ 202\ \ 225\ \ 243\ \ 256\ \ 264\ \ 270\ \ 280\ \ 285\ \ 273)\cdot kip\cdot ft$

Live Load Impact: (STD 3.8.2.1)

Flexure Impact Factor

$L_f := L_{span} = 30.75\,ft$ (STD 3.8.2.2c)

$$I_f := 1 + \min\left(0.30, \frac{50ft}{L_f + 125ft}\right) = 1.30$$

Shear Impact Factor (STD 3.8.2.2d)

$L_v := \left(L_{span} - x_e\right)$

$$I_v := 1 + \min\left(0.30, \frac{50ft}{L_v + 125ft}\right) = 1.30$$

Multiple Presence Factor

$N_L := \text{floor}\left[\left(width_{deck} - 2\cdot 1.67ft\right) \div 12ft\right] = 2.00$ number of lanes that can be loaded (no shoulder)

$MP := 1.0$ for one or two lanes loaded (STD 3.12.1)

Live Load Distribution Factors:

Flexural Distribution Factors (STD 3.23.2)

$d_e := 1ft$ distance from center of exterior girder to the location of the centroid of the outermost wheel group

Exterior Beam

$$DF_{extf_{1,1}} := \begin{cases} \frac{S}{7ft} & \text{if } S \le 10ft \\ 1 + \frac{d_e}{S} - \frac{3ft}{S} & \text{otherwise} \end{cases} = 1.286$$

wheels/beam, for 1 lane loaded, but:

$DF_{extf_{1,1}} := 0.5 \cdot DF_{extf_{1,1}} = 0.64$ lanes/beam

$$DF_{extf_{1,2}} := \begin{cases} \frac{S}{5.5ft} & \text{if } S \le 14ft \\ 1 + \frac{d_e}{S} - \frac{3ft}{S} & \text{otherwise} \end{cases} = 1.636$$

wheels/beam, for 2+ lanes loaded, but:

$DF_{extf_{1,2}} := 0.5 \cdot DF_{extf_{1,2}} = 0.82$ lanes/beam

Interior Beam

$$DF_{intf_{1,1}} := \begin{cases} \frac{S}{7ft} & \text{if } S \le 10ft \\ 1 - \frac{3ft}{S} & \text{otherwise} \end{cases} = 1.286$$

wheels/beam, for 1 lane loaded, but:

$DF_{intf_{1,1}} := 0.5 \cdot DF_{intf_{1,1}} = 0.64$ lanes/beam

$$DF_{intf_{1,2}} := \begin{cases} \frac{S}{5.5ft} & \text{if } S \le 14ft \\ \frac{3}{2} - \frac{5ft}{S} & \text{otherwise} \end{cases} = 1.636$$

wheels/beam, for 2+ lanes loaded, but:

$DF_{intf_{1,2}} := 0.5 DF_{intf_{1,2}} = 0.82$ lanes/beam

Shear Distribution Factors (STD 3.23.1)

$d_e := 1ft$ distance from center of exterior girder to the location of the centroid of the outermost wheel group

Exterior Beam

$$DF_{extv_{1,1}} := \begin{cases} \frac{S}{7ft} & \text{if } S \le 10ft \\ 1 + \frac{d_e}{S} - \frac{3ft}{S} & \text{otherwise} \end{cases} = 1.286$$

wheels/beam, for 1 lane loaded, but:

$DF_{extv_{1,1}} := 0.5 \cdot DF_{extv_{1,1}} = 0.64$ lanes/beam

$$DF_{extv_{1,2}} := \begin{cases} \frac{S}{5.5ft} & \text{if } S \le 14ft \\ 1 + \frac{d_e}{S} - \frac{3ft}{S} & \text{otherwise} \end{cases} = 1.636$$

wheels/beam, for 2+ lanes loaded, but:

$DF_{extv_{1,2}} := 0.5 \cdot DF_{extv_{1,2}} = 0.82$ lanes/beam

Interior Beam

$$DF_{intv_{1,1}} := \begin{cases} \frac{S}{7ft} & \text{if } S \le 10ft \\ 1 - \frac{3ft}{S} & \text{otherwise} \end{cases} = 1.286$$

wheels/beam, for 1 lane loaded, but:

$DF_{intv_{1,1}} := 0.5 \cdot DF_{intv_{1,1}} = 0.64$ lanes/beam

$$DF_{intv_{1,2}} := \begin{cases} \frac{S}{5.5ft} & \text{if } S \le 14ft \\ \frac{3}{2} - \frac{5ft}{S} & \text{otherwise} \end{cases} = 1.636$$

wheels/beam, for 2+ lanes loaded, but:

$DF_{intv_{1,2}} := 0.5 DF_{intv_{1,2}} = 0.82$ lanes/beam

Distribution Factor Summary

Lanes: 1 2+

$DF_{intf} = (0.64 \quad 0.82)$ Moment DF $DF_f := if(BeamType = "interior", max(DF_{intf}), max(DF_{extf})) = 0.82$

$DF_{extf} = (0.64 \quad 0.82)$

$DF_{intv} = (0.64 \quad 0.82)$ Shear DF $DF_v := if(BeamType = "interior", max(DF_{intv}), max(DF_{extv})) = 0.82$

$DF_{extv} = (0.64 \quad 0.82)$

Factored Loads: (STD 3.22.1)

$M_{u_z} := 1.3 \cdot \left[1.0 \cdot \left(M_{DL_z}\right) + 1.67 \cdot \left(I_f \cdot DF_f \cdot M_{LL_z}\right)\right]$

$M_u^T = (-0 \quad 57 \quad 200 \quad 266 \quad 330 \quad 446 \quad 549 \quad 639 \quad 716 \quad 779 \quad 829 \quad 865 \quad 891 \quad 926 \quad 947 \quad 931) \cdot kip \cdot ft$

$V_{u_z} := 1.3 \cdot \left[1.0 \cdot \left(V_{DL_z}\right) + 1.67 \cdot \left(I_v \cdot DF_v \cdot \left|V_{LL_z}\right|\right)\right]$

$V_u^T = (155 \quad 152 \quad 144 \quad 140 \quad 136 \quad 128 \quad 120 \quad 112 \quad 104 \quad 96 \quad 88 \quad 80 \quad 72 \quad 64 \quad 57 \quad 33) \cdot kip$

B.3 Abutment Design, Construction, and Material Properties

Abutments to support the laboratory bridge were designed to meet two objectives. First, the abutments needed to be modular so that each abutment section was under the 15 ton weight limit of the overhead crane. Second, the abutments needed to resist the 375 kip reaction from an interior girder that was conservatively estimated as 85 percent of the possible 440 kip loading applied directly over that interior girder. This resulted in each abutment consisting of two 17 ft 4 in. long concrete sections post-tensioned together to form each abutment.

Reinforcement design for the bridge abutments was completed using a strut-and-tie model approach as outlined in Appendix A of the American Concrete Association (ACI) 318-11 Building Code and Commentary (2011). The final strut-and-tie capacity, including nodal zones, was checked using the free Computer Aided Strut-and-Tie (CAST) (2004) software available from the University of Illinois at Urbana-Champaign. Analysis of the strut-and-tie model along the 17 ft 4 in. block length required that top longitudinal No. 4 bars and bottom longitudinal No. 5 bars be spaced at 8 in. to carry tension tie forces. Details of the abutment reinforcement can be seen in Figure B-1 and Figure B-2. The No. 4 stirrup spacing of 6 in. and No. 5 single legged stirrup spacing of 12 in. was selected after considering the 375 kip applied to an interior girder of the bridge. Analysis along the 17 ft 4 in. length of the block included many point loads from each girder and from load frame reactions whereas analysis in the 3 ft 7 in. cross section considered only one girder reaction and one load frame reaction.

Two 2.5 in. diameter schedule 40 PVC tubes were placed along the 17 ft 4 in. length to allow for post-tensioning the two blocks together, 2 in. diameter schedule 40 PVC tubing was placed vertically (west abutment blocks) or horizontally (east abutment blocks, for use with 45 degree steel props) oriented to connect the abutments to the laboratory strong floor, and pairs of 1.5 in. diameter plain finish B7 continuous threaded rod were used to connect to the load frame column base plates to the abutments. Abutment formwork was designed and donated for use by Advanced Shoring and installed with lumber formwork pieces built at the University of Minnesota. Details are shown in Figure B-3 and Figure B-4. Formwork was constructed using 1 ft, 4 ft, and 8 ft sections of MEVA crane-set forming panels. A false floor constructed of 2x12 lumber and ¾ in. plyform plywood was added to the

formwork to adjust for the correct abutment block height. A ½ in. plyform plywood liner was used at one end of the formwork and at various locations along the length of the formwork to support both the longitudinal PVC and the horizontal PVC, respectively. Furthermore, a ¼ in. plyform plywood liner was used at one end of each abutment block to make the total length ¼ in. less than the specified 17 ft 4 in. This was done such that when each individual block was correctly orientated in the Theodore V. Galambos Structural Engineering Laboratory there was a ½ in. gap between two adjacent abutment blocks. This gap was grouted prior to post-tensioning the east and west abutments.

Approximately 7.5 yd^3 of concrete were placed for each of the four abutment blocks between May 9, 2013 and May 30, 2013 in the loading dock of the Civil Engineering building at the University of Minnesota. Concrete was delivered at 8 am and placed in the formwork using the concrete truck chute. Placement, finishing, and fabrication of cylinder test specimens was completed by researchers from the University of Minnesota. The concrete was cured outdoors covered with polyethylene plastic.

The four abutment blocks were placed in the laboratory, on ½ in. wooden shims, to form the east and west abutments. Prior to load testing, the gap under the abutments and the gap between two adjacent blocks was grouted using USG Ultracal 30 gypsum cement mixed by weight at a ratio of 38 parts water to 100 parts gypsum cement. The grout compressive strength was assumed to be approximately 6,000 psi and the density at wet use consistency was assumed to be 115 pcf. When mixing, the plaster was allowed to soak in the water for approximately one minute before mixing the batch for approximately one minute. Two days after grouting, adjacent blocks were post-tensioned together to form the 34 ft 8 in. long east and west abutments, two individual sections were post-tensioned together using two 1 in. diameter 150 ksi all-thread bars from Williams Form Engineering Corporation and a 30 ton hydraulic jack donated for use by Lametti & Sons, Inc. Each rod was individually post-tensioned to approximately 60 kips ($0.46f_{pu}$) and had an elongation of approximately 1 in. Abutments were tied to the strong floor using 1 in. diameter B7 threaded rod placed through holes in the 30 in. thick laboratory strong floor.

The concrete specified for the abutment blocks was chosen to meet three criteria: a 28-day nominal compressive strength of 6,000 psi, a slump of 6 in. for ease of placement in the congested formwork, and a ¾ in. maximum aggregate size. Engineers at Cemstone

Concrete were able to provide a concrete mix (mix designation 6066P) that met the compressive strength requirement and was appropriate for placement in the loading dock of the Civil Engineering building at the University of Minnesota. Specified mix details and information for the four 7.5 cubic yard batches are given in Table B-1. The fresh and hardened concrete mix properties are given in Table B-2.

B.4 Bridge Construction Formwork Details

Bridge Deck

Deck formwork was designed and installed following the same procedures used by bridge construction contractors. All dead load from fresh concrete and reinforcement was supported by the girders. Figure B-5 shows the formwork layout. Formwork constructed with ¾ in. plyform plywood and 2x4 lumber was installed in 8 ft (either length or width) sections to match the typical size of plywood sheets and lumber. Dayton Superior overhang brackets with type 8-A hangers (exterior beams) and type 8 hangers with a pair of 8 ft 2x12 ledgers (interior beams) were installed every 3 ft 8 in. on center. Vertical formwork to create a 9 in. deck thickness was created using ¾ in. plyform plywood and 2x4 lumber studs at 18 in. on center. Horizontal support was added with 2x4 kickers spaced at 36 in. on center. A safety guardrail was constructed on the North and South sides of the bridge deck using Dayton Superior C52 guard rail receptacles and 2x4 lumber (5 ft vertical pieces, 10 ft rail pieces). All of the formwork was sprayed with form release oil and all coil rod sections cast in the concrete were coated with Crisco for ease of removal after placing concrete. Additionally, 2.5 in. diameter schedule 40 PVC tubing 9 in. tall was installed at midspan to create holes for the load frame tie down system needed when loading the bridge to near ultimate capacity. All non-lumber formwork was donated for use on this project by Advance Shoring.

Single Girder Bridge Deck

Single girder deck formwork was designed and installed following the same procedures used by bridge construction contractors. All dead load from fresh concrete and reinforcement was supported by the girders. Details can be seen in Figure B-6. Formwork constructed with ¾ in. plyform plywood and 2x4 lumber was installed in 8 ft sections to match the typical size of plywood sheets and lumber. Dayton Superior overhang brackets with type 8 hangers were installed every 4 ft on center. Vertical formwork to create a 9 in. deck thickness was created using ¾ in. plyform plywood and 2x4 lumber studs at 18 in. on center. Horizontal support was added with 2x4 kickers spaced at 36 in. on center. All of the formwork was sprayed with form release oil and all coil rod sections cast in the concrete (shown in Figure B-6) were coated with Crisco for ease of removal after placing concrete.

Additionally, 2 in. diameter PVC tubing 9 in. tall was installed 2 ft from beam ends to enable moving the composite section with the overhead crane after placing concrete. All non-lumber formwork was donated for use on this project by Advance Shoring.

End Diaphragm

End diaphragm formwork was designed and installed following the same procedures used by bridge construction contractors. All dead load from fresh concrete and reinforcement was supported by the girders. Details can be seen in Figure B-7 and Figure B-8. Formwork was constructed with ¾ in. plyform plywood and either 2x4 or 2x8 lumber and was installed between girders to form the end diaphragm. Three SL610 Spanall beams, donated for use by Advanced Shoring, were used between each girder to support the end diaphragm formwork and fresh concrete. Additional horizontal stability was added to the formwork with three pairs of two 3/8 in. threaded rods in the longitudinal bridge direction between each girder (shown in Figure B-8). All of the formwork was sprayed with form release oil prior to placing concrete.

Barrier

Formwork for the barrier was temporarily loaned to the University of Minnesota by PCiRoads. Four inclined (front) and four vertical (rear) sections of metal formwork were delivered in 10 ft segments. Details can be seen in Figure B-9. Each individual 10 ft section was initially secured to the bridge deck using a minimum of three ¼ in. diameter by 2 in. length Red Head Hammer-Set Anchors, and three bolts were used to connect each adjacent piece of formwork. Each front/rear set of formwork were fastened down to prevent uplift by hooking a J-shaped coil rod to the No. 5 bar hoops protruding from the deck and tightening against two 2x4 strongbacks located at mid-length of the formwork. Additional horizontal stability was added to each front/rear set of formwork sections with three pairs of two 1/2 in. coil rods in the transverse direction. Furthermore, a piece of 2.5 in. diameter schedule 40 PVC tubing was installed at midspan to create a hole for the load frame tie down system in case the tie down system was required for testing in the northeast quadrant.

Table B-1. Abutment Concrete Mix Design

	Specified	Truck 1	Truck 1	Truck 1	Truck 1
	Qty / cy	Batch Qty	Batch Qty	Batch Qty	Batch Qty
Mix Name	6066P	6066P	6066P	6066P	6066P
Mix Date/Time	10/23/04	5/9/13 7:25 AM	5/16/13 7:49 AM	5/24/13 7:50 AM	5/30/13 9:32 AM
Lafarge at Davenport, IA Type I Cement (lb)	675	5055	5025	n/a	5055
Aggregate Industries 3/4 in. Aggregate (lb)	1714	12941	12880	n/a	13020
Aggregate Industries Larson Plant Sand (lb)	1200	9400	9380	n/a	9520
Flyash from Coal Creek at Underwood, ND (lb)	125	925	925	n/a	930
Water (gal)	32.7	238	239	n/a	238
BASF MB AE 90 Air Entrainer (oz)	2.5	37	30	n/a	30
BASF Glenium 7500 HRWR (oz)	24	140	200	n/a	200
BASF Polyheed 1020 MRWR (oz)	24	117	177	n/a	177
Cylinder Count	----	4	4	4	4

Table B-2. Fresh and Hardened Abutment Concrete Properties

	Specified	Truck 1	Truck 1	Truck 1	Truck 1
Mix Name	6066P	6066P	6066P	6066P	6066P
Date/Time	----	5/9/13 7:25 AM	5/16/13 7:49 AM	5/24/13 7:50 AM	5/30/13 9:32 AM
Air (%)	5.0 ± 1.5	----	----	----	----
Slump (in.)	6.0	6.25	7.25	10	8
W/C Ratio	0.34	0.332	0.335	n/a	0.331
Unit Wt. (pcf)	146	----	----	----	----
Average Compressive Strength of Three Cylinders, f'_c (psi)					
28 day	6,000	7,083	6,211	6,507	6,090

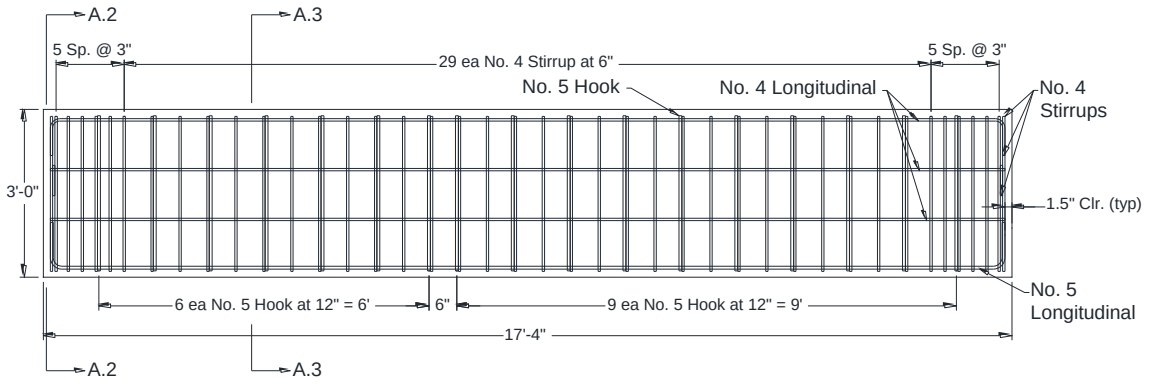

Figure B-1. Abutment Reinforcement Details

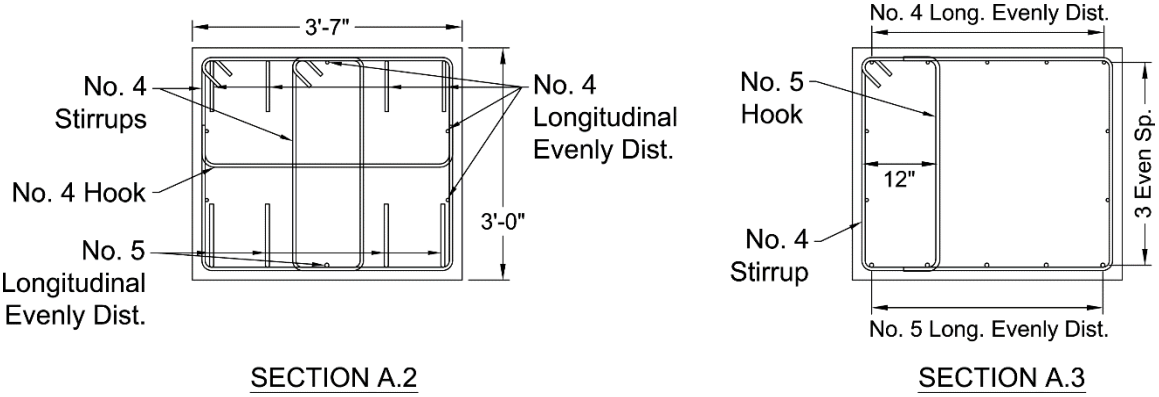

Figure B-2. Section of Abutment Reinforcement Details

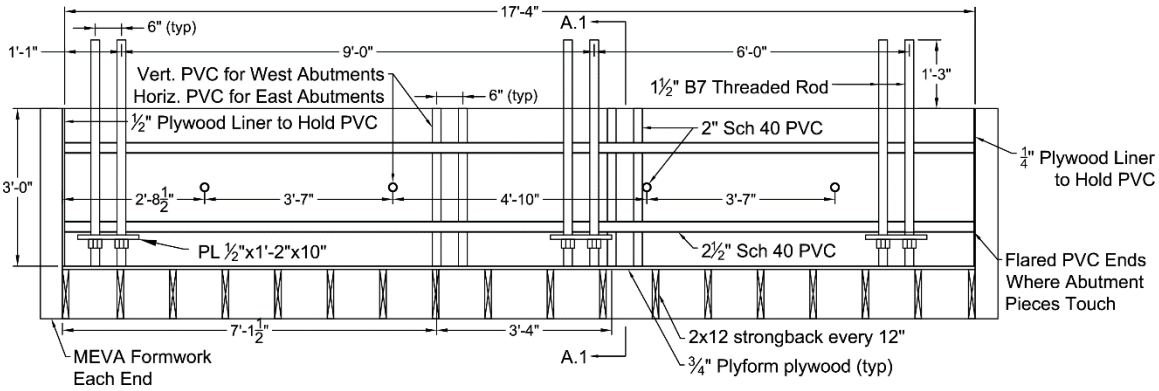

Figure B-3. Abutment Formwork and Non-Reinforcement Details

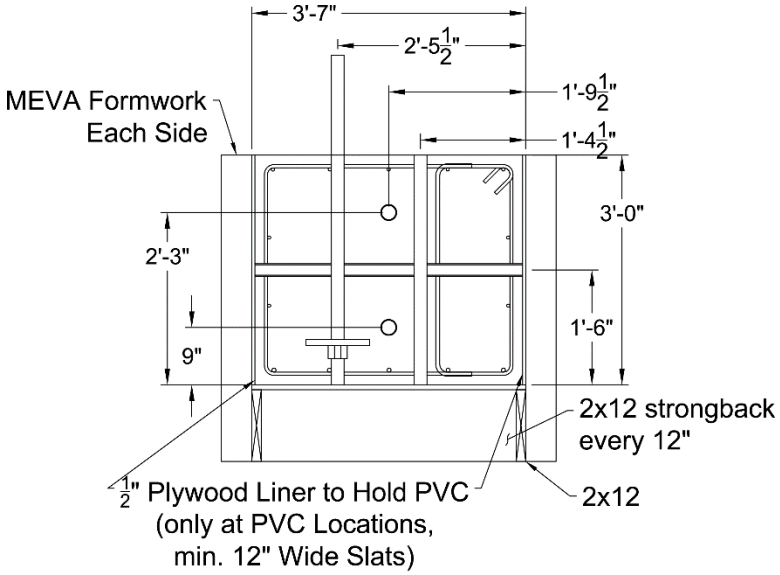

Figure B-4. Cross Section of Abutment Formwork and Non-Reinforcement Details

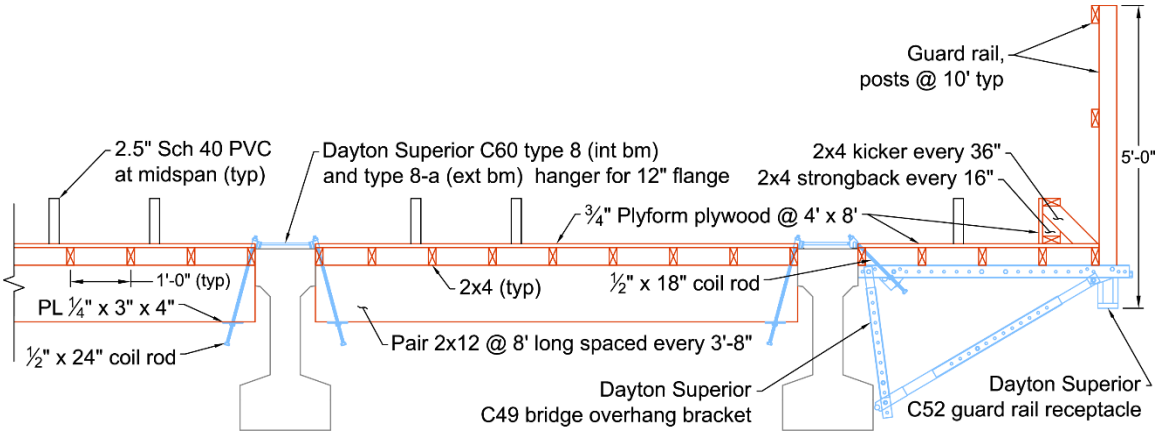

Figure B-5. Half Bridge Deck Formwork Transverse Section at Midspan

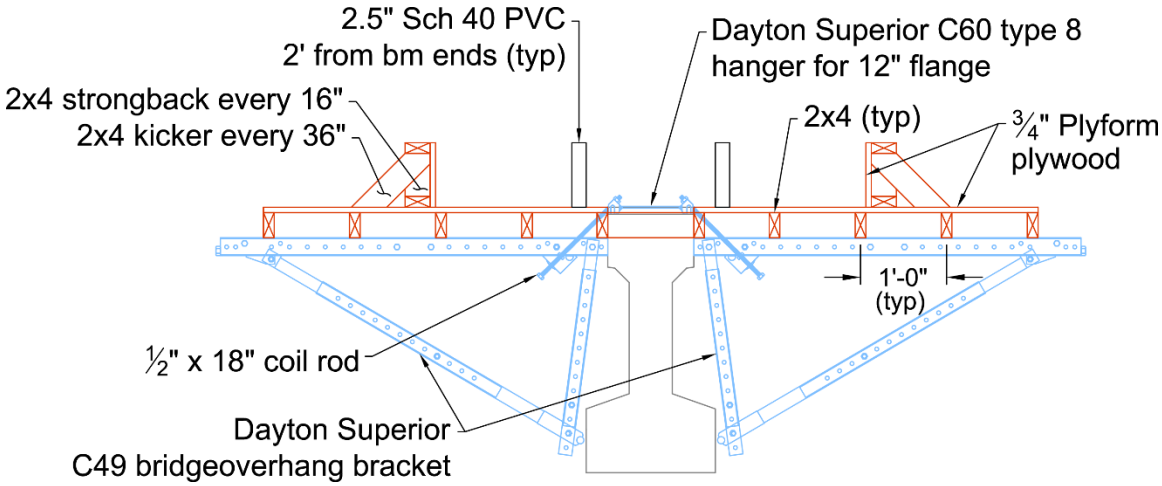

Figure B-6. Single Girder Deck Formwork Transverse Section

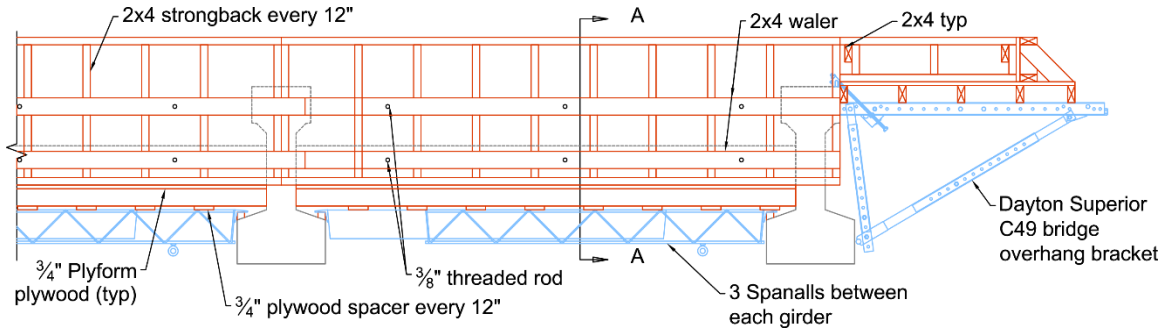

Figure B-7. Half End View of Diaphragm Formwork

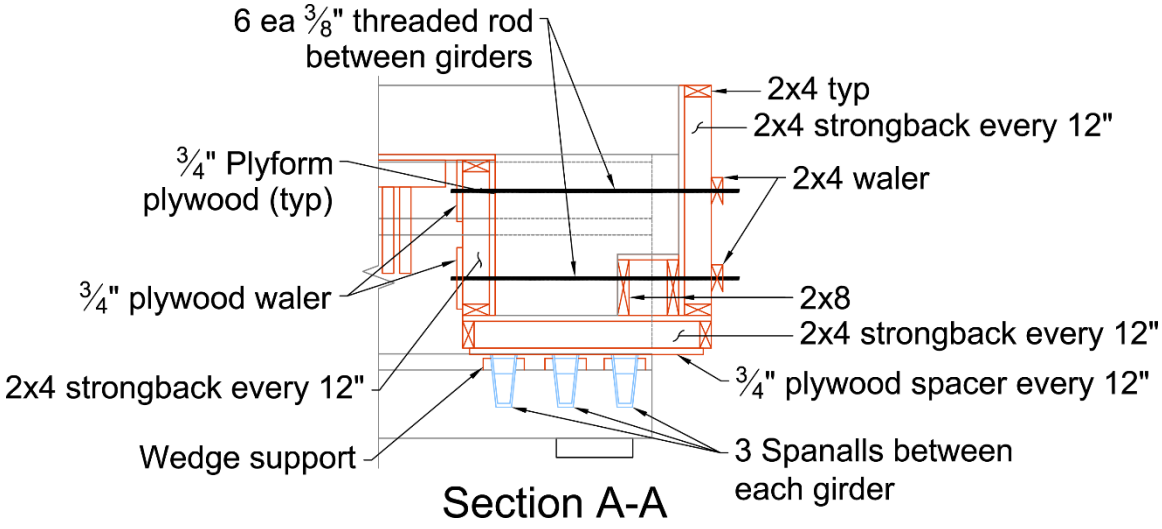

Figure B-8. Cross Section of End Diaphragm Formwork

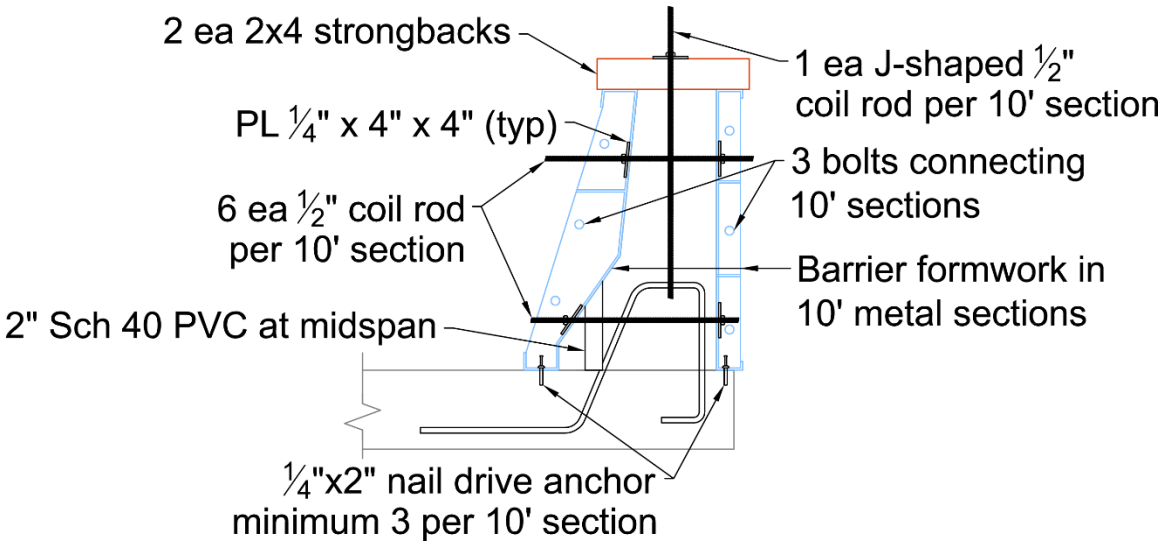

Figure B-9. Barrier Formwork Transverse Section

APPENDIX C. EXPERIMENTAL INSTRUMENTATION DETAILS

Appendix C includes details related to the instrumentation and data acquisition used for laboratory experiments. Section C.1 lists the types of instruments used in the laboratory and the manufacturer. Section C.2 describes the technique used to apply vibrating wire strain gages to concrete surfaces in this project. Section C.3 describes the techniques used to apply foil strain gages to concrete and steel surfaces in this project. Section C.4 through C.6 have sample CR1000 programs used at the following times: during laboratory and field testing to collect VWG strains, during bridge girder fabrication to collect strains from gages installed on prestressing strand, and during ultimate testing to collect stirrup strains in the laboratory bridge girders.

C.1 Instrumentation Manufacturer and Model Number Details

Instrument Description	Manufacturer	Model No.	Calibration Factor **	Length / Range	Experimental Use	DAQ
Linear foil strain gage *	Tokyo Sokki Kenkyujo (Texas Measurements)	FLA-3-11-5LT	2.10	3 mm	Embedded stirrup strain, stirrup yield strength	CR1000
Linear foil strain gage	Tokyo Sokki Kenkyujo (Texas Measurements)	FLK-1-11-5LT	2.11	1 mm	Initial prestress force, strand yield strength	CR1000
Vibrating wire strain gage	Geokon	4200	G1: 0.97 G2-G4: 0.98	6 in.	Prestress losses	GK-403
Vibrating wire strain gage	Geokon	4000	0.96	6 in.	Box-type rosette, neutral axis	CR1000
Foil strain gage rosette	Tokyo Sokki Kenkyujo (Texas Measurements)	FRA-6-11-5LT	2.10	6 mm	Single girder shear strain	CE DAQ
LVDTs	Measurement Specialties (Schaevitz Sensors)	n/a	Varies	± 0.5, 1, and 3 inch	Vertical and horizontal displacement	CE DAQ
Tiltmeter	Jewell Instruments (Applied Geomechanics)	800	0.05	± 1 degree	Girder end rotation	CE DAQ
Linear foil strain gage	Tokyo Sokki Kenkyujo (Texas Measurements)	FLA-30-11-5LT	2.12	30 mm	Barrier and girder neutral axis	CE DAQ
Foil strain gage rosette	Tokyo Sokki Kenkyujo (Texas Measurements)	PFLR-30-11	2.11	30 mm	Laboratory bridge shear strain	CE DAQ

* All foil gages were 120 ohm

** Calibration factors apply to individual sensors and are therefore only applicable to this experimental study

C.2 Vibrating Wire Strain Gage Application Techniques

VWGs in the box-type rosette were applied in a repeatable fashion to the web of the prestressed concrete girders using the steps outlined below. The following Loctite Industrial products were used to attach the VWGs to the concrete surface: Loctite 410 Prism Instant Adhesive and Loctite 7452 Tak Pak Accelerator.

	Application Step Description	Visual Depiction
1.	Measure critical locations from the support face and mark a vertical line on the web at each location.	----
2.	Prepare girder web concrete surface (approximately 12 in. square) with an electric grinder and knot wire cup brush attachment.	
3.	Clean prepared surface with acetone, rag, and dry with a can of compressed air.	----
4.	Place blank aluminum plate on top of 2 ft level that was 2.25 in. tall and balanced on the bottom flange/web interface. Apply epoxy to lower corner mounts and touch to web. Remove aluminum plate from web to leave epoxy marks. Spray epoxy marks located on web with accelerant and replace blank aluminum plate in same location to permanently attach.	
5.	Carefully remove blank aluminum plate from lower corner mounts. Apply strain relief aluminum angle to the right or left of the lower corner mount with same epoxy/accelerant method.	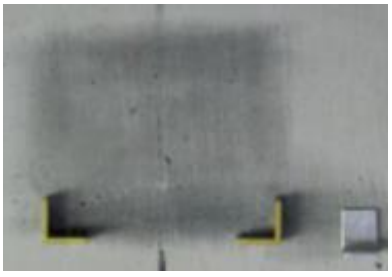

6. Place VWG jig into corner mounts. Set four VWGs into jig while flush against web (with spacer set screws). Secure VWG with set screws. Tilt away from web and apply epoxy to mounting blocks of VWG. Touch mounting blocks to web using corner mounts and spacer set screws as guide.

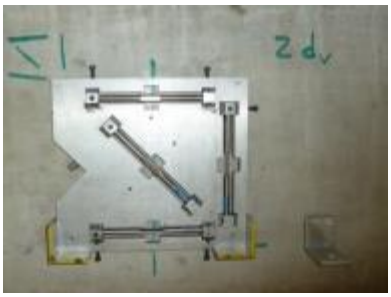

7. Tilt away from web and spray epoxy marks located on web with accelerant. Replace VWGs in same location using corner mounts and spacer set screws as guide to permanently attach VWGs.

8. Remove lower corner mounts prior to removing VWG jig for ease. Install VWG wire with small hose clamp. Write VWG wire number on concrete web surface. Zip tie VWG wires to strain relief aluminum angle.

9. Record VWG location and wire number on appropriate data sheet.

C.3 Foil Strain Gage Application Techniques on Steel and Concrete

The initial technique is described for installing strain gages on rebar and modifications are noted for other steel surface applications. Strain gages were installed using adhesives and coating materials produced by Tokyo Sokki Kenkyujo Co., Ltd, according to the following procedure:

1. Grind a thin layer from the bar surface, preferably not on a rib, using a sanding grinder wheel. In this case a Weiler Vortec Pro zirconium grit size 60 was used.
2. Sand the steel surface using 100, 220 and 400 grit sand paper, in that order.
3. Mark exact strain gage location with ballpoint pen.
4. Clean steel surface with acetone leaving a small groove from ballpoint pen.
5. Align and move strain gage from clean surface to rebar surface using clear scotch tape. In this case PCT-2M Gage Installation Tape was used from Vishay Micro-Measurements.
6. Peel gage back from steel surface using scotch tape, place approximately two drops of CN adhesive on the rebar spread even over the desired area. Mount strain gage and hold down for approximately 30 seconds.
7. Remove scotch tape after adhesive dried.
8. Place a small piece of electrical tape to separate the exposed copper strain gage wires from the rebar.
9. Use zip tie to provide strain relief to the gage.
10. Cover the entire strain gage area with SB tape.
11. Wrap strain gage area and SB tape with aluminum foil tape.
12. Seal edges of aluminum foil tape with Araldite two part epoxy to give a hard shell-like cover to provide mechanical protection during the concrete placing operation. Allow the epoxy to dry for 24 hours.

Note:

For application to prestressing strands exposed to environmental conditions, exclude step 1 and exclude step 11 if speed is critical.

The second technique is described for installing foil strain gages on concrete surfaces. Strain gages were installed using adhesives and coating materials produced by Tokyo Sokki Kenkyujo Co., Ltd, according to the following procedure:

1. Apply a thin layer of PS adhesive, which is a two-component room-temperature-curing polyester adhesive, to the concrete face to provide a suitable gage-bonding surface. This should fill any small voids in the concrete face. Allow the adhesive to dry for 24 hours.
2. Sand the thin adhesive layer with 320 or 400 grit sand paper until the base concrete material is exposed.
3. Mark exact strain gage location with ballpoint pen or pointed metal rod.
4. Clean surface with acetone leaving a small groove from marking utensil.
5. Align and move strain gage from clean surface to concrete surface using clear scotch tape.
6. Peel gage back from concrete surface using scotch tape, place approximately two drops of CN adhesive (or CN-E adhesive for longer gage length gages) on the strain gage. Mount strain gage and hold down for approximately 60 seconds.
7. Remove scotch tape after adhesive is dry.
8. Provide strain relief to the gage wires using J-B Weld SteelStik epoxy putty.

C.4 CR1000 Program used for VWGs during Laboratory and Field Bridge Testing

```
'CR1000 Vibrating wire sensor program
'Used 8-29-2013 by Ben Dymond at the University of Minnesota.
'This program will measure up to 80 vibrating wire sensors wired to 5 AM16/32 multiplexers,
'interfaced through 2- AVW4 vibrating wire interfaces.
'*******************************************************************************
'CR1000 Analog Input Channel assignments were made to ease field verification
'and/or for any troubleshooting necessary.

'CR1000 Differential channel #1 measures the vibrating wire sensors from multiplexer MP #1.
'CR1000 Differential channel #2 measures the vibrating wire sensors from multiplexer MP #2.
'CR1000 Differential channel #3 measures the vibrating wire sensors from multiplexer MP #3.
'CR1000 Differential channel #4 measures the vibrating wire sensors from multiplexer MP #4.
'CR1000 Differential channel #5 measures the vibrating wire sensors from multiplexer MP #5.

'CR1000 Digital Control Port assignments were also made to ease any troubleshooting or verification.
'CR1000 Control Port #1 is used to Enable (turn ON or activate) multiplexer #1.
'CR1000 Control Port #2 is used to Enable (turn ON or activate) multiplexer #2.
'CR1000 Control Port #3 is used to Enable (turn ON or activate) multiplexer #3.
'CR1000 Control Port #4 is used to Enable (turn ON or activate) multiplexer #4.
'CR1000 Control Port #5 is used to Enable (turn ON or activate) multiplexer #5.

'CR1000 Control Port #8 is used globally with all 5 multiplexers to clock each multiplexer.
'(advance relays to next channel)

'AM16/32 channel wiring   to  AVW4 #1 Wiring inputs => =>  AVW4 Outputs  to =>  CR1000 Analog Input channels
'MP#1  ODD H(high) --->----  T1 +  ------->--------->----- T1 ------->--------   SE #1
'MP#1  ODD L(Odd)  --->----  T1 -  ------->--------->----- T1                    (single input)
'MP#1  EVEN H(high)--->----  C1 +  ------->--------->----- F1 ------->--------   SE #2
'MP#1  Even L(high) -->----  C1 -  ------->--------->----- F1                    (single input)
'
'AM16/32 channel wiring   to  AVW4 #1 Wiring inputs => =>  AVW4 Outputs  to  => CR1000 Analog Input channels
'MP#2  ODD H(high) --->----  T2 +  ------->--------->----- T2 ------->--------   SE #3
'MP#2  ODD L(Odd)  --->----  T2 -  ------->--------->----- T2                    (single input)
'MP#2  EVEN H(high)--->----  C2 +  ------->--------->----- F2 ------->--------   SE #4
'MP#2  Even L(high) -->----  C2 -  ------->--------->----- F2                    (single input)
'
'AM16/32 channel wiring   to  AVW4 #1 Wiring inputs => =>  AVW4 Outputs  to =>  CR1000 Analog Input channels
'MP#3  ODD H(high) --->----  T3 +  ------->--------->----- T3 ------->--------   SE #5
'MP#3  ODD L(Odd)  --->----  T3 -  ------->--------->----- T3                    (single input)
'MP#3  EVEN H(high)--->----  C3 +  ------->--------->----- F3 ------->--------   SE #6
'MP#3  Even L(high) -->----  C3 -  ------->--------->----- F3                    (single input)
'
'AM16/32 channel wiring   to  AVW4 #1 Wiring inputs => =>  AVW4 Outputs  to  => CR1000 Analog Input channels
'MP#4  ODD H(high) --->----  T4 +  ------->--------->----- T4 ------->--------   SE #7
'MP#4  ODD L(Odd)  --->----  T4 -  ------->--------->----- T4                    (single input)
'MP#4  EVEN H(high)--->----  C4 +  ------->--------->----- F4 ------->--------   SE #8
'MP#4  Even L(high) -->----  C4 -  ------->--------->----- F4                    (single input)
'
'AM16/32 channel wiring   to  AVW4 #2 Wiring inputs => =>  AVW4 Outputs to  => CR1000 Analog Input channels
'MP#5  ODD H(high) --->----  T1 +  ------->--------->----- T1 ------->--------   SE #9
'MP#5  ODD L(Odd)  --->----  T1 -  ------->--------->----- T1                    (single input)
'MP#5  EVEN H(high)--->----  C1 +  ------->--------->----- F1 ------->--------   SE #10
'MP#5  Even L(high) -->----  C1 -  ------->--------->----- F1                    (single input)

'PROGRAM BEGINS HERE.

'Declare program constants

Const ScanInt = 88          'Scan Interval in Seconds
Const NumLoops = 5          'Number of Loops to Read VWGs
Const SFreq_VW = 450        'Start Frequency in Hertz for Geokon
Const EFreq_VW = 1250       'End Frequency in Hertz for Geokon
Const VW_ConstG = 4062      'Vibrating Wire Gage Constant (G) Multiply by 1000
Const VW_Offset = 0.0       'Vibrating Wire Gage Offset
Const VW_TempMult = 2.5     'Vibrating Wire Gage Temperature Reading Multiplier
Const VW_TempOffset = 0.0   'Vibrating Wire Gage Temper
```

```
Const VW_BatchB = 0.96      'Vibrating Wire Gage batch factor
Const NumSensorsMP1 = 16    'Number of Sensors on MP #1
Const NumSensorsMP2 = 16    'Number of Sensors on MP #2
Const NumSensorsMP3 = 16    'Number of Sensors on MP #3
Const NumSensorsMP4 = 16    'Number of Sensors on MP #4
Const NumSensorsMP5 = 16    'Number of Sensors on MP #5

'Declare program variables.

Public DAQ_Batt                 'Data Acquisition Battery Voltage
Public DAQ_Temp                 'Data Acquisition Temperature
Public TestID As String * 20    'Test ID for load test only. (Enter the name in Public Field Monitor Table)
Public Flag(8)                  'General use flags for stopping/starting scan

Public TempMP1(NumSensorsMP1)   'Declare 16 Variables for Multiplexer 1 (Temp and VW Coils).
Public CoilMP1(NumSensorsMP1)
Public TempMP2(NumSensorsMP2)   'Declare 16 Variables for Multiplexer 2 (Temp and VW Coils).
Public CoilMP2(NumSensorsMP2)
Public TempMP3(NumSensorsMP3)   'Declare 16 Variables for Multiplexer 3 (Temp and VW Coils).
Public CoilMP3(NumSensorsMP3)
Public TempMP4(NumSensorsMP4)   'Declare 16 Variables for Multiplexer 4 (Temp and VW Coils).
Public CoilMP4(NumSensorsMP4)
Public TempMP5(NumSensorsMP5)   'Declare 12 Variables for Multiplexer 5 (Temp and VW Coils).
Public CoilMP5(NumSensorsMP5)

Alias TempMP1(1) = T1MP1      :Alias CoilMP1(1)   = G1MP1
Alias TempMP1(2) = T2MP1      :Alias CoilMP1(2)   = G2MP1
Alias TempMP1(3) = T3MP1      :Alias CoilMP1(3)   = G3MP1
Alias TempMP1(4) = T4MP1      :Alias CoilMP1(4)   = G4MP1
Alias TempMP1(5) = T5MP1      :Alias CoilMP1(5)   = G5MP1
Alias TempMP1(6) = T6MP1      :Alias CoilMP1(6)   = G6MP1
Alias TempMP1(7) = T7MP1      :Alias CoilMP1(7)   = G7MP1
Alias TempMP1(8) = T8MP1      :Alias CoilMP1(8)   = G8MP1
Alias TempMP1(9) = T9MP1      :Alias CoilMP1(9)   = G9MP1
Alias TempMP1(10) = T10MP1    :Alias CoilMP1(10)  = G10MP1
Alias TempMP1(11) = T11MP1    :Alias CoilMP1(11)  = G11MP1
Alias TempMP1(12) = T12MP1    :Alias CoilMP1(12)  = G12MP1
Alias TempMP1(13) = T13MP1    :Alias CoilMP1(13)  = G13MP1
Alias TempMP1(14) = T14MP1    :Alias CoilMP1(14)  = G14MP1
Alias TempMP1(15) = T15MP1    :Alias CoilMP1(15)  = G15MP1
Alias TempMP1(16) = T16MP1    :Alias CoilMP1(16)  = G16MP1

Alias TempMP2(1)  = T17MP2    :Alias CoilMP2(1)   = G17MP2
Alias TempMP2(2)  = T18MP2    :Alias CoilMP2(2)   = G18MP2
Alias TempMP2(3)  = T19MP2    :Alias CoilMP2(3)   = G19MP2
Alias TempMP2(4)  = T20MP2    :Alias CoilMP2(4)   = G20MP2
Alias TempMP2(5)  = T21MP2    :Alias CoilMP2(5)   = G21MP2
Alias TempMP2(6)  = T22MP2    :Alias CoilMP2(6)   = G22MP2
Alias TempMP2(7)  = T23MP2    :Alias CoilMP2(7)   = G23MP2
Alias TempMP2(8)  = T24MP2    :Alias CoilMP2(8)   = G24MP2
Alias TempMP2(9)  = T25MP2    :Alias CoilMP2(9)   = G25MP2
Alias TempMP2(10) = T26MP2    :Alias CoilMP2(10)  = G26MP2
Alias TempMP2(11) = T27MP2    :Alias CoilMP2(11)  = G27MP2
Alias TempMP2(12) = T28MP2    :Alias CoilMP2(12)  = G28MP2
Alias TempMP2(13) = T29MP2    :Alias CoilMP2(13)  = G29MP2
Alias TempMP2(14) = T30MP2    :Alias CoilMP2(14)  = G30MP2
Alias TempMP2(15) = T31MP2    :Alias CoilMP2(15)  = G31MP2
Alias TempMP2(16) = T32MP2    :Alias CoilMP2(16)  = G32MP2

Alias TempMP3(1)  = T33MP3    :Alias CoilMP3(1)   = G33MP3
Alias TempMP3(2)  = T34MP3    :Alias CoilMP3(2)   = G34MP3
Alias TempMP3(3)  = T35MP3    :Alias CoilMP3(3)   = G35MP3
Alias TempMP3(4)  = T36MP3    :Alias CoilMP3(4)   = G36MP3
Alias TempMP3(5)  = T37MP3    :Alias CoilMP3(5)   = G37MP3
Alias TempMP3(6)  = T38MP3    :Alias CoilMP3(6)   = G38MP3
Alias TempMP3(7)  = T39MP3    :Alias CoilMP3(7)   = G3
```

```
Alias TempMP3(8)  = T40MP3    :Alias CoilMP3(8)   = G40MP3
Alias TempMP3(9)  = T41MP3    :Alias CoilMP3(9)   = G41MP3
Alias TempMP3(10) = T42MP3    :Alias CoilMP3(10)  = G42MP3
Alias TempMP3(11) = T43MP3    :Alias CoilMP3(11)  = G43MP3
Alias TempMP3(12) = T44MP3    :Alias CoilMP3(12)  = G44MP3
Alias TempMP3(13) = T45MP3    :Alias CoilMP3(13)  = G45MP3
Alias TempMP3(14) = T46MP3    :Alias CoilMP3(14)  = G46MP3
Alias TempMP3(15) = T47MP3    :Alias CoilMP3(15)  = G47MP3
Alias TempMP3(16) = T48MP3    :Alias CoilMP3(16)  = G48MP3

Alias TempMP4(1)  = T49MP4    :Alias  CoilMP4(1)  = G49MP4
Alias TempMP4(2)  = T50MP4    :Alias  CoilMP4(2)  = G50MP4
Alias TempMP4(3)  = T51MP4    :Alias  CoilMP4(3)  = G51MP4
Alias TempMP4(4)  = T52MP4    :Alias  CoilMP4(4)  = G52MP4
Alias TempMP4(5)  = T53MP4    :Alias  CoilMP4(5)  = G53MP4
Alias TempMP4(6)  = T54MP4    :Alias  CoilMP4(6)  = G54MP4
Alias TempMP4(7)  = T55MP4    :Alias  CoilMP4(7)  = G55MP4
Alias TempMP4(8)  = T56MP4    :Alias  CoilMP4(8)  = G56MP4
Alias TempMP4(9)  = T57MP4    :Alias  CoilMP4(9)  = G57MP4
Alias TempMP4(10) = T58MP4    :Alias  CoilMP4(10) = G58MP4
Alias TempMP4(11) = T59MP4    :Alias  CoilMP4(11) = G59MP4
Alias TempMP4(12) = T60MP4    :Alias  CoilMP4(12) = G60MP4
Alias TempMP4(13) = T61MP4    :Alias  CoilMP4(13) = G61MP4
Alias TempMP4(14) = T62MP4    :Alias  CoilMP4(14) = G62MP4
Alias TempMP4(15) = T63MP4    :Alias  CoilMP4(15) = G63MP4
Alias TempMP4(16) = T64MP4    :Alias  CoilMP4(16) = G64MP4

Alias TempMP5(1)  = T65MP5    :Alias  CoilMP5(1)  = G65MP5
Alias TempMP5(2)  = T66MP5    :Alias  CoilMP5(2)  = G66MP5
Alias TempMP5(3)  = T67MP5    :Alias  CoilMP5(3)  = G67MP5
Alias TempMP5(4)  = T68MP5    :Alias  CoilMP5(4)  = G68MP5
Alias TempMP5(5)  = T69MP5    :Alias  CoilMP5(5)  = G69MP5
Alias TempMP5(6)  = T70MP5    :Alias  CoilMP5(6)  = G70MP5
Alias TempMP5(7)  = T71MP5    :Alias  CoilMP5(7)  = G71MP5
Alias TempMP5(8)  = T72MP5    :Alias  CoilMP5(8)  = G72MP5
Alias TempMP5(9)  = T73MP5    :Alias  CoilMP5(9)  = G73MP5
Alias TempMP5(10) = T74MP5    :Alias  CoilMP5(10) = G74MP5
Alias TempMP5(11) = T75MP5    :Alias  CoilMP5(11) = G75MP5
Alias TempMP5(12) = T76MP5    :Alias  CoilMP5(12) = G76MP5
Alias TempMP5(13) = T77MP5    :Alias  CoilMP5(13) = G77MP5
Alias TempMP5(14) = T78MP5    :Alias  CoilMP5(14) = G78MP5
Alias TempMP5(15) = T79MP5    :Alias  CoilMP5(15) = G79MP5
Alias TempMP5(16) = T80MP5    :Alias  CoilMP5(16) = G80MP5

Public i
Public NumScans

Dim VWMult1(NumSensorsMP1)
Dim VWOffset1(NumSensorsMP1)
Dim TmpMult1(NumSensorsMP1)
Dim TmpOffset1(NumSensorsMP1)

Dim VWMult2(NumSensorsMP2)
Dim VWOffset2(NumSensorsMP2)
Dim TmpMult2(NumSensorsMP2)
Dim TmpOffset2(NumSensorsMP2)

Dim VWMult3(NumSensorsMP3)
Dim VWOffset3(NumSensorsMP3)
Dim TmpMult3(NumSensorsMP3)
Dim TmpOffset3(NumSensorsMP3)

Dim VWMult4(NumSensorsMP4)
Dim VWOffset4(NumSensorsMP4)
Dim TmpMult4(NumSensorsMP4)
Dim TmpOffset4(NumSensorsMP4)
```

```
Dim VWMult5(NumSensorsMP5)
Dim VWOffset5(NumSensorsMP5)
Dim TmpMult5(NumSensorsMP5)
Dim TmpOffset5(NumSensorsMP5)

'Define Data Table
DataTable (DataSamples,1,-1)
  DataInterval (0,ScanInt,Sec,10)
  Sample (1,TestID,String)
  Sample (1,NumScans,FP2)
  Minimum (1,DAQ_Batt,FP2,0,0)
  Sample (1,DAQ_Temp,FP2)
  Sample (NumSensorsMP1,TempMP1(),IEEE4)
  Sample (NumSensorsMP1,CoilMP1(),IEEE4)
  Sample (NumSensorsMP2,TempMP2(),IEEE4)
  Sample (NumSensorsMP2,CoilMP2(),IEEE4)
  Sample (NumSensorsMP3,TempMP3(),IEEE4)
  Sample (NumSensorsMP3,CoilMP3(),IEEE4)
  Sample (NumSensorsMP4,TempMP4(),IEEE4)
  Sample (NumSensorsMP4,CoilMP4(),IEEE4)
  Sample (NumSensorsMP5,TempMP5(),IEEE4)
  Sample (NumSensorsMP5,CoilMP5(),IEEE4)
EndTable

DataTable (DataAverage,NumScans=NumLoops,1000)
  Sample (1,TestID,String)
  Average (NumSensorsMP1,TempMP1(),IEEE4,0)
  Average (NumSensorsMP1,CoilMP1(),IEEE4,0)
  Average (NumSensorsMP2,TempMP2(),IEEE4,0)
  Average (NumSensorsMP2,CoilMP2(),IEEE4,0)
  Average (NumSensorsMP3,TempMP3(),IEEE4,0)
  Average (NumSensorsMP3,CoilMP3(),IEEE4,0)
  Average (NumSensorsMP4,TempMP4(),IEEE4,0)
  Average (NumSensorsMP4,CoilMP4(),IEEE4,0)
  Average (NumSensorsMP5,TempMP5(),IEEE4,0)
  Average (NumSensorsMP5,CoilMP5(),IEEE4,0)
EndTable

'Main Program
BeginProg

  'Multiplexer 1
  VWMult1(1) =VW_ConstG : VWOffset1(1) =0.0   : TmpMult1(1) =2.5 : TmpOffset1(1) =0.0
  VWMult1(2) =VW_ConstG : VWOffset1(2) =0.0   : TmpMult1(2) =2.5 : TmpOffset1(2) =0.0
  VWMult1(3) =VW_ConstG : VWOffset1(3) =0.0   : TmpMult1(3) =2.5 : TmpOffset1(3) =0.0
  VWMult1(4) =VW_ConstG : VWOffset1(4) =0.0   : TmpMult1(4) =2.5 : TmpOffset1(4) =0.0
  VWMult1(5) =VW_ConstG : VWOffset1(5) =0.0   : TmpMult1(5) =2.5 : TmpOffset1(5) =0.0
  VWMult1(6) =VW_ConstG : VWOffset1(6) =0.0   : TmpMult1(6) =2.5 : TmpOffset1(6) =0.0
  VWMult1(7) =VW_ConstG : VWOffset1(7) =0.0   : TmpMult1(7) =2.5 : TmpOffset1(7) =0.0
  VWMult1(8) =VW_ConstG : VWOffset1(8) =0.0   : TmpMult1(8) =2.5 : TmpOffset1(8) =0.0
  VWMult1(9) =VW_ConstG : VWOffset1(9) =0.0   : TmpMult1(9) =2.5 : TmpOffset1(9) =0.0
  VWMult1(10)=VW_ConstG : VWOffset1(10)=0.0   : TmpMult1(10)=2.5 : TmpOffset1(10)=0.0
  VWMult1(11)=VW_ConstG : VWOffset1(11)=0.0   : TmpMult1(11)=2.5 : TmpOffset1(11)=0.0
  VWMult1(12)=VW_ConstG : VWOffset1(12)=0.0   : TmpMult1(12)=2.5 : TmpOffset1(12)=0.0
  VWMult1(13)=VW_ConstG : VWOffset1(13)=0.0   : TmpMult1(13)=2.5 : TmpOffset1(13)=0.0
  VWMult1(14)=VW_ConstG : VWOffset1(14)=0.0   : TmpMult1(14)=2.5 : TmpOffset1(14)=0.0
  VWMult1(15)=VW_ConstG : VWOffset1(15)=0.0   : TmpMult1(15)=2.5 : TmpOffset1(15)=0.0
  VWMult1(16)=VW_ConstG : VWOffset1(16)=0.0   : TmpMult1(16)=2.5 : TmpOffset1(16)=0.0

  'Multiplexer 2
  VWMult2(1) =VW_ConstG : VWOffset2(1) =0.0   : TmpMult2(1) =2.5 : TmpOffset2(1) =0.0
  VWMult2(2) =VW_ConstG : VWOffset2(2) =0.0   : TmpMult2(2) =2.5 : TmpOffset2(2) =0.0
  VWMult2(3) =VW_ConstG : VWOffset2(3) =0.0   : TmpMult2(3) =2.5 : TmpOffset2(3) =0.0
  VWMult2(4) =VW_ConstG : VWOffset2(4) =0.0   : TmpMult2(4) =2.5 : TmpOffset2(4) =0.0
  VWMult2(5) =VW_ConstG : VWOffset2(5) =0.0   : TmpMult2(5) =2.5 : TmpOffset2(5) =0.0
```

```
VWMult2(6) =VW_ConstG : VWOffset2(6) =0.0   : TmpMult2(6) =2.5 : TmpOffset2(6) =0.0
VWMult2(7) =VW_ConstG : VWOffset2(7) =0.0   : TmpMult2(7) =2.5 : TmpOffset2(7) =0.0
VWMult2(8) =VW_ConstG : VWOffset2(8) =0.0   : TmpMult2(8) =2.5 : TmpOffset2(8) =0.0
VWMult2(9) =VW_ConstG : VWOffset2(9) =0.0   : TmpMult2(9) =2.5 : TmpOffset2(9) =0.0
VWMult2(10)=VW_ConstG : VWOffset2(10)=0.0   : TmpMult2(10)=2.5 : TmpOffset2(10)=0.0
VWMult2(11)=VW_ConstG : VWOffset2(11)=0.0   : TmpMult2(11)=2.5 : TmpOffset2(11)=0.0
VWMult2(12)=VW_ConstG : VWOffset2(12)=0.0   : TmpMult2(12)=2.5 : TmpOffset2(12)=0.0
VWMult2(13)=VW_ConstG : VWOffset2(13)=0.0   : TmpMult2(13)=2.5 : TmpOffset2(13)=0.0
VWMult2(14)=VW_ConstG : VWOffset2(14)=0.0   : TmpMult2(14)=2.5 : TmpOffset2(14)=0.0
VWMult2(15)=VW_ConstG : VWOffset2(15)=0.0   : TmpMult2(15)=2.5 : TmpOffset2(15)=0.0
VWMult2(16)=VW_ConstG : VWOffset2(16)=0.0   : TmpMult2(16)=2.5 : TmpOffset2(16)=0.0

'Multiplexer 3
VWMult3(1) =VW_ConstG : VWOffset3(1) =0.0   : TmpMult3(1) =2.5 : TmpOffset3(1) =0.0
VWMult3(2) =VW_ConstG : VWOffset3(2) =0.0   : TmpMult3(2) =2.5 : TmpOffset3(2) =0.0
VWMult3(3) =VW_ConstG : VWOffset3(3) =0.0   : TmpMult3(3) =2.5 : TmpOffset3(3) =0.0
VWMult3(4) =VW_ConstG : VWOffset3(4) =0.0   : TmpMult3(4) =2.5 : TmpOffset3(4) =0.0
VWMult3(5) =VW_ConstG : VWOffset3(5) =0.0   : TmpMult3(5) =2.5 : TmpOffset3(5) =0.0
VWMult3(6) =VW_ConstG : VWOffset3(6) =0.0   : TmpMult3(6) =2.5 : TmpOffset3(6) =0.0
VWMult3(7) =VW_ConstG : VWOffset3(7) =0.0   : TmpMult3(7) =2.5 : TmpOffset3(7) =0.0
VWMult3(8) =VW_ConstG : VWOffset3(8) =0.0   : TmpMult3(8) =2.5 : TmpOffset3(8) =0.0
VWMult3(9) =VW_ConstG : VWOffset3(9) =0.0   : TmpMult3(9) =2.5 : TmpOffset3(9) =0.0
VWMult3(10)=VW_ConstG : VWOffset3(10)=0.0   : TmpMult3(10)=2.5 : TmpOffset3(10)=0.0
VWMult3(11)=VW_ConstG : VWOffset3(11)=0.0   : TmpMult3(11)=2.5 : TmpOffset3(11)=0.0
VWMult3(12)=VW_ConstG : VWOffset3(12)=0.0   : TmpMult3(12)=2.5 : TmpOffset3(12)=0.0
VWMult3(13)=VW_ConstG : VWOffset3(13)=0.0   : TmpMult3(13)=2.5 : TmpOffset3(13)=0.0
VWMult3(14)=VW_ConstG : VWOffset3(14)=0.0   : TmpMult3(14)=2.5 : TmpOffset3(14)=0.0
VWMult3(15)=VW_ConstG : VWOffset3(15)=0.0   : TmpMult3(15)=2.5 : TmpOffset3(15)=0.0
VWMult3(16)=VW_ConstG : VWOffset3(16)=0.0   : TmpMult3(16)=2.5 : TmpOffset3(16)=0.0

'Multiplexer 4
VWMult4(1) =VW_ConstG : VWOffset4(1) =0.0   : TmpMult4(1) =2.5 : TmpOffset4(1) =0.0
VWMult4(2) =VW_ConstG : VWOffset4(2) =0.0   : TmpMult4(2) =2.5 : TmpOffset4(2) =0.0
VWMult4(3) =VW_ConstG : VWOffset4(3) =0.0   : TmpMult4(3) =2.5 : TmpOffset4(3) =0.0
VWMult4(4) =VW_ConstG : VWOffset4(4) =0.0   : TmpMult4(4) =2.5 : TmpOffset4(4) =0.0
VWMult4(5) =VW_ConstG : VWOffset4(5) =0.0   : TmpMult4(5) =2.5 : TmpOffset4(5) =0.0
VWMult4(6) =VW_ConstG : VWOffset4(6) =0.0   : TmpMult4(6) =2.5 : TmpOffset4(6) =0.0
VWMult4(7) =VW_ConstG : VWOffset4(7) =0.0   : TmpMult4(7) =2.5 : TmpOffset4(7) =0.0
VWMult4(8) =VW_ConstG : VWOffset4(8) =0.0   : TmpMult4(8) =2.5 : TmpOffset4(8) =0.0
VWMult4(9) =VW_ConstG : VWOffset4(9) =0.0   : TmpMult4(9) =2.5 : TmpOffset4(9) =0.0
VWMult4(10)=VW_ConstG : VWOffset4(10)=0.0   : TmpMult4(10)=2.5 : TmpOffset4(10)=0.0
VWMult4(11)=VW_ConstG : VWOffset4(11)=0.0   : TmpMult4(11)=2.5 : TmpOffset4(11)=0.0
VWMult4(12)=VW_ConstG : VWOffset4(12)=0.0   : TmpMult4(12)=2.5 : TmpOffset4(12)=0.0
VWMult4(13)=VW_ConstG : VWOffset4(13)=0.0   : TmpMult4(13)=2.5 : TmpOffset4(13)=0.0
VWMult4(14)=VW_ConstG : VWOffset4(14)=0.0   : TmpMult4(14)=2.5 : TmpOffset4(14)=0.0
VWMult4(15)=VW_ConstG : VWOffset4(15)=0.0   : TmpMult4(15)=2.5 : TmpOffset4(15)=0.0
VWMult4(16)=VW_ConstG : VWOffset4(16)=0.0   : TmpMult4(16)=2.5 : TmpOffset4(16)=0.0

'Multiplexer 5
VWMult5(1) =VW_ConstG : VWOffset5(1) =0.0   : TmpMult5(1) =2.5 : TmpOffset5(1) =0.0
VWMult5(2) =VW_ConstG : VWOffset5(2) =0.0   : TmpMult5(2) =2.5 : TmpOffset5(2) =0.0
VWMult5(3) =VW_ConstG : VWOffset5(3) =0.0   : TmpMult5(3) =2.5 : TmpOffset5(3) =0.0
VWMult5(4) =VW_ConstG : VWOffset5(4) =0.0   : TmpMult5(4) =2.5 : TmpOffset5(4) =0.0
VWMult5(5) =VW_ConstG : VWOffset5(5) =0.0   : TmpMult5(5) =2.5 : TmpOffset5(5) =0.0
VWMult5(6) =VW_ConstG : VWOffset5(6) =0.0   : TmpMult5(6) =2.5 : TmpOffset5(6) =0.0
VWMult5(7) =VW_ConstG : VWOffset5(7) =0.0   : TmpMult5(7) =2.5 : TmpOffset5(7) =0.0
VWMult5(8) =VW_ConstG : VWOffset5(8) =0.0   : TmpMult5(8) =2.5 : TmpOffset5(8) =0.0
VWMult5(9) =VW_ConstG : VWOffset5(9) =0.0   : TmpMult5(9) =2.5 : TmpOffset5(9) =0.0
VWMult5(10)=VW_ConstG : VWOffset5(10)=0.0   : TmpMult5(10)=2.5 : TmpOffset5(10)=0.0
VWMult5(11)=VW_ConstG : VWOffset5(11)=0.0   : TmpMult5(11)=2.5 : TmpOffset5(11)=0.0
VWMult5(12)=VW_ConstG : VWOffset5(12)=0.0   : TmpMult5(12)=2.5 : TmpOffset5(12)=0.0
VWMult5(13)=VW_ConstG : VWOffset5(13)=0.0   : TmpMult5(13)=2.5 : TmpOffset5(13)=0.0
VWMult5(14)=VW_ConstG : VWOffset5(14)=0.0   : TmpMult5(14)=2.5 : TmpOffset5(14)=0.0
VWMult5(15)=VW_ConstG : VWOffset5(15)=0.0   : TmpMult5(15)=2.5 : TmpOffset5(15)=0.0
VWMult5(16)=VW_ConstG : VWOffset5(16)=0.0   : TmpMult5(16)=2.5 : TmpOffset5(16)=0.0
```

```
  NumScans = 0

  Do
    While Flag(1) = false: Loop
      '********************************** MP #1 VW SENSOR LOOP ****************************************

      Scan (ScanInt,Sec,0,5)  'Start the main scan of the program.
        PanelTemp (DAQ_Temp, 250)
        Battery (DAQ_Batt)

        PortSet(1,1)  'Enable MP 1 using Control Port #1
        i=0
        SubScan(0,0,NumSensorsMP1)    'Use constant NumSensorsMP1 to determine # of passes through loop.
          Delay (0,10,msec)
          PortSet(8,1)                 'Clock MP to start at channel 1, using Control Port #8.
          Delay(0,20,mSec)
          PortSet(8,0)
          '++++++++++++++++++++++++++++++++++++++++++++++++++++++++++++++++++++++++++++++++++++++++++++++
          Delay(0,500,mSec)
          'AVW4 CHANNEL 1 MP LOOP
          i=i+1

          'MEASURE TEMP
          'Measure the temperature of the sensor
          'Half Bridge measurement is Ratio/Metric,
          'must set the multiplier at V_excitation/1000 or 2500/1000 = 2.5
          'BrHalf(Dest,Reps,Range,SEChan,ExChan,MeasPEx,ExmV,RevEx,SettlingTime,Integ,Mult,Offset)
          BrHalf(TempMP1(i),1,mV2500,1,Vx1,1,2500,True,20000,_60Hz,TmpMult1(i),TmpOffset1(i))
          'questions: settling time, reverse excitation,
          'BrHalf(TempMP1(i),1,mV5000,1,Vx1,1,2500,false,200,250,TmpMult1(i)(),TmpOffset1(i)())

          'MEASURE VW SENSOR
          'Note:  Actual Multiplier and Offset will vary depending upon Sensor calibration.
          'Start and Stop Frequencies are determined by the sensor model
          'VibratingWire(Dest,Reps,Range,SeChan,ExChan,StartFreq,EndFreq,TSweep,Steps,DelMeas,NumCycles,DelReps,M
ult,Offset)
          VibratingWire(CoilMP1(i),1,mV2_5,2,Vx1,SFreq_VW,EFreq_VW,150,-1,100000,100,0,VWMult1(i),VWOffset1(i))
          'questions: same
          'VibratingWire(CoilMP1(i),1,mV2_5,2,1,800,2500,50,30,10000,300,0,1,0)

          'TEMP COMPENSATION CALCULATION
          'Calculate temperature based upon the 5 coefficients (5th order polynomial)
          'Polynomial  F(X)= C0 + C1(X)+ C2(X^2) + C3(X^3) + C4(X^4) + C5(X^5)
          'NOTE: These coefficients are for reference only and will vary from Sensor to Sensor.
          'C0= -104.78  C1= 378.11  C2= -611.59  C3= 544.27  C4= -240.91  C5= 43.089
          TempMP1(i)=-104.78+((378.11*TempMP1(i))+(-611.59*TempMP1(i)^2)+(544.27*TempMP1(i)^3)+(-240.91*TempMP1(i
)^4)+(43.089*TempMP1(i)^5))

          Delay (0,10,mSec)
        NextSubScan
        PortSet(1,0) 'Turn Off Port #1 to disable MP #1.

        '********************************** MP #2 VW SENSOR Loop ****************************************

        PortSet(2,1)  'Enable MP 2, using Control Port #2.
        i=0
        SubScan(0,0,NumSensorsMP2)    'Use constant NumSensorsMP2 to determine # of passes through loop.
          Delay (0,10,msec)
          PortSet(8,1)                 'Clock MP to start at channel 1, using Control Port #8.
          Delay(0,20,mSec)
          PortSet(8,0)
          '++++++++++++++++++++++++++++++++++++++++++++++++++++++++++++++++++++++++++++++++++++++++++++++
          Delay(0,500,mSec)
          'AVW4 CHANNEL 2 MP Loop
          i=i+1
```

```
          'MEASURE TEMP
          'Measure the temperature of the sensor
          'Half Bridge measurement is Ratio/Metric,
          'must set the multiplier at V_excitation/1000 or 2500/1000 = 2.5
          'BrHalf(Dest,Reps,Range,SEChan,ExChan,MeasPEx,ExmV,RevEx,SettlingTime,Integ,Mult,Offset)
          BrHalf(TempMP2(i),1,mV5000,3,Vx1,1,2500,True,20000,_60Hz,TmpMult2(i),TmpOffset2(i))

          'MEASURE VW SENSOR
          'Note:  Actual Multiplier and Offset will vary depending upon Sensor calibration.
          'Start and Stop Frequencies are determined by the sensor model
          'VibratingWire(Dest,Reps,Range,SeChan,ExChan,StartFreq,EndFreq,TSweep,Steps,DelMeas,NumCycles,DelReps,M
ult,Offset)
          VibratingWire(CoilMP2(i),1,mV2_5,4,Vx1,SFreq_VW,EFreq_VW,150,-1,100000,100,0,VWMult2(i),VWOffset2(i))

          'TEMP COMPENSATION CALCULATION
          'Calculate temperature based upon the 5 coefficients (5th order polynomial)
          'Polynomial  F(X)= C0 + C1(X)+ C2(X^2) + C3(X^3) + C4(X^4) + C5(X^5)
          'NOTE: These coefficients are for reference only and will vary from Sensor to Sensor.
          'C0= -104.78  C1= 378.11  C2= -611.59  C3= 544.27  C4= -240.91  C5= 43.089
          TempMP2(i)=-104.78+((378.11*TempMP2(i))+(-611.59*TempMP2(i)^2)+(544.27*TempMP2(i)^3)+(-240.91*TempMP2(i
)^4)+(43.089*TempMP2(i)^5))

          Delay (0,10,mSec)
        NextSubScan
        PortSet(2,0) 'Turn Off Port #2 to disable multiplexer MP #2.

        '************************************ MP #3 VW SENSOR Loop ***************************************

        PortSet(3,1)  'Enable MP 3, using Control Port #3.
        i=0
        SubScan(0,0,NumSensorsMP3)    'Use constant NumSensorsMP3 to determine # of passes through loop.
          Delay (0,10,msec)
          PortSet(8,1)                 'Clock MP to start at channel 1, using Control Port #8.
          Delay(0, 20, mSec)
          PortSet(8,0)
          '+++++++++++++++++++++++++++++++++++++++++++++++++++++++++++++++++++++++++++++++++++++++++++++++++++
          Delay(0,500,mSec)
          'AVW4 CHANNEL 3 MP Loop
          i=i+1

          'MEASURE TEMP
          'Measure the temperature of the sensor
          'Half Bridge measurement is Ratio/Metric,
          'must set the multiplier at V_excitation/1000 or 2500/1000 = 2.5
          'BrHalf(Dest,Reps,Range,SEChan,ExChan,MeasPEx,ExmV,RevEx,SettlingTime,Integ,Mult,Offset)
          BrHalf(TempMP3(i),1,mV5000,5,Vx1,1,2500,True,20000,_60Hz,TmpMult3(i),TmpOffset3(i))

          'MEASURE VW SENSOR
          'Note:  Actual Multiplier and Offset will vary depending upon Sensor calibration.
          'Start and Stop Frequencies are determined by the sensor model
          'VibratingWire(Dest,Reps,Range,SeChan,ExChan,StartFreq,EndFreq,TSweep,Steps,DelMeas,NumCycles,DelReps,M
ult,Offset)
          VibratingWire(CoilMP3(i),1,mV2_5,6,Vx1,SFreq_VW,EFreq_VW,150,-1,100000,100,0,VWMult3(i),VWOffset3(i))

          'TEMP COMPENSATION CALCULATION
          'Calculate temperature based upon the 5 coefficients (5th order polynomial)
          'Polynomial  F(X)= C0 + C1(X)+ C2(X^2) + C3(X^3) + C4(X^4) + C5(X^5)
          'NOTE: These coefficients are for reference only and will vary from Sensor to Sensor.
          'C0= -104.78  C1= 378.11  C2= -611.59  C3= 544.27  C4= -240.91  C5= 43.089
          TempMP3(i)=-104.78+((378.11*TempMP3(i))+(-611.59*TempMP3(i)^2)+(544.27*TempMP3(i)^3)+(-240.91*TempMP3(i
)^4)+(43.089*TempMP3(i)^5))

          Delay (0,10,mSec)
        NextSubScan
        PortSet(3,0) 'Turn Off Port #3 to disable multiplexer MP #3
```

```
'************************************ MP #4 VW SENSOR Loop ***************************************

PortSet(4,1)  'Enable MP 4, using Control Port #4.
i=0
SubScan(0,0,NumSensorsMP4)    'Use constant NumSensorsMP4 to determine # of passes through loop.
  Delay (0,10,msec)
  PortSet(8,1)                 'Clock MP to start at channel 1, using Control Port #8.
  Delay(0,20,mSec)
  PortSet(8,0)
  '+++++++++++++++++++++++++++++++++++++++++++++++++++++++++++++++++++++++++++++++++++++++++++++++
  Delay(0, 500, mSec)
  'AVW4 CHANNEL 4 MP Loop
  i=i+1

  'MEASURE TEMP
  'Measure the temperature of the sensor
  'Half Bridge measurement is Ratio/Metric,
  'must set the multiplier at V_excitation/1000 or 2500/1000 = 2.5
  'BrHalf(Dest,Reps,Range,SEChan,ExChan,MeasPEx,ExmV,RevEx,SettlingTime,Integ,Mult,Offset)
  BrHalf(TempMP4(i),1,mV5000,7,Vx1,1,2500,True,20000,_60Hz,TmpMult4(i),TmpOffset4(i))

  'MEASURE VW SENSOR
  'Note:  Actual Multiplier and Offset will vary depending upon Sensor calibration.
  'Start and Stop Frequencies are determined by the sensor model
  'VibratingWire(Dest,Reps,Range,SeChan,ExChan,StartFreq,EndFreq,TSweep,Steps,DelMeas,NumCycles,DelReps,M
ult,Offset)
  VibratingWire(CoilMP4(i),1,mV2_5,8,Vx1,SFreq_VW,EFreq_VW,150,-1,100000,100,0,VWMult4(i),VWOffset4(i))

  'TEMP COMPENSATION CALCULATION
  'Calculate temperature based upon the 5 coefficients (5th order polynomial)
  'Polynomial  F(X)= C0 + C1(X)+ C2(X^2) + C3(X^3) + C4(X^4) + C5(X^5)
  'NOTE: These coefficients are for reference only and will vary from Sensor to Sensor.
  'C0= -104.78  C1= 378.11  C2= -611.59  C3= 544.27  C4= -240.91  C5= 43.089
  TempMP4(i)=-104.78+((378.11*TempMP4(i))+(-611.59*TempMP4(i)^2)+(544.27*TempMP4(i)^3)+(-240.91*TempMP4(i
)^4)+(43.089*TempMP4(i)^5))

  Delay (0,10,mSec)
NextSubScan
PortSet(4,0) 'Turn Off Port #4 to disable multiplexer MP #4.

'************************************ MP #5 VW SENSOR Loop ***************************************

PortSet(5,1)  'Enable MP 5, using Control Port #5.
i=0
SubScan(0,0,NumSensorsMP5)    'Use constant NumSensorsMP5 to determine # of passes through loop.
  Delay (0,10,msec)
  PortSet(8,1)                 'Clock MP to start at channel 1, using Control Port #8.
  Delay(0, 20, mSec)
  PortSet(8,0)
  '+++++++++++++++++++++++++++++++++++++++++++++++++++++++++++++++++++++++++++++++++++++++++++++++
  Delay(0,500,mSec)
  'AVW4 CHANNEL 5 MP Loop
  i=i+1

  'MEASURE TEMP
  'Measure the temperature of the sensor
  'Half Bridge measurement is Ratio/Metric,
  'must set the multiplier at V_excitation/1000 or 2500/1000 = 2.5
  'BrHalf(Dest,Reps,Range,SEChan,ExChan,MeasPEx,ExmV,RevEx,SettlingTime,Integ,Mult,Offset)
  BrHalf(TempMP5(i),1,mV5000,9,Vx2,1,2500,True,20000,_60Hz,TmpMult5(i),TmpOffset5(i))

  'MEASURE VW SENSOR
  'Note:  Actual Multiplier and Offset will vary depending upon Sensor calibration.
  'Start and Stop Frequencies are determined by the sensor model
  'VibratingWire(Dest,Reps,Range,SeChan,ExChan,StartFreq,EndFreq,TSweep,Steps,DelMeas,NumCycles,DelReps,M
ult,Offset)
```

```
          VibratingWire(CoilMP5(i),1,mV2_5,10,Vx2,SFreq_VW,EFreq_VW,150,-1,100000,100,0,VWMult5(i),VWOffset5(i))

          'TEMP COMPENSATION CALCULATION
          'Calculate temperature based upon the 5 coefficients (5th order polynomial)
          'Polynomial  F(X)= C0 + C1(X)+ C2(X^2) + C3(X^3) + C4(X^4) + C5(X^5)
          'NOTE: These coefficients are for reference only and will vary from Sensor to Sensor.
          'C0= -104.78  C1= 378.11  C2= -611.59  C3= 544.27  C4= -240.91  C5= 43.089
          TempMP5(i)=-104.78+((378.11*TempMP5(i))+(-611.59*TempMP5(i)^2)+(544.27*TempMP5(i)^3)+(-240.91*TempMP5(i
)^4)+(43.089*TempMP5(i)^5))

          Delay (0,10,mSec)
        NextSubScan
        PortSet(5,0) 'Turn Off Port #5 to disable multiplexer MP #5.

        NumScans = NumScans + 1

        '****************************************** STORE VALUES TO THE OUTPUT TABLE *********************
        'Call the tables after the arrays have been filled within the subscans.  The SubScan protocol will
        'try filling the arrays each subscan. For instance: if in the 1st subscan loop, 16 values would be
        'written every pass through the loop, with only 1 measurement value per each
        '(15 empty values each pass through).
        CallTable DataSamples
        CallTable DataAverage

        If NumScans = NumLoops Then
          NumScans = 0
          Flag(1) = false
        EndIf

      NextScan
    Loop
  EndProg
```

C.5 CR1000 Program used for Foil Gages on Prestressing Strand

```
'CR1000 sensor program
'Used 6-25-2013 by Ben Dymond at the University of Minnesota.
'This program will measure 35 - 120 ohm foil gages wired to
'three AM16/32 multiplexers, interfaced through one AVW4 vibrating wire interface.
'*****************************************************************************
'CR1000 Analog Input Channel assignments were made to ease field verification
'and/or for any troubleshooting necessary.

'CR1000 Differential channel #1 measures the sensors from multiplexer MP #1.
'CR1000 Differential channel #2 measures the sensors from multiplexer MP #2.
'CR1000 Differential channel #3 measures the sensors from multiplexer MP #3.

'CR1000 Digital Control Port assignments were also made to ease any troubleshooting or verification.
'CR1000 Control Port #1 is used to Enable (turn ON or activate) multiplexer #1.
'CR1000 Control Port #2 is used to Enable (turn ON or activate) multiplexer #2.
'CR1000 Control Port #3 is used to Enable (turn ON or activate) multiplexer #3.

'** CR1000 Control Port #8 is used globally with all 3 multiplexers to clock each multiplexer.
'(advance relays to next channel)

'AM16/32 channel wiring to AVW4 #1 Wiring inputs => AVW4 Outputs => 4WFBS TIM => CR1000 Analog Input channels
'MP#1  ODD H(high) --->----  T1 +  ------->--------->----- T1 ------->--------   SE #1
'MP#1  ODD L(Odd)  --->----  T1 -  ------->--------->----- T1                    (single input)
'MP#1  EVEN H(high)--->----  C1 +  ------->--------->----- F1 ------->--------   SE #2
'MP#1  Even L(high) -->----  C1 -  ------->--------->----- F1                    (single input)
'
'AM16/32 channel wiring to AVW4 #1 Wiring inputs => AVW4 Outputs => 4WFBS TIM => CR1000 Analog Input channels
'MP#2  ODD H(high) --->----  T2 +  ------->--------->----- T2 ------->--------   SE #3
'MP#2  ODD L(Odd)  --->----  T2 -  ------->--------->----- T2                    (single input)
'MP#2  EVEN H(high)--->----  C2 +  ------->--------->----- F2 ------->--------   SE #4
'MP#2  Even L(high) -->----  C2 -  ------->--------->----- F2                    (single input)
'
'AM16/32 channel wiring to AVW4 #1 Wiring inputs => AVW4 Outputs to => CR1000 Analog Input channels
'MP#3  ODD H(high) --->----  T3 +  ------->--------->----- T3 ------->--------   SE #5
'MP#3  ODD L(Odd)  --->----  T3 -  ------->--------->----- T3                    (single input)
'MP#3  EVEN H(high)--->----  C3 +  ------->--------->----- F3 ------->--------   SE #6
'MP#3  Even L(high) -->----  C3 -  ------->--------->----- F3                    (single input)

'PROGRAM BEGINS HERE.

'Declare program constants

Const ScanInt = 20          'Scan Interval in Seconds
Const NumLoops = 1          'Number of Loops to Read gages

Const FoilMult = 2.11       'Gage factor for 120 ohm foil gages
Const FoilOff = 0.0         'Offset for 120 ohm foil gages

Const NumSensorsMP1 = 16    'Number of Sensors on MP #1
Const NumSensorsMP2 = 16    'Number of Sensors on MP #2
Const NumSensorsMP3 = 3     'Number of Sensors on MP #3

'Declare program variables.

Public DAQ_Batt                 'Data Acquisition Battery Voltage
Public DAQ_Temp                 'Data Acquisition Temperature
Public TestID As String * 20    'Test ID for load test only. (Enter the name in Public Field Monitor Table)
Public Flag(8)                  'General use flags for stopping/starting scan

Public FoilMP1(NumSensorsMP1)   'Declare Variables for Multiplexer 1 (Foil gages)
Public Vr1000MP1(NumSensorsMP1)
Public GFAdjMP1(NumSensorsMP1)
Public BRZeroMP1(NumSensorsMP1)
Public CKnownMP1(NumSensorsMP1)
Public CIndex
Public CAvg
```

```
Public FCLoaded
Public QBSSMode
Public GFRaw
Public ZMode1

Public FoilMP2(NumSensorsMP2)   'Declare Variables for Multiplexer 2 (Foil gages)
Public VR1000MP2(NumSensorsMP2)
Public GFAdjMP2(NumSensorsMP2)
Public BRZeroMP2(NumSensorsMP2)
Public CKnownMP2(NumSensorsMP2)
Public ZMode2

Public FoilMP3(NumSensorsMP3)   'Declare Variables for Multiplexer 3 (Foil gages)
Public VR1000MP3(NumSensorsMP3)
Public GFAdjMP3(NumSensorsMP3)
Public BRZeroMP3(NumSensorsMP3)
Public CKnownMP3(NumSensorsMP3)
Public ZMode3

Alias FoilMP1(1) = G1MP1
Alias FoilMP1(2) = G2MP1
Alias FoilMP1(3) = G3MP1
Alias FoilMP1(4) = G4MP1
Alias FoilMP1(5) = G5MP1
Alias FoilMP1(6) = G6MP1
Alias FoilMP1(7) = G7MP1
Alias FoilMP1(8) = G8MP1
Alias FoilMP1(9) = G9MP1
Alias FoilMP1(10) = G10MP1
Alias FoilMP1(11) = G11MP1
Alias FoilMP1(12) = G12MP1
Alias FoilMP1(13) = G13MP1
Alias FoilMP1(14) = G14MP1
Alias FoilMP1(15) = G15MP1
Alias FoilMP1(16) = G16MP1

Alias FoilMP2(1)  = G17MP2
Alias FoilMP2(2)  = G18MP2
Alias FoilMP2(3)  = G19MP2
Alias FoilMP2(4)  = G20MP2
Alias FoilMP2(5)  = G21MP2
Alias FoilMP2(6)  = G22MP2
Alias FoilMP2(7)  = G23MP2
Alias FoilMP2(8)  = G24MP2
Alias FoilMP2(9)  = G25MP2
Alias FoilMP2(10) = G26MP2
Alias FoilMP2(11) = G27MP2
Alias FoilMP2(12) = G28MP2
Alias FoilMP2(13) = G29MP2
Alias FoilMP2(14) = G30MP2
Alias FoilMP2(15) = G31MP2
Alias FoilMP2(16) = G32MP2

Alias FoilMP3(1)  = G33MP3
Alias FoilMP3(2)  = G34MP3
Alias FoilMP3(3)  = G35MP3
'Alias FoilMP3(4) = G36MP3
'Alias FoilMP3(5) = G37MP3
'Alias FoilMP3(6) = G38MP3
'Alias FoilMP3(7) = G39MP3
'Alias FoilMP3(8) = G40MP3
'Alias FoilMP3(9) = G41MP3
'Alias FoilMP3(10) = G42MP3
'Alias FoilMP3(11) = G43MP3
'Alias FoilMP3(12) = G44MP3
'Alias FoilMP3(13) = G45MP3
```

```
'Alias FoilMP3(14) = G46MP3
'Alias FoilMP3(15) = G47MP3
'Alias FoilMP3(16) = G48MP3

Public i
Public j

Public FoilMult1(NumSensorsMP1)
Public FoilOffset1(NumSensorsMP1)

Public FoilMult2(NumSensorsMP2)
Public FoilOffset2(NumSensorsMP2)

Public FoilMult3(NumSensorsMP3)
Public FoilOffset3(NumSensorsMP3)

'Define Data Table
DataTable (DataSamples,1,-1)
  DataInterval (0,ScanInt,Sec,10)
  Sample (1,TestID,String)
  Minimum (1,DAQ_Batt,FP2,0,0)
  Sample (1,DAQ_Temp,FP2)
  Sample (NumSensorsMP1,FoilMP1(),IEEE4)
  Sample (NumSensorsMP2,FoilMP2(),IEEE4)
  Sample (NumSensorsMP3,FoilMP3(),IEEE4)
EndTable

DataTable (DataAverage,Flag(1)=true,1000)
  Sample (1,TestID,String)
  Average (NumSensorsMP1,FoilMP1(),IEEE4,0)
  Average (NumSensorsMP2,FoilMP2(),IEEE4,0)
  Average (NumSensorsMP3,FoilMP3(),IEEE4,0)
EndTable

'Main Program
BeginProg

  'Multiplexer 1
  FoilMult1(1) =FoilMult : FoilOffset1(1) =FoilOff
  FoilMult1(2) =FoilMult : FoilOffset1(2) =FoilOff
  FoilMult1(3) =FoilMult : FoilOffset1(3) =FoilOff
  FoilMult1(4) =FoilMult : FoilOffset1(4) =FoilOff
  FoilMult1(5) =FoilMult : FoilOffset1(5) =FoilOff
  FoilMult1(6) =FoilMult : FoilOffset1(6) =FoilOff
  FoilMult1(7) =FoilMult : FoilOffset1(7) =FoilOff
  FoilMult1(8) =FoilMult : FoilOffset1(8) =FoilOff
  FoilMult1(9) =FoilMult : FoilOffset1(9) =FoilOff
  FoilMult1(10)=FoilMult : FoilOffset1(10)=FoilOff
  FoilMult1(11)=FoilMult : FoilOffset1(11)=FoilOff
  FoilMult1(12)=FoilMult : FoilOffset1(12)=FoilOff
  FoilMult1(13)=FoilMult : FoilOffset1(13)=FoilOff
  FoilMult1(14)=FoilMult : FoilOffset1(14)=FoilOff
  FoilMult1(15)=FoilMult : FoilOffset1(15)=FoilOff
  FoilMult1(16)=FoilMult : FoilOffset1(16)=FoilOff

  'Multiplexer 2
  FoilMult2(1) =FoilMult : FoilOffset2(1) =FoilOff
  FoilMult2(2) =FoilMult : FoilOffset2(2) =FoilOff
  FoilMult2(3) =FoilMult : FoilOffset2(3) =FoilOff
  FoilMult2(4) =FoilMult : FoilOffset2(4) =FoilOff
  FoilMult2(5) =FoilMult : FoilOffset2(5) =FoilOff
  FoilMult2(6) =FoilMult : FoilOffset2(6) =FoilOff
  FoilMult2(7) =FoilMult : FoilOffset2(7) =FoilOff
  FoilMult2(8) =FoilMult : FoilOffset2(8) =FoilOff
  FoilMult2(9) =FoilMult : FoilOffset2(9) =FoilOff
  FoilMult2(10)=FoilMult : FoilOffset2(10)=FoilOff
```

```
FoilMult2(11)=FoilMult : FoilOffset2(11)=FoilOff
FoilMult2(12)=FoilMult : FoilOffset2(12)=FoilOff
FoilMult2(13)=FoilMult : FoilOffset2(13)=FoilOff
FoilMult2(14)=FoilMult : FoilOffset2(14)=FoilOff
FoilMult2(15)=FoilMult : FoilOffset2(15)=FoilOff
FoilMult2(16)=FoilMult : FoilOffset2(16)=FoilOff

'Multiplexer 3
FoilMult3(1) =FoilMult : FoilOffset3(1) =FoilOff
FoilMult3(2) =FoilMult : FoilOffset3(2) =FoilOff
FoilMult3(3) =FoilMult : FoilOffset3(3) =FoilOff
'  FoilMult3(4) =FoilMult : FoilOffset3(4) =FoilOff
'  FoilMult3(5) =FoilMult : FoilOffset3(5) =FoilOff
'  FoilMult3(6) =FoilMult : FoilOffset3(6) =FoilOff
'  FoilMult3(7) =FoilMult : FoilOffset3(7) =FoilOff
'  FoilMult3(8) =FoilMult : FoilOffset3(8) =FoilOff
'  FoilMult3(9) =FoilMult : FoilOffset3(9) =FoilOff
'  FoilMult3(10)=FoilMult : FoilOffset3(10)=FoilOff
'  FoilMult3(11)=FoilMult : FoilOffset3(11)=FoilOff
'  FoilMult3(12)=FoilMult : FoilOffset3(12)=FoilOff
'  FoilMult3(13)=FoilMult : FoilOffset3(13)=FoilOff
'  FoilMult3(14)=FoilMult : FoilOffset3(14)=FoilOff
'  FoilMult3(15)=FoilMult : FoilOffset3(15)=FoilOff
'  FoilMult3(16)=FoilMult : FoilOffset3(16)=FoilOff

'Initialize calibration variables for
'Quarter Bridge Strain, 3-wire 120 ohm with 4WFBS120 TIM measurement 'Vr1000()'
CIndex=1 : CAvg=1
For j = 1 To NumSensorsMP1
  GFAdjMP1(j)=FoilMult1(j)
Next

For j = 1 To NumSensorsMP2
  GFAdjMP2(j)=FoilMult2(j)
Next

For j = 1 To NumSensorsMP3
  GFAdjMP3(j)=FoilMult3(j)
Next

Do
  While Flag(1) = false: Loop
    '********************************** MP #1 SENSOR LOOP *********************************************
    'Load the most recent calibration values from the CalHist table
    FCLoaded=LoadFieldCal(True)

    Scan (ScanInt,Sec,0,NumLoops)  'Start the main scan of the program.
      PanelTemp (DAQ_Temp, 250)
      Battery (DAQ_Batt)

      PortSet(1,1)  'Enable MP 1 using Control Port #1
      i=1
      SubScan(0,0,NumSensorsMP1)    'Use constant NumSensorsMP1 to determine # of passes through loop.
        Delay (0,10,msec)
        PortSet(8,1)                 'Clock MP to start at channel 1, using Control Port #8.
        Delay(0,20,mSec)
        PortSet(8,0)
        '+++++++++++++++++++++++++++++++++++++++++++++++++++++++++++++++++++++++++++++++++++++++++++++++++++++++
        Delay(0,500,mSec)
        'AVW4 CHANNEL 1 MP LOOP

        'Quarter Bridge Strain, 3-wire 120 ohm with 4WFBS120 TIM measurement 'Vr1000()'
        '************************use an intergration values of _60Hz ************************************
        BrFull(Vr1000MP1(i),1,mV25,1,Vx3,1,2500,True,True,0,_60Hz,1,0)
        i=i+1
        Delay (0,10,mSec)
```

```
NextSubScan

'Quarter Bridge Strain, 3-wire 120 ohm with 4WFBS120 TIM measurement 'Vr1000()'
StrainCalc(FoilMP1(),NumSensorsMP1,Vr1000MP1(),BRZeroMP1(),-1,GFAdjMP1(),0)
'Quarter bridge strain shunt calibration for Quarter Bridge Strain,
'3-wire 120 ohm with 4WFBS120 TIM measurement 'Vr1000()'
FieldCalStrain(13,FoilMP1(),1,GFAdjMP1(),0,QBSSMode,CKnownMP1(),CIndex,CAvg,FoilMult1(),0)
'Zeroing calibration for Quarter Bridge Strain, 3-wire 120 ohm with 4WFBS120 TIM measurement 'Vr1000()'
FieldCalStrain(10,Vr1000MP1(),NumSensorsMP1,0,BRZeroMP1(),ZMode1,0,CIndex,CAvg,0,FoilMP1())

Delay (0,10,mSec)
PortSet(1,0) 'Turn Off Port #1 to disable MP #1.

'********************************** MP #2 VW SENSOR Loop ****************************************

PortSet(2,1)  'Enable MP 2, using Control Port #2.
i=1
SubScan(0,0,NumSensorsMP2)    'Use constant NumSensorsMP2 to determine # of passes through loop.
  Delay (0,10,msec)
  PortSet(8,1)                 'Clock MP to start at channel 1, using Control Port #8.
  Delay(0,20,mSec)
  PortSet(8,0)
  '++++++++++++++++++++++++++++++++++++++++++++++++++++++++++++++++++++++++++++++++++++++++++++++++
  Delay(0,500,mSec)
  'AVW4 CHANNEL 2 MP Loop

  'Quarter Bridge Strain, 3-wire 120 ohm with 4WFBS120 TIM measurement 'Vr1000()'
  '************************use an intergration values of _60Hz ************************************
  BrFull(VR1000MP2(i),1,mV25,2,Vx3,1,2500,True,True,0,_60Hz,1,0)
  i=i+1
  Delay (0,10,mSec)
NextSubScan

'Quarter Bridge Strain, 3-wire 120 ohm with 4WFBS120 TIM measurement 'Vr1000()'
StrainCalc(FoilMP2(),NumSensorsMP2,VR1000MP2(),BRZeroMP2(),-1,GFAdjMP2(),0)
'Quarter bridge strain shunt calibration for
'Quarter Bridge Strain, 3-wire 120 ohm with 4WFBS120 TIM measurement 'Vr1000()'
FieldCalStrain(13,FoilMP2(),1,GFAdjMP2(),0,QBSSMode,CKnownMP2(),CIndex,CAvg,FoilMult2(),0)
'Zeroing calibration for
'Quarter Bridge Strain, 3-wire 120 ohm with 4WFBS120 TIM measurement 'Vr1000()'
FieldCalStrain(10,VR1000MP2(),NumSensorsMP2,0,BRZeroMP2(),ZMode2,0,CIndex,CAvg,0,FoilMP2())

Delay (0,10,mSec)
PortSet(2,0) 'Turn Off Port #2 to disable multiplexer MP #2.

'********************************** MP #3 VW SENSOR Loop ****************************************

PortSet(3,1)  'Enable MP 3, using Control Port #3.
i=1
SubScan(0,0,NumSensorsMP3)    'Use constant NumSensorsMP3 to determine # of passes through loop.
  Delay (0,10,msec)
  PortSet(8,1)                 'Clock MP to start at channel 1, using Control Port #8.
  Delay(0, 20, mSec)
  PortSet(8,0)
  '++++++++++++++++++++++++++++++++++++++++++++++++++++++++++++++++++++++++++++++++++++++++++++++++
  Delay(0,500,mSec)
  'AVW4 CHANNEL 3 MP Loop

  'Quarter Bridge Strain, 3-wire 120 ohm with 4WFBS120 TIM measurement 'Vr1000()'
  '************************use an intergration values of _60Hz ************************************
  BrFull(VR1000MP3(i),1,mV25,3,Vx3,1,2500,True,True,0,_60Hz,1,0)
  i=i+1
  Delay (0,10,mSec)
NextSubScan
```

```
      'Quarter Bridge Strain, 3-wire 120 ohm with 4WFBS120 TIM measurement 'Vr1000()'
      StrainCalc(FoilMP3(),NumSensorsMP3,VR1000MP3(),BRZeroMP3(),-1,GFAdjMP3(),0)
      'Quarter bridge strain shunt calibration for
      'Quarter Bridge Strain, 3-wire 120 ohm with 4WFBS120 TIM measurement 'Vr1000()'
      FieldCalStrain(13,FoilMP3(),1,GFAdjMP3(),0,QBSSMode,CKnownMP3(),CIndex,CAvg,FoilMult3(),0)
      'Zeroing calibration for
      'Quarter Bridge Strain, 3-wire 120 ohm with 4WFBS120 TIM measurement 'Vr1000()'
      FieldCalStrain(10,VR1000MP3(),NumSensorsMP3,0,BRZeroMP3(),ZMode3,0,CIndex,CAvg,0,FoilMP3())

      Delay (0,10,mSec)
      PortSet(3,0) 'Turn Off Port #3 to disable multiplexer MP #3.

      '********************************** STORE VALUES TO THE OUTPUT TABLE *********************************
      'Call the tables after the arrays have been filled within the subscans.  The SubScan protocol will try
      'filling the arrays each subscan. For instance: if in the 1st subscan loop, 16 values would be written
      'every pass through the loop, with only 1 measurement value per each (15 empty values each pass through).
      CallTable DataSamples
      CallTable DataAverage

    NextScan
  Loop
EndProg
```

C.6 CR1000 Program used to Collect Stirrup Strains during Lab Testing

```
'CR1000 sensor program created in Short Cut (2.9)
'Used 12-17-2015 by Ben Dymond at the University of Minnesota.
'This program will measure 48 - 120 ohm foil gages wired to
'three AM16/32 multiplexers

'Declare Variables and Units
Public BattV
Public FCLoaded
Public PTemp_C

Public CReps
Public ZMode
Public QBSSMode
Public CIndex
Public CAvg
Public LCount
Public Strain(16)
Public Vr1000(16)
Public GFAdj(16)
Public BrZero(16)
Public CKnown(16)

Public CReps_2
Public ZMode_2
Public QBSSMode_2
Public CIndex_2
Public CAvg_2
Public LCount_2
Public Strain_2(16)
Public Vr1000_2(16)
Public GFAdj_2(16)
Public BrZero_2(16)
Public CKnown_2(16)

Public CReps_3
Public ZMode_3
Public QBSSMode_3
Public CIndex_3
Public CAvg_3
Public LCount_3
Public Strain_3(16)
Public Vr1000_3(16)
Public GFAdj_3(16)
Public BrZero_3(16)
Public CKnown_3(16)

'Public RTempC
'Public Temp_F(25)
'Public RTempC_2
'Public Temp_F_2(25)

Public GFsRaw(16) = {2.10,2.10,2.10,2.10,2.10,2.10,2.10,2.10,2.10,2.10,2.10,2.10,2.10,2.10,2.10,2.10}
Public GFsRaw_2(16)={2.10,2.10,2.10,2.10,2.10,2.10,2.10,2.10,2.10,2.10,2.10,2.10,2.10,2.10,2.10,2.10}
Public GFsRaw_3(16)={2.10,2.10,2.10,2.10,2.10,2.10,2.10,2.10,2.10,2.10,2.10,2.10,2.10,2.10,2.10,2.10}

Public TestID As String * 20    'Test ID for load test only. (Enter the name in Public Field Monitor Table)
Public Flag(8)                  'General use flags for stopping/starting scan

Public SEVolt11        'North CivE 110k load cell
Public ScaledLoadN11
Public SEVolt13        'Middle CivE 220k load cell
Public ScaledLoadM13
Public SEVolt15        'South CivE 110k load cell
Public ScaledLoadS15

Alias  SEVolt11 = F110kN
```

```
Alias  SEVolt13 = F220kM
Alias  SEVolt15 = F110kS

Const DatInt=10    'Seconds
Const ScanInt=10    'Seconds

Units BattV=Volts
Units PTemp_C=Deg C

Units Strain=microstrain
Units Vr1000=mV/V
Units GFAdj=unitless
Units BrZero=mV/V

Units Strain_2=microstrain
Units Vr1000_2=mV/V
Units GFAdj_2=unitless
Units BrZero_2=mV/V

Units Strain_3=microstrain
Units Vr1000_3=mV/V
Units GFAdj_3=unitless
Units BrZero_3=mV/V

'Define Data Tables
DataTable(StrainTable,True,-1)
  DataInterval(0,DatInt,Sec,10)

  Sample (1,TestID,String)
  Minimum (1,BattV,FP2,0,0)
  Sample (1,PTemp_C,FP2)
  Sample (1,SEVolt11,FP2)
  Sample (1,SEVolt13,FP2)
  Sample (1,SEVolt15,FP2)

  Average(1,Strain(1),IEEE4,False)
  Average(1,Strain(2),IEEE4,False)
  Average(1,Strain(3),IEEE4,False)
  Average(1,Strain(4),IEEE4,False)
  Average(1,Strain(5),IEEE4,False)
  Average(1,Strain(6),IEEE4,False)
  Average(1,Strain(7),IEEE4,False)
  Average(1,Strain(8),IEEE4,False)
  Average(1,Strain(9),IEEE4,False)
  Average(1,Strain(10),IEEE4,False)
  Average(1,Strain(11),IEEE4,False)
  Average(1,Strain(12),IEEE4,False)
  Average(1,Strain(13),IEEE4,False)
  Average(1,Strain(14),IEEE4,False)
  Average(1,Strain(15),IEEE4,False)
  Average(1,Strain(16),IEEE4,False)

  Average(1,Strain_2(1),IEEE4,False)
  Average(1,Strain_2(2),IEEE4,False)
  Average(1,Strain_2(3),IEEE4,False)
  Average(1,Strain_2(4),IEEE4,False)
  Average(1,Strain_2(5),IEEE4,False)
  Average(1,Strain_2(6),IEEE4,False)
  Average(1,Strain_2(7),IEEE4,False)
  Average(1,Strain_2(8),IEEE4,False)
  Average(1,Strain_2(9),IEEE4,False)
  Average(1,Strain_2(10),IEEE4,False)
  Average(1,Strain_2(11),IEEE4,False)
  Average(1,Strain_2(12),IEEE4,False)
  Average(1,Strain_2(13),IEEE4,False)
  Average(1,Strain_2(14),IEEE4,False)
```

```
  Average(1,Strain_2(15),IEEE4,False)
  Average(1,Strain_2(16),IEEE4,False)

  Average(1,Strain_3(1),IEEE4,False)
  Average(1,Strain_3(2),IEEE4,False)
  Average(1,Strain_3(3),IEEE4,False)
  Average(1,Strain_3(4),IEEE4,False)
  Average(1,Strain_3(5),IEEE4,False)
  Average(1,Strain_3(6),IEEE4,False)
  Average(1,Strain_3(7),IEEE4,False)
  Average(1,Strain_3(8),IEEE4,False)
  Average(1,Strain_3(9),IEEE4,False)
  Average(1,Strain_3(10),IEEE4,False)
  Average(1,Strain_3(11),IEEE4,False)
  Average(1,Strain_3(12),IEEE4,False)
  Average(1,Strain_3(13),IEEE4,False)
  Average(1,Strain_3(14),IEEE4,False)
  Average(1,Strain_3(15),IEEE4,False)
  Average(1,Strain_3(16),IEEE4,False)
EndTable

'Main Program
BeginProg
  'Initialize calibration variables for
  'Quarter Bridge Strain, 3-wire 120 ohm with 4WFBS120 TIM measurement 'Vr1000()'
  CIndex=1 : CAvg=1 : CReps=16
  For LCount = 1 To 16
    GFAdj(LCount)=GFsRaw(LCount)
  Next

  'Initialize calibration variables for
  'Quarter Bridge Strain, 3-wire 120 ohm with 4WFBS120 TIM measurement 'Vr1000_2()'
  CIndex_2=1 : CAvg_2=1 : CReps_2=16
  For LCount_2 = 1 To 16
    GFAdj_2(LCount_2)=GFsRaw_2(LCount_2)
  Next

  'Initialize calibration variables for
  'Quarter Bridge Strain, 3-wire 120 ohm with 4WFBS120 TIM measurement 'Vr1000_3()'
  CIndex_3=1 : CAvg_3=1 : CReps_3=16
  For LCount_3 = 1 To 16
    GFAdj_3(LCount_3)=GFsRaw_3(LCount_3)
  Next

  Do
    While Flag(1) = false: Loop
      'Load the most recent calibration values from the CalHist table
      FCLoaded=LoadFieldCal(True)
      'Main Scan
      Scan(ScanInt,Sec,0,1)
        'Default Datalogger Battery Voltage measurement 'BattV'
        Battery(BattV)
        'Default Wiring Panel Temperature measurement 'PTemp_C'
        PanelTemp(PTemp_C,_60Hz)

        'Generic Single-Ended Voltage measurements 'VoltSE'
        'VoltSE(Dest,Reps,Range,SEChan,MeasOff,SettlingTime,Integ,Mult,Offset)
        VoltSe(SEVolt11,1,mV5000,11,True,0,_60Hz,1,0)
        VoltSe(SEVolt13,1,mV5000,13,True,0,_60Hz,1,0)
        VoltSe(SEVolt15,1,mV5000,15,True,0,_60Hz,1,0)

        'User Entered Calculations
        ScaledLoadN11 = SEVolt11*(12)*2/1000
        ScaledLoadM13 = SEVolt13*(24)*2/1000
        ScaledLoadS15 = SEVolt15*(12)*2/1000
```

```
'Turn AM16/32 Multiplexer On
PortSet(1,1)
Delay(0,150,mSec)
LCount=1
SubScan(0,uSec,16)
  'Switch to next AM16/32 Multiplexer channel
  PulsePort(8,10000)
  'Quarter Bridge Strain, 3-wire 120 ohm with 4WFBS120 TIM measurement 'Vr1000()'
  BrFull(Vr1000(LCount),1,mV7_5,1,Vx1,1,2500,True,True,0,_60Hz,1,0)
  LCount=LCount+1
NextSubScan
'Calculated strain result 'Strain()' for
'Quarter Bridge Strain, 3-wire 120 ohm with 4WFBS120 TIM measurement 'Vr1000()'
StrainCalc(Strain(),16,Vr1000(),BrZero(),-1,GFAdj(),0)
'Quarter bridge strain shunt calibration for
'Quarter Bridge Strain, 3-wire 120 ohm with 4WFBS120 TIM measurement 'Vr1000()'
FieldCalStrain(13,Strain(),1,GFAdj(),0,QBSSMode,CKnown(),CIndex,CAvg,GFsRaw(),0)
'Zeroing calibration for
'Quarter Bridge Strain, 3-wire 120 ohm with 4WFBS120 TIM measurement 'Vr1000()'
FieldCalStrain(10,Vr1000(),CReps,0,BrZero(),ZMode,0,CIndex,CAvg,0,Strain())
'Turn AM16/32 Multiplexer Off
PortSet(1,0)
Delay(0,150,mSec)

'Turn AM16/32 Multiplexer On
PortSet(2,1)
Delay(0,150,mSec)
LCount_2=1
SubScan(0,uSec,16)
  'Switch to next AM16/32 Multiplexer channel
  PulsePort(8,10000)
  'Quarter Bridge Strain, 3-wire 120 ohm with 4WFBS120 TIM measurement 'Vr1000_2()'
  BrFull(Vr1000_2(LCount_2),1,mV7_5,2,Vx1,1,2500,True,True,0,_60Hz,1,0)
  LCount_2=LCount_2+1
NextSubScan
'Calculated strain result 'Strain_2()' for
'Quarter Bridge Strain, 3-wire 120 ohm with 4WFBS120 TIM measurement 'Vr1000_2()'
StrainCalc(Strain_2(),16,Vr1000_2(),BrZero_2(),-1,GFAdj_2(),0)
'Quarter bridge strain shunt calibration for
'Quarter Bridge Strain, 3-wire 120 ohm with 4WFBS120 TIM measurement 'Vr1000_2()'
FieldCalStrain(13,Strain_2(),1,GFAdj_2(),0,QBSSMode_2,CKnown_2(),CIndex_2,CAvg_2,GFsRaw_2(),0)
'Zeroing calibration for
'Quarter Bridge Strain, 3-wire 120 ohm with 4WFBS120 TIM measurement 'Vr1000_2()'
FieldCalStrain(10,Vr1000_2(),CReps_2,0,BrZero_2(),ZMode_2,0,CIndex_2,CAvg_2,0,Strain_2())
'Turn AM16/32 Multiplexer Off
PortSet(2,0)
Delay(0,150,mSec)

'Turn AM16/32 Multiplexer On
PortSet(3,1)
Delay(0,150,mSec)
LCount_3=1
SubScan(0,uSec,16)
  'Switch to next AM16/32 Multiplexer channel
  PulsePort(8,10000)
  'Quarter Bridge Strain, 3-wire 120 ohm with 4WFBS120 TIM measurement 'Vr1000_3()'
  BrFull(Vr1000_3(LCount_3),1,mV7_5,3,Vx1,1,2500,True,True,0,_60Hz,1,0)
  LCount_3=LCount_3+1
NextSubScan
'Calculated strain result 'Strain_3()' for
'Quarter Bridge Strain, 3-wire 120 ohm with 4WFBS120 TIM measurement 'Vr1000_3()'
StrainCalc(Strain_3(),16,Vr1000_3(),BrZero_3(),-1,GFAdj_3(),0)
'Quarter bridge strain shunt calibration for
'Quarter Bridge Strain, 3-wire 120 ohm with 4WFBS120 TIM measurement 'Vr1000_3()'
FieldCalStrain(13,Strain_3(),1,GFAdj_3(),0,QBSSMode_3,CKnown_3(),CIndex_3,CAvg_3,GFsRaw_3(),0)
'Zeroing calibration for
```

```
      'Quarter Bridge Strain, 3-wire 120 ohm with 4WFBS120 TIM measurement 'Vr1000_3()'
      FieldCalStrain(10,Vr1000_3(),CReps_3,0,BrZero_3(),ZMode_3,0,CIndex_3,CAvg_3,0,Strain_3())
      'Turn AM16/32 Multiplexer Off
      PortSet(3,0)
      Delay(0,150,mSec)

      'Call Data Tables and Store Data
      CallTable(StrainTable)
    NextScan
  Loop
EndProg
```

APPENDIX D. DATA MEASURED DURING GIRDER FABRICATION

D.1 Measured Prestressing Strand Force

Two methods were considered for estimating the initial tensioning force in the prestressing strands: linear foil strain gages attached to the strand prior to tensioning and the pressure sensor on the hydraulic jack used by Cretex Concrete Products. The data collected from the linear foil strain gages were unreliable due to a high noise to signal ratio, with noise levels of approximately ±200 με. It was determined that one possible cause for the poor signal to noise ratio was a low integration time in the Campbell Scientific program. An integration constant should be selected to filter 60 Hz noise. Therefore, the initial jacking force applied to each strand was based on the pressure gage on the hydraulic jack.

The naming convention for the prestressing strands is shown in Figure D-1 as a cross-sectional view looking toward the live end of the prestressing bed. The strands were numbered from 1 to 22 starting from the bottom row and the left column. The initial prestress applied to each strand is summarized in Table D-1. These values were necessary for the measured elongation correction and were based on the applied jacking force measured by Cretex, the manufacturer provided prestressing strand area, and an assumed seating/slip loss of 6.6 ksi which could not be accounted for using the Cretex pressure gage. The seating/slip loss was calculated using the 3792 in. length of Cretex prestressing Bed 1, a manufacturer provided prestressing strand modulus of elasticity of 28,700 ksi, and assuming the following: a live end seating loss of 3/8 in. as recommended by PCI (1997) and AASHTO (2010), a dead end slip of 1/8 in., and an abutment movement of 3/8 in. The seating loss, dead end slip, and abutment movement values were those typically used by Cretex Concrete design engineers when calculating the required pressure gage and required elongation values for stressing. The total initial prestress after seating/slip loss, calculated by dividing the total prestress force of 22 strands by the total area of strand, was $0.59f_{pu}$ (158.6 ksi) for each of the five girders.

Table D-1 shows that the draped strands were stressed to approximately 16.75 kips in the field as recorded by Cretex personnel. Discussion with Cretex design engineers after fabrication indicated that this lower prestressing value was selected because the force in the strands increases when the draped strands, initially laid flat in the prestressing bed, are lifted and secured at the lift point between beams. The lift point between beams and the

hold down points at mid-length of the beams are used to create the correct drape angle in the girders.

Vibrating wire strain gages were installed at midspan in each of the four laboratory bridge girders to measure prestress losses due to elastic shortening, creep, and shrinkage. The vibrating wire gages were placed near the vertical centroid of the prestressing strands, as shown in Figure D-1. Elastic shortening losses were estimated using the change in strain measured by the embedded vibrating wire gage prior to and after transfer of the prestressing force at the centroid of the prestressing strands. It was assumed that, with adequate bond between prestressing strand and concrete, the change in concrete strain recorded by the VWG was equivalent to the change in strain of the prestressing strand.

The apparent VWG strain readings were converted to mechanical strain values using the following equation:

$$\varepsilon_M = (G_1 - G_0)B + (T_1 - T_0)\,(CF_s - CF_c) \tag{C.1}$$

where ε_M is the mechanical strain, G_1 is the VWG strain reading at any time after the initial reading, G_0 is the initial VWG strain reading, B is the batch factor, T_1 is the VWG thermistor temperature at any time after the initial reading, T_0 is the initial VWG thermistor temperature reading, CR_s is the thermal coefficient of expansion of steel (assumed to be 12.2 με/°C), CR_c is the thermal coefficient of expansion of concrete (assumed to be 10.4 με/°C). The mechanical strain values were converted to stress using the manufacturer provided prestressing strand modulus of elasticity of 28,700 ksi. Batch factors of 0.97 for Girder 1 and 0.98 for Girders 2, 3, and 4 were used in the calculations. The values used to calculate the elastic shortening loss are given in Table D-2.

Two methods were used to reproduce the measured VWG strain in the concrete at the level of the strand centroid as shown in the design calculations. The effective prestress force, P_i, required was determined assuming net sections, a neutral axis location at the centroid of the net section, and a concrete modulus of elasticity of 3,879 ksi based on $33w_c^{1.5}\sqrt{f'_{ci}}$, where the unit weight concrete was recorded as 144.6 pcf and an average f'_{ci} was 4,571 psi. Furthermore, the required jacking prestress force, P_{jreqd}, after accounting for anchorage losses, was calculated based on transformed sections and a neutral axis location

at the centroid of the transformed section. Both methods produced the same result and are discussed in depth by Al-Omaishi et al. (2009).

Table D-3 summarizes measured long-term losses, specifically creep and shrinkage, using the vibrating wire gages. Six time steps for calculation of prestress losses were included. The first time step, from strand tensioning to release, includes only prestressing strand relaxation which cannot be measured by the VWGs. The remaining time steps included the following: (2) release to single beam deck placement, (3) single beam deck placement to single beam testing, (4) single beam testing to bridge deck placement, (5) bridge deck placement to elastic testing, and (6) elastic testing to inelastic testing.

Steel relaxation could not be measured by the VWGs installed at midspan of the beams and had to be estimated using a time-step method. Results were calculated using the methods outlined by the PCI committee (Preston 1975) at six time steps: (1) strand tensioning to release, (2) release to single beam deck placement, (3) single beam deck placement to single beam testing, (4) single beam testing to bridge deck placement, (5) bridge deck placement to elastic testing, and (6) elastic testing to inelastic testing. Steel relaxation losses were calculated based on the prestressing force applied to the strands as measured by Cretex. Table D-4 highlights the relaxation losses at each time step for the bridge girders.

D.2 Measured Girder Camber

The five girders were cast on June 27, 2013 at Cretex Concrete Products in Elk River, MN. On June 29, 2013 the formwork was removed after the concrete reached the required concrete compressive strength for release. The first camber measurements, shown in Table D-5, were taken immediately following release of the strands at midspan of each beam. An additional set of camber measurements were taken on July 3, 2013 prior to moving and bunking the beams in the Cretex Concrete storage yard. No more camber measurements were taken after this time. Camber data was not used to predict the prestress levels at transfer due to potential error when recording small magnitude camber measurements resulting from the low prestress levels and short beam lengths.

Table D-1. Strand Stress and Force after Seating and Slip

Strand Number	Cretex Jacking Force (k)	Equivalent Draped Force (k)	Prestress After Seating (ksi)	Force After Seating (k)
1	25.25	----	158.6	24.2
2	25.25	----	158.6	24.2
3	25.25	----	158.6	24.2
4	25.25	----	158.6	24.2
5	25.25	----	158.6	24.2
6	25.25	----	158.6	24.2
7	25.25	----	158.6	24.2
8	25.25	----	158.6	24.2
9	25.25	----	158.6	24.2
10	25.25	----	158.6	24.2
11	25.25	----	158.6	24.2
12	25.25	----	158.6	24.2
13	25.25	----	158.6	24.2
14	25.25	----	158.6	24.2
15	25.25	----	158.6	24.2
16	25.25	----	158.6	24.2
17	16.75	25.25	158.6	24.2
18	16.75	25.25	158.6	24.2
19	16.75	25.25	158.6	24.2
20	16.75	25.25	158.6	24.2
21	16.75	25.25	158.6	24.2
22	16.75	25.25	158.6	24.2
			Total Strand Sum:	533.2

Table D-2. VWG Elastic Shortening Data

		Raw Strain	T (°C)	ε_M (με)	σ_M (ksi)
Girder 1					
Pre-release*	6/29/13 11:50 AM	3490.8	30.8	-71.0	-2.0
Post-release	6/29/13 12:25 PM	2905.1	30.7	-639.1	-18.3
Difference between post- and pre-release:				-568.1	-16.3
Girder 2					
Pre-release*	6/29/13 11:50 AM	3588.7	33.1	-99.7	-2.9
Post-release	6/29/13 12:25 PM	2996.7	32.8	-679.8	-19.5
Difference between post- and pre-release:				-580.2	-16.7
Girder 3					
Pre-release*	6/29/13 11:50 AM	3606.6	32.4	-337.2	-9.7
Post-release	6/29/13 12:25 PM	3038.5	32.3	-894.0	-25.7
Difference between post- and pre-release:				-556.7	-16.0
Girder 4					
Pre-release*	6/29/13 11:50 AM	3159.2	32.7	-170.7	-4.9
Post-release	6/29/13 12:25 PM	2602.2	32.5	-716.6	-20.6
Difference between post- and pre-release:				-545.9	-15.7

* Pre-release data represent a zero reading and the differences represent a change in strain due to elastic shortening

Table D-3. VWG Long-Term Losses after Elastic Shortening

Time Step	Event	Date	Raw Strain	T (°C)	ε_M (με)	σ_M (ksi)	Time Step Diff. (ksi)
Girder 1							
1	Post-release	6/29/2013	2905.1	30.7	-639.1	-18.3	----
2	Single beam deck	11/5/2013	2219.3	4.5	-1304.4	-37.4	-19.1
3	Single beam test	1/28/2014	2104.7	18.6	-1415.5	-40.6	-3.2
----	Pre-bridge deck	3/5/2014	2038.3	18.1	-1479.9	-42.5	----
4	Post-bridge deck	3/5/2014	2081.8	16.5	-1437.7	-41.3	-0.6
				Bridge deck prestress gains:	42.2	1.2	----
5	Elastic Testing	5/8/2014	2051.5	20.5	-1467.1	-42.1	-0.8
6	Inelastic Testing	12/8/2014	1997.6	17.0	-1519.4	-43.6	-1.5
				Long-term losses after release:	-880.3	-25.3	----
Girder 2							
1	Post-release	6/29/2013	2996.7	32.8	-679.8	-19.5	----
2	Single beam deck	11/5/2013	2321.7	5.1	-1341.3	-38.5	-19.0
3	Single beam test	1/28/2014	2238.7	18.5	-1422.7	-40.8	-2.3
----	Pre-bridge deck	3/5/2014	2167.3	17.9	-1492.6	-42.8	----
4	Post-bridge deck	3/5/2014	2212.3	16.3	-1448.5	-41.6	-0.7
				Bridge deck prestress gains:	44.1	1.3	----
5	Elastic Testing	5/8/2014	2180.2	20.5	-1480.0	-42.5	-0.9
6	Inelastic Testing	12/8/2014	2131.9	16.7	-1527.3	-43.8	-1.4
				Long-term losses after release:	-847.5	-24.3	----
Girder 3							
1	Post-release	6/29/2013	3038.5	32.3	-894.0	-25.7	----
2	Single beam deck	11/5/2013	2331.8	4.8	-1586.5	-45.5	-19.9
3	Single beam test	1/28/2014	2238.5	18.8	-1678.0	-48.2	-2.6
----	Pre-bridge deck	3/5/2014	2169.5	18.1	-1745.6	-50.1	----
4	Post-bridge deck	3/5/2014	2214.9	16.3	-1701.1	-48.8	-0.7
				Bridge deck prestress gains:	44.5	1.3	----
5	Elastic Testing	5/8/2014	2183.4	20.9	-1732.0	-49.7	-0.9
6	Inelastic Testing	12/8/2014	2136.9	16.9	-1777.5	-51.0	-1.3
				Long-term losses after release:	-883.6	-25.4	----
Girder 4							
1	Post-release	6/29/2013	2602.2	32.5	-716.6	-20.6	----
2	Single beam deck	11/5/2013	1926.8	4.9	-1378.5	-39.6	-19.0
3	Single beam test	1/28/2014	1827.7	18.8	-1475.6	-42.3	-2.8
----	Pre-bridge deck	3/5/2014	1758.4	18.1	-1543.5	-44.3	----
4	Post-bridge deck	3/5/2014	1802.2	16	-1500.6	-43.1	-0.7
				Bridge deck prestress gains:	42.9	1.2	----
5	Elastic Testing	5/8/2014	1750.4	20.9	-1551.3	-44.5	-1.5
6	Inelastic Testing	12/8/2014	1672.6	17.0	-1627.6	-46.7	-2.2
				Long-term losses after release:	-911.0	-26.1	----

Table D-4. PCI Committee Method Steel Relaxation Losses

Time Step	RE Loss (ksi)
(1) Tensioning to release	0.72
(2) Release to single beam deck	0.24
(3) Single beam deck to test single beam	0.03
(4) Test single beam to bridge deck	0.01
(5) Bridge deck to elastic testing	0.01
(6) Elastic testing to inelastic testing	0.03
Sum:	1.04

Table D-5. Girder Camber Measurements (in.)

Girder No.	1	2	3	4	5
6/29/13 1:06 PM	15/32	1/4	1/8	1/4	1/4
7/3/13 8:14 AM	5/8	3/8	3/8	15/32	1/2

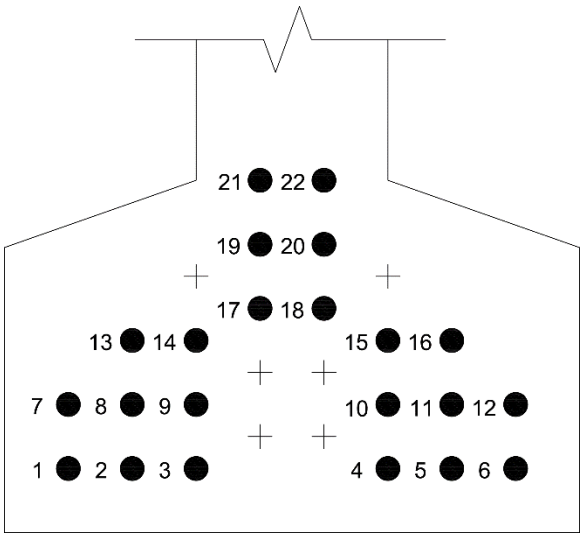

Figure D-1. Prestressing Strand Numbering Looking Toward Live End

APPENDIX E. DATA FROM LABORATORY EXPERIMENTS

Appendix E includes data from tests of the laboratory bridge in both the elastic and inelastic ranges. Section E.1 includes detailed elastic loading histories for tests completed in the southeast quadrant (no barrier, no end diaphragm), the northeast quadrant (barrier, no end diaphragm), the northwest quadrant (barrier, end diaphragm), and the southwest quadrant (no barrier, end diaphragm). Section E.2 contains rotation data collected during inelastic testing of both ends of the laboratory bridge. Section E.3 contains bearing pad vertical displacement data collected during inelastic testing of both ends of the laboratory bridge. Section E.4 contains results from the neoprene bearing pad material property study conducted to understand the bearing pad vertical displacement data. Section E.5 contains stirrup yielding data collected during inelastic testing of both ends of the laboratory bridge.

E.1 Detailed Elastic Loading Histories

This section contains the detailed loading histories for the force-controlled testing conducted in each of the four bridge quadrants:

Lab Bridge Elastic South East (LBESE) – no barrier; no end diaphragm

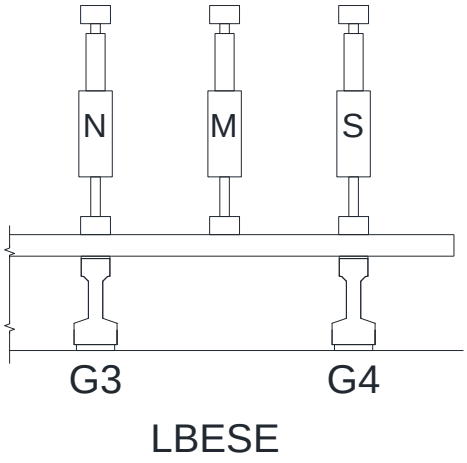

LBESE

Test Date	Test Nomenclature	Test Description and Notes
5/8/2014	----	Many tests were run between 5/8/14 and 8/1/14 to solve issues related to elastic load steps, load and unload rates, torsional effects, and malfunctioning instrumentation.
8/1/2014	LBESE_4d_M(HSS5)	Rerun test Middle actuator at $4d_v$ to 50k, 75k after adding HSS tube at 4d and SP at BP, 4d
8/21/2014	LBESE_4d_M(HSS7)	Rerun test Middle actuator at $4d_v$ to 50k, 75k after adding HSS tube below BF at 4d and SP at BP, 4d
8/25/2014	LBESE_4d_M	Initial test Middle actuator at $4d_v$ to 50k, 75k. Foil rosettes opposite VWGs, no HSS tube, and SP at BP, 4d for remainder of tests
8/26/2014	LBESE_4d_S	Initial test South actuator at $4d_v$ to 50k, 75k
8/26/2014	LBESE_4d_N	Initial test North actuator at $4d_v$ to 50k, 75k
8/26/2014	LBESE_4d_NM	Initial test North & Middle Actuator at $4d_v$ to 50k, 75k
8/26/2014	LBESE_4d_SM	Initial test South & Middle Actuator at $4d_v$ to 50k, 75k
8/26/2014	LBESE_4d_SMN	Initial test South, Middle, and North Actuators at $4d_v$ to 50k
8/26/2014	LBESE_2d_M	Initial test Middle actuator at $2d_v$ to 50k, 75k
8/27/2014	LBESE_2d_S	Initial test South actuator at $2d_v$ to 50k, 75k
8/27/2014	LBESE_2d_N	Initial test North actuator at $2d_v$ to 50k, 75k
8/27/2014	LBESE_2d_NM	Initial test North & Middle Actuator at $2d_v$ to 50k, 75k
8/27/2014	LBESE_2d_SM	Initial test South & Middle Actuator at $2d_v$ to 50k, 75k
8/27/2014	LBESE_2d_SMN	Initial test South, Middle, and North Actuators at $2d_v$ to 50k

Lab Bridge Elastic North East (LBENE) – barrier; no end diaphragm

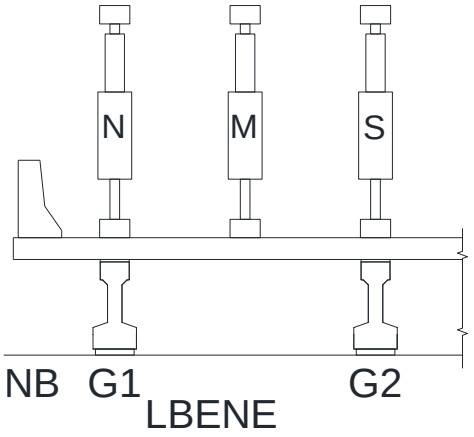

Test Date	Test Nomenclature	Test Description and Notes
9/9/2014	LBENE_4d_M	Second test Middle actuator at $4d_v$ to 50k, 75k
9/9/2014	LBENE_4d_S	Second test South actuator at $4d_v$ to 50k, 75k
9/10/2014	LBENE_4d_N	Initial test North actuator at $4d_v$ to 50k, 75k
9/10/2014	LBENE_4d_NM	Initial test North & Middle actuator at $4d_v$ to 50k, 75k
9/10/2014	LBENE_4d_SM	Initial test South & Middle actuator at $4d_v$ to 50k, 75k
9/10/2014	LBENE_4d_SMN(2)	Second test South & Middle & North actuator at $4d_v$ to 50k
9/10/2014	LBENE_2d_M	Initial test Middle actuator at $2d_v$ to 50k, 75k
9/10/2014	LBENE_2d_S	Initial test South actuator at $2d_v$ to 50k, 75k
9/10/2014	LBENE_2d_N	Initial test North actuator at $2d_v$ to 50k, 75k
9/11/2014	LBENE_2d_NM	Initial test North & Middle actuator at $2d_v$ to 50k, 75k
9/11/2014	LBENE_2d_SM	Initial test South & Middle actuator at $2d_v$ to 50k, 75k
9/11/2014	LBENE_2d_SMN	Initial test South & Middle & North actuator at $2d_v$ to 50k

Lab Bridge Elastic North West (LBENW) – barrier; end diaphragm

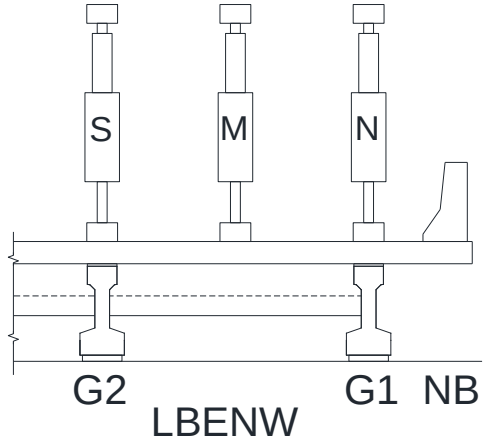

Test Date	Test Nomenclature	Test Description and Notes
10/14/2014	LBENW_2d_M	Second test Middle actuator at $2d_v$ to 50k, 75k
10/14/2014	LBENW_2d_S	Second test South actuator at $2d_v$ to 50k, 75k
10/14/2014	LBENW_2d_N	Second test North actuator at $2d_v$ to 50k, 75k
10/14/2014	LBENW_2d_NM	Second test North & Middle actuator at $2d_v$ to 50k, 75k
10/14/2014	LBENW_2d_SM	Second test South & Middle actuator at $2d_v$ to 50k, 75k
10/14/2014	LBENW_2d_SMN	Second test South & Middle & North actuator at $2d_v$ to 50k
10/15/2014	LBENW_4d_M	Second test Middle actuator at $4d_v$ to 50k, 75k
10/15/2014	LBENW_4d_S	Second test South actuator at $4d_v$ to 50k, 75k
10/15/2014	LBENW_4d_N	Second test North actuator at $4d_v$ to 50k, 75k
10/15/2014	LBENW_4d_NM	Second test North & Middle actuator at $4d_v$ to 50k, 75k
10/15/2014	LBENW_4d_SM	Second test South & Middle actuator at $4d_v$ to 50k, 75k
10/15/2014	LBENW_4d_SMN	Second test South & Middle & North actuator at $4d_v$ to 50k
10/23/2014	LBENW_4d_M(bar)	Third test Middle actuator at $4d_v$ to 50k, 75k, barrier VWG instrumentation modified
10/23/2014	LBENW_4d_N(bar)	Third test North actuator at $4d_v$ to 50k, 75k, barrier VWG instrumentation modified
10/23/2014	LBENW_4d_NM(bar)	Third test North & Middle actuator at $4d_v$ to 50k, 75k, barrier VWG instrumentation modified
10/23/2014	LBENW_4d_SMN(bar)	Third test South & Middle & North actuator at $4d_v$ to 50k, barrier VWG instrumentation modified

Lab Bridge Elastic South West (LBESW) – no barrier; end diaphragm

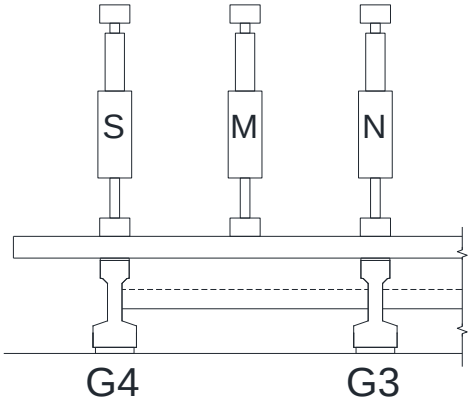

LBESW

Test Date	Test Nomenclature	Test Description and Notes
11/4/2014	LBESW_4d_S	Initial test South actuator at $4d_v$ to 50k, 75k, barrier instrumentation removed for all tests, 1.0dOG4 VWG missing
11/4/2014	LBESW_4d_N	Initial test North actuator at $4d_v$ to 50k, 75k, 1.0dOG4 VWG missing
11/4/2014	LBESW_4d_NM	Initial test North & Middle actuator at $4d_v$ to 50k, 75k, 1.0dOG4 VWG missing
11/4/2014	LBESW_4d_SM	Initial test South & Middle actuator at $4d_v$ to 50k, 75k, 1.0dOG4 VWG missing
11/4/2014	LBESW_4d_SMN	Initial test South & Middle & North actuator at $4d_v$ to 50k, 1.0dOG4 VWG missing
11/5/2014	LBESW_2d_M	Initial test Middle actuator at $2d_v$ to 50k, 75k
11/5/2014	LBESW_2d_N	Initial test North actuator at $2d_v$ to 50k, 75k
11/5/2014	LBESW_2d_NM	Initial test North & Middle actuator at $2d_v$ to 50k, 75k
11/5/2014	LBESW_2d_SM	Initial test South & Middle actuator at $2d_v$ to 50k, 75k
11/5/2014	LBESW_2d_SMN	Initial test South & Middle & North actuator at $2d_v$ to 50k
11/6/2014	LBESW_2d_S(2)	Second test South actuator at $2d_v$ to 50k, 75k
11/10/2014	LBESW_4d_M(2)	Second test Middle actuator at $4d_v$ to 50k, 75k

E.2 Girder Rotation during Inelastic Testing

A tiltmeter was placed at the west end of each girder during LBUW testing and at the east end of each girder during LBUE testing to record the rotation. Figure E-1 and Figure E-2 show that Girder 3 (LBUW) and Girder 2 (LBUE) had the most end rotation, while adjacent girders also experienced rotation that caused downward deflection as the load increased. The tiltmeter exceeded the maximum working range in Girder 3 during LBUW and on Girder 2 during LBUE. No useful data were recorded after the beam rotated approximately 0.5 degrees and caused downward deflection. During both LBUW and LBUE, the end rotation of the girder farthest from the loaded beam were near zero and indicated that the rotation caused slight upward deflection during testing.

E.3 Bearing Pad Vertical Displacement during Inelastic Testing

Four LVDTs per bearing pad at the loaded end of the bridge were used to collect bearing pad displacement data during LBUW and LBUE testing. An LVDT was placed at each corner of the bearing pad to collect data assuming the bearing pad would not uniformly displace downward as load was applied. Figure E-3 and Figure E-4 show bearing pad behavior during LBUW testing of the loaded beam (G3) and the exterior adjacent beam (G4), respectively. The loaded beam deflected in the same manner transversely (i.e., all four corners deflected downward, which is positive in Figure E-3), but the corners of the bearing longitudinally nearest the applied load deflected more than those furthest from the applied load. Bearing pads supporting beams adjacent to the loaded girder deflected approximately the same longitudinally but, transversely, the side of the bearing pad nearest the loaded girder deflected more than the side furthest from the loaded girder. The BP_Avg and BP_PlaneAvg data shown in Figure E-3 and Figure E-4 is discussed in the following paragraph.

Figure E-5 and Figure E-6 show the averaged LVDT data from each of the four transducers on each of the four girders for LBUW and LBUE, respectively. The data indicated that the loaded girder during both LBUW (Girder 3) and LBUE (Girder 2) had the most bearing pad displacement while the adjacent interior and exterior girder displaced approximately the same magnitude during loading. During both LBUW and LBUE testing, data from the exterior girder furthest from the loaded beam indicated that the bearing pad experienced slight decompression during testing. During LBUW testing, the bearing pad LVDT on the southeast corner of Girder 2 was not securely attached throughout the testing process, so its readings were not indicative of the bearing pad displacement at that point. Figure E-5 shows the average data for each of the girders that had working LVDTs (labeled BP_Avg), but data for the southeast corner of Girder 2 was reproduced using the results of just three LVDTs assuming the bearing pad remained planar during deformation. The validity of this assumption was determined by examining the behavior of the bearing pads under G3 and G4 to determine if the average displacement could be accurately predicted by using only three of the four LVDTs attached to the bearing pad. Figure E-3 and Figure E-4 show bearing pad behavior of the loaded beam (G3) and the exterior adjacent beam (G4), including two averaged data sets: the average of data from all four working LVDTs

(labeled BP_Avg), and an average of data that included three of the LVDTs and a fourth data point for the corner without an LVDT calculated assuming a rigid plane connected all four corners of the bearing pad (labeled BP_PlaneAvg). The data indicate a good match between the two averages and confidence for predicting the G2 bearing pad displacement using the three working LVDTs.

The distribution of girder reactions throughout the LBUW testing program provided insight regarding how the shear forces were distributed to the supports at ultimate strength. Applied pressure (or stress) versus displacement data from testing the 2.5 in. thick neoprene bearing pad discussed in Section E.4 was used to estimate the girder reactions using bearing pad LVDT displacement data. Data from the pressure versus displacement curve in Section E.4 was collected from zero initial applied load, but the bridge bearing pads were precompressed prior to load testing by the dead load due to the self-weight of each girder, a tributary width of bridge deck, and a tributary width of end diaphragm on the west side of the bridge. Steps used to estimate the girder reactions included:

1. The dead load precompression was equal to a reaction of 26.7 kips on the west end of the bridge assuming a unit weight of concrete equal to 150 pcf.
2. The dead load reaction was divided by the area of the 160 $in.^2$ bearing pad to obtain a dead load stress of 0.16 or 0.17 ksi in the pad for the exterior or interior girder, respectively.
3. Data from pressure versus displacement curves in Section E.4 indicated the dead load stress was equivalent to a displacement of 0.020 or 0.021 in. downward for the exterior or interior girder, respectively.
4. The equivalent dead load displacement value was added to the average LVDT displacement data from each step of live loading to obtain the total bearing pad displacement.
5. The total bearing pad displacement was converted to a dead load plus live load pressure using data from Section E.4.
6. The reaction due to live load only was obtained by converting the dead load plus live load pressure to a force using the bearing pad area and subtracting the dead load reaction due to the girder, deck, and end diaphragm self-weight.

Figure E-7 shows the total applied load versus the calculated girder reactions due to live load. The reaction due to self-weight was removed. The sum of all four girder reactions were also compared to the west reaction from a 2D beam-line analysis of the bridge with an applied point load. Converting the averaged bearing pad displacement data from four LVDTs to a girder reaction did not yield the expected results. The sum of the four calculated reactions did not align with the anticipated reaction data calculated using beam line statics.

The distribution of girder reactions throughout the LBUE testing program were generated in the same manner as LBUW data. The dead load precompression was equal to a reaction of 22.8 kips on the east end of the bridge (with no end diaphragm). The dead load reaction was divided by the area of the 160 $in.^2$ bearing pad to obtain a dead load stress of 0.13 or 0.14 ksi for the exterior or interior girder, respectively. Data from pressure versus displacement curves in Section E.4 indicated the dead load stress was equivalent to a displacement of 0.018 or 0.019 in. downward for the exterior or interior girder, respectively. Figure E-8 shows the total applied load versus the calculated girder reactions for LBUE. The sum of all four girder reactions were compared to the east reaction from a 2D beam-line analysis of the bridge. Similar to the reaction data from LBUW testing, converting the averaged bearing pad displacement data from four LVDTs to a girder reaction did not yield the expected results. There are three potential reasons that the calculated reaction data did not align with the data from statics.

First, the stress versus displacement curve from the neoprene bearing pad material property study described in Section E.4 was generated with pure compression applied to the bearing pads. Very little bending was induced during the sample bearing pad tests and uniform compression was achieved. However, uniform compression from an axial load was likely never present in the laboratory bridge. The patch live load was applied directly above Girder 3, and the bearing pad subjected to a larger reaction force compressed more along the transverse edge closest to the point load when compared to the transverse edge furthest from the point load. This type of bearing pad displacement profile was representative of the curvature profile in Girder 3. Beams adjacent to Girder 3 experienced more compression on both the transverse edge closest to the point load and the longitudinal edge closest to Girder 3. These displacement profiles in the bearing pads were not

uniformly downward and a different correlation between stress and displacement may exist.

Second, data from the neoprene bearing pad material property study assumed that the entire bottom face of a bearing pad was always in contact with the bottom support surface. This was the case in the 200 kip capacity MTS testing frame when using the swivel supported steel plates. However, during inelastic live loading of the laboratory bridge, the entire bottom surface of the bearing pad may not have stayed in contact with the concrete abutment. Average LVDT data indicated that some of the girder bearing pads (or specific corners of bearing pads) experienced reduced compression (i.e., lost some of the dead load compression) during testing. These effects would negate the assumption that applied stress and reactions are related by the entire bearing pad cross sectional area, but the stress and reactions would be related by a dynamic bearing pad area that was non-rectangular and changed over the course of testing.

Third, interaction between the girder, bearing pad, and concrete abutment was more complex than pure compression due to an applied live load. As more curvature was induced in the loaded girder, and to a lesser extent in the adjacent girders, the bearing pads also experienced a horizontal shear force as shown in Figure E-9. This complex behavior was not present in the neoprene bearing pad material property study discussed in Section E.4 because the 200 kip capacity MTS testing frame was not able to apply simultaneous compression and horizontal shear forces.

The discussions above outline potential reasons that the calculated girder reactions did not align with predicted values.

E.4 Neoprene Bearing Pad Material Property Study

Three bearing pad samples of different thickness were tested to determine the relationship between the applied load and the displacement. The test was completed in the 200 kip capacity MTS testing frame using the test setup shown in Figure E-10. Load was monitored using the CE DAQ and an average bearing pad displacement was calculated from data recorded by four DC powered displacement transducers (DCDTs) as shown in Figure E-10. The DCDTs were mounted to each corner of the top steel plate. The plunger rested on the bottom steel plate and contracted as the bearing pad was compressed. Each of the three samples were cut from a larger bearing pad to fit in the 200 kip MTS testing frame. Each sample was square and had an approximate side length of 8 in. The bearing pad height and width were measured at three different locations. The bearing pad thickness was measured at three locations along each of the four sides to obtain average data as shown in Table E-1.

Each bearing pad specimen was tested three times with different loading rates. Two tests were done in accordance with ASTM D4014 (2012) which specified loading increments of one-fifth of the design load of the bearing pad. In this test setup, the design load for the bearing pads was 200 kips which was limited by the capacity of the MTS test frame. Therefore, a maximum load of 200 kips was achieved after load was applied in increments of 40 kips; after each 40 kip increment, the applied load was sustained for 30 seconds. The initial test was completed with a load rate of 40 kips per 1.4 minutes (28.6 kips/min) and the second test was completed with a load rate of 40 kips per 2.6 minutes (15.4 kips/min). Completing the load increments in 1.4 minutes and 2.6 minutes was in accordance with the lower and upper bounds specified by ASTM D4014 (2012). The third test was completed using the same five load steps and corresponding increments of 40 kips, but each load increment was applied over 20 minutes for a loading rate of 40 kips per 20 minutes (2 kips/min). The slower rate was comparable to the anticipated loading rate for testing of the laboratory bridge. Photographs of specimen bulging, load versus displacement results, and pressure versus displacement results for each of the three specimens are shown in Figure E-11 through Figure E-19.

E.5 Stirrup Yielding during Inelastic Testing

Figure 5-13 and Figure 5-19 showed that 12 of the 15 stirrup strain gages within the shear span exceeded the predicted yield strain for LBUW and that 8 of the 15 stirrup strain gages within the shear span exceeded the predicted yield strain for LBUE, respectively. The predicted yield strain, ε_y, of 0.0024 was calculated based on the measured stirrup yield strain as provided in Table 4-12. Figure E-20 through Figure E-23 show the shear at the reaction (applied shear) versus stirrup strain for stirrups J, I, H, and G during LBUW testing. Figure E-24 through Figure E-27 show the shear at the reaction (applied shear) versus stirrup strain for stirrups A, B, C, and D during LBUE testing. Data in each figure indicated the onset of yielding from most of the strain gages on these eight stirrups. Figure E-25 shows that the middle (M) strain gage on stirrup B did not record data during LBUE and was likely damaged during girder or bridge construction.

For both LBUW and LBUE, the strain gages indicated near zero tensile strain in the stirrups prior to observation of web-shear cracking. Immediately after web-shear cracking, the stirrups continued to exhibit elastic behavior and did not reach the yield strain. All strain gages on stirrups I and H yielded prior to the peak applied shear during LBUW and all strain gages on stirrups A, B, C, and D yielded prior to the peak applied shear during LBUE. However, the strain gages on stirrups J and G yielded after the peak load was applied to the girder during LBUW and the bottom strain gage on stirrup C yielded after the peak load was applied to the girder during LBUE. No stirrups in girders adjacent to Girder 3 for LBUW and Girder 2 for LBUE yielded and the stirrups in adjacent beams exhibited linear elastic behavior during LBUW and LBUE.

Table E-1. Measured Bearing Pad Dimensions and Properties

Bearing Pad Property	Nominal Thickness		
	1-3/8 in.	2-1/2 in.	4-3/8 n.
Average Measured Thickness (in.)	1.354	2.563	4.375
Average Width (in.)	8.000	8.042	8.042
Average Height (in.)	8.063	7.979	7.938
Weight (lb)	7.050	13.372	23.502
Density ($lb/in.^3$)	0.0807	0.0813	0.0842
No. of cover rubber layers	2	2	2
Thickness of cover rubber (in.)	0.3125	0.25	0.25
No. of interior rubber layers	1	3	6
Thickness of interior rubber layers (in.)	0.4375	0.5	0.5
No. of interior steel layers	2	4	7
Thickness of interior steel plates (in.)	0.125	0.125	0.125

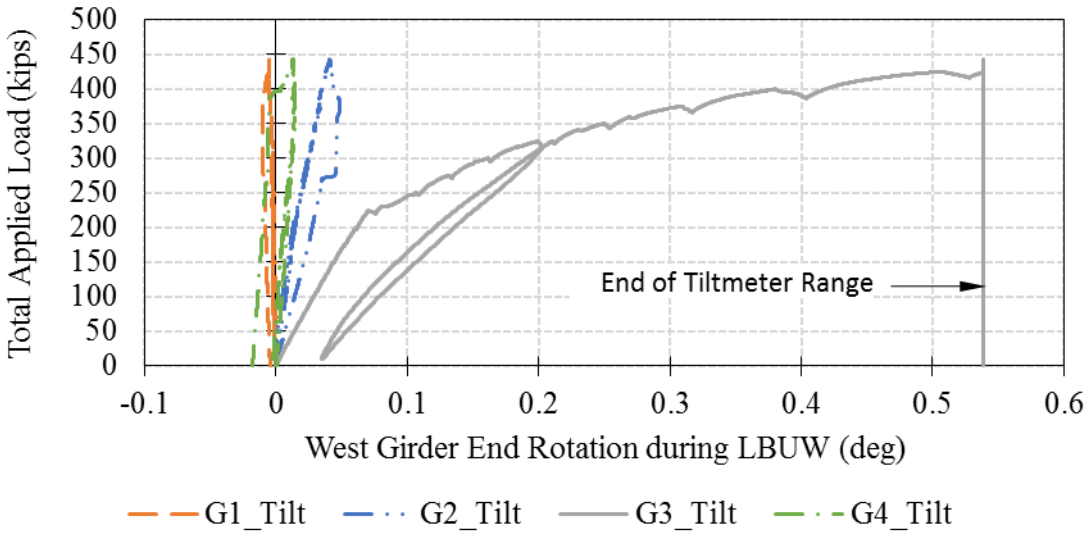

Figure E-1. End Rotation of Girders during LBUW

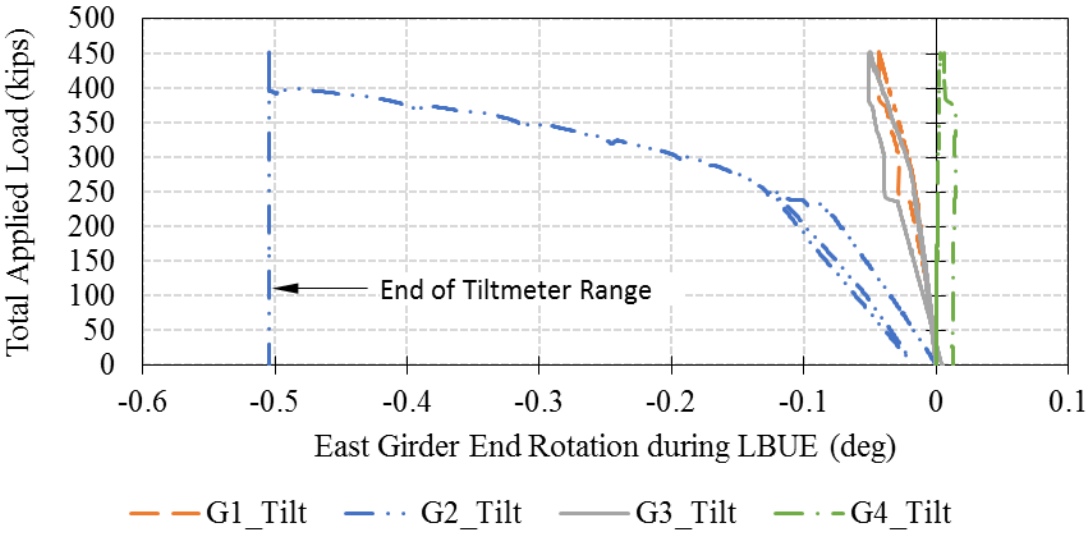

Figure E-2. End Rotation of Girders during LBUE

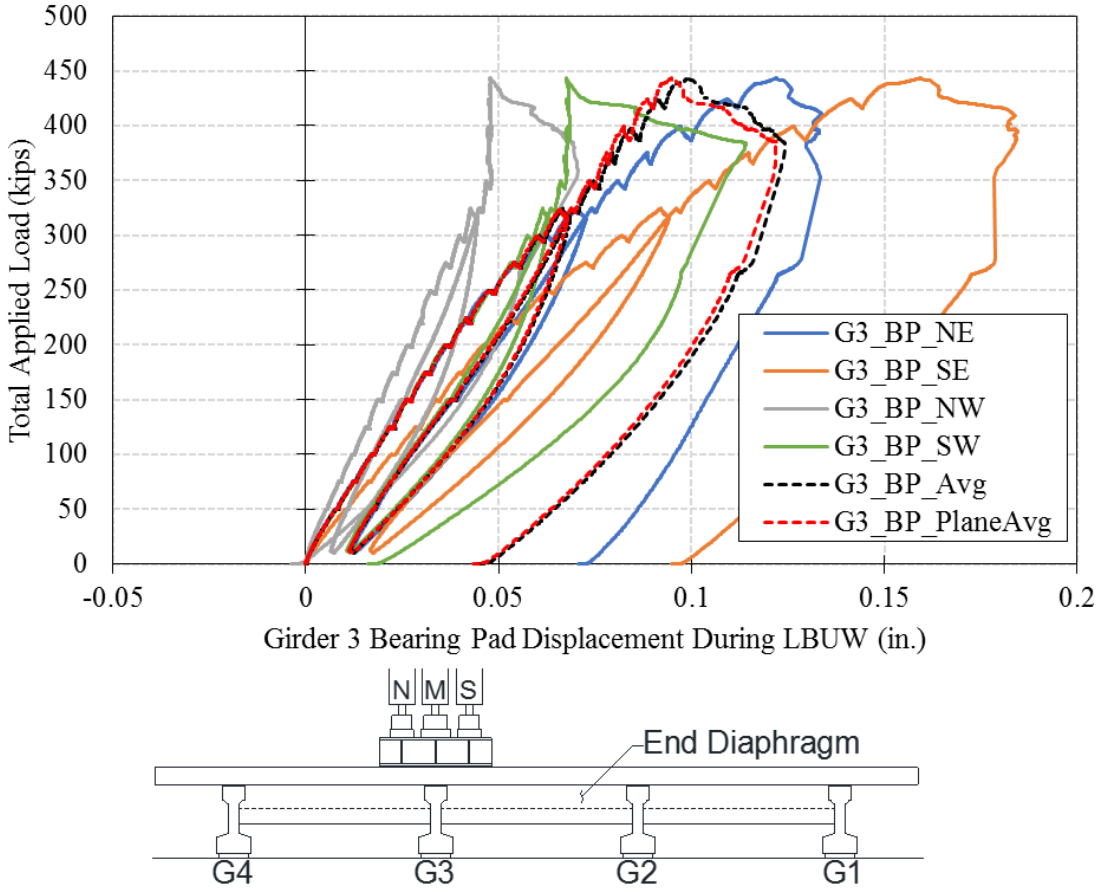

Figure E-3. Girder 3 Bearing Pad Displacement during LBUW

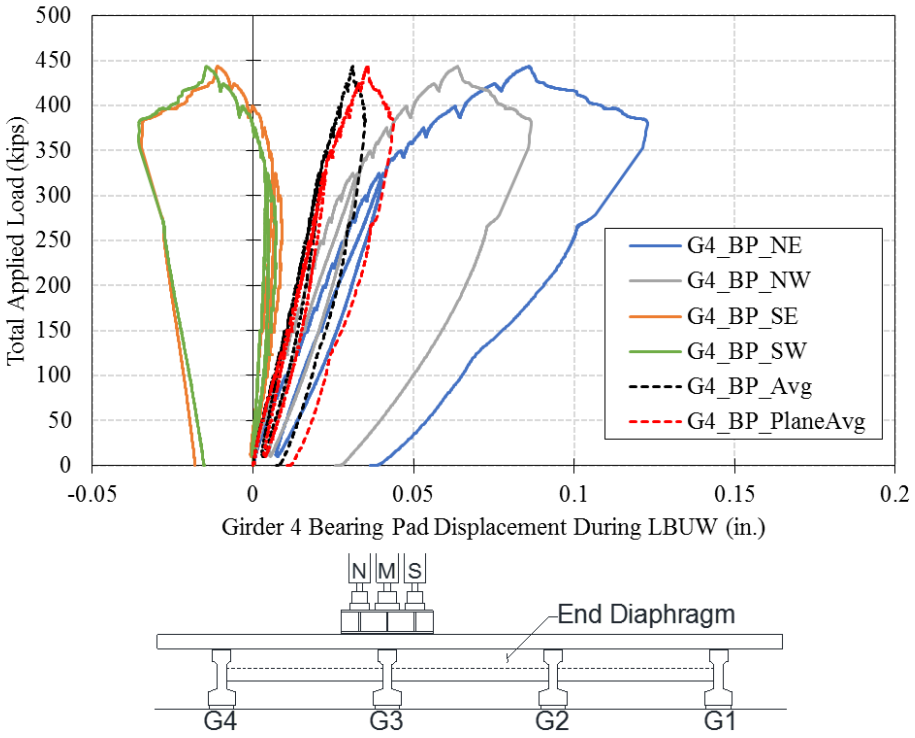

Figure E-4. Girder 4 Bearing Pad Displacement during LBUW

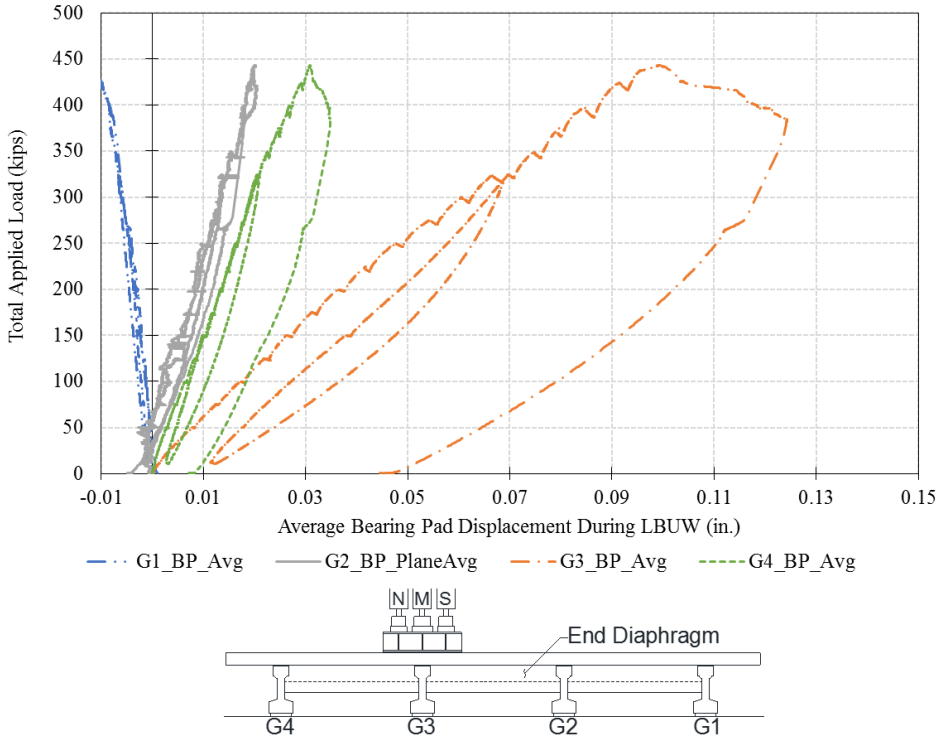

Figure E-5. Average Bearing Pad Displacements during LBUW

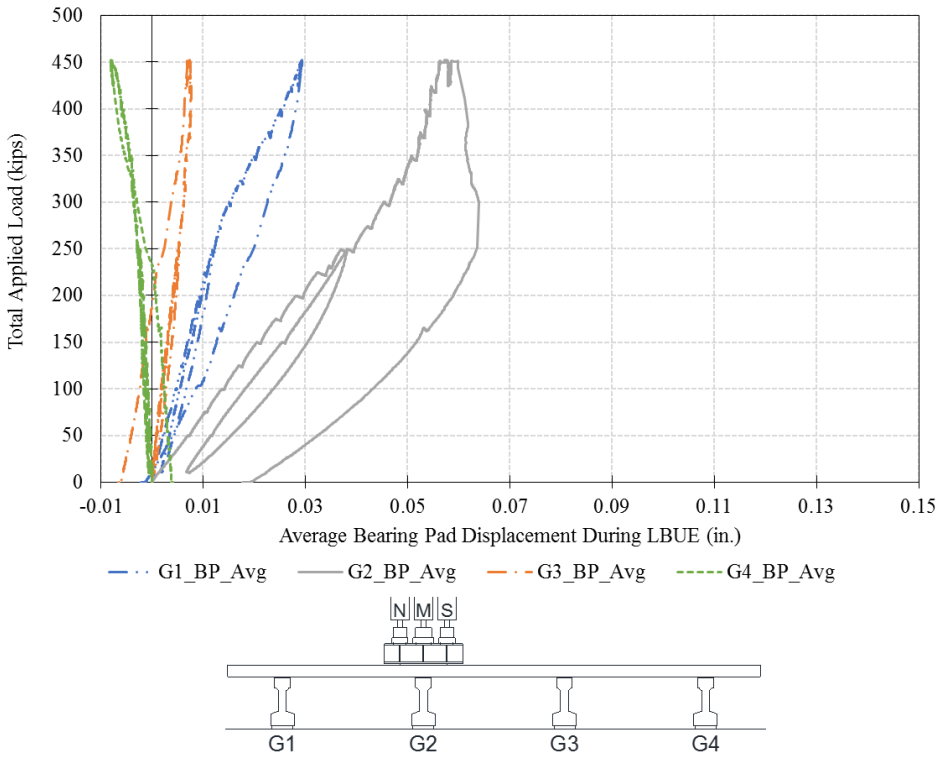

Figure E-6. Average Bearing Pad Displacements during LBUE

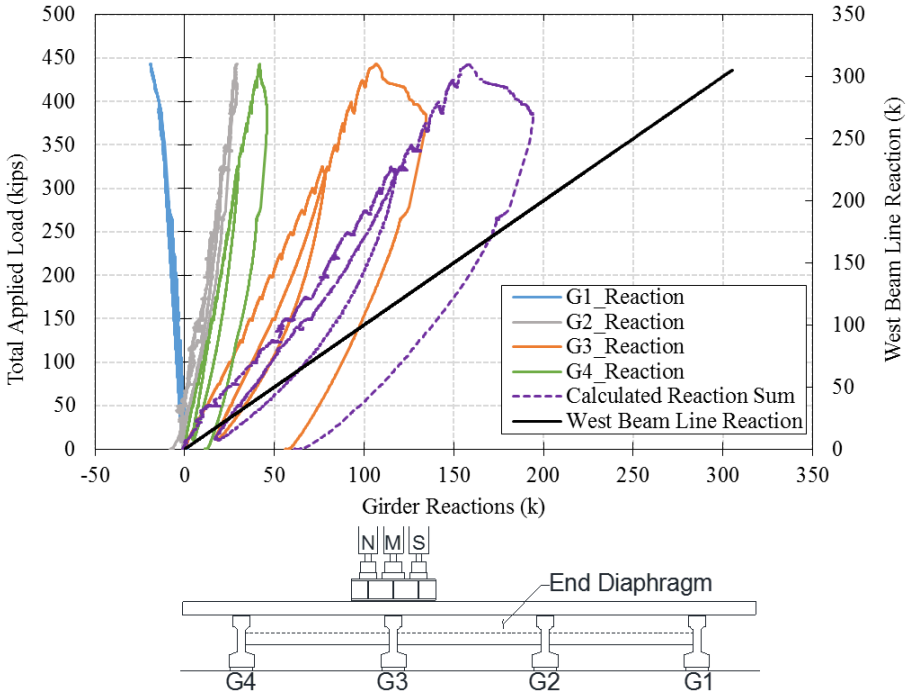

Figure E-7. Girder Reactions Estimated with Bearing Pad LVDT Data for LBUW

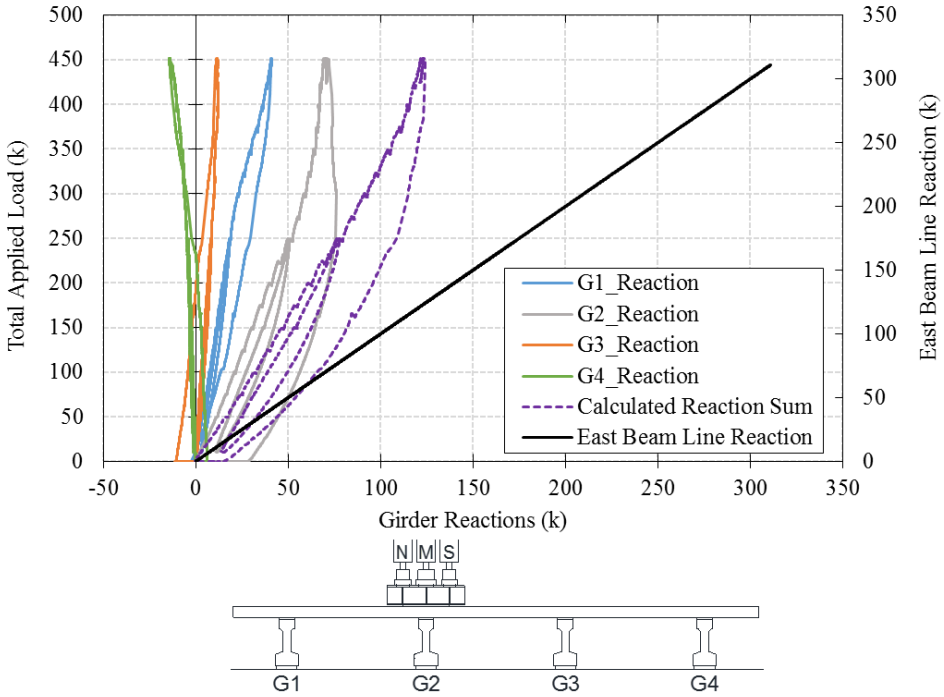

Figure E-8. Girder Reactions Estimated with Bearing Pad LVDT Data for LBUE

Figure E-9. Bearing Pad Horizontal Shear Behavior during Ultimate Testing

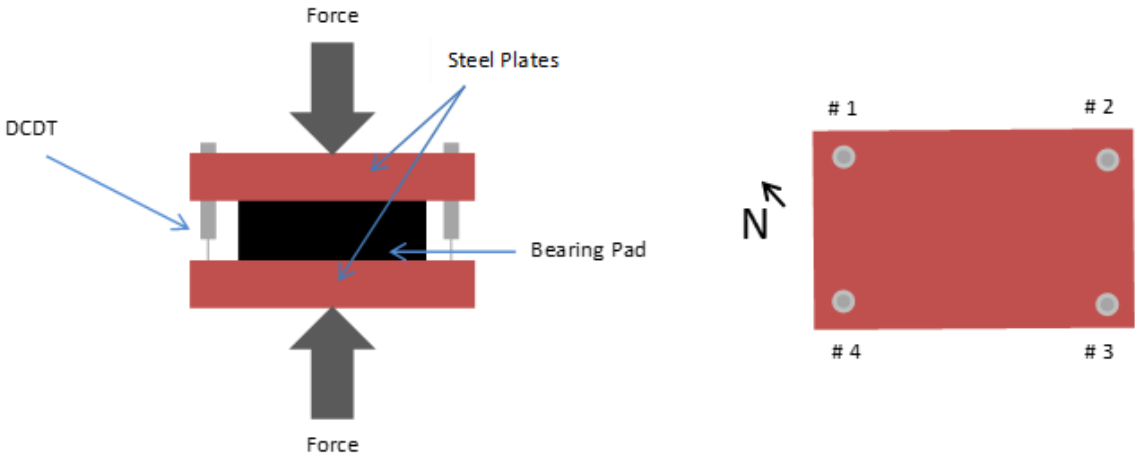

Figure E-10. Bearing Pad Test Setup Elevation (left) and Top (right) View

Figure E-11. Bulging Observed in 1-3/8 in. Bearing Pad

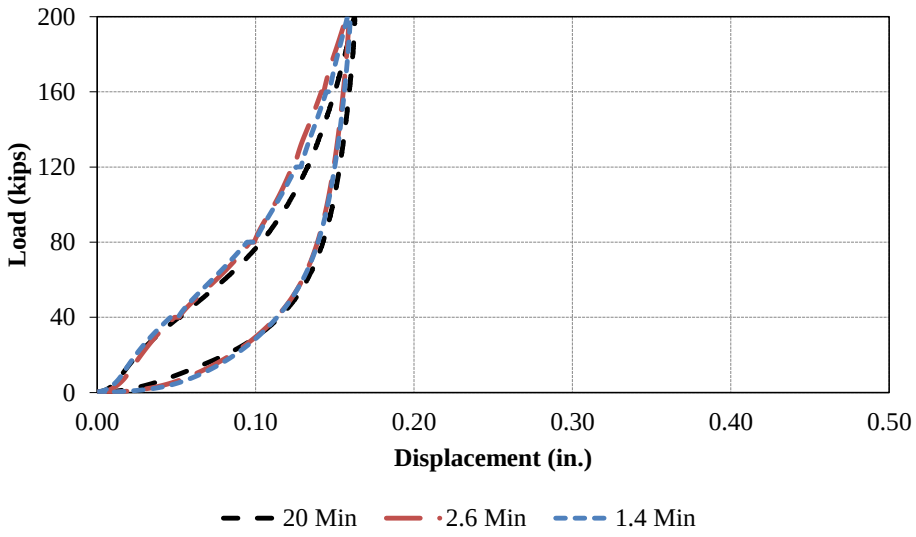

Figure E-12. Load vs. Displacement for 1-3/8 in. Bearing Pad

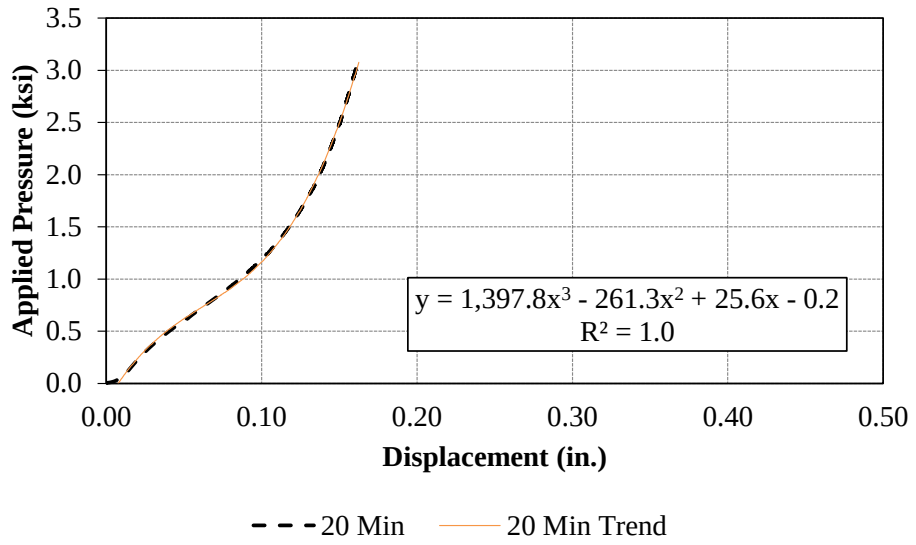

Figure E-13. Pressure vs. Displacement for 1-3/8 in. Bearing Pad

Figure E-14. Bulging Observed in 2-1/2 in. Bearing Pad

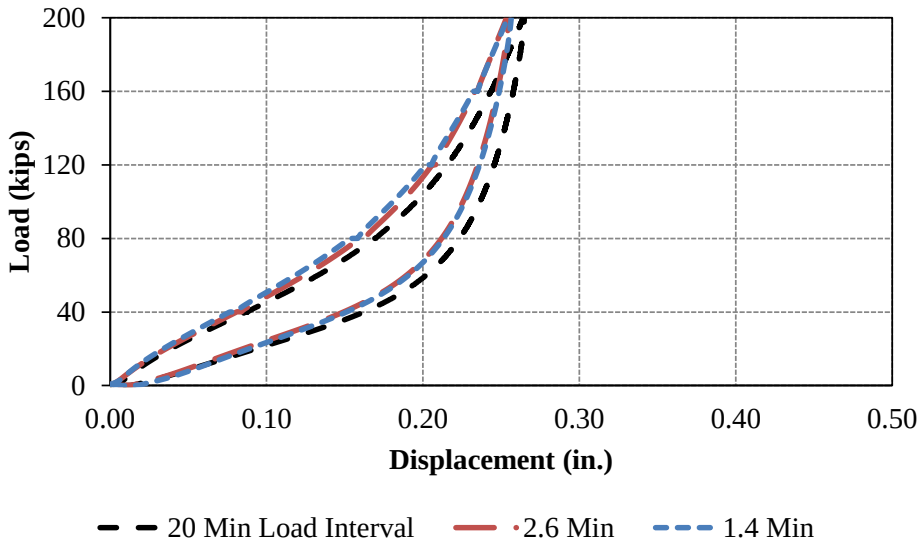

Figure E-15. Load vs. Displacement for 2-1/2 in. Bearing Pad

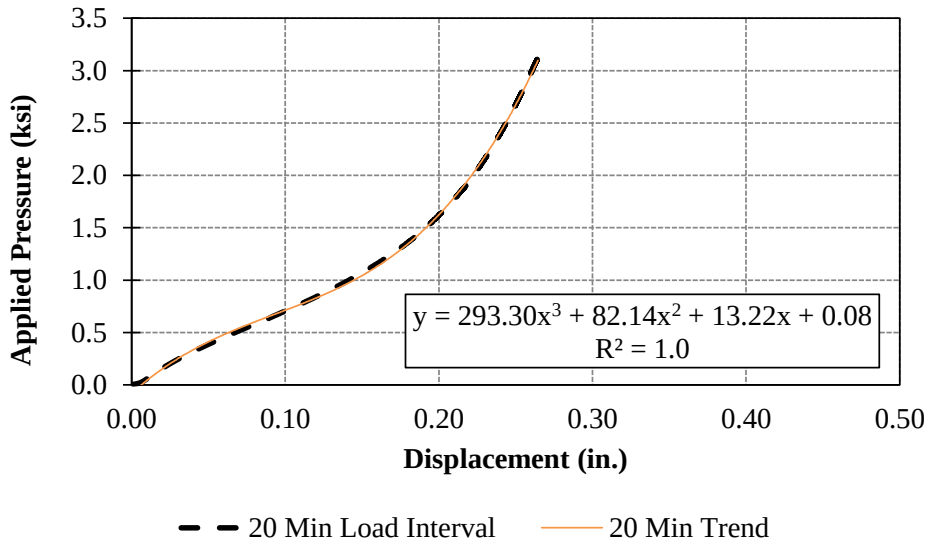

Figure E-16. Pressure vs. Displacement for 2-1/2 in. Bearing Pad

Figure E-17. Bulging Observed in 4-3/8 in. Bearing Pad

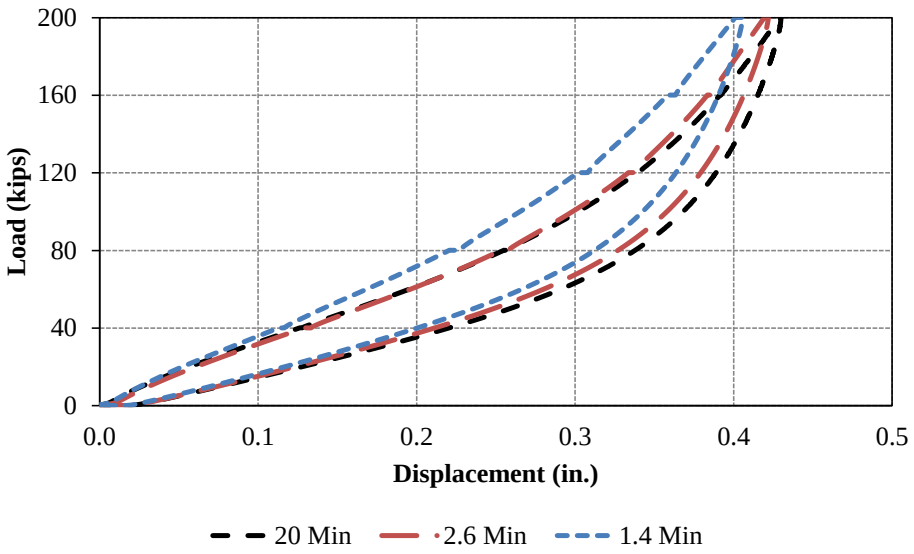

Figure E-18. Load vs. Displacement for 4-3/8 in. Bearing Pad

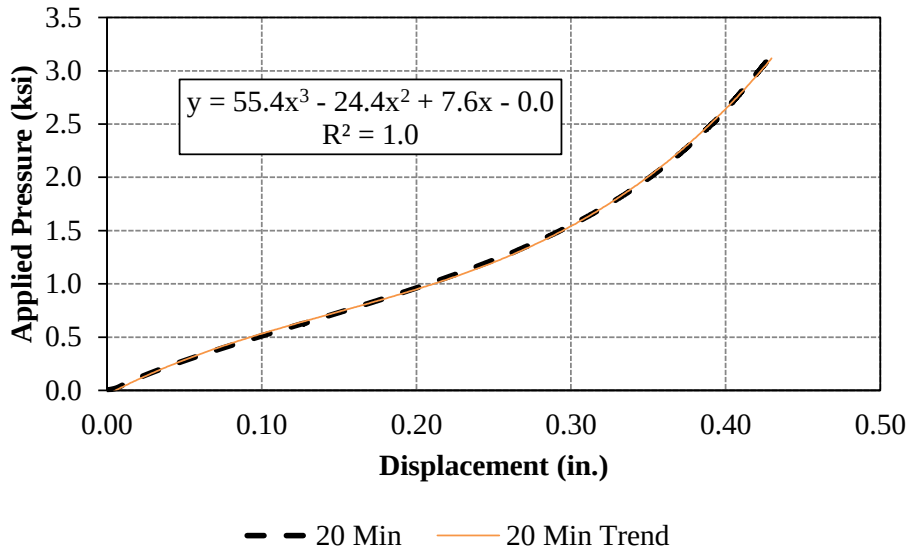

Figure E-19. Pressure vs. Displacement for 4-3/8 in. Bearing Pad

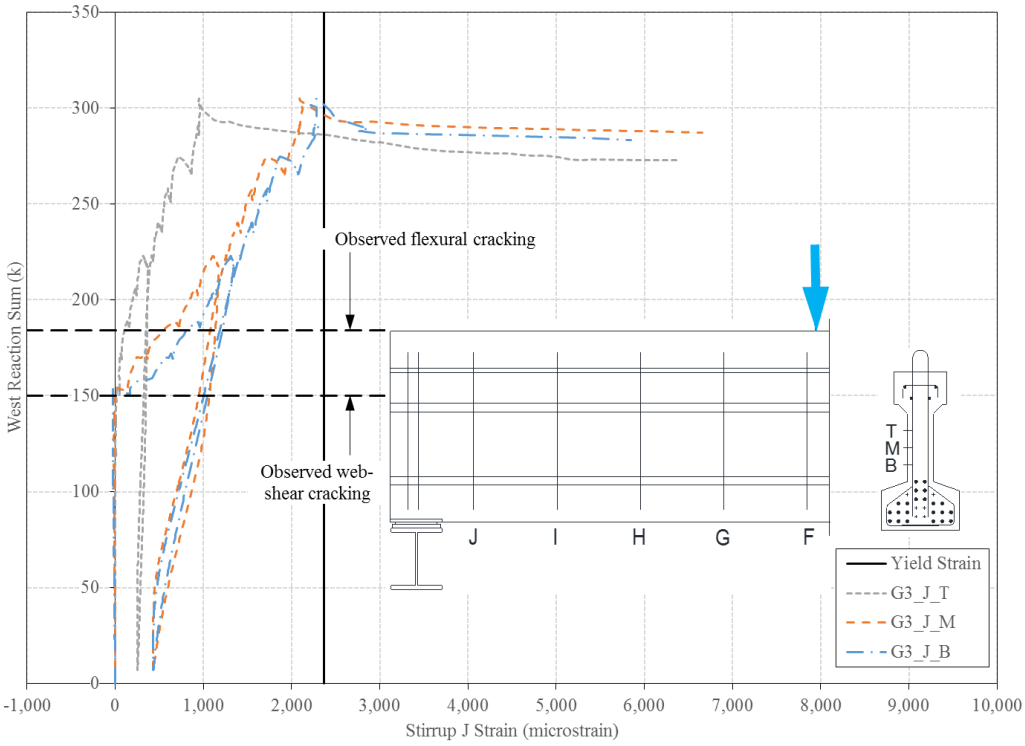

Figure E-20. Sum of West Girder Reactions vs. Stirrup J Strain for LBUW

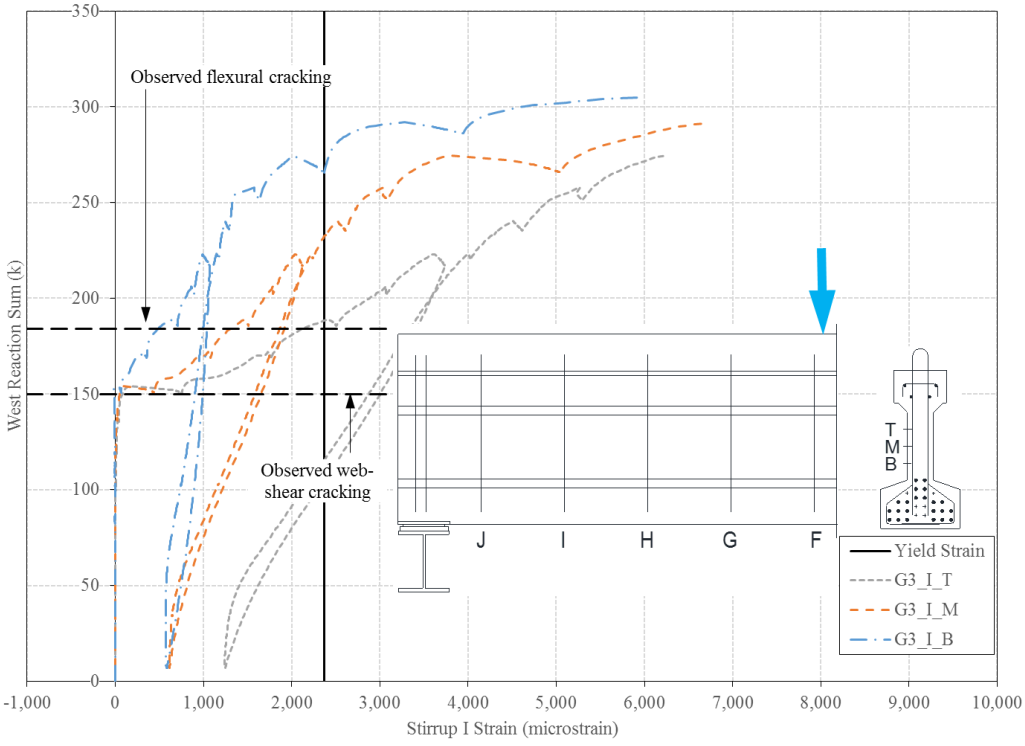

Figure E-21. Sum of West Girder Reactions vs. Stirrup I Strain for LBUW

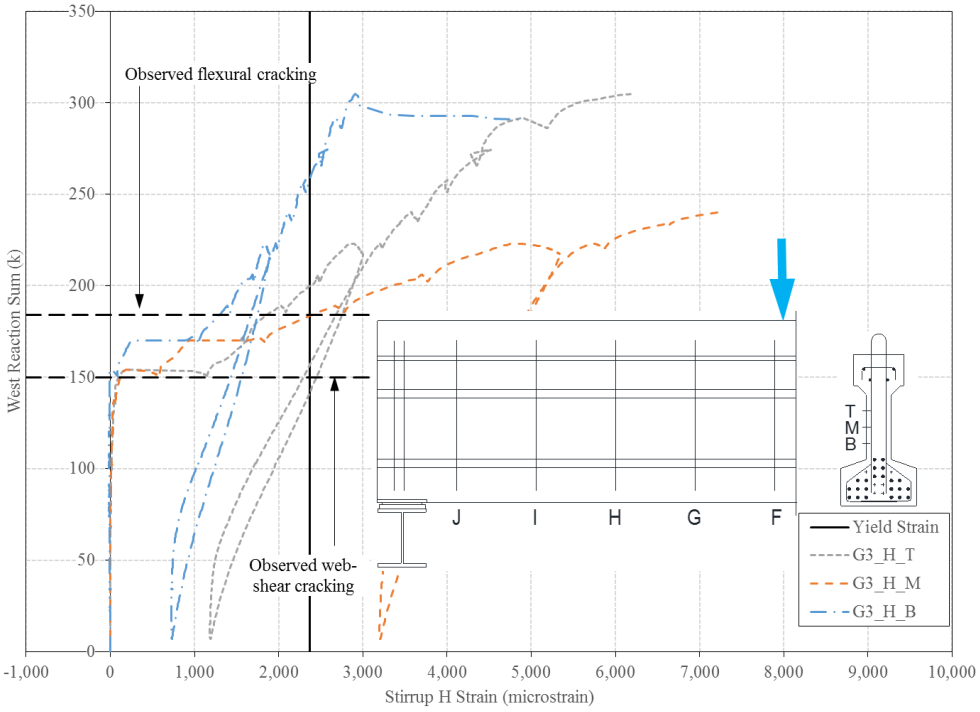

Figure E-22. Sum of West Girder Reactions vs. Stirrup H Strain for LBUW

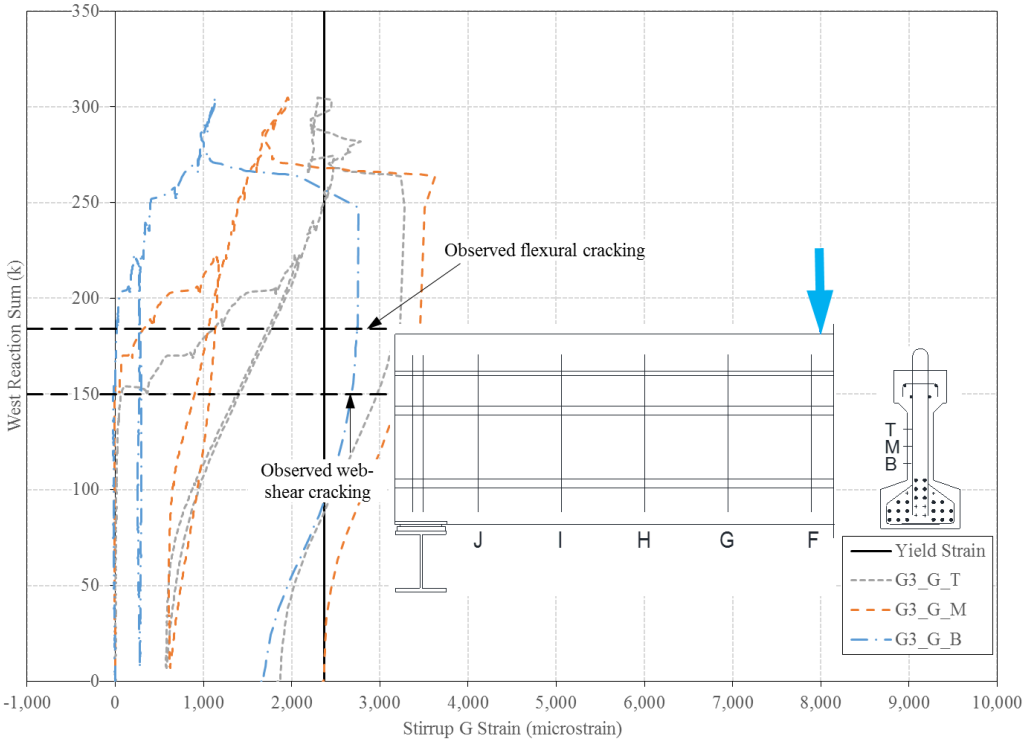

Figure E-23. Sum of West Girder Reactions vs. Stirrup G Strain for LBUW

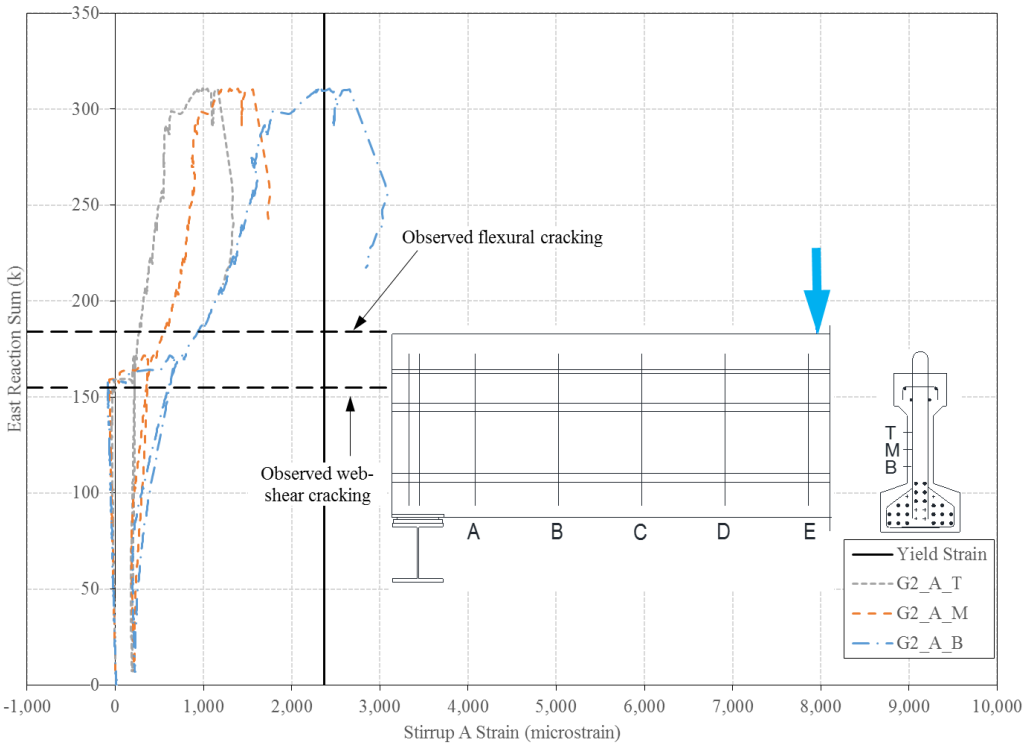

Figure E-24. Sum of East Girder Reactions vs. Stirrup A Strain for LBUE

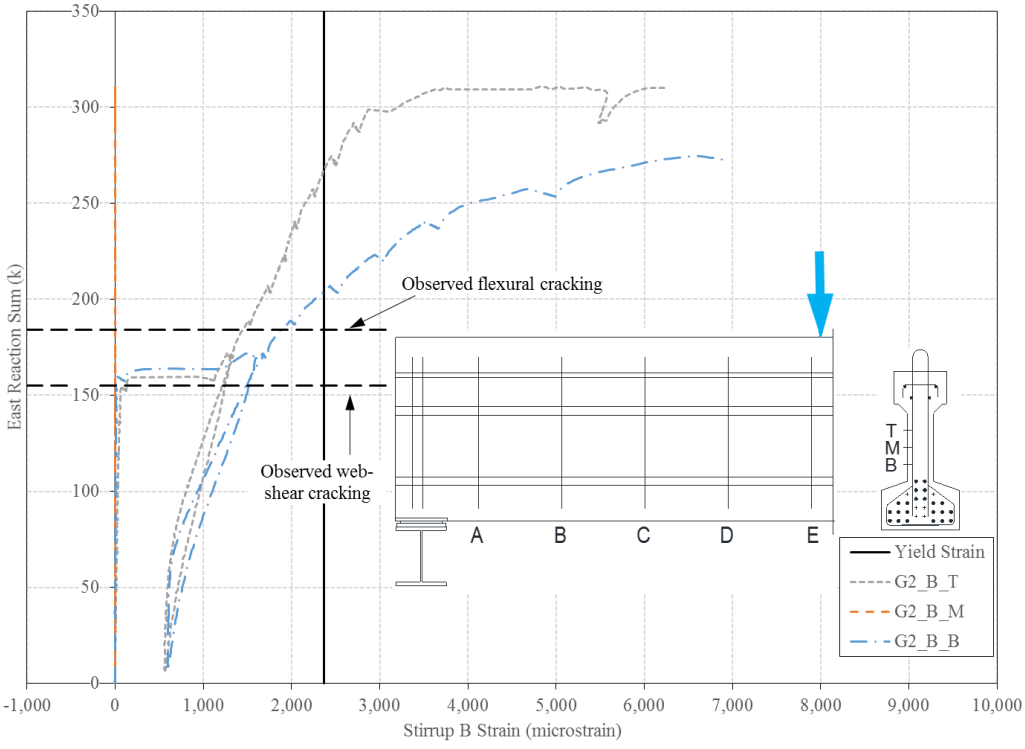

Figure E-25. Sum of East Girder Reactions vs. Stirrup B Strain for LBUE

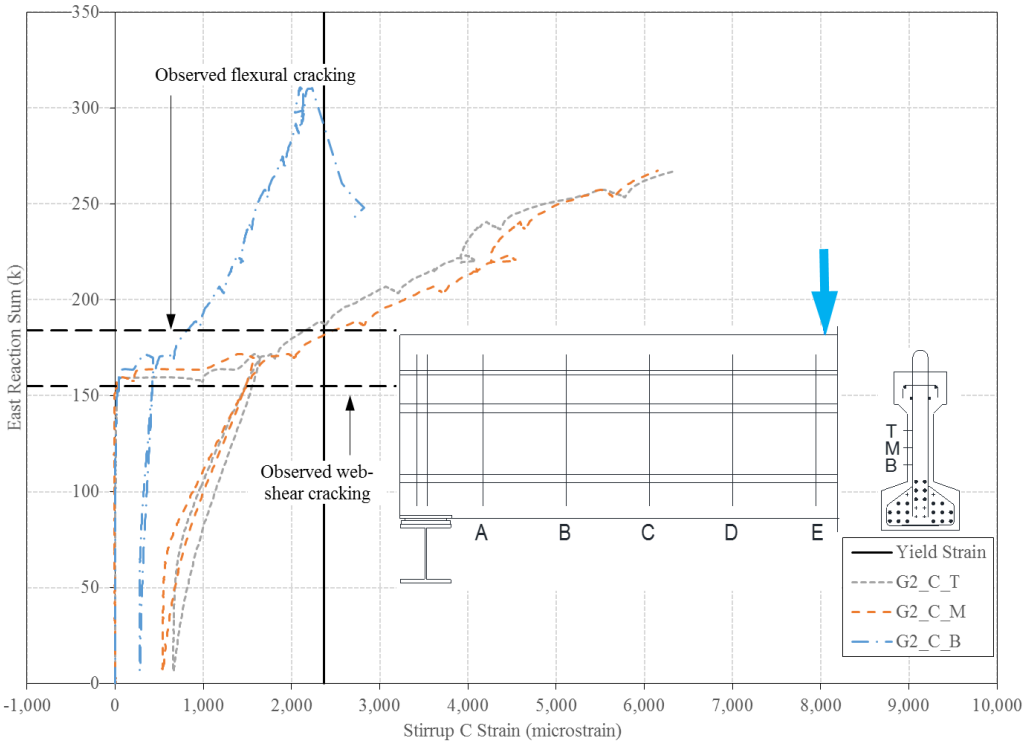

Figure E-26. Sum of East Girder Reactions vs. Stirrup C Strain for LBUE

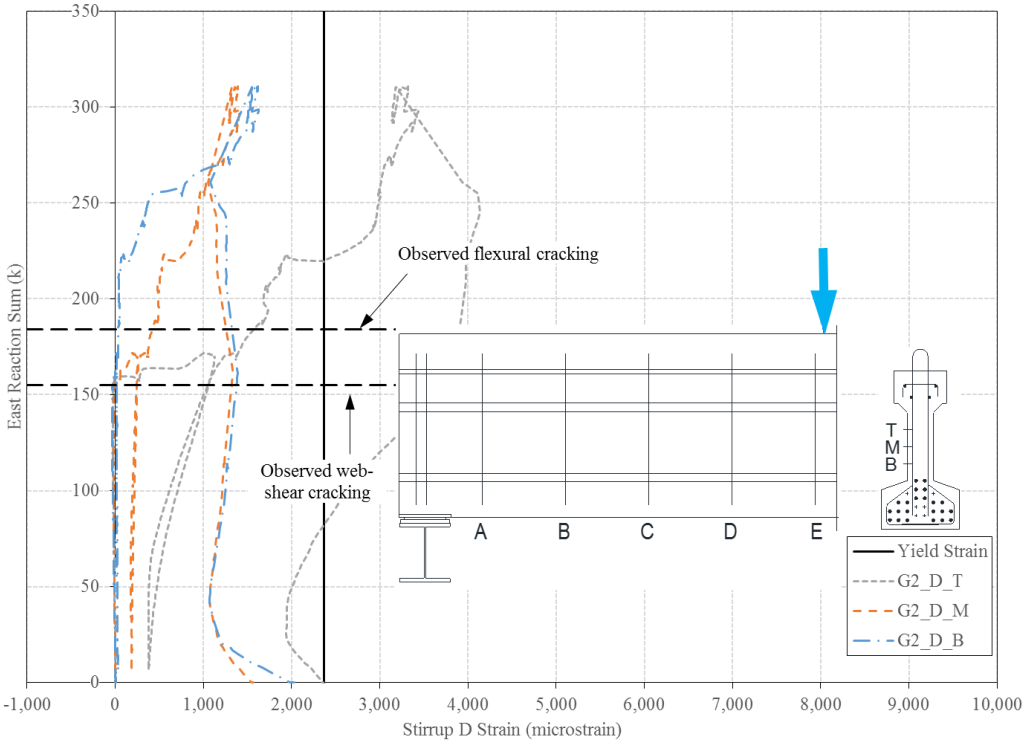

Figure E-27. Sum of East Girder Reactions vs. Stirrup D Strain for LBUE

APPENDIX F. FIELD SINGLE GIRDER TESTING AND RESULTS

F.1 Girder Specifications, Composite Deck, and Test Setup

F.2 Testing Results

This Appendix left intentionally blank. Final details included in the MnDOT Final Report.

APPENDIX G. FIELD BRIDGE TESTING DETAILS

Appendix G provides information related to the truck weights and axle dimensions used for live load field testing. Furthermore, Appendix G provides detail related to the testing protocols created for each field bridge. The end span and focus corner for live load testing were selected based on their accessibility. The field test protocol girder numbering was selected to align with the girder numbering on the bridge plans. However, to be consistent across six bridges, the girder numbering was changed after data collection. After re-numbering, Girder 1 (G1) was always the exterior girder in the focus corner of the bridge.

Furthermore, the longitudinal back-to-back truck locations for each test (Loc 3, 5, 7, 9, and 11.) were selected such that the back-to-back rear tandem axles were all located past a transverse line of gages. Typically, the transverse gage locations discussed in Section 6.3 corresponded to longitudinal truck locations discussed in 6.4 and given in Table 6-3. However, to be consistent across six bridges, the back-to-back truck locations for Bridge 09002 and Bridge 65006 were renamed after data collection due to adoption of the wrong numbering scheme in the initial testing protocol. For Bridge 09002, the original truck locations of Loc 5, Loc 9, and Loc 11 shown in Section G.6 were renamed as Loc 3, Loc 11, and Loc 7, respectively, for use in the main body of the report. For Bridge 65006, the original truck location of Loc 5 shown in Section G.7 was renamed as Loc 3 for use in the main body of the report.

G.1 Live Load Truck Dimensions and Weights

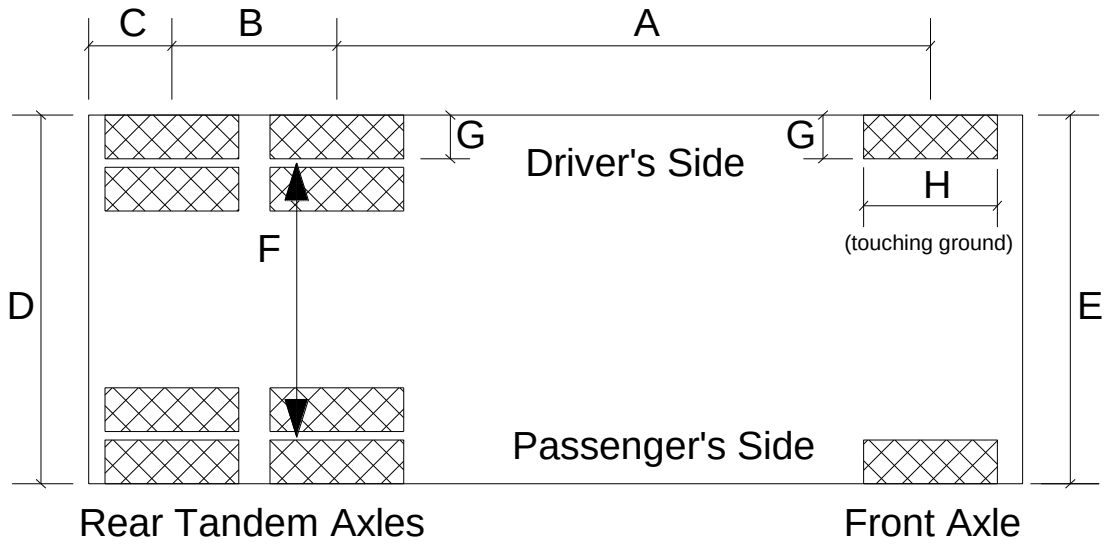

Bridge No.	73852		73872		62826		08011		09002		65006	
Truck No.	**99044**	**97137**	**96416**	**99044**	**98409**	**208551**	**205584**	**207586**	**202559**	**207656**	**202585**	**211566**
Lead Vehicle		x	x		x		x			x		x
A (in.)	181	183	177	177	183	187	183	181	182	183	182	187
B (in.)	56	53	55	55	54	55	55	55	55	55	55	55
C (in.)	55	45	38	38	39	40	47	45	39	40	39	39
D (in.)	94	94	94	94	96	96	95	94	96	95	95	95
E (in.)	96	92	95	95	96	96	96	98	98	98	97	98
F (in.)	74	72.5	73	73	72	73	74	73	73	73	73	73
G (front, in.)	12	12	12.5	12.5	12	12	12	12	12	12	12	12
G (rear, in.)	8.5	8.5	8.5	8.5	8.5	8.5	8.5	8.5	8.5	8.5	9	9
H (in.)	8	8	8	8	9	9	8	8	8	8	8	8
Front Axle (lb)	15,560	15,720	13,940	15,020	15,820	15,980	14,260	14,740	16,140	14,000	16,900	16,900
Tandem (lb)	35,480	35,340	36,320	35,140	33,620	33,520	34,540	35,660	33,840	36,060	33,100	33,200
Total (lb)	50,920	51,100	50,120	50,220	49,440	49,800	48,800	50,400	49,980	50,060	50,000	50,100

G.2 Bridge 73852 Testing Protocol

Bridge Information:

Bridge Number:	73852
Starting Date/Time:	June 25th 2012, 6:00 am
Location:	County Highway 136 over I-94 WB in Stearns County, near St. Cloud, MN (Decimal degrees of Latitude, Longitude: 45.498699, -94.198893)
Year Built:	1976
End Diaphragm:	Partial Depth
Skew:	2 degrees
End Span Geometry:	4 girders spaced at 11 ft with span length 63 ft
d_s:	50 in.

Objectives for Bridge 73852 Live Load Tests

Objective 1: Static Load Testing

Static tests are planned to verify transverse shear distribution near the north abutment and the northern most pier (pier 3), if accessible by bucket truck or manlift. Shear distribution tests will be performed on the north end span of the structure (span 4), shown in Figure 1, and will include loading the structure in both the north and south bound lanes. Load will be applied with two MnDOT sand trucks filled so that their total weight is approximately 50 kips. The trucks will be parked on the bridge at various locations for data collection. Additional static tests are planned to verify transverse flexural distribution at midspan. Two longitudinal strain gages will be placed at midspan of each girder to determine the flexural strain and vertical strain distribution (for neutral axis calculation).

Figure 1. Bridge 73852

Objective 2: Visual Inspection of End Regions for Shear Cracks

Bridge 73852 has an inventory shear rating less than unity. Applying maximum truck load provides the opportunity to investigate possible shear cracks that may exist on the girders. These girders would most likely only be visible under the application of load. Visual inspection will be done on both an interior and exterior girder when the back-to-back truck configuration is parked at a maximum applied shear location. Any visible shear cracks will be recorded and photographed.

Planning for Bridge 73852 Live Load Tests

The truck tests are planned to occur between June 25 and June 28, 2012. Instrumentation of all bridge girders near the abutment will occur in the first day. Truck tests near the abutment will all occur in the second day. The third day will be used to instrument all girders near the first interior pier using a snooper truck. Truck tests near the first interior pier will occur on the fourth day. The fourth day also includes removing the strain gages applied with a snooper truck. The tests should be completed rain or shine unless the weather is terrible. The following tasks need to be completed in preparation for the truck tests on day two. The responsibility for each of the tasks is identified below.

Task 1: Mark Truck Locations (UMN)

The locations where the trucks are to be positioned for the various static tests should be marked on the bridge prior to the truck tests. The use of marking paint should be used for a semi-permanent testing profile which will provide an outline for chalking the test grid on the day of testing.

Task 2: Arrange for Loaded Trucks (MnDOT)

Two loaded sand trucks will be needed for performing the static tests. Each truck should nominally weigh 50 kips and have a front axle to back axle length of approximately 19'-8". Each truck will need to be weighed prior to testing and after testing. Weight information should be obtained for the front axle only, the rear tandem axles only, and the entire truck. A volunteer should fill out the "truck record sheet." The trucks should be tarped over the course of the testing week to assure that no rain adds weight to the truck.

Task 3: Plan and Implement Traffic Control (MnDOT)/ (UMN)

Day 1 – Instrumentation: The bridge does not need to be closed at all, but UMN will close the shoulder using cones to mark the deck.

Day 2 – Truck Tests: The bridge will need to be periodically closed during each static test (which should last approximately 15 minutes). Scheduled tests must take place when MnDOT traffic control crews are at the site, between 6 AM and 4:30 PM, for a total of 10.5 hours of partial bridge closure. The first testing day will include all static tests done near the north abutment

Day 3 – Instrumentation: The bridge will need single lane closures to allow for the use of a snooper truck to instrument all four girders near the pier. During this lane closure, marking of the deck testing grid will also take place.

Day 4 – Truck Tests: The second day of testing will consist of static tests performed near the first pier. The same loaded sand trucks should be used for all tests, regardless of day. Near the end of the day, truck testing will stop so that instrumentation can be removed using the snooper truck.

Schedule for Bridge 73852 Live Load Tests

Testing should be completed in four days. The schedule for the first day of testing is presented in Table 1 on the next page. The diagrams that describe the testing locations for each test description are shown in Figure 2 through Figure 5.

Row	Start Time	Actual Start Time	Test	Duration (min)	Details	Priority	Completed?	Traffic Control	Notes
1	6:00 AM		Abutment Start	60	Begin MnDOT travel & traffic control	0		None	
2	6:30 AM		Zero 1	15	Take measurements with no load before traffic control	0		None	
3	7:15 AM		G4 BB Loc 3	15	G4 back-to-back, rear axle south truck at Loc 3	1		Periodically Close Bridge	
4	7:30 AM		G4 ST Loc 0	15	G4 single north truck, rear axle positioned at Loc 0	1		"	
5	7:45 AM		G4 BB Loc 5	15	G4 back-to-back, rear axle south truck at Loc 5	1		"	
6	8:00 AM		G4 ST Loc 1	15	G4 single north truck, rear axle positioned at Loc 1	1		"	
7	8:15 AM		Zero 2	15	Take measurements with no load	1		"	
8	8:30 AM		G4 BB Loc 7	15	G4 back-to-back, rear axle south truck at Loc 7	1		"	
9	8:45 AM		G4 SS Loc 7	15	G4 side-by-side, rear axles centered at Loc 7	2		"	
10	9:00 AM		G4 SS Loc 8	15	G4 side-by-side, rear axles centered at Loc 8	2		"	
11	9:15 AM		G3 BB Loc 3	15	G3 back-to-back, rear axle south truck at Loc 3	1		"	repeatability test
12	9:30 AM		Zero 3	15	Take measurements with no load	1		"	
13	9:45 AM		G3-G4 BB Loc 3	15	G3-G4 split back-to-back, rear axle south truck at Loc 3	1		"	
14	10:00 AM		G3-G4 ST Loc 0	15	G3-G4 split single north truck, rear axle at Loc 0	1		"	
15	10:15 AM		G3-G4 BB Loc 5	15	G3-G4 split back-to-back, rear axle south truck at Loc 5	1		"	
16	10:30 AM		G3-G4 ST Loc 1	15	G3-G4 split single north truck, rear axle at Loc 1	1		"	
17	10:45 AM		Zero 4	15	Take measurements with no load	1		"	
18	11:00 AM		G3-G4 BB Loc 7	15	G3-G4 split back-to-back, rear axle south truck at Loc 7	1		"	
19	11:15 AM		G3-G4 SS Loc 7	15	G3-G4 split side-by-side, rear axles centered at Loc 7	2		"	
20	11:30 AM		G3-G4 SS Loc 8	15	G3-G4 split side-by-side, rear axles centered at Loc 8	2		"	
21	11:45 AM		G4 BB Loc 3	15	G4 back-to-back, rear axle south truck at Loc 3	1		"	repeatability test
22	12:00 PM		Zero 5	15	Take measurements with no load	1		"	
23	12:15 PM		G3 BB Loc 3	15	G3 back-to-back, rear axle south truck at Loc 3	1		"	
24	12:30 PM		G3 ST Loc 0	15	G3 single north truck, rear axle at Loc 0	1		"	
25	12:45 PM		G3 BB Loc 5	15	G3 back-to-back, rear axle south truck at Loc 5	1		"	
26	1:00 PM		G3 ST Loc 1	15	G3 single north truck, rear axle at Loc 1	1		"	
27	1:15 PM		G3 BB Loc 7	15	G3 back-to-back, rear axle south truck at Loc 7	1		"	
28	1:30 PM		Zero 6	15	Take measurements with no load	1		"	
29	1:45 PM		G2 BB Loc 3	15	G2 back-to-back, rear axle south truck at Loc 3	1		"	
30	2:00 PM		G2 BB Loc 5	15	G2 back-to-back, rear axle south truck at Loc 5	1		"	
31	2:15 PM		G2-G1 BB Loc 3	15	G2-G1 split back-to-back, rear axle south truck at Loc 3	1		"	
32	2:30 PM		G2-G1 BB Loc 5	15	G2-G1 split back-to-back, rear axle south truck at Loc 5	1		"	
33	2:45 PM		Zero 7	15	Take measurements with no load	1		"	
34	3:00 PM		G1 BB Loc 3	15	G1 back-to-back, rear axle south truck at Loc 3	1		"	
35	3:15 PM		G1 BB Loc 5	15	G1 back-to-back, rear axle south truck at Loc 5	1		"	
36	3:30 PM		G4 BB Loc 3	15	G4 back-to-back, rear axle south truck at Loc 3	1		"	thermal repeatability test
37	3:45 PM		Zero 8	45	Take measurements with no load, MnDOT leaves	0		Remove	
38	4:30 PM		Day 2 Complete		Testing complete and traffic control removed	0		None	

The test locations in the table below are extra day 1 tests if time permits.

39	Extra		G3W BB Loc 3	15	G3W back-to-back, rear axle south truck at Loc 3	1		"	
40	Extra		G3W ST Loc 0	15	G3W single north truck, rear axle at Loc 0	3		"	
41	Extra		G3W BB Loc 5	15	G3W back-to-back, rear axle south truck at Loc 5	1		"	
42	Extra		G3W ST Loc 1	15	G3W single north truck, rear axle at Loc 1	3		"	
43	Extra		G3W BB Loc 7	15	G3W back-to-back, rear axle south truck at Loc 7	1		"	
44	Extra		G3E BB Loc 3	15	G3E back-to-back, rear axle south truck at Loc 3	1		"	
45	Extra		G3E ST Loc 0	15	G3E single north truck, rear axle at Loc 0	3		"	
46	Extra		G3E BB Loc 5	15	G3E back-to-back, rear axle south truck at Loc 5	1		"	
47	Extra		G3E ST Loc 1	15	G3E single north truck, rear axle at Loc 1	3		"	
48	Extra		G3E BB Loc 7	15	G3E back-to-back, rear axle south truck at Loc 7	1		"	
49	Extra		G3-G2 BB Loc 3	15	G3-G2 split back-to-back, rear axle south truck at Loc 3	1		"	
50	Extra		G3-G2 BB Loc 5	15	G3-G2 split back-to-back, rear axle south truck at Loc 5	1		"	

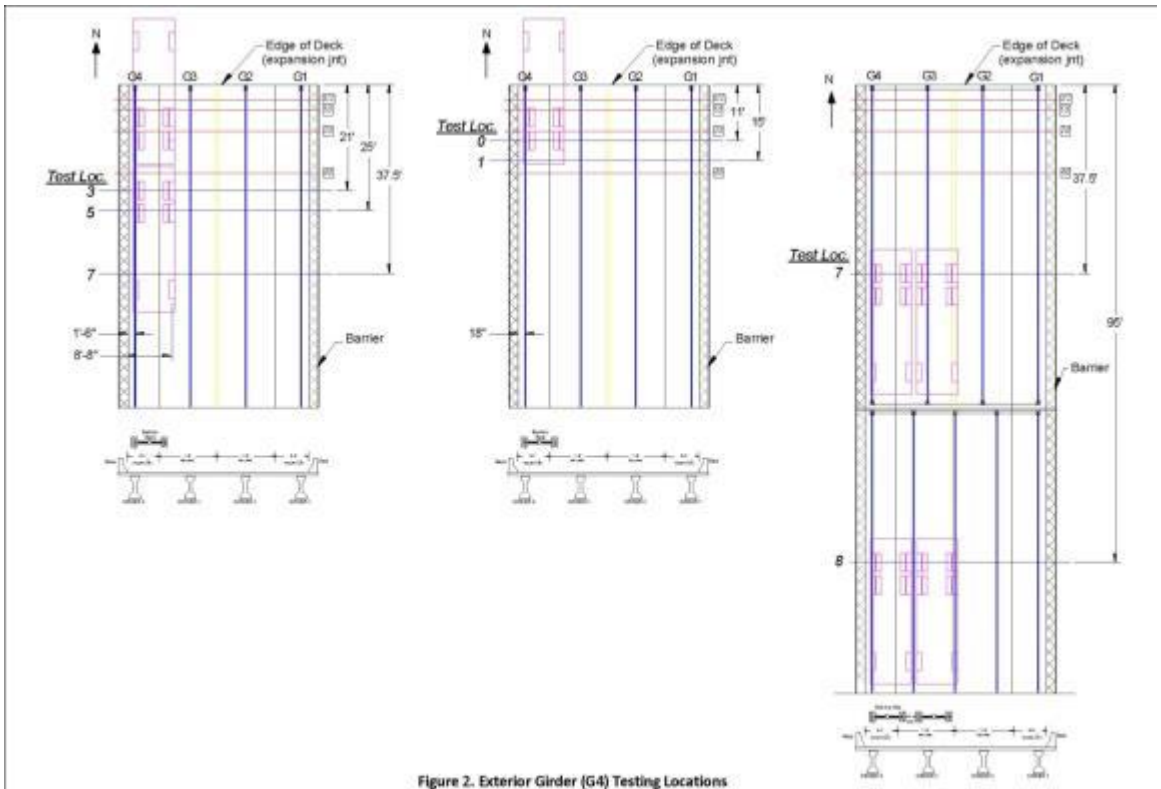

Figure 2. Exterior Girder (G4) Testing Locations

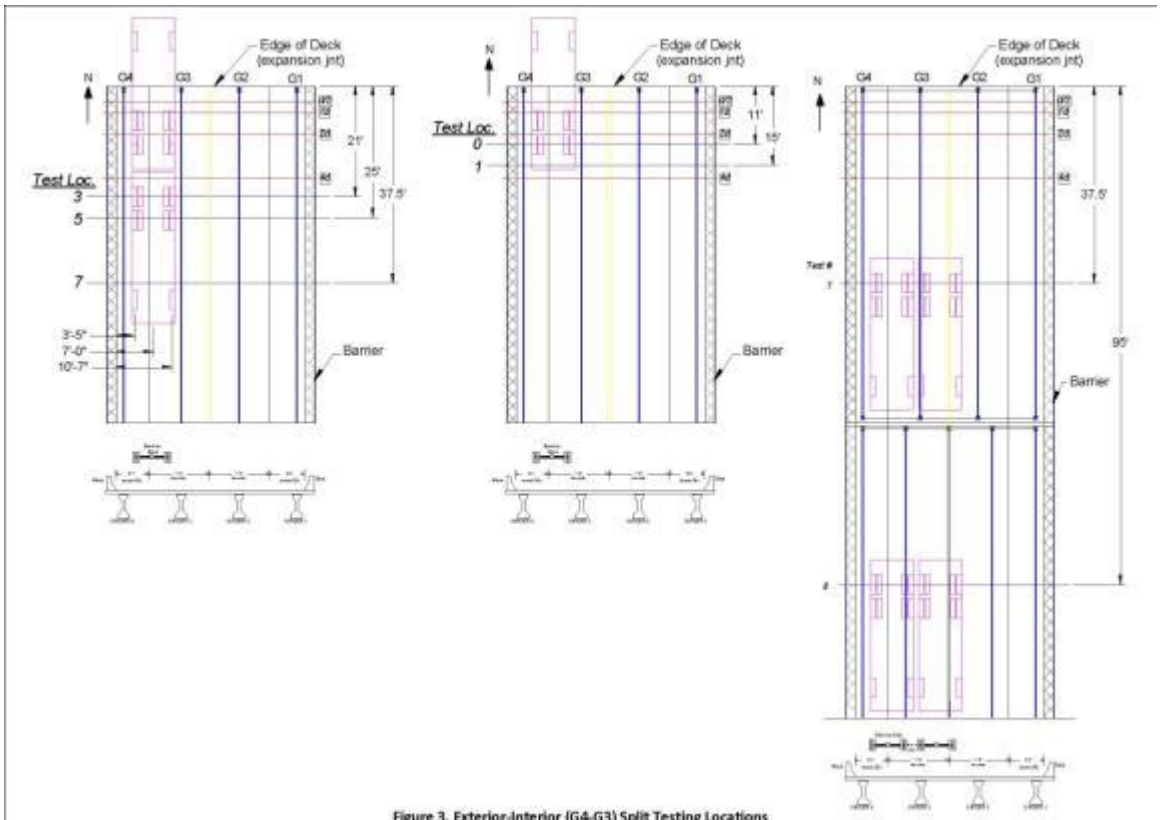

Figure 3. Exterior-Interior (G4-G3) Split Testing Locations

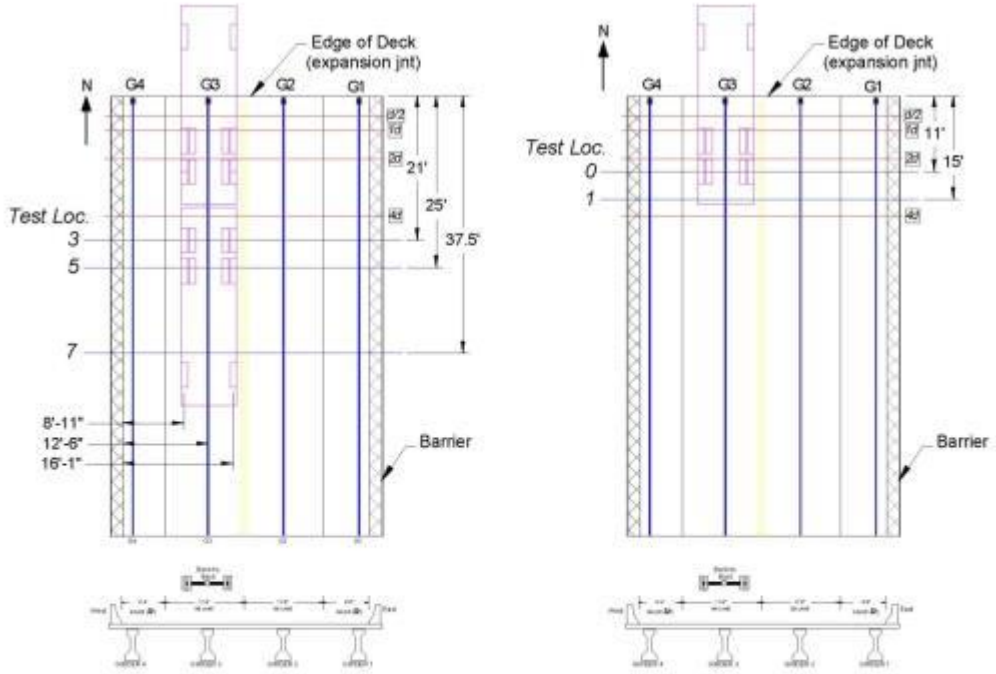

Figure 4. Interior Girder (G3) Testing Locations

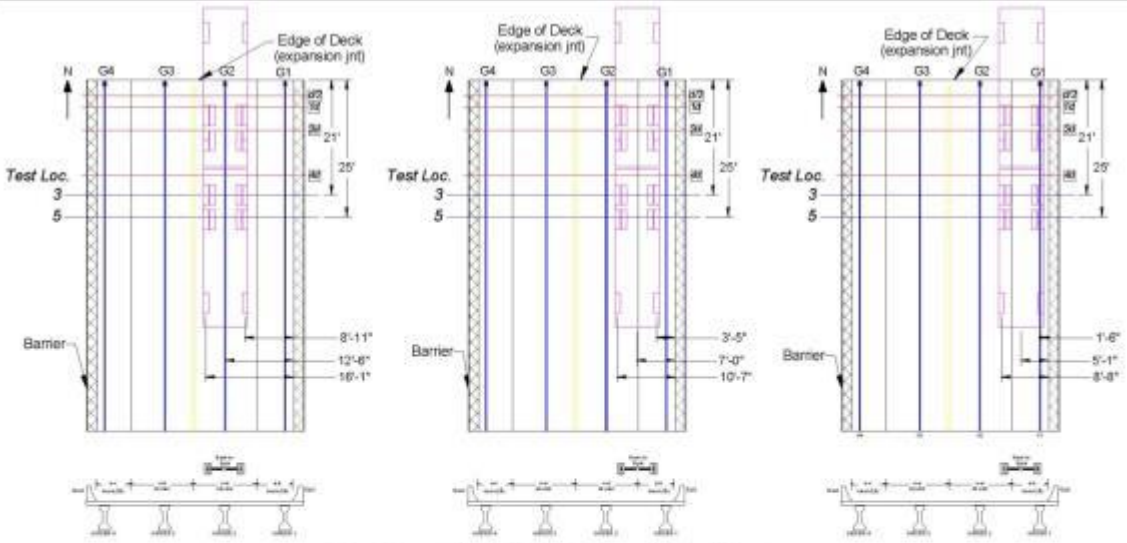

Figure 5. Symmetric Girder (G2, G2-G1 split, and G1) Testing Locations

The schedule for the second day of testing is presented in Table 2 on the next page. The diagrams that describe the testing locations for each test description are shown in Figure 6 through Figure 9.

Row	Start Time	Actual Start Time	Test	Duration (min)	Details	Priority	Completed?	Traffic Control	Notes
1	6:00 AM		Abutment Start	60	Begin MnDOT travel & traffic control	0		None	
2	6:30 AM		Zero 1	15	Take measurements with no load before traffic control	0		None	
3	7:15 AM		G4 BB Loc 3	15	G4 back-to-back, rear axle north truck at Loc 3	1		Periodically Close Bridge	
4	7:30 AM		G4 ST Loc 0	15	G4 single south truck, rear axle positioned at Loc 0	1		"	
5	7:45 AM		G4 BB Loc 5	15	G4 back-to-back, rear axle north truck at Loc 5	1		"	
6	8:00 AM		G4 ST Loc 1	15	G4 single south truck, rear axle positioned at Loc 1	1		"	
7	8:15 AM		Zero 2	15	Take measurements with no load	1		"	
8	8:30 AM		G4 BB Loc 7	15	G4 back-to-back, rear axle north truck at Loc 7	1		"	
9	8:45 AM		G4 SS Loc 8	15	G4 side-by-side, rear axles centered at Loc 8	2		"	
10	9:00 AM		G3 BB Loc 3	15	G3 back-to-back, rear axle north truck at Loc 3	1		"	repeatability test
11	9:15 AM		Zero 3	15	Take measurements with no load	1		"	
12	9:30 AM		G3-G4 BB Loc 3	15	G3-G4 split back-to-back, rear axle north truck at Loc 3	1		"	
13	9:45 AM		G3-G4 ST Loc 0	15	G3-G4 split single south truck, rear axle at Loc 0	1		"	
14	10:00 AM		G3-G4 BB Loc 5	15	G3-G4 split back-to-back, rear axle north truck at Loc 5	1		"	
15	10:15 AM		G3-G4 ST Loc 1	15	G3-G4 split single south truck, rear axle at Loc 1	1		"	
16	10:30 AM		Zero 4	15	Take measurements with no load	1		"	
17	10:45 AM		G3-G4 BB Loc 7	15	G3-G4 split back-to-back, rear axle north truck at Loc 7	1		"	
18	11:00 AM		G3-G4 SS Loc 8	15	G3-G4 split side-by-side, rear axles centered at Loc 8	2		"	
19	11:15 AM		G4 BB Loc 3	15	G4 back-to-back, rear axle north truck at Loc 3	1		"	repeatability test
20	11:30 AM		Zero 5	15	Take measurements with no load	1		"	
21	11:45 AM		G3 BB Loc 3	15	G3 back-to-back, rear axle north truck at Loc 3	1		"	
22	12:00 PM		G3 ST Loc 0	15	G3 single south truck, rear axle at Loc 0	1		"	
23	12:15 PM		G3 BB Loc 5	15	G3 back-to-back, rear axle north truck at Loc 5	1		"	
24	12:30 PM		G3 ST Loc 1	15	G3 single south truck, rear axle at Loc 1	1		"	
25	12:45 PM		G3 BB Loc 7	15	G3 back-to-back, rear axle north truck at Loc 7	1		"	
26	1:00 PM		Zero 6	15	Take measurements with no load	1		"	
27	1:15 PM		G2 BB Loc 5	15	G2 back-to-back, rear axle north truck at Loc 5	1		"	
28	1:30 PM		G2-G1 BB Loc 5	15	G2-G1 split back-to-back, rear axle north truck at Loc 5	1		"	
29	1:45 PM		G1 BB Loc 5	15	G1 back-to-back, rear axle north truck at Loc 5	1		"	
30	2:00 PM		Zero 7	15	Take measurements with no load	1		"	
31	2:15 PM		De-Instrument	90	Snooper truck used to take down pier instrumentation	0		"	
32	3:45 PM		Stop Traffic Control	45	MnDOT traffic control leaves	0		Remove	
33	4:30 PM		Day 4 Complete		Testing complete and traffic control removed	0		None	

The test locations in the table below are extra day 2 tests if time permits.

34	Extra		G2 BB Loc 3	15	G2 back-to-back, rear axle north truck at Loc 3	2		"	
35	Extra		G2-G1 BB Loc 3	15	G2-G1 split back-to-back, rear axle north truck at Loc 3	2		"	
36	Extra		G1 BB Loc 3	15	G1 back-to-back, rear axle north truck at Loc 3	2		"	
37	Extra		G3W BB Loc 3	15	G3W back-to-back, rear axle north truck at Loc 3	2		"	
38	Extra		G3W ST Loc 0	15	G3W single south truck, rear axle at Loc 0	3		"	
39	Extra		G3W BB Loc 5	15	G3W back-to-back, rear axle north truck at Loc 5	2		"	
40	Extra		G3W ST Loc 1	15	G3W single south truck, rear axle at Loc 1	3		"	
41	Extra		G3W BB Loc 7	15	G3W back-to-back, rear axle north truck at Loc 7	2		"	
42	Extra		G3E BB Loc 3	15	G3E back-to-back, rear axle north truck at Loc 3	2		"	
43	Extra		G3E ST Loc 0	15	G3E single south truck, rear axle at Loc 0	3		"	
44	Extra		G3E BB Loc 5	15	G3E back-to-back, rear axle north truck at Loc 5	2		"	
45	Extra		G3E ST Loc 1	15	G3E single south truck, rear axle at Loc 1	3		"	
46	Extra		G3E BB Loc 7	15	G3E back-to-back, rear axle north truck at Loc 7	2		"	
47	Extra		G3-G2 BB Loc 3	15	G3-G2 split back-to-back, rear axle north truck at Loc 3	3		"	
48	Extra		G3-G2 BB Loc 5	15	G3-G2 split back-to-back, rear axle north truck at Loc 5	3		"	

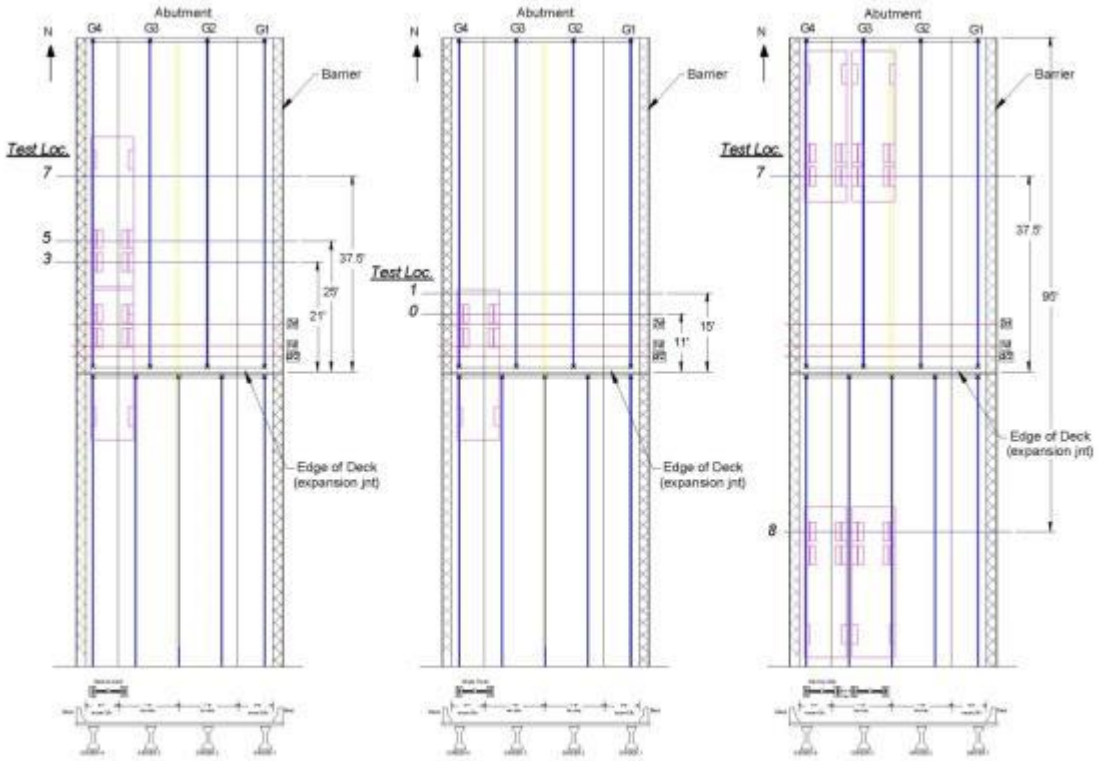

Figure 6. Exterior Girder (G4) Testing Locations

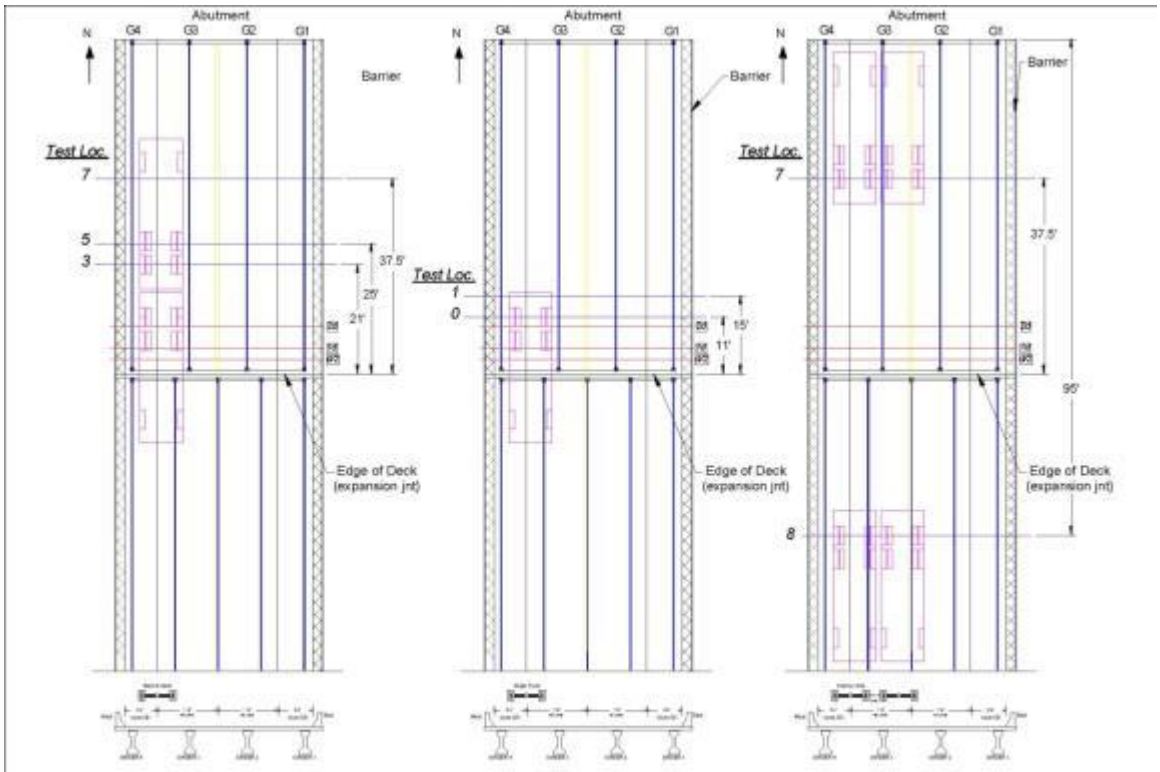

Figure 7. Exterior-Interior (G4-G3) Split Testing Locations

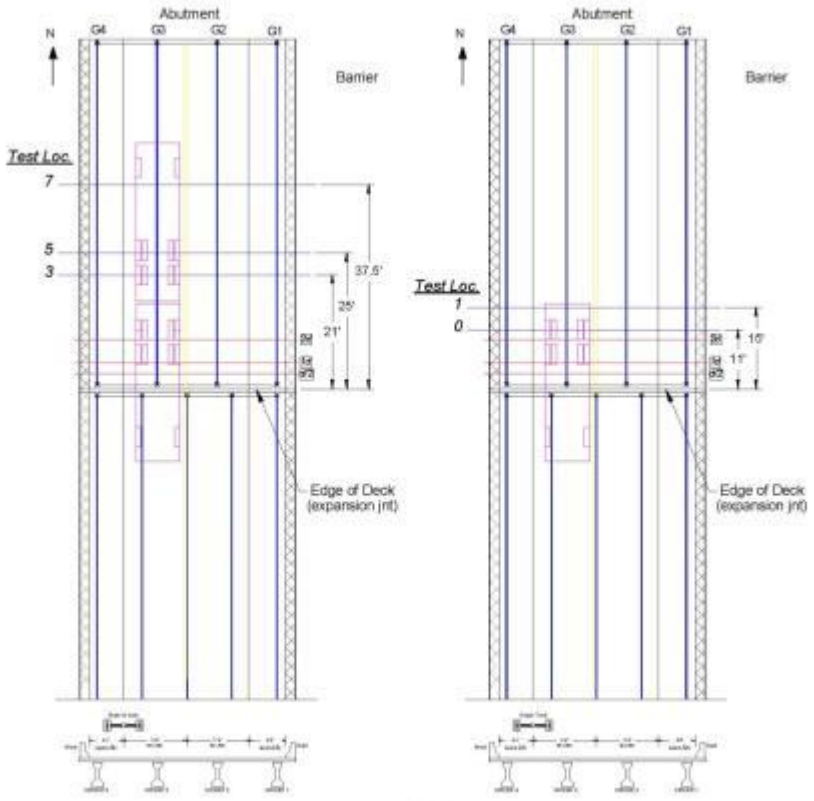

Figure 8. Interior Girder (G3) Testing Locations

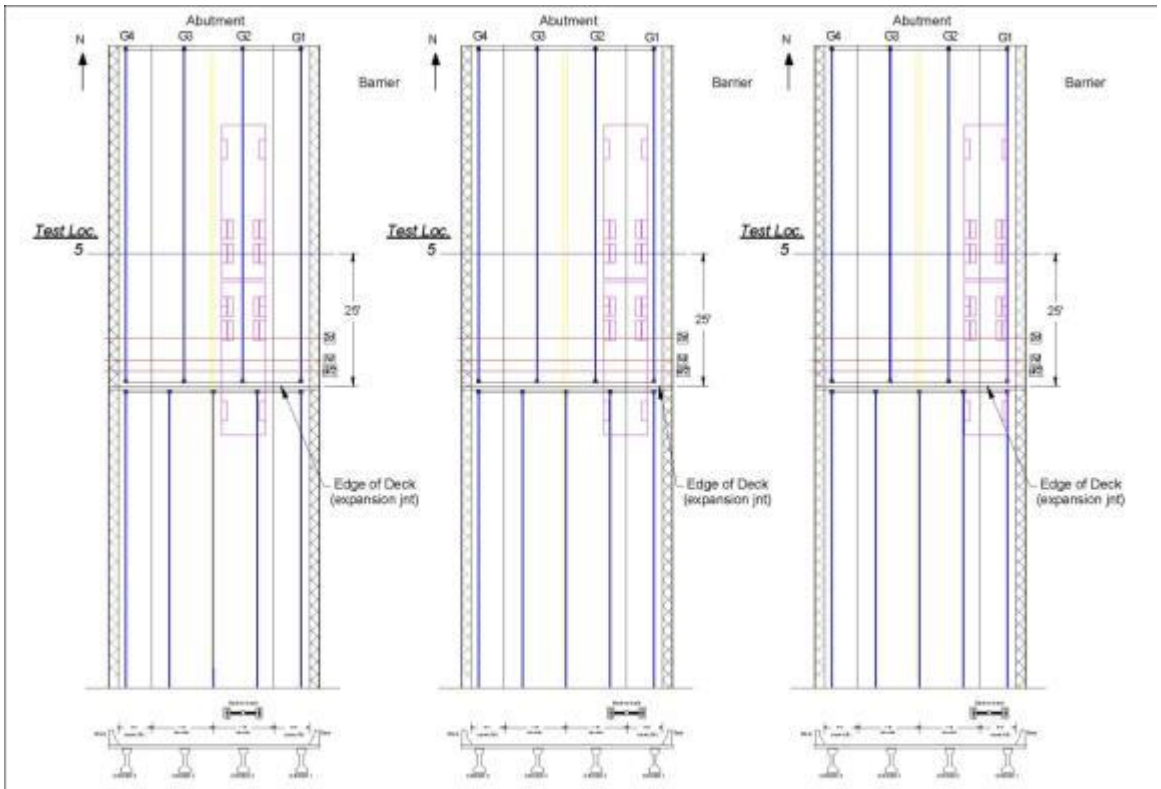

Figure 9. Symmetric Girder (G2, G2-G1 split, and G1) Testing Locations

Instrumentation and Data Collection for Bridge 73852 Live Load Tests

For all static testing, Geokon vibrating wire strain gage data will be collected using a Campbell Scientific CR1000 data acquisition system. All channels will be scanned five times per truck stop which takes approximately 8 minutes.

Instrumentation will be installed on all four girders, as labeled in Figure 10 and Figure 11 and the western barrier. Girder instrumentation plans are shown in Figure 12 through Figure 15.

Figure 10. North Abutment Girder Numbering

Figure 11. Pier 3 Girder Numbering

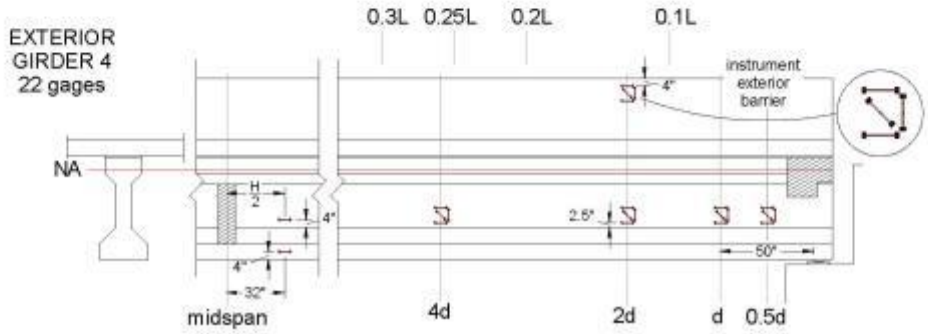

Figure 12. Girder 4 Instrumentation

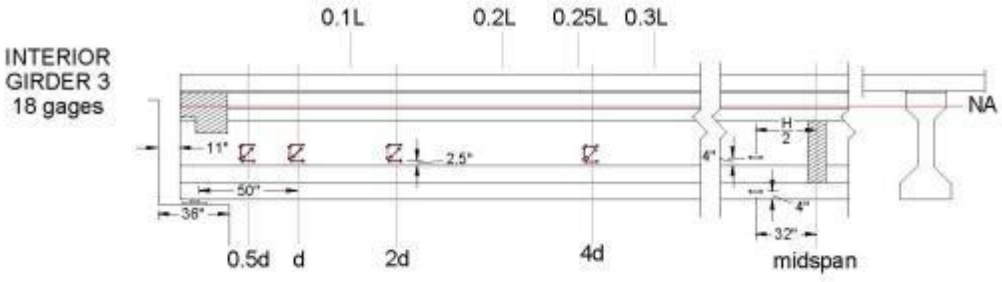

Figure 13. Girder 3 Instrumentation

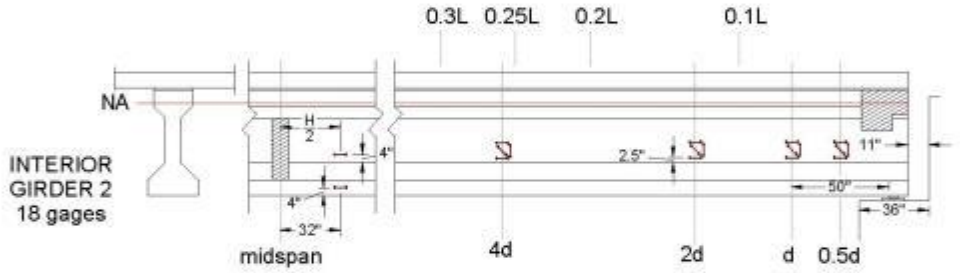

Figure 14. Girder 2 Instrumentation

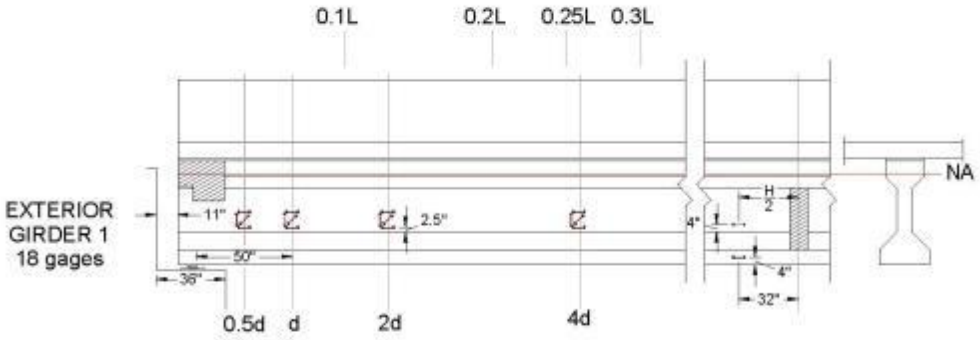

Figure 15. Girder 1 Instrumentation

The vibrating wire strain gage wires are all pulled to a set of boards where the ends are attached to terminal blocks. Most of the strain gage wires are 10 feet in length and will be used near the abutment, as shown in Figure 16. The wires running from gages located at 4d and from the barrier are longer, spliced wires. The length of the wire splices are shown in Figure 16.

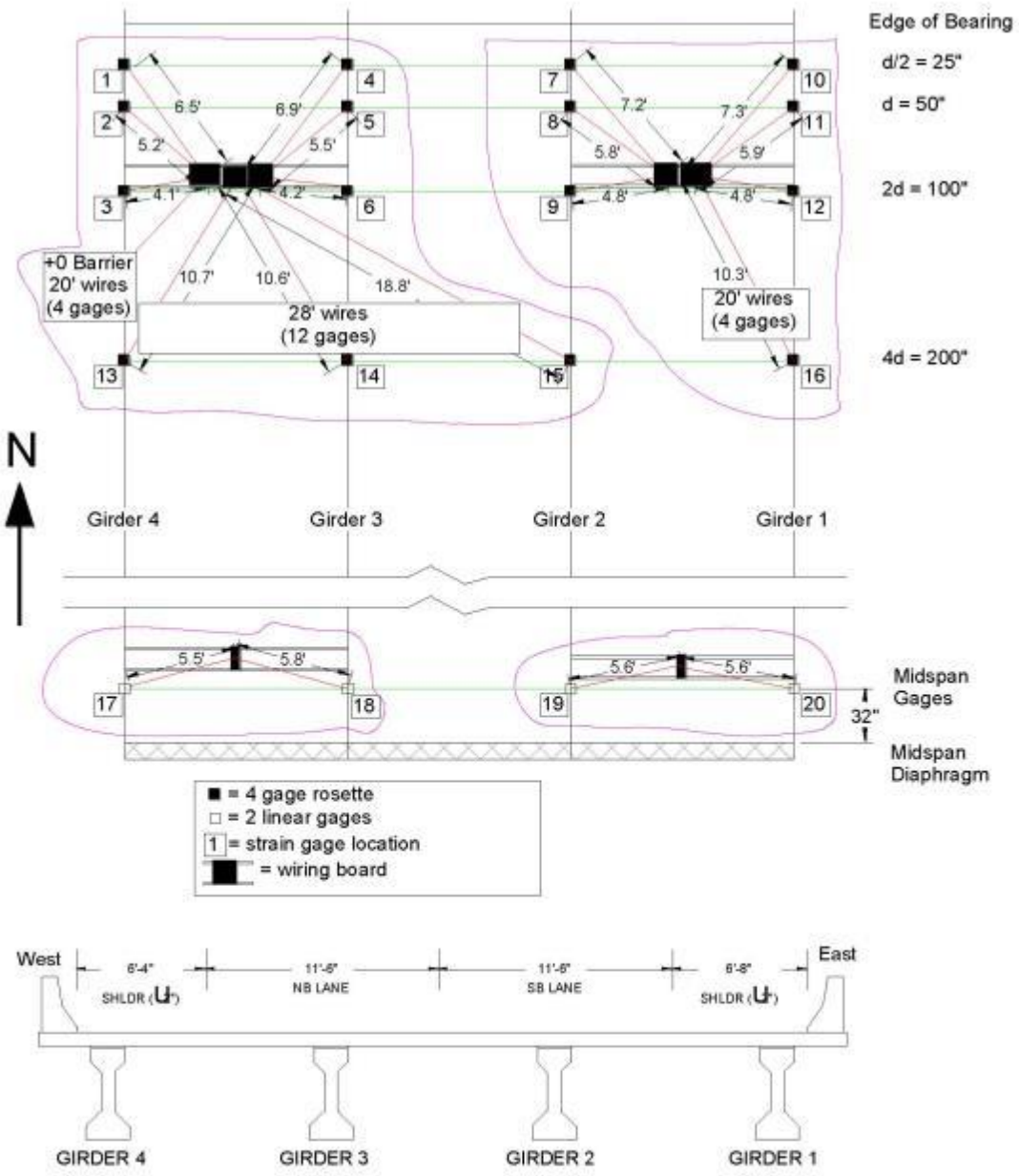

Figure 16. VWG Wiring Diagram

Volunteers and Workers for Bridge 73852 Live Load Tests

Abutment Test Setup – Day 1 (Monday June 25th):

- Van and Brock's car *leave* University Avenue Parking Ramp at **6 am (be there earlier)**
- Bridge shoulder closure with UMN cones

Ben Dymond (612-219-1548)	Operations Director
Andrew Morgan (715-214-4596)	Prep Team-Ladder
Brock Hedegaard (406-489-1985)	Install Team 1-Support
Daniel Morton (574-210-3653)	Install Team 1-Ladder
Damien Teichner (612-644-4745)	Install Team 2-Support
Katsiaryna (Kate) Talkachova (315-254-3693)	Prep Team-Support
Andrew Gastineau (507-273-6683)	Install Team 2-Ladder
Paul Bergson (651-470-9732)	Safety Coordinator & Deck Shoulder Marking
Carol Shield	Safety Coordinator & Pictures

Abutment Truck Tests – Day 2 (Tuesday June 26th):

- Van and Andrew G's car *leave* University Avenue Parking Ramp at **5 am (be there earlier)**
- Bridge lane closure and periodic bridge closures with MnDOT

Ben Dymond (612-219-1548)	Operations/Truck Director
Andrew Morgan (715-214-4596)	Data Sheet Recorder
Brock Hedegaard (406-489-1985)	Data Collection
Damien Teichner (612-644-4745)	Visual Shear Crack Inspector & Pictures
Andrew Gastineau (507-273-6683)	Data Sheet Recorder & Pictures
Carol Shield	Safety Coordinator & Visual Shear Crack Inspector

Pier Instrumentation – Day 3 (Wednesday June 27th):

- Van and Ben's (or Brocks's) car *leave* University Avenue Parking Ramp at **5 am (be there earlier)**
- Bridge lane closure with MnDOT snooper for gage installation

Ben Dymond (612-219-1548)	Operations Director & Pictures
Andrew Morgan (715-214-4596)	Prep/Install Team
Brock Hedegaard (406-489-1985)	Prep/Install Team
Damien Teichner (612-644-4745)	Prep/Install Team
Katsiaryna (Kate) Talkachova (315-254-3693)	Prep/Install Team & Wiring Guru
Cathy French (763-227-6575)	Safety Coordinator

Pier Truck Tests & Gage Removal – Day 4 (Thursday June 28th):

- Van and Ben's (or Brocks's) car *leave* University Avenue Parking Ramp at **5 am (be there earlier)**
- Bridge lane closure and periodic bridge closures with MnDOT, snooper for uninstalling gages
    - All volunteers for uninstallation

Ben Dymond (612-219-1548)	Operations/Truck Director
Andrew Morgan (715-214-4596)	Data Sheet Recorder
Brock Hedegaard (406-489-1985)	Data Collection
Damien Teichner (612-644-4745)	Shear Crack Inspector & Pictures
Daniel Morton (574-210-3653)	Data Sheet Recorder
Cathy French (763-227-6575)	Safety Coordinator & Shear Crack Inspection (if feasible)

Appendix A –Record Sheets

(next page)

Field Testing Bridge 73852 Deck Marking Record Sheet

Abutment Girders and Transverse Testing Locations

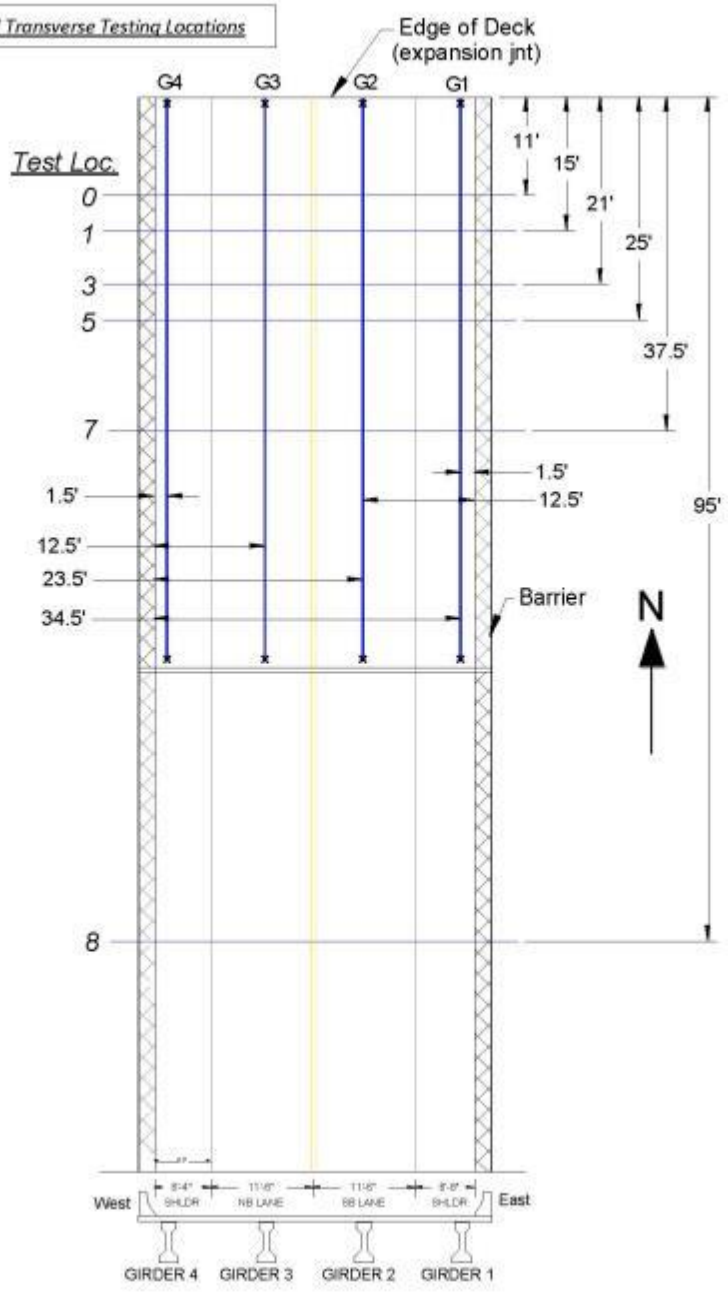

19

Field Testing Bridge 73852 Deck Marking Record Sheet

Driver's Tire Longitudinal Lines (7'-2" wheel spacing)

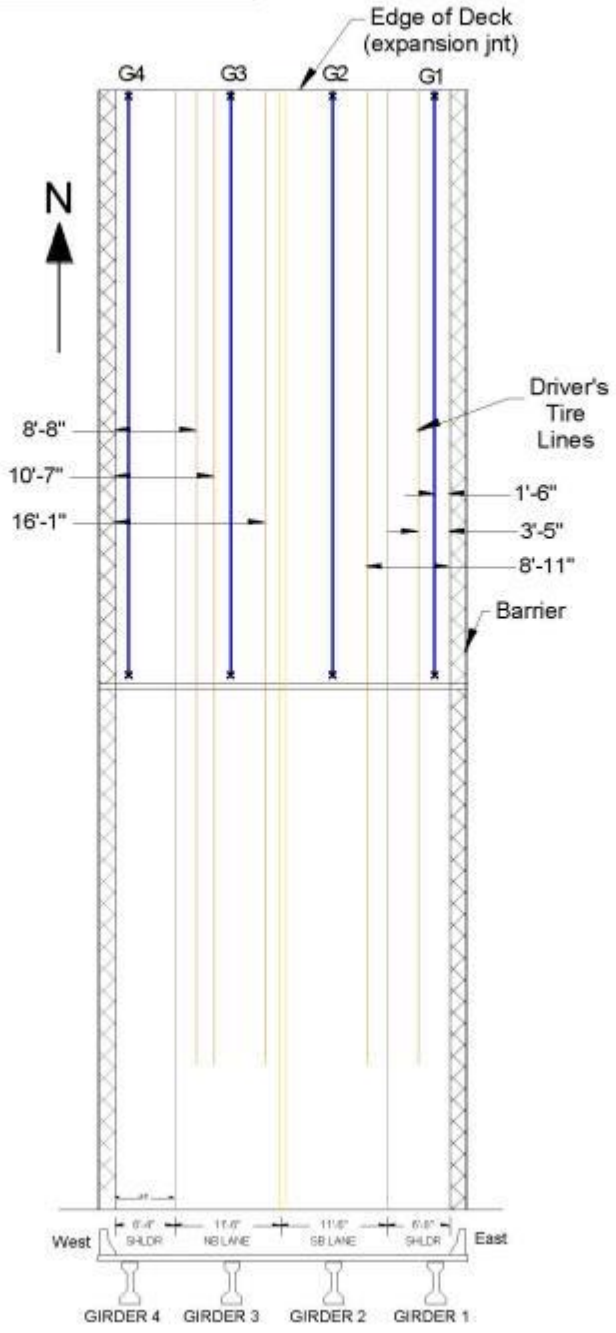

Field Testing Bridge 73852 Deck Marking Record Sheet

Pier Transverse Testing Locations

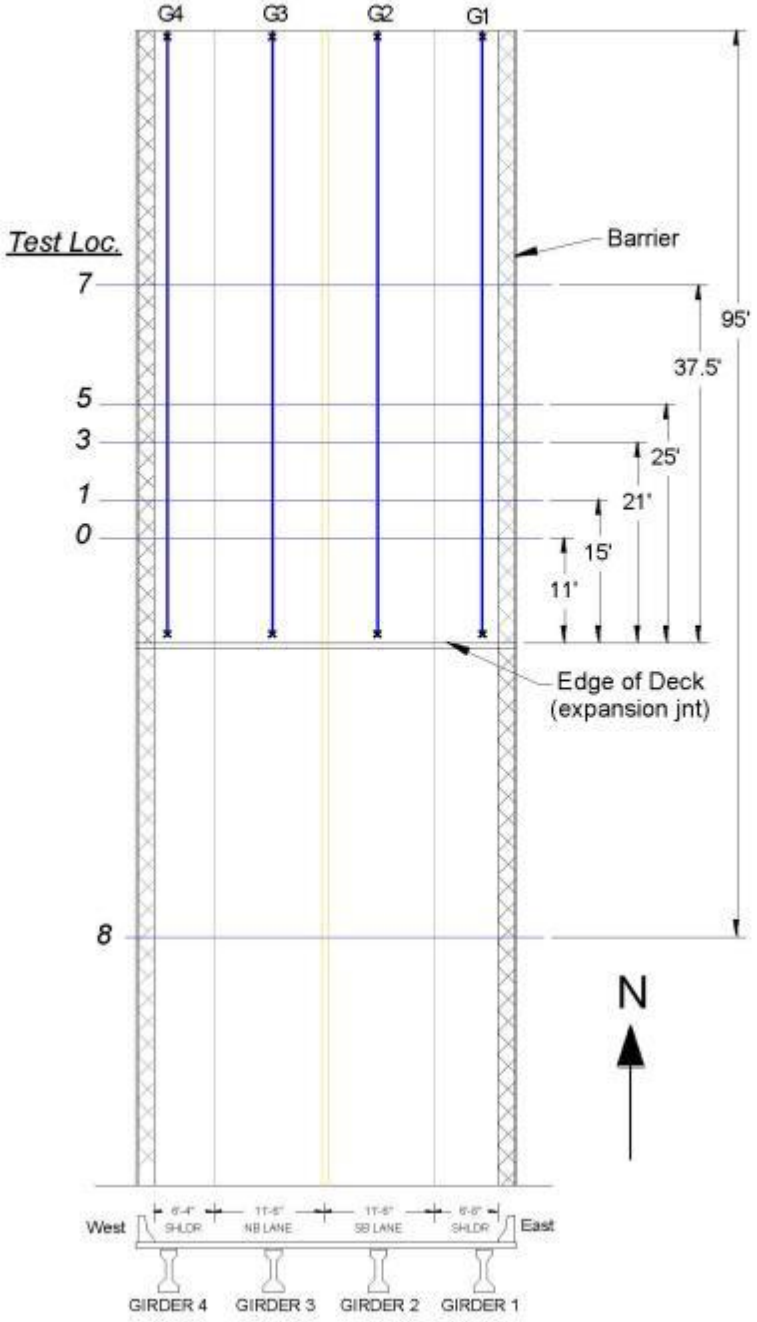

G.3 Bridge 73872 Testing Protocol

Bridge Information:

Bridge Number:	73872
Starting Date/Time:	August 6th 2012, 6:00 am
Location:	County Road 159 over I-94 WB, in Stearns County, near St. Cloud, MN (Decimal degrees of Latitude, Longitude: 45.601132,-94.389227)
Year Built:	1976
End Diaphragm:	Full Depth
Skew:	0 degrees
End Span Geometry:	4 girders spaced at 14'-8" with span length 58 ft
d_s:	50 in.

Objectives for Bridge 73872 Live Load Tests

Objective 1: Static Load Testing

Static tests are planned to verify transverse shear distribution near the north abutment and the northern most pier (pier 3), if accessible by bucket truck or manlift. Shear distribution tests will be performed on the north end span of the structure (span 4), shown in Figure 1, and will include loading the structure in both the north and south bound lanes. Load will be applied with two MnDOT sand trucks filled so that their total weight is approximately 50 kips each. The trucks will be parked on the bridge at various locations for data collection. Additional static tests are planned to verify transverse flexural distribution at midspan. Two strain gages will be placed at midspan of each girder to determine the flexural strain and vertical strain distribution (for neutral axis calculation).

Objective 2: Visual Inspection of End Regions for Shear Cracks

Bridge 73872 has an inventory shear rating less than unity. Applying maximum truck load provides the opportunity to investigate possible shear cracks that may exist on the girders. These girders would most likely only be visible under the application of load. Visual inspection will be done on both an interior and exterior girder when the back-to-back truck configuration is parked at a maximum applied shear location. Any visible shear cracks will be recorded and photographed.

Figure 1. Bridge 73872

Planning for Bridge 73872 Live Load Tests

The truck tests are planned to occur between August 6 and August 25, 2012. Instrumentation of all bridge girders near the abutment will occur in the first day. Truck tests near the abutment will all occur in the second day. The third day will be used to instrument all girders near the first interior pier using a snooper truck. Truck tests near the first interior pier will occur on the fourth day. The fourth day also includes removing the pier strain gages applied with a snooper truck. The tests should be completed rain or shine unless the weather is terrible. The following tasks need to be completed in preparation for the truck tests on day two. The responsibility for each of the tasks is identified below.

Task 1: Mark Truck Locations (UMN)

The locations where the trucks are to be positioned for the various static tests should be marked on the bridge prior to the truck tests. The use of marking paint should be used for a semi-permanent testing profile which will provide an outline for chalking the test grid on the day of testing.

Task 2: Arrange for Loaded Trucks (MnDOT)

Two loaded sand trucks will be needed for performing the static tests. Each truck should nominally weigh 50 kips and have a front axle to back axle length of approximately 19'-8". Each truck will need to be weighed prior to testing and after testing. Weight information should be obtained on the front axle load (by itself), rear most rear axle (by itself), the rear tandem axle load (all four back wheels), and total load for each truck. A volunteer should fill out the "truck record sheet." The trucks should be tarped over the course of the testing week to assure that no rain adds weight to the truck.

Task 3: Plan and Implement Traffic Control (MnDOT)/ (UMN)

Day 1 – Instrumentation: The bridge does not need to be closed at all, but UMN will close the shoulder using cones to mark the deck.

Day 2 – Truck Tests: The bridge will need to be periodically closed during each static test (which should last approximately 15 minutes). Scheduled tests must take place when MnDOT traffic control crews are at the site, between 6 AM and 4:30 PM, for a total of 10.5 hours of partial bridge closure. The first testing day will include all static tests done near the north abutment.

Day 3 – Instrumentation: The bridge will need single lane closures to allow for the use of a snooper truck to instrument all four girders near the pier. During this lane closure, marking of the deck testing grid will also take place.

Day 4 – Truck Tests: The bridge will need to be periodically closed during each static test (which should last approximately 15 minutes). A bumper truck and cones will be required on I-94 WB to protect the computer van from oncoming traffic. Scheduled tests must take place when MnDOT traffic control crews are at the site, between 6 AM and 4:30 PM, for a total of 10.5 hours of partial bridge closure. The second day of testing will consist of static tests performed near the first pier. The same loaded sand trucks should be used for all tests, regardless of day. Near the end of the day, truck testing will stop so that instrumentation can be removed using the snooper truck.

Schedule for Bridge 73872 Live Load Tests

Testing should be completed in four days. The schedule for the first day of testing is presented in Table 1. The diagrams that describe the testing locations for each test description are shown in Figure 2 through Figure 5.

Row	Time	Start Time	Test	Duration (min)	Details	Priority	End Time	Traffic Control	Notes
1	6:00 AM		Abutment Start	75	Begin MnDOT travel & traffic control	0		None	
2	7:15 AM		Zero 1	15	Take measurements with no load before traffic control	0		None	
3	7:30 AM		G4 BB Loc 3	15	G4 back-to-back, rear axle south truck at Loc 3	1		Periodically Close Bridge	
4	7:45 AM		G4 ST Loc 0	15	G4 single north truck, rear axle positioned at Loc 0	1		"	
4	8:00 AM		G4 BB Loc 5	15	G4 back-to-back, rear axle south truck at Loc 5	1		"	
5	8:15 AM		G4 ST Loc 1	10	G4 single north truck, rear axle positioned at Loc 1	1		"	
6	8:25 AM		Zero 2	15	Take measurements with no load	1		"	
7	8:40 AM		G4 BB Loc 7	15	G4 back-to-back, rear axle south truck at Loc 7	1		"	
8	8:55 AM		G4 SS Loc 7	15	G4 side-by-side, rear axles centered at Loc 7	2		"	
9	9:10 AM		G3 BB Loc 3	10	G3 back-to-back, rear axle south truck at Loc 3	1		"	repeatability test
10	9:20 AM		Zero 3	15	Take measurements with no load	1		"	
11	9:35 AM		G3-G4 BB Loc 3	15	G3-G4 split back-to-back, rear axle south truck at Loc 3	1		"	
12	9:50 AM		G3-G4 ST Loc 0	15	G3-G4 split single north truck, rear axle at Loc 0	1		"	
13	10:05 AM		G3-G4 BB Loc 5	15	G3-G4 split back-to-back, rear axle south truck at Loc 5	1		"	
14	10:20 AM		G3-G4 ST Loc 1	10	G3-G4 split single north truck, rear axle at Loc 1	1		"	
15	10:30 AM		Zero 4	15	Take measurements with no load	1		"	
16	10:45 AM		G3-G4 BB Loc 7	15	G3-G4 split back-to-back, rear axle south truck at Loc 7	1		"	
17	11:00 AM		G3-G4 SS Loc 7	10	G3-G4 split side-by-side, rear axles centered at Loc 7	2		"	
18	11:10 AM		G3-G4 SS Loc 8	10	G3-G4 split side-by-side, rear axles centered at Loc 8	2		"	
19	11:20 AM		G4 BB Loc 3	10	G4 back-to-back, rear axle south truck at Loc 3	1		"	repeatability test
20	11:30 AM		Zero 5	15	Take measurements with no load	1		"	
21	11:45 AM		G3 BB Loc 3	15	G3 back-to-back, rear axle south truck at Loc 3	1		"	
22	12:00 PM		G3 ST Loc 0	15	G3 single north truck, rear axle at Loc 0	1		"	
23	12:15 PM		G3 BB Loc 5	15	G3 back-to-back, rear axle south truck at Loc 5	1		"	
24	12:30 PM		G3 ST Loc 1	15	G3 single north truck, rear axle at Loc 1	1		"	
25	12:45 PM		G3 BB Loc 7	10	G3 back-to-back, rear axle south truck at Loc 7	1		"	
26	12:55 PM		Zero 6	15	Take measurements with no load	1		"	
27	1:10 PM		G2 BB Loc 3	10	G2 back-to-back, rear axle south truck at Loc 3	1		"	
28	1:20 PM		G2 BB Loc 5	15	G2 back-to-back, rear axle south truck at Loc 5	1		"	
29	1:35 PM		G2-G1 BB Loc 3	10	G2-G1 split back-to-back, rear axle south truck at Loc 3	2		"	
30	1:45 PM		G2-G1 BB Loc 5	10	G2-G1 split back-to-back, rear axle south truck at Loc 5	1		"	
31	1:55 PM		Zero 7	15	Take measurements with no load	1		"	
32	2:10 PM		G1 BB Loc 3	10	G1 back-to-back, rear axle south truck at Loc 3	2		"	
33	2:20 PM		G1 BB Loc 5	15	G1 back-to-back, rear axle south truck at Loc 5	1		"	
34	2:35 PM		G3 BB Loc 3	15	G3 back-to-back, rear axle south truck at Loc 3	1		"	repeatability test
35	2:50 PM		G3-G4 BB Loc 3	15	G3-G4 split back-to-back, rear axle south truck at Loc 3	1		"	repeatability test
36	3:05 PM		G4 BB Loc 3	10	G4 back-to-back, rear axle south truck at Loc 3	1		"	repeatability test
37	3:15 PM		Zero 8	75	Take measurements with no load, MnDOT leaves	0		Remove	
38	4:30 PM		Day 2 Complete		Testing complete and traffic control removed	0		None	

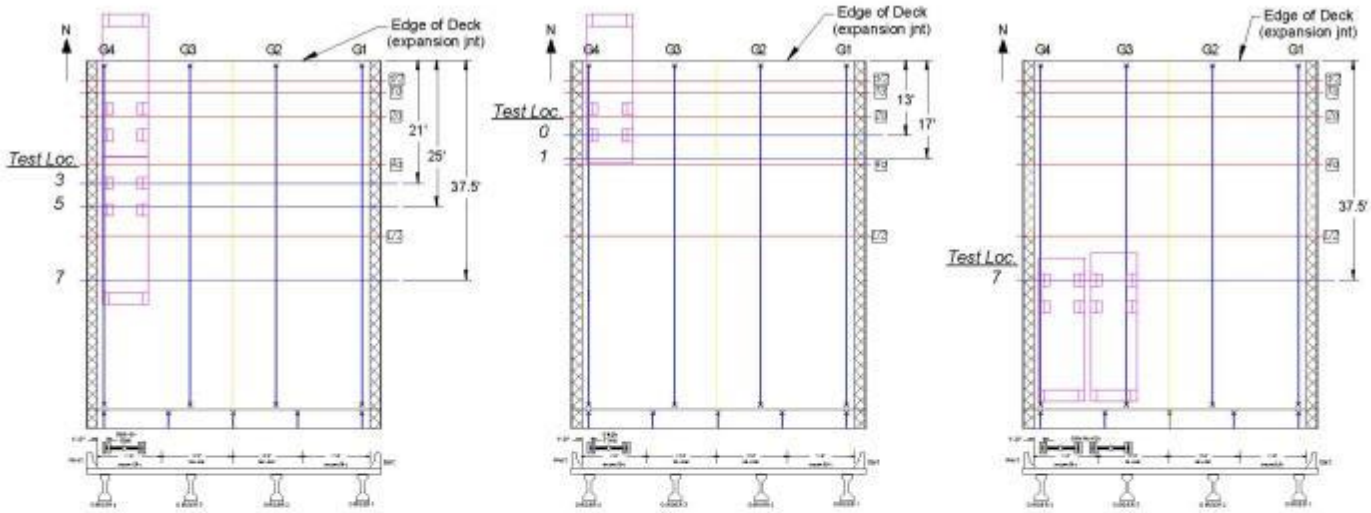

Figure 2. Exterior Girder (G4) Abutment Testing Locations

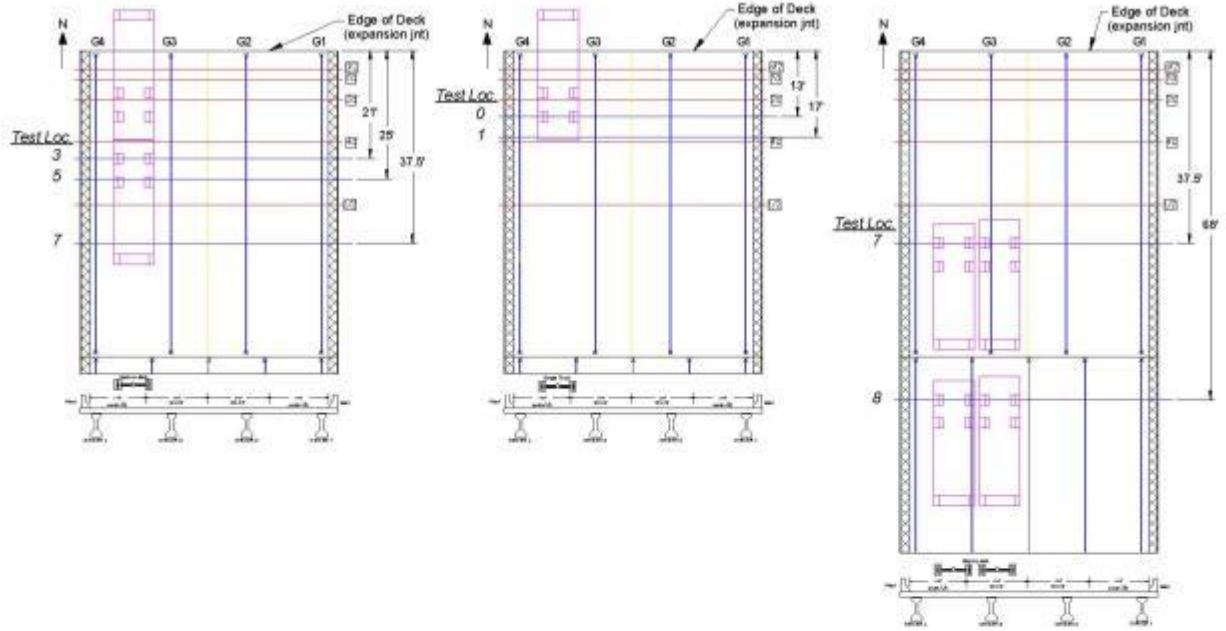

Figure 3. Exterior-Interior (G4-G3) Split Abutment Testing Locations

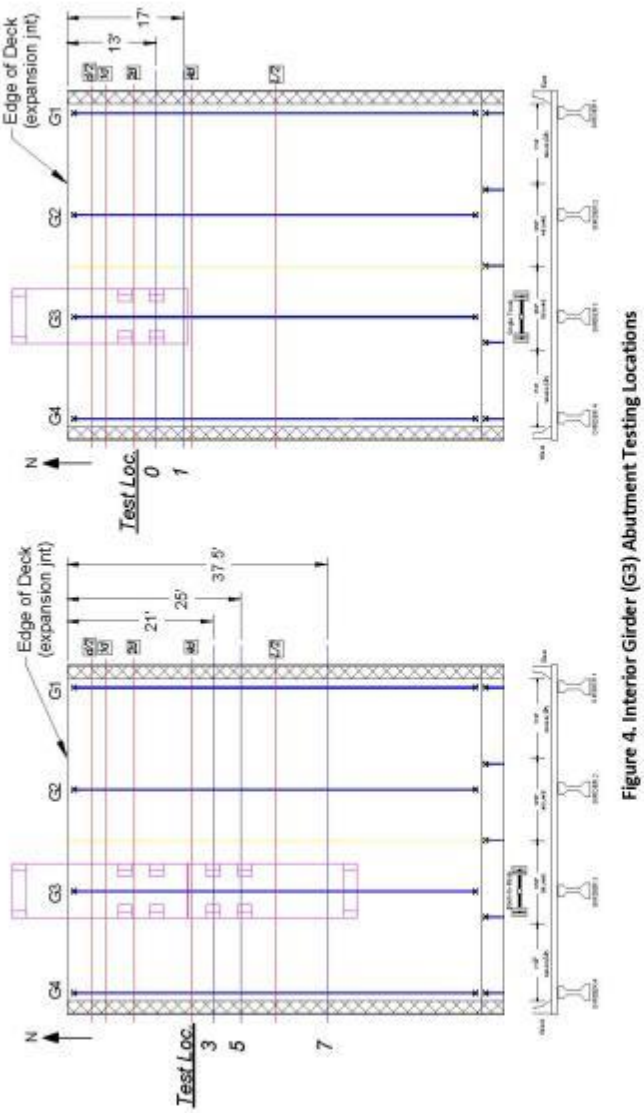

Figure 4. Interior Girder (G3) Abutment Testing Locations

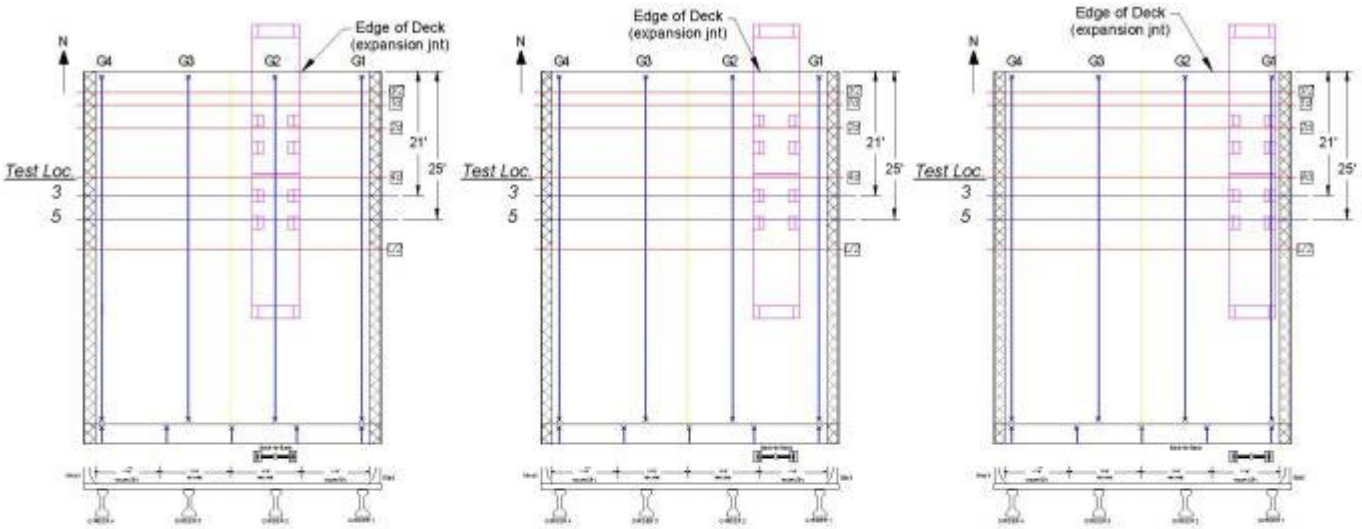

Figure 5. Symmetric Girder (G2, G2-G1 split, and G1) Abutment Testing Locations

The schedule for the second day of testing is presented in Table 2 on the next page. The diagrams that describe the testing locations for each test description are shown in Figure 6 through Figure 9.

Row	Time	Start Time	Test	Duration (min)	Details	Priority	End Time	Traffic Control	Notes
1	6:00 AM		Abutment Start	120	Begin MnDOT travel & traffic control	0		None	
2	8:00 AM		Zero 1	15	Take measurements with no load before traffic control	0		None	
3	8:15 AM		G4 BB Loc 3	10	G4 back-to-back, rear axle north truck at Loc 3	1		Periodically Close Bridge	
4	8:25 AM		G4 ST Loc 0	15	G4 single south truck, rear axle positioned at Loc 0	1		"	
5	8:40 AM		G4 BB Loc 5	10	G4 back-to-back, rear axle north truck at Loc 5	1		"	
6	8:50 AM		G4 ST Loc 1	10	G4 single south truck, rear axle positioned at Loc 1	1		"	
7	9:00 AM		Zero 2	15	Take measurements with no load	1		"	
8	9:15 AM		G4 BB Loc 7	15	G4 back-to-back, rear axle north truck at Loc 7	1		"	
9	9:30 AM		G3 BB Loc 3	15	G3 back-to-back, rear axle north truck at Loc 3	1		"	repeatability test
10	9:45 AM		G3-G4 BB Loc 3	10	G3-G4 split back-to-back, rear axle north truck at Loc 3	1		"	
11	9:55 AM		G3-G4 ST Loc 0	15	G3-G4 split single south truck, rear axle at Loc 0	1		"	
12	10:10 AM		G3-G4 BB Loc 5	10	G3-G4 split back-to-back, rear axle north truck at Loc 5	1		"	
13	10:20 AM		G3-G4 ST Loc 1	10	G3-G4 split single south truck, rear axle at Loc 1	1		"	
14	10:30 AM		Zero 3	15	Take measurements with no load	1		"	
15	10:45 AM		G3-G4 BB Loc 7	15	G3-G4 split back-to-back, rear axle north truck at Loc 7	1		"	
16	11:00 AM		G3-G4 SS Loc 8	15	G3-G4 split side-by-side, rear axles centered at Loc 8	2		"	
17	11:15 AM		G4 BB Loc 3	10	G4 back-to-back, rear axle north truck at Loc 3	1		"	repeatability test
18	11:25 AM		Zero 4	15	Take measurements with no load	1		"	
19	11:40 AM		G3 BB Loc 3	10	G3 back-to-back, rear axle north truck at Loc 3	1		"	
20	11:50 AM		G3 ST Loc 0	15	G3 single south truck, rear axle at Loc 0	1		"	
21	12:05 PM		G3 BB Loc 5	10	G3 back-to-back, rear axle north truck at Loc 5	1		"	
22	12:15 PM		G3 ST Loc 1	15	G3 single south truck, rear axle at Loc 1	1		"	
23	12:30 PM		G3 BB Loc 7	10	G3 back-to-back, rear axle north truck at Loc 7	1		"	
24	12:40 PM		Zero 5	15	Take measurements with no load	1		"	
25	12:55 PM		G2 BB Loc 5	15	G2 back-to-back, rear axle north truck at Loc 5	1		"	
26	1:10 PM		G2-G1 BB Loc 5	15	G2-G1 split back-to-back, rear axle north truck at Loc 5	1		"	
27	1:25 PM		G1 BB Loc 5	15	G1 back-to-back, rear axle north truck at Loc 5	1		"	
28	1:40 PM		G3-G4 BB Loc 3	15	G3-G4 split back-to-back, rear axle north truck at Loc 3	1		"	repeatability test
29	1:55 PM		G3-G4 BB Loc 3 R	10	G3-G4 split back-to-back, rear axle north truck at Loc 3	2		"	repeatability test
30	2:05 PM		Zero 6	10	Take measurements with no load	1		"	
31	2:15 PM		De-Instrument	90	Snooper truck used to take down pier instrumentation	0		"	
32	3:45 PM		Stop Traffic Control	45	MnDOT traffic control leaves	0		Remove	
33	4:30 PM		Day 4 Complete		Testing complete and traffic control removed	0		None	

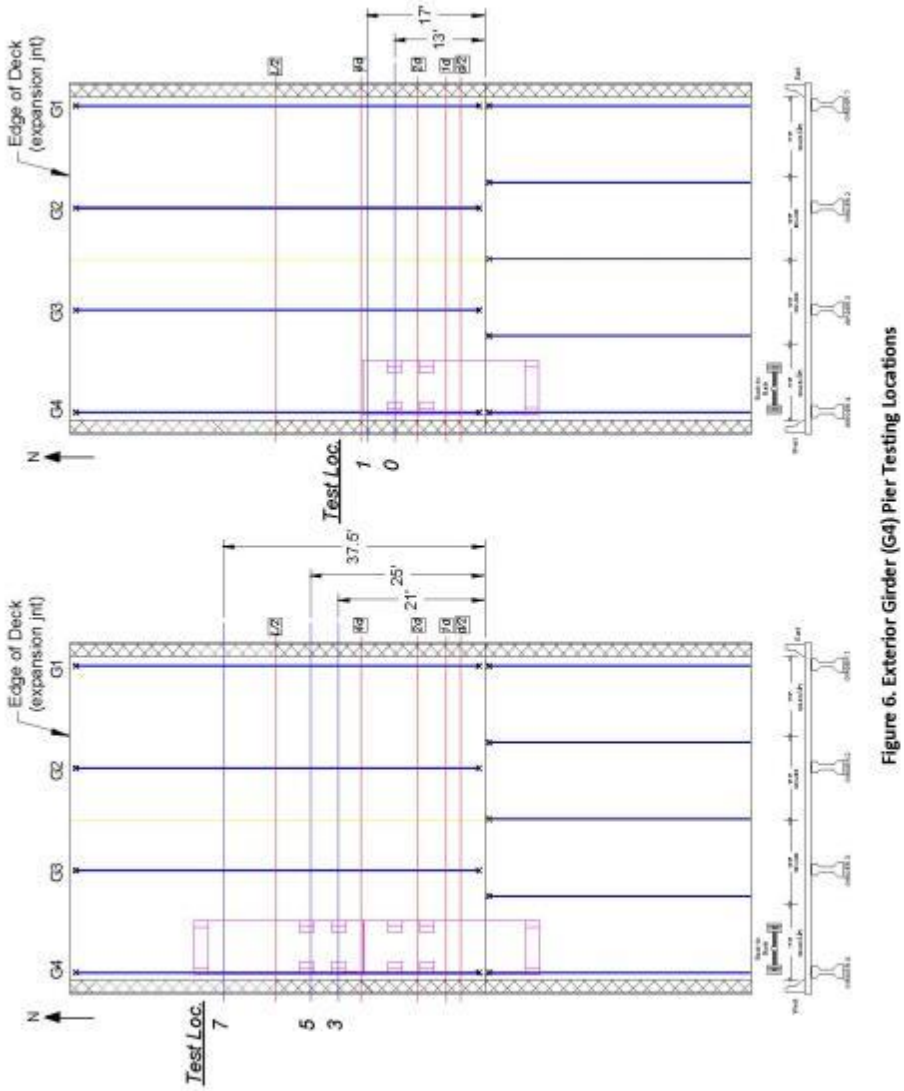

Figure 6. Exterior Girder (G4) Pier Testing Locations

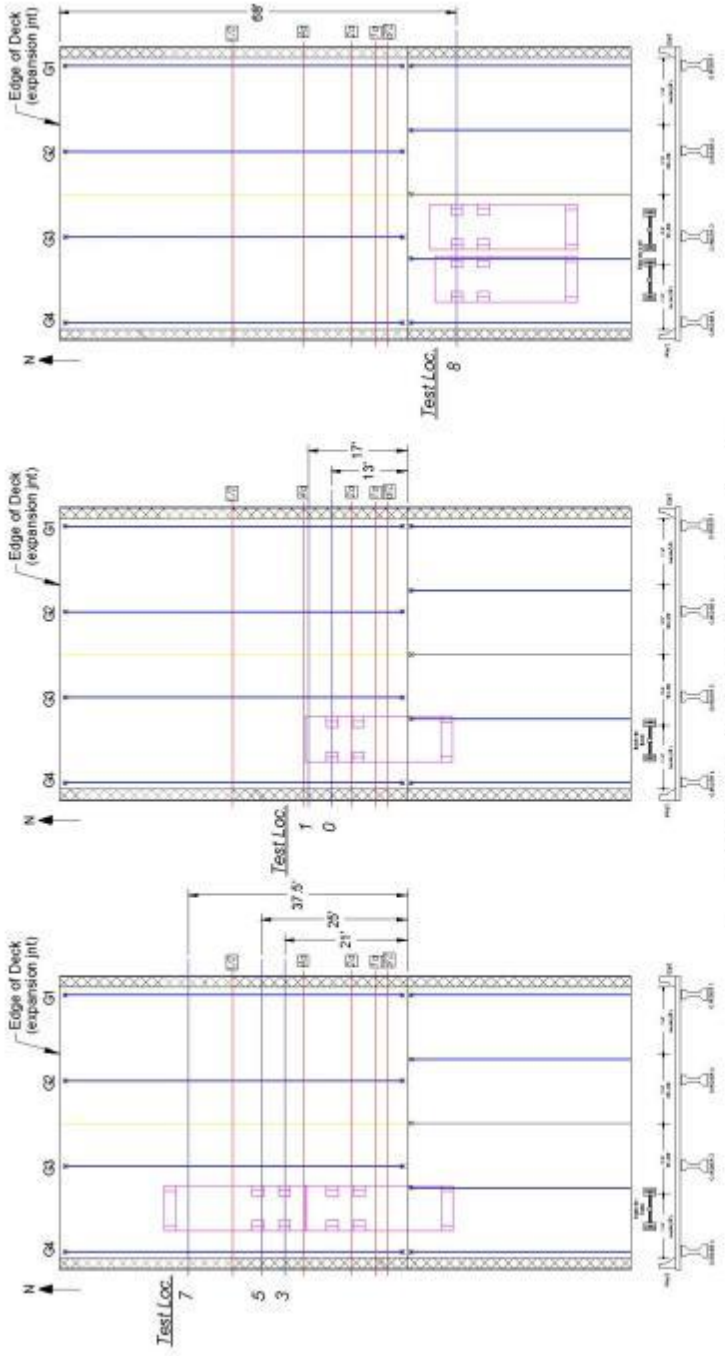

Figure 7. Exterior-Interior (G4-G3) Split Pier Testing Locations

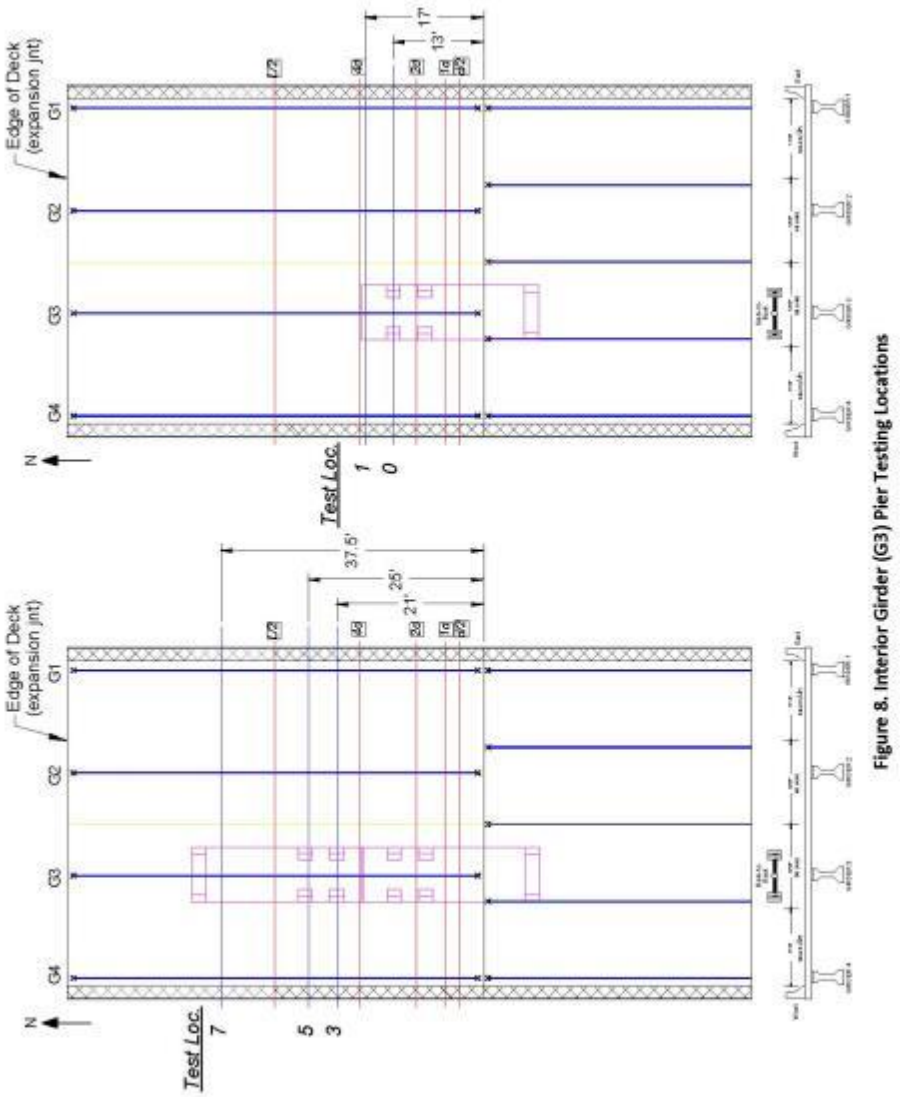

Figure 8. Interior Girder (G3) Pier Testing Locations

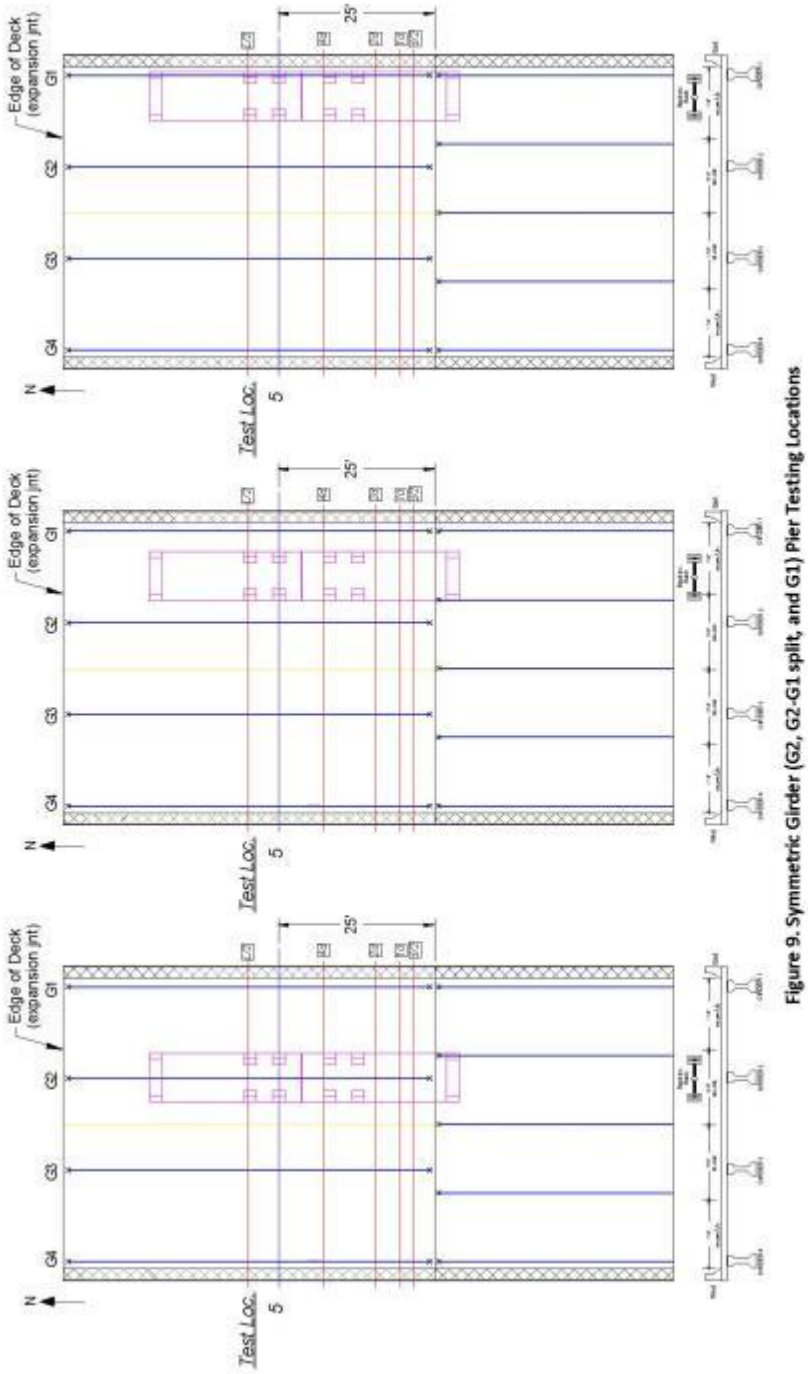

Figure 9. Symmetric Girder (G2, G2-G1 split, and G1) Pier Testing Locations

Instrumentation and Data Collection for Bridge 73872 Live Load Tests

For all static testing, Geokon vibrating wire strain gage data will be collected using a Campbell Scientific CR1000 data acquisition system. All channels will be scanned five times per truck stop which takes approximately 8 minutes.

Instrumentation will be installed on all four girders, as labeled in Figure 10 and Figure 11 and the western barrier. Girder instrumentation plans are shown in Figure 12 through Figure 15.

Figure 10. North Abutment Girder Numbering

Figure 11. Pier 3 Girder Numbering

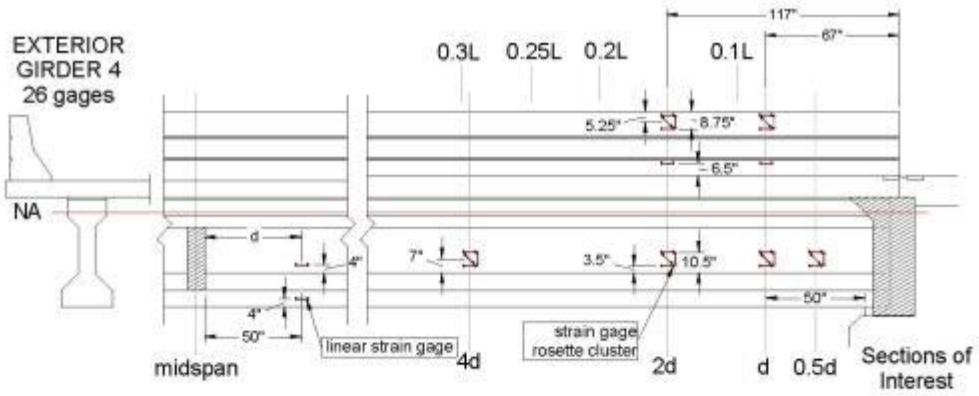

Figure 12. Girder 4 Instrumentation

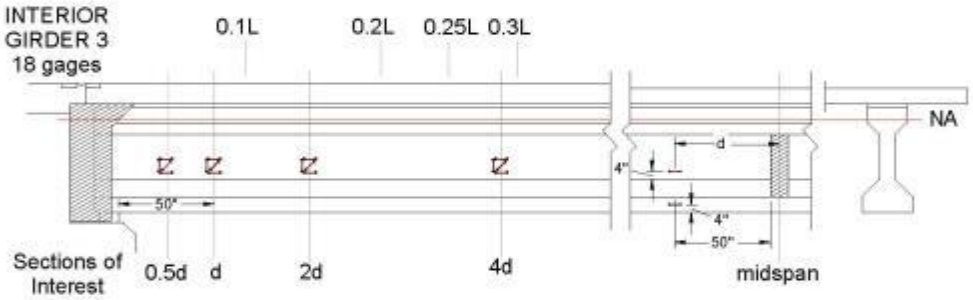

Figure 13. Girder 3 Instrumentation

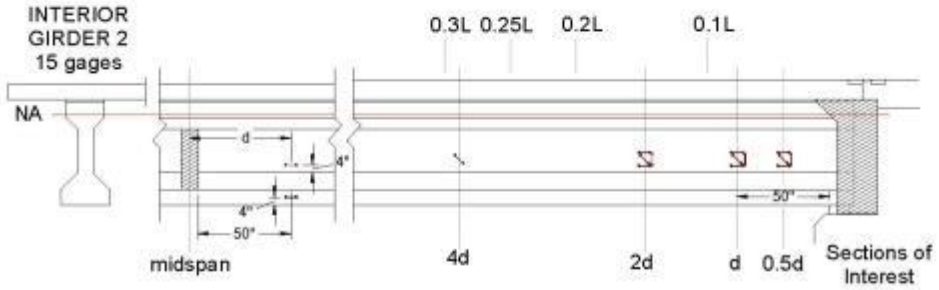

Figure 14. Girder 2 Instrumentation

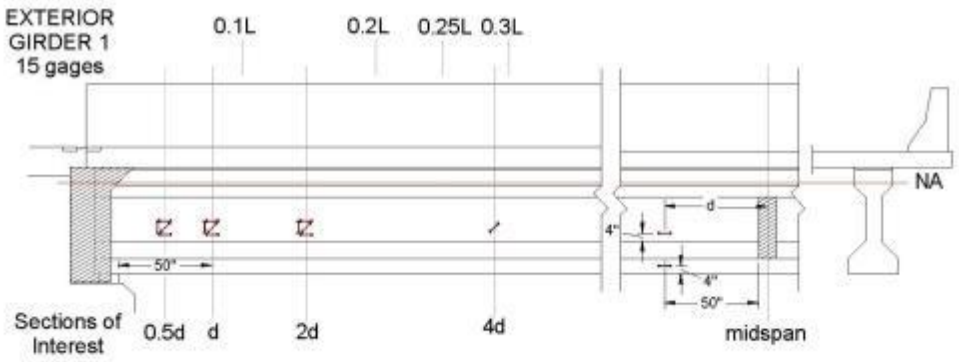

Figure 15. Girder 1 Instrumentation

The vibrating wire strain gage wires are all pulled to a set of boards where the ends are attached to terminal blocks. Most of the strain gage wires are 10 feet in length and will be used near the abutment, as shown in Figure 16. The wires running from gages located at 4d, from the barrier, and at midspan are longer, spliced wires. The length of the wire splices are shown in Figure 16.

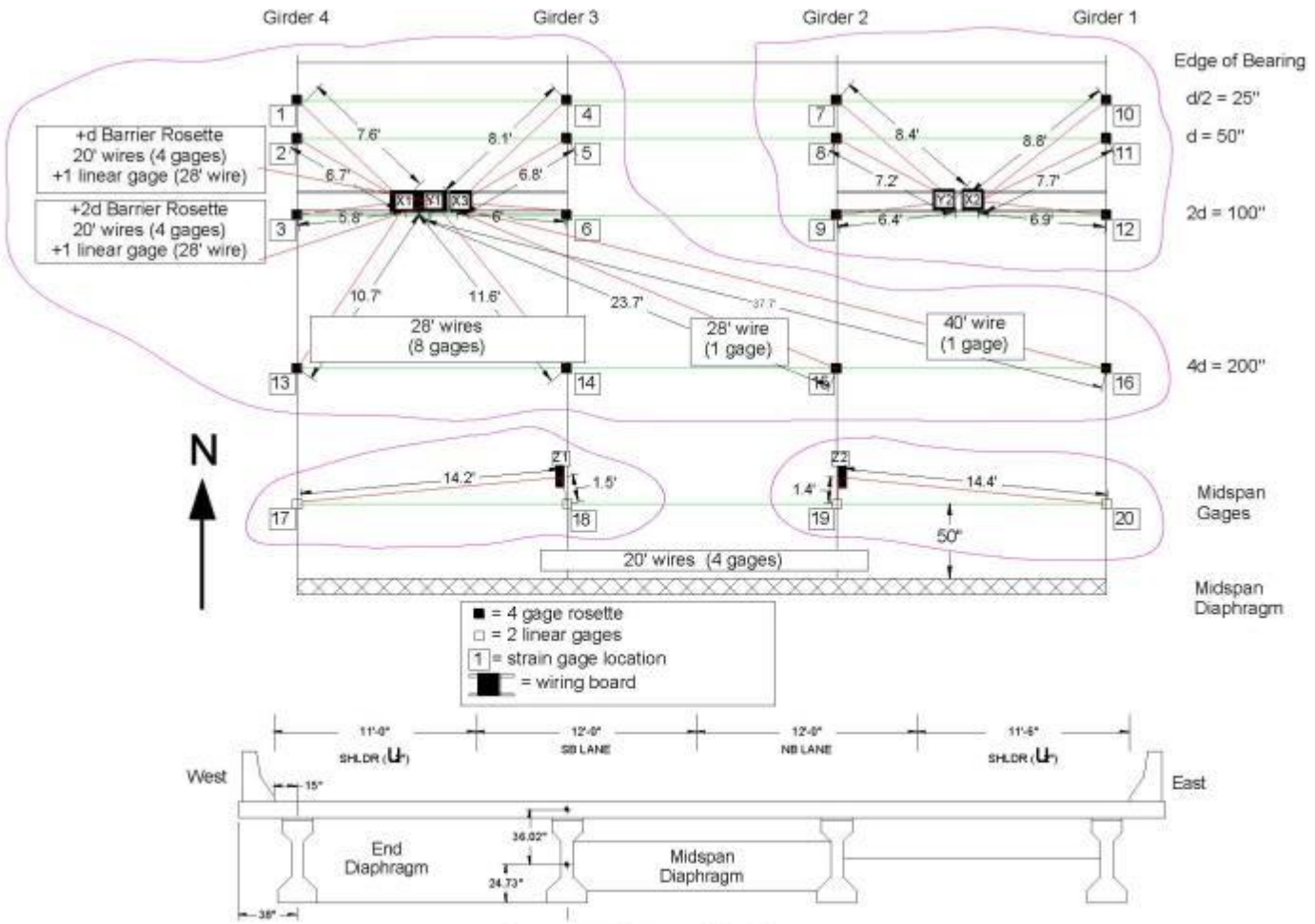

Figure 16. Strain Gage Wiring Diagram

Volunteers and Workers for Bridge 73872 Live Load Tests

Abutment Test Setup – Day 1 (Monday August 6th):

- Van and Daniel's car *leave* CivE Loading Dock at **6 am (be there earlier)**
- Bridge shoulder closure with UMN cones

Ben Dymond (612-219-1548)	Operations Director & Wiring
Andrew Morgan (715-214-4596)	Prep Team-Ladder
Brock Hedegaard (406-489-1985)	Install Team 1-Support
Daniel Morton (574-210-3653)	Install Team 1-Ladder
Damien Teichner (612-644-4745)	Install Team 2-Support
Brian Mathys (651-235-0744)	Prep Team-Support
Andrew Gastineau (507-273-6683)	Install Team 2-Ladder & Deck Shoulder Marking
Rachel Gaulke (651-336-6042)	Safety Coordinator & Deck Shoulder Marking

Abutment Truck Tests – Day 2 (Tuesday August 7th):

- Van and Brock's car *leave* CivE Loading Dock at **5 am (be there earlier)**
- Bridge lane closure and periodic bridge closures with MnDOT

Ben Dymond (612-219-1548)	Operations/Truck Director & Shear Crack Inspector
Andrew Morgan (715-214-4596)	Data Sheet Recorder
Brock Hedegaard (406-489-1985)	Data Collection
Brian Mathys (651-235-0744)	Data Sheet Recorder & Pictures
Cathy French (763-227-6575)	Safety Coordinator

Pier Instrumentation – Day 3 (Wednesday August 8th):

- Van and Ben's (or Brian's) car *leave* CivE Loading Dock at **5 am (be there earlier)**
- Bridge lane closure with MnDOT snooper for gage installation

Ben Dymond (612-219-1548)	Operations Director & Install Team
Andrew Morgan (715-214-4596)	Prep Team
Damien Teichner (612-644-4745)	Install Team
Brian Mathys (651-235-0744)	Prep Team & Pictures
Cathy French (763-227-6575)	Safety Coordinator

Pier Truck Tests & Gage Removal – Day 4 (Thursday August 9th):

- Van and Brocks's (or Daniel's) car *leave* CivE Loading Dock at **5 am (be there earlier)**
- Bridge lane closure and periodic bridge closures with MnDOT, snooper for uninstalling gages
    - All volunteers for uninstallation

Ben Dymond (612-219-1548)	Operations/Truck Director
Andrew Morgan (715-214-4596)	Data Sheet Recorder
Brock Hedegaard (406-489-1985)	Data Collection
Daniel Morton (574-210-3653)	Data Sheet Recorder
Cathy French (763-227-6575)	Safety Coordinator

Appendix A –Record Sheets

(next page)

Abutment Girders and Transverse Testing Locations

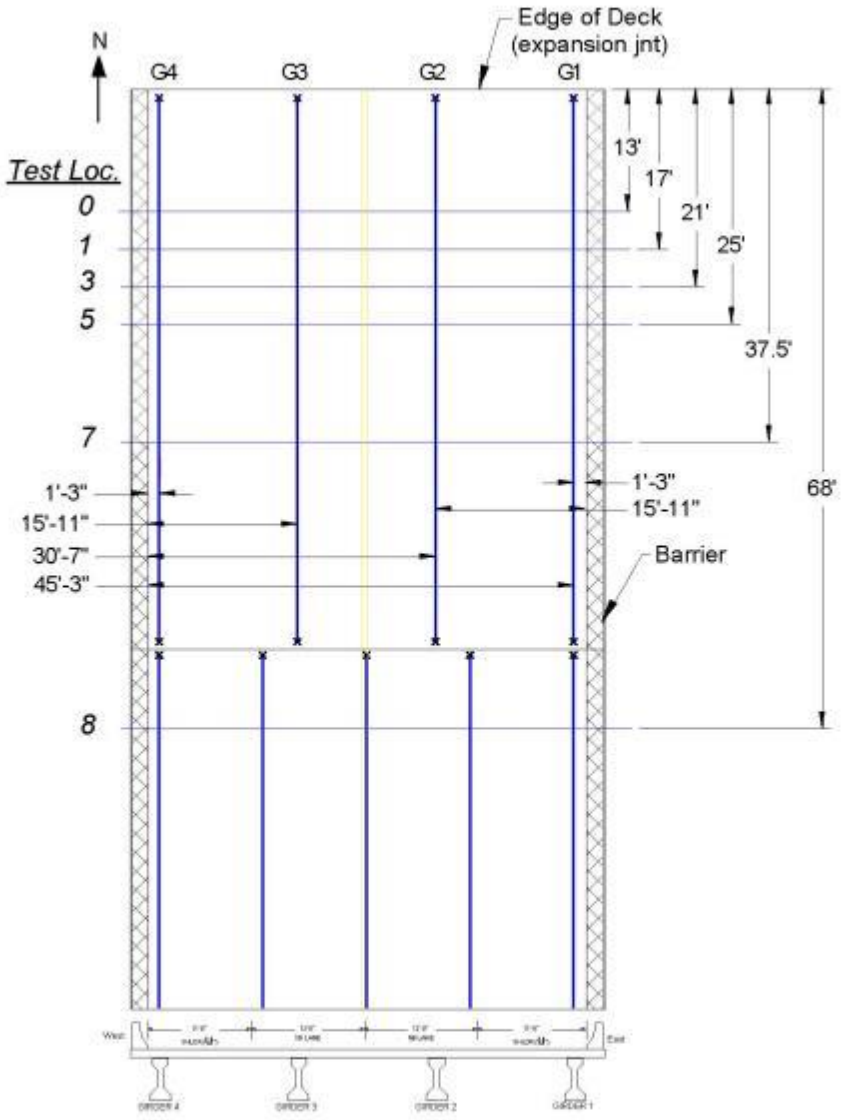

Field Testing Bridge 73872 Girder Board Wiring Record Sheet

Driver's Tire Longitudinal Lines

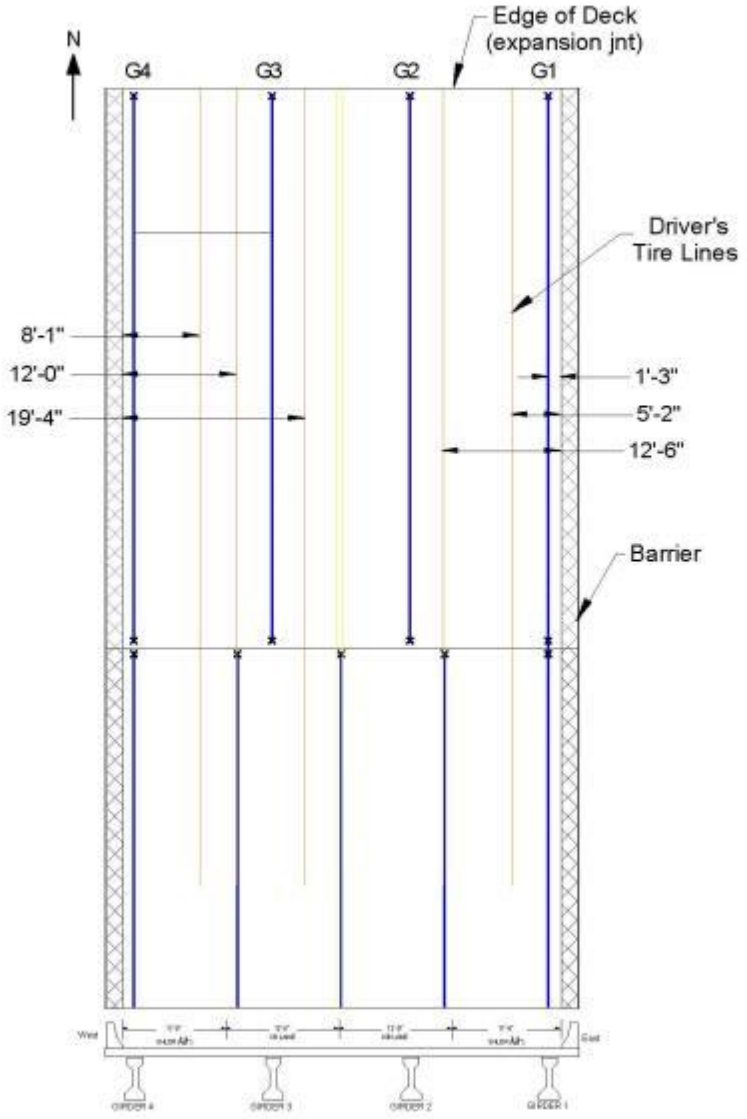

19

Field Testing Bridge 73872

Girder Board Wiring Record Sheet

Pier Transverse Testing Locations

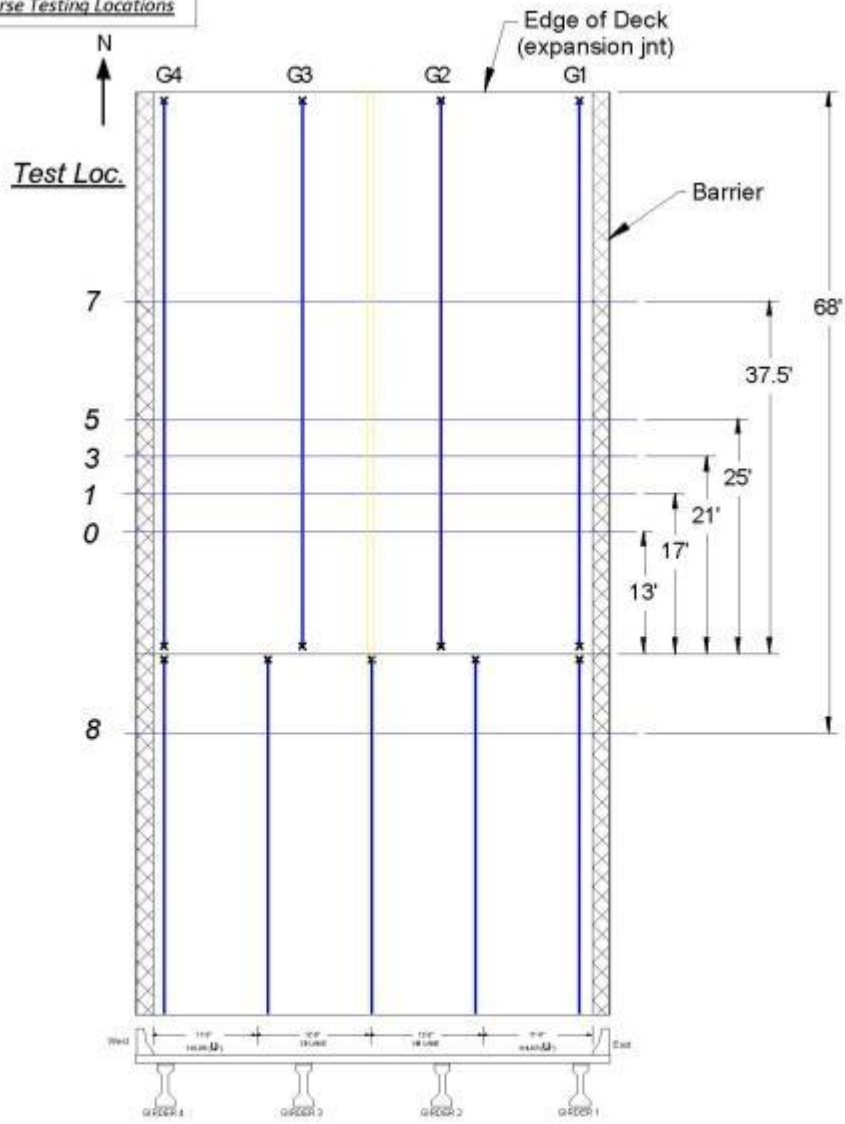

G.4 Bridge 62826 Testing Protocol

Bridge Information:

Bridge Number:	62826
Starting Date/Time:	October 18th 2012, 9:00 am
Location:	I-694 EB over White Bear Ave, in Ramsey County, near North St. Paul, MN (Decimal degrees of Latitude, Longitude: 45.037171,-93.017668)
Year Built:	1969
End Diaphragm:	Full Depth
Skew:	1 degree
End Span Geometry:	4 girders spaced at 12'-6" with span length 38 ft
d_v:	40 in.

Objectives for Bridge 62826 Live Load Tests

Objective 1: Static Load Testing

Static tests are planned to verify transverse shear distribution near the west abutment. Shear distribution tests will be performed on the west end span of the structure (span 1), shown in Figure 1, and will include loading the structure in both east bound lanes. Load will be applied with two MnDOT sand trucks filled so that their total weight is approximately 50 kips each. The trucks will be parked on the bridge at various locations for data collection. Additional static tests are planned to verify transverse flexural distribution near midspan. One supplemental horizontal strain gage will be placed at 4d (which is near d_v away from midspan) of each girder to determine the flexural strain and vertical strain distribution (for neutral axis calculation).

Objective 2: Visual Inspection of End Regions for Shear Cracks

Bridge 62826 has an inventory shear rating less than unity. Applying maximum truck load provides the opportunity to investigate possible shear cracks that may exist on the girders. These girders would most likely only be visible under the application of load. Visual inspection will be done on both an interior and exterior girder when the back-to-back truck configuration is parked at a maximum applied shear location. Any visible shear cracks will be recorded and photographed.

Figure 1. Bridge 62826

Planning for Bridge 62826 Live Load Tests

The truck tests are planned to occur between October 18 and October 19, 2012. Instrumentation of all bridge girders near the abutment will occur between 8 am and 8 pm on October 18th. Truck tests near the abutment will all occur during the night between 8 pm (October 18th) and 5 am (October 19th). The instrumentation will also be removed from the bridge after completion of truck testing on October 19th. The tests should be completed rain or shine unless the weather is terrible. The following tasks need to be completed in preparation for the truck tests overnight. The responsibility for each of the tasks is identified below.

Task 1: Mark Truck Locations (UMN)

The locations where the trucks are to be positioned for the various static tests should be marked on the bridge prior to the truck tests. The use of marking paint should be used for a semi-permanent testing profile which will provide an outline for supplemental chalking prior to night testing.

Task 2: Arrange for Loaded Trucks & Lights (MnDOT)

Two loaded sand trucks will be needed for performing the static tests. Each truck should nominally weigh 50 kips and have a front axle to back axle length of approximately 19'-8". Each truck will need to be weighed prior to testing and after testing. Weight information should be obtained on the front axle load (by itself), rear most rear axle (by itself), the rear tandem axle load (all four back wheels), and total load for each truck. A volunteer should fill out the "truck record sheet." The trucks should be tarped over the course of the testing week to assure that no rain adds weight to the truck.

MnDOT is also responsible for providing construction flood lights to illuminate the bridge deck area during live load tests.

Task 3: Plan and Implement Traffic Control (MnDOT)/ (UMN)

Day – Instrumentation: The bridge is already closed due to construction. No additional traffic control is needed.

Overnight – Truck Tests: The bridge is already closed due to construction. No additional traffic control is needed. Scheduled tests must take place when MnDOT truck crews are at the site, between 7:30 PM and 5:30 AM, for a total of 10 hours of live load testing. The night testing will include all static tests done near the west abutment. Truck testing will stop so that instrumentation can be removed no later than 5:30 AM. MnDOT employees are not needed to remove the instrumentation, but UMN volunteers must not interfere with construction traffic.

Schedule for Bridge 62826 Live Load Tests

Testing should be completed in 24 hours. The schedule for the abutment testing is presented in Table 1. The diagrams that describe the testing locations for each test description are shown in Figure 2 through Figure 5.

Row	Time	Start Time	Test	Duration (min)	Details	Priority	End Time	Traffic Control	Notes
1	7:30 PM		Abutment Start	90	Begin MnDOT travel & traffic control	0		None	
2	9:00 PM		Zero 1	10	Take measurements with no load before traffic control	0		None	
3	9:10 PM		G4 BB Loc 3	15	G4 back-to-back, rear axle south truck at Loc 3	1		Bridge is Closed	
4	9:25 PM		G4 ST Loc 0	15	G4 single north truck, rear axle positioned at Loc 0	1		"	
5	9:40 PM		Zero 2	15	Take measurements with no load	1		"	
6	9:55 PM		G4 BB Loc 5	15	G4 back-to-back, rear axle south truck at Loc 5	1		"	
7	10:10 PM		G4 ST Loc 1	15	G4 single north truck, rear axle positioned at Loc 1	1		"	
8	10:25 PM		G4 BB Loc 7	10	G4 back-to-back, rear axle south truck at Loc 7	1		"	
9	10:35 PM		Zero 3	15	Take measurements with no load	1		"	
*** Save Test Data, Close RTDAQ, Restart RTDAQ and open Flags & Data --- Should prevent tests where not all data is captured ***									
10	10:45 PM		G3 BB Loc 3	15	G3 back-to-back, rear axle south truck at Loc 3	1		"	repeatability test
11	11:00 PM		G3-G4 BB Loc 3	15	G3-G4 split back-to-back, rear axle south truck at Loc 3	1		"	
12	11:15 PM		G3-G4 ST Loc 0	15	G3-G4 split single north truck, rear axle at Loc 0	1		"	
13	11:30 PM		G3-G4 BB Loc 5	15	G3-G4 split back-to-back, rear axle south truck at Loc 5	1		"	
14	11:45 PM		G3-G4 ST Loc 1	15	G3-G4 split single north truck, rear axle at Loc 1	1		"	
15	12:00 AM		G3-G4 BB Loc 7	10	G3-G4 split back-to-back, rear axle south truck at Loc 7	1		"	
16	12:15 AM		Zero 4	15	Take measurements with no load	1		"	
17	12:25 AM		G4 BB Loc 3	15	G4 back-to-back, rear axle south truck at Loc 3	1		"	repeatability test
18	12:40 AM		G3 BB Loc 3	15	G3 back-to-back, rear axle south truck at Loc 3	1		"	
19	12:55 AM		G3 ST Loc 0	15	G3 single north truck, rear axle at Loc 0	1		"	
20	1:10 AM		G3 BB Loc 5	15	G3 back-to-back, rear axle south truck at Loc 5	1		"	
21	1:25 AM		G3 ST Loc 1	15	G3 single north truck, rear axle at Loc 1	1		"	
22	1:40 AM		G3 BB Loc 7	10	G3 back-to-back, rear axle south truck at Loc 7	1		"	
23	1:50 AM		Zero 5	15	Take measurements with no load	1		"	
*** Save Test Data, Close RTDAQ, Restart RTDAQ and open Flags & Data --- Should prevent tests where not all data is captured ***									
24	2:05 AM		G2 BB Loc 3	15	G2 back-to-back, rear axle south truck at Loc 5	1		"	
25	2:20 AM		G2 BB Loc 5	15	G2 back-to-back, rear axle south truck at Loc 5	2		"	
26	2:35 AM		G2-G1 BB Loc 3	15	G2-G1 split back-to-back, rear axle south truck at Loc 5	1		"	
27	2:50 AM		G2-G1 BB Loc 5	10	G2-G1 split back-to-back, rear axle south truck at Loc 5	2		"	
28	3:00 AM		G1 BB Loc 3	15	G1 back-to-back, rear axle south truck at Loc 5	1		"	
29	3:15 AM		G1 BB Loc 5	15	G1 back-to-back, rear axle south truck at Loc 5	2		"	
30	3:30 AM		G3 BB Loc 3	15	G3 back-to-back, rear axle south truck at Loc 3	1		"	repeatability test
31	3:45 AM		G3-G4 BB Loc 3	15	G3-G4 split back-to-back, rear axle south truck at Loc 3	1		"	repeatability test
32	4:00 AM		G4 BB Loc 3	10	G4 back-to-back, rear axle south truck at Loc 3	1		"	repeatability test
33	4:10 AM		Zero 6	10	Take measurements with no load	0		Remove	
34	4:20 AM		Day 2 Complete		Testing complete and MnDOT leaves	0		None	

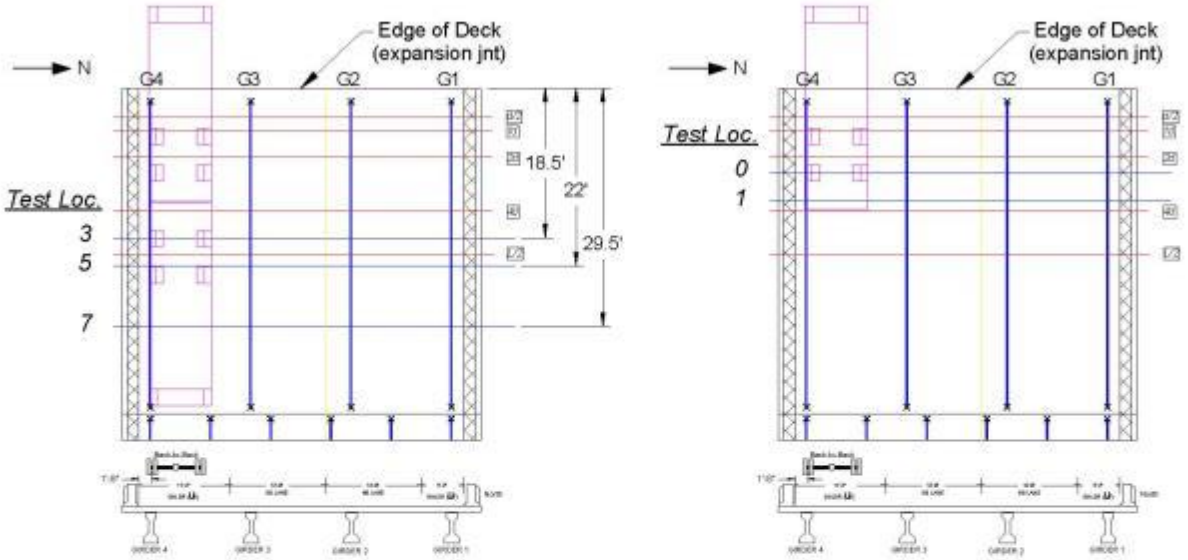

Figure 2. Exterior Girder (G4) Abutment Testing Locations

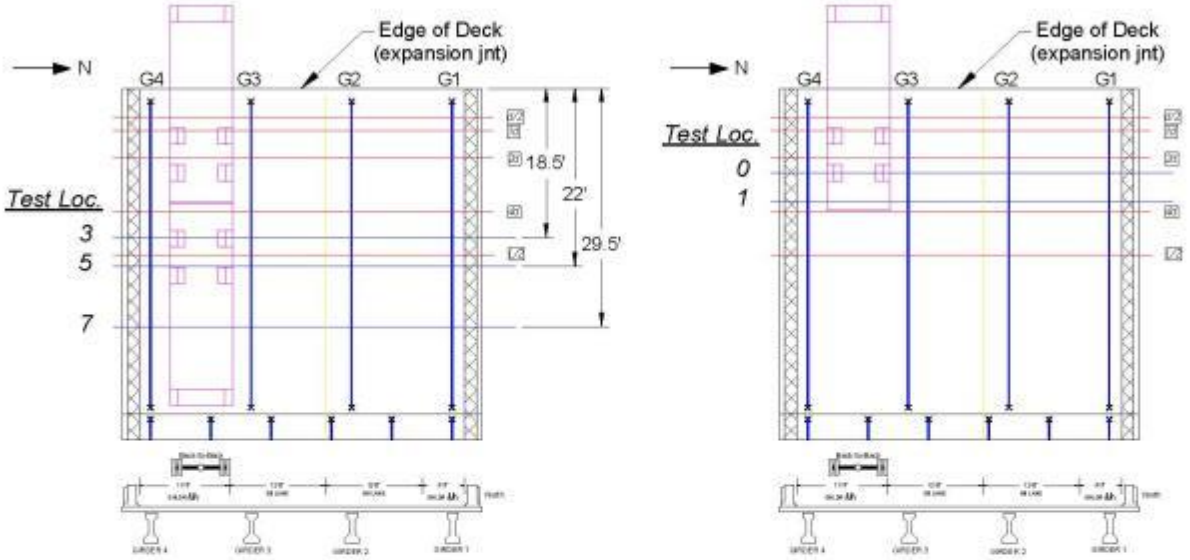

Figure 3. Exterior-Interior (G4-G3) Split Abutment Testing Locations

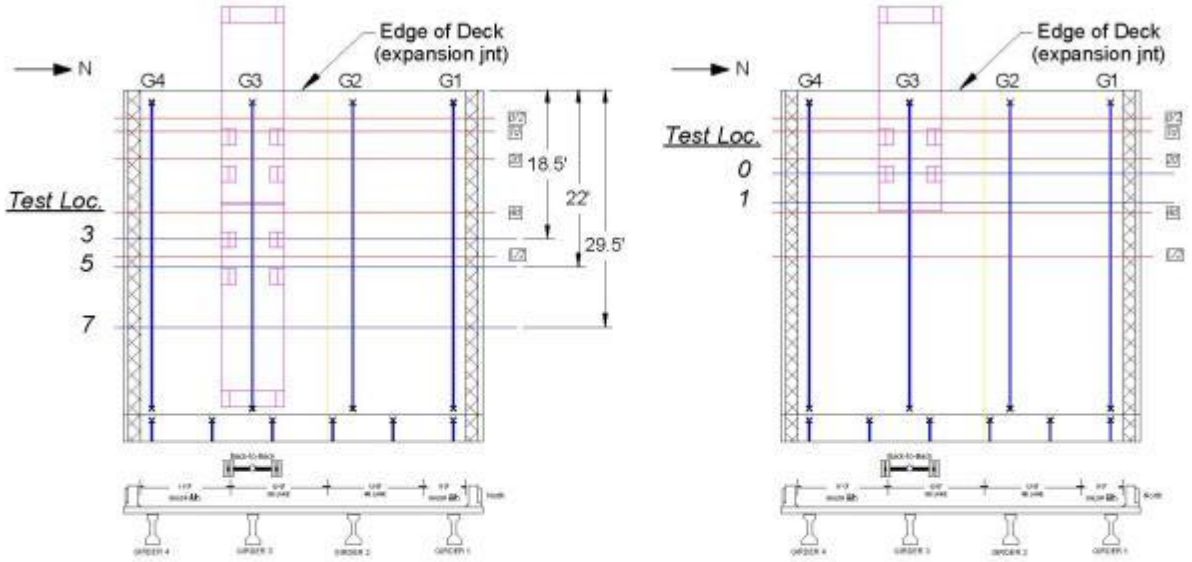

Figure 4. Interior Girder (G3) Abutment Testing Locations

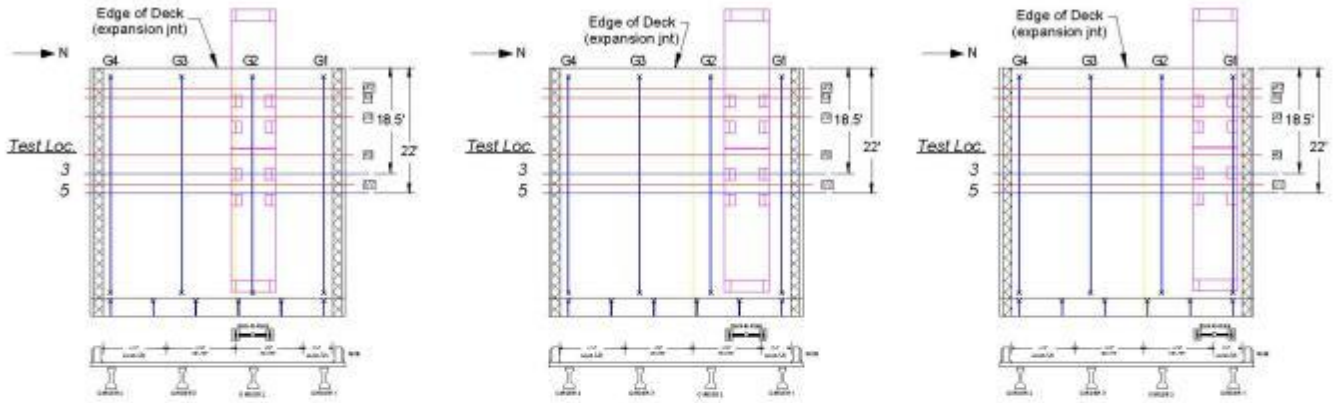

Figure 5. Symmetric Girder (G2, G2-G1 split, and G1) Abutment Testing Locations

Instrumentation and Data Collection for Bridge 62826 Live Load Tests

For all static testing, Geokon vibrating wire strain gage data will be collected using a Campbell Scientific CR1000 data acquisition system. All channels will be scanned five times per truck stop which takes approximately 8 minutes.

Instrumentation will be installed on all four girders, as labeled in Figure 6, and the southern barrier. Girder instrumentation plans are shown in Figure 7 through Figure 10.

Figure 6. West Abutment Girder Numbering

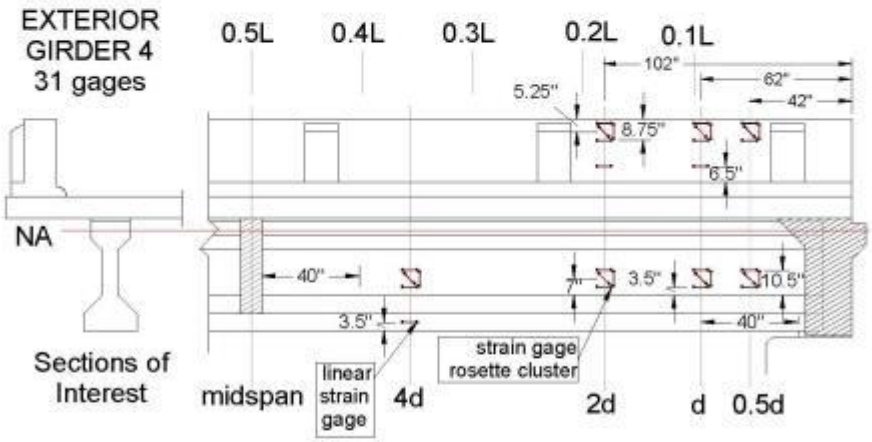

Figure 7. Girder 4 Instrumentation

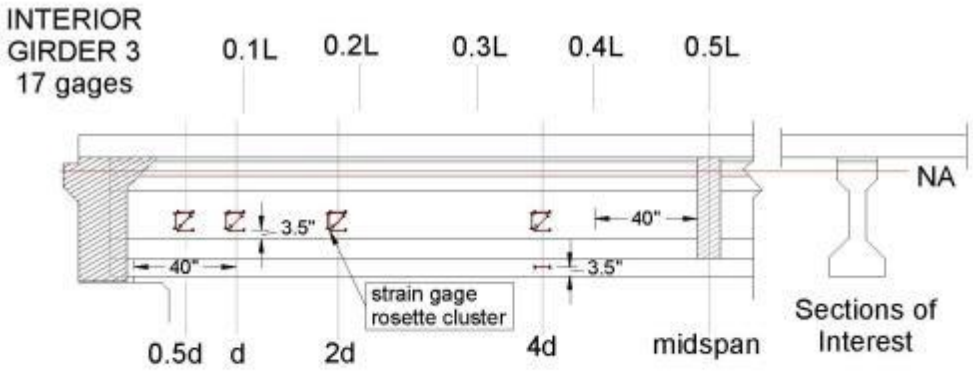

Figure 8. Girder 3 Instrumentation

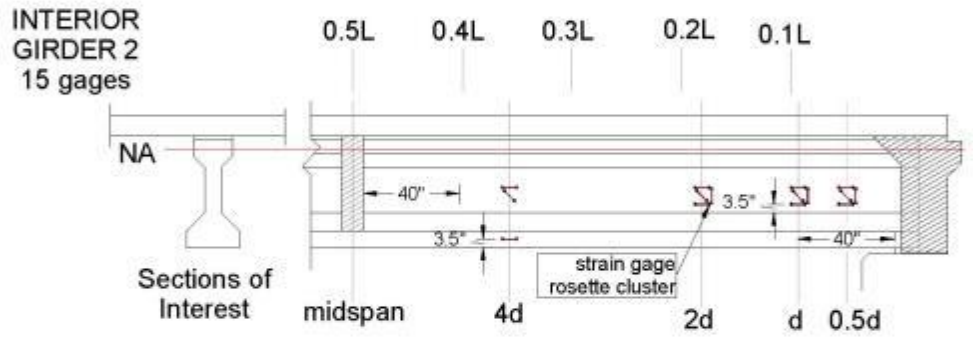

Figure 9. Girder 2 Instrumentation

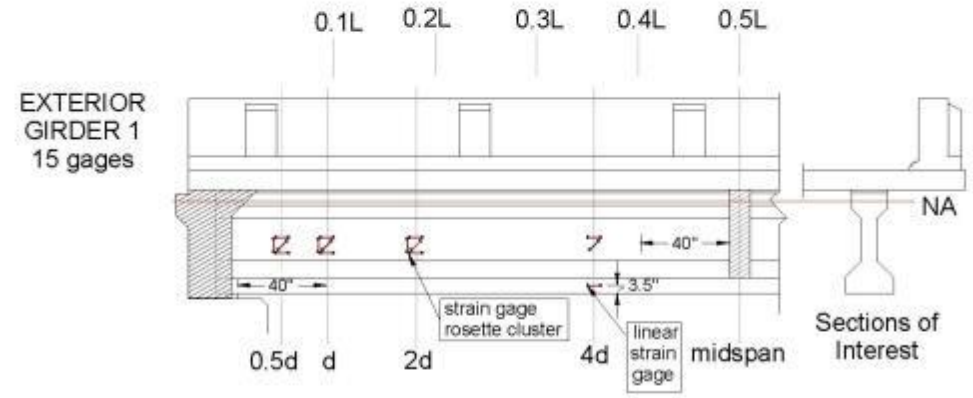

Figure 10. Girder 1 Instrumentation

The vibrating wire strain gage wires are all pulled to a set of boards where the ends are attached to terminal blocks. Most of the strain gage wires are 10 feet in length and will be used near the abutment, as shown in Figure 11. The wires running from gages located at 4d, from the barrier, and at midspan are longer, spliced wires. The length of the wire splices are shown in Figure 11.

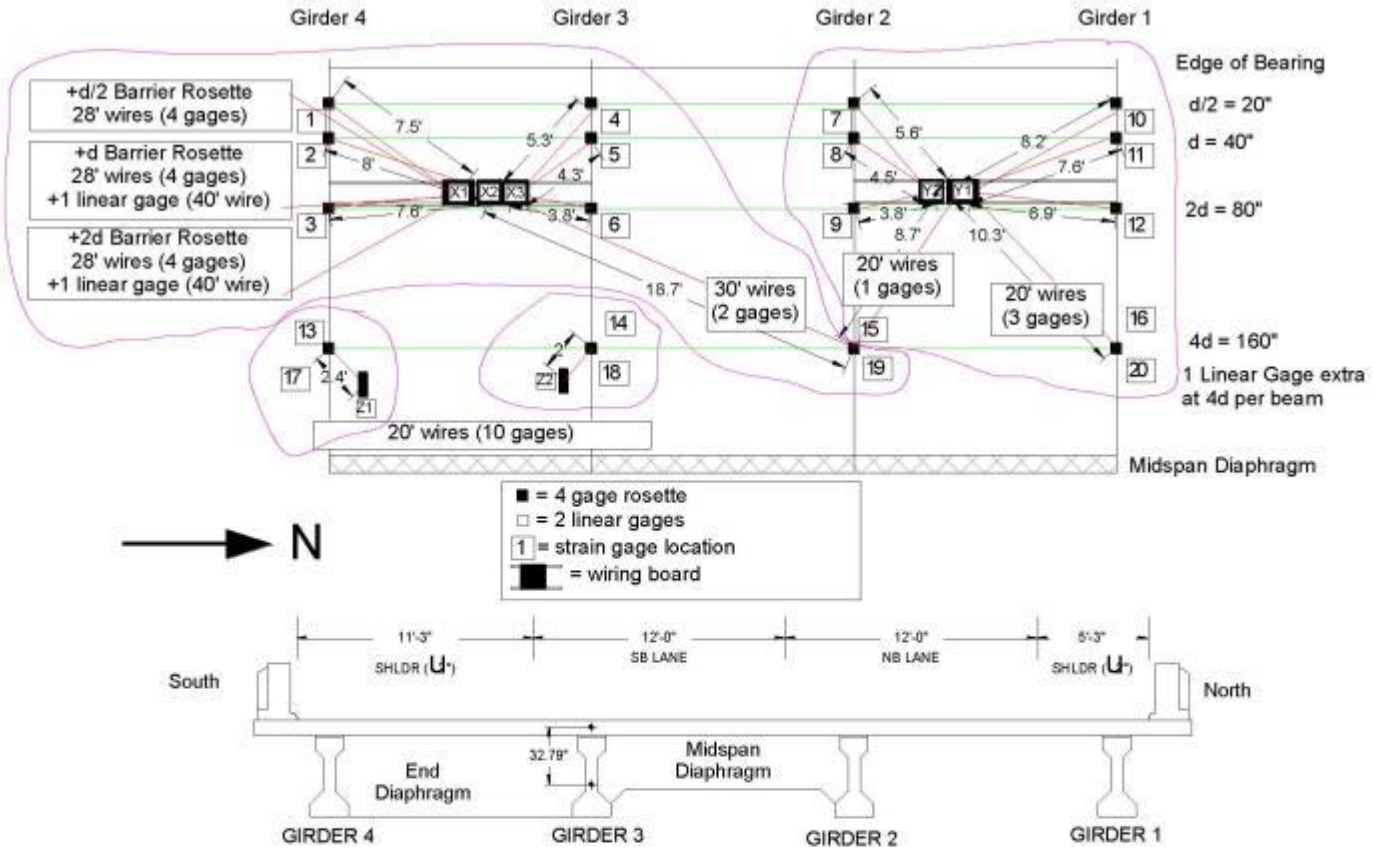

Figure 11. Strain Gage Wiring Diagram

Volunteers and Workers for Bridge 62826 Live Load Tests

Abutment Test Setup – Daytime (Thursday October 18th):

- Arrive at bridge by **9:00 AM**, van will bring supplies

Ben Dymond (612-219-1548)	Prep Team & Wiring
Brian Mathys (651-235-0744)	Prep Team
Andrew Gastineau (507-273-6683)	Install Team
Brock Hedegaard (406-489-1985)	Install Team
Melynda Jensen (952-564-4178)	Deck Marking & Pictures
Paul Bergson (651-470-9732)	Safety Coordinator & Deck Marking

Abutment Truck Tests – Overnight (starting Thursday October 18th):

- Arrive at bridge by **7:30 PM**, van will bring supplies

Ben Dymond (612-219-1548)	Operations/Truck Director
Andrew Morgan (715-214-4596)	Data Sheet Recorder
Krista Morris (651-269-2665)	Data Sheet Recorder & Pictures
Carol Shield	Computer Data Collection

Abutment Test Take-down – Daytime (Friday October 19th):

- Arrive at bridge by **10:00 AM**, van will bring supplies

Ben Dymond (612-219-1548)
Daniel Morton (574-210-3653)
Melynda Jensen (952-564-4178)
Paul Bergson (651-470-9732)

Appendix A –Record Sheets
(next page)

Abutment Girders and Transverse Testing Locations

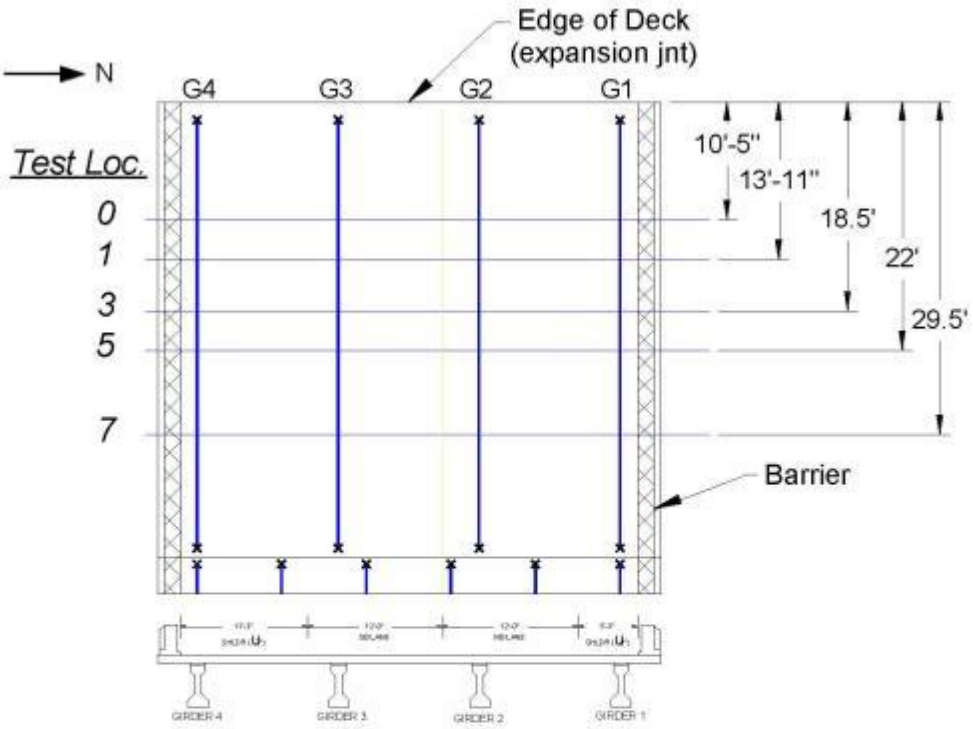

Field Testing Bridge 62826 Deck Marking Record Sheet

Driver's Tire Longitudinal Lines

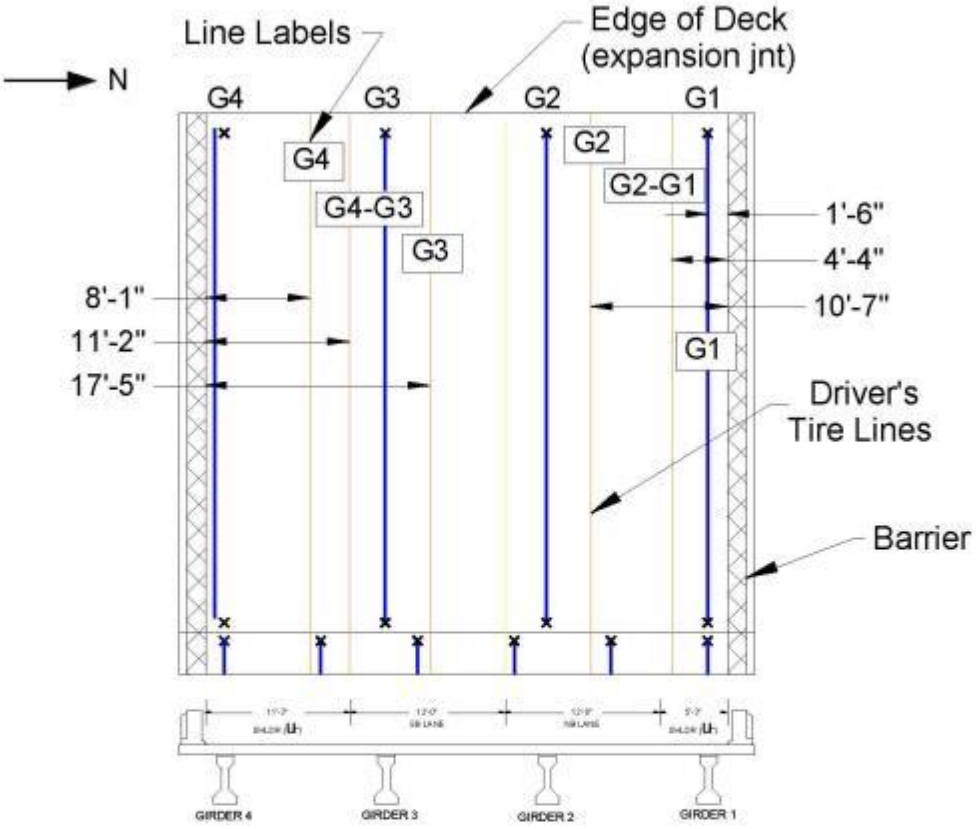

G.5 Bridge 08011 Testing Protocol

Bridge Information:

Bridge Number:	08011
Starting Date/Time:	July 17th 2013, 7 am
Location:	Hwy 15 over Little Cottonwood River, in Brown County, near New Ulm, MN (Decimal degrees of Latitude, Longitude: 44.238697,-94.434759)
Year Built:	1988
End Diaphragm:	Partial Depth
Skew:	0 degrees
End Span Geometry:	5 girders spaced at 11' with span length 76 ft
d_v:	41.7" (assumed to be 40" for ease)

Objectives for Bridge 08011 Live Load Tests

Objective 1: Static Load Testing

Static tests are planned to verify transverse shear distribution near the abutment. Shear distribution tests will be performed on the north end span of the structure (span 2), shown in Figure 1, and will include loading the structure in both lanes. Load will be applied with two MnDOT sand trucks filled so that their total weight is approximately 50 kips each. The trucks will be parked on the bridge at various locations for data collection.

Figure 1. Bridge 08011

Additional static tests are planned to verify transverse flexural distribution near L/4. One supplemental horizontal strain gage will be placed at 6d (which is near L/4) of each girder to determine the flexural strain and vertical strain distribution (for neutral axis calculation).

Objective 2: Visual Inspection of End Regions for Shear Cracks

Bridge 08011 has an inventory shear rating less than unity. Applying maximum truck load provides the opportunity to investigate possible shear cracks that may exist on the girders. These girders would most likely only be visible under the application of load. Visual inspection will be done on both an interior and exterior girder when the back-to-back truck configuration is parked at a maximum applied shear location. Any visible shear cracks will be recorded and photographed.

Planning for Bridge 08011 Live Load Tests

The truck tests are planned to occur on July 17 and July 18, 2013. Instrumentation of all bridge girders near the abutment will occur between 7 am and 7 pm on July 17, 2013. Truck tests near the abutment will occur during the day on July 18, 2013. The instrumentation will also be removed from the bridge after completion of truck testing on July 18, 2013. The tests should be completed rain or shine unless the weather is terrible. The following tasks need to be completed in preparation for the truck tests overnight. The responsibility for each of the tasks is identified below.

Task 1: Mark Truck Locations (UMN)
The locations where the trucks are to be positioned for the various static tests should be marked on the bridge prior to the truck tests. The use of marking paint should be used for a semi-permanent testing profile which will provide an outline for supplemental chalking prior to night testing.

Task 2: Arrange for Loaded Trucks (MnDOT)
Two loaded sand trucks will be needed for performing the static tests. Each truck should nominally weigh 50 kips and have a front axle to back axle length of approximately 19'-8". Each truck will need to be weighed prior to testing and after testing. Weight information should be obtained on the front axle load (by itself), the rear tandem axle load (all four back wheels), and total load for each truck. A volunteer should fill out the "truck record sheet." The trucks should be tarped over the course of the testing to assure that no rain adds weight to the truck.

Task 3: Plan and Implement Traffic Control (MnDOT)/ (UMN)
Day 1 – Instrumentation: The bridge does not need to be closed at all, but UMN will close the shoulder using cones to mark the deck.

Day 2 – Truck Tests: The bridge will need to be periodically closed during each static test (which should last approximately 10 minutes). Scheduled tests must take place when MnDOT traffic control crews are at the site, between 7 AM and 5:30 PM, for a total of 10.5 (really 7.5 hours of work time) of partial bridge closure. The first testing day will include all static tests done near the north abutment.

Schedule for Bridge 08011 Live Load Tests

Testing should be completed in 7.5 hours. The schedule for the abutment testing is presented in Table 1. The diagrams that describe the testing locations for each test description are shown in Figure 2 through Figure 7.

Row	Time	Start Time	Test	Duration (min)	Details	Priority	End Time	Traffic Control	Notes
1	7:00 AM		Abutment Start	90	Begin MnDOT travel & traffic control	0		None	
2	8:30 AM		Zero 1	12	Take measurements with no load before traffic control	0		None	
3	8:42 AM		G5 BB Loc 5	15	G5 back-to-back, rear axle south truck at Loc 5	1		Bridge is Closed	
4	8:57 AM		G5 ST Loc 0	12	G5 single north truck, rear axle positioned at Loc 0	1		"	
5	9:09 AM		G5 BB Loc 9	12	G5 back-to-back, rear axle south truck at Loc 9	1		"	
6	9:21 AM		G5 ST Loc 1	10	G5 single south truck, front rear axle positioned at Loc 1	1		"	
7	9:31 AM		Zero 2	12	Take measurements with no load	1		"	
8	9:43 AM		G4 BB Loc 5	12	G4 back-to-back, rear axle south truck at Loc 5	1		"	
9	9:55 AM		G4 ST Loc 0	12	G4 single north truck, rear axle positioned at Loc 0	1		"	
10	10:07 AM		G4 BB Loc 9	12	G4 back-to-back, rear axle south truck at Loc 9	1		"	
11	10:19 AM		G4 ST Loc 1	10	G4 single south truck, front rear axle positioned at Loc 1	1		"	
12	10:29 AM		Zero 3	12	Take measurements with no load	1		"	
*** Save Test Data, Close RTDAQ, Restart RTDAQ, Start Monitoring Table and open Flags & Data ---- Should prevent tests where not all data is captured ***									
12	10:41 AM		G3-G4 BB Loc 5	12	G3-G4 split back-to-back, rear axle south truck at Loc 5	1		"	
13	10:53 AM		G3-G4 ST Loc 0	12	G3-G4 single north truck, rear axle positioned at Loc 0	1		"	
14	11:05 AM		G3-G4 BB Loc 9	12	G3-G4 split back-to-back, rear axle south truck at Loc 9	1		"	
15	11:17 AM		G3-G4 ST Loc 1	10	G3-G4 single south truck, front rear axle positioned at Loc 1	1		"	
16	11:27 AM		Zero 4	12	Take measurements with no load	1		"	
17	11:39 AM		G3 BB Loc 5	12	G3 back-to-back, rear axle south truck at Loc 5	1		"	
18	11:51 AM		G3 ST Loc 0	12	G3 single north truck, rear axle positioned at Loc 0	1		"	
19	12:03 PM		G3 BB Loc 9	12	G3 back-to-back, rear axle south truck at Loc 9	1		"	
20	12:15 PM		G3 ST Loc 1	10	G3 single south truck, front rear axle positioned at Loc 1	1		"	
21	12:25 PM		Zero 5	12	Take measurements with no load	1		"	
22	12:37 PM		G2 BB Loc 5	12	G1 back-to-back, rear axle south truck at Loc 5	1		"	
23	12:49 PM		G2 BB Loc 9	12	G1 back-to-back, rear axle south truck at Loc 9	1		"	
24	1:01 PM		G5 BB Loc 5	12	G5 back-to-back, rear axle south truck at Loc 5	1		"	repeatability test
25	1:13 PM		G5 BB Loc 9	10	G5 back-to-back, rear axle south truck at Loc 9	1		"	repeatability test
26	1:23 PM		Zero 6	12	Take measurements with no load	1		"	
*** Save Test Data, Close RTDAQ, Restart RTDAQ, Start Monitoring Table and open Flags & Data ---- Should prevent tests where not all data is captured ***									
24	1:35 PM		G4 BB Loc 5	12	G4 back-to-back, rear axle south truck at Loc 5	1		"	repeatability test
25	1:47 PM		G4 BB Loc 9	12	G4 back-to-back, rear axle south truck at Loc 9	1		"	repeatability test
26	1:59 PM		G3-G4 BB Loc 5	12	G3-G4 split back-to-back, rear axle south truck at Loc 5	1		"	repeatability test
27	2:11 PM		G3-G4 BB Loc 9	10	G3-G4 split back-to-back, rear axle south truck at Loc 9	1		"	repeatability test
28	2:21 PM		Zero 7	12	Take measurements with no load	1		"	
29	2:33 PM		G3 BB Loc 5	12	G3 back-to-back, rear axle south truck at Loc 5	1		"	repeatability test
30	2:45 PM		G3 BB Loc 9	12	G3 back-to-back, rear axle south truck at Loc 9	1		"	repeatability test
31	2:57 PM		G2 BB Loc 5	12	G1 back-to-back, rear axle south truck at Loc 5	***1.5***		"	repeatability test
32	3:09 PM		G2 BB Loc 9	12	G1 back-to-back, rear axle south truck at Loc 9	***1.5***		"	repeatability test
33	3:21 PM		Zero 8	10	G4-G5 split single north truck, rear axle at Loc 0	1		"	

*** Save Test Data, Close RTDAQ, Restart RTDAQ, Start Monitoring Table and open Flags & Data ---- Should prevent tests where not all data is captured ***									
34	3:31 PM		G4-G5 BB Loc 5	12	G4-G5 split back-to-back, rear axle south truck at Loc 5	2		"	
35	3:43 PM		G4-G5 ST Loc 0	12	G4-G5 split single north truck, rear axle at Loc 0	2		"	
36	3:55 PM		G4-G5 BB Loc 9	12	G4-G5 split back-to-back, rear axle south truck at Loc 9	2		"	
37	4:07 PM		G4-G5 ST Loc 1	10	G4-G5 split single south truck, front rear axle at Loc 1	2		"	
38	4:17 PM		Zero 9	10	Take measurements with no load	0		"	
39	4:27 PM		Day 2 Complete		Testing complete and MnDOT leaves	0		None	

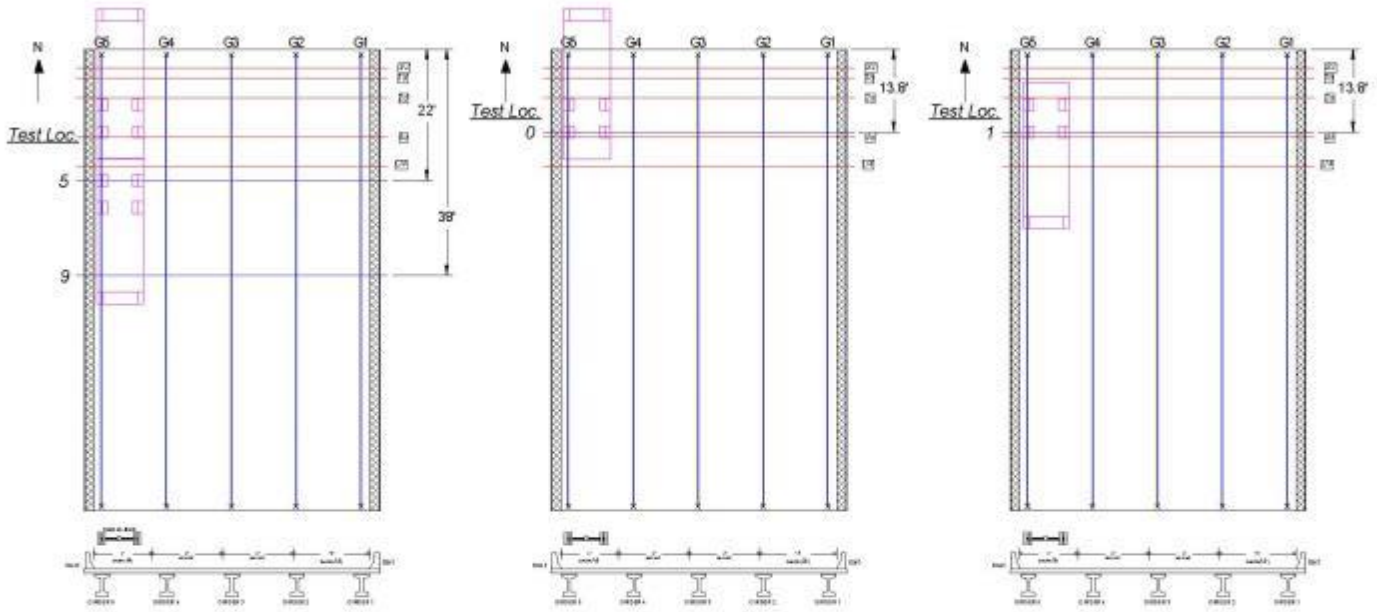

Figure 2. Exterior Girder (G5) Abutment Testing Locations

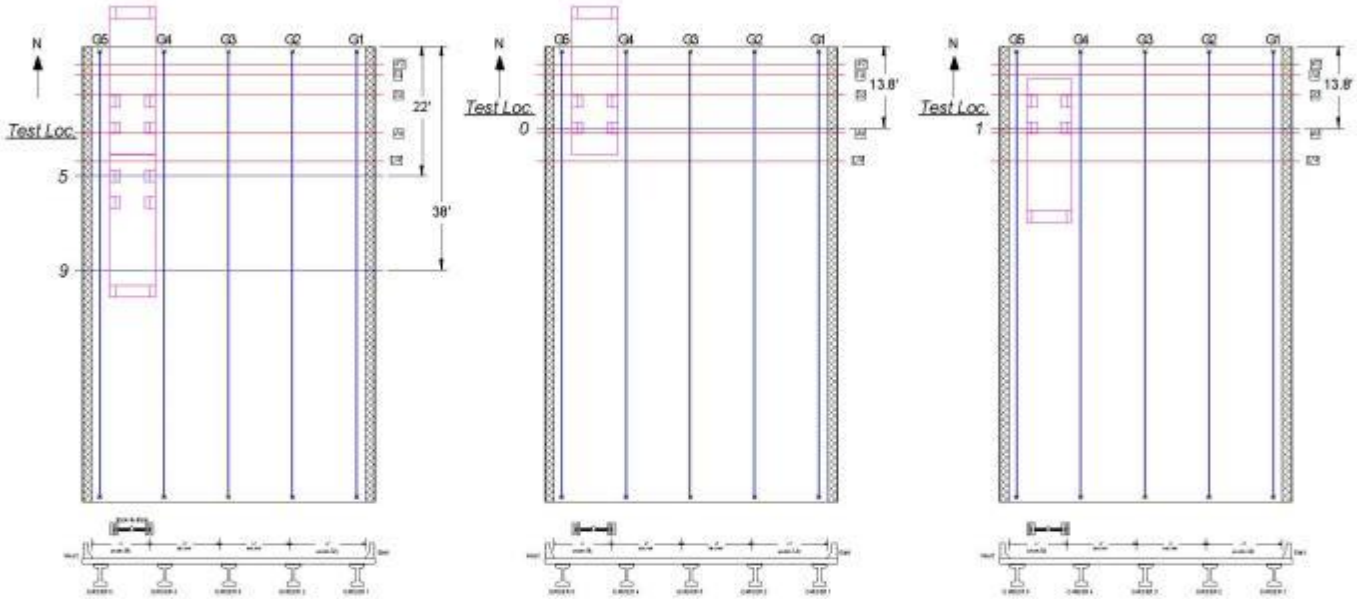

Figure 3. Exterior-Interior (G5-G4) Split Abutment Testing Locations

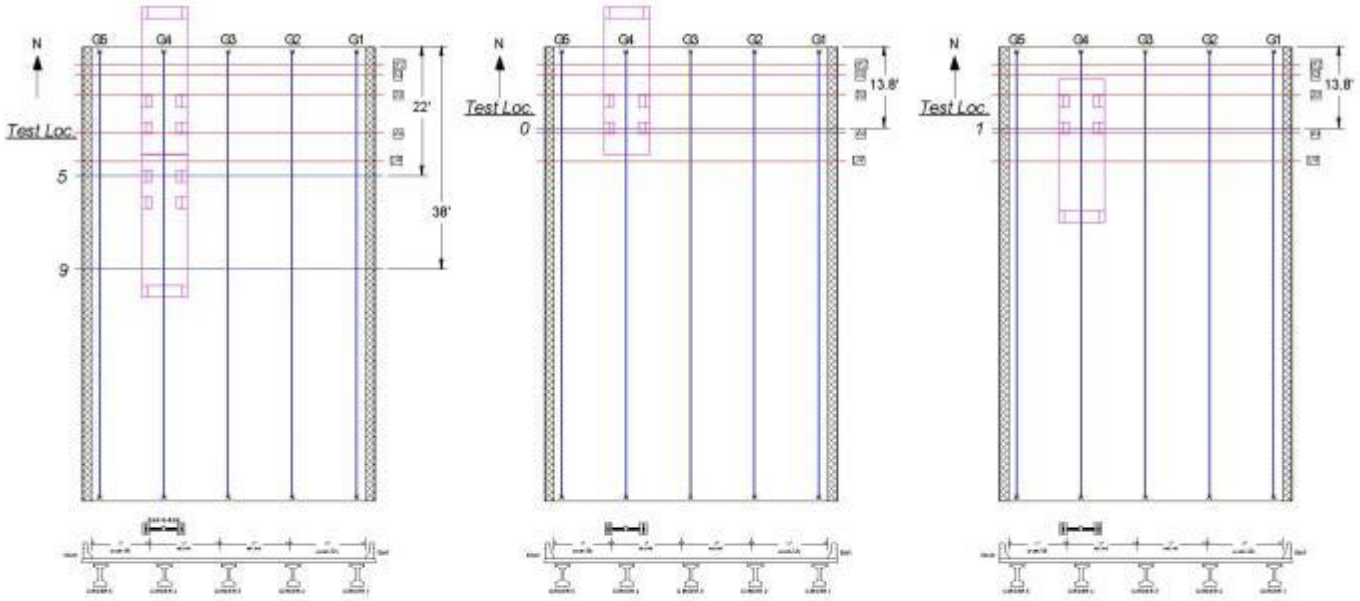

Figure 4. Interior (G4) Abutment Testing Locations

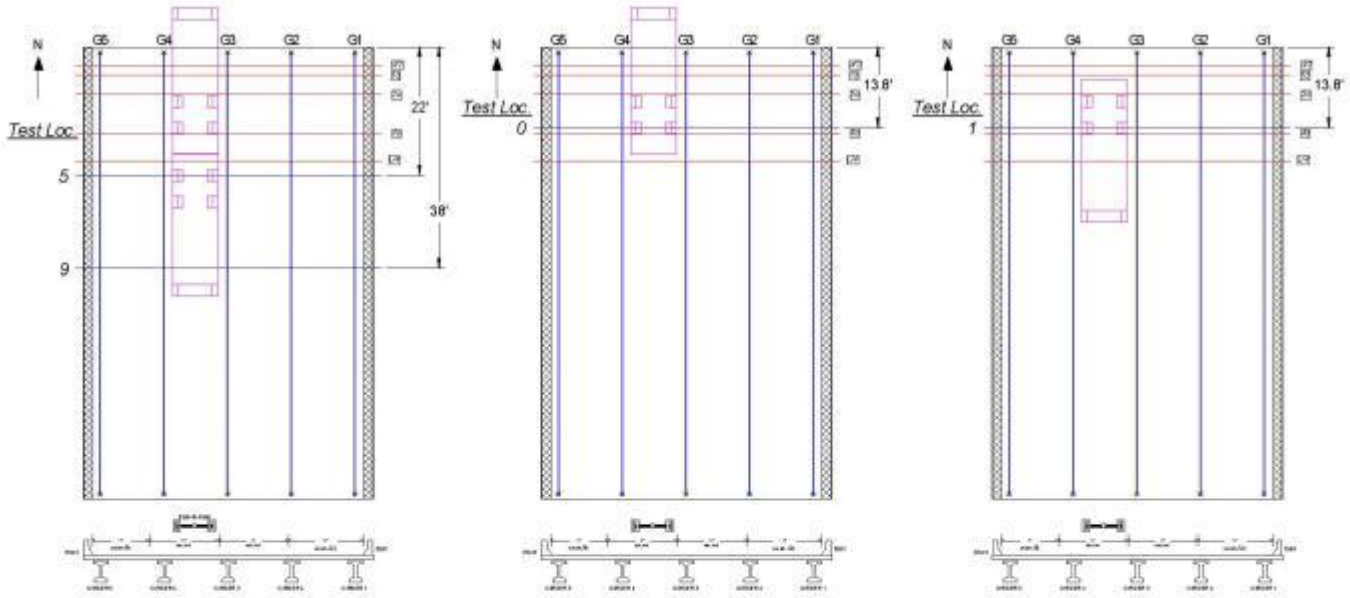

Figure 5. Interior-Interior Girder (G4-G3) Split Abutment Testing Locations

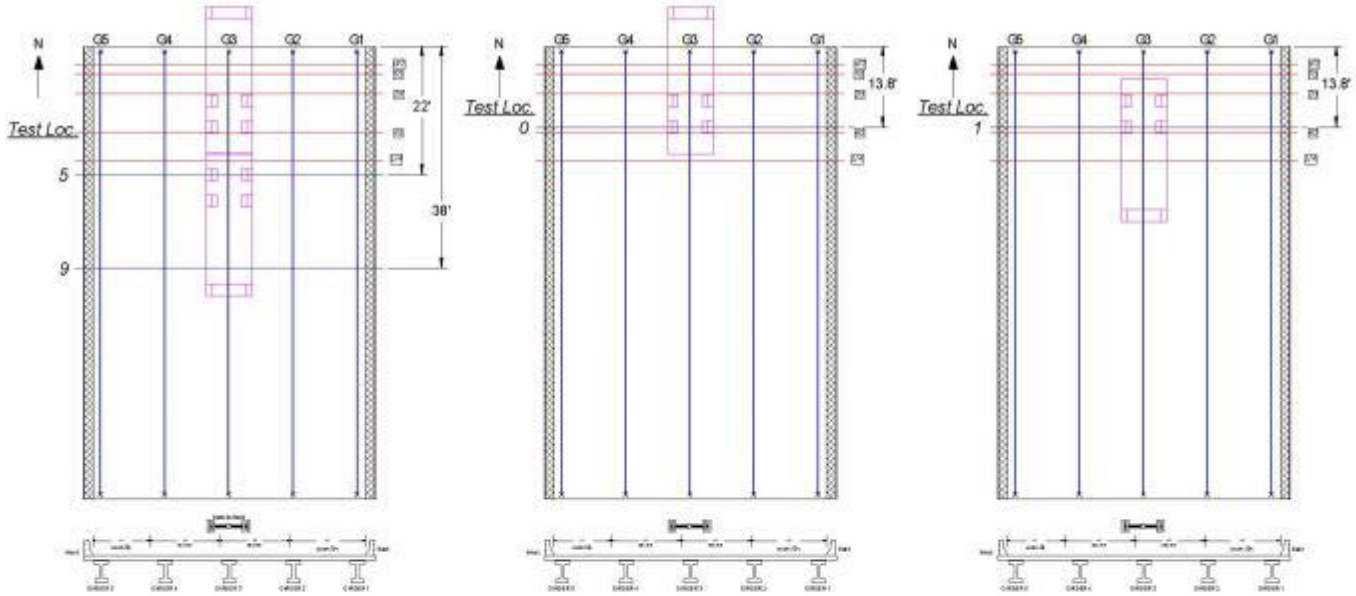

Figure 6. Interior Girder (G3) Abutment Testing Locations

Figure 7. Interior (G2) Girder Abutment Testing Locations

Instrumentation and Data Collection for Bridge 08011 Live Load Tests

For all static testing, Geokon vibrating wire strain gage data will be collected using a Campbell Scientific CR1000 data acquisition system. All channels will be scanned five times per truck stop which takes approximately 8 minutes.

Instrumentation will be installed on all five girders, as labeled in Figure 8, and the western barrier. Girder instrumentation plans are shown in Figure 9 through Figure 13.

Figure 8. North Abutment Girder Numbering

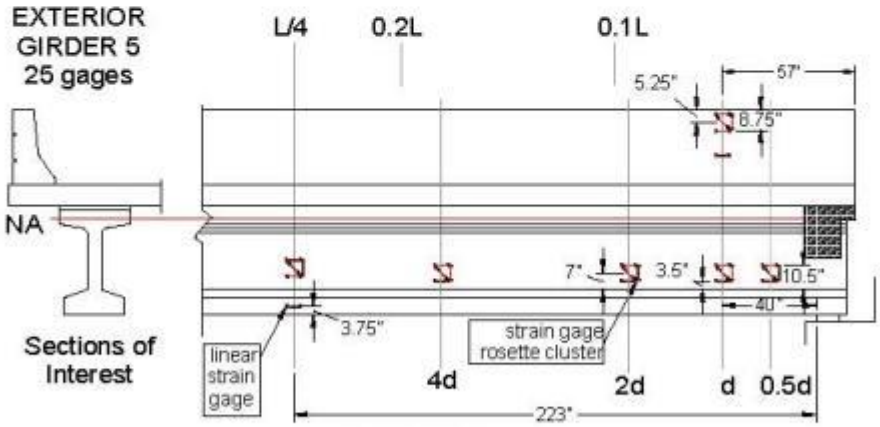

Figure 9. Girder 5 Instrumentation

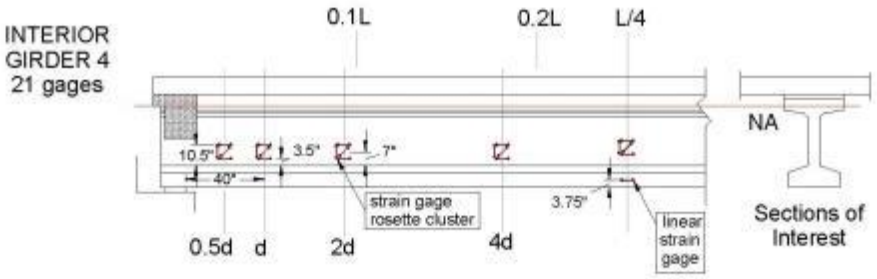

Figure 10. Girder 4 Instrumentation

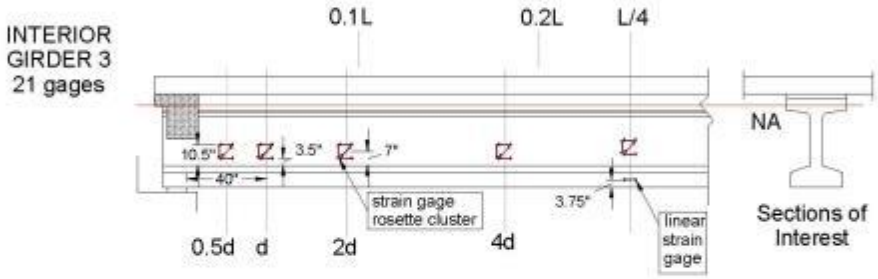

Figure 11. Girder 3 Instrumentation

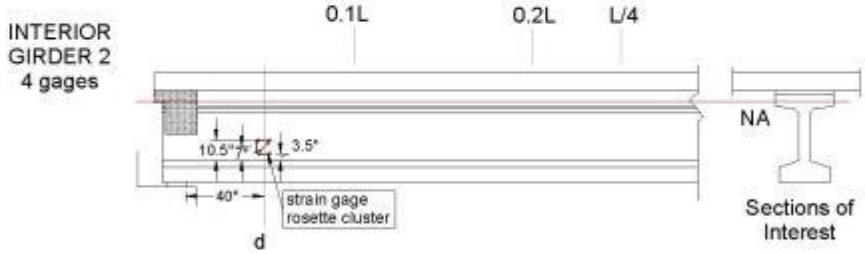

Figure 12. Girder 2 Instrumentation

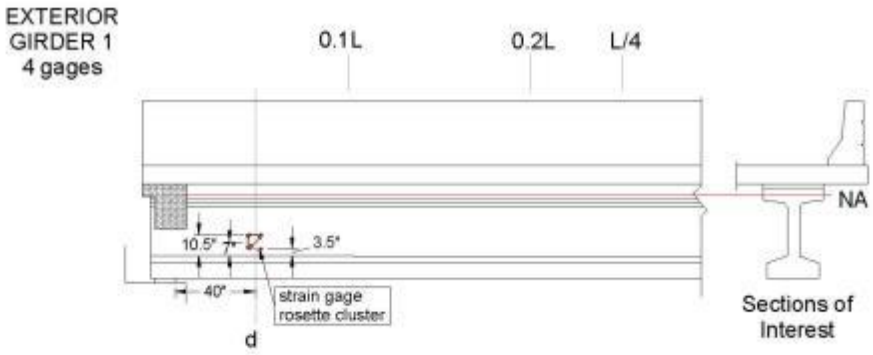

Figure 13. Girder 1 Instrumentation

The vibrating wire strain gage wires are all pulled to a set of boards where the ends are attached to terminal blocks. Most of the strain gage wires are 10 feet in length and will be used near the abutment, as shown in Figure 14.

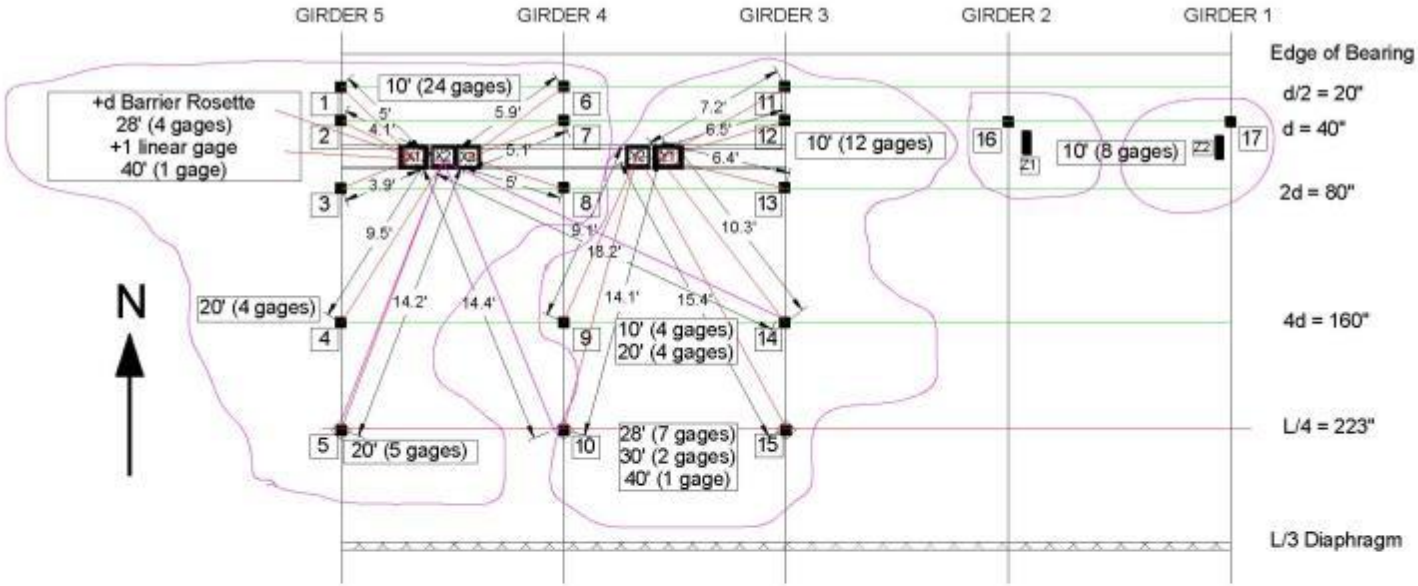

Figure 14. Strain Gage Wiring Diagram

Volunteers and Workers for Bridge 08011 Live Load Tests

Abutment Test Setup – Daytime (Wednesday July 17th):

- Meet at Brian Mathys' house by **5:00 AM**, van will bring supplies

Ben Dymond (612-219-1548)	Prep Team, Install Team & Wiring
Sam Konieczny (763-843-6082)	Prep Team & Pictures
Brock Hedegaard (406-489-1985)	Prep Team
Mike Larson (920-344-5789)	Install Team
Brian Mathys (651-235-0744)	Install Team
Carol Shield	Safety Coordinator & Deck Marking

Abutment Truck Tests – Daytime (Thursday July 18th):

- Leave hotel by **7:00 AM**, vans will bring supplies

Ben Dymond (612-219-1548)	Operations/Truck Director
Sam Konieczny (763-843-6082)	Data Sheet Recorder
Mike Larson (920-344-5789)	Data Sheet Recorder
Brian Mathys (651-235-0744)	Data Sheet Recorder & Pictures
Brock Hedegaard (406-489-1985)	Computer Data Collection
Carol Shield	Safety Coordinator & Computer Data Collection

Appendix A –Record Sheets

(next page)

Field Testing Bridge 08011 Deck Marking Record Sheet

Transverse Testing Locations

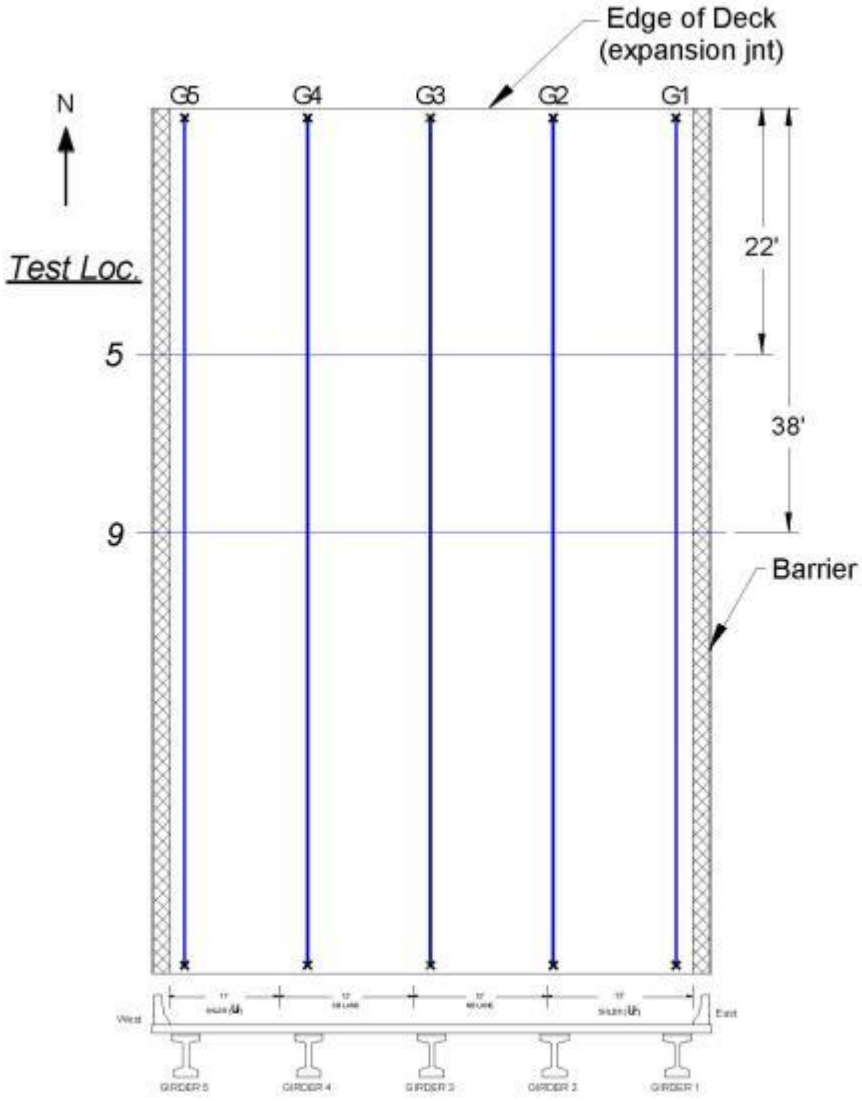

16

Field Testing Bridge 08011 Deck Marking Record Sheet

Driver's Tire Longitudinal Lines

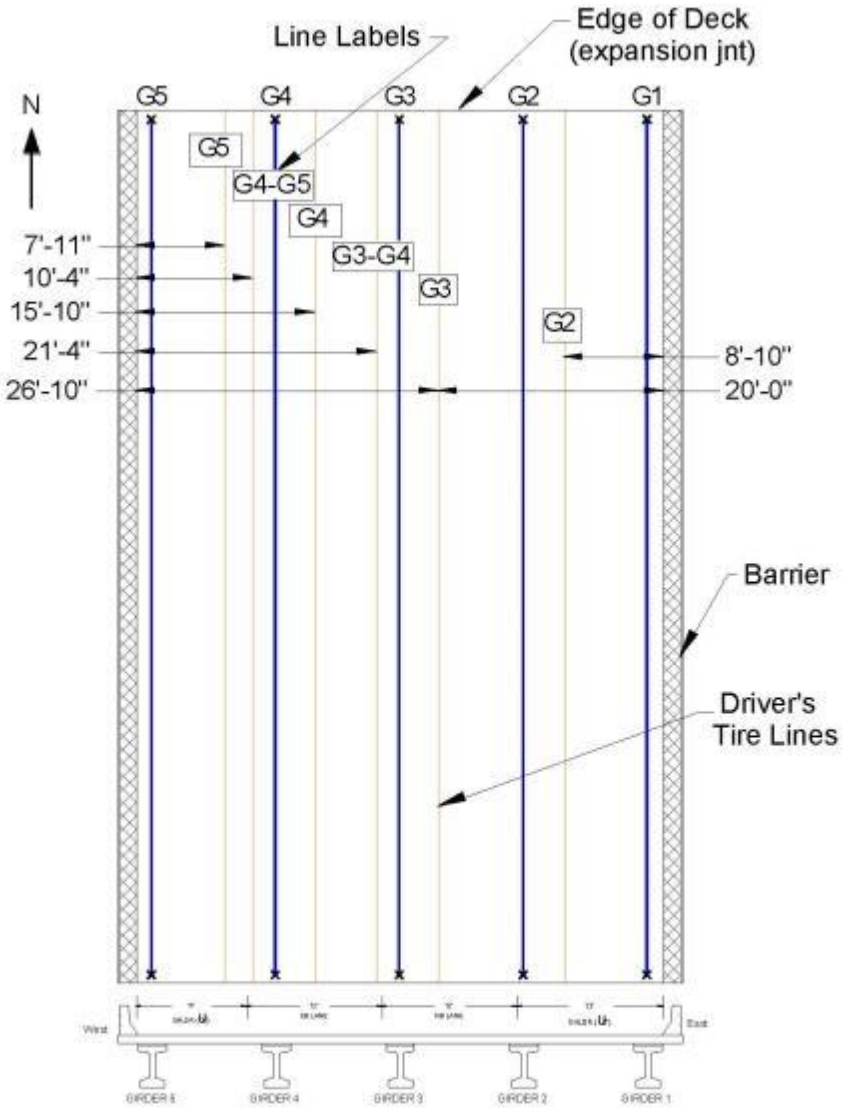

G.6 Bridge 09002 Testing Protocol

Bridge Information:

Bridge Number:	09002
Starting Date/Time:	August 14th 2013, 7 am
Location:	MN Hwy 27 over Moose Horn River, in Carlton County, near Moose Lake, MN (Decimal degrees of Latitude, Longitude: 46.457846,-92.751496)
Year Built:	1970
End Diaphragm:	Partial Depth
Skew:	0 degrees
End Span Geometry:	5 girders spaced at 11.5' with span length 39 ft
d_v:	34"

Objectives for Bridge 09002 Live Load Tests

Objective 1: Static Load Testing

Static tests are planned to verify transverse shear distribution near the abutment. Shear distribution tests will be performed on the east end span of the structure (span 3), shown in Figure 1, and will include loading the structure in both lanes. Load will be applied with two MnDOT sand trucks filled so that their total weight is approximately 50 kips each. The trucks will be parked on the bridge at various locations for data collection.

Figure 1. Bridge 09002

Additional static tests are planned to verify transverse flexural distribution near L/2. One supplemental horizontal strain gage will be placed at 4d of two girders to determine the flexural strain and vertical strain distribution (for neutral axis calculation).

Objective 2: Visual Inspection of End Regions for Shear Cracks

Bridge 09002 has an inventory shear rating less than unity. Applying maximum truck load provides the opportunity to investigate possible shear cracks that may exist on the girders. These girders would most likely only be visible under the application of load. Visual inspection will be done on both an interior and exterior girder when the back-to-back truck configuration is parked at a maximum applied shear location. Any visible shear cracks will be recorded and photographed.

Planning for Bridge 09002 Live Load Tests

The truck tests are planned to occur on August 14 and August 15, 2013. Instrumentation of all bridge girders near the abutment will occur between 7 am and 7 pm on August 14, 2013. Truck tests near the abutment will occur during the day on August 15, 2013. The instrumentation will also be removed from the bridge after completion of truck testing on August 15, 2013. The tests should be completed rain or shine unless the weather is terrible. The following tasks need to be completed in preparation for the truck tests overnight. The responsibility for each of the tasks is identified below.

Task 1: Mark Truck Locations (UMN)
The locations where the trucks are to be positioned for the various static tests should be marked on the bridge prior to the truck tests. The use of marking paint should be used for a semi-permanent testing profile which will provide an outline for supplemental chalking prior to testing.

Task 2: Arrange for Loaded Trucks (MnDOT)
Two loaded sand trucks will be needed for performing the static tests. Each truck should nominally weigh 50 kips and have a front axle to back axle length of approximately 19'-8". Each truck will need to be weighed prior to testing and after testing. Weight information should be obtained on the front axle load (by itself), the rear tandem axle load (all four back wheels), and total load for each truck. A volunteer should fill out the "truck record sheet." The trucks should be tarped over the course of the testing to assure that no rain adds weight to the truck.

Task 3: Plan and Implement Traffic Control (MnDOT)/ (UMN)
Day 1 – Instrumentation: The bridge does not need to be closed at all, but UMN will close the shoulder using cones to mark the deck.

Day 2 – Truck Tests: The bridge will need to be periodically closed during each static test (which should last approximately 10 minutes). Scheduled tests must take place when MnDOT traffic control crews are at the site, between 6:30 AM and 5:00 PM, for a total of 10.5 (really 7.5 hours of work time) of partial bridge closure. The first testing day will include all static tests done near the east abutment.

Schedule for Bridge 09002 Live Load Tests

Testing should be completed in 7.5 hours. The schedule for the abutment testing is presented in Table 1. The diagrams that describe the testing locations for each test description are shown in Figure 2 through Figure 7.

Row	Time	Start Time	Test	Duration (min)	Details	Priority	End Time	Traffic Control	Notes
1	6:30 AM		Abutment Start	60	Begin MnDOT travel & traffic control	0		None	
2	7:30 AM		Zero 1	12	Take measurements with no load before traffic control	0		None	
3	7:42 AM		G1 BB Loc 5	12	G1 back-to-back, rear axle west truck at Loc 5	1		Bridge is Closed	
4	7:54 AM		G1 ST Loc 0	12	G1 single east truck, rear axle positioned at Loc 0	1		"	
5	8:06 AM		G1 BB Loc 9	12	G1 back-to-back, rear axle west truck at Loc 9	1		"	
6	8:18 AM		G1 BB Loc 11	12	G1 back-to-back, rear axle west truck at Loc 11	1		"	
7	8:30 AM		Zero 2	12	Take measurements with no load	1		"	
*** Save Test Data, Close RTDAQ, Restart RTDAQ, Start Monitoring Table and open Flags & Data ---- Should prevent tests where not all data is captured ***									
8	8:42 AM		G2-G1 BB Loc 5	12	G2-G1 split back-to-back, rear axle west truck at Loc 5	1		"	
9	8:54 AM		G2-G1 ST Loc 0	12	G2-G1 split single east truck, rear axle at Loc 0	1		"	
10	9:06 AM		G2-G1 BB Loc 9	12	G2-G1 split back-to-back, rear axle west truck at Loc 9	1		"	
11	9:18 AM		G2-G1 ST Loc 1	10	G2-G1 split single west truck, front rear axle at Loc 1	1		"	
12	9:28 AM		Zero 3	12	Take measurements with no load	1		"	
*** Save Test Data, Close RTDAQ, Restart RTDAQ, Start Monitoring Table and open Flags & Data ---- Should prevent tests where not all data is captured ***									
13	9:40 AM		G2 BB Loc 5	12	G2 back-to-back, rear axle west truck at Loc 5	1		"	
14	9:52 AM		G2 ST Loc 0	12	G2 single east truck, rear axle positioned at Loc 0	1		"	
15	10:04 AM		G2 BB Loc 9	12	G2 back-to-back, rear axle west truck at Loc 9	1		"	
16	10:16 AM		G2 ST Loc 1	10	G2 single west truck, front rear axle positioned at Loc 1	1		"	
17	10:26 AM		Zero 3	12	Take measurements with no load	1		"	
*** Save Test Data, Close RTDAQ, Restart RTDAQ, Start Monitoring Table and open Flags & Data ---- Should prevent tests where not all data is captured ***									
18	10:38 AM		G3-G2 BB Loc 5	12	G3-G2 split back-to-back, rear axle west truck at Loc 5	1		"	
19	10:50 AM		G3-G2 ST Loc 0	12	G3-G2 single east truck, rear axle positioned at Loc 0	1		"	
20	11:02 AM		G3-G2 BB Loc 9	12	G3-G2 split back-to-back, rear axle west truck at Loc 9	1		"	
21	11:14 AM		G1 BB Loc 11	12	G1 back-to-back, rear axle west truck at Loc 11	1		"	
22	11:26 AM		Zero 4	12	Take measurements with no load	1		"	
*** Save Test Data, Close RTDAQ, Restart RTDAQ, Start Monitoring Table and open Flags & Data ---- Should prevent tests where not all data is captured ***									
23	11:38 AM		G3 BB Loc 5	12	G3 back-to-back, rear axle west truck at Loc 5	1		"	
24	11:50 AM		G3 ST Loc 0	12	G3 single east truck, rear axle positioned at Loc 0	1		"	
25	12:02 PM		G3 BB Loc 9	12	G3 back-to-back, rear axle west truck at Loc 9	1		"	
26	12:14 PM		G3 ST Loc 1	10	G3 single west truck, front rear axle positioned at Loc 1	1		"	
27	12:24 PM		Zero 5	12	Take measurements with no load	1		"	
*** Save Test Data, Close RTDAQ, Restart RTDAQ, Start Monitoring Table and open Flags & Data ---- Should prevent tests where not all data is captured ***									

28	12:36 PM		G1 BB Loc 5	12	G1 back-to-back, rear axle west truck at Loc 5	1		"	repeatability test
29	12:48 PM		G1 ST Loc 0	12	G1 single east truck, rear axle positioned at Loc 0	1		"	repeatability test
30	1:00 PM		G2-G1 BB Loc 5	12	G2-G1 split back-to-back, rear axle west truck at Loc 5	1		"	repeatability test
31	1:12 PM		G2-G1 ST Loc 0	10	G2-G1 split single east truck, rear axle at Loc 0	1		"	repeatability test
32	1:22 PM		Zero 6	12	Take measurements with no load	1		"	
*** Save Test Data, Close RTDAQ, Restart RTDAQ, Start Monitoring Table and open Flags & Data — Should prevent tests where not all data is captured ***									
33	1:34 PM		G2 BB Loc 5	12	G2 back-to-back, rear axle west truck at Loc 5	1		"	repeatability test
34	1:46 PM		G2 ST Loc 0	12	G2 single east truck, rear axle positioned at Loc 0	1		"	repeatability test
35	1:58 PM		G3-G2 BB Loc 5	12	G3-G2 split back-to-back, rear axle west truck at Loc 5	1		"	repeatability test
36	2:10 PM		G3-G2 ST Loc 0	10	G3-G2 single east truck, rear axle positioned at Loc 0	1		"	repeatability test
37	2:20 PM		Zero 7	12	Take measurements with no load	1		"	
*** Save Test Data, Close RTDAQ, Restart RTDAQ, Start Monitoring Table and open Flags & Data — Should prevent tests where not all data is captured ***									
38	2:32 PM		G3 BB Loc 5	12	G3 back-to-back, rear axle west truck at Loc 5	1		"	repeatability test
39	2:44 PM		G3 ST Loc 0	12	G3 single east truck, rear axle positioned at Loc 0	1		"	repeatability test
40	2:56 PM		G4 BB Loc 5	12	G4 back-to-back, rear axle west truck at Loc 5	2		"	
41	3:08 PM		G4 BB Loc 9	10	G4 back-to-back, rear axle west truck at Loc 9	2		"	
42	3:18 PM		Zero 8	12	Take measurements with no load	1		"	
43	3:30 PM		Day 2 Complete		Testing complete and MnDOT leaves	0		None	

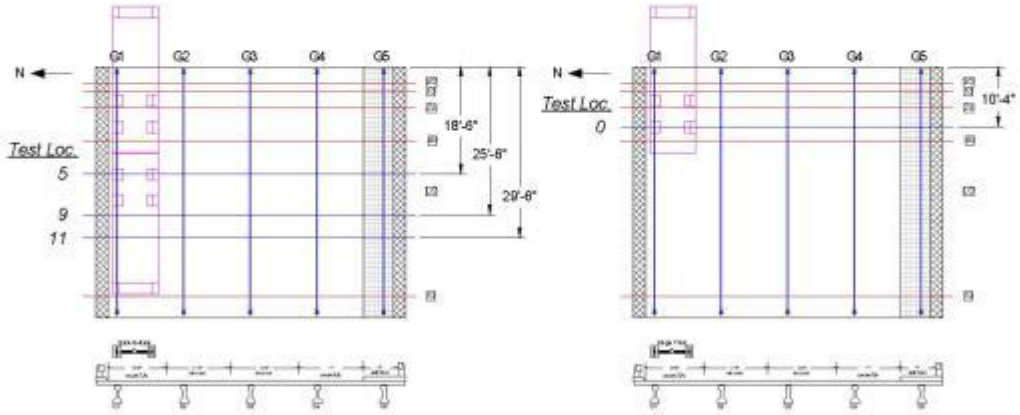

Figure 2. Exterior Girder (G1) Abutment Testing Locations

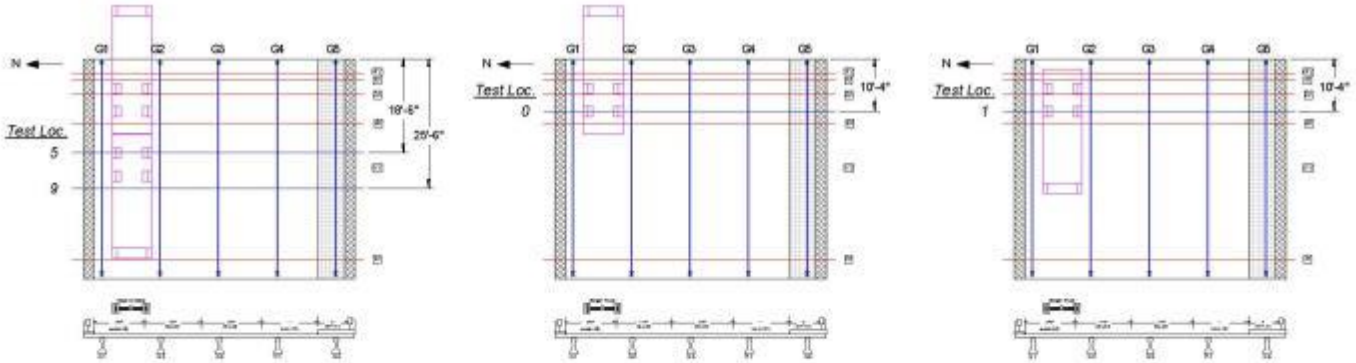

Figure 3. Interior-Exterior Girder (G2-G1) Split Abutment Testing Locations

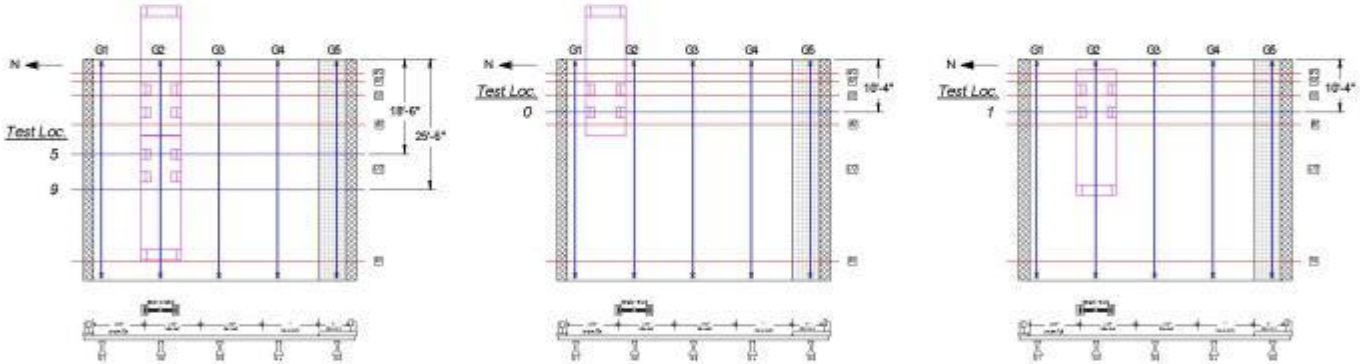

Figure 4. Interior Girder (G2) Abutment Testing Locations

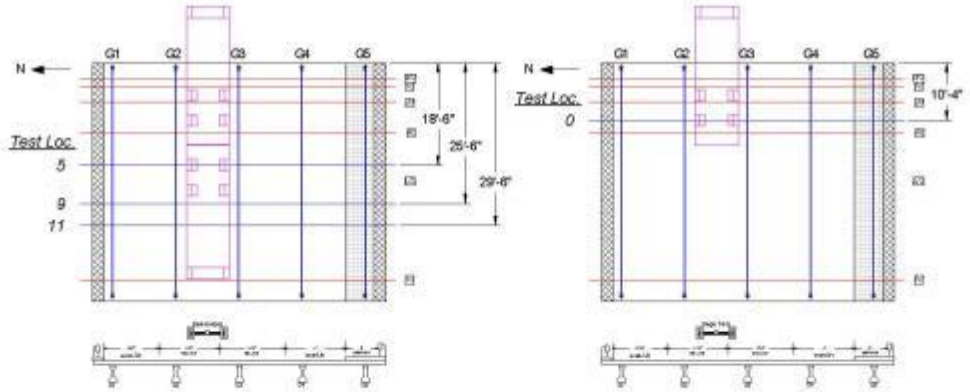

Figure 5. Interior-Interior Girder (G3-G2) Split Abutment Testing Locations

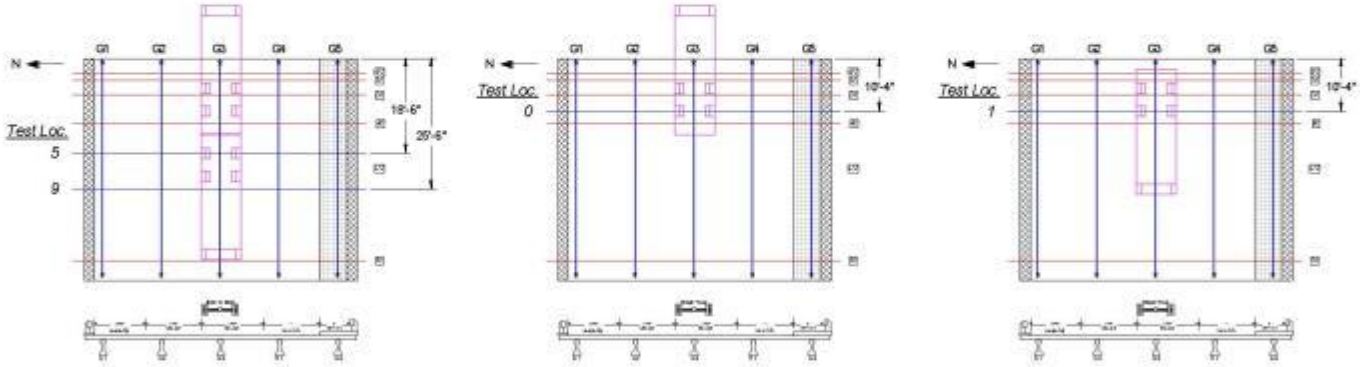

Figure 6. Interior Girder (G3) Abutment Testing Locations

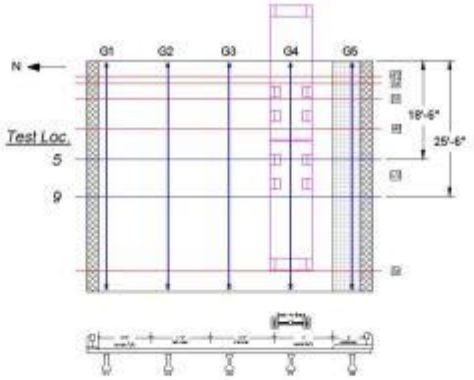

Figure 7. Interior Girder (G4) Abutment Testing Locations

Instrumentation and Data Collection for Bridge 09002 Live Load Tests

For all static testing, Geokon vibrating wire strain gage data will be collected using a Campbell Scientific CR1000 data acquisition system. All channels will be scanned five times per truck stop which takes approximately 8 minutes.

Instrumentation will be installed on all five girders, as labeled in Figure 8. Girder instrumentation plans are shown in Figure 9 through Figure 13.

Figure 8. East Abutment Girder Numbering

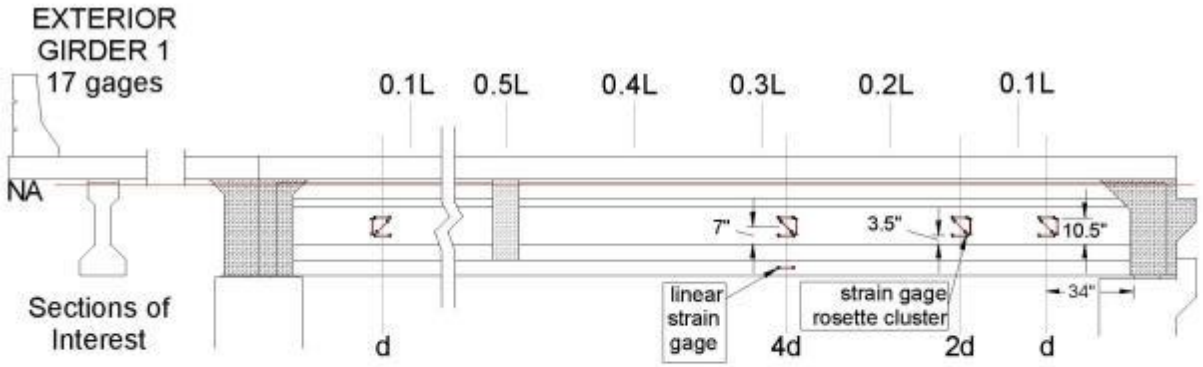

Figure 9. Girder 1 Instrumentation

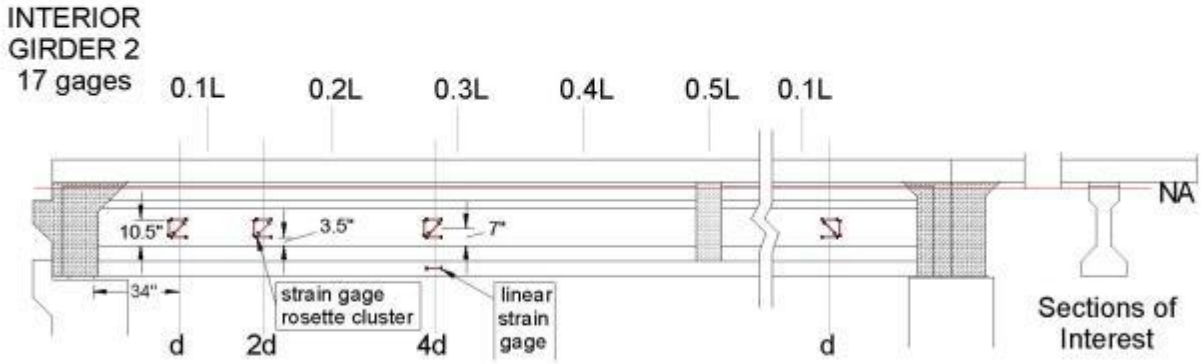

Figure 10. Girder 2 Instrumentation

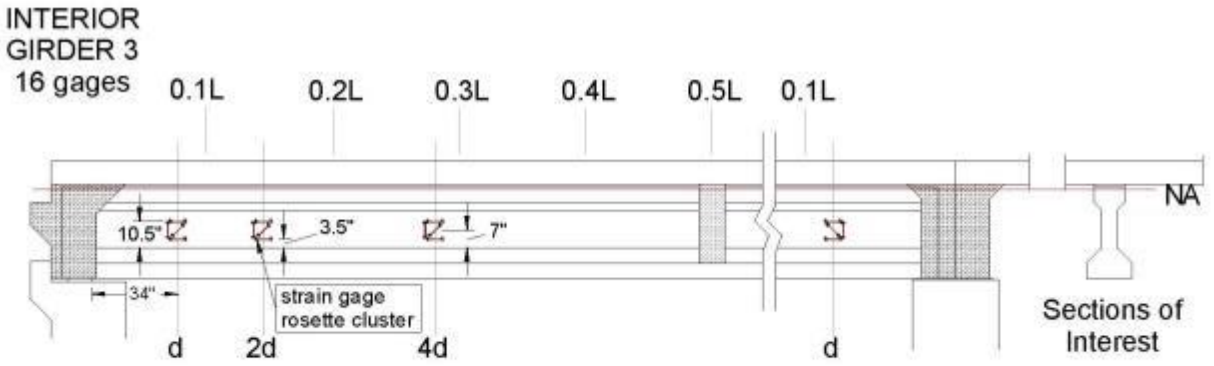

Figure 11. Girder 3 Instrumentation

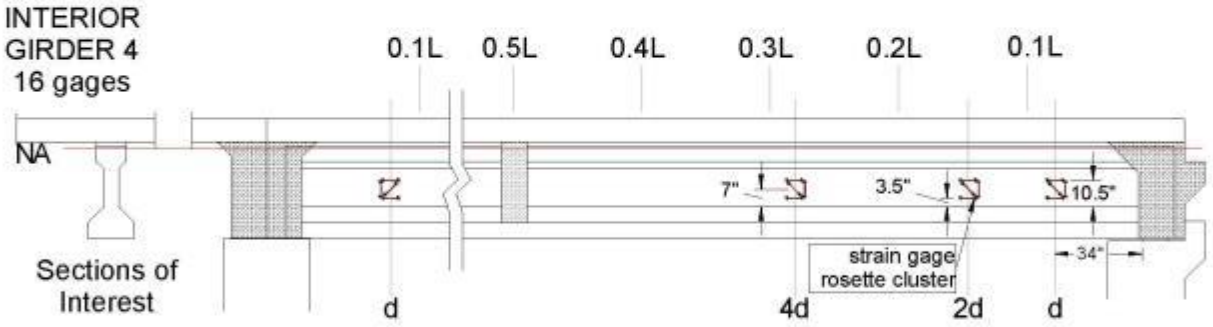

Figure 12. Girder 4 Instrumentation

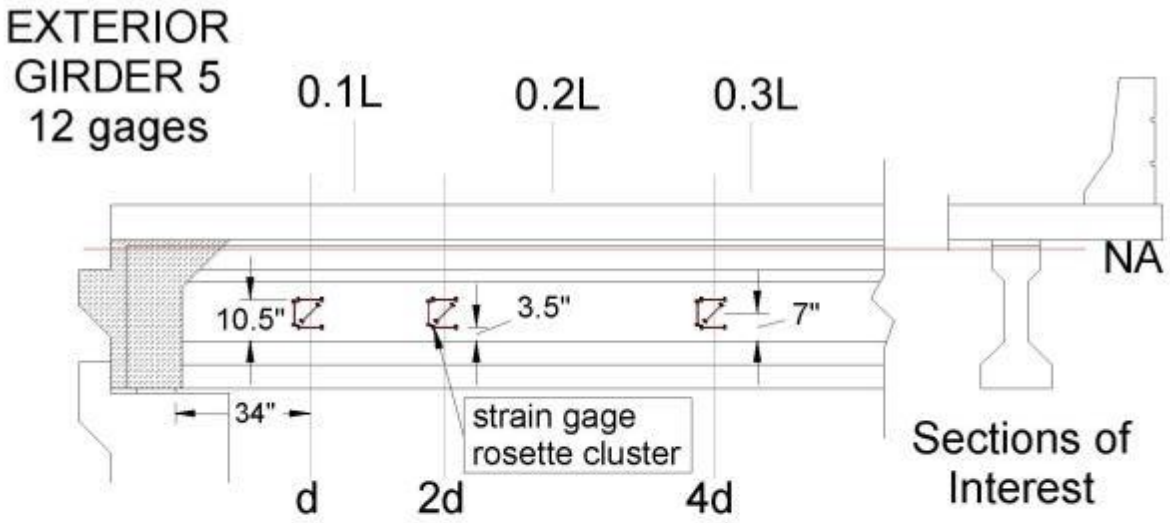

Figure 13. Girder 5 Instrumentation

The vibrating wire strain gage wires are all pulled to a set of boards where the ends are attached to terminal blocks. Most of the strain gage wires are 10 feet in length and will be used near the abutment, as shown in Figure 14.

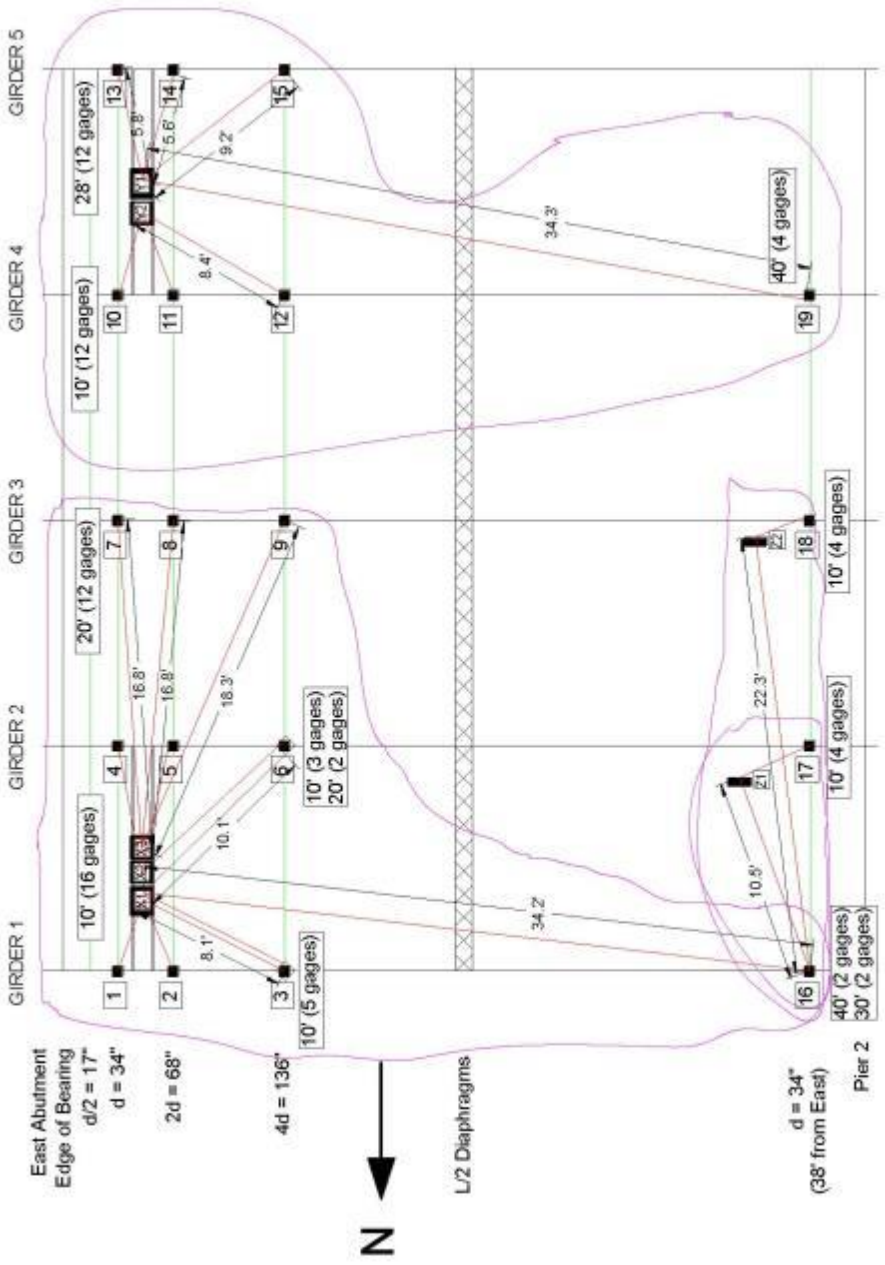

Figure 14. Strain Gage Wiring Diagram

Volunteers and Workers for Bridge 09002 Live Load Tests

Abutment Test Setup – Daytime (Wednesday August 14th):

- Meet at Brian Mathys' house by **6:00 AM**, van will bring supplies

Ben Dymond (612-219-1548)	Prep Team, Install Team & Wiring
Sam Konieczny (763-843-6082)	Prep Team & Pictures & Wiring
Mike Larson (920-344-5789)	Install Team
Brian Mathys (651-235-0744)	Install Team & Wiring
Paul Bergson (651-470-9732)	Safety Coordinator & Deck Marking

Abutment Truck Tests – Daytime (Thursday August 15th):

- Leave hotel by **6:45 AM**, van will bring supplies

Ben Dymond (612-219-1548)	Operations/Truck Director
Sam Konieczny (763-843-6082)	Data Sheet Recorder
Mike Larson (920-344-5789)	Data Sheet Recorder
Brian Mathys (651-235-0744)	Computer Data Collection
Paul Bergson (651-470-9732)	Safety Coordinator

Appendix A –Record Sheets
(next page)

Field Testing Bridge 09002 Deck Marking Record Sheet

Transverse Testing Locations

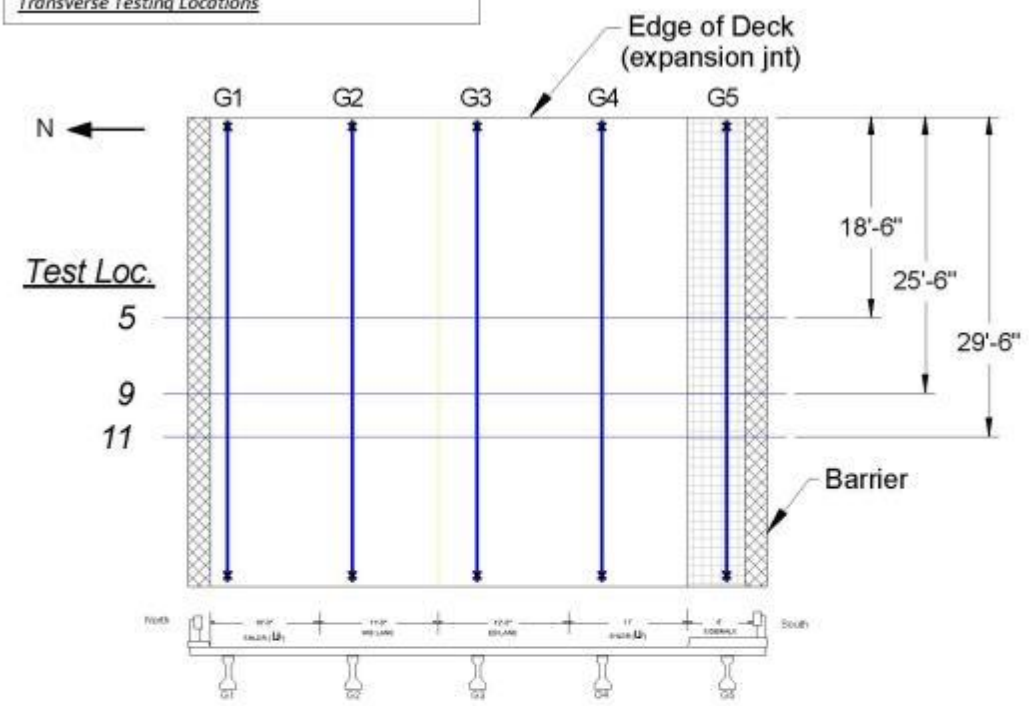

13

Field Testing Bridge 09002 Deck Marking Record Sheet

Driver's Tire Longitudinal Lines

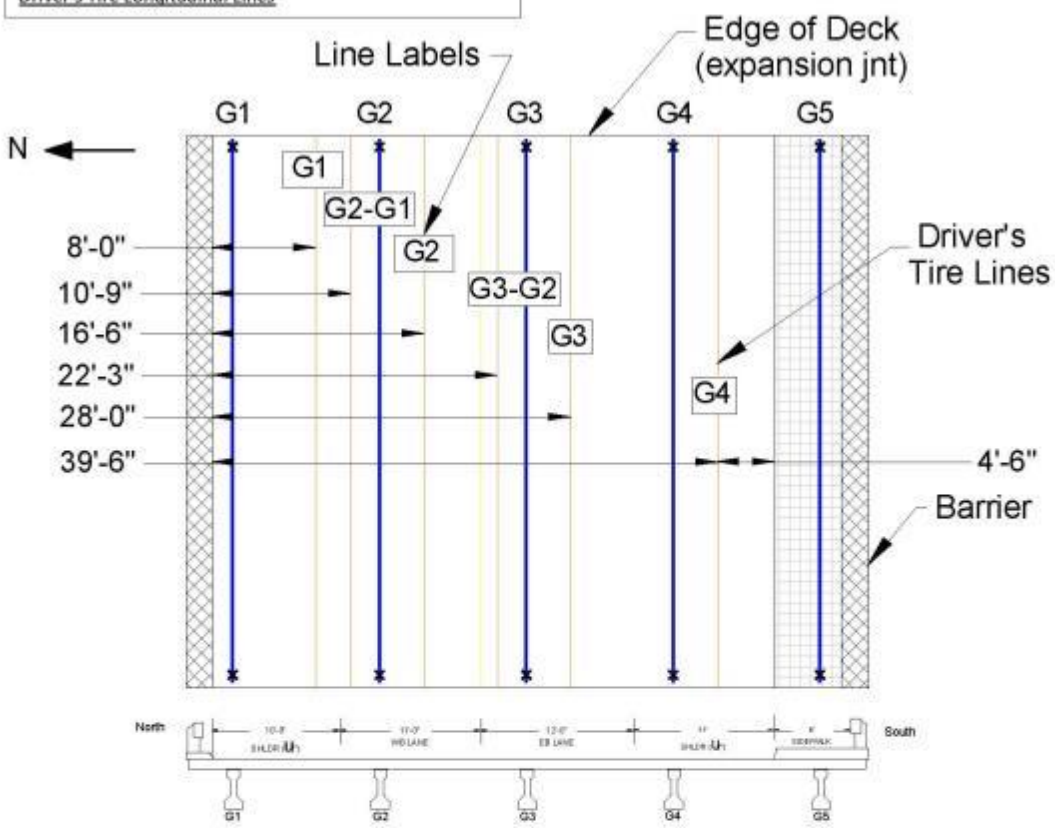

G.7 Bridge 65006 Testing Protocol

Bridge Information:

Bridge Number:	65006
Starting Date/Time:	August 28th 2013, 8 am
Location:	MN Hwy 19 over Birch Coulee Creek, in Renville County, near Morton, MN (Decimal degrees of Latitude, Longitude: 44.541754,-94.953718)
Year Built:	1983
End Diaphragm:	Partial Depth
Skew:	30 degrees
End Span Geometry:	5 girders spaced at 11.0' with span length 45 ft
d_c	34"

Objectives for Bridge 65006 Live Load Tests

Objective 1: Static Load Testing

Static tests are planned to verify transverse shear distribution near the . Shear distribution tests will be performed on the west end span of the structure (span 1), shown in Figure 1, and will include loading the structure in both lanes. Load will be applied with two MnDOT sand trucks filled so that their total weight is approximately 50 kips each. The trucks will be parked on the bridge at various locations for data collection.

Figure 1. Bridge 65006

Additional static tests are planned to verify transverse flexural distribution near L/2. One supplemental horizontal strain gage will be placed at 4d of two girders to determine the flexural strain and vertical strain distribution (for neutral axis calculation).

Objective 2: Visual Inspection of End Regions for Shear Cracks

Bridge 65006 has an inventory shear rating less than unity. Applying maximum truck load provides the opportunity to investigate possible shear cracks that may exist on the girders. These girders would most likely only be visible under the application of load. Visual inspection will be done on both an interior and exterior girder when the back-to-back truck configuration is parked at a maximum applied shear location. Any visible shear cracks will be recorded and photographed.

Planning for Bridge 65006 Live Load Tests

The truck tests are planned to occur on August 28 and August 29, 2013. Instrumentation of all bridge girders near the abutment will occur between 7 am and 7 pm on August 28, 2013. Truck tests near the abutment will occur during the day on August 29, 2013. The instrumentation will also be removed from the bridge after completion of truck testing on August 29, 2013. The tests should be completed rain or shine unless the weather is terrible. The following tasks need to be completed in preparation for the truck tests overnight. The responsibility for each of the tasks is identified below.

Task 1: Mark Truck Locations (UMN)

The locations where the trucks are to be positioned for the various static tests should be marked on the bridge prior to the truck tests. The use of marking paint should be used for a semi-permanent testing profile which will provide an outline for supplemental chalking prior to testing.

Task 2: Arrange for Loaded Trucks (MnDOT)

Two loaded sand trucks will be needed for performing the static tests. Each truck should nominally weigh 50 kips and have a front axle to back axle length of approximately 19'-8". Each truck will need to be weighed prior to testing and after testing. Weight information should be obtained on the front axle load (by itself), the rear tandem axle load (all four back wheels), and total load for each truck. A volunteer should fill out the "truck record sheet." The trucks should be tarped over the course of the testing to assure that no rain adds weight to the truck.

Task 3: Plan and Implement Traffic Control (MnDOT)/ (UMN)

Day 1 – Instrumentation: The bridge does not need to be closed at all, but UMN will close the shoulder using cones to mark the deck.

Day 2 – Truck Tests: The bridge will be closed during the day. Scheduled tests must take place when MnDOT traffic control crews are at the site, between 6:30 AM and 5:00 PM, for a total of 10.5 (really 7.5 hours of work time) of partial bridge closure. The first testing day will include all static tests done near the west abutment.

Schedule for Bridge 65006 Live Load Tests

Testing should be completed in 7.5 hours. The schedule for the abutment testing is presented in Table 1. The diagrams that describe the testing locations for each test description are shown in Figure 2 through Figure 7.

Row	Time	Start Time	Test	Duration (min)	Details	Priority	End Time	Traffic Control	Notes
1	6:30 AM		Abutment Start	80	Begin MnDOT travel & traffic control	0		None	
2	7:50 AM		Zero 1	12	Take measurements with no load before traffic control	0		None	
3	8:02 AM		G1 BB Loc 5	12	G1 back-to-back, rear axle east truck at Loc 5	1		Bridge is Closed	
4	8:14 AM		G2-G1 BB Loc 5	10	G2-G1 split back-to-back, rear axle east truck at Loc 5	1		"	
5	8:24 AM		G2-G1 ST Loc 0	12	G2-G1 split single west truck, rear axle at Loc 0	1		"	
6	8:36 AM		G2-G1 BB Loc 11	10	G2-G1 split back-to-back, rear axle east truck at Loc 11	1		"	
7	8:46 AM		Zero 2	12	Take measurements with no load	1		"	
*** Save Test Data, Close RTDAQ, Restart RTDAQ, Start Monitoring Table and open Flags & Data ---- Should prevent tests where not all data is captured ***									
8	8:58 AM		G2 BB Loc 5	12	G2 back-to-back, rear axle east truck at Loc 5	1		"	
9	9:10 AM		G3-G2 BB Loc 5	12	G3-G2 split back-to-back, rear axle east truck at Loc 5	1		"	
10	9:22 AM		Zero 3	12	Take measurements with no load	1		"	
*** Save Test Data, Close RTDAQ, Restart RTDAQ, Start Monitoring Table and open Flags & Data ---- Should prevent tests where not all data is captured ***									
11	9:34 AM		G3 BB Loc 5	10	G3 back-to-back, rear axle east truck at Loc 5	1		"	
12	9:44 AM		G3 ST Loc 0	12	G3 single west truck, rear axle positioned at Loc 0	1		"	
13	9:56 AM		G3 BB Loc 11	10	G3 back-to-back, rear axle east truck at Loc 11	1		"	
14	10:06 AM		Zero 4	12	Take measurements with no load	1		"	
*** Save Test Data, Close RTDAQ, Restart RTDAQ, Start Monitoring Table and open Flags & Data ---- Should prevent tests where not all data is captured ***									
15	10:18 AM		G4-G3 BB Loc 5	12	G4-G3 back-to-back, rear axle east truck at Loc 5	1		"	
16	10:30 AM		G4 BB Loc 5	10	G4 back-to-back, rear axle east truck at Loc 5	1		"	
17	10:40 AM		Zero 5	12	Take measurements with no load	1		"	
*** Save Test Data, Close RTDAQ, Restart RTDAQ, Start Monitoring Table and open Flags & Data ---- Should prevent tests where not all data is captured ***									
18	10:52 AM		G5-G4 BB Loc 5	10	G5-G4 back-to-back, rear axle east truck at Loc 5	1		"	
19	11:02 AM		G5-G4 ST Loc 0	12	G5-G4 back-to-back, rear axle east truck at Loc 5	1		"	
20	11:14 AM		G5-G4 BB Loc 11	12	G5-G4 split back-to-back, rear axle east truck at Loc 11	1		"	
21	11:26 AM		G5 BB Loc 5	10	G5 back-to-back, rear axle east truck at Loc 5	1		"	
22	11:36 AM		Zero 6	12	Take measurements with no load before traffic control	1		"	
*** Save Test Data, Close RTDAQ, Restart RTDAQ, Start Monitoring Table and open Flags & Data ---- Should prevent tests where not all data is captured ***									

23	11:48 AM		G1 BB Loc 5	12	G1 back-to-back, rear axle east truck at Loc 5	1		"	repeatability test
24	12:00 PM		G2-G1 BB Loc 5	10	G2-G1 split back-to-back, rear axle east truck at Loc 5	1		"	repeatability test
25	12:10 PM		G2-G1 ST Loc 0	12	G2-G1 split single west truck, rear axle at Loc 0	1		"	repeatability test
26	12:22 PM		G2-G1 BB Loc 11	10	G2-G1 split back-to-back, rear axle east truck at Loc 11	1		"	repeatability test
27	12:32 PM		Zero 7	12	Take measurements with no load	1		"	
*** Save Test Data, Close RTDAQ, Restart RTDAQ, Start Monitoring Table and open Flags & Data ---- Should prevent tests where not all data is captured ***									
28	12:44 PM		G2 BB Loc 5	12	G2 back-to-back, rear axle east truck at Loc 5	1		"	repeatability test
29	12:56 PM		G3-G2 BB Loc 5	10	G3-G2 split back-to-back, rear axle east truck at Loc 5	1		"	repeatability test
30	1:06 PM		Zero 8	12	Take measurements with no load	1		"	
*** Save Test Data, Close RTDAQ, Restart RTDAQ, Start Monitoring Table and open Flags & Data ---- Should prevent tests where not all data is captured ***									
31	1:18 PM		G3 BB Loc 5	10	G3 back-to-back, rear axle east truck at Loc 5	1		"	repeatability test
32	1:28 PM		G3 ST Loc 0	12	G3 single west truck, rear axle positioned at Loc 0	1		"	repeatability test
33	1:40 PM		G3 BB Loc 11	10	G3 back-to-back, rear axle east truck at Loc 11	1		"	repeatability test
34	1:50 PM		Zero 9	12	Take measurements with no load	1		"	
*** Save Test Data, Close RTDAQ, Restart RTDAQ, Start Monitoring Table and open Flags & Data ---- Should prevent tests where not all data is captured ***									
35	2:02 PM		G4-G3 BB Loc 5	12	G4-G3 back-to-back, rear axle east truck at Loc 5	1		"	repeatability test
36	2:14 PM		G4 BB Loc 5	10	G4 back-to-back, rear axle east truck at Loc 5	1		"	repeatability test
37	2:24 PM		Zero 10	12	Take measurements with no load	1		"	
*** Save Test Data, Close RTDAQ, Restart RTDAQ, Start Monitoring Table and open Flags & Data ---- Should prevent tests where not all data is captured ***									
38	2:36 PM		G5-G4 BB Loc 5	10	G5-G4 back-to-back, rear axle east truck at Loc 5	1		"	repeatability test
39	2:46 PM		G5-G4 ST Loc 0	12	G5-G4 back-to-back, rear axle east truck at Loc 5	1		"	repeatability test
40	2:58 PM		G5-G4 BB Loc 11	12	G5-G4 split back-to-back, rear axle east truck at Loc 11	1		"	repeatability test
41	3:10 PM		G5 BB Loc 5	10	G5 back-to-back, rear axle east truck at Loc 5	1		"	repeatability test
42	3:20 PM		Zero 11	12	Take measurements with no load	0		"	
43	3:32 PM		Day 2 Complete		Testing complete and MnDOT leaves	0		None	

508

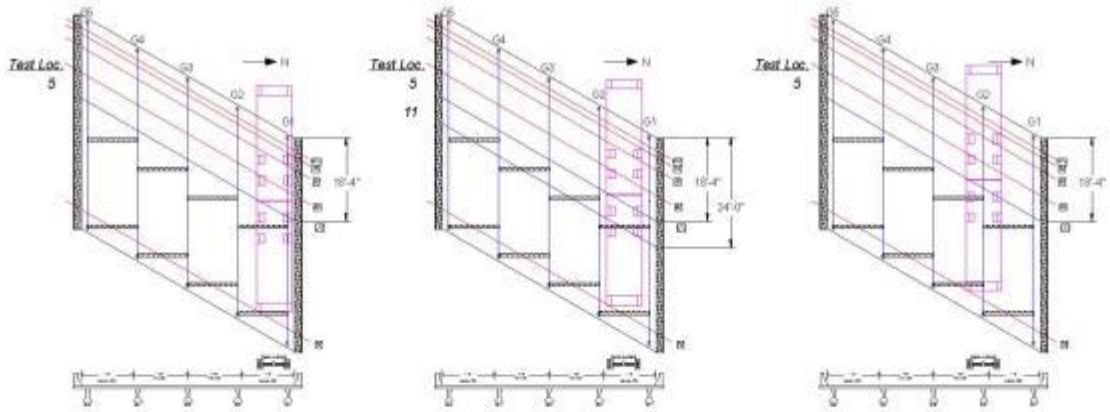

Figure 2. Exterior Girder (G1), Interior-Exterior Girder (G2-G1) Split, and Interior Girder (G2) Abutment Testing Locations

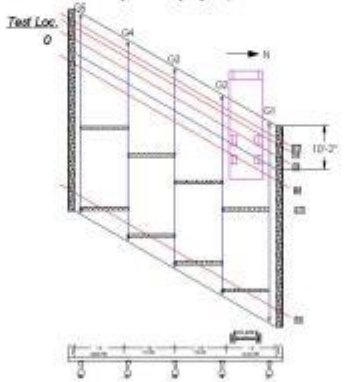

Figure 3. Interior-Exterior Girder (G2-G1) Split Abutment Single Truck Testing Location

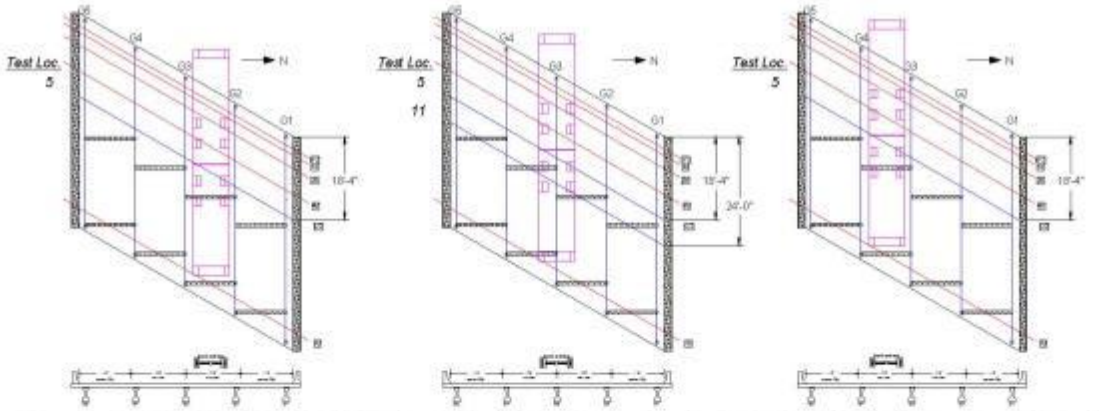

Figure 4. Interior-Interior Girder (G3-G2) Split, Interior Girder (G3), and Interior-Interior Girder (G3-G2) Split Abutment Testing Locations

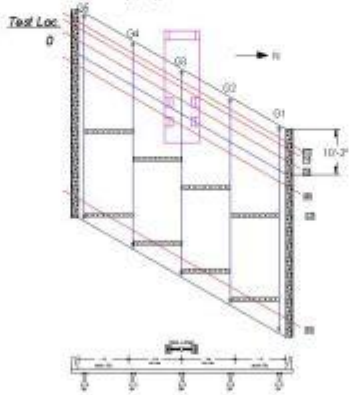

Figure 5. Interior Girder (G3) Abutment Single Truck Testing Location

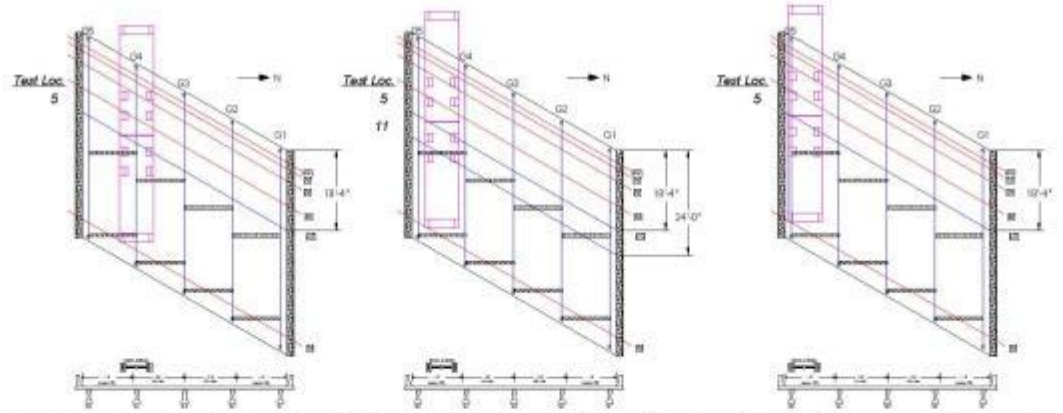

Figure 6. Interior Girder (G4), and Interior-Exterior Girder (G5-G4) Split, and Exterior Girder (G5) Abutment Testing Locations

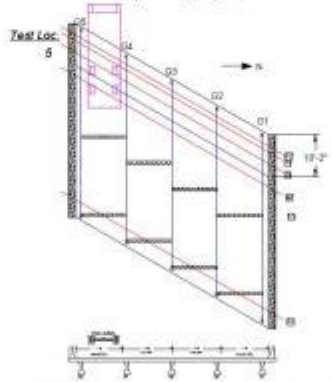

Figure 7. Interior-Exterior Girder (G5-G4) Split Abutment Single Truck Testing Location

511

Instrumentation and Data Collection for Bridge 65006 Live Load Tests

For all static testing, Geokon vibrating wire strain gage data will be collected using a Campbell Scientific CR1000 data acquisition system. All channels will be scanned five times per truck stop which takes approximately 8 minutes.

Instrumentation will be installed on all five girders, as labeled in Figure 8. Girder instrumentation plans are shown in Figure 9 through Figure 13.

Figure 8. West abutment Girder Numbering

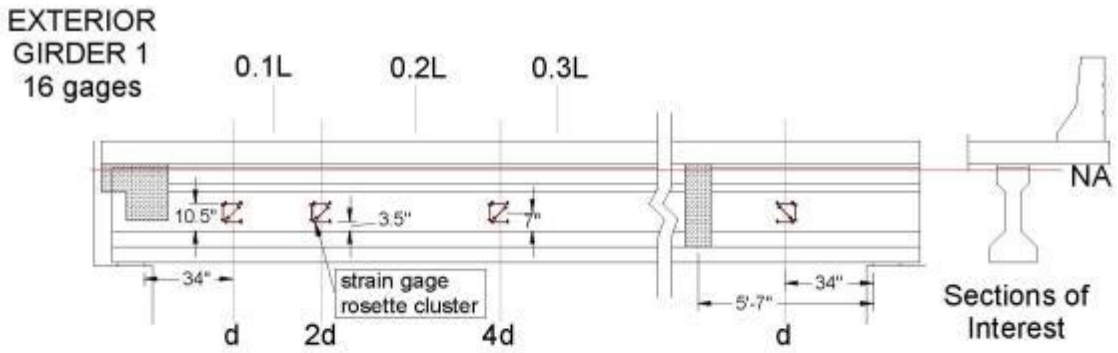

Figure 9. Girder 1 Instrumentation

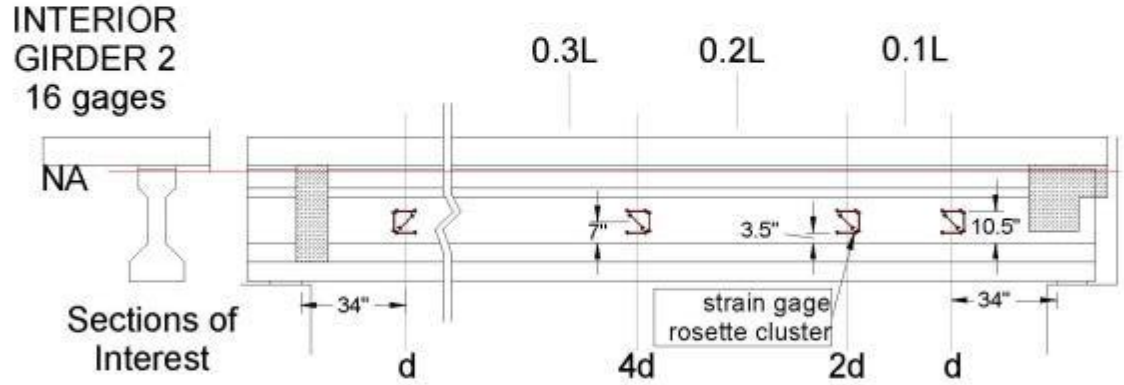

Figure 10. Girder 2 Instrumentation

513

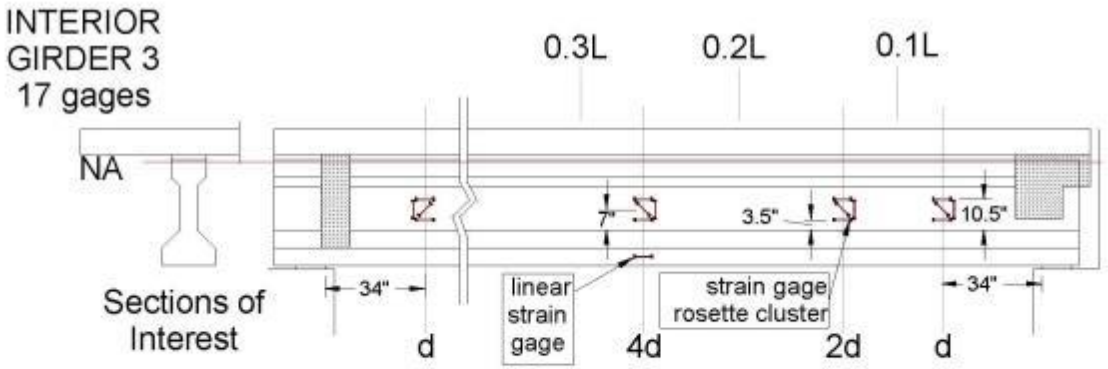

Figure 11. Girder 3 Instrumentation

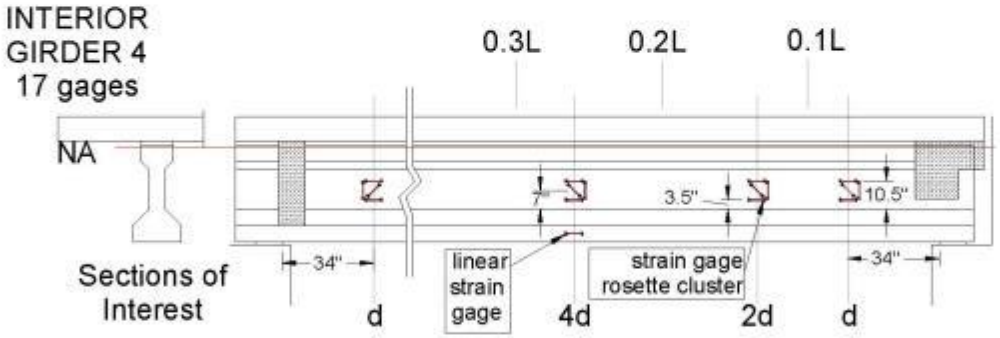

Figure 12. Girder 4 Instrumentation

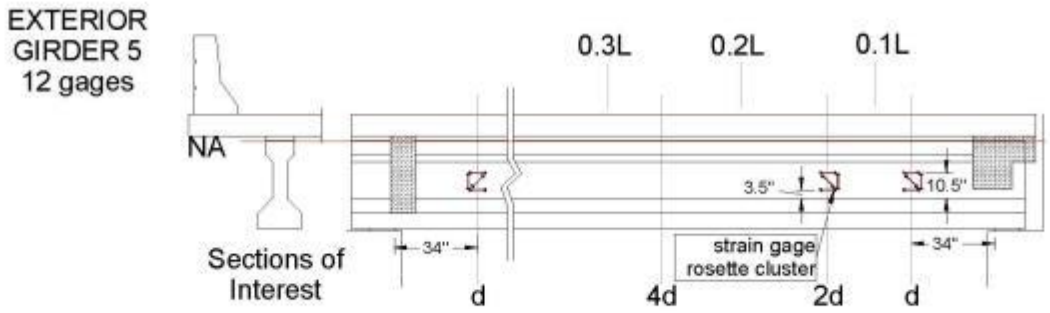

Figure 13. Girder 5 Instrumentation

The vibrating wire strain gage wires are all pulled to a set of boards where the ends are attached to terminal blocks. Most of the strain gage wires are 10 feet in length and will be used near the abutment, as shown in Figure 14.

515

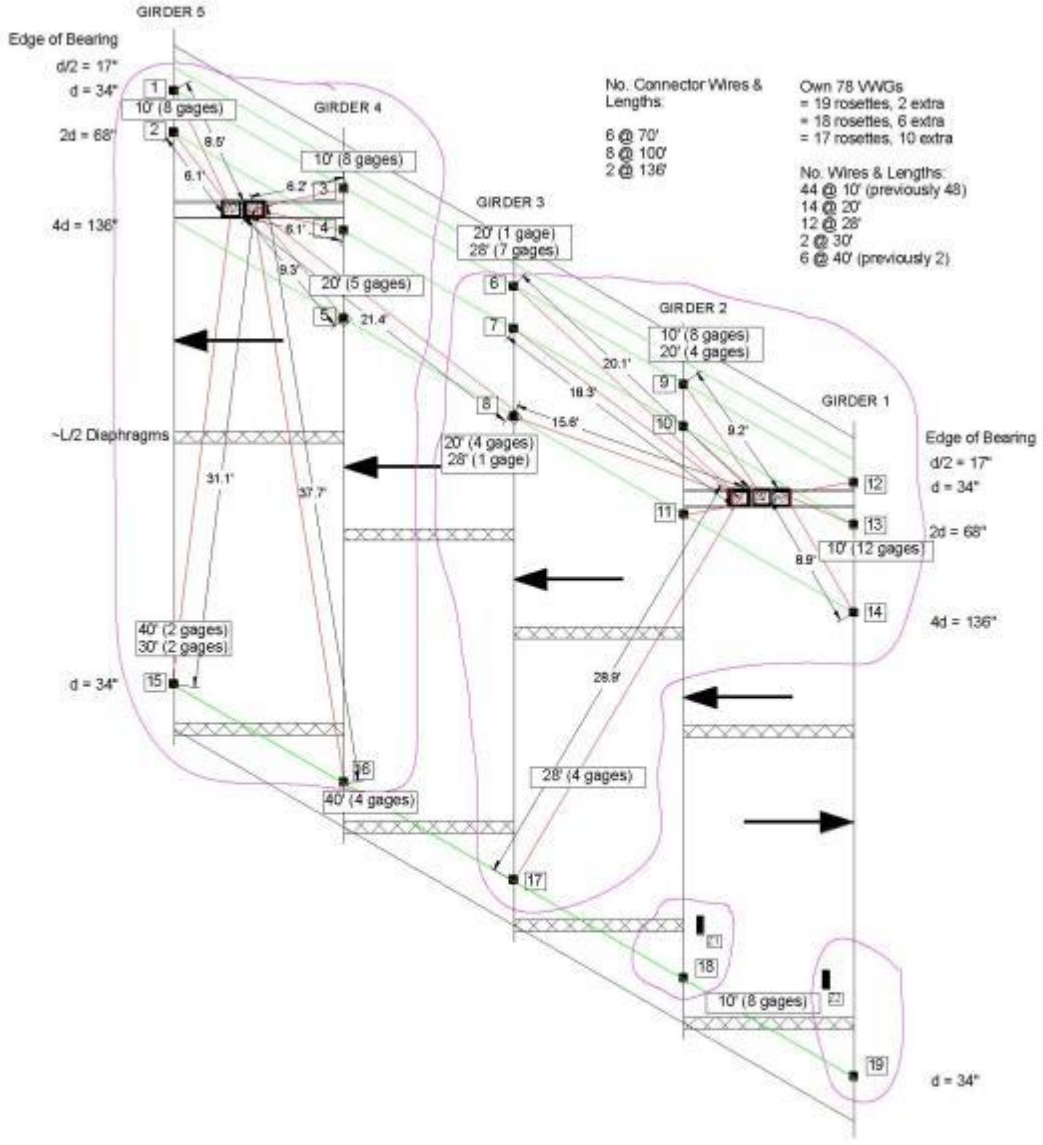

Figure 14. Strain Gage Wiring Diagram

Volunteers and Workers for Bridge 65006 Live Load Tests

Abutment Test Setup – Daytime (Wednesday August 28th):

- Meet at Brian Mathys' house by **6:00 AM**, van will bring supplies

Ben Dymond (612-219-1548)	Install Team & Wiring & Deck Marking
Sam Konieczny (763-843-6082)	Prep Team & Pictures
Mike Larson (920-344-5789)	Install Team & Board Construction
Brian Mathys (651-235-0744)	Prep Team & Wiring
Brock Hedegaard (406-489-1985)	Wiring & Deck Marking

Abutment Truck Tests – Daytime (Thursday August 29th):

- Leave hotel by **6:45 AM**, van will bring supplies

Ben Dymond (612-219-1548)	Operations/Truck Director
Sam Konieczny (763-843-6082)	Data Sheet Recorder
Mike Larson (920-344-5789)	Data Sheet Recorder
Brock Hedegaard (406-489-1985)	Computer Data Collection
Brian Mathys (651-235-0744)	Computer Data Collection
Cathy French (763-227-6575))	Safety Coordinator
Ken Ito (612-747-5023)	

Appendix A –Record Sheets

(next page)

Field Testing Bridge 65006

Deck Marking Sheets

Transverse Testing Locations

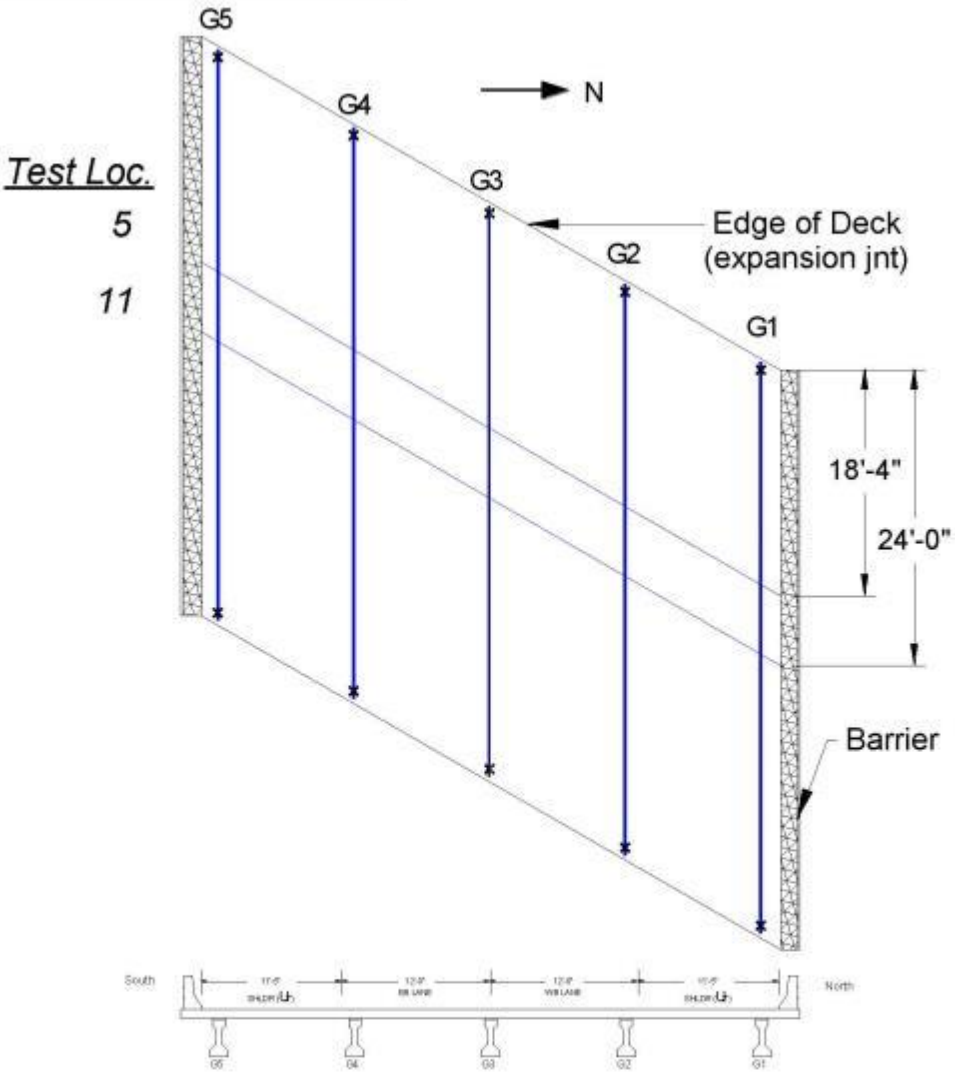

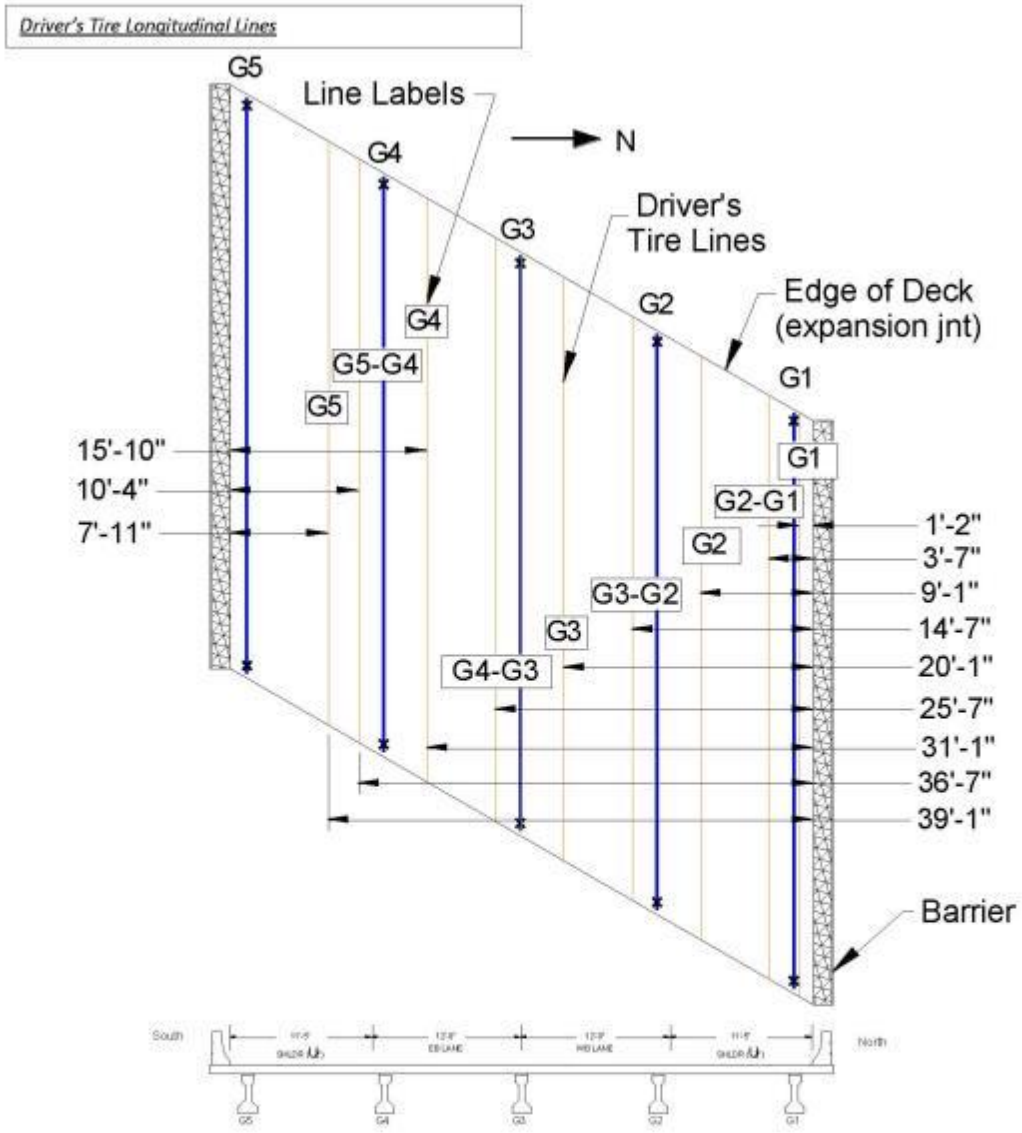
Driver's Tire Longitudinal Lines
G5
Line Labels
N
G4
Driver's
Tire Lines
G3
G2
Edge of Deck
(expansion jnt)
G1
G4
G5-G4
G5
15'-10"
10'-4"
7'-11"
G1
G2-G1
G2
G3-G2
G3
G4-G3
1'-2"
3'-7"
9'-1"
14'-7"
20'-1"
25'-7"
31'-1"
36'-7"
39'-1"
Barrier
South
North

G.8 Data Sheets Typical of all Bridges (taken from Br. 65006)

Task Descriptions

- Prep Team

  Use blank aluminum plate to install LOWER (only) corner mounts for dog bone jig plate

  1. Prep surface with water, wire brush, and rag
  2. Set blank aluminum plate on top of 2° level that is balanced on the bottom flange/web interface
  3. Apply epoxy to LOWER corner mounts and touch to web
  4. Remove aluminum plate from web to leave epoxy marks
  5. Spray epoxy marks located on web with accelerant
  6. Reapply aluminum plate with LOWER corner mounts in same location to permanently attached (epoxied)
  7. Apply strain relief aluminum angle to the right (when abutment on right) or left (when abutment on left) of the LOWER corner mount with same epoxy method

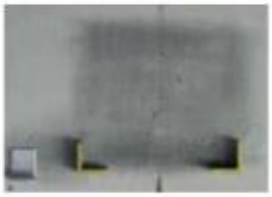

- Install Team

  Use pre-installed LOWER corner mounts and dog bone jig to install strain gages in rosette pattern (4 gages)

  1. Set four VWGs into dog bone jig while flush with web (in corner mounts with spacer set screws)
  2. Secure VWG with set screws
  3. Apply epoxy to mounting blocks of VWG, touch to web using corner mounts and spacer set screws as guide
  4. Remove
  5. Spray epoxy marks located on web with accelerant
  6. Reapply VWG in same location using dog bone jig with corner mounts and spacer set screws as guide to permanently attach VWG (epoxied)
  7. Trace border of dog bone jig with permanent marker for future use
  8. Remove LOWER corner mounts prior to removing dog bone jig for ease
  9. Install VWG wire with small hose clamp after complete
  10. Write VWG wire number on concrete surface
  11. Record VWG location and wire number on data sheets
  12. Zip tie 4 VWG wires to strain relief aluminum angle

- Wiring

  Gather all VWG wires after zip tied to strain relief, pull towards girder boards, attached to terminal end blocks on girder boards X, Y, Z.

  1. Record which VWG is attached to which location in rosette pattern
     a. 0.5d-G4-B at location 0.5d, on Girder 4, and in the Bottom rosette position
     b. 1.0d-G3-T at location 1.0d, on Girder 3, and in the Top rosette position

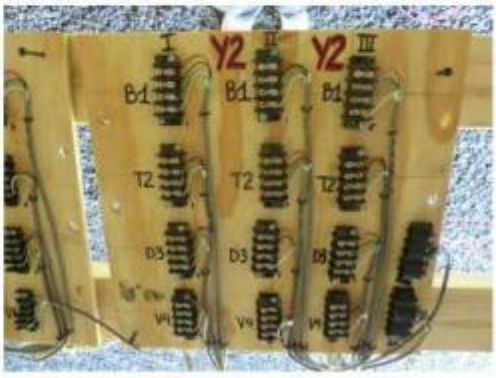

c. 2.0d-G2-D at location 2.0d, on Girder 2, and in the Diagonal rosette position
d. 4.0d-G1-V at location 4.0d, on Girder 1, and in the Vertical rosette position

2. Use wiring guide data sheets to attach VWG wires to appropriate girder board
3. Record which VWG location is wired to which girder board

- Computer Data Collection

In charge of the laptop computer and CR1000 system/cart. Collect data from each truck location test and record the test name and test time.

1. Turn on generator.
2. Plug computer and CR1000 into power strip from generator extension cord.
3. Run RTDAQ in the field monitor mode.
4. Use Flag Control to start each test cycle.
5. Name each 5 cycle test with the appropriate test name after cycle starts.
6. Record start time for each test on paper form.
7. Append (save) each test's data to the large .dat file after each test.

- Data Sheet Recorder

Use data sheets to record every test's precise truck position (along length of bridge and perpendicular to length of bridge). Use chalk grid on deck as reference.

1. Use provided data sheets.
2. Record time that the truck(s) are in position under the appropriate truck test
3. Record how far the rear axle tires are off the grid lines along the length of the bridge and perpendicular to the length of the bridge, for every truck test.

- Deck Shoulder Marker

Use grid reference sheet to layout the bridge deck grid for truck tests.

1. Mark positions of grid at the outside edge of the shoulder, near barrier, with white marking spray paint when the shoulder is closed (also near expansion joint).
2. Prior to testing use chalk to grid lines along bridge deck in direction of traffic and perpendicular to direction of traffic.

- Shear Crack Inspector

While truck loads are on bridge over particular girder, check that girder with flashlight for shear cracks near support.

1. During truck tests, when trucks are over each individual girder throughout day, check the web of the girder near support with flashlight for diagonal shear cracks that might open when load is applied.

- Pictures

Take more pictures than you have ever taken in your life. Literally, take a picture of everything, even things we are not adding, modifying, or working near. Spin circles and take pictures.

1. strain gage locations
   a. process of application
      i. corner mounting angles, dog bone jig, epoxy process
   b. end product strain gage configuration

    c. strain relief angles w/ and w/o wires
2. girder naming convention
3. deck marking/grid layout
4. ladder usage and safety equipment
5. lighting
6. sand trucks for testing
    a. from every angle
    b. axles
    c. positions during every test location
        i. position
        ii. back-to-back, side-by-side, one truck only
7. snooper truck usage for instrumentation, removal, etc.
8. data collection system
    a. CR1000, cart, connector wires, girder boards
9. pictures of bridge in general
10. LITERALLY, PICTURES OF ANYTHING AND EVERYTHING!

Equipment for Bridge 65006 Live Load Tests

Instrumentation

VW Gages and Accessories

- VW Gages (78 extra)
- Extra end blocks (2 cylinders full)
- Red VWG testing box and power cord
- Allen Wrenches (3)
  - size for VWG end blocks
- Loctite Epoxy (***refrigerator***) and Accelerant (4)
- Adjustable (water pump) pliers (2)
- Cans of Compressed Air (2)
- Small/Medium Adjustable Wrench
- ~~Hammers (2)~~
- Phillips Head Screw Driver (4)
- Flat Head Screw Driver (4)
- Acetone
- Small Plastic tub (2)
- Rags
- Spray water bottles & water (2)
- Dog bone mounting jig (2)
- Blank plate mounting jig (2)
- Aluminum corner tabs for mounting jig (80)
- Strain relief aluminum angles with large hole (40)

Connectors and wiring boards

- Wiring boards X1, X2, X3, Y1, Y2, Z1, Z2
- Pipe clamps (7)
- Long Connector wires – 2 @ 136', 8 @ 100', 6 @ 70' for 16 total
  - ~~spool rod to unreel the long cables~~
- Connector crimpers and extra supplies
- Wiring board 2x4 supports at 10' long (4)
  - Battery powered drill
  - Drywall screws (1" max length)
- Wiring board 2x4 support extensions at 3' long (8)
- Six foot 2x4 for ladder to hold 2' level for corner mounts
- Extra 100' of Belden wire
- Extra terminal blocks (2)

Data Acquisition Setup

- Plastic to cover van door with computer
- CR1000 cart with power cord
  - grounding wire and rod
- Computer with power cord and USB connection cord
  - Thumb drive
- Small CSi Screwdrivers (2)
- Generator
- ~~AC/DC car converter~~
- Small gas can
- Extension Cords (2)
- Power strip
- Wire cutters
- Wire strippers

Instrumentation Layout

- Small Sledge Hammer
- ~~Threaded rod (8)~~
  - with 2x4 blocks (12)
- Sidewalk Chalk
- White marking paint (2)
- ~~Walkie Talkies~~
- 150' Measuring Tape (1)
- Tape Measures (3)
- Framing square (2)
- 20-24' ladder (2)
- Ladder Extenders
- Long chain and key lock

Miscellaneous

- Water proof wading boots in hard hat cabinet (2 pair)
- 6' long 2x10 or 2x12
- WD-40
- Zip Ties (small and large)
- Duct Tape (red and silver)
- Camera (Ben's and lab)
- ~~Hand saw~~
- ~~Electric Circular Saw~~
- ~~Hammer Drill~~
  - ~~5/32" concrete drill bit~~
- 5/16" hex head drill bit
- Grinder with wire brush wheel to clear concrete
  - Dust mask (2-3)
  - Face guard for grinding
  - ~~or use battery operated drill with wire brush adapter~~
- Hammer
- 12" Irwin clamps (2)
- Torpedo Levels (2)
- Pink String
- Safety harness and tie off for working on snooper (3)
- Flux
- Solder
- Solder tools

- Electrical Tape (orange and black)
- Trash bags/Target bags
- Flash lights (2) for shear crack inspection
    - Batteries for flashlights
- Permanent Markers
- Pen, Paper
- Clip boards (4)
- Data sheets
- Notebook from old bridge test
- Stop and Yield signs
- Traffic Cones (~5)
- Snapping chalk line
- ~~Set of synced watches from Carol's office~~
- Safety equipment
    - Reflective vests (6)
    - Reflective pants (6)
    - Hard hats (6)
    - Safety glasses (3-4)
    - Long pants
    - Steel toe boots

Field Testing Bridge 65006

Truck Measurement Sheet

Recorder: _____ **Date:** _____

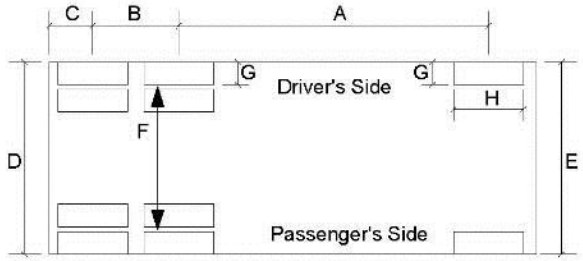

Dim A = CL of front axle to CL of middle axle on driver's side
Dim B = CL of middle axle to CL of rear axle on driver's side
Dim C = CL of rear axle to end of truck
Dim D = out-to-out of rear tire treads
Dim E = out-to-out of front tire treads
Dim F = center-to-center distance between rear tandem
Dim G = front tire tread width / rear tire tread width
Dim H = front tire tread length / rear tire tread length (touching ground)

Truck No.	Driver Name	Truck Model	Dim A	Dim B	Dim C	Dim D	Dim E	Dim F	Dim G	Dim H	Front Axle Weight	Rear Tandem Axle Weight (Rear + Middle)	Total Weight
									/	/			
									/	/			

Field Testing Bridge 65006 Truck Record Sheet

Recorder: _____ **Date:** _____ **Focus Girder:** G3

Truck Test Name: _____ **Start Test Time:** _____

Description: _____

Truck Position:

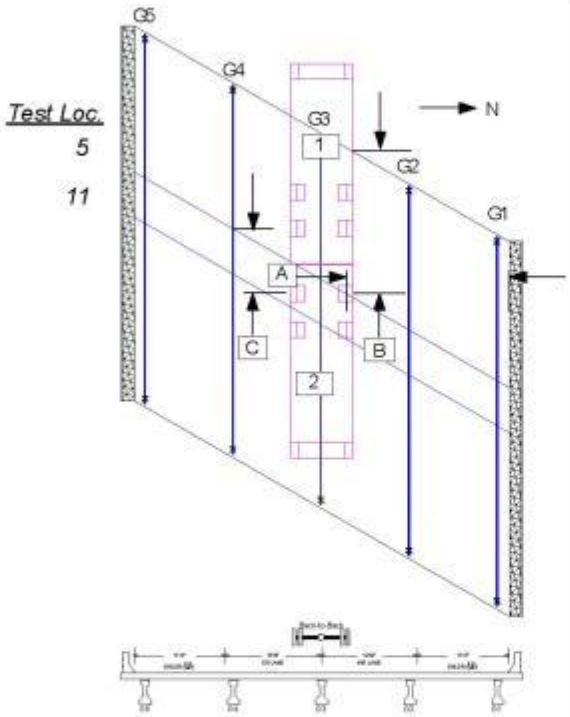

MnDOT Truck Number

1 = _____

2 = _____

Dimensions

A = Distance from center line rear tandem on eastern truck (truck 2) to inside face of barrier.

B = Distance from center line rear axle on eastern truck (truck 2) to pier joint

C = Distance from center line rear axle on western truck (truck 2) to center line rear axle on western truck (truck 1)

Test	Dim A	Dim B	Dim C
G3 BB Loc 5			
G3 ST Loc 0			--------
G3 BB Loc 11			

Field Testing Bridge 65006 Rosette Record Sheet

Recorder: _____ **Date:** _____

End of Span: _____
(abutment or pier)

Rosette Position: _____ **Girder Number:** _____
(d/2=17", d=34", 2d=68", 4d=136") (1, 2, 3, 4, or 5)

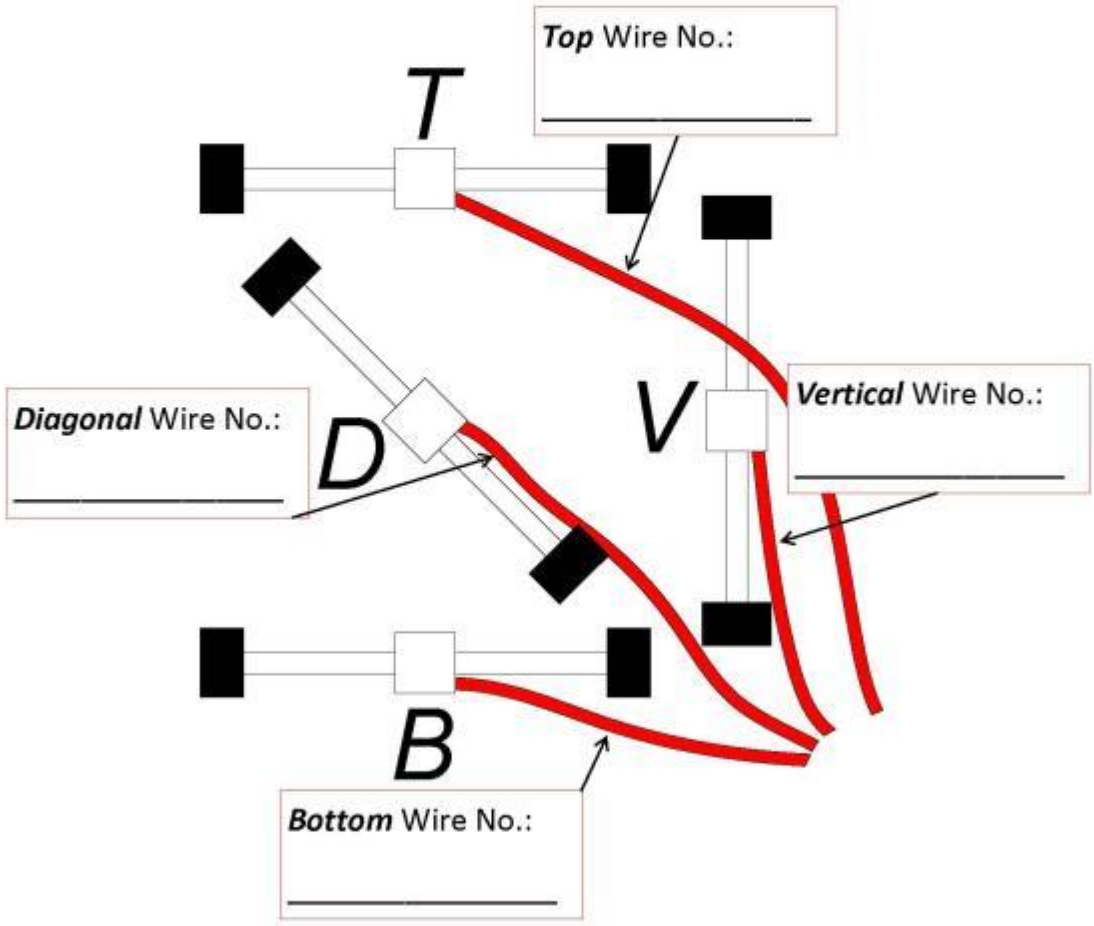

Field Testing Bridge 65006 Rosette Record Sheet

Recorder: _____ **Date:** _____

End of Span: _____
(abutment or pier)

Gage Position: _____ **Girder Number:** _____
(4d=136") (1, 2, 3, 4, or 5)

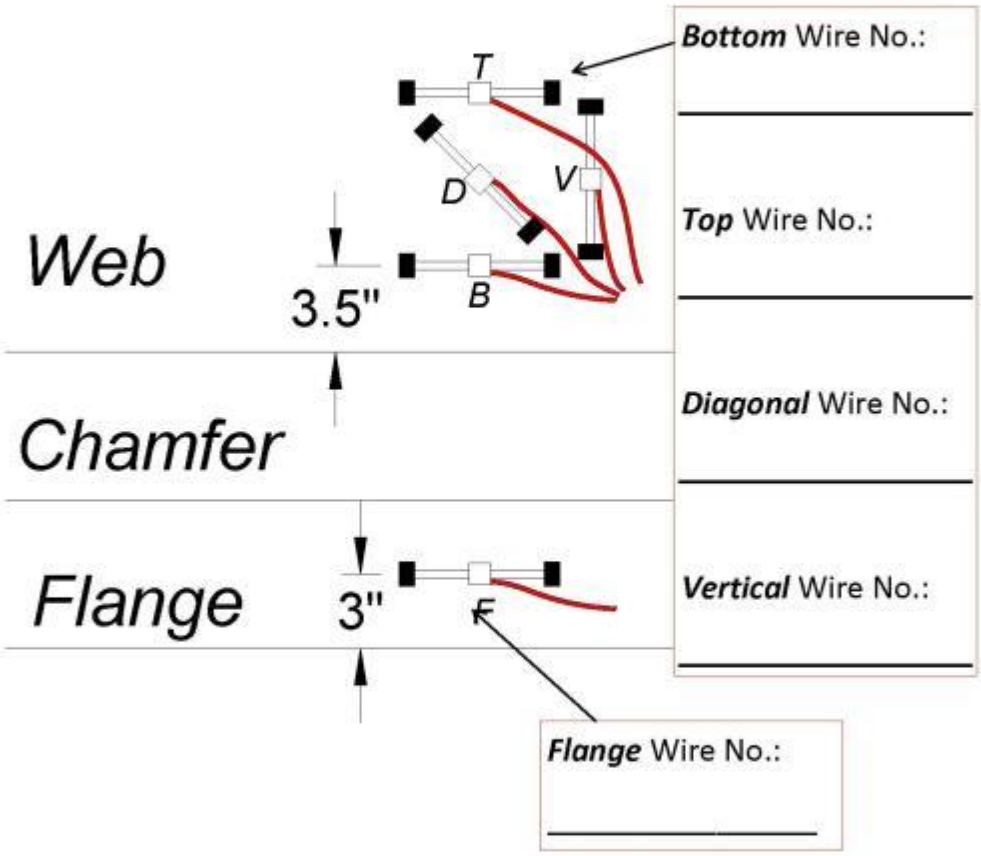

Field Testing Bridge 65006 Rosette Record Sheet

Recorder: _____ **Date:** _____

End of Span: _____
(abutment or pier)

Rosette Position: _____ **Girder Number:** _____
(d/2=17", d=34", 2d=68", 4d=136") (1, 2, 3, 4, or 5)

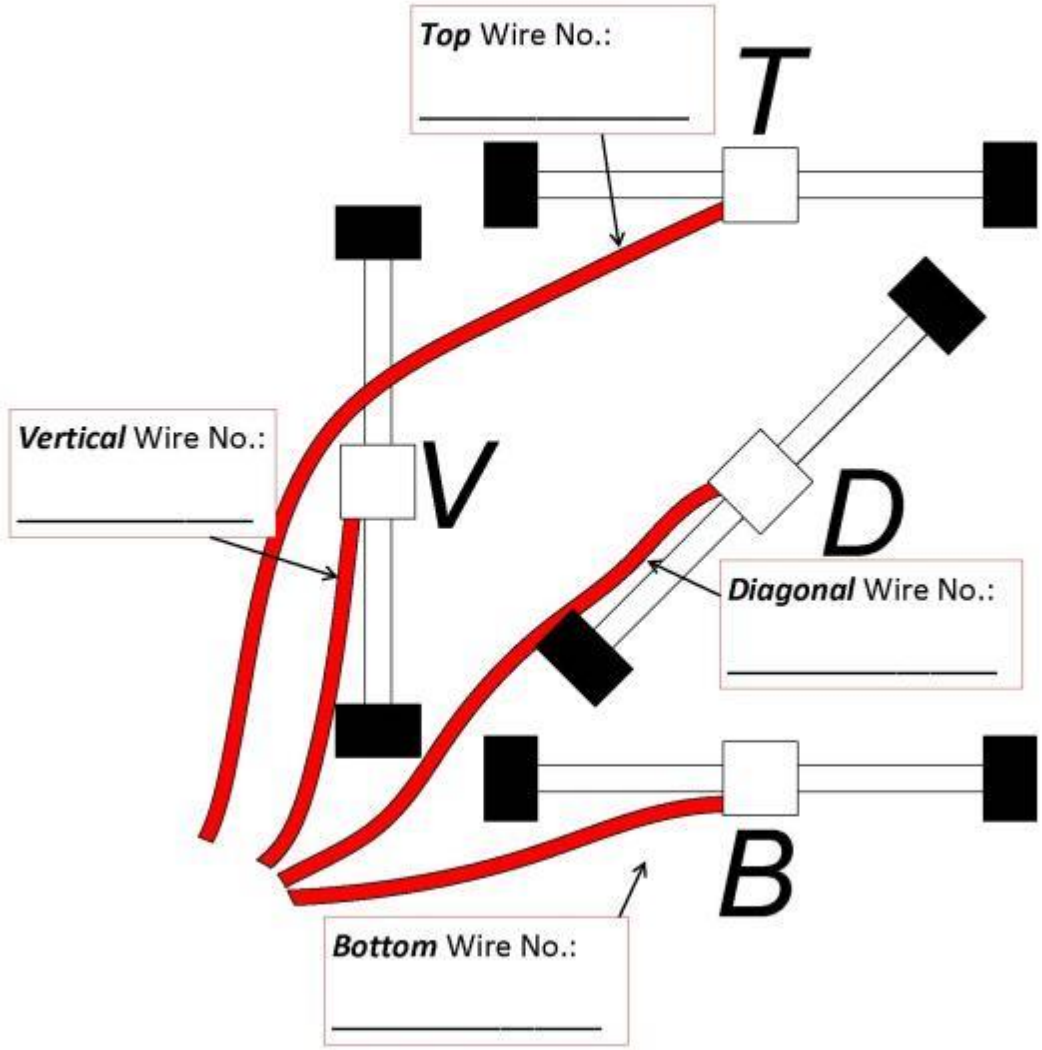

Field Testing Bridge 65006 Rosette Record Sheet

Recorder: _____ **Date:** _____

End of Span: _____
(abutment or pier)

Gage Position: _____ **Girder Number:** _____
(4d=136") (1, 2, 3, 4, or 5)

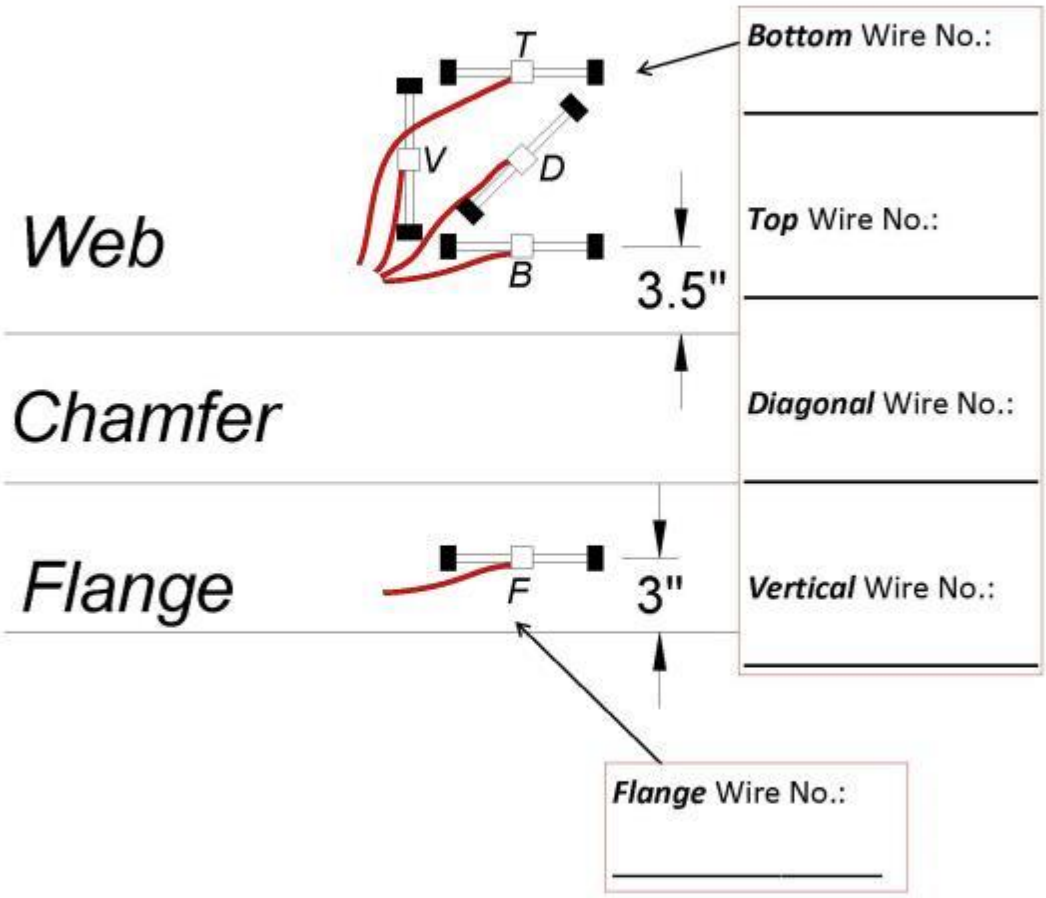

Field Testing Bridge 65006 **Abutment** Channel Record Sheet

Board	Conn	Rosette	Location	Channel #	Board	Conn	Rosette	Location	Channel #
				1					41
				2					42
				3					43
				4					44
				5					45
				6					46
				7					47
				8					48
				9					49
				10					50
				11					51
				12					52
				13					53
				14					54
				15					55
				16					56
				17					57
				18					58
				19					59
				20					60
				21					61
				22					62
				23					63
				24					64
				25					65
				26					66
				27					67
				28					68
				29					69
				30					70
				31					71
				32					72
				33					73
				34					74
				35					75
				36					76
				37					77
				38					78
				39					79
				40					80

Field Testing Bridge 65006

Field Data Record Sheet

Loc	Rosette Position	Abutment																	
		Girder 5				Girder 4				Girder 3				Girder 2				Girder 1			
		Chnl	Strain - 3 Test ID's			Chnl	Strain - 3 Test ID's			Chnl	Strain - 3 Test ID's			Chnl	Strain - 3 Test ID's			Chnl	Strain - 3 Test ID's		
d	B																				
	T																				
	D																				
	V																				
2d	B																				
	T																				
	D																				
	V																				
4d	B																				
	T																				
	D																				
	V																				
d	B																				
	T																				
	D																				
	V																				
	F																				
Pier																					

Field Testing Bridge 65006 CPU Board Record Sheet

Recorder: _____ **Date:** _____

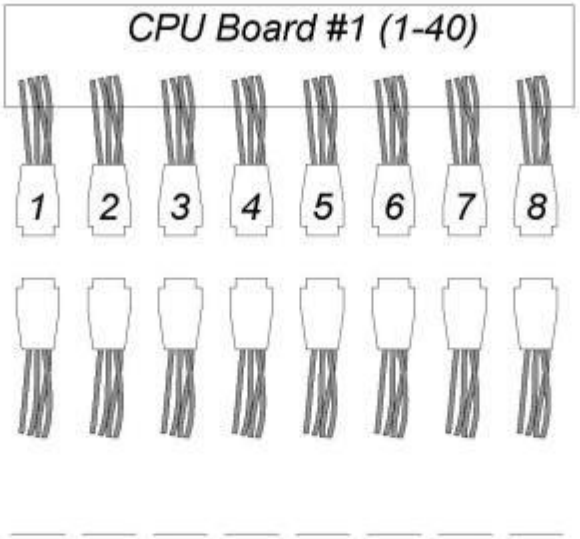

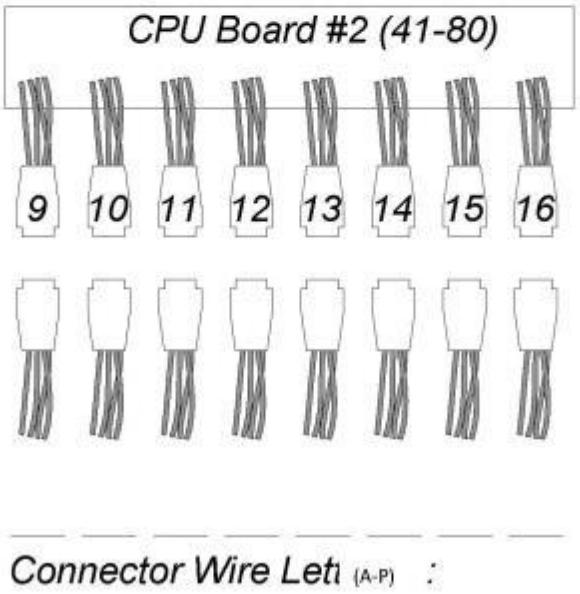

Field Testing Bridge 65006
Recorder: _____

CPU Board Record Sheet
Date: _____

Testing End (abutment or pier): _____

Board X1

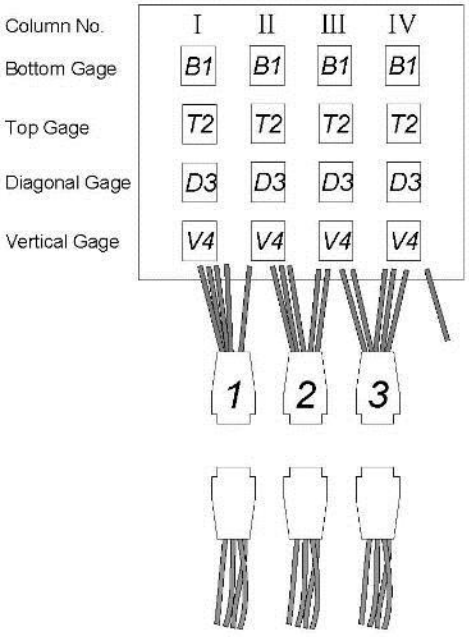

Connector Wire Lettering:
(A-P)

Board Loc.	Strain Gage Wire No.	Girder No. / Gage Position
X1-I-B1		
X1-I-T2		
X1-I-D3		
X1-I-V4		
X1-II-B1		
X1-II-T2		
X1-II-D3		
X1-II-V4		
X1-III-B1		
X1-III-T2		
X1-III-D3		
X1-III-V4		
X1-IV-B1		
X1-IV-T2		
X1-IV-D3		
X1-IV-V4		

Field Testing Bridge 65006 CPU Board Record Sheet

Recorder: _____ **Date:** _____

Testing End (abutment or pier): _____

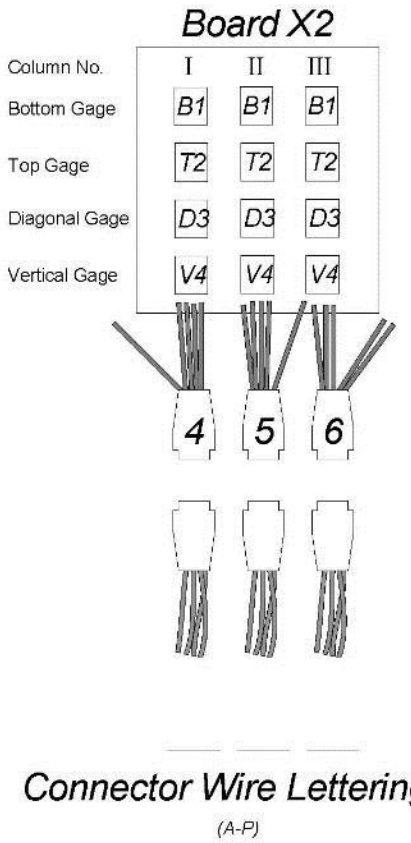

Board Loc.	Strain Gage Wire No.	Girder No. / Gage Position
X2-I-B1		
X2-I-T2		
X2-I-D3		
X2-I-V4		
X2-II-B1		
X2-II-T2		
X2-II-D3		
X2-II-V4		
X2-III-B1		
X2-III-T2		
X2-III-D3		
X2-III-V4		

Field Testing Bridge 65006 CPU Board Record Sheet

Recorder: _____ **Date:** _____

Testing End (abutment or pier): _____

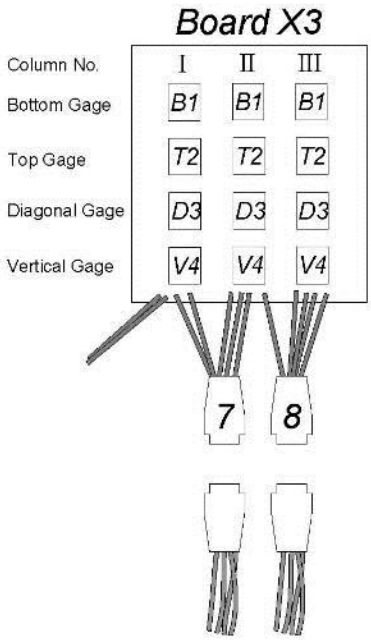

Connector Wire Lettering:

(A-P)

Board Loc.	Strain Gage Wire No.	Girder No. / Gage Position
X3-I-B1		
X3-I-T2		
X3-I-D3		
X3-I-V4		
X3-II-B1		
X3-II-T2		
X3-II-D3		
X3-II-V4		
X3-III-B1		
X3-III-T2		
X3-III-D3		
X3-III-V4		

Field Testing Bridge 65006 CPU Board Record Sheet

Recorder: _____ **Date:** _____

Testing End (abutment or pier): _____

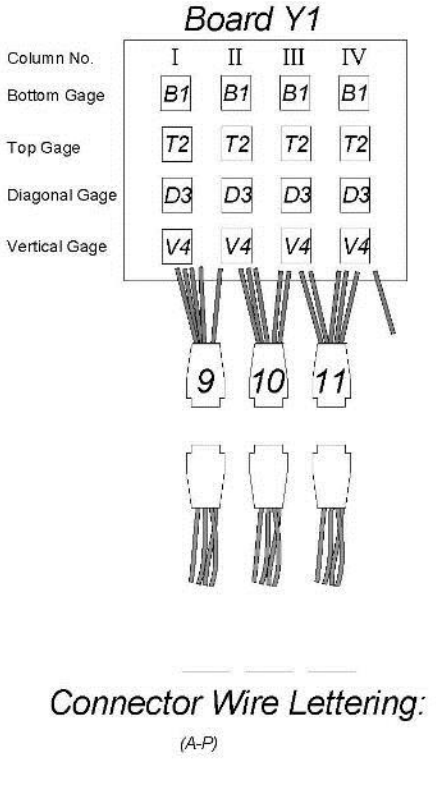

Board Loc.	Strain Gage Wire No.	Girder No. / Gage Position
Y1-I-B1		
Y1-I-T2		
Y1-I-D3		
Y1-I-V4		
Y1-II-B1		
Y1-II-T2		
Y1-II-D3		
Y1-II-V4		
Y1-III-B1		
Y1-III-T2		
Y1-III-D3		
Y1-III-V4		
Y1-IV-B1		
Y1-IV-T2		
Y1-IV-D3		
Y1-IV-V4		

Field Testing Bridge 65006 CPU Board Record Sheet

Recorder: _____ **Date:** _____

Testing End (abutment or pier): _____

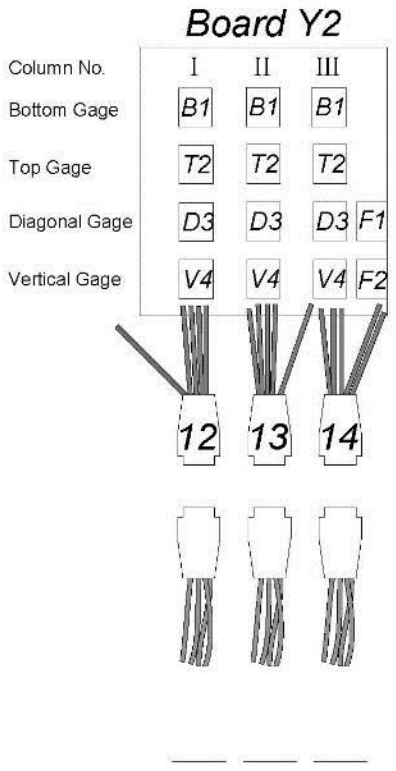

Connector Wire Lettering:

(A-P)

Board Loc.	Strain Gage Wire No.	Girder No. / Gage Position
Y2-I-B1		
Y2-I-T2		
Y2-I-D3		
Y2-I-V4		
Y2-II-B1		
Y2-II-T2		
Y2-II-D3		
Y2-II-V4		
Y2-III-B1		
Y2-III-T2		
Y2-III-D3		
Y2-III-V4		
Y2-IV-F1		
Y2-IV-F2		

Field Testing Bridge 65006 CPU Board Record Sheet

Recorder: _____ **Date:** _____

Testing End (abutment or pier): _____

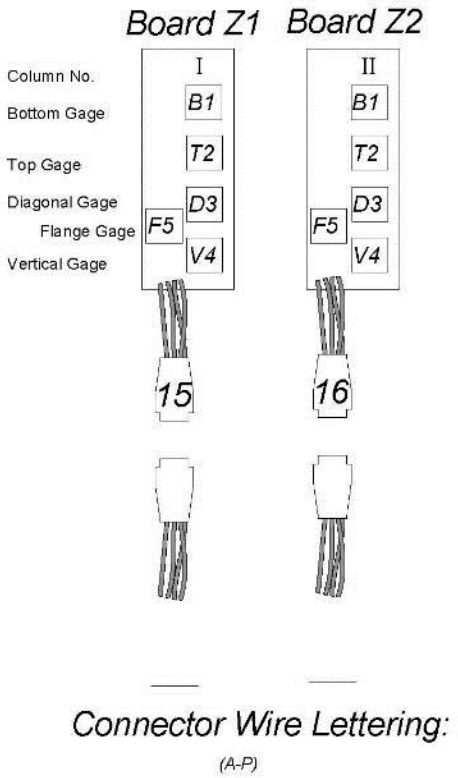

Board Loc.	Strain Gage Wire No.	Girder No. / Gage Position
Z1-I-B1	_____	_____
Z1-I-T2	_____	
Z1-I-D3	_____	
Z1-I-V4	_____	
Z1-I-F5	_____	
Z2-II-B1	_____	_____
Z2-II-T2	_____	
Z2-II-D3	_____	
Z2-II-V4	_____	
Z2-II-F5	_____	

APPENDIX H. CONCRETE CORE MATERIAL PROPERTY STUDY

Drilled concrete core specimens from 13 bridges removed from service in the MnDOT inventory were provided to UMN. None of the drilled core specimens were from structures considered in the field bridge live load testing portion of this research. Three to six cores were taken from each bridge. Details about the core date and location on the structure are listed in Table H-1. Material testing was completed on 50 samples to determine concrete compressive strength, f'_c, and modulus of elasticity, E_c. The design of all bridges in this study were governed by the MnDOT July 1st, 1947 Specification along with "Supplement No. 1" dated April 15, 1953.

Core specimens provided by MnDOT were drilled from the web of the bridge girders and had a diameter of 3.75 in. and length between 6 in. and 7.5 in. Detail regarding the core dimensions and necessary modifications as specified by ASTM C39 (2012) are listed in Table H-2. Prior to testing, each core was capped using a sulfur capping compound in accordance with ASTM C617 (2012). Compressive strength and modulus testing, highlighted in Figure H-1 were completed using the following procedure. A single core from each bridge was initially broken using a Forney testing machine to determine the compressive strength following the procedure outlined in ASTM C39 (2012), with an average loading rate of 475 pounds per second. The initial concrete compressive strength from each bridge was used to determine the parameters for the modulus of elasticity test for the remaining cores from that structure.

The modulus of elasticity test was conducted in accordance with ASTM C469 (2010). Load was applied and recorded using a Forney testing machine, highlighted in Figure H-1. Vertical displacement of the concrete core was measured using a compressometer apparatus as shown in Figure H-2 with a linear variable differential transformer (LVDT) oriented along the longitudinal axis of the cylinder. The LVDT was calibrated prior to testing. The setup was verified by measurement on an aluminum cylinder with a known modulus of elasticity. Results from this test indicated that the elastic modulus test apparatus provided accurate data. Displacement was measured with the LVDT over a gauge length of 2.63 in. which satisfied ASTM C469-10 for the tested concrete core size.

The modulus of elasticity results were generated in accordance with ASTM C469 (2010). The procedure and data collection were repeated four times for each cylinder. As

outlined in ASTM C469 (2010), the data from the first cycle was not used and the modulus measured in the subsequent three cycles was averaged. Following completion of the elastic modulus testing, the three cores used to generate the results were broken in compression according to ASTM C39 (2012) to obtain an average concrete compressive strength. The densities of 24 cylinders from six of the bridges were measured in accordance with ASTM C42 (2013) and are given in Table H-3. The average measured densities for the six bridges ranged from 146 pcf to 151 pcf, with an overall average of 148 pcf. The cylinders used to measure densities were not used to determine the reported concrete compressive strengths or moduli of elasticity.

Concrete compressive strength and modulus of elasticity results from each bridge are summarized in Table H-4. As outlined in the appropriate ASTM standards, compressive strength results were rounded to the nearest 10 psi and modulus of elasticity results were rounded to the nearest 50 ksi. For comparison to measured values, the theoretical modulus of elasticity was calculated using the equation $33 w_c^{1.5} \sqrt{f'_c}$ discussed by Pauw (1960). Table H-4 lists the bridge specific unit weight, w_c, used to calculate the modulus of elasticity. The average unit weight of 148 pcf was used when bridge specific data was not available. Table H-4 also shows that, on average, the Pauw (1960) equation provided an accurate estimate of measured concrete elastic modulus.

Table H-5 compares the average measured concrete compressive strength to a range of theoretical specified compressive strengths because the research team could not locate records of the measured 28-day concrete compressive strengths. Discussion with the TAP indicated that the specified concrete compressive strength was likely 5,000 psi for all structures in this study. Additionally, the value of f'_c equal to 5,000 psi is what MnDOT currently uses as a material property in *Virtis* for these structures. Table H-5 highlights that the differences between specified 28-day strengths and measured 28-day strengths can be calculated using applicable statistical bias factors, λ, as discussed by Nowak and Szerszen (2003) and verified for MnDOT specified concretes by Dereli et al. (2010). Furthermore, Table H-5 shows the concrete compressive strength with the statistical bias factor and an additional minimum 20 percent strength gain over time as observed by Wood (1991) and verified for MnDOT specified concretes by Dereli et al. (2010). Table H-5 shows that the long-term measured concrete compressive strength can be well, but conservatively,

predicted by multiplying the specified concrete strength by 1.2*λ for the range of assumed specified strengths between 5,000 and 6,000 psi. The prediction is still accurate, but slightly unconservative, if the specified concrete strength was 6,500 psi.

Table H-1. Core Sample Location and Date Cored

Bridge No.	Year Built	Core No. or Desc.	Location of Core	Date Cored
9310	1959	1A	N. Fascia, W. Span, Middle	11/26/12
9310	1959	2A	N. Fascia, W. Span, Middle	11/26/12
9310	1959	3A	N. Fascia, W. Span, Middle	11/26/12
9312	1959	1	Beam 5, E. Span	8/8/12
9312	1959	2	Beam 5, E. Span	8/8/12
9312	1959	3	Beam 5, E. Span	8/8/12
9301	1959	1	E. Span, S. Fascia Beam	8/8/12
9301	1959	2	E. Span, S. Fascia Beam	8/8/12
9301	1959	3	E. Span, S. Fascia Beam	8/8/12
9448	1959	1B	W. Fascia, Center Span, Middle	11/26/12
9448	1959	2B	W. Fascia, Center Span, Middle	11/26/12
9448	1959	3B	W. Fascia, Center Span, Middle	11/26/12
9447	1959	1	Span 3, E. Fascia Beam	10/13/11
9447	1959	2	Span 3, E. Fascia Beam	10/13/11
9447	1959	3	Span 3, E. Fascia Beam	10/13/11
9311	1959	1	E. Span, Middle	11/26/12
9311	1959	2	E. Span, Middle	11/26/12
9311	1959	3	E. Span, Middle	11/26/12
9302	1959	2 top	E. Span, S. Fascia	8/10/12
9302	1959	1 middle	E. Span, S. Fascia	8/10/12
9302	1959	3 bottom	E. Span, S. Fascia	8/10/12
6510	1958	Roselawn, G1, 1	105 in. from N. end, 20 in. up from BF, span 3	7/2/14
6510	1958	Roselawn, G1, 3	85 in. from N. end, 14 in. up from BF, span 3	7/2/14
6510	1958	Roselawn, G2, 1	75 in. from N. end, 20 in. up from BF, span 3	7/2/14
6510	1958	Roselawn, G2, 3	80 in. from N. end, 18 in. up from BF, span 3	7/2/14
6510	1958	Roselawn, G3, 2	75 in. from N. end, 14 in. up from BF, span 3	7/2/14
6510	1958	Roselawn, G3, 3	75 in. from N. end, 25 in. up from BF, span 3	7/2/14
6511	1958	Wheelock, G3, 1	49 in. from W. end, 24 in. up from BF, span 4	3/8/14
6511	1958	Wheelock, G3, 2	73 in. from W. end, 24 in. up from BF, span 4	3/8/14
6511	1958	Wheelock, G3, 3	85 in. from W. end, 24 in. up from BF, span 4	3/8/14
6514	1958	Larpenteur, G2, 1	41.5 in. from E. end, 14 in. up from BF, span 3	6/7/14
6514	1958	Larpenteur, G2, 2	41.5 in. from E. end, 19 in. up from BF, span 3	6/7/14
6514	1958	Larpenteur, G2, 3	49 in. from E. end, 14 in. up from BF, span 3	6/7/14
6514	1958	Larpenteur, G4, 3	48 in. from E. end, 14 in. up from BF, span 3	6/7/14
6514	1958	Larpenteur, G6, 1	50 in. from E. end, 14 in. up from BF, span 3	6/7/14
6514	1958	Larpenteur, G6, 3	60.5 in. from E. end, 14 in. up from BF, span 3	6/7/14
6579	1958	Arlington, G1, 1	83 in. from W. end, 24 in. up from BF, span 4	3/7/14
6579	1958	Arlington, G4, 3	75 in. from W. end, 26 in. up from BF, span 4	3/7/14
9118	1958	County B, G1, 1	83 in. from N. end, 14 in. up from BF, span 3	6/30/14
9118	1958	County B, G3, 1	75 in. from N. end, 20 in. from BF, span 3	6/30/14
9118	1958	County B, G3, 3	80 in. from N. end, 18 in. up from BF, span 3	6/30/14
9118	1958	County B, G4, 1	105 in. from N. end, 20 in. up from BF, span 3	6/30/14
9118	1958	County B, G4, 3	85 in. fom N. end, 14 in. up from BF, span 3	6/30/14
9118	1958	County B, G4, 3	96 in. from N. end, 21 in. up from BF, span 3	6/30/14
9120	1958	Hwy 36, G1, 2	73 in. from N. end, 12 in. up from BF, span 3	6/28/14
9120	1958	Hwy 36, G2, 1	76 in. from N. end, 22 in. up from BF, span 3	6/28/14
9120	1958	Hwy 36, G2, 3	80 in. from N. end, 17 in. up from BF, span 3	6/28/14
9120	1958	Hwy 36, G3, 1	108 in. from N. end, 22 in. up from BF, span 3	6/28/14
9120	1958	Hwy 36, G3, 2	94 in. from N. end, 20 in. up from BF, span 3	6/28/14
9120	1958	Hwy 36, G3, 3	88 in. from N. end, 14 in. up from BF, span 3	6/28/14

Note: N, S, W, E = appropriate cardinal direction, BF = bottom flange

Table H-2. Core Sample Dimensions and ASTM C39-12 Correction Factors

Bridge No.	Year Built	Core No. or Desc.	Length L (in.)	Diameter d (in.)	L/d	$L/d \leq 1.75$ (factor reqd)	Correction Factor on f'_c
9310	1959	1A	7.063	3.75	1.883	no	1.000
9310	1959	2A	7.063	3.75	1.883	no	1.000
9310	1959	3A	7.063	3.75	1.883	no	1.000
9312	1959	1	6.063	3.75	1.617	yes	0.969
9312	1959	2	6.094	3.75	1.625	yes	0.970
9312	1959	3	6.156	3.75	1.642	yes	0.971
9301	1959	1	6.688	3.75	1.783	no	1.000
9301	1959	2	6.688	3.75	1.783	no	1.000
9301	1959	3	6.750	3.75	1.800	no	1.000
9448	1959	1B	7.219	3.75	1.925	no	1.000
9448	1959	2B	7.219	3.75	1.925	no	1.000
9448	1959	3B	7.219	3.75	1.925	no	1.000
9447	1959	1	7.250	3.75	1.933	no	1.000
9447	1959	2	7.375	3.75	1.967	no	1.000
9447	1959	3	7.375	3.75	1.967	no	1.000
9311	1959	1	6.125	3.75	1.633	yes	0.971
9311	1959	2	6.125	3.75	1.633	yes	0.971
9311	1959	3	6.156	3.75	1.642	yes	0.971
9302	1959	2 top	7.063	3.75	1.883	no	1.000
9302	1959	1 middle	7.063	3.75	1.883	no	1.000
9302	1959	3 bottom	7.063	3.75	1.883	no	1.000
6510	1958	Roselawn, G1, 1	6.239	3.75	1.66	yes	0.973
6510	1958	Roselawn, G1, 3	6.161	3.75	1.64	yes	0.971
6510	1958	Roselawn, G2, 1	6.219	3.76	1.65	yes	0.972
6510	1958	Roselawn, G2, 3	6.260	3.75	1.67	yes	0.974
6510	1958	Roselawn, G3, 2	6.259	3.75	1.67	yes	0.974
6510	1958	Roselawn, G3, 3	6.275	3.75	1.67	yes	0.974
6511	1958	Wheelock, G3, 1	6.150	3.74	1.64	yes	0.972
6511	1958	Wheelock, G3, 2	6.129	3.74	1.64	yes	0.971
6511	1958	Wheelock, G3, 3	6.130	3.74	1.64	yes	0.971
6514	1958	Larpenteur, G2, 1	6.092	3.73	1.63	yes	0.971
6514	1958	Larpenteur, G2, 2	6.210	3.73	1.66	yes	0.973
6514	1958	Larpenteur, G2, 3	6.069	3.73	1.63	yes	0.970
6514	1958	Larpenteur, G4, 3	6.142	3.76	1.63	yes	0.971
6514	1958	Larpenteur, G6, 1	6.185	3.74	1.65	yes	0.972
6514	1958	Larpenteur, G6, 3	6.159	3.73	1.65	yes	0.972
6579	1958	Arlington, G1, 1	6.183	3.83	1.61	yes	0.969
6579	1958	Arlington, G4, 3	5.355	2.77	1.93	no	1.000
9118	1958	County B, G1, 1	6.000	3.74	1.60	yes	0.968
9118	1958	County B, G3, 1	6.083	3.75	1.62	yes	0.970
9118	1958	County B, G3, 3	6.041	3.74	1.62	yes	0.969
9118	1958	County B, G4, 1	6.106	3.75	1.63	yes	0.970
9118	1958	County B, G4, 3	6.031	3.75	1.61	yes	0.969
9118	1958	County B, G4, 3	6.069	3.75	1.62	yes	0.969
9120	1958	Hwy 36, G1, 2	6.155	3.75	1.64	yes	0.971
9120	1958	Hwy 36, G2, 1	6.175	3.74	1.65	yes	0.972
9120	1958	Hwy 36, G2, 3	6.120	3.75	1.63	yes	0.971
9120	1958	Hwy 36, G3, 1	6.180	3.75	1.65	yes	0.972
9120	1958	Hwy 36, G3, 2	6.121	3.73	1.64	yes	0.971
9120	1958	Hwy 36, G3, 3	6.116	3.75	1.63	yes	0.970

Table H-3. Core Sample Location and Unit Weight

Bridge No.	Year Built	Core No. or Desc.	Length *L* (in.)	Diameter *d* (in.)	Weight (lb)	Volume (ft^3)	Unit Wt. (pcf)	Avg Unit Wt. (pcf)
6510	1958	Roselawn, G1, 2	6.1250	3.76	5.7370	0.039	146	146
6510	1958	Roselawn, G2, 2	6.1250	3.80	5.8340	0.040	145	
6510	1958	Roselawn, G3, 1	6.0625	3.75	5.6885	0.039	147	
6511	1958	Wheelock, G1, 1	6.1250	2.76	3.1900	0.021	150	151
6511	1958	Wheelock, G1, 2	6.1250	2.77	3.1930	0.021	149	
6511	1958	Wheelock, G1, 3	6.0625	2.77	3.2085	0.021	152	
6511	1958	Wheelock, G2, 1	6.0625	2.77	3.1900	0.021	151	
6511	1958	Wheelock, G2, 2	6.1250	2.77	3.2045	0.021	150	
6511	1958	Wheelock, G2, 3	6.1250	2.76	3.2090	0.021	151	
6514	1958	Larpenteur, G4, 1	6.0000	3.74	5.8635	0.038	154	150
6514	1958	Larpenteur, G4, 2	6.1250	3.73	5.8065	0.039	150	
6514	1958	Larpenteur, G6, 2	6.1875	3.73	5.7385	0.039	147	
6579	1958	Arlington, G1, 2	6.1250	2.77	3.1660	0.021	148	148
6579	1958	Arlington, G1, 3	6.1250	2.76	3.1430	0.021	148	
6579	1958	Arlington, G2, 1	6.0625	2.76	3.1155	0.021	148	
6579	1958	Arlington, G2, 2	6.0625	2.77	3.1435	0.021	149	
6579	1958	Arlington, G2, 3	6.1250	2.77	3.1565	0.021	148	
6579	1958	Arlington, G4, 1	6.0625	2.77	3.1370	0.021	148	
6579	1958	Arlington, G4, 2	6.0625	2.76	3.1095	0.021	148	
9118	1958	County B, G1, 2	6.0625	3.75	5.6410	0.039	146	146
9118	1958	County B, G1, 3	6.1250	3.75	5.7515	0.039	147	
9118	1958	County B, G3, 2	6.0625	3.74	5.6645	0.039	147	
9120	1958	Hwy 36, G1, 1	6.1250	3.73	5.7365	0.039	148	149
9120	1958	Hwy 36, G2, 2	6.0625	3.73	5.7075	0.038	149	
9120	1958	Hwy 36, G2, 3	6.1250	3.75	5.8615	0.039	150	
							Avg:	148
							Std Dev:	2

Table H-4. Concrete Compressive Strength and Modulus of Elasticity Results

Bridge No.	Year Built	Core No. or Desc.	Date of f'_c Test (2014)	f'_c (psi)	Date of E Test (2014)	E_{avg} (ksi)	$33w_c^{1.5}\sqrt{f'_c}$ (ksi)	w_c (pcf)
9310	1959	1A	6/4	7,540	--	--	5,200	n/a
9310	1959	2A	8/5	7,280	7/17	4,750	5,100	
9310	1959	3A	8/5	8,690	7/17	5,200	5,550	
9312	1959	1	7/14	10,800	--	--	6,200	n/a
9312	1959	2	8/5	9,620	7/14	5,550	5,850	
9312	1959	3	8/5	9,010	7/14	5,600	5,650	
9301	1959	1	7/14	8,490	--	--	5,500	n/a
9301	1959	2	8/5	9,720	7/14	6,300	5,900	
9301	1959	3	8/5	8,820	7/14	5,600	5,600	
9448	1959	1B	6/5	8,700	--	--	5,550	n/a
9448	1959	2B	8/5	9,640	7/17	5,000	5,850	
9448	1959	3B	n/a	n/a	7/17	5,250	n/a	
9447	1959	1	6/6	9,370	--	--	5,750	n/a
9447	1959	2	8/6	7,930	7/17	4,400	5,300	
9447	1959	3	8/6	9,180	7/17	4,900	5,700	
9311	1959	1	7/14	9,320	--	--	5,750	n/a
9311	1959	2	8/6	8,690	7/14	5,700	5,550	
9311	1959	3	8/6	8,630	7/14	5,800	5,550	
9302	1959	2 top	7/14	8,480	--	--	5,500	n/a
9302	1959	1 middle	8/6	7,260	7/14	4,650	5,100	
9302	1959	3 bottom	8/6	9,040	7/14	4,850	5,650	
6510	1958	Roselawn, G1, 1	8/22	8,320	8/22	5,900	5,300	146
6510	1958	Roselawn, G1, 3	8/22	7,010	8/22	5,500	4,850	
6510	1958	Roselawn, G2, 1	8/22	8,950	--	--	5,500	
6510	1958	Roselawn, G2, 3	8/22	7,320	8/22	5,150	5,000	
6510	1958	Roselawn, G3, 2	8/22	8,380	8/22	5,750	5,300	
6510	1958	Roselawn, G3, 3	8/22	8,110	8/22	5,350	5,250	
6511	1958	Wheelock, G3, 1	8/22	9,060	--	--	5,800	151
6511	1958	Wheelock, G3, 2	8/22	7,950	8/22	5,350	5,450	
6511	1958	Wheelock, G3, 3	8/22	7,930	8/22	5,850	5,450	
6514	1958	Larpenteur, G2, 1	8/22	9,550	8/22	4,900	5,950	150
6514	1958	Larpenteur, G2, 2	8/22	7,750	--	--	5,350	
6514	1958	Larpenteur, G2, 3	10/16	9,130	8/22	5,050	5,800	
6514	1958	Larpenteur, G4, 3	8/22	9,050	8/22	5,200	5,750	
6514	1958	Larpenteur, G6, 1	8/22	8,880	8/22	5,200	5,700	
6514	1958	Larpenteur, G6, 3	8/22	8,510	8/22	5,800	5,600	
6579	1958	Arlington, G1, 1	10/16	9,350	9/18	5,650	5,750	148
6579	1958	Arlington, G4, 3	9/4	9,350	--	--	5,750	
9118	1958	County B, G1, 1	8/22	8,220	8/22	5,700	5,300	146
9118	1958	County B, G3, 1	8/22	9,570	8/22	5,400	5,700	
9118	1958	County B, G3, 3	8/22	8,840	8/22	5,750	5,500	
9118	1958	County B, G4, 1	8/22	7,330	8/22	5,250	5,000	
9118	1958	County B, G4, 3	8/22	9,570	8/22	5,600	5,700	
9118	1958	County B, G4, 3	8/22	8,900	--	--	5,500	
9120	1958	Hwy 36, G1, 2	8/25	8,430	--	--	5,500	149
9120	1958	Hwy 36, G2, 1	10/16	9,870	9/18	5,700	5,950	
9120	1958	Hwy 36, G2, 3	10/16	8,040	10/16	4,350	5,400	
9120	1958	Hwy 36, G3, 1	10/16	9,880	9/18	4,800	5,950	
9120	1958	Hwy 36, G3, 2	10/16	8,340	9/18	5,250	5,500	
9120	1958	Hwy 36, G3, 3	10/16	8,080	9/18	5,100	5,400	
			Avg:	8,690		5,350	5,550	148
			Std Dev:	810		450	300	2

Table H-5. Average Measured f'_c vs. Specified f'_c and Statistically Increased f'_c

Avg Meas f'_c (psi)	Spec f'_c (psi)	λ	λ * Spec f'_c (psi)	1.2* λ	1.2* λ * Spec f'_c (psi)	Avg Meas f'_c / 1.2* λ * Spec f'c
8,690	5,000	1.38	6,900	1.66	8,280	1.05
	5,500	1.19	6,545	1.43	7,854	1.11
	6,000	1.16	6,960	1.39	8,352	1.04
	6,500	1.14	7,410	1.37	8,892	0.98

Figure H-1. Sulfur Cap and Compression Testing (left) and Modulus of Elasticity Test Setup (right)

Figure H-2. Compressometer and LVDT Used to Measure Displacement

APPENDIX I. DATA FROM PARAMETRIC STUDY

Appendix I presents plots of shear per unit load in the interior girder versus the location of interest for shear along the span length. Cases include both one lane loaded (Figure I-1 through Figure I-7 in Section I.1) and two lanes loaded (Figure I-8 through Figure I-14 in Section I.2) for each parametric study bridge and two lanes loaded for each bridge from the MnDOT inventory used to verify the screening tool ratio results from the parametric study (Figure I-15 through Figure I-19 in Section I.3). Bridge data for structures from the MnDOT inventory were taken from MnDOT Report 2010-03 authored by Dereli et al. (2010). The methodology used to create the plots was discussed in section 7.2.1 and the results were generated using a 3D FEM.

I.1 Shear Distribution Results for One Lane Loaded

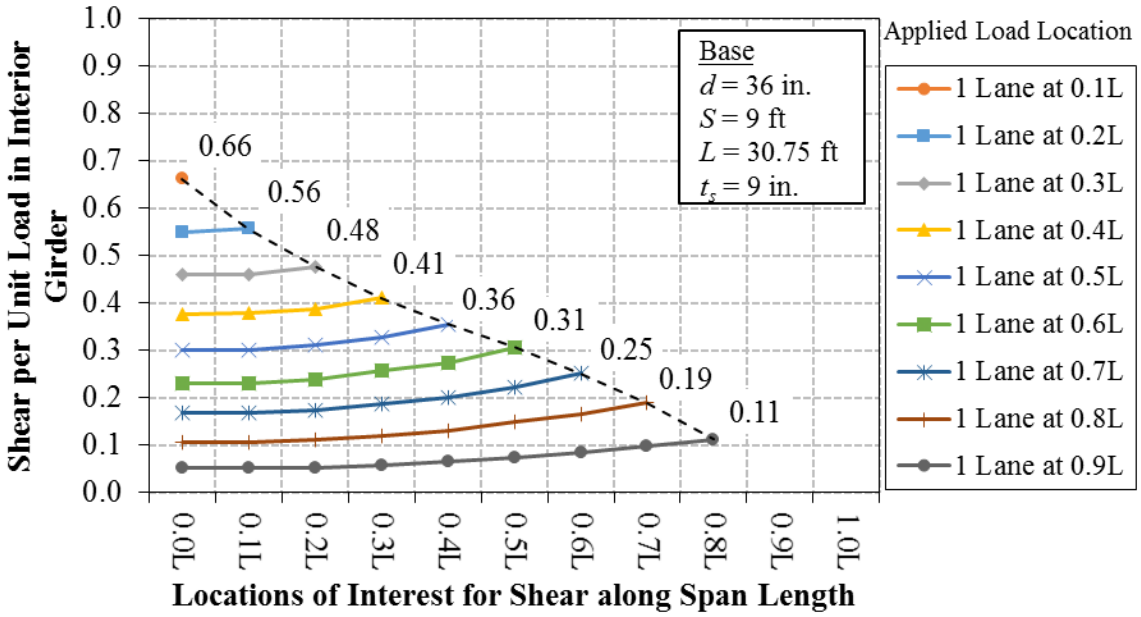

Figure I-1. Base Case Shear per Unit Load vs. Span Length for 1 Lane Loaded

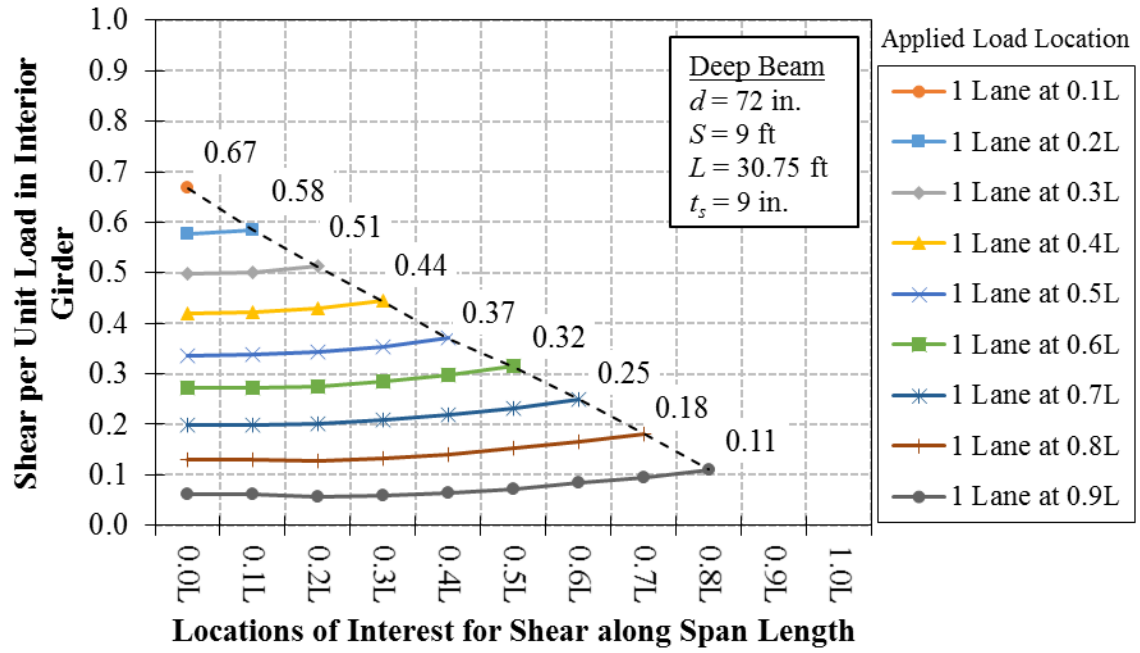

Figure I-2. Deep Beam Shear per Unit Load vs. Span Length for 1 Lane Loaded

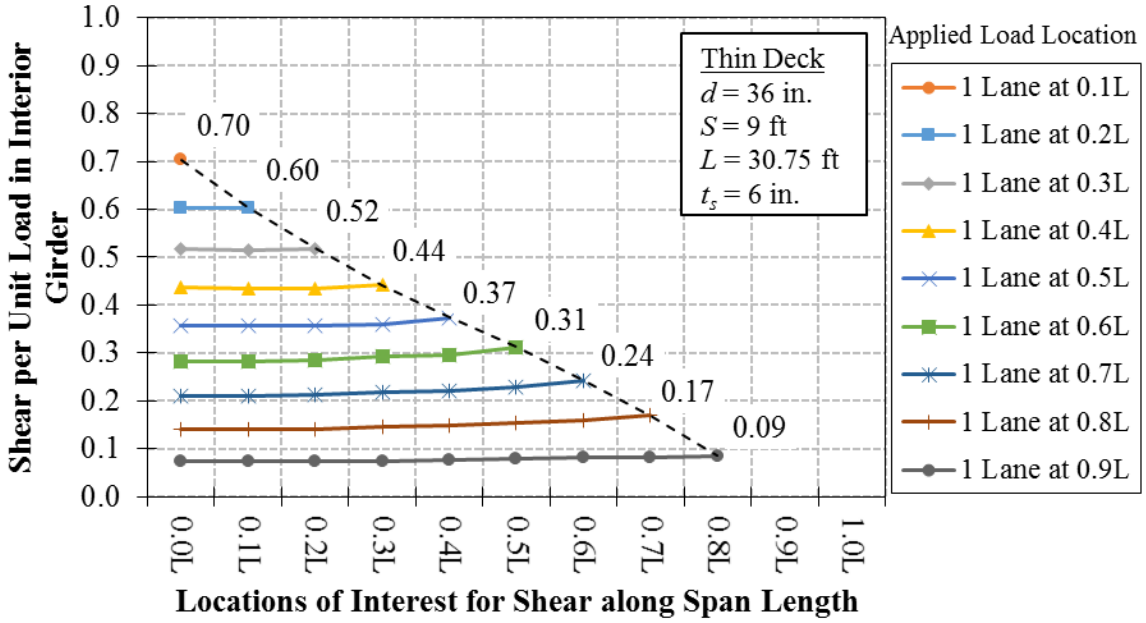

Figure I-3. Thin Deck Shear per Unit Load vs. Span Length for 1 Lane Loaded

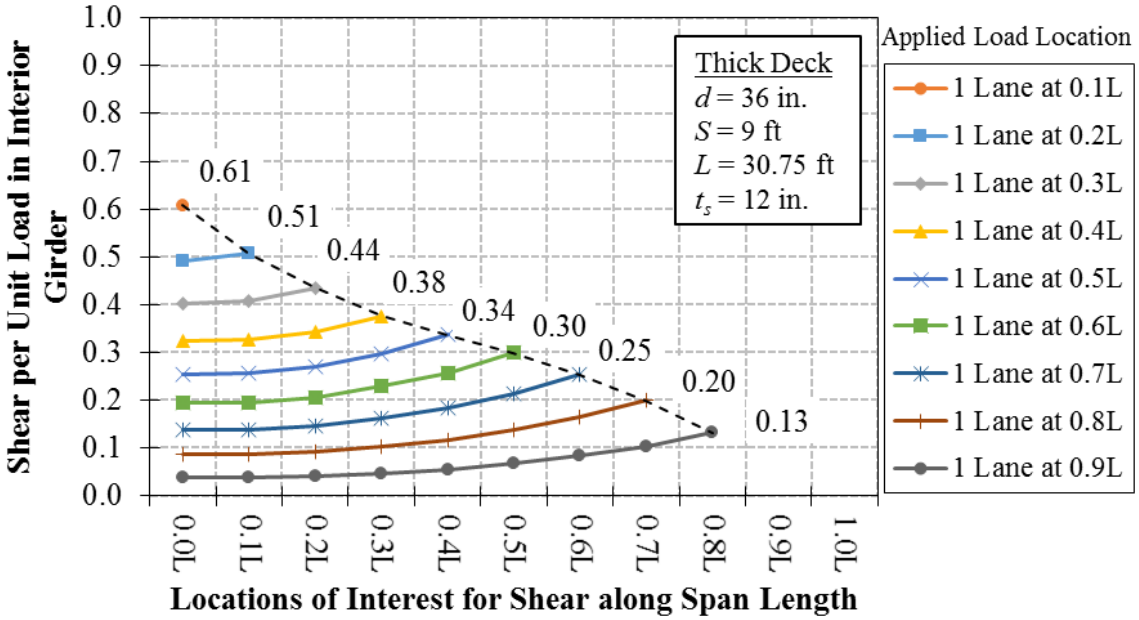

Figure I-4. Thick Deck Shear per Unit Load vs. Span Length for 1 Lane Loaded

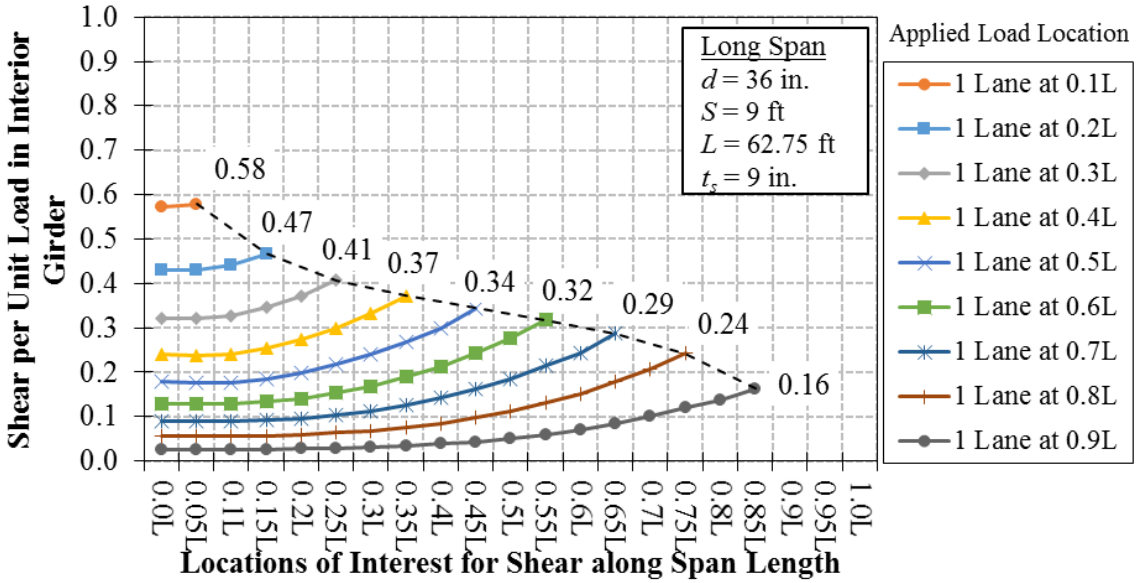

Figure I-5. Long Span Shear per Unit Load vs. Span Length for 1 Lane Loaded

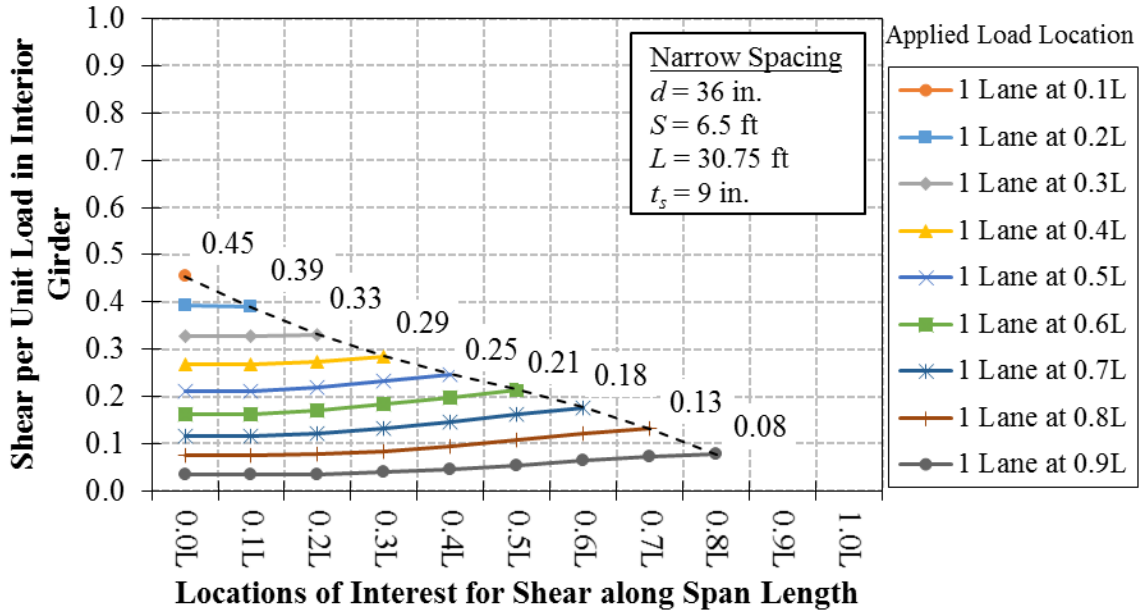

Figure I-6. Narrow Spacing Shear per Unit Load vs. Span Length for 1 Lane Loaded

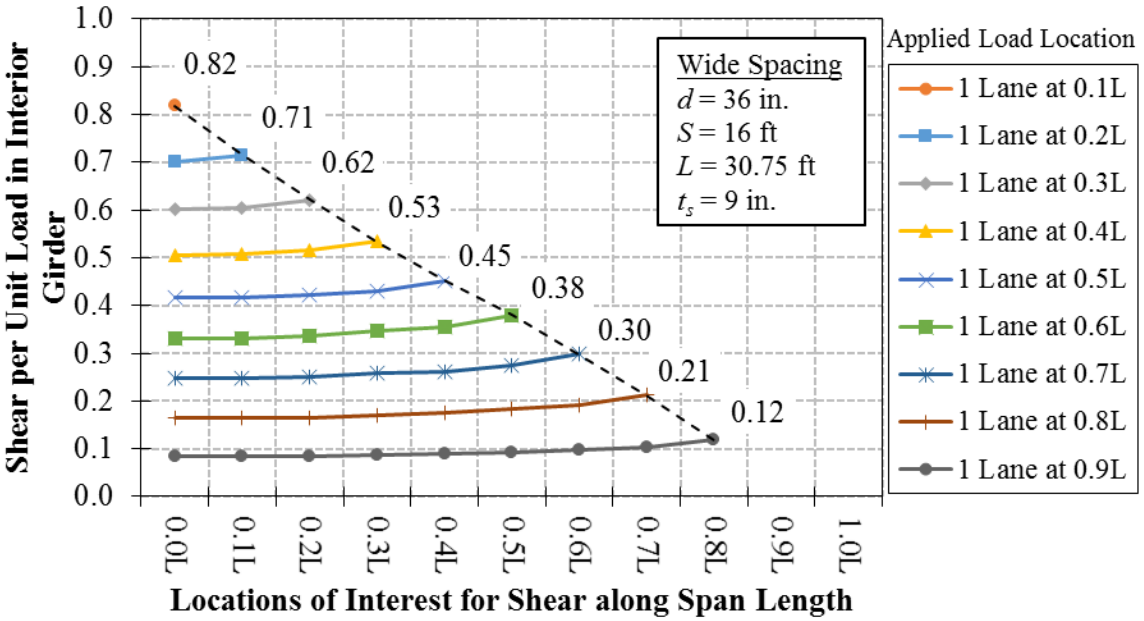

Figure I-7. Wide Spacing Shear per Unit Load vs. Span Length for 1 Lane Loaded

I.2 Shear Distribution Results for Two Lanes Loaded

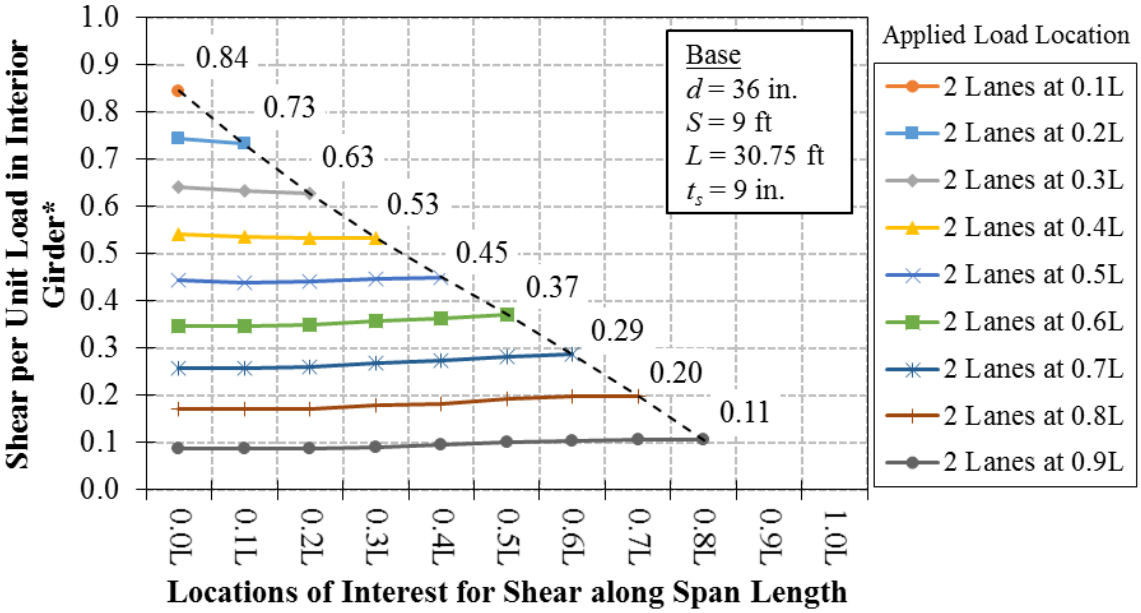

*The Shear per Unit Load in Interior Girder values already account for the presence of two axles.

Figure I-8. Base Case Shear per Unit Load vs. Span Length for 2 Lanes Loaded

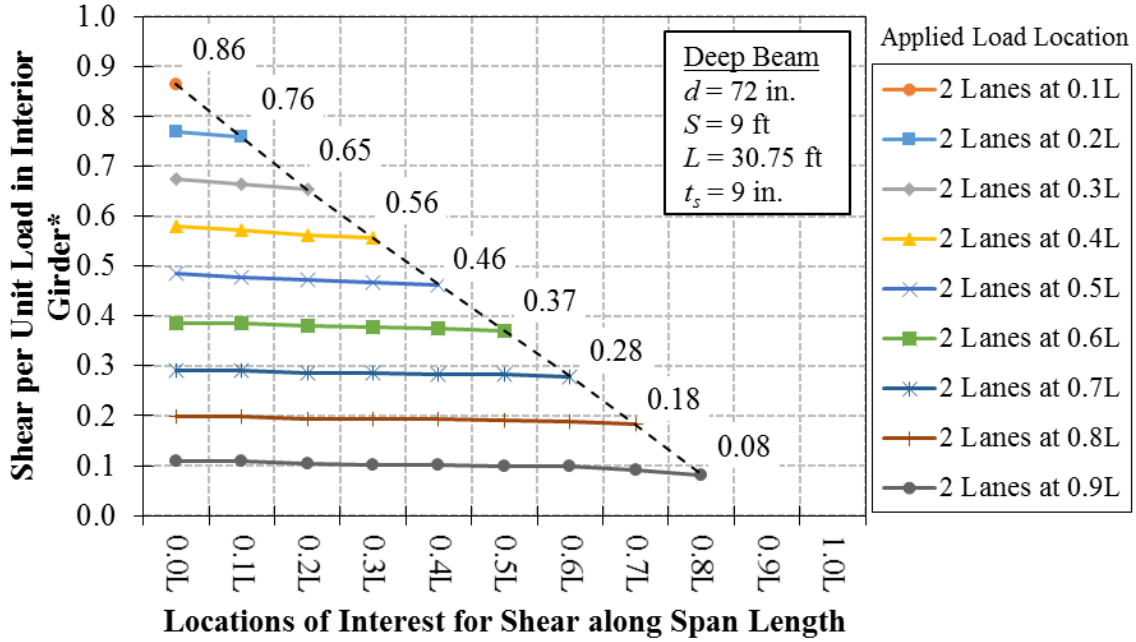

*The Shear per Unit Load in Interior Girder (%) values already account for the presence of two axles.

Figure I-9. Deep Beam Shear per Unit Load vs. Span Length for 2 Lanes Loaded

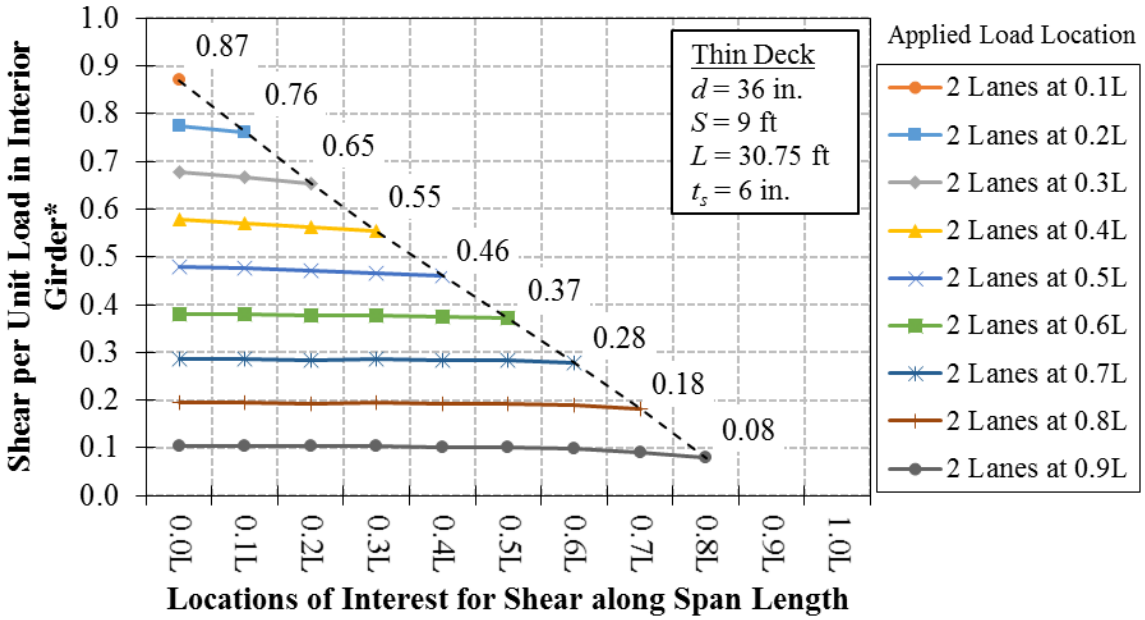

*The Shear per Unit Load in Interior Girder values already account for the presence of two axles.

Figure I-10. Thin Deck Shear per Unit Load vs. Span Length for 2 Lanes Loaded

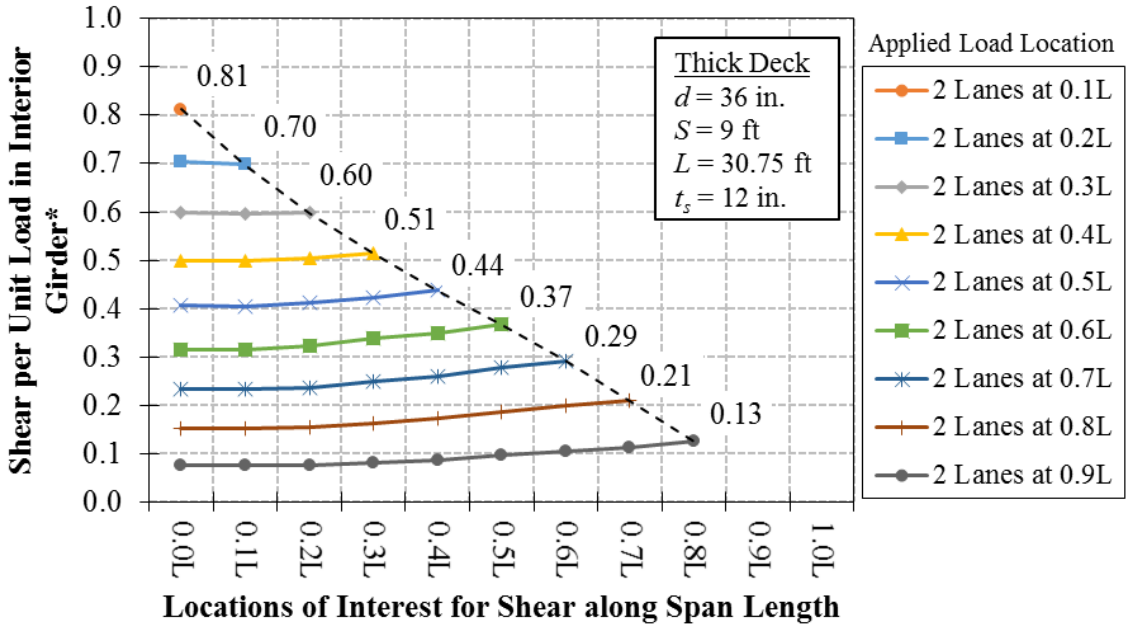

*The Shear per Unit Load in Interior Girder values already account for the presence of two axles.

Figure I-11. Thick Deck Shear per Unit Load vs. Span Length for 2 Lanes Loaded

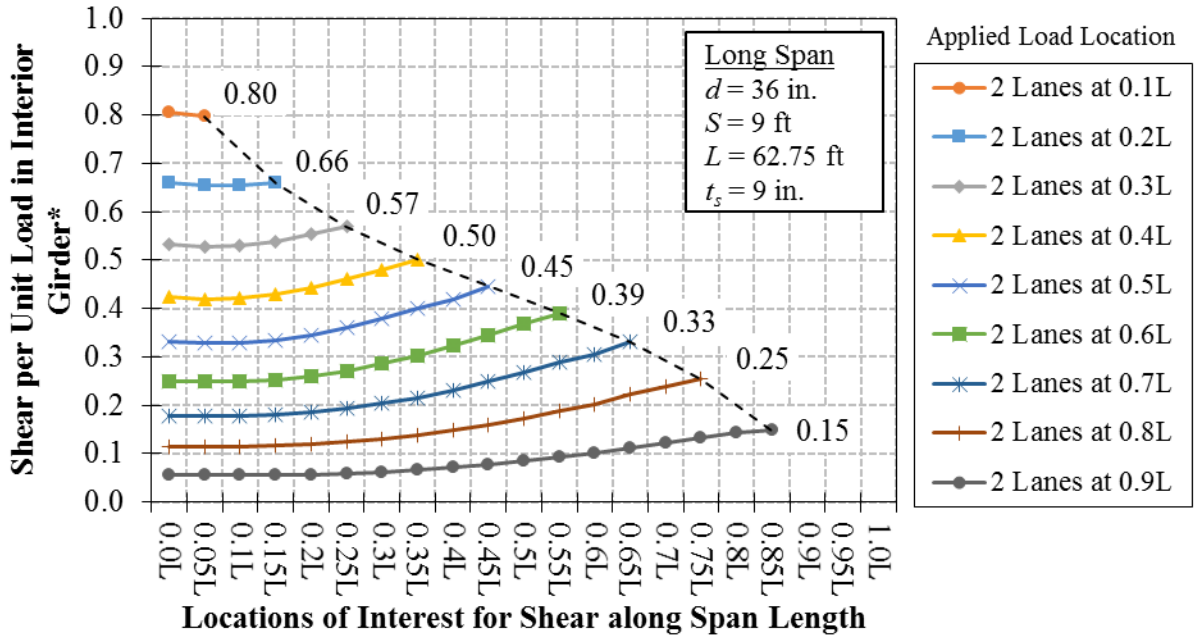

*The Shear per Unit Load in Interior Girder values already account for the presence of two axles.

Figure I-12. Long Span Shear per Unit Load vs. Span Length for 2 Lanes Loaded

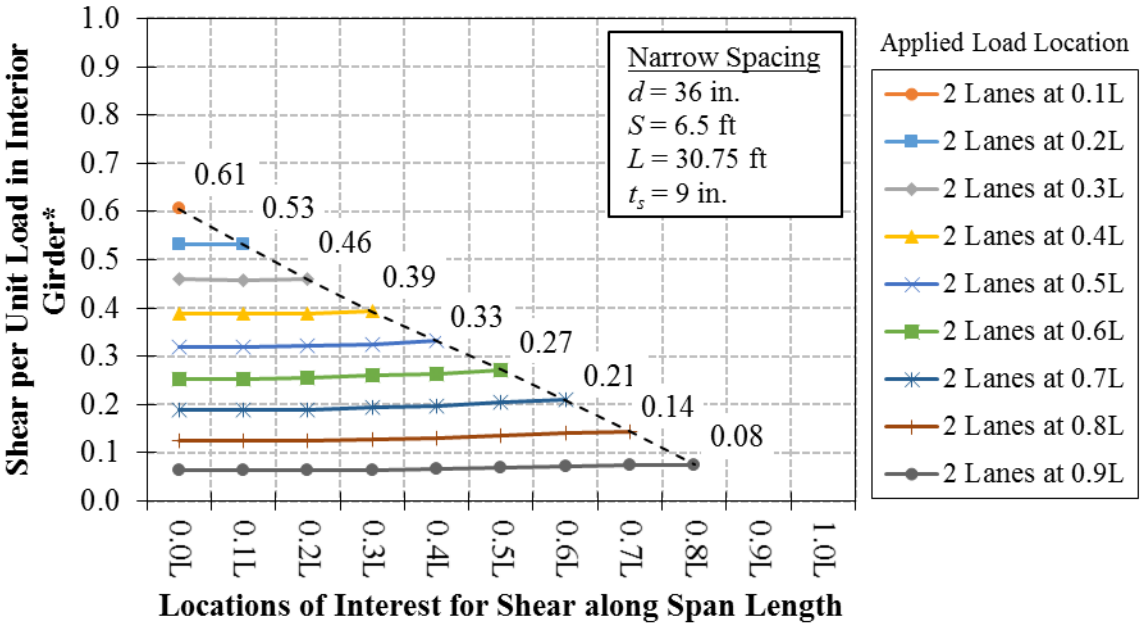

*The Shear per Unit Load in Interior Girder values already account for the presence of two axles.

Figure I-13. Narrow Spacing Shear per Unit Load vs. Span Length for 2 Lanes Loaded

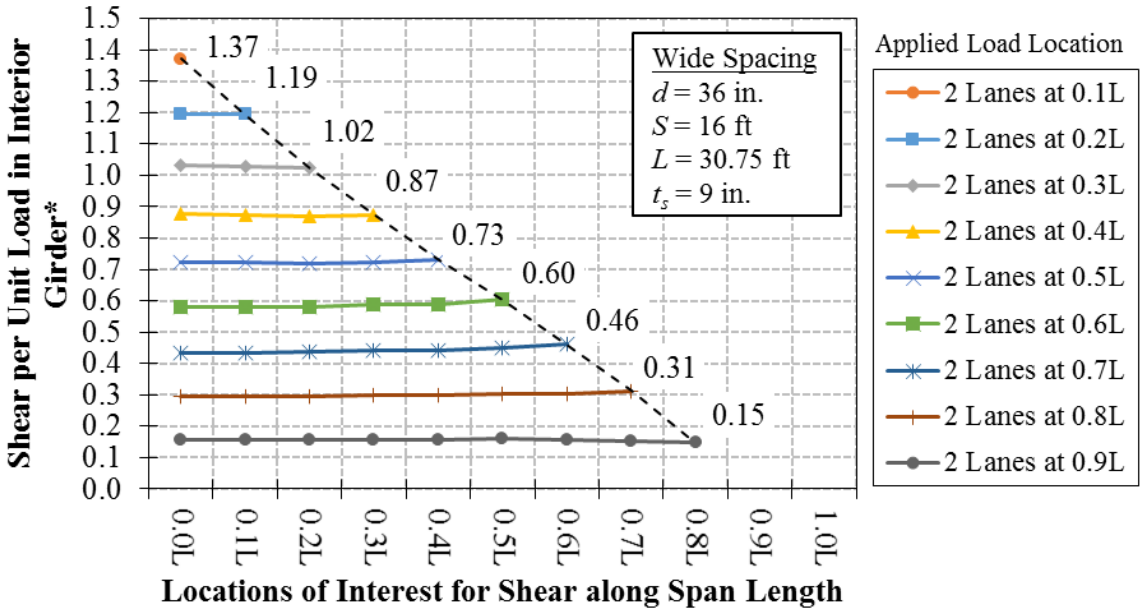

*The Shear per Unit Load in Interior Girder values already account for the presence of two axles.

Figure I-14. Wide Spacing Shear per Unit Load vs. Span Length for 2 Lanes Loaded

I.3 Shear Distribution Results from MnDOT Verification Bridges

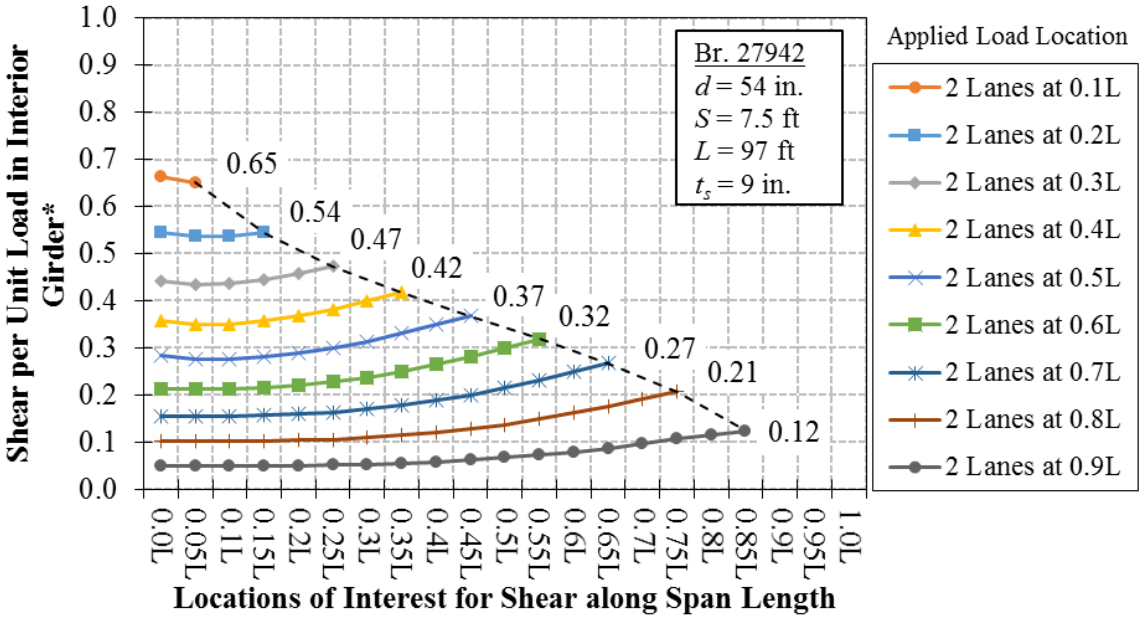

*The Shear per Unit Load in Interior Girder values already account for the presence of two axles.

Figure I-15. Br. 27942 Shear per Unit Load vs. Span Length for 2 Lanes Loaded

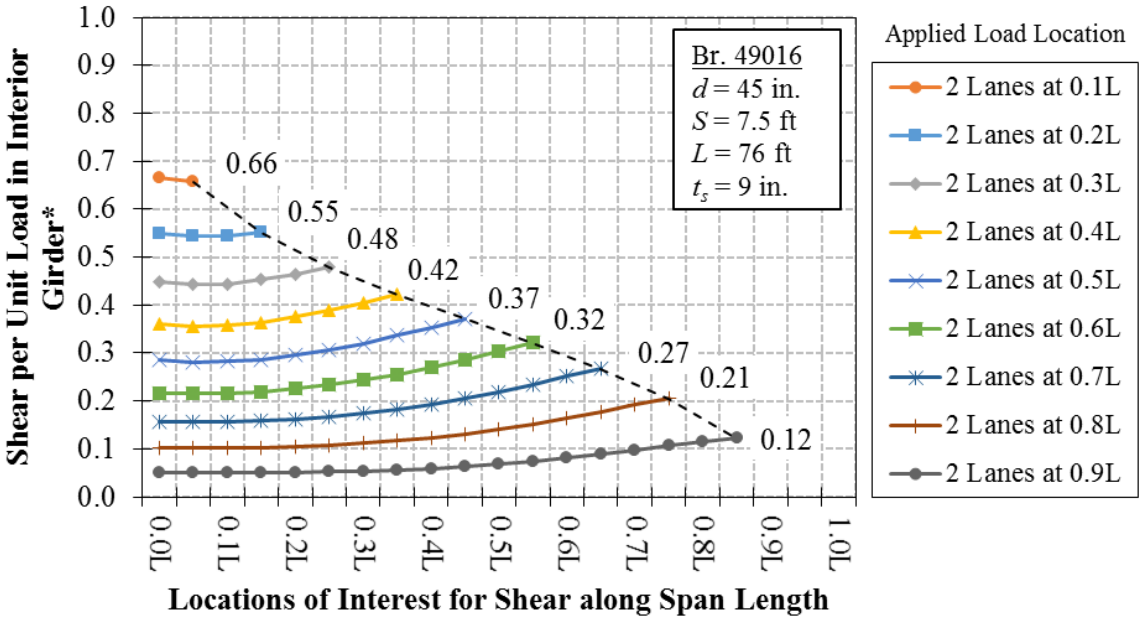

*The Shear per Unit Load in Interior Girder values already account for the presence of two axles.

Figure I-16. Br. 49016 Shear per Unit Load vs. Span Length for 2 Lanes Loaded

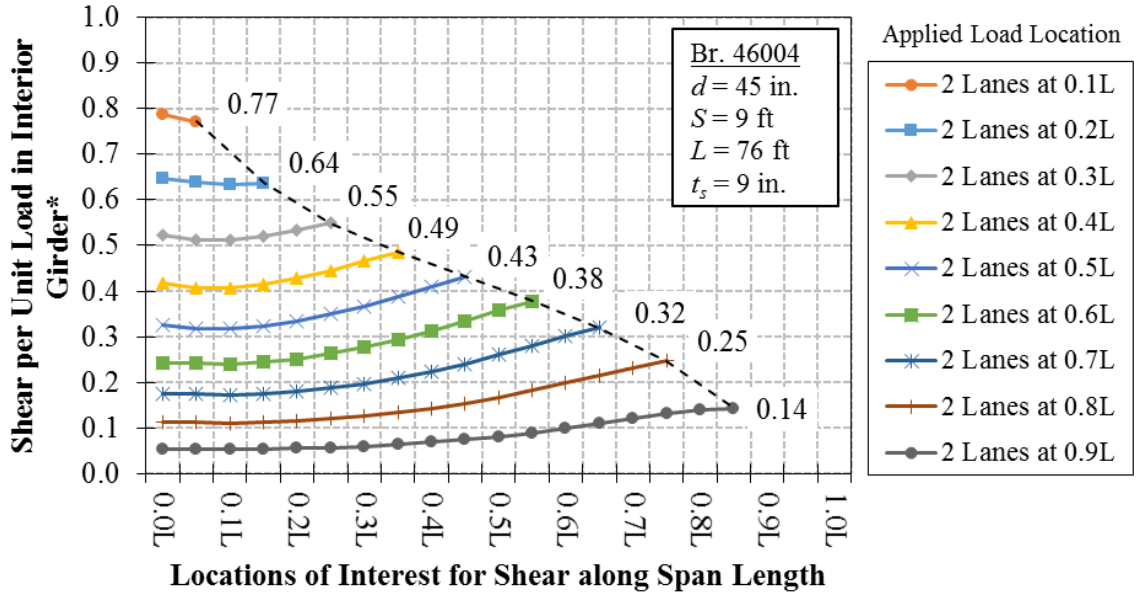

*The Shear per Unit Load in Interior Girder values already account for the presence of two axles.

Figure I-17. Br. 46004 Shear per Unit Load vs. Span Length for 2 Lanes Loaded

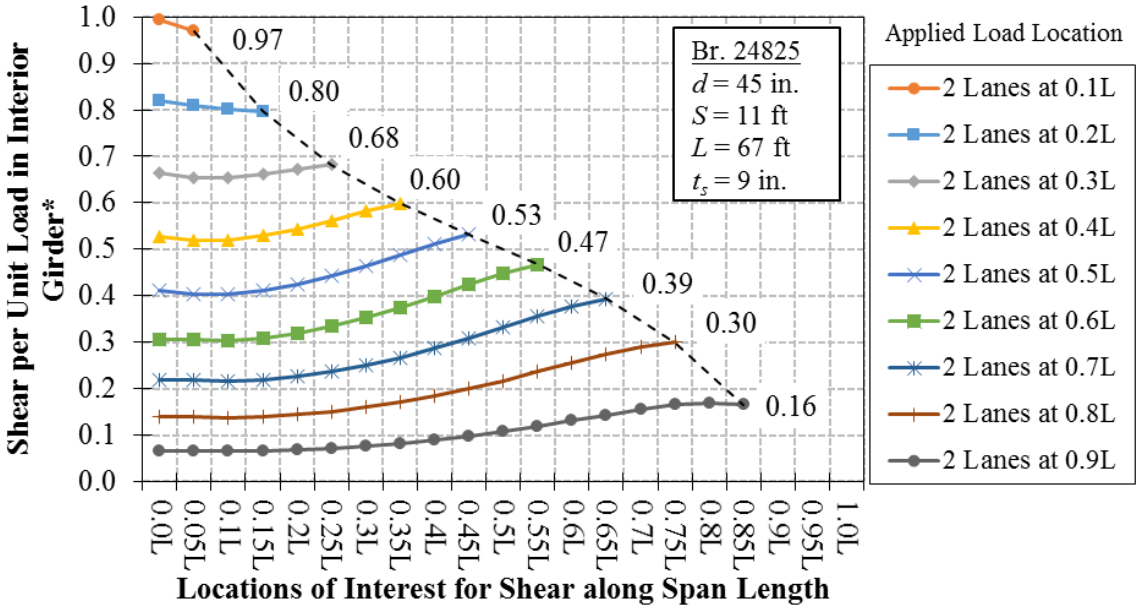

*The Shear per Unit Load in Interior Girder values already account for the presence of two axles.

Figure I-18. Br. 24825 Shear per Unit Load vs. Span Length for 2 Lanes Loaded

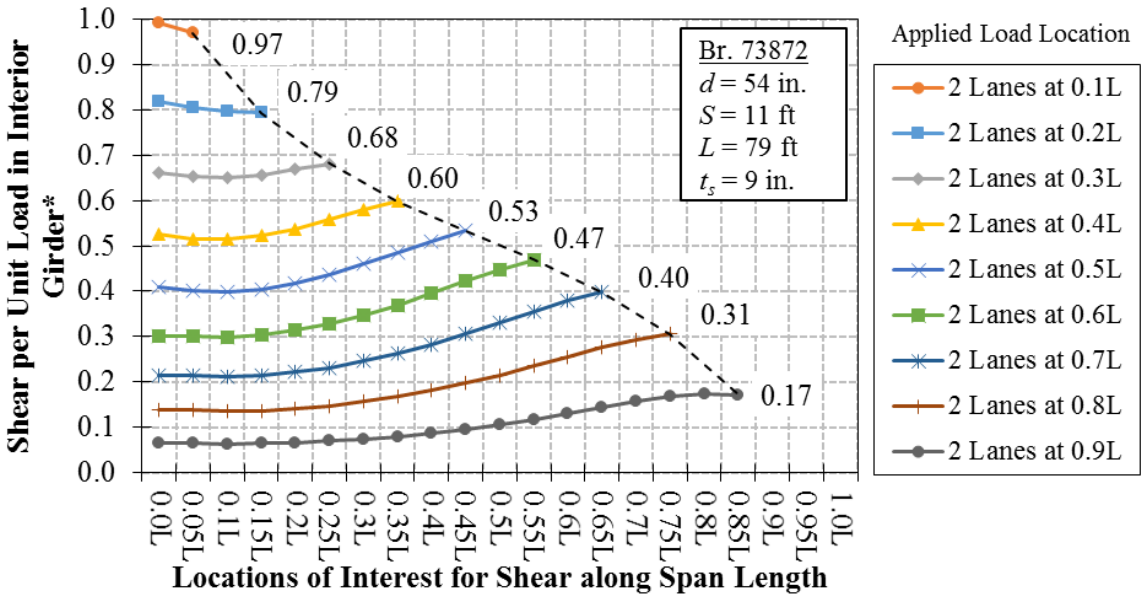

*The Shear per Unit Load in Interior Girder values already account for the presence of two axles.

Figure I-19. Br. 73872 Shear per Unit Load vs. Span Length for 2 Lanes Loaded